UNIVERSITY OF
KWAZULU-NATAL

INYUVESI
YAKWAZULU-NATALI

APPLICATIONS OF FLUOROCARBONS FOR SUPERCRITICAL EXTRACTION IN THE PETROLEUM INDUSTRY

Mark Duncan Williams-Wynn

[MSc. (Eng.)]

Submitted in fulfilment of the requirements for the degree of Doctor of Philosophy in the School of Engineering at the University of KwaZulu-Natal

March 2016

Advisors: Prof. D Ramjugernath

Prof. P. Naidoo

DECLARATION

I, Mark Duncan Williams-Wynn, Student number: 207500314, declare that

(i) The research reported in this thesis, except where otherwise indicated, is my original work.

(ii) This thesis has not been submitted for any degree or examination at any other university.

(iii) This thesis does not contain other persons' data, pictures, graphs or other information, unless specifically acknowledged as being sourced from other persons.

(iv) This thesis does not contain other persons' writing, unless specifically acknowledged as being sourced from other researchers. Where other written sources have been quoted, then:

a) their words have been re-written but the general information attributed to them has been referenced;

b) where their exact words have been used, their writing has been placed inside quotation marks, and referenced.

(v) This thesis does not contain text, graphics or tables copied and pasted from the Internet, unless specifically acknowledged, and the source being detailed in the thesis and in the References sections.

Signed: _____ Date: _____

As the candidate's supervisor I agree to the submission of this thesis.

_____ _____

Prof. D. Ramjugernath Prof. P. Naidoo

DETAILS OF CONTRIBUTION TO PUBLICATIONS that form part and/or include research presented in this thesis (include publications in preparation, submitted, in press and published and give details of the contributions of each author to the experimental work and writing of each publication)

Publication 1: **Williams-Wynn, M.D., Naidoo, P., Ramjugernath, D. (2016). Isothermal (vapour + liquid) equilibrium data for binary systems of (n-hexane + CO_2 or CHF_3), J. Chem. Thermodyn. 94, pp. 31-42**
Williams-Wynn: Undertook all experimental work and modelling and wrote the paper.
Naidoo: Provided advice for the measurements and modelling and proof-read the manuscript.
Ramjugernath: Provided advice for the measurements and modelling, proof-read the manuscript and undertook administration for submission of the manuscript.

Publication 2: **Williams-Wynn, M.D., Naidoo, P., Ramjugernath, D. (xxxx). Isothermal vapour-liquid equilibrium data for the binary systems of (CHF_3 or C_2F_6) and n-heptane, J. Chem. Thermodyn., submitted**
Williams-Wynn: Undertook all experimental work and modelling and wrote the paper.
Naidoo: Provided advice for the measurements and modelling and proof-read the manuscript.
Ramjugernath: Provided advice for the measurements and modelling, proof-read the manuscript and undertook administration for submission of the manuscript.

Publication 3: **Williams-Wynn, M.D., Naidoo, P., Ramjugernath, D. (xxxx). Isothermal vapour-liquid equilibrium data for the binary systems of (CHF_3 or C_2F_6) and n-octane, J. Chem. Eng. Data, to be submitted**
Williams-Wynn: Undertook all experimental work and modelling and wrote the paper.
Naidoo: Provided advice for the measurements and modelling and proof-read the manuscript.
Ramjugernath: Provided advice for the measurements and modelling, proof-read the manuscript and undertook administration for submission of the manuscript.

Publication 4: **Williams-Wynn, M.D., Naidoo, P., Ramjugernath, D. (xxxx). Isothermal vapour-liquid equilibrium data for the binary systems of CHF_3 with (n-nonane, n-decane, or n-undecane) and (C_2F_6 + n-decane), Fluid Phase Equilibria, to be submitted**
Williams-Wynn: Undertook all experimental work and modelling and wrote the paper.
Naidoo: Provided advice for the measurements and modelling and proof-read the manuscript.
Ramjugernath: Provided advice for the measurements and modelling, proof-read the manuscript and undertook administration for submission of the manuscript.

Publication 5: **Williams-Wynn, M.D., Naidoo, P., Ramjugernath, D. (xxxx). Isothermal vapour-liquid equilibrium data for binary systems of (CHF_3 or C_2F_6) with (1-hexene or 3-methylpentane), J. Chem. Thermodyn., to be submitted**
Williams-Wynn: Undertook all experimental work and modelling and wrote the paper.
Naidoo: Provided advice for the measurements and modelling and proof-read the manuscript.
Ramjugernath: Provided advice for the measurements and modelling, proof-read the manuscript and undertook administration for submission of the manuscript.

Publication 6: **Williams-Wynn, M.D., Naidoo, P., Ramjugernath, D. (xxxx). Isothermal vapour-liquid equilibrium data for binary systems of (CHF_3 or C_2F_6) with (methylcyclohexane or toluene), J. Chem. Eng. Data, to be submitted**

Williams-Wynn: Undertook all experimental work and modelling and wrote the paper.
Naidoo: Provided advice for the measurements and modelling and proof-read the manuscript.
Ramjugernath: Provided advice for the measurements and modelling, proof-read the manuscript and undertook administration for submission of the manuscript.

ACKNOWLEDGEMENTS

- All glory to my Lord, Jesus Christ.
- An acknowledgement of the assistance and guidance of the supervisors of the research undertaken, Prof. Deresh Ramjugernath and Prof. Paramespri Naidoo, is necessary.
- The financial support of the South African Research Chairs Initiative of the Department of Science and Technology and the National Research Foundation is acknowledged.
- The assistance of the Thermodynamic Research Unit's laboratory and workshop technicians, Mr Ayanda Khanyile, Mr Leon Augustyn and Mr Lindenkosi Mkize, as well as the School of Engineering's electronics technician, Mr Sanjay Deeraj was appreciated.
- The assistance of Dr Wayne Nelson in becoming proficient in the measurement of high pressure phase equilibrium measurements is appreciated.
- The use of the facilities at the Centre Thermodynamique des Procédés at the École Nationale Supérieure des Mines de Paris (MINES ParisTech) for the measurement of the critical points of mixtures is acknowledged.
- The assistance and guidance of Dr Christophe Coquelet, Mr Alain Valtz, Dr Paolo Stringari and other staff members at the Centre Thermodynamique des Procédés at the École Nationale Supérieure des Mines de Paris (MINES ParisTech) is acknowledged.

ABSTRACT

The majority of supercritical processes utilise carbon dioxide (CO_2) as the principal solvent, because CO_2 has many attributes that make it an ideal supercritical fluid (SCF) solvent. This study investigates the possibility of replacing CO_2 with trifluoromethane or hexafluoroethane, because of the poor performance of CO_2 in cases where more polar and heavier molecular weight solutes must be extracted. Several applications in the petroleum industry, such as oil sludge treatment and the treatment of contaminated soils, are discussed.

Due to the large number hydrocarbons present in such applications, a selection of solutes that could be used to simulate a simplified stream were chosen for these investigations. These selected solutes were n-hexane, n-heptane, n-octane, n-nonane, n-decane, n-undecane, 1-hexene, 3-methylpentane, methylcyclohexane, toluene and water. High-pressure vapour-liquid equilibria and vapour-liquid-liquid equilibria for binary systems containing either trifluoromethane or hexafluoroethane, with these solutes were measured using a static-analytic apparatus at temperatures of between (272.9 and 313.2) K. For several systems, the phase equilibria data were verified using bubble-point pressures measured with a static-synthetic, variable-volume cell.

Parameters for thermodynamic models were obtained by regression of the experimental data for the binary systems. The models provide a good representation of the majority of the systems investigated, and were therefore also used to estimate portions of the critical locus curves. These critical locus curves were compared to the critical loci that were extrapolated from the sub-critical coexistence data as well as critical loci that were measured with a critical point determination apparatus. There is satisfactory agreement between the calculated, the extrapolated and the measured critical loci.

The thermodynamic models were used to simulate the separation of several hydrocarbon-water emulsions using either CO_2, trifluoromethane, hexafluoroethane or mixtures thereof. The simulations confirmed that trifluoromethane, hexafluoroethane as well as mixtures thereof, provide improved performances (recoveries and yields) when used as alternative solvents in the SCF extraction of these systems. An economic analysis of a SCF extraction process was performed to investigate the performance of the solvents, and if such SCF extraction processes, using a mixture of trifluoromethane and hexafluoroethane, would provide an economically competitive treatment process for hydrocarbon-water emulsions.

CONTENTS

LIST OF FIGURES

LIST OF TABLES

1. INTRODUCTION

Many specialist separation techniques have been developed specifically with petroleum refineries in mind. The numerous complexities present in the separation of the components of crude oil have promoted innovative and efficient separation schemes. There remain further process advances for the petroleum industry that are yet to be developed. This is most pertinently the case with the processing of petroleum waste streams.

Supercritical fluids (SCFs) are a fairly new field. Many new technologies have been envisaged with the use of a SCF solvent as the chief innovation. The applications of SCFs range from extraction processes to particle formation processes.

The purpose of this chapter is to provide a background into some of the difficult separations found in the petroleum industry, to which supercritical fluid extraction (SCFE) could possibly be applied. The advantages in the use of SCFs are discussed, along with several current applications of SCFs in industry. Finally, the possible applicability of SCFs to effect difficult separations found in the petroleum industry are reviewed.

1.1. PETROLEUM INDUSTRY PROCESSES

The feedstock to any crude oil refinery is possibly one of the most complex mixtures for which a separation is required. A large fleet of processes is required in order to fractionate and convert the raw feedstock into the required products. Research is ongoing in attempts to develop new and improved processes to separate a given feedstock into the required products. This is especially challenging given the dramatic variability of the feedstock. The fleet of processes used on a crude oil refinery produce a vast number of intermediate process streams, product streams and waste streams. A new interest, in an effort to improve the efficiency and to reduce the environmental impact of the petroleum industry, is the development of new methods for the processing of streams, with little value, that were previously seen as waste. Examples of these waste streams include oil sludge and contaminated soils.

1.1.1. OIL SLUDGE

Oil sludge, or refinery sludge, describes a broad range of residues that are produced by the oil and petroleum industries. The mixture of petroleum residues, water and sand which is produced during exploration and development of oil fields is known as oil sludge (Jing et al., 2011). So too is the sludge from the wastewater treatment facility of an oil refinery (Güngören et al., 2007), as well as the sludge

removed from the bottom of crude oil storage tanks (Ávila-Chávez et al., 2007). In general, therefore, an oil sludge is any stable colloidal suspension containing oil-in-water or water-in-oil emulsions along with suspended solids and a number of other minor components arising from activities related to the petroleum industry (Jing et al., 2011). The sludge often also contains small concentrations of toxic heavy metals, which means that care has to be taken during oil sludge processing and disposal (Kriipsalu et al., 2008).

Due to the broad spectrum of sources of oil sludge, it is difficult to present a generalised characteristic for all oil sludge. Each process produces a different sludge, with the composition of the oil sludge also being highly dependent upon the crude oil from which it is produced (Schmidt, 1986). Regardless of this fact, information on the components present in a sludge and the concentration of each component in the oil sludge are vital for the design of efficient processes for the recovery of valuable components.

It is therefore necessary to analyse the characteristics of each of the oil sludges that are to be processed. This has led to a substantial number of investigations into the characteristics of oil sludge from numerous of sources. Examples of several of these investigations are given in Table 1.1.

Table 1.1: Investigations characterising various oil sludge.

Authors	Investigation
Altgelt and Boduszynski (1994)	Reviewed modern methods for the analysis of heavy petroleum fractions
Carbognani et al. (1999)	Characterised the oils and separated solids from Venezuelan oil wells and storage tanks
Carbognani et al. (2001)	Characterised the crude oil and solid deposits from the PST crude oil field in eastern Venezuela
Kriipsalu et al. (2008)	Performed a component-based analysis of the oily sludge from the flocculation-flotation unit of a waste water treatment plant of a Swedish oil refinery
Heidarzadeh et al. (2010)	Evaluated several oil sludge samples from a Tehran oil refinery
Wang et al. (2010)	Determined the compositions of oil sludges from two Chinese oil fields
Zhang et al. (2011)	Characterised the oil sludge from an electric hydrator

1.1.1.1. SOURCES

Oil sludge is produced during the extraction of the crude oil (oil field sludge) and in the refining of the crude oil (refinery sludge).

Refinery Sludge

van Oudenhoven et al. (1995) listed the main sources of oily sludge in an oil refinery as:

- Process water and surface run-off via flocculation-flotation units,
- Excess activated sludge, and
- Accumulated sludge in the bottoms of rail, truck and storage tanks.

Van Oudenhoven et al. estimated that sludge produced by refineries account for as much as 0.12% of their throughput. Based on this estimate, an average 100 000 barrel per day refinery would produce 120 b/d, or 14.3 m^3/d, of oil sludge.

A number of different units within the oil refinery utilise or produce water within the process. Examples of these processes include the desalination and the cracking processes. Much of this water can be recycled, but a substantial amount must also be disposed of, or at the least, the oil sludge must be removed from this water before reuse. All of the storm-water run-off from the process areas of oil refineries must also be collected and treated (Da Silva et al., 2012). The volume of the oil sludge that is collected from the plant must be reduced in pre-treatment processes to enable easier processing and disposal. The pre-treatment processes include gravity separators, flocculation-flotation units, centrifuges, filters, and thermal, electrical or acoustic dewatering units (dehydrators) (van Oudenhoven et al., 1995; Zhang et al., 2011).

Alongside the oil and water emulsions, oil sludge also contains solids, such as mineral particles, which are formed during the drilling of the oil wells and are entrained in the crude oil during production. These particles are very fine, and remain in suspension during transportation of the crude oil, until such time as they are stored in storage tanks (Wang et al., 2010). Asphaltenes present in crude oil are absorbed onto any hydrophilic solid particles present at the oil-water interface (Kriipsalu et al., 2008). As these particles absorb the asphaltenes, they become larger and heavier and settle to the bottom of the tank as a sludge. This sludge accumulates at the bottom of any tank containing crude oil, and must occasionally be removed, as the tank capacity would otherwise be reduced.

Due to the few possibilities for the disposal or recycling of oil sludge, many refineries and other crude processing facilities have large stockpiles, which are stored in semi-permanent land-fills or sludge ponds (Kam, 2001).

1.1.1.2. Formation Mechanics

The two most common hydrocarbon components that are found in oil sludge are asphaltenes and paraffinic waxes. Asphaltenes were defined by Pfeiffer and Saal (1940) as the heptane-insoluble,

toluene-soluble fraction of petroleum. The main building blocks of asphaltenes are polynuclear aromatic rings. Attached to these aromatic rings are alkyl side chains and heteroatoms such as oxygen, nitrogen and sulphur. Asphaltenes are generally the most polar components in crude oil (Yang and Kilpatrick, 2005). The paraffinic waxes are the most aliphatic and non-polar components found in the crude oil, but they generally have extremely high molecular weights and marginal solubilities in the crude oil itself (Yang and Kilpatrick, 2005).

Currently, there is no widespread consensus or understanding on which components in a crude oil stream will precipitate or deposit, and therefore, what the exact composition of an oil sludge derived from a specific crude oil would be. The initialisation steps for the formation of the oil sludge are also not well understood. This poor understanding is due to the complex nature of the crude oil and of the asphaltenes and paraffinic waxes therein (Musser and Kilpatrick, 1998). Some of the current reasonings for the formation of the sludge are discussed in Table 1.2.

Table 1.2. Oil sludge formation theories.

Asphaltenes	The polar portions of the functional groups present in the asphaltenes are suspected to be responsible for the aggregation of the asphaltenes, and thus the formation of oil sludge (Yang and Kilpatrick, 2005). Wang et al. (2010) found that oil sludge generally contains higher concentrations of asphaltenes and polar molecules than the crude oils from which they were derived. This indicates that there is a definite aggregation and accumulation of the asphaltenes, creating the sludge. The polar asphaltenic molecules also accumulate preferentially at the oil-water interface, and are therefore likely to be responsible for the formation of the oil-water emulsion in the sludge.
Paraffinic Waxes	Some of the waxes precipitate out of the crude oil when the thermodynamic solid-liquid boundary is crossed. These precipitating waxes entrain other shorter chained paraffins in the process (Yang and Kilpatrick, 2005), resulting in them being found in the oil sludge.
Mineral Particles	Yang and Kilpatrick (2005) and Sztukowski and Yarranton (2005) claimed that along with the asphaltenes, any fine solids present in the crude oil were also responsible for the stability of an oil-water emulsion. Langevin et al. (2004) reported that mineral particles can become oil-wet after lengthy contact with the crude oil. These particles, if sufficiently tiny, stabilise the oil-water emulsion. However, during long term storage, it is suspected that the droplets from the emulsion aggregate and settle to the bottom of the tank, forming emulsified sludge.

1.1.1.3. TREATMENT TECHNIQUES

There are many different oil sludge treatment techniques available, although this number has diminished over the years due to economic and environmental reasons (Kam, 2001). Simultaneously, not many alternative processes have been developed, which has led to limited options being available for the treatment and disposal of oil sludge.

The recovery of hydrocarbons by each of the treatment process differs substantially. Some processes, such as incineration and land-farming, do not intrinsically allow for the recovery of hydrocarbons, but are simply a means of waste reduction and disposal. Other techniques, such as pyrolysis and extraction, were developed with the aim of recovering at least a portion of the useful components. Brief descriptions of some of the more common treatment techniques are given in Table 1.3.

Table 1.3. A brief summary of current oil sludge treatment techniques

Process	Description
Centrifugation	Centrifugation is used to separate a gaseous phase, an aqueous phase and a hydrocarbon phase from the oil sludge (Da Silva et al., 2012). The separation is dependent on the different densities of the phases present in the mixture. This technique is not capable of processing 'oil-wet' mineral particles.
Electro-demulsification	A voltage is applied across an oil sludge, causing the fine particles that are absorbed at the droplet surface to precipitate (Elektorowicz and Habibi, 2005). Once these particles are removed, the separation of the phases can proceed, because the applied voltage also reduces the interfacial surface tensions.
Extraction	A liquid or a supercritical solvent is used to extract the hydrocarbon components from the sludge. When using liquid solvents, the recovery of the solvents is often difficult. The solvent is therefore often re-processed alongside the extracted solutes. Several investigations have been undertaken into the use of SCFs to perform the extraction.
Incineration	The incineration of oil sludge is a simple method for reducing the volume of waste. However, there are no reusable products and the combustion is also highly polluting, producing both a flue gas and a fly ash. The presence of heavy metals in the oil sludge means that the combustion products are often toxic.
Landfill	The oil sludge is buried underground, within impermeable 'cells'. These cells prevent the sludge from entering and contaminating any underground water sources. The sludge is allowed to decompose naturally. This is one of the most cost effective sludge disposal techniques, but requires availability of empty land for the landfill, and does not allow for the hydrocarbon portion of the sludge to be recovered.

Process	Description
Land Farming	In land farming, the oil sludge is added to the top layer of soil in small concentrations, and the sludge is degraded by microorganisms and by natural weathering. This technique can only be used where there are large tracts of unused lands, which is generally in areas where the climate does not allow the land to be used for agricultural activities, such as in arid deserts.
Pyrolysis	The oil sludge is heated to high temperatures in the absence of air,producing light hydrocarbons from the hydrocarbon portion of the sludge. The light hydrocarbons can be utilised as a synthesis gas. A small amount of fly ash is also produced, which must be disposed of safely.

A more detailed description of these techniques for the treatment of oil sludge is given in Appendix A.1.

1.1.2. Contaminated Soils

During the production, transportation and refining of crude oil and its products, spillages and leaks are unfortunately commonplace. These spillages and leaks, if not contained lead to the contamination of the surrounding soil. If soil contamination occurs, techniques for its remediation are required. The recovery of the valuable hydrocarbons from the contaminated soils being remediated is sometimes also of interest. The established conventions and regulations with regards to soil remediation, either in-situ, on-site or elsewhere, vary drastically from country to country (Wilson and Jones, 1993). Many regulations are concerned with how the remediation process affects the surrounding environment. Established conventions are often based upon the cost of the various techniques. In many soil remediation applications, the cost remains one of the most important considerations.

1.1.2.1. Compositions and Soil Structures

In controlled studies of soil rehabilitation, two distinct types of contaminated soils are usually investigated; those containing “total petroleum hydrocarbons” (TPH), and those containing only “polycyclic aromatic hydrocarbons”, or PAH (Ávila-Chávez and Trejo, 2010). The contaminated soils used in the studies are often created by the addition of a hydrocarbon mixture to a ‘clean’ soil, in a technique known as spiking. TPH contaminated soils contain a broad spectrum of hydrocarbons, which are comparable to the compositions of crude oil, and include both aliphatic and aromatic components (Michelsen and Boyce, 1993; Kostecki, 1999). PAH contaminated soils are soils that have been contaminated with only heavy, polycyclic aromatics. The removal of these high molecular weight

aromatics from soil matrices is the most difficult soil remediation application, and according to Wilson and Jones (1993), has not as yet been performed to a satisfactory degree with current technology.

The structure and type of the soil matrix that has been contaminated also contributes towards the ease with which the hydrocarbons can be separated from it. The unique properties of soils from different locations mean that no two separations will be the same (Brady et al., 1987). The differences in the soils are further enhanced by environmental factors, such as temperature, amount of rainfall and amount of sunlight. Many contaminated soils form complex matrices with the contaminating hydrocarbons due to weathering. The separation of such weathered contaminated soils cannot be adequately analysed by using "spiked" soils (Barnabas et al., 1995). Laboratory studies are therefore made more difficult, as real samples are needed in order to obtain authentic results.

1.1.2.2. TREATMENT TECHNIQUES

Although there is a necessity for the treatment of soils and sediments contaminated with petroleum products, there are not very many economically and technically feasible technologies available (Anitescu and Tavlarides, 2006). A fair number of processes have been suggested, but many of these have been shown to be financially unsustainable, or damaging to the environment. Some techniques are performed in situ, and do not require removal of the soil, whereas other techniques require the soil to be excavated for treatment. Several techniques that have been used on a large scale are described in Table 1.4.

Table 1.4. A brief summary of the treatment techniques for contaminated soils

Technique	Description
Biodegradation	Although this technique is essentially a case of leaving the contaminated soil 'as-is', the degradation of the contaminants can be accelerated by aeration of the soils, or by the addition of nutrients for the microorganisms.
Excavation and landfill	The contaminated soil is excavated and disposed of in a landfill site. Soil that has been sourced from elsewhere is used to replace the excavated soil. This technique is by far the fastest and simplest option, but can often be costly.
Incineration	The contaminated soil is excavated and is burned in a furnace. Any combustible organic material present in the soil is combusted. This is an expensive treatment technique, and is generally only used for the treatment of small amounts of soil. This process is also highly polluting, unless scrubbing of the flue gas is performed, in which case, it becomes substantially more expensive.

Technique	Description
Liquid extraction	The contaminated soil is washed with a liquid solvent. The solvent must then be separated from the soil by filtration and drying. Residual amounts of the solvent will remain in the soil, and the contaminants must be separated from the solvent by further separation processes, making this technique unpopular.
Phyto-remediation	Phytoremediation is similar to biodegration in that it uses natural processes to degrade the contaminants. The difference being that vegetation, rather than micro-organic activity, is used to perform the degradation. This technique is slow, but is also cheap to implement.
Soil washing or flushing	Surfactants are added, in situ, to the contaminated soil in an aqueous solution. The surfactants improve the solubility of the organic contaminants in the water. The 'wash liquid' is then removed from the soil through wells that are drilled into the ground. This technique is not favoured, as it is not possible to remove all of the wash water from the soil, and this could enter underground water sources, contaminating them with the surfactant.
Supercritical extraction	A SCF is used to extract the contaminants from the soil. The high pressures required for the SCF mean that this technique cannot be undertaken in-situ. The contaminants are easily separated from the solvent, by altering the pressure or temperature of the solution, thereby reducing their solubilities in the solvent. A large number of laboratory scale SCF treatments have been performed, but there have been few industrial scale processes reported that make use of this technique.

Further discussions on these techniques for the treatment of contaminated soil are provided in Appendix A.2.

1.1.3. Desulphurisation of Crude Oil

Hiyoshi et al. (2010) proposed that supercritical carbon dioxide (CO_2) could be used to remove aromatic sulphur components from fuel oils. These components require removal because they contribute towards sulphur oxide emissions ensuing the combustion of the fuel oils. The present desulphurisation process, catalytic hydrodesulphurisation, uses a Ni-Mb or Co-Mb catalyst, in conjunction with high temperatures and pressures, to remove the sulphur as hydrogen sulphide, H_2S (Topsøe et al., 1996). The H_2S formed in the catalytic hydrodesulphurisation process is toxic, and therefore must be separated from the off-gases by means of a scrubber.

The study of Hiyoshi et al. focused on the removal of the aromatic sulphur components, as these were found, by Wang and Prins (2009), to be least reactive in hydrodesulphurisation, and therefore the

most difficult to remove. It was found that supercritical CO_2 could be used to reduce the concentration of aromatic sulphur compounds in a mixture with hydrocarbons. The question remains, however, as to whether this process would be economically feasible, particularly when including all of the ancillary equipment required for the recovery of the solvent.

1.1.4. Dehydration and Desalination of Crude Oil

Untreated crude oil contains substantial amounts of water and salts, which are entrained during the production and transportation of the crude oil. The salts, which consist mostly of chlorides of sodium, magnesium and calcium, are dissolved either in any water droplets present in the crude oil, or else in the water portion of the emulsion (ASTM Committee D-2, 1949). The water, along with the dissolved salts, must be removed before distillation, as the salts, in the presence of water, can undergo hydrolysis upon heating, forming hydrogen chloride (HCl). The HCl causes corrosion of the process piping where accumulation occurs. Even salts that do not undergo hydrolysis can be damaging to the integrity of the process equipment, as they can cause fouling or catalyst deactivation.

1.1.4.1. Current Techniques

The most commonly used technology at present for the removal of the water and the accompanying dissolved salts from the crude oil is electric demulsification, in which an electric field is passed through the crude oil, causing the coalescence of the water droplets. Further details into the theory behind the operation of an electrical demulsification unit are given by Ichikawa (2007). If the water content in the crude oil is too high, the efficiency of electrical demulsification is reduced. This is because of an increased electrical conductivity of the fluid between the electrodes. Samedova et al. (2011) proposed a pre-treatment process for cases such as this to desalinate and dehydrate crude oil before sending it to the crude oil fractionation column. Their process utilised supercritical carbon dioxide.

Samedova et al. did not present any mechanisms behind their dehydration and desalinisation technique. It was therefore not possible to ascertain whether the supercritical CO_2 was used as a solvent to selectively extract the water and dissolved salts, or whether it was used as a coagulant, reducing the surface tension of the water droplets, and allowing their coalescence. The likelihood of carbon dioxide having a higher selectivity for water than for the hydrocarbons, at any given process conditions, is low. It is therefore more likely that, for this process to function, the supercritical CO_2 at high pressures performs the role of a coagulant. A major concern with the use of supercritical CO_2 with a fluid with high water content would be the formation of carbonic acid. Curiously, no mention of the acidity of the solution was made by Samedova et al.

A pilot plant for this process was constructed, and Samedova et al. (2011) claim that the technical-economical calculations for this new dehydration and desalinisation process reveal a substantially lower energy expenditure. This would equate to lowered operational costs for a refinery using this process.

1.1.5. Oil Sands

The unconventional crude oil that can be obtained from oil sands is of a low-grade and requires significant upgrading before it can be used in conventional petroleum applications (Brough et al., 2010). Oil sands contain a mixture of sand and clay with water and bitumen. There are substantial variances in the physical and chemical properties of the bitumen with location (Subramanian and Hanson, 1998). For oil sands processing, there have been two fields in which the use of SCFs has been investigated. The first area is the separation of the bitumen from the sand, clay and water as was investigated by numerous authors, such as Subramanian and Hanson (1998), Kotlyar et al. (1990) and Hartzell and Guigard (2012). The second area of interest is the use of SCFs in the upgrading of the bitumen into lower molecular weight hydrocarbons, as investigated by Brough et al. (2010).

1.1.5.1. Current Techniques

Some of the processes that are currently used for the extraction of the bitumen from oil sands are damaging to the environment, and improved techniques must be developed, to reduce the impact of petroleum extraction on the environment. An example of one of the current, environmentally damaging, separation techniques is the method used to extract the bitumen from the Athabasca oil sands in Northern Alberta, Canada (Hartzell and Guigard, 2012). This technique comprises treating the oil sands with a 'hot water extraction process', which uses large volumes of hot water to separate the bitumen from the sands (Government of Alberta, 2014). Unfortunately, in this process, not all of the water can be recycled due to economic restraints. Another example is the extraction of bitumen from Utah oil sands, also using a hot water process (Miller and Misra, 1982). There are a number of differences between these two processes, due to the different oil sand properties. However, both of these processes have high water consumption rates, as well as high operational temperatures in common (Subramanian and Hanson, 1998). In both processes, the spent oil sands and water are sent as slurry to large, environmentally hazardous, tailings dams.

SCFs have also been used to extract the bitumen from the oil sands in a manner similar to the method of extracting hydrocarbons from oil sludge. The main solvents that have been investigated are pure carbon dioxide, carbon dioxide with a co-solvent (Hartzell and Guigard, 2012), ethane (Rose et al., 2000) and propane (Subramanian and Hanson, 1998). Some of the advantages of using a supercritical

solvent to separate the bitumen from the oil sands are the ability to recycle and reuse a much greater percentage of the solvent, the reduction in the temperature of the process, and the improved yield and quality of the bitumen (Hartzell and Guigard, 2012). These advantages could lead to a reduction in the environmental impact of the process, as well as improving the economics of the process. The biggest problem with the solvents that have been investigated thus far are their low polarities, which results in low solubilities, and therefore high solvent to feed ratio requirements.

1.2. Supercritical Fluids: An Advantage

As seen with some of the examples from the petroleum industry, SCFs offer an alternative to conventional solvents. According to Erkey (2000), the disadvantages of the commonly used industrial solvents include:

- High viscosities,
- Specific gravities of close to unity, making the separation of the product from the solvents more complex,
- The solvents that are used are often surface active agents (surfactants) and therefore form emulsions,
- The amount of solvent that must be used must be of a substantially greater volume than the volume of the product, thus requiring large amounts of solvent, and
- There is often residual contamination of the products and by-products with the solvent.

The difficulties with the high viscosities, the specific gravities of close to one, and the amount of solvent required, can most often be overcome by using diluents. The use of diluents does not, however, prevent the residual contamination of the products with the organic solvent (Erkey, 2000; Perrut, 2000).

With SCF processes, the solvents are generally gases at lower pressures (Adrian et al., 1997). This gives SCF processes an advantage in solvent recovery, and inhibits residual solvent contamination of the products. A reduction in the pressure of the extract stream causes the solvent to leave the supercritical state, in turn causing a substantial decrease in the mutual solubilities of the product in the solvent and the solvent in the product (Palmer and Ting, 1995). The amount of residual solvent remaining in the product is substantially less than when a liquid solvent is utilised, and the solvent recovery is correspondingly increased (Jonas and Lamb, 1987).

Rizvi et al. (1986) list some of the important characteristics of SCFs which make them useful for industrial processes. These were said to include, “their high densities, low viscosities and diffusivities

that are intermediate between gases and liquids". The densities of SCFs are of the same magnitude as liquid densities. This leads to enhanced solubilities of the solutes in the SCFs in comparison to conventional solvents (Jonas and Lamb, 1987).

Sheng et al. (1992) listed some of the factors that should be considered in the selection of a SCF solvent as:

- The cost and availability of the solvent,
- The operational pressures required,
- The toxicity of the solvent, and
- The flammability of the solvent.

The major disadvantage in the use of SCFs are the high pressures that are required to achieve the supercritical state. These high pressures are often a deterrent from using SCFs in industry. This is due to the high costs for the construction of process equipment capable of withstanding these pressures, and the safety concerns that accompany the high pressure operations. Chordia (2008) reasoned that, in order for SCFs to become accepted in mainstream chemical processing, they need to be applied in high-volume, low capital cost technologies. This was disputed by Teja and Eckert (2000), who instead suggested that the niche markets in which SCFs have a foothold could become substantially more common in the future, thereby increasing the contribution of SCFs to industry.

1.3. Industrial Applications of Supercritical Fluids

Although solvent extraction is by far the most common application of SCFs, there are a large number of alternative processes in which they offer improvements over conventional processes. Some advantages of using SCFs are due to the comparatively high diffusivities and densities that are obtainable. Other advantages are linked to the large variations in the fluid properties that are achievable with only small changes in the process conditions close to the critical point. Additionally, supercritical processes are often viewed as belonging to the field of 'green chemistry' (Poliakoff et al., 1999), which makes them popular in the so-called 'green' industries.

Green chemistry was defined by Anastas and Warner (1998) as the development of novel processes that produce similar volumes of chemical products, but use and generate less hazardous substances, than the original process. Most of the research into SCF processes could therefore be classified as 'green chemistry', as the aim is to replace conventional solvents with SCFs, which are generally less hazardous and generate less waste products.

Desimone and Tumas (2003) identified carbon dioxide as one of the principal solvents with which green chemistry can be achieved. Since the early 1980's, carbon dioxide has become the 'ultimate solvent' for supercritical processes, mainly because it satisfies all of the desired criteria for a supercritical solvent (Sheng et al., 1992). There has therefore been little impetus for research into other gases for use as supercritical solvents. However, over the last few decades, it has been advocated that the increased release of "greenhouse gases" such as carbon dioxide, methane and other refrigerants, into the atmosphere are responsible for climate change (Osman et al., 2012). The greenhouse effect theory has meant that the opinion of SCF processes, especially those using solvents with high greenhouse warming potentials (GWPs), such as carbon dioxide have become tarnished. These SCF processes now require additional solvent capture after the extraction processes, to prevent the emission of so-called 'greenhouse gases'.

Some applications of SCFs, alternative to extraction, are given below in Table 1.5. It is believed that there is further scope, even within these applications, for different supercritical solvents that exhibit affinities for solutes that differ from those exhibited by CO_2.

Table 1.5. Applications of SCFs in industry

Application	Description
Analytical applications	SCFs are used in a number of analytical applications (Saito, 2013). The most common of these applications is supercritical fluid chromatography (SCFC). It is seen in some cases to be an extension of high pressure liquid chromatography (HPLC). Advantages of SCFC include the abilities to separate chiral components and the high throughput capabilities (Taylor, 2009). However, SCFC with non-polar CO_2 as the principle solvent does not provide a good separation of polar compounds.
Dry cleaning	SCFs have been used to dry clean a number of different items. An interesting application of SCF dry cleaning is its use to clean antique textiles without causing damage to the fibres (Sousa et al., 2007).
Extraction	The most common application of SCFs in industry is for extraction processes. The SCFs are used as replacements for conventional liquid solvents. Extraction processes could take the form of a single stage extraction or a multiple stage fractionation.
Painting and dyeing	SCFs have been used to reduce the viscosity of thick liquid coatings. The solution can then sprayed on a surface with ease, achieving a good, even distribution of the coating (Hoy, 1991). SCFs have also been used as a solvent for dyeing fabrics, improving the efficiency of the process, and reducing the amount of waste that is produced.

Application	Description
Particle production	SCFs have been used to form particles with very particular and uniform properties, as well as to produce particles that are free from any residual solvent (Tom and Debenedetti, 1991). There are a number of different techniques that are used to form the particles. The technique that is used depends on the properties of the substrate and the desired properties of the particles.
Polymer manufacture	Similarly to the use of SCFs in particle production, they can also be used for polymer manufacture to produce polymers with altered properties or structures (Teja and Eckert, 2000). The polymers that are formed with SCFs as the solvent have very narrow molecular weight distributions, and therefore, high degrees of polymerisation are possible. A special capability when using SCF solvents is the production of co-polymers containing two polymers that are mutually insoluble in conventional solvents.
Preservative Infusion	SCFs can be used to infuse pesticides, biocides and preservatives into the structure of wood (Acda et al., 1996). The infusion of these chemicals into the wood protects the wood from any internal damage, which is not possible when the chemicals are applied only to the surface.
Reaction Medium	A new application of SCFs is their use as a reaction medium (Machida et al., 2011). The reactions are performed in the SCFs, which have far higher mass transfer rates and molecular densities than conventional solvents. Thus, the reaction rates, the selectivity and the yield are all improved. The separation of the products from the solvent is also simplified with SCFs.

A more detailed discussion of these applications is presented in Appendix A.3.

1.4. SUPERCRITICAL FLUID EXTRACTION

In solvent extraction, a liquid solvent is contacted with the solid or liquid from which some of the components are to be obtained. These components are soluble in the liquid and therefore dissolve and can be recovered from the solvent. With SCFE processes, the liquid solvent is replaced with a fluid, which, at the high pressures at which the plant is operated, is in its supercritical state.

The majority of industrial SCFE processes are involved in the extraction and purification of nutraceuticals, food supplements and active pharmaceutical ingredients from solid raw materials (Sihvonen et al., 1999; Teja and Eckert, 2000). Palmer and Ting (1995) provided a comprehensive update on this industry up until 1995. Other reviews of SCFs were performed by Rozzi and Singh (2002), and by King (2014). Many of the applications for the food industry were developed as a

response to pressure applied by government regulations and consumer demands, encouraging the replacement of organic solvents with more benign alternatives (Teja and Eckert, 2000). Carbon dioxide is by far the most prevalent solvent used in the current applications, and will likely remain as such for the foreseeable future, as consumers will have no reservations about consuming a product that could contain residual quantities of carbon dioxide (Teja and Eckert, 2000). There would, however, remain many reservations if the solvent was a more 'exotic' gas, such as a hydrocarbon or a fluorinated hydrocarbon refrigerant. For this reason, the investigation was limited to processes in which the products would not be used for human consumption.

SCFE uses the solubilities of various solutes in the SCF, at specified temperatures and pressures, to remove them from their original solution. The two applications of SCFE are the production of a product containing chosen solutes from a mixture which also contains insoluble components, or the separation of solutes based upon their different solubilities in the SCF. The first application is by far the most common, and is considered the principal application of SCFs within industry. The second application, known as supercritical fluid fractionation (SCFF), remains a relatively obscured technique, with little industrial penetration. Examples of research into SCFF include the proposal of Espinosa et al. (2002) for the separation of fish oil fatty acid ethyl esters by SCFF, and the SCFF scheme of Crause and Nieuwoudt (2003) for the separation of heavy paraffin waxes.

One of the major advantages of SCFE is the ability to operate at temperatures close to ambient temperature. These temperatures mean that SCFs are attractive for use with heat sensitive systems (Nieuwoudt, 1996; Wypych, 2001). There is also a substantial saving in utility heating costs that can be achieved if operating a process at near ambient temperatures as opposed to the elevated temperatures often used in conventional processes. These reduced energy costs for heating are one of the factors that make SCFs economically viable.

1.5. SCFE IN THE PETROLEUM INDUSTRY

The petroleum industry is well versed in the construction, operation and maintenance of high pressure equipment. The high pressure requirements for SCFE cannot therefore be seen as a deterrent for the petroleum industry. A lack of understanding of the properties and fundamentals of SCFs, and how they behave in separation processes, is likely the major reason behind them not being used commonly in the petroleum industry.

There are a large number of possibilities for using SCFE in the petroleum industry, with most of the processes discussed in Section 1.1 being likely candidates for improvement by using SCFE. SCFE has an advantage over other solvent extraction techniques in that the solvent recovery can be achieved

simply by altering the process conditions. With liquid solvents, the usual practice is to blend the extract stream (both the solvent and the solutes) with the feed to a given fractionation column (Biceroglu, 1994; Trowbridge and Holcombe, 1995). This increased feed to the fractionation column reduces the volumes of fresh feed that can be processed, or alternatively, a column with a larger diameter is required. The larger throughput in such a column would also require increased utility useage and thus increased processing costs.

The solubilities of various components in SCFs are highly sensitive to the temperature and pressure at which the extraction is being performed (Palmer and Ting, 1995). This is useful for obtaining very specific splits of products. It also raises the possibility of producing multiple products of different compositions from a single extract. In cases such as the treatment of contaminated soils, where it is desired to treat a component such that it can be returned to the environment, the extremely low residuals remaining after SCFE provide a huge advantage over conventional liquid solvent extraction.

2. SUPERCRITICAL FLUIDS

The thermodynamic critical point for a pure component is the combination of pressure and temperature at which the separation between the vapour and the liquid phases suddenly ceases to exist. Figure 2.1 gives the *P*-*V*-*T* diagram of a pure substance, extracted from the work of Brignole and Pereda (2013). On the *P*-T plane projection given in this figure, it can clearly be observed that for a given pure component, any combination of temperature and pressure above the critical point will generate only a single fluid phase, termed a 'supercritical fluid'.

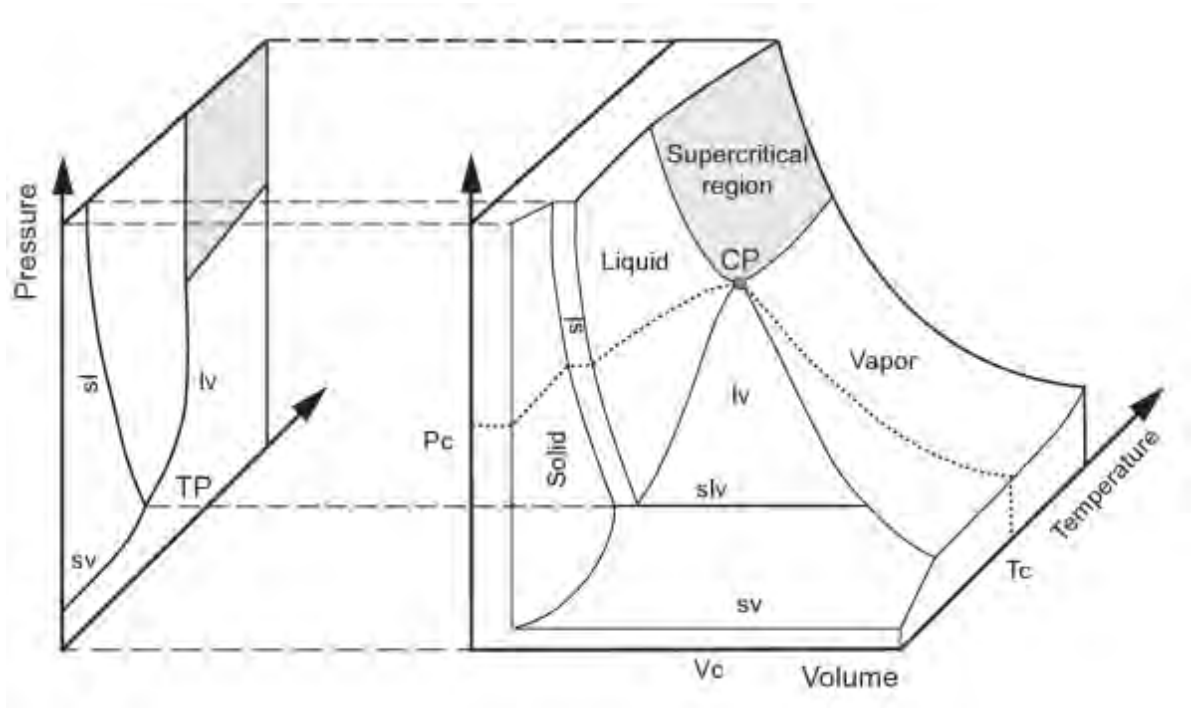

Figure 2.1. *P*-*V*-*T* diagram of a pure substance and its projection on the *P*-*T* and *P*-*V* planes (Brignole and Pereda, 2013)

Supercritical fluids display some properties that are usually attributed only to gases, in that they have no phase boundaries, and therefore have no surface tension, and yet have densities that are closer to the densities of liquids than those of vapours (Berche et al., 2009).

2.1. HISTORY

Supercritical fluids were first discovered by Cagniard de la Tour in 1822 by the heating of a sealed glass tube, filled with ethanol under pressure (Cagniard de la Tour, 1822). Cagniard de la Tour found that, at first, the liquid expanded, and thereafter, at a certain temperature, the demarcation between the liquid and vapour phases simply disappeared. Upon cooling of the tube, first a cloudiness (critical opalescence) appeared and thereafter the liquid meniscus re-appeared.

Andrews (1869) investigated the pressure-volume relationship of the 'vapour-liquid co-existence line' using carbonic acid. It was found that, upon increasing the pressure to partially liquefy the carbonic acid, and thereafter, heating it, "the surface demarcation between the liquid and the gas became fainter, lost its meniscus and thereafter disappeared entirely". The temperature and pressure at this point was named the 'critical point'. Andrews noted that if the pressure or the temperature were to be suddenly decreased, the fluid that formed demonstrated a phenomenon of moving and flickering bands and lines (striate). An interesting observation that was made by Andrews was that it was possible to take a fluid from its vapour state to its liquid state without any 'breaches of continuity', simply by manipulation of the temperature and the pressure.

The discovery of a 'fourth phase of matter' was considered, at the time, to be a phenomenon peculiar to the substances involved. However, Curie (1891) showed that the concept was in actual fact a universal phenomenon while investigating the demagnetisation effect on ferromagnetic materials at temperatures above the critical temperature.

Hannay and Hogarth (1879) expanded upon the investigation of Andrews (1869), by examining the solvent properties of SCFs for non-volatile solids. The solubilities of a number of solids in a supercritical solvent were compared to the solubilities in the same solvent in its liquid and vapour states. Hannay and Hogarth showed that the presence of a solid in the solution altered the critical pressure and temperature of the solution.

After the initial discovery of supercritical fluids, little interest was shown in using SCF for industrial applications (Schwarz, 2001). Other than the research conducted by Todd and Elgin (1955), into the solubilities of solids in supercritical ethylene, little research was conducted with regards to SCFs until the 1970's. A notable process developed in the 1970's by the Kerr-McGee Corporation was the "Residual Oil Supercritical Extraction" (ROSE) process of Gearhart and Garwin (1976). Authors such as Zosel (1978), Hubert and Vitzthum (1978), Schneider (1978) and Peter and Brunner (1978) then began to recognise the advantages that were posed by using supercritical carbon dioxide as a solvent.

In 1981, Worthy published a paper where SCF solvents were suggested as useful for effecting separations within the chemical processing industry (Worthy, 1981). Shortly thereafter, research into supercritical fluids began to gain traction with Bott (1980), Brunner and Peter (1981), Brogle (1982) and Randall (1982) all publishing papers relating to supercritical fluid extraction with carbon dioxide. During the 1980s, the majority of research into supercritical fluids related to the extraction of natural products, and was conducted in Germany. At the time, there was very little competition from elsewhere (Perrut, 2000).

Despite the research that was gaining traction in Germany, Basta and McQueen (1985) questioned four years later why there had still been no major new industrial applications of supercritical fluids. One of their hypotheses was that one of the major deterrents for industry in adopting supercritical processes was the unfamiliarity with the design and operation of high pressure equipment.

Most SCF research branched into two streams after the early discoveries. These two fields were the phase behaviour of a fluid in and around its supercritical state and the industrial applications of SCFs (Squires and Paulaitis, 1987). These two fields were not merged up until the 1980s, when researchers began to utilise phase behaviour measurements to predict the separation efficiencies of SCFE. This merging of the two fields has led to SCF research becoming a more conventional branch of chemistry research.

From the late 1980's and forward, a substantial amount of research was conducted into SCFE, beginning with authors such as McHugh and Krukonis (1986), Charpentier and Sevenants (1988) and Lira (1988). As more and more systems are investigated, the complexity of the systems under investigation has also increased (Johnston et al., 1989). Additional applications of SCFs, apart from SCFE have been developed as the properties and behaviour of SCFs have become better understood.

2.2. THERMODYNAMIC BEHAVIOUR

To understand the solubilities of solutes in different supercritical solvents, the behaviour of the solvent-solute binary system around the critical region needs to be understood (Knox, 2005). van Konynenburg and Scott (1980) utilised the van der Waals Equation of State (vdW EOS) to predict the phase diagrams for a wide range of binary mixtures. They determined the binary critical locus in the pressure-temperature-composition space by solving exactly a series of equations.

The various types of loci that were obtained, yielded a number of possible phase diagrams, which van Konynenburg and Scott classified according to their characteristic projections onto the P-T plane. This gave rise to the van Konynenburg and Scott (VKS) classification system. The projections of the loci yielded a number of interesting phenomena, such as lower and upper critical solution temperatures, lower and upper critical end points (LCEPs/UCEPs) and tri-critical points.

A lower critical solution temperature (LCST) occurs when a homogeneous phase separates into two distinct phases upon an increase in the temperature of the solution. The LCST is the minimum temperature on the isobaric co-existence curve. An upper critical solution temperature (UCST) occurs when two phases become a single phase solution with an increase in the temperature. The maximum temperature along the isobaric co-existence curve is the UCST. Systems with large positive molar excess enthalpies are most likely to exhibit UCSTs, whereas systems with negative excess enthalpies and large positive excess Gibbs free energies are most likely to exhibit LCSTs.

In a binary system, the critical end points occur at the intersection of a VLLE line and a critical locus curve (O'Connell and Haile, 2005). The critical locus curve could contain loci of liquid-liquid critical points or of vapour-liquid critical points. In the case of the occurrence of a liquid-liquid critical locus curve, the vapour phase and one liquid phase from the three phase solution become homogeneous, whereas in the case of the occurrence of a vapour-liquid critical locus curve, the two liquid phases in the heterogeneous solution become homogeneous or miscible. The UCEP occurs at a maximum temperature on the VLLE line, whereas a LCEP occurs at a minimum temperature on the VLLE line. Tricritical points are those points at which three coexisting phases become identical (Widom, 1973; Griffiths, 1974)

The system classifications that were proposed by van Konynenburg and Scott (1980) are divided into three distinct classes. The first class of systems exhibit a continuous critical locus, which joins the two pure component critical points. In the second class of systems, which are usually binary systems containing two components with very different critical temperatures, there is no continuous line joining the individual pure component critical points in the *P-T-x* space. As well as this discontinuity in the critical locus curve of class II systems, these systems could also exhibit LCSTs, which are caused by strong interactions between the two components. These theoretical LCSTs are often found at temperatures lower than the melting temperature of the solution (Heidemann and Khalil, 1980), meaning that these systems are difficult to distinguish from one another.

The VKS classifications of phase diagrams for binary systems with equal sized molecules are given in Table 2.1 and Table 2.2. Table 2.1 describes the class 1 types of phase diagrams and Table 2.2 describes the class 2 types of phase diagrams.

Table 2.1. VKS class 1 classification of van Konynenburg and Scott (1980) for binary systems consisting of equally sized molecules.

Type	VKS Description	Explanation
I	One critical line: C_1 to C_2 ($g = l$)	The simplest possible phase behaviour. The critical locus curve occurs between the critical points of the individual pure components.
II	Two critical lines: C_1 to C_2 ($g = l$); C_m to UCEP [$g + (l_1 = l_2)$]	This phase diagram consists of a gas-liquid critical locus between the pure component critical points, and a second critical line; the locus describing the UCSTs, starting at a fictitious 'critical point at infinite pressure', and ending at an upper critical end point (UCEP). This is the upper temperature limit of the three phase equilibrium region.

Table 2.2: VKS class 2 classification of van Konynenburg and Scott (1980) for binary systems consisting of equally sized molecules

Type	VKS Description	Explanation
III	Two critical lines: C_1 to UCEP [l_1 + (g = l_2)]; C_m to C_2 [(l = l) to (g = l)]. Three phase line: (*P*,*T*)=(0,0) to UCEP	Two critical locus curves are present in this type of system. The first curve moves from the critical point of the first component to a gas-liquid UCEP. The second curve occurs between the critical point of the second component and a critical point at infinite pressure. This locus curve transitions from a liquid-liquid critical loci to a gas-liquid critical loci along its length. A three phase line runs from a UCEP to P = 0, T = 0 between the pure component vapour pressure curves.
III-HA	Three phase line: (*P*,*T*) = (0,0) to UCEP does not lie between the pure component vapour pressure curves.	The three phase line runs from a UCEP to a point at (P, T = 0 MPa, 0 K) at lower temperatures than the one component vapour pressure curves, producing 'heteroazeotropic' behaviour.
IV	Three critical lines: C_1 to UCEP [l_1 + (g = l_2)]; LCEP to C_2 [(l = l) to (g = l)]; C_m to UCEP [g + (l_1 = l_2)]	For this type of system, the first critical locus curve (gas-liquid) moves from the critical point of component one to the UCEP. The second (liquid-liquid) curve moves from the UCEP to a critical locus at infinite pressure. The third critical locus curve travels from the critical point of the second component to a LCEP. This curve changes from gas-liquid critical loci to liquid-liquid critical loci along its length.
V	Two critical lines: C_1 to UCEP [l_1 + (g = l_2)]; LCEP to C_2 [(l = l) to (g = l)]	The lack of the low temperature UCST (C_m to UCEP) is the only difference between type IV and type V phase diagrams. It is often difficult to distinguish between type IV and type V diagrams because the UCST critical line could be hidden below the melting point of the solution.

In addition to these classes, type I, II and V systems also have subclasses, denoted I-A, II-A and V-A in which azeotropic behaviour is observed at sub-critical conditions. The type I azeotropes are negative, whereas the type II-A and V-A azeotropes are positive. With a negative azeotrope, at a fixed pressure, the boiling temperature of the azeotrope is greater than the boiling temperatures of the individual components. With a positive azeotrope, the opposite is true.

The graphical explanation of these types of systems is provided in the form of several global phase behaviour plots on the *P*-*T* plane in Figure 2.2 from the work of Martinez (2007).

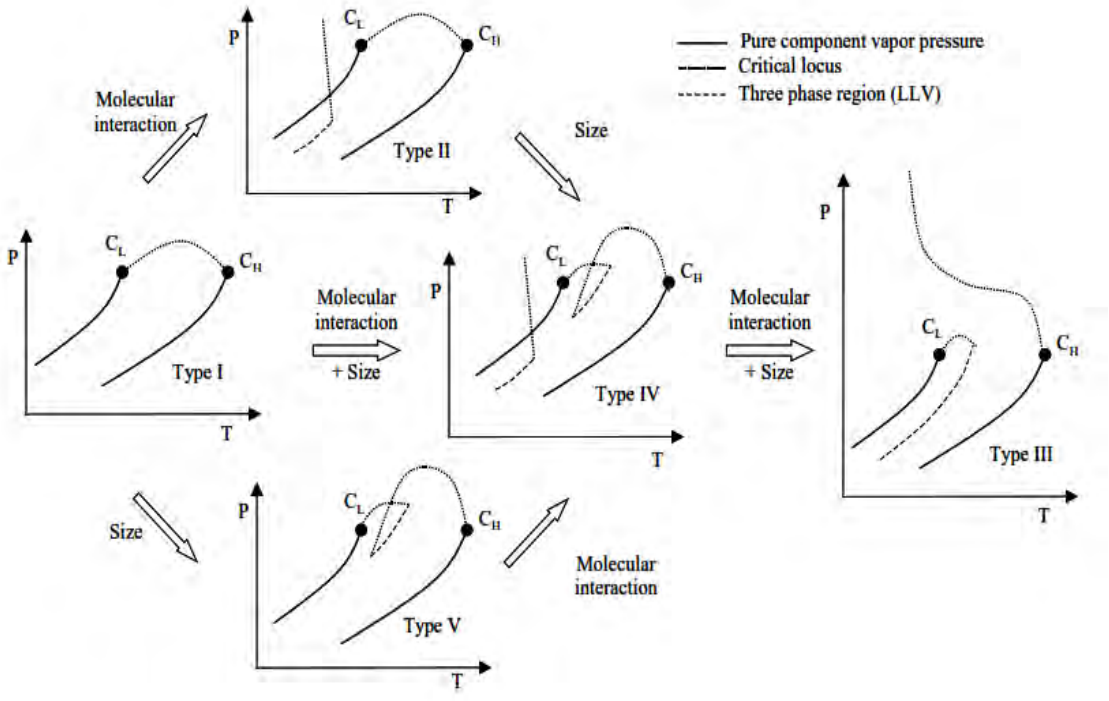

Figure 2.2. P-T planes of the global phase behaviour diagrams for the VKS classification system (Martinez, 2007)

van Konynenburg and Scott (1980) also predicted the phase behaviour of binary mixtures containing molecules of unequal sizes, but they found that the phase diagrams that were developed did not differ substantially from those identified using equal sized molecules. The unequally sized molecules did however mean that the azeotropic composition became a function of both the temperature and the pressure. There were also a number of cases in which double azeotropes were predicted.

Three important and occasionally useful phenomena that occur with supercritical fluids are critical opalescence, retrograde condensation and the 'cross-over' effect.

2.2.1. Critical Opalescence

Critical opalescence is a light scattering phenomenon that occurs universally at the critical point of a fluid (pure or multi-component). This causes the fluid to appear opaque, often with striae moving through the fluid, caused by the large fluctuations in the properties of the fluid in the approach to the critical point (Gopal, 2000). The occurrence of critical opalescence allows easier observation of the critical point. A more detailed explanation of the critical opalescence phenomenon was given by Gopal (2000).

2.2.2. RETROGRADE CONDENSATION

Retrograde condensation occurs at temperatures and pressures close to the critical region (Palmer and Ting, 1995), and is the formation of a liquid phase upon a decrease in pressure while the temperature remains constant (Park et al., 1987). With retrograde condensation, at a given temperature (always greater than the critical solution temperature), an increase in pressure results in a decrease in the solubility of the solute in the supercritical fluid. This can be observed in Figure 2.3, which is reproduced from the work of Park et al. (1987).

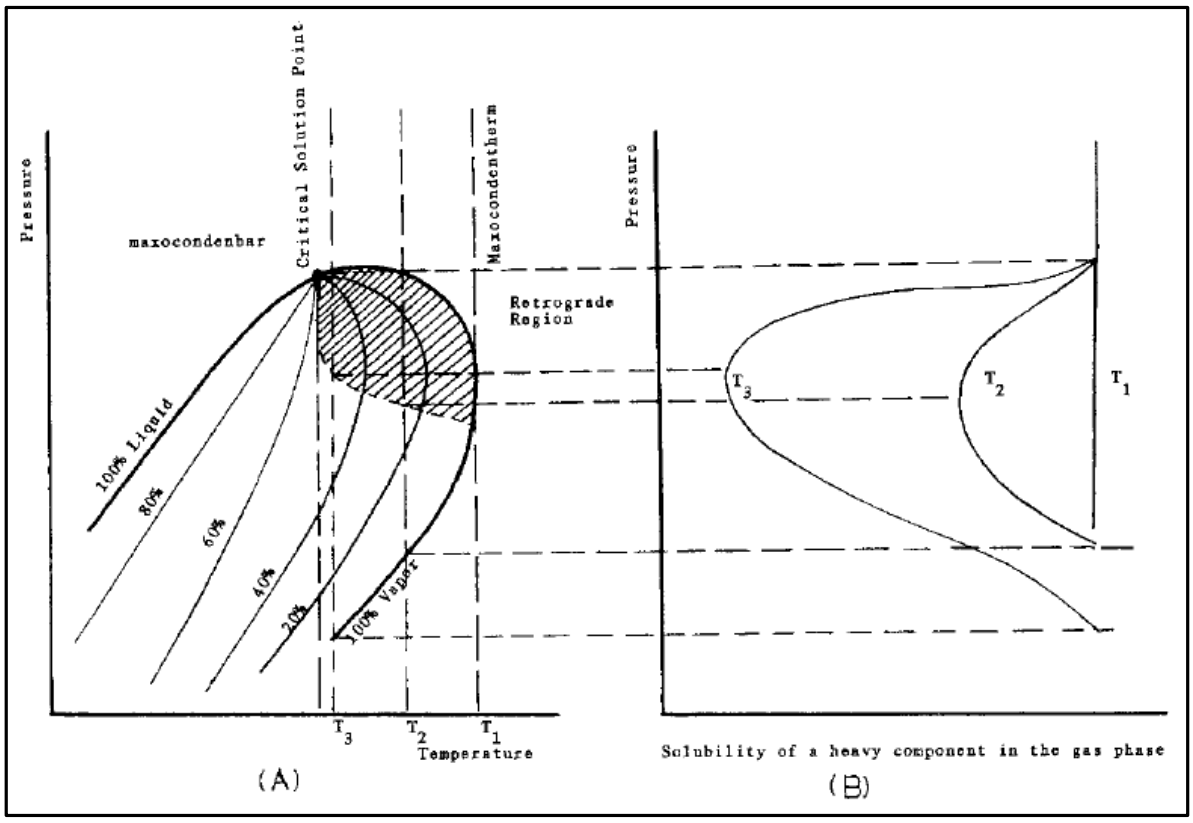

Figure 2.3: (A) The pressure-temperature plot and (B) the corresponding pressure-composition plot for a fluid exhibiting retrograde condensation. This figure is reproduced from the work of Park et al. (1987).

2.2.3. THE CROSS-OVER EFFECT

The 'cross-over' effect is a phenomenon in which, for the simplified case of a binary mixture, one solute will have a higher solubility in the supercritical fluid at all pressures up to a certain point, after which the solubility of the second solute becomes greater than that of the first (Park et al., 1987). This 'cross-over' effect is extremely useful, as it means that a process can be designed which would require only small pressure swings in order to obtain completely different separations.

2.3. DENSITY AND TRANSPORT PROPERTIES

The solubility of a component in a supercritical solvent has a complex dependency upon the temperature, pressure and density of the fluid (Haghbakhsh et al., 2013). Investigations into the

variations in the density of a SCF as a function of the temperature and pressure can provide insight into the conditions required to achieve the desired solubilities (Chrastil, 1982). The subcritical and supercritical densities, of both the pure component, and of the mixture, are therefore important. Generally, the solubility of a compound in a SCF increases as the density of the fluid increases. The subcritical densities can be predicted fairly accurately by thermodynamic models, but for supercritical densities, the current models are empirical, and rely on being tuned using experimental data. These correlations include those of Chrastil (1982), Guigard and Stiver (1998) and Hernández et al. (2011), to name a few.

The transport properties of the SCFs are of importance in the design of a SCF process (Lavanchy et al., 2006). As well as being useful in the design of the pumping and piping requirements of a plant, these properties also play an integral role in the dynamics behind any extraction or reaction that occurs. Utilising the equilibrium conditions of the process makes the assumption that equilibrium is attained immediately. In almost all cases, however, there is a period of time required for the equilibrium conditions to be attained. Transport properties, such as the diffusivities, viscosities and surface tensions of the mixtures are thus of importance, as they affect the speed at which equilibrium is attained. Many of the transport properties are also interdependent.

The viscosity of a fluid is a measure of the extent to which energy is lost by the fluid when it is forced to flow, and is strongly dependent upon the temperature (Stephan and Lucas, 1979). This temperature dependency is, however, influenced by the density of the fluid (Zabaloy et al., 2005). According to Zabaloy et al., the viscosity of a fluid at high densities will decrease as temperature increases, whereas the viscosity of a fluid at a low density will increase as temperature increases. At intermediate densities, there is the possibility for local extrema in viscosity to occur. Upon heating of a sample of a liquid, the viscosity of the liquid will decrease rapidly as the critical temperature is approached. Once the sample becomes a SCF, changes in the viscosity with changes in temperature are very small, when compared to those occurring in the liquid phase. These variations can be observed in Figure 2.4 from the work of Chen et al. (2014). In this plot, the temperature and pressure dependency of the dynamic viscosity can be observed. A 2.5 MPa variance in the pressure of the fluid near to the critical locus could cause the viscosity of the fluid to double. This phenomenon is useful in tailoring the conditions for a specific SCF application.

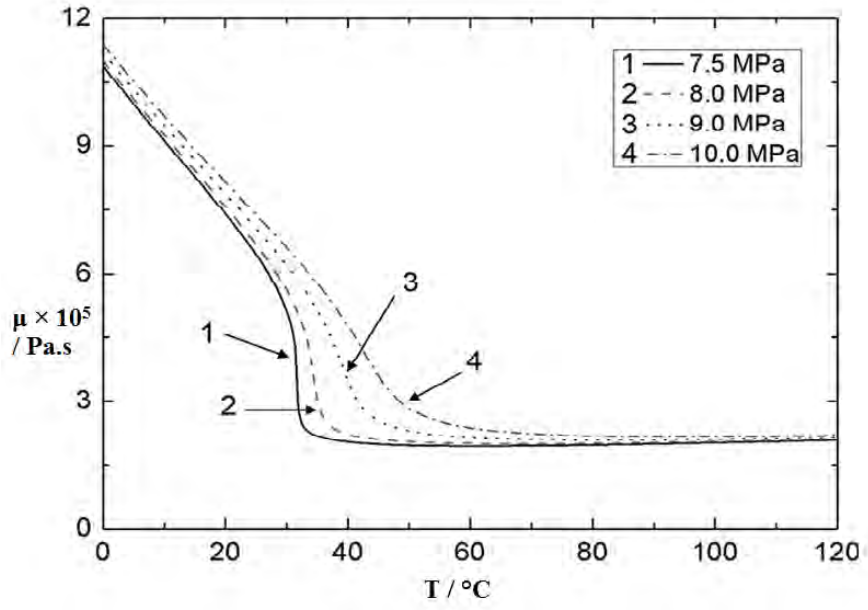

Figure 2.4. The temperature and pressure dependency of CO_2 viscosities at pressures of: —, 7.5 MPa; – –, 8.0 MPa; · ·, 9.0 MPa; – · – · –, 10 MPa. This plot was extracted from the work of Chen et al. (2014).

Although from Figure 2.4, it appears as if the viscosity of the supercritical fluid remains fairly constant with variations of temperature and pressure, Figure 2.5, obtained from the work of Zabaloy et al. (2005) proves otherwise. This plot demonstrates that the viscosity of CO_2 continues to decrease as the temperature is increased. At the same time, however, increases in the pressure at isothermal conditions can cause the viscosity to increase.

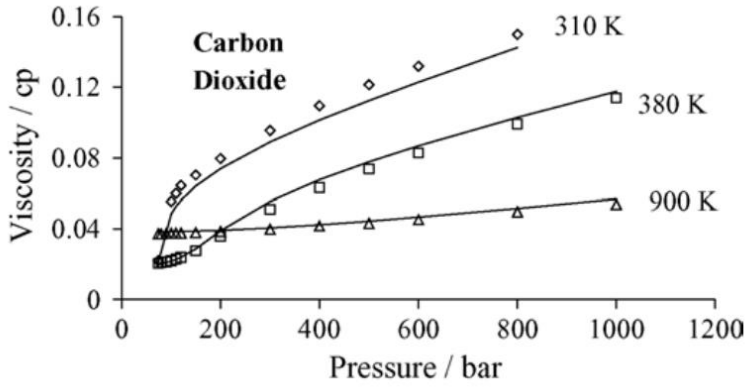

Figure 2.5. Viscosity-pressure plot for CO_2 at temperatures of between (310 and 900) K, as reported by Zabaloy et al. (2005). Experimental data (◊, □, Δ) was from the study of Stephan and Lucas (1979), with the fitted curves calculated using the correlation of Zabaloy et al.

2.4. SOLVENTS

A number of considerations must be made when selecting a supercritical solvent system. These include safety and operational considerations. Additionally, solvent selection must be based upon the supercritical properties of the solvent and its ability to perform the required separation.

2.4.1. SOLVENT SELECTION

An imperative for a SCF solvent is that its critical temperature be in close proximity to room temperature. Without this, any SCF process would require additional heating, which would impact on the economic viability of the process. The operational temperatures therefore drastically reduce the number of solvents that can be utilised, as there are only a handful of compounds that fulfil the requirement. Some of the more likely candidates as SCF solvents are low molecular weight hydrocarbons, such as ethane. Freons were also suggested by Hawthorne et al. (1992) as alternative fluids for SCFE, as some Freons exhibit most of the properties desired for SCF solvents.

2.4.2. POLAR SOLVENTS

Wirths and Schneider (1985) investigated the effect that polarity had on the critical phase behaviour by observing the critical behaviour of a number of hydrocarbons in CF_4 (a non-polar compound) and CHF_3 (a highly polar solvent with a dipole of $\mu = 1.65$ D). Their investigation provided data points at fixed compositions (isopleths), with varied pressures and temperatures.

Wirths and Schneider discovered that CHF_3 in binary mixtures with straight chained alkanes behaved differently to CF_4 systems with the same straight chained hydrocarbons. In contrast, the phase behaviour of CHF_3, and CF_4 in binary mixtures with decalin, squalane and tetralin had many similarities. The systems containing CF_4 exhibited higher mutual solubilities with shorter chained n-alkanes, but, as the n-alkane chain length increased, the solubility of n-alkanes in CHF_3 became greater than the solubility in CF_4. These two observations were explained by Wirths and Schneider as being due to the poor miscibility between fluorocarbons and hydrocarbons, the temperature dependence of CHF_3 self-association, and the occurrence of dipole or induced dipole interactions between CHF_3 and segments of the n-alkane chains. The similarity between the phase behaviour of the systems containing either of the two solvents with the cyclic hydrocarbons, in comparison to the straight chained alkanes is possibly due to the inability of CHF_3 to induce a dipole moment within the cyclic hydrocarbons, thereby giving them similar interactions as with the non-polar CF_4.

2.4.3. CO-SOLVENTS

As an alternative to the replacement of the entire solvent system, many processes have overcome low solvent polarities by the addition of a polar co-solvent to the solvent.

Kurnik and Reid (1982) were some of the first authors to investigate the use of co-solvents, in a study into the solubility of synthetic mixtures of solids in supercritical CO_2. They found that the solubility of some of the solids was enhanced by up to 300% when in a multicomponent solute system, as compared to the solubility of the solute in the pure solvent without additional components present. This was attributed to the co-solvent effect. Brunner (1983) also found that the solvent power and the solubility were improved upon addition of a co-solvent or 'entrainer'.

Dobbs et al. (1986) measured the solubility of a number of solids in supercritical CO_2, with the addition of liquid alkane co-solvents. They discovered that the solubility of the solids in the solvent mixture was significantly increased, even with the addition of only small amounts of co-solvents. It was postulated that this phenomenon was due to the fact that supercritical CO_2 is less polarisable than all of the hydrocarbons other than methane, and therefore the addition of the co-solvents enhanced the 'polarisability' of the solvents.

The addition of the co-solvents was found to further enhance the solubility with an increased chain length of the co-solvent. It was theorised that this enhanced solubility was due to the attractive forces, caused by the improved 'polarisability', outweighing the increased repulsive forces related to the van der Waals volume (Dobbs et al., 1986).

LIQUID CO-SOLVENTS

The most common type of co-solvents that are used are polar organic liquids, such as short chain-length alcohols. According to Kordikowski and Schneider (1993), when using liquid co-solvents, the following criteria are necessary for co-solvency effects to occur.

- The components with low volatility (i.e. the solute and the co-solvent) must be chemically different and should contain different functional groups.
- The differences between the critical pressures of the constituent binary systems must be small for isothermal co-solvency effects.
- There must be no specific interactions such as hydrogen bonding between the components.

Scheidgen and Schneider (2000) provided a ternary isothermal phase prism for the CO_2 + 1-octanol + hexadecane system at 313 K to depict the co-solvency effects. The phase prism for this system, as reported by Scheidgen and Schneider (2000), is given in Figure 2.6.

With this system, the two non-volatile components are chemically different, with one being an alcohol and the other an n-alkane. The critical pressures of the binary border systems are fairly close (15.8 MPa against 16.4 MPa), and there is therefore a substantial co-solvency effect. The minimum critical pressure of the ternary system is 10.4 MPa, 5.4 MPa less than the critical pressure of the CO_2 + 1-octanol binary mixture.

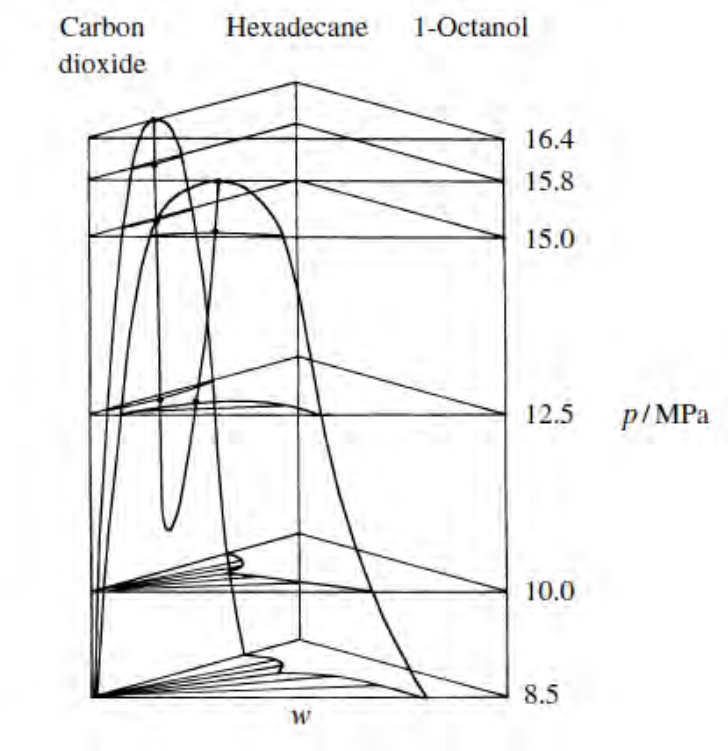

Figure 2.6: Isothermal phase prism for the carbon dioxide + 1-octanol + hexadecane system at 313 K. This figure was reproduced from the work of Scheidgen and Schneider (2000).

Co-solvency effects can result in complex systems in which closed, homogeneous regions (miscible regions) are completely surrounded by heterogeneous regions (immiscible regions) on an isobaric diagram. According to Pöhler et al. (1996) and Kordikowski and Schneider (1993), the largest miscibility windows occur when the shapes of the critical locus curves of each of the binary border systems are similar.

Supercritical Co-Solvents

Rather than the use of a liquid co-solvent, there is also a possibility to use a gaseous co-solvent. An example is an azeotropic mixture of CO_2 and a refrigerant. The addition of a polar refrigerant as a co-solvent could possibly improve the efficiency of the separation, while at the same time; lower the pressure at which the separation must be performed. The addition of azeotrope forming co-solvents to the CO_2 could result in a solvent that is 'green' and is easy to recover (Beckman, 2004). At present, not much investigative work has been conducted into this type of co-solvent. There have been,

however, a number of phase equilibrium measurements conducted for binary CO_2 and refrigerant systems (Roth et al., 1992; Shiflett and Sandier, 1998; Valtz et al., 2007; Nasrifar et al., 2008), although most of these measurements were undertaken in attempts to discover improved refrigerants.

2.5. Sub-Critical Thermodynamic Modelling

Sub-critical modelling is a relatively mature field, with a large number of reviews and summaries having been conducted over the years. A number of highly detailed reviews of chemical thermodynamics, have been conducted by authors including Walas (1985), Raal and Mühlbauer (1998) and Prausnitz et al. (1999).

2.5.1. Modelling Method

There are a number of approaches to the modelling of sub-critical systems. The simplest model for describing the sub-critical behaviour of a system is Raoult's law (equation 2.1.), as given by Smith et al. (2005). Raoult's law does not allow for any 'non-idealities' within the system, and therefore can only be applied with a measure of success to systems at low pressure and with highly similar components. Examples of such systems include those containing isomers or adjacent members of a homologous series.

$$y_i P = x_i P_i^0 \qquad 2.1$$

If the assumption that the liquid phase is an ideal solution is abandoned, and an activity coefficient term (γ_i) is included in the model, to describe the liquid phase 'non-idealities', the modified Raoult's law is produced (equation 2.2). This liquid phase activity coefficient is evaluated from excess Gibbs' energy (G^E) expressions.

$$y_i P = x_i \gamma_i P_i^0 \qquad 2.2$$

The modified Raoult's law still does not have the ability to account for vapour phase 'non-idealities', and therefore also only applies to low pressure systems. A more generalised model for vapour-liquid equilibria would also require a term to account for the vapour phase 'non-ideality'. If the vapour-phase fugacity coefficient (ϕ_i) is utilised, then the gamma-phi (γ-ϕ) model is developed (equation 2.3).

$$y_i \phi_i P = x_i \gamma_i P_i^0 \qquad 2.3$$

An alternative approach to the gamma-phi method is to introduce the fugacity coefficient to describe the non-idealities of both the vapour (ϕ_i^v) and liquid phases (ϕ_i^l). For this method, termed the phi-phi (ϕ-ϕ) approach, the fugacity coefficients for both phases are calculated using equations of state (EOS).

For high pressure phase equilibria, either the gamma-phi or the phi-phi (equation 2.4) models can be used to describe the systems.

$$y_i \phi_i^v = x_i \phi_i^l \qquad 2.4$$

One difficulty of the gamma-phi method occurs when the system temperature is above the critical temperature of at least one of the components (Smith et al., 2005). Since a fluid does not have a vapour pressure when it is in its supercritical state, the fugacity of the pure liquid cannot be calculated, since the fugacity is a function of the vapour pressure. This does not, however, prevent the fugacity of a sub-critical mixture at temperatures and pressures above the critical points of the pure component from being calculated.

2.5.2. Equations of State

For this work, cubic EOS were utilised to evaluate the fugacity coefficients describing the vapour phase non-ideality. Two of the more commonly used EOS are the Soave-Redlich-Kwong and the Peng-Robinson EOS (Table 2.3).

Soave-Redlich-Kwong (SRK) EOS

The Redlich-Kwong (RK) EOS (Redlich and Kwong, 1949) was a precursor to the SRK EOS (Soave, 1972), but it could not always perform accurate vapour-liquid equilibrium calculations because the liquid phase non-ideality could not be accurately calculated.

Soave (1972) modified the equation, improving the accuracy of the correlation of vapour-liquid equilibrium (VLE) data for non-polar and slightly polar systems as well as the vapour pressure calculation of hydrocarbons. A further modification of the temperature dependence of the attraction term of the EOS (Soave et al., 1993) meant that the calculation of the vapour pressures for both polar and non-polar solvents was also improved.

The SRK EOS still has a number of limitations, most notably, the inability to accurately predict the specific volume of the liquid phase. The SRK EOS over predicts the specific volume of the liquid phase by up to 27% in certain cases (Peng and Robinson, 1976). Another shortfall of the SRK EOS was the decreased accuracy of the predictions at points close to the critical point.

Peng-Robinson (PR) EOS

Peng and Robinson (1976) proposed an alternative modification to the cubic EOS of van der Waal, in an attempt to satisfactorily predict the liquid density and to improve the accuracy of predictions close to the critical point.

The PR EOS did not full address the issues of poor prediction of the liquid density, but it did allow a good prediction of the VLE of hydrocarbon systems close to the critical point. A large number of further short fallings of the SRK EOS and the PR EOS were discussed by both Abbott (1979) and by Martin (1979).

Table 2.3. A summary of the SRK and the PR EOS.

Equation of state	Mathematical form	
Soave-Redlich-Kwong (SRK)	$P = \frac{RT}{(V-b)} - \frac{a(T)}{V(V+b)}$	2.5
Peng-Robinson (PR)	$P = \frac{RT}{(V-b)} - \frac{a(T)}{V(V+b)+b(V-b)}$	2.6

ALPHA FUNCTION

Several authors have suggested the alteration of the alpha function for the cubic EOS in attempts to improve the accuracy of the correlation of phase equilibria data for mixtures (Twu et al., 1991). The standard PR alpha functions are "adequate for hydrocarbons and other non-polar compounds", but lack accuracy for polar compounds (Aspen Technology, 2012). For any light gases at high temperatures (T/T_c > 5), the standard alpha function also provides unrealistic results.

The reason for these unrealistic results is theorised to be due to the boundary conditions used for the derivation of the function. The function was developed on the basis that attractions between molecules become infinitesimal as temperature increases. The value for alpha would therefore correspondingly trend towards zero as temperature was to increase. This assumption was corrected by Boston and Mathias (1980) in their proposed alpha function.

Alpha functions that provide improved accuracies above the critical point are the Twu generalised alpha function (Twu et al., 1991; 1992) and the Mathias-Copeman (MC) alpha function (Mathias and Copeman, 1983). Other alpha functions, such as the Schwartzentruber-Renon-Watanasiri (SRW) alpha function (Schwartzentruber et al., 1990) and the Boston-Mathias (BM) alpha function (Boston and Mathias, 1980) are not capable of functioning above the critical points of the pure components, due to their formulations.

Twu Generalised alpha function (Twu et al., 1991; 1992)

The Twu generalised alpha function is currently recognised as the best available alpha function (Aspen Technology, 2012). It is a theoretically derived function. It behaves the best of the available alpha functions at supercritical conditions when the system exhibits large acentric factors. There is, however, no limit on the minimum value for the acentric factor, making this a versatile alpha function.

Mathias-Copeman alpha function (Mathias and Copeman, 1983)

The Mathias-Copeman (MC) alpha function provides accurate correlations of the vapour pressure for polar compounds. There are two forms of the MC alpha function, that for below the critical temperature and that for above the critical temperature. For the use of the MC alpha function above the critical point of one of the components, the second term and higher must be neglected by setting them equal to zero.

Both the Twu alpha function and the Mathias-Copeman alpha function are described in Table 2.4. An important note to make when using these generalised alpha functions capable of being applied to any cubic EOS is that the regressed parameters will differ for different EOS with the same component.

Table 2.4. A summary of the alpha functions discussed in this study.

Alpha function	Mathematical form	
Twu generalised alpha function	$\alpha_i(T_{r,i}, \omega_i) = {T_r}^{N(M-1)} exp\left[L\left(1 - {T_r}^{NM}\right)\right]$	2.7
	where *L*, *M* and *N* are fitted parameters	
Mathias-Copeman alpha function	$\alpha_i(T_{r,i}, \omega_i) = \left[1 + \kappa_1\left(1 - \sqrt{T_{r,i}}\right) + \kappa_2\left(1 - \sqrt{T_{r,i}}\right)^2 + \kappa_3\left(1 - \sqrt{T_{r,i}}\right)^3\right]$	2.8
	where κ_1, κ_2, and κ_3 are fitted parameters	

2.5.3. Mixtures and Mixing Rules

The original EOS were developed to describe the phase behaviour of single component systems without needing any phase equilibrium data. As such, they require only the pure component critical point (P_c, T_c) to enable them to describe the properties of a pure component. For multiple component systems, the pure component parameters must be combined by using empirical mixing rules.

There have been many mixing rules that have been developed over the years, each with different applications and peculiarities. Raal and Mühlbauer (1998) reviewed a number of the more common mixing rules. All of the available mixing rules are empirical, as no theory has been developed to relate the composition dependence of the parameters from EOS to the molecular interactions within a system.

van der Waals Mixing Rules

The simplest of the mixing rules are the van der Waals (VDW) mixing rules (Smith et al., 2005). These mixing rules use a quadratic equation to calculate a_m, and a linear equation to calculate b_m. For simple binary systems, the geometric mean of the pure component parameters provides satisfactory results.

SOAVE MIXING RULES

Soave (1972) made use of the van der Waals mixing rules, but rather than using a geometric mean combining rule, defined a new combining rule.

WONG-SANDLER (WS) MIXING RULES

In their findings, referred to as the Michelsen-Kistenmacher Syndrome, Michelsen and Kistenmacher (1990) pointed out a problems with regards to invariance and dilution effects, when the original VDW mixing rules are applied to multi-component mixtures (Hernández-Garduza et al., 2001). These problems were also identified by Adachi and Sugie (1986) and Stryjek and Vera (1986).

To overcome the problem with most mixing rules that was highlighted by Michelsen and Kistenmacher, Wong and Sandler (1992) made use of the excess Helmholtz free energy, rather than the more conventionally used excess Gibbs' energy. The excess Helmholtz free energy at infinite pressure was equated to that calculated from an activity coefficient model. This ensured that the model provided the correct low and high density limits, while remaining independent of the density. An activity coefficient model is used within the mixing rules in order to describe the excess Helmholtz free energy at infinite dilution. This improved the accuracy of the model in the dilute regions.

The binary interaction parameter, k_{ij}, for this mixing rule, must be obtained from the regression of experimental VLE data.

2.5.4. LIQUID PHASE NON-IDEALITY

The liquid phase 'non-ideality' is described by the activity coefficient in thermodynamic phase equilibria calculations. The activity coefficient is most often determined from correlations for the excess Gibbs' energy. The excess Gibbs' energy describes the deviation from ideal mixing behaviour of the system, and is primarily a function of composition and system temperature (Oonk and Tamarit, 2005).

As with the EOS, there are a vast array of available correlations for calculating the excess Gibbs energy of a system. These correlations can be divided into three classes; empirical models, local composition models and group contribution models. The group contribution models are sometimes looked upon as a subset of local composition models (Mollerup, 1981; Smith et al., 2005). Mollerup (1981) showed that all of the local composition models developed up until 1981 could be derived from a local composition version of the van der Waals EOS, simply by altering the assumptions that were made.

Empirical models for the excess Gibbs' energy include the Margules equations, the van Laar equation and the Redlich/Kister expansion (Redlich et al., 1952). These models have little to no theoretical footing, and therefore are not often used, because of their poor ability to predict the behaviour of

multicomponent systems (Smith et al., 2005). They are, however, substantially simpler than the local composition or group composition models.

The local composition models attempt to account for any differences in the molecular sizes of the different components, as well as any the intermolecular forces that occur (Wilson, 1964). The model that was proposed by Wilson (1964) was one of the first of this series of activity coefficient models. The local composition models have an advantage in their application to multi-component systems, as no additional parameters are required for multi-component systems other than those required for each of the constituent binary systems (Smith et al., 2005).

Other popular local composition models that have been developed include the **N**on-**R**andom **T**wo-**L**iquid (NRTL) equation (Renon and Prausnitz, 1968) and the **Uni**versal **Qua**si-**C**hemical (UNIQUAC) equation (Abrams and Prausnitz, 1975). Both of these equations are complex, with the UNIQUAC equation being considerably more so.

WILSON MODEL

The Wilson equation was proposed by Wilson (1964) for the representation of the excess free energy of mixing of a system. The Wilson activity coefficient model contains two parameters, Λ_{12} and Λ_{21}, which must be regressed from experimental phase equilibrium data. Interestingly, the Wilson equation conforms to the Henry's and Raoult's laws at limits of $x_i = 0$ and $x_i = 1$ respectively.

NON-RANDOM TWO-LIQUID (NRTL) MODEL

The three adjustable parameters for the NRTL equation are α, b_{12}, and b_{21}. The binary interaction parameters, b_{12} and b_{21}, are obtained by the regression of experimental data. Renon and Prausnitz (1968) provided some guidelines for selecting values for α, which describes the randomness of the mixture. Raal and Mühlbauer (1998) claimed that there was no conclusive evidence for the selection of a value for α, and that it should rather also be fitted by the regression of experimental data. Previous to this, Walas (1985) had suggested that, if an estimate of α had to be made, a value of 0.3 should be used for non-aqueous systems and a value of 0.4 be used for systems containing both aqueous and organic components.

As is inferred by its name, the NRTL equation is able to predict immiscibility in the liquid phase, and because it takes into account the sizes of the molecules, as well as the interaction between them, it is capable of representing highly non-ideal systems. Walas (1985) also showed that the NRTL equation can be used to represent systems for which the plot of the natural logarithm of the activity coefficients against the liquid mole fraction has either a maximum or a minimum.

Universal Quasi-Chemical (UNIQUAC) Model

The UNIQUAC model, developed by Abrams and Prausnitz (1975) uses a combination term, g^C and a residual term, g^R, in the calculation of the excess Gibbs energy of a system. The calculation of the binary interaction parameters, τ_{ij}, introduces a temperature dependency to the model. The binary interaction parameters are not equal, and the parameters must be obtained by the regression of binary experimental data. The calculations of the activity coefficients for a binary mixture with the UNIQUAC model are substantially more complex that those of the Wilson and the NRTL models.

Anderson and Prausnitz (1978) modified the original UNIQUAC model for systems which contained water or shorter chain length alcohols. This model is known as the modified UNIQUAC method. The modification made use of optimised values for the relative molecular surface area, denoted q_i', to improve the agreement between experimental data and the fitted models.

2.5.5. Regression Routines

A number of different regression routines have been developed for the regression of the parameters of thermodynamic models to VLE data. The regression routines include the objective functions that are used, the algorithm used to minimise these objective functions, and the types of parameters that are fitted.

Objective Function

Many objective functions exist, but the choice of the objective function is based upon the data that is being regressed. Aspen Plus V8.0 (Aspen Technology, 2012) provides several objective function options, including maximum likelihood, ordinary least squares, Barker's method and modified Barker's method objective functions. Other more specialised objective functions are also provided for, such as those formed using activity coefficients or equilibrium constants. The objective functions that are of interest for this study are listed in Table 2.5.

In this study, the modified Barker's method objective function, which is a form of a bubble flash calculation, was utilised for the regression of (*P*-*x*-*y*) VLE data and the Barker's method was used for the regression of (*P*-*x*) bubble pressure data. This enabled a similar type of method to be used for both types of data that was available.

Table 2.5. Some of the objective functions available in Aspen Plus V8.0.

Objective function	Fitted variables	Fixed variables	Comments
Maximum likelihood	*P, T, x, y*	none	Residuals from all four variables must be considered when evaluating a model fitted to experimental data with the maximum likelihood objective function. Temperature is often found to be over flexible, due to its relative magnitude.
Ordinary least squares (bubble flash)	*P, y*	*T, x*	Residuals of *P* and *y* need to be evaluated.
Ordinary least squares (dew flash)	*P, x*	*T, y*	Residuals of *P* and *x* need to be evaluated.
Barker's method (Barker, 1953)	*P*	*T, y, x*	Only a single fitted variable, but still able to correlate VLE data precisely (Abbott and Van Ness, 1975). Useful for the correlation of bubble pressure (*P-x*) data.
Modified Barker's method (Barker, 1953)	*P, y*	*T, x*	Similar to the ordinary least squares bubble flash objective function, but with the ability to correlate VLE data precisely (Abbott and Van Ness, 1975).

Regression Algorithm

In addition to the choice of the objective function, three regression algorithms are available within Aspen Plus V8.0 (Aspen Technology 2012). These algorithms are the Britt-Lueke algorithm, the Deming algorithm and a weighted least squares algorithm. The Britt-Lueke algorithm is recommended by Aspen Technologies, and is a rigorous maximum likelihood method. The least-squares algorithm is available, but appears to not be favoured by Aspen Technologies. Ideally, each of the algorithms should be utilised until such time as the absolute minimum of the objective function is obtained.

Temperature Dependency

The parameters for the thermodynamic models can be regressed either as temperature dependent or temperature independent parameters. In the case of isothermal data being regressed with temperature dependent parameters, all of the isothermal data sets are regressed simultaneously. On the other hand, with temperature independent parameters being regressed, each isotherm must be regressed separately. The binary interaction parameter from the mixing rule, k_{ij}, is used to include the temperature dependence into the model. The temperature dependent binary interaction parameter is directly proportional to the temperature.

2.6. Critical Point Modelling and Estimation

The prediction of the critical point of a multi-component system is important for thermodynamic phase equilibrium measurements, as the accuracy of thermodynamic models often decreases as the critical point is approached. It is also difficult to accurately determine the critical point of the multi-component systems experimentally.

A number of techniques have therefore been developed for the prediction of the critical point or critical loci of mixtures. These techniques can be divided into three categories; empirical methods, indirect methods and direct methods (Stockfleth and Dohrn, 1998).

Empirical methods use 'pseudo-averages' of the critical temperatures and molar volumes of the pure components within an EOS to determine the critical pressure of the mixture. The use of purely empirical methods was predicted by Hicks and Young (1975), to decrease as progress was made with the theoretical prediction. These methods only apply to the system types for which they were developed (Elliott and Daubert, 1987), most of which are simple systems (Kolář and Kojima, 1996).

Spencer et al. (1973) conducted an investigation into the performance of a number of empirical methods for determining the critical locus points of multi-component systems. They recommended methods for both multi-component hydrocarbon systems and 'hydrocarbon + non-hydrocarbon mixtures'. For the critical temperature, the method of Li (1971) was recommended; for the critical pressure, the method of Kreglewski and Kay (1969) was recommended, and if all three critical properties were required for a non-polar mixture, it was recommended that the method proposed by Chueh and Prausnitz (1967) be used.

The indirect methods involve the extrapolation of experimental phase envelope data up to the critical point. These methods are less common than the empirical or direct methods, as they involve a large number of phase equilibrium calculations for the determination of a single critical point (Stockfleth and Dohrn, 1998). These methods are also generally not as accurate as the direct method. An example of an indirect critical locus point estimation technique is the indirect scaling law of Ungerer et al. (2005), as used by El Ahmar et al. (2011).

The direct method involves the use of rigorous thermodynamic criteria to determine the critical points of a system. An example of a direct method is the method of Heidemann and Khalil (1980). This method uses an EOS fitted to subcritical experimental data to determine the critical locus points of multicomponent systems, and was based upon the earlier work of Gibbs between 1876 and 1878, as detailed by Gibbs and Bumstead (1906). This method was shown to be more efficient and more robust than other methods and was further optimised by Michelsen and Heidemann (1981).

Elliott and Daubert (1987) compared several of the direct and empirical methods for determining the critical loci of mixtures with data obtained from a number of sources, including the compilation of Hicks and Young (1975). They found that the critical pressure calculations for binary systems were substantially more accurate when the direct method was used than when other methods were used. For the determination of the critical temperature of binary mixtures, there was no single method providing the most accurate results. In the case of determining the critical volume of a binary mixture, none of the direct methods or empirical methods provided results similar to the experimental values. Modifications to the direct method, by the inclusion of a correction factor were required in order to obtain reasonable critical volume values.

Overall, Elliott and Daubert found that the direct methods appeared to be more reliable, as well as offering better versatility. They are also useful for the prediction of anomalies that empirical methods are not capable of correlating. On the other hand, these methods are generally substantially more computationally intensive. They also importantly rely on the fit of the thermodynamic model to the experimental data.

2.6.1. The Heidemann and Khalil Direct Method

The derivation of the method which was proposed by Heidemann and Khalil (1980) begins with Gibbs' condition for thermodynamic stability (Gibbs and Bumstead, 1906). A criterion for the critical point is derived from this condition, such that, the tangent plane distance, *D*, is positive for any isothermal change.

$$D = \left[A - A_0 + P_0(V - V_0) - \sum_{i=1}^{m} \mu_{i0}(n_i - n_{i0})\right]_{T_0} \qquad 2.9$$

where *A* is the Helmholtz energy of the system, *P* is the system pressure, *V* is the system volume, μ_i is the chemical potential of component *I*, and n_i is the number of moles of component *i*. The subscript *'0'* denotes the conditions of a phase that is stable for any isothermal change as long as *D* is positive, and *'m'* denotes the number of components present in the mixture.

The Helmholtz energy, *A*, is expanded to two terms in a Taylor series expansion around the 'zero' state, at a constant total volume, and the thermodynamic identity relating the fugacity to the Helmholtz energy (equation 2.10) is used in this expansion.

$$RT\left(\frac{\partial(\ln f_i)}{\partial n_i}\right)_{T,V,n_{l\neq j}} = \left(\frac{\partial^2 A}{\partial n_i \partial n_j}\right)_{T,V,n_{l\neq i,j}} \qquad 2.10$$

where f_i is the fugacity of component *i*.

The expansion of equation 2.9, using equation 2.10 yields equation 2.11.

$$\frac{1}{2}\Delta n_i \Delta n_j \sum_{j=1}^{m}\sum_{i=1}^{m}\left(\frac{\partial(\ln f_i)}{\partial n_j}\right)_{T,V,n_{l\neq j}} + \frac{1}{6}\Delta n_i \Delta n_j \Delta n_k \sum_{k=1}^{m}\sum_{j=1}^{m}\sum_{i=1}^{m}\left(\frac{\partial^2(\ln f_i)}{\partial n_j \partial n_k}\right)_{T,V,n_{l\neq j,k}} + \frac{R_3}{RT} > 0 \qquad 2.11$$

The double summation portion of equation 2.11 can be expressed in matrix-vector notation, as expressed by the three equivalent equations, 2.12, 2.13 and 2.14. This portion of the equation must vanish, and therefore the solutions must be found such that all three equations are satisfied.

$$\tfrac{1}{2}\Delta \boldsymbol{n}^T \boldsymbol{Q} \Delta \boldsymbol{n} = 0 \qquad 2.12$$

$$det(\boldsymbol{Q}) = 0 \qquad 2.13$$

$$\boldsymbol{Q}\Delta \boldsymbol{n} = \boldsymbol{0} \qquad 2.14$$

If there is a non-zero $\Delta \boldsymbol{n}$ that provides a solution to the above equations, then the triple summation portion of equation 2.11 need be considered. In the work of Michelsen (1984), it was suggested that the triple summation be re-written in the form that is given by equation 2.15.

$$\sum_{k=1}^{m}\sum_{j=1}^{m}\sum_{i=1}^{m}\left(\frac{\partial^2(\ln f_i)}{\partial n_j \partial n_k}\right)_{T,V,n_{l\neq j,k}} \Delta n_i \Delta n_j \Delta n_k \sum_{i=1}^{m}\sum_{j=1}^{m}\left[\Delta n_i \Delta n_j \sum_{k=1}^{m}\left(\frac{\partial q_{ij}}{\partial n_k}\right)_{T,V,n_{l\neq k}} \Delta n_k\right] \qquad 2.15$$

From this form, the triple summation can be calculated as a double summation (equation 2.16), which reduces the computational requirements.

$$\sum_{k=1}^{m}\sum_{j=1}^{m}\sum_{i=1}^{m}\left(\frac{\partial^2(\ln f_i)}{\partial n_j \partial n_k}\right)_{T,V,n_{l\neq j,k}} \Delta n_i \Delta n_j \Delta n_k = \sum_{i=1}^{m}\sum_{j=1}^{m} \Delta n_i \Delta n_j q^*_{i,j} = 0 \qquad 2.16$$

Stockfleth and Dohrn (1998) provided a detailed flowsheet of the computational procedure proposed by Heidemann and Khalil for solving equations 2.12 to 2.14. This procedure estimates the critical temperature and critical molar volume of the system using an EOS for which the parameters have been obtained from the regression of experimental data. The starting value for V_C is *3.85 b*, where *b* is the volume correction term from the EOS. The starting point for T_C is $1.5\sum_i z_i T_{C,i}$. The flowsheet for the Heidemann and Khalil calculation as given by Stockfleth and Dohrn (1998) is reproduced in Figure 2.7.

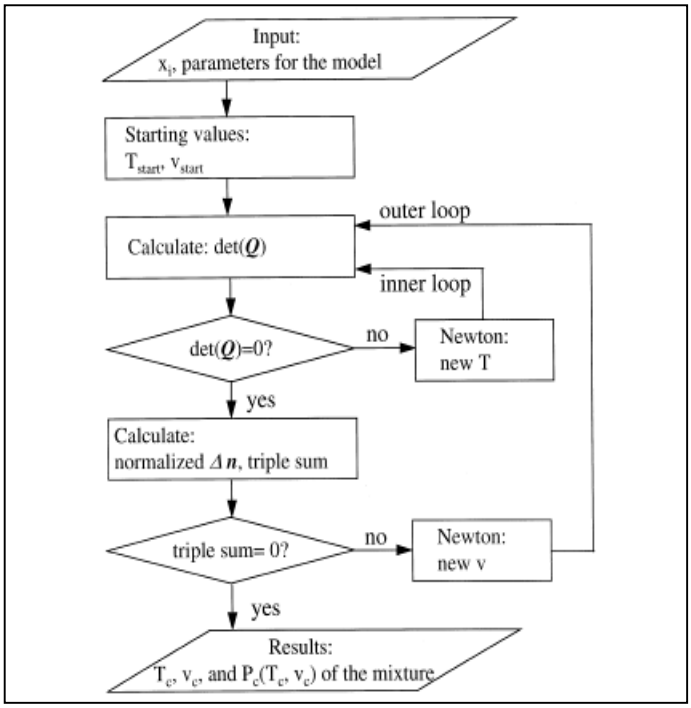

Figure 2.7. The Heidemann and Khalil critical point calculation procedure, as presented by Stockfleth and Dohrn (1998)

This procedure has two optimisation loops, both of which utilise the Newton-Raphson method to search for the critical values that solve equations 2.12 to 2.14 or equation 2.16. According to Stockfleth and Dohrn, this computational procedure converges in almost all cases involving vapour-liquid critical points. For liquid-liquid critical points, different starting points for the critical temperature and molar volume must be chosen. The method for choosing these different starting points was, however, not disclosed.

The elements of matrix ***Q***, (calculated to satisfy equations 2.12 to 2.14) in the first step must be calculated using numerical differentiation. A four point differencing scheme was suggested by Stockfleth and Dohrn (1998) for both differentiations.

El Ahmar et al. (2011) showed that this calculation procedure tended to over-predict their critical loci. This over-prediction was in all likelihood due to the thermodynamic model that was applied to the system, rather than due to the calculation procedure. The dependency of this method upon the thermodynamic model used to describe the sub-critical phase behaviour is probably its biggest weakness. When the thermodynamic model is capable of describing the sub-critical data with high accuracy, the calculation procedure provides accurate critical locus curves. If the model poorly describes the system, then the predicted critical loci could differ substantially from the real values.

2.6.2. The Indirect Extended Scaling Laws

El Ahmar et al. (2011) used the extended scaling laws of Ungerer et al. (2005) to determine the critical loci for binary mixtures consisting of a perfluorocarbon and an n-alkane. This method predicted the critical points with a reasonable degree of accuracy.

The method of Ungerer et al. uses the 'near-critical scaling law', extending it with a linear term. The new extended scaling law is given as equations 2.17 and 2.18.

$$y - x = \lambda_1(P_c - P) + \mu(P_c - P)^{\beta} \qquad 2.17$$

$$\frac{y + x}{2} - x_c = \lambda_2(P_c - P) \qquad 2.18$$

The coefficients for the extended scaling laws, λ_1, λ_2, μ, and β, are regressed by fitting a set of co-existence points (*P, x, y*) from the vapour-liquid equilibria below the critical point. The equations are then used to solve for x_c and P_c.

The extended scaling laws, though being an indirect method, provide a fairly accurate approximation ($\pm$ 5 %) of the critical point with low computational requirements. This accuracy is highly dependent upon the amount of data that is available, as well as the proximity of this data to the critical point.

2.6.3. The Direct PSRK Critical Point Prediction Method

The disadvantage of most of the direct critical point calculation methods is that they require equilibrium data to be available for the system, in order to obtain parameters for the EOS. Sadus (1992) attempted to apply conformal solution theory to binary systems containing non-polar or only weakly polar components, in order to predict the critical properties of the mixtures. This attempt was shown to provide good agreement between the predicted and experimental critical properties. Unfortunately, this only applied to non-polar and slightly polar systems, and there was therefore a lack of a direct method for predicting the critical properties of highly non-ideal systems.

Kolář and Kojima (1996) therefore proposed the use of the Predictive Soave-Redlich-Kwong (PSRK) EOS using the critical point calculation procedure of Heidemann and Khalil (1980) and the further developments of Michelsen (1984) and Mollerup and Michelsen (1992) in order to predict the critical points of multicomponent systems.

The PSRK method is based upon a revised form of the original UNIFAC Gibbs excess energy model (Hansen et al., 1991). The UNIFAC group parameters were fitted to experimental data measured at near ambient temperatures. The non-linear character of the PSRK functions results in frequent

overprediction of the critical points, when extrapolating from near ambient temperatures to the temperatures at which the mixture critical points exist. This overprediction can only be prevented by regressing experimental critical point data (Kolář and Kojima, 1996), which contradicts the original aims of predicting the mixture critical properties.

In the work of García-Sánchez et al. (1992), the PSRK critical point predictions provided similar relative average deviations from experimental data to those from the calculation of the critical properties using the SRK EOS.

2.6.4. Redlich-Kister Type Equations

Soo et al. (2010) utilised Redlich-Kister (RK) type equations (Redlich and Kister, 1948) to obtain a model describing the critical locus curves of binary mixtures. The equations for the mixture critical temperature and pressure are given by equations 2.19 and 2.20 respectively.

$$T_{c,12} = x_1 T_{c,1} + x_2 T_{c,2} + \sum_{j=1}^{n} a_j x_1 x_2 (2x_1 - 1)^{j-1} \quad 2.19$$

$$P_{c,12} = x_1 P_{c,1} + x_2 P_{c,2} + \sum_{j=1}^{n} b_j x_1 x_2 (2x_1 - 1)^{j-1} \quad 2.20$$

Where $T_{c,ij}$ and $P_{c,ij}$ are the mixture critical temperature and pressure, $T_{c,i}$ and $P_{c,i}$ are the pure component critical temperature and pressure, x_i is the mole fraction of component i, n is the order of the equation and b_1, b_2, …, b_n are the empirical parameters for the equation. The parameters can be fitted to the data by minimising the sum of the mean relative deviations between the model and the data. Generally, the order of the equation is increased until a reasonable fit of the correlation to the data is achieved. These equations are entirely empirical in nature, and it is therefore not recommended to infer too many conclusions from this model.

3. SYSTEMS OF INTEREST

This chapter details the process behind the selection of the systems for which measurements were to be undertaken for this study. Initially, the fluorocarbon solvents that had characteristics that were best suited to the purposes of this study were selected. These desired characteristics are given in Section 1.5.1. Thereafter, the solutes that would be most representative of systems encountered in the petroleum industry were chosen. Solutes for which phase equilibrium data was available with currently used SC solvents (such as CO_2 and ethane) were given preference in the selection process.

The phase equilibrium data for CO_2 with the chosen solutes was important for this study, as the performance of the new solvents would have to be benchmarked against the performance of CO_2 as a SC solvent. The various authors who have reported phase equilibrium data of CO_2 with the chosen solutes were therefore presented, and their measurements were described. Lastly, it was equally important to obtain literature data involving the selected solvents, in order to ascertain the methods that have been used to measure and model this data. This data was useful in ensuring that measurements that have been previously undertaken were not repeated.

3.1. SOLVENT SELECTION

A list of some of the possible candidates for SCFE is given in Table 3.1, alongside their critical properties, their dipole moments and their NFPA 704 codes (National Fire Protection Asociation, 2012).

Of the solvents listed in this table, three had dipole moments greater than zero, with the remainder of the gases being theoretically non-polar. The three polar gases of interest were 1,1-difluoroethene (R-1132a), chlorotrifluoromethane (R-13) and trifluoromethane (R-23). As one of the aims of this study was to remove the necessity for a polar co-solvent, it was desirable that one of these three polar solvents be investigated as a SCF solvent.

The toxicity, flammability and stability of the various gases are categorised according to the NFPA 704 codes. The values of each of the three codes (health, flammability and stability/reactivity) for the proposed candidates are tabulated in Table 3.1. These values characterise some of the important characteristics for SCF solvents discussed in section 1.2. The values range from 0 (no risk) to 4 (highest risk). The codes were used to determine which gases would be best suited as SCF solvents.

Table 3.1: Solvent candidates for SCFE

	ASHRAE No.	T_c / K [a]	P_c / MPa [a]	Dipole Moment / D	Health Code [b]	Fire Code [b]	Instability Code [b]
1,1-Difluoroethene	R-1132a	302.85	4.460	1.3893	1	4	2
Carbon dioxide	R-744	304.26	7.377	0	3	0	0
Chlorotrifluoro-methane	R-13	292.59	4.185	0.5	2	0	1
Ethane	R-170	305.35	4.884	0	1	4	0
Ethylene	R-1150	282.65	5.076	0	1	4	2
Hexafluoroethane	R-116	292.85	2.980	0	1	0	0
Trifluoromethane	R-23	299.07	4.836	1.65	1	0	1

[a] *Data obtained from Lide (2004)*

[b] *National Fire Protection Association Standard 704: Standard System for the Identification of the Hazards of Materials for Emergency Response*

R-13, although appearing to be a promising candidate as a SCF solvent, is considered harmful to the ozone layer, and has subsequently been banned by the Montreal Protocol (UNEP, 2003). There was therefore no logical purpose in pursuing any further investigation with this gas, as it would not be possible to use it industrially. Of the two remaining polar gases, the use of R-23 posed significantly fewer hazards than the use of R-1132a. This was due to the much lower flammability and reactivity of the R-23, compared to the R-1132a.

Although hexafluoroethane (R-116) has a dipole moment of 0 D, which is due to the symmetry of the molecule; the fluorine atoms present in the molecule are more electronegative than the carbon backbone. Because of this, very weak intermolecular forces could still be present in solutions containing R-116. Additionally, the low NFPA 704 ratings for R-116 make it a promising candidate. The performance of R-116 as a SCF solvent was therefore also investigated in this study.

Consideration must also be given to the greenhouse warming potential (GWP) and the atmospheric lifetime of the solvents, as these will also play an important factor in the selection of suitable SC solvent. The GWP is an estimate of the global warming that could be induced by the molecules of the given compound in the atmosphere when compared to the same mass of CO_2 molecules (Perrut, 2010). The atmospheric lifetime is the average time taken for molecules of the compound to decompose when they are released into the environment. The GWP and atmospheric lifetimes for the solvent candidates are presented in Table 3.2.

Table 3.2. Greenhouse warming potentials and atmospheric lifetimes for the SCF solvent candidates

	ASHRAE No.	GWP	atmospheric lifetime / years
1,1-Difluoroethene [a]	R-1132a	4	unknown
Carbon dioxide [b]	R-744	1	>10 000
Chlorotrifluoromethane [c]	R-13	14 420	640
Ethane [c]	R-170	5.5	12
Ethylene [c]	R-1150	3.7	1.45
Hexafluoroethane [b]	R-116	9200	10 000
Trifluoromethane [c]	R-23	11 700	270

[a] Low and Sharratt (2015)
[b] Calm and Hourahan (2007)
[c] Forster et al. (2007)

The hydrocarbons, ethane and ethylene, exhibit the lowest GWP and atmospheric lifetime of those listed in the table. R-23, although having a high GWP has a relatively short atmospheric lifetime, and is probably the best halogenated compound. R-1132a has a low GWP, but due to poor fire and instability codes, it was not considered as a supercritical solvent in this study.

Carbon dioxide, ethane, propane and a butane/pentane mixture have all been used previously as SC solvents. The advantages and disadvantages of these gases are discussed below.

3.1.1. Carbon Dioxide

Carbon dioxide is cheap and readily available. It is also non-toxic and non-flammable. For these reasons, it is by far the most common solvent used in supercritical fluid systems (McHugh and Krukonis, 1986; Sheng et al., 1992). Carbon dioxide was, for many years, also considered to be an environmentally friendly solvent, and was therefore seen as the best solvent for use in SCFE.

Rizvi et al. (1986) showed that dense CO_2 is more selective of low molecular weight lipophilic compounds. These are those compounds that have an affinity for dissolving in lipids or non-polar solvents, such as hydrocarbons, esters, aldehydes, etc. Schultz and Randall (1970) showed for liquid CO_2, and Stahl et al. (1988) for dense gaseous CO_2, that within a homologous series of lipophilic substances, the selectivity decreased with increased molecular weight or upon the addition of polar groups to the molecules.

The major drawback for the use of carbon dioxide as the solvent for supercritical extraction is its low polarity (Li et al., 2003). Because of the low polarity of CO_2, additional co-solvents must be added to

the solvent, in order to increase the polarity and thereby improve the extraction yields of the more polar solutes (Knox, 2005). In systems in which water is present, the carbon dioxide dissolved in the water can dissociate to form a slightly acidic carbonic acid solution (Wiebe and Gaddy, 1940). The lowered pH of this solution is problematic when the process involves pH sensitive components, such as enzymes (Beckman, 2004). Additionally, a reduced pH could result in unwanted side-reactions or corrosion of the equipment. Carbon dioxide and water systems are therefore often avoided. In addition to this, due to the relatively large solubility of water in CO_2, systems with a water content in the feed greater than 15 wt. % are usually dried prior to extraction to improve the yield (Shariaty-Niassar et al., 2009). A further discussion of CO_2 is provided in section 3.3.

3.1.2. ETHANE

Investigations into the use supercritical ethane for extraction purposes have been undertaken to a far lesser extent than the use of carbon dioxide. Authors who have investigated ethane as a supercritical solvent include Moradinia and Teja Amyn (1987), Ávila-Chávez et al. (2007), Ávila-Chávez and Trejo (2010) and Zamudio et al. (2011). Additionally, Singh et al. (2000) reported the critical temperature and pressure for C_6 to C_{10} n-alkanes in ethane at concentrations of up to 5.2 mol. %. Ethane has a critical temperature that is close to room temperature, making it a useful supercritical solvent. However, it is also non-polar and its use is therefore plagued by the same disadvantages as with the use of carbon dioxide.

An additional hazard when working with flammable solvents such as ethane, is the control system that must be implemented to prevent combustion or explosion. These controls are even more important when considering the high pressures of operation. Ramírez et al. (2011) compared the Dow Fire and Explosion Indices (FEI) for a number of SCFE processes with different solvents. They found that the FEI for extraction processes using supercritical propane was of an order of magnitude higher than when using supercritical carbon dioxide. The risks of operating with supercritical ethane would be of a similar magnitude to using supercritical propane.

3.1.3. PROPANE

Propane was investigated as a supercritical solvent by Peters et al. (1992), Subramanian and Hanson (1998) and on numerous occasions by Schwarz et al. (Schwarz and Knoetze, 2007; Schwarz et al., 2008; Schwarz et al., 2011). Propane, however, has a critical temperature of 369.8 K (Ambrose and Tsonopoulos, 1995), and is therefore not particularly useful as an alternative solvent, as the process would require significant heating. Supercritical propane also has substantially higher fire and explosion risks than CO_2 (Ramírez et al., 2011).

3.1.4. BUTANE/PENTANE

The ROSE Process of KBR Technologies Inc. (2007) makes use of either butane or pentane to separate very heavy crudes or residues from tar sand bitumens into an asphalt fraction and a deasphalted heavy oil fraction (Knox, 2005). The conventional process for the upgrading of these very heavy oils is delayed coking (Gearhart and Nelson, 1983). The utility costs for the operation of the ROSE® Process are approximately one third of the costs of delayed coking. The solvent to feed ratio for the process is approximately 5 to 1, but most of the solvent is recovered, and low utility costs are maintained through process integration. Although the process has to be operated at temperatures above the critical temperature of n-butane or n-pentane, these temperatures are still lower than those used in delayed coking.

3.1.5. TRIFLUOROMETHANE

A small amount of research into the use of R-23 as a SCF solvent has been reported in literature. These research activities are presented in Table 3.3 below.

Table 3.3. Examples of investigations into the use of supercritical R-23 as a solvent

Author	Investigation
Taylor and King (1994)	Investigated the use of SC R-23 to recover organochlorine pesticides from food and agricultural products without co-extracting fats. There was found to be a 100-fold decrease in the co-extraction of fats with SC R-23 when compared to extraction with SC CO_2.
Hillmann and Bächmann (1995)	Compared the SCF extraction rates of polar and non-polar pesticides from silanized glass beads with either CO_2 or R-23 as the solvent. They found that R-23 provided a higher recovery rate of the pesticides, but the selectivities of polar and non-polar pesticides did not appear to differ.
Goldfarb and Corti (2000)	Analysed the performance of R-23 as a SC solvent for organic electrolytes. They found that the organic electrolytes that were investigated exhibited solubilities and electrical conductivities that were sufficiently high in the SC R-23 to enable its use.
Cabañas et al. (2003)	Used SC R-23 to deposit copper films, used in the microelectronics industry, by the chemical fluid deposition technique.
Helfgen et al. (2003)	Investigated the RESS solid preparation technique with a SC CO_2 and SC R-23 as solvents. Smaller particles were obtained when using R-23 as the solvent.

No pilot-plant or full-scale investigations into R-23 have been reported in open literature. Further discussions on R-23 are given in section 3.4.

3.1.6. HEXAFLUOROETHANE

The little research that has been conducted into the use of R-116 as a SC solvent has primarily been into its use as a solvent in the electronics industry and in particle manufacture. Examples of the research into SC R-116 are given in Table 3.4.

Table 3.4. Examples of investigations into the use of supercritical R-116 as a solvent

Author	Investigation
Gallagher et al. (1995)	Patented a process for the use of R-116 as a supercritical solvent for gas anti-solvent (GAS) recrystallization of solids. The SCF was added to an organic solution containing the dissolved solids inducing nucleation of the dissolved solids.
Cabañas et al. (2003)	Used supercritical R-116 to deposit copper films, used in the microelectronics industry, by the chemical fluid deposition technique.
McDermott et al. (2008)	Patented a process for the removal of contaminants from the surfaces of semiconductor electronic components using supercritical R-116.
Kim et al. (2011)	Patented a process using supercritical R-116 for the transport of a quantum dot precursor fluid to the surface of a thin metal oxide layer for the fabrication of transparent electrodes in the manufacture of quantum dot sensitised solar cells.

There have also been no pilot-plant or full-scale-scale investigations into R-116 as a SC solvent. R-116 is further discussed in section 3.5.

3.2. SOLUTE SELECTION

In research into petroleum extraction and separation techniques, a number of authors, such as Nagarajan et al. (1990), Polishuk et al. (2003), and Jiménez-Gallegos et al. (2006), have used members of the n-alkane series to model various petroleum streams. Moradinia and Teja (1986; 1987) reported that the odd- and even-numbered n-alkanes exhibited different trends in their properties. It was therefore decided that it would be prudent to include a number of components from the n-alkane series (both odd- and even- numbered) as solutes for these investigations.

Additionally, the behaviour of several solutes with additional functional groups was also of interest. Therefore, one branched alkane, one alkene, one cycloalkane and one aromatic were also included in the study.

It was also desirable to be able to benchmark the performance of the proposed solvents to the performance of currently used solvents such as carbon dioxide or ethane. Above and beyond the selection of solutes that would provide a good model system for a petroleum stream, emphasis was

also placed upon choosing solutes for which binary phase equilibrium data with solvents such as carbon dioxide or ethane was available. A literature search was performed, using the NIST ThermoLit Literature Report Builder for these systems. Table 3.5 provides the systems for which literature data was available with either carbon dioxide or ethane as the second component in the binary mixture.

Table 3.5. Possible solutes for representative measurements with the number of studies that have been conducted with systems of CO_2 or ethane and the solute.

Solute	No. of Carbon Atoms	CO_2 + solute	Ethane + solute
n-propane	3	15	16
n-butane	4	16	8
n-pentane	5	7	4
3-methylpentane *	6	1	0
1-hexene *	6	3	0
benzene	6	13	4
cyclohexane	6	12	2
n-hexane *	6	13	4
1-heptene	7	1	0
methylcyclohexane *	7	3	1
n-heptane *	7	10	5
toluene *	7	32	1
n-octane *	8	14	4
n-nonane *	9	3	1
n-decane *	10	14	5
n-undecane *	11	2	1
n-dodecane	12	4	6
n-tridecane	13	3	0
n-tetradecane	14	6	1
n-pentadecane	15	5	0

* Solutes that were chosen for this study.

Water was included in addition to the ten solutes that were selected above, as many of the processes for which SCF could be used in the petroleum industry would contain a water fraction.

3.3. Carbon Dioxide

A large amount of property data is available for binary CO_2 systems. This data includes phase equilibrium data, densities, diffusivities and viscosities. CO_2 is also relatively cheap and easy to obtain.

3.3.1. Phase Equilibria

There have been a substantial number of high pressure phase equilibria studies conducted for systems involving carbon dioxide with liquid hydrocarbons. Several of the authors that have reported data for CO_2 with the solutes chosen for this study have been presented in Table 3.6. This table provides the

temperature ranges at which the data was measured, the number of data points provided, the equipment type and the data modelling approach used by each of the authors.

Table 3.6. Authors who have reported phase equilibrium data for CO_2 with the solutes chosen for this study.

System	Author	T / K	Data	Equipment [a]	Modelling Technique
CO_2 + n-hexane	Ohgaki and Katayama (1976)	298.09 to 313.09	20	SA cell	RK EOS with Lewis rule
	Li et al. (1981)	313.2 to 393.2	39	VV SA cell	SRK EOS, flash-type objective function
	Wagner and Wichterle (1987)	303.14 to 323.14	26	SA cell	PR EOS with classical mixing rules, maximum likelihood objective function
	Chen and Chen (1992)	303.15 to 323.15	25		
CO_2 + n-heptane	Kalra et al. (1978)	310.7 to 477.2	64	VV SA cell	Henry's constants evaluated
	Lay (2010)	293.15 to 313.15	25	VV SS cell	PR EOS with 1 temperature dependent parameter
CO_2 + n-octane	Weng and Lee (1992)	313.15 to 348.15	22	DA cell	Soave (1972), Patel-Teja (1982) and Iwai-Margerum-Lu (Iwai et al., 1988) EOS with quadratic mixing rules. Equilibrium ratio errors objective function with Levenberg-Marquardt algorithm
	Jiménez-Gallegos et al. (2006)	322.29 to 372.53	28	SA cell	PR EOS using both classical and WS/NRTL mixing rule, Ordinary least squares objective function
	Yu et al. (2006)	313.2 to 393.2	47	VV SA cell	PR, Peng-Robinson-Stryjek-Vera and Heilig-Franck EOSs, with VDW and Panagiotopolous-Reid mixing rules Objective function minimised pressure deviations
	Tochigi et al. (2010)	313.14	7	SA cell	Modified SRK EOS (Sandarusi et al., 1986) with Adachi and Sugie (1986) mixing rule Least squares objective function
CO_2 + n-nonane	Jennings and Schucker (1996)	343.25	6	DA cell	
	Camacho-Camacho et al. (2007)	315.12 to 418.82	38	SA cell	PR EOS using classical and WS mixing rule with NRTL model, Minimised ordinary least squares objective function

System	Author	T / K	Data	Equipment [a]	Modelling Technique
CO_2 + n-decane	Reamer and Sage (1963)	292.9 to 510.9	82	VV SS cell	
	Nagarajan and Robinson (1986)	344.3 to 377.6	45	VV SA cell	
	Chou et al. (1990)	344.25 to 377.15	8	SA cell, vapour recirculation	
	Iwai et al. (1994)	311.0 to 344.3	5	DA with sampling	The PR EOS with classical mixing rules Objective function minimised composition deviations
	Shaver et al. (2001)	344.3	26	SA cell	Data smoothing with Wilson-Wegner expansion (Charoensombut-amon and Kobayashi, 1986)
	Jiménez-Gallegos et al. (2006)	319.11 to 372.94	29	SA cell	PR EOS using both classical and WS mixing rules, NRTL model Ordinary least squares objective function.
CO_2 + n-undecane	Camacho-Camacho et al. (2007)	314.98 to 418.30	42	SA cell	PR EOS using both classical and WS mixing rules, NRTL model Ordinary least squares objective function minimised by Levenberg-Marquardt method.
CO_2 + 3-methyl pentane	Mutelet et al. (2005)	293.15 to 383.15	49	VV SS cell	The Predictive Peng-Robinson (PPR78) EOS with classical mixing rules
CO_2 + 1-hexene	Vera and Orbey (1984)	303.15 to 343.15	25	SA cell	The PR EOS with classical mixing rules
	Wagner and Wichterle (1987)	303.15 to 323.15	22	SA cell	PR with classical mixing rules Maximum likelihood objective function
	Jennings and Teja (1989)	309.3 to 332.3	45	DA with recirculation of vapour liquid	Patel-Teja and Treble-Bishnoi EOS with classical mixing rules Objective function minimised composition deviations
CO_2 + methyl-cyclohexane	Ng and Robinson (1979)	311.0 to 477.2	31	SA cell	PR EOS
	Nasrifar et al. (2003)	269.17 to 308.2	63	SS cell (Cailletet apparatus)	PSRK EOS with MC alpha parameter, Holderbaum and Gmehling mixing rules and UNIQUAC activity coefficient Objective function minimised pressure deviations

System	Author	T / K	Data	Equipment [a]	Modelling Technique
CO_2 + toluene	Ng and Robinson (1978)	311.25 to 477.05	34	SA cell	PR EOS
	Sebastian et al. (1980)	393.3 to 542.9	21	DA cell	
	Fink and Hershey (1990)	308.16 to 353.18	50	DA cell	PR EOS with 1 or 2 interaction parameters Two objective functions: Minimised deviations in relative volatility and vapour phase composition or minimised pressure residuals
	Muhlbauer and Raal (1991)	352.15	9	SA cell	Combined method using the PR EOS with the UNIQUAC equation or the truncated virial EOS with the UNIQUAC equation
	Naidoo et al. (2008)	283.15 to 391.45	43	VV SA cell	PR EOS + Stryjek-Vera alpha function, WS/NRTL model Ordinary least squares objective function minimised by Marquardt method
CO_2+ water	King and Coan (1971)	298.15 to 373.15	22	DA cell	Virial coefficients
	Bamberger et al. (2000)	323.2 to 353.1	29	DA cell	Modified PR EOS (Melhem et al., 1989), with Panagiotopoulos and Reid (1986) mixing rules Minimised vapour and liquid composition deviations
	Valtz et al. (2004)	278.22 to 318.23	47	SA cell	PR EOS with van der Waals mixing rule PR EOS with MC alpha function, WS mixing rule and NRTL activity coefficient model Square-well version of SAFTR-VR theory Objective function minimised composition uncertainties by Simplex algorithm

[a] DA, dynamic-analytic; SA, static-analytic; SS, static-synthetic; VV, variable-volume

3.3.2. Critical Loci and System Classification

Martinez (2007) investigated systems containing CO_2 and n-alkanes with various carbon chain lengths. It was found that systems involving carbon dioxide and n-alkanes with up to 12 carbon atoms were VKS type II systems, while those containing C_{12} to C_{14} n-alkanes were most likely type IV systems. Above this, the systems were estimated to be type V systems. The observations used by Martinez to make these estimations were presented by Martinez in the plot shown in Figure 3.1.

With the higher carbon numbers (above C_{22}), the dissection of the solid-liquid-liquid-vapour equilibrium (SLLVE) line and the UCEP line means that the UCEP becomes obscured by solidification of

the alkane. This point of dissection is clearly visible in Figure 3.1. The obscuring of the UCEP makes it impossible to verify that binary systems with higher n-alkane chain lengths are indeed type V systems.

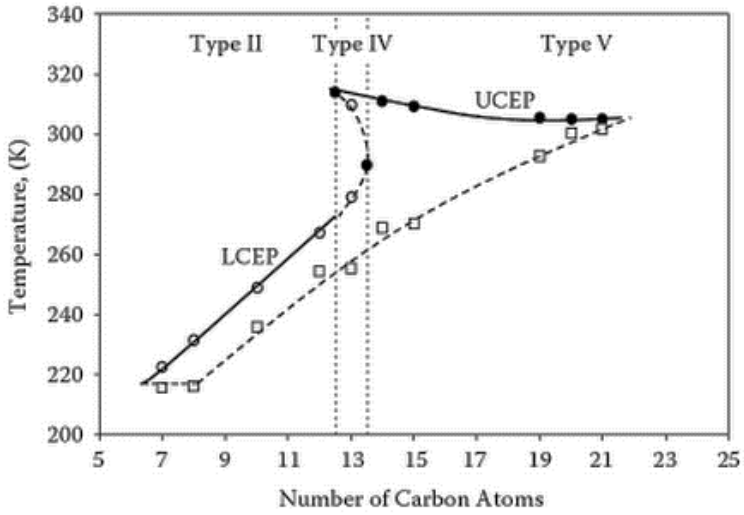

Figure 3.1. Phase transitions for binaries of CO_2 with n-alkanes plotted as a function of number of carbon atoms and temperature. The plot includes the VKS type classification of the systems. UCEP, upper critical end point; LCEP, lower critical end point; □ and dashed line, solid-liquid-liquid-vapour equilibria.

3.3.3. Density and Viscosity

As of 2013, there were more than 1240 measured pure SC CO_2 densities (with the corresponding system conditions) that had been reported. These densities were measured at temperatures of between (308 and 523) K, and at pressures of between (7.5062 and 46.8) MPa (Haghbakhsh et al., 2013).

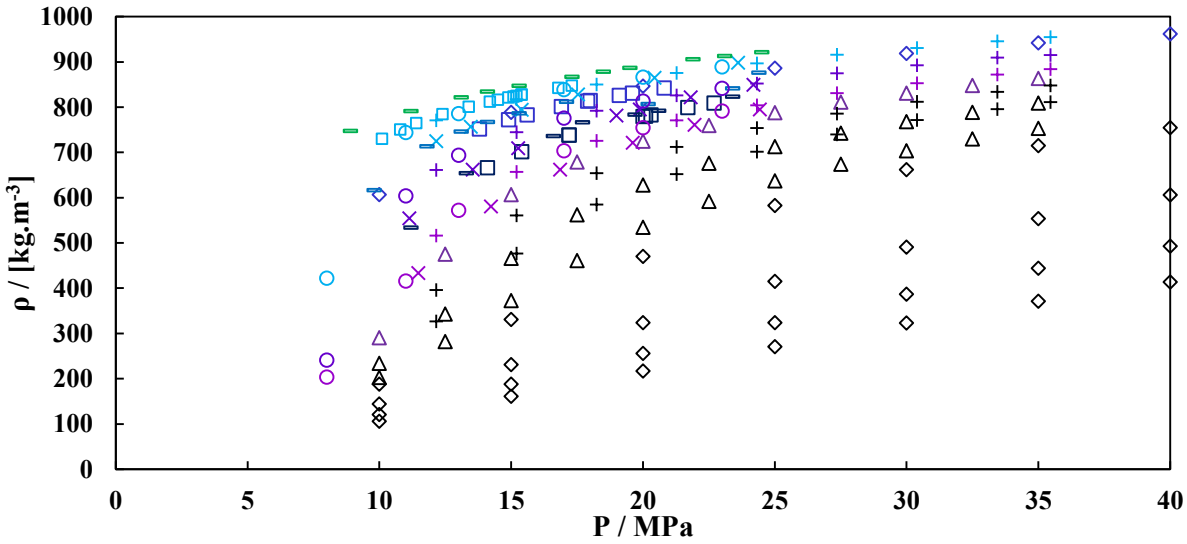

Figure 3.2. Densities as a function of pressure for supercritical CO_2. □, Laitinen and Jäntti (1996); ◊, Miller et al. (1996); Δ, García-González et al. (2001); ×, Cheng et al. (2002); ‖, Duarte et al. (2004); +, Hojjati et al. (2007).

Temperature Colour Scheme: ■, (300-305) K; ■, (305-310) K; ■, (310-315) K; ■, (315-320) K; ■, (320-325) K; ■, (325-330) K; ■, (330-335) K; ■, above 335 K.

The densities of SC CO_2 as a function of pressure and temperature from several of these authors (Laitinen and Jäntti, 1996; Miller et al., 1996; García-González et al., 2001; Cheng et al., 2002; Duarte et al., 2004; Hojjati et al., 2007) are plotted in Figure 3.2. The densities of SC CO_2 are the highest at temperatures close to the critical temperature and at high pressures. The largest density gradients with changes in the pressure and temperature occur in the region close to the critical point.

In addition to the SC densities, there are an additional 204 sub-critical CO_2 densities reported by the NIST ThermoData Engine (2013). These have been measured at temperatures of between (217 and 304.16) K. A substantial amount of density data was also available for sub-critical binary mixtures of CO_2 with the solutes of interest in this study (NIST ThermoData Engine, 2013). A fair amount of this data was measured at low solute concentrations, in the regions at which operation of a SCF process would be expected to operate. Several authors also measured the densities along the full composition scale, from pure solvent to pure solute.

The viscosity of SC CO_2 has been measured by a number of authors, with several correlations having been fitted to the data. Vesovic et al. (1990) provided an in depth discussion on these viscosities. At a temperature of 298.15 K, and as the density approaches zero, CO_2 was shown by Vesovic et al. to have a dynamic viscosity of approximately 1.5×10^{-5} Pa·s.

3.3.4. Sources

The major sources of CO_2 are by-products of a number of different industrial processes, such as the production of ammonia and ethanol and the processing of natural gas (Parsons Brinckerhoff, 2011). The CO_2 that is produced by power generation plants (the single largest source) is generally not captured, as the technology for capture of CO_2 from flue gases remains expensive. The fact that there remain largely untapped sources of CO_2 points to an abundant supply, which is not expected to come under pressure from any increases in demand.

The major problem with the supply of CO_2 is the balancing the regional supply and demand. Often the sources of CO_2 are far removed from where the demand exists (IHS Inc., 2015), and this causes pricing disparities across regions. This should be considered when the location of a plant requiring a supply of CO_2 is being selected.

3.3.5. Emission Mitigation

At present, the release of carbon dioxide in volumes as utilised in SCFE processes is not covered by any protocols or legislation. Thus it remains the most viable option to vent any carbon dioxide that cannot feasibly be recycled.

3.3.6. COSTS

The cost of gases such as CO_2 is dependent upon the willing buyer, willing seller principle, and can therefore vary fairly dramatically from sale to sale. A handbook produced by SRI Consulting (2010) provided approximate prices for CO_2. The prices for bulk CO_2 from a variety of sources (ranging from ammonia production facilities to coal gasification facilities) ranged between US$3 and US$20 per metric ton. These prices include the transport costs via pipeline. These prices are for contracts involving thousands of metric tons of CO_2, and would therefore be substantially lower than the prices that would be paid for the relatively small throughput of a SCFE plant.

Costs for the supply of only several tons per annum would incur significantly higher transport costs per mass unit than larger supply contracts, as the gas would have to be transported by road, rather than by a pipeline. Conservative estimates of the costs of CO_2 would therefore be between US$100 and US$200 per metric ton.

3.4. TRIFLUOROMETHANE SYSTEMS

Very little property data has been measured for binary systems containing R-23 as one of the constituents. There is, however, a fair amount of pure component data. Most of this has been measured for the characterisation of the refrigeration performance of R-23.

3.4.1. PHASE EQUILIBRIA

A few authors have investigated the phase equilibrium of R-23 with hydrocarbons, CO_2 and water. These authors and a description of their study are listed below in Table 3.7.

Table 3.7. Authors who have measured phase equilibrium data for systems involving R-23

Author	Investigation
Wirths and Schneider (1985)	Measured pressure-temperature phase boundary curves for isopleths of binary R-23 + hydrocarbon (n-hexane, n-octane, n-decane) systems at temperatures of between (273 and 630) K and at pressures of up to 250 MPa. The optical, high pressure autoclave of Alwani and Schneider (1969) was used. No thermodynamic modelling was performed.

Author	Investigation
Zheng et al. (1997)	Measured the solubility of R-23 in water at temperatures of (278.15, 308.15 and 338.15) K and pressures less than 0.1 MPa. A stirred glass equilibrium cell was used, with the solubility being determined from the PVT relationship. Modelling approach of Zuo and Guo (1991), with both the SRK with VDW mixing roles and the modified Debye-Hűckel model.
Poot and de Loos (1999)	Reported VLLE pressure-temperature relationships for binary systems of R-23 with n-alkanes (C_6, C_7 and C_8), phenylalkanes (C_3, C_4, C_5, and C_8) and octanol at temperatures of between (248 and 315) K and at pressures up to 5.86 MPa. Glass tube Cailletet apparatus used (static synthetic). No thermodynamic modelling. Determination of van Konynenburg and Scott classification.
Miguel et al. (2000)	Measured the solubility of R-23 in water as a function of temperature between (288 and 303) K, at atmospheric pressure. The simple glass absorption vessel of Silva et al. (1997) was used. The *P-V-T* relationship was used to determine the amount of gas absorbed. A modified version of the PR EOS was used to model the data.
Zhang et al. (2006)	Measured isothermal VLE data for ethane and R-23 at temperatures of between (188.31 and 243.76) K and at pressures of up to 1.62 MPa. Used a ± 300 cm^3 stainless steel equilibrium cell with vapour phase recirculation and vapour and liquid sampling capabilities. SRK EOS with Huron-Vidal (HV) mixing rule and NRTL model used to correlate data.
Nasrifar et al. (2008)	Measured the bubble and dew point curves for the binary system of CO_2 and R-23 at temperatures of between 263 K and the mixture critical point and pressures of up to 7.02 MPa. Used a Cailletet apparatus (static-synthetic). PR EOS with Stryjek and Vera modification (PRSV) and a Margules-type binary interaction parameter.
Bogatu et al. (2009; 2010a; 2010b; 2011)	Measured the bubble pressure phase equilibrium data for systems containing R-23 with (1-phenylpropane, (2-methylpropyl) benzene, 1-phenyloctane or 1-phenyltetradecane) at temperatures of between (245 and 400) K and at pressures of up to 15 MPa. Used a Cailletet apparatus (static-synthetic). Either the PR EOS or the SRK EOS with 1 or 2 parameter classical (VDW) mixing rules. All four systems were said to exhibit type III behaviour of the van Konynenburg and Scott classification.

Author	Investigation
Ju et al. (2009)	Measured the binary isothermal VLE data of R-23 with n-propane and n-butane at temperatures of between (283.15 and 313.15) K and pressures of up to 4.78 MPa. A 200 cm^3 stainless steel equilibrium cell with two viewing windows and recirculation of both liquid and vapour phases was used. Sampling of vapour and liquid phases was performed with sample valves. PR EOS with WS mixing rules and NRTL model was used to correlate the data.

A few interesting observations can be drawn from these summaries. Several of the investigations measured only bubble pressure data using static-synthetic equipment. This was possible due to the low solubilities of the liquids in the subcritical R-23. Other authors reported only the pressure-temperature phase boundary curves, measured with a static-synthetic type of equipment. The compositions of the phases present in the cell were not reported by these authors, as the equipment did not have sampling capabilities. The only two authors who have reported isothermal *P-x-y* data both used equipment that provided recirculation of the vapour phase, presumably to hasten the approach to equilibrium. This suggests a slow absorbance of the refrigerant into the liquid phase.

The PR EOS and the SRK EOS were most commonly used to describe the phase behaviour of the systems. Most of the authors combined the EOS with some form of mixing rules and an activity coefficient model. Only Miguel et al. (2000) and Bogatu et al. (2009, 2010a, 2010b, 2011) used an EOS with the classical (VDW) mixing rules, although the model of Bogatu et al. utilised two parameters for the mixing rules.

Bogatu et al. (2010a) mention that the PR and SRK EOS were used because of 'good qualitative results in VLE calculations for highly non-ideal asymmetric systems'. Their reasoning for using the VDW two parameter mixing rules stems from the fact that Polishuk et al. (1999) showed that a cubic EOS coupled with a two parameter VDW mixing rule was capable of predicting the pressure-temperature behaviour of VKS type I to type V systems. The VDW mixing rule with a single parameter was not capable of providing a good prediction of the phase behaviour.

The VKS classification type for the systems was suggested by Poot and de Loos (1999) and Bogatu et al. (2009, 2010a, 2010b, 2011). Both set of authors proposed that type II or III behaviour was displayed by the binary systems. The systems with the second component having shorter carbon chain lengths were classified as type II systems, and those with longer carbon chain length as type III systems. Poot and de Loos stated that the R-23 + n-hexane system was a type II system, whereas the R-23 + n-heptane was a type III system. They investigated the system type of a quasi-binary R-23 + n-hexane + n-heptane system, describing it as a type IV system. Thus, they propose that with the binary systems

of R-23 with the homologous series of n-alkanes, the transition from type II systems to type III systems occurs via an intermediate type IV system. A similar phenomenon was found with CO_2 with the n-alkane homologous series (Enick et al., 1985; Fall and Luks, 1985), as shown in Figure 3.1, reproduced from the work of Martinez (2007).

3.4.2. Density and Viscosity

At least 216 sub-critical density data points for R-23 have been reported, measured at temperatures of between (124.71 and 299) K. Measurements of the supercritical densities of trifluoromethane have been undertaken by a small number of authors, including Hou and Martin (1959), Hori et al. (1982), Ohgaki et al. (1990), Aizpiri et al. (1991) and Kamiya et al. (1995). There is no data reported in literature of supercritical densities of mixtures involving R-23.

The data reported by Aizpiri et al. (1991) are plotted in Figure 3.3. A few sub-critical data points were included in this work, and these are included in the plot. For this system, similarly to the CO_2 system, the value for $\left(\partial\rho/\partial P\right)_T$ is large around the critical point. The SCF densities of R-23 are substantially larger than those of CO_2 (approximately 1200 kg m^{-3} for R-23 at 20 MPa in comparison to approximately 850 kg m^{-3} for CO_2). This suggests that the solubilities of the solutes will be higher in R-23 than in CO_2, so long as the dependency of the solubility on the density of the fluid applies for these systems.

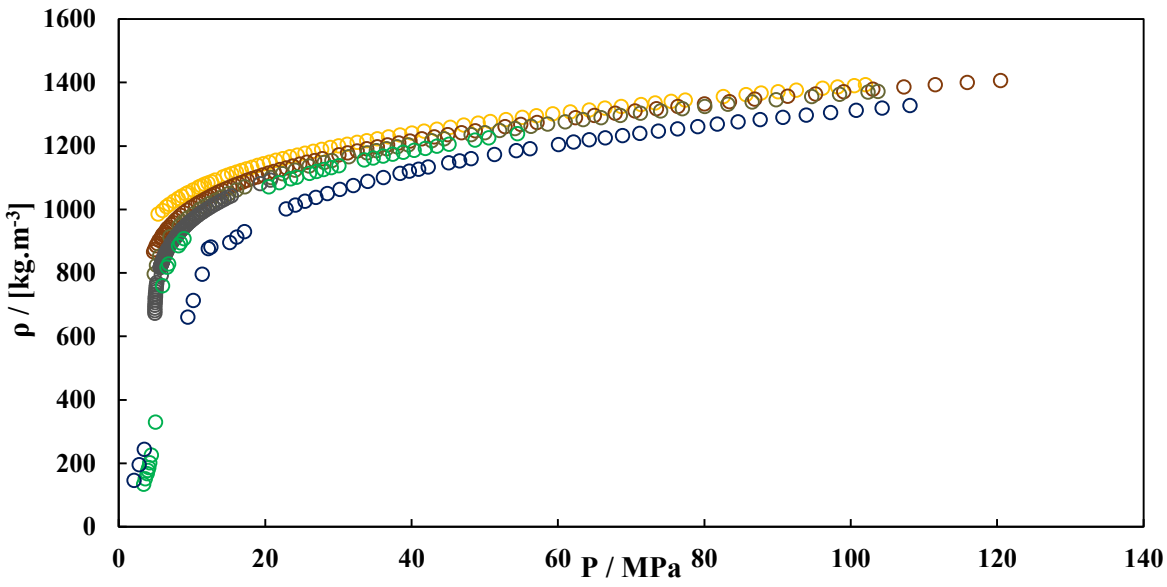

Figure 3.3. Density as a function of pressure for supercritical R23 as reported by Aizpiri et al. (1991). Temperature colour scheme: ■, (285-290) K; ■, (290-295) K; ■, (295-300) K; ■, (300-305) K; ■, (305-310) K; ■, (310-315) K; ■, (315-320) K; ■, (320-325) K.

The dynamic viscosity of R-23 gas at 298.15 K was reported to be 1.462×10^{-5} Pa.s by Dunlop (1994). Although the temperature that the viscosity was measured was slightly above the critical temperature

of R-23, the pressure was approximately atmospheric pressure, and therefore the fluid that was measured was in its gaseous form.

3.4.3. SOURCES

The major source of trifluoromethane is as a by-product in the production of chlorodifluoromethane (R-22) (McCulloch, 2004). The production of R-23 by this process has been minimised to a great extent by process optimisation, but a considerable amount of R-23 is still produced. This must be captured to be either sold or destroyed. In the R-22 production process, the R-23 is most commonly separated from the R-22 in a distillation column, where the R-23 is removed as the distillate. Another newly proposed capture process makes use of a zeolite molecular sieve to capture the R-23 (Corbin and Shiflett, 2015).

Most uses of R-22 in the developed world are being phased out due to the restrictions of its use by the Montreal Protocol (UNEP, 2003). These restrictions do not, however, apply to developing countries, and China, in particular, has therefore recently experienced burgeoning production abilities (McCulloch, 2004). In addition to this, the Montreal Protocol allows the indefinite use of R-22 in the manufacture of polytetrafluoroethylene (PTFE). There is a substantial worldwide consumption of PTFE, with annual production expected to reach 240 thousand tons by 2017 (Global Industry Analysts Inc., 2014). The production of PTFE is expected to continue being buoyed by new opportunities for its use that continue to be discovered. The sustained production rates of PTFE that are expected translate into the continued production of R-22 and, as a consequence, R-23.

3.4.4. EMISSION MITIGATION

Whatever R-23 is to be sold is diverted from the recovered R-23 rich stream exiting the separation process of a R-22 production facility. The remaining R-23 is destroyed in gas fired incinerators (McCulloch, 2004). The R-23 must be incinerated because it is one of the gases of which emissions are heavily controlled by the Kyoto Protocol (United Nations Framework Convention on Climate Change, 1997). Were R-23 to be used as a SC solvent, a possible scenario for the prevention of the emissions of the R-23 into the atmosphere downstream of the extraction process would be to incinerate whatever R-23 could not be recovered in an economically feasible manner. The incineration would produce products very similar to those from the combustion of the R-23 off-gases in the production of R-22. Thus the use of the R-23 as a supercritical solvent would simply be a temporary diversion of the R-23 between the capture and incineration stages.

3.4.5. COSTS

The typical price for R-22 in the USA and Western Europe ranges between $2100 and $2400 per ton. Since R-23 is simply an unwanted side-product of the production of R-22, it would be expected that

the R-23 would be available at price levels below or equal to those of the R-22. The likelihood of this increases when considering that costs would be incurred in destroying the R-23, unless alternative uses can be developed for it.

As a conservative estimate, allowing for transport and storage costs, it was considered that the R-23 would be available at the same price as the R-22 ($2400). The price of R-23 would therefore be approximately 12 times that of CO_2.

3.5. HEXAFLUOROETHANE SYSTEMS

As with R-23, the main understanding of the thermodynamic and transport properties of R-116 comes from investigation into its use as a refrigerant.

3.5.1. PHASE EQUILIBRIA

There are less phase equilibrium data available for systems involving R-116 than is the case for systems involving R-23. The few measurements that are described in open literature are listed in Table 3.8 below.

Table 3.8. Studies of the phase equilibrium data for systems involving R-116.

Author	Investigation
Miller (1968)	Measured the solubility of R-116 in cyclohexane at temperatures of between (280.1 and 305.5) K and at a pressure of 1 atmosphere. The apparatus of Dymond and Hildebrand (1967) was used. No thermodynamic modelling was performed.
Park et al. (1982)	Investigated the solubility of 6 Freons, among them R-116, in water, at 298 K and 100 kPa. A modified version of microgasometric apparatus of Scholander (1947) was used. No thermodynamic modelling was performed.
Zhang et al. (2005)	Measured isothermal VLE data for ethane and R-116 at temperatures of between (199.64 and 242.93) K and at pressures of up to 1.26 MPa. Used a ± 300 cm^3 stainless steel equilibrium cell with vapour phase recirculation and vapour and liquid sampling capabilities. PR EOS with the Panagiotopoulos-Reid mixing rule used to model the system.

Author	Investigation
Valtz et al. (2007)	Measured 6 VLE isotherms for the R-116 and CO_2 system at temperatures of between (253.29 and 296.72) K and at pressures of between (1.05 and 6.45) MPa. A static-analytic cell with liquid and vapour phase sampling capabilities with two ROLSI™ samplers was used. PR EOS with MC alpha function, WS mixing rules and NRTL model used to correlate the experimental data.
Ramjugernath et al. (2009)	Measured 6 VLE isotherms for the system of R-116 and propane at temperatures of between (263.3 and 323.2) K and a pressure range of between (0.344 and 3.851) MPa. Measurements undertaken in a ± 12 cm^3 static-analytic microcell with pneumatic capillary samplers for sampling both liquid and vapour phases. PR EOS with MC alpha function, WS mixing rules and NRTL activity coefficient model used to correlate data.
Ramjugernath et al. (2015a)Ramjugernath et al. (2015b)	Measured VLE isotherms for the binary systems of R-116 with n-butane at temperatures of between (273 and 323) K. Used the same apparatus and modelling approach as Ramjugernath et al. (2009).
Ramjugernath et al. (2015b)Ramjugernath et al. (2015a)	Measured VLE isotherms for the binary systems of R-116 with n-pentane or n-hexane at temperatures of between (288 and 297) K. Used the same apparatus and modelling approach as Ramjugernath et al. (2009).

For the phase equilibrium measurements of systems containing R-116, four authors have measured *P-x-y* data, and the remaining two only measured the solubilities of R-116 in water and cyclohexane at atmospheric pressure. The *P-x-y* measurements were correlated with the PR EOS with an associated mixing rule. Zhang et al. (2005) made use of the Panagiotopolous and Reid mixing rule, while Ramjugernath et al. used the WS mixing rule with the NRTL activity coefficient model. The PR EOS was used because it provides a good accuracy, and its use is widespread in the chemical industry.

In a precursory work to that of Valtz et al. (2007), Coquelet et al. (2003) showed that their experimental data for the difluoromethane + propane system was well represented by the PR EOS with the WS mixing rules. This difluoromethane + propane system had similar behaviour to the R-116 + CO_2 system measured by Valtz et al. The WS mixing rules required a model to provide the excess Gibbs energy, and Valtz et al. used the NRTL activity coefficient model.

3.5.2. Density and Viscosity

There are only 42 data points that have been measured, and reported in literature for the density of sub-critical pure R-116. These densities were measured at temperatures of between (175.01 and

292.85) K. For the R-116, no experimentally measured SC densities were discovered. Data, which were calculated from a model, were available (Lemmon et al., 2011). These data are presented in Figure 3.4. The density of supercritical R-116 was shown to be similar to that of R-23, suggesting that the solubilities of the various components that are to be investigated in this study will be similar with these solvents.

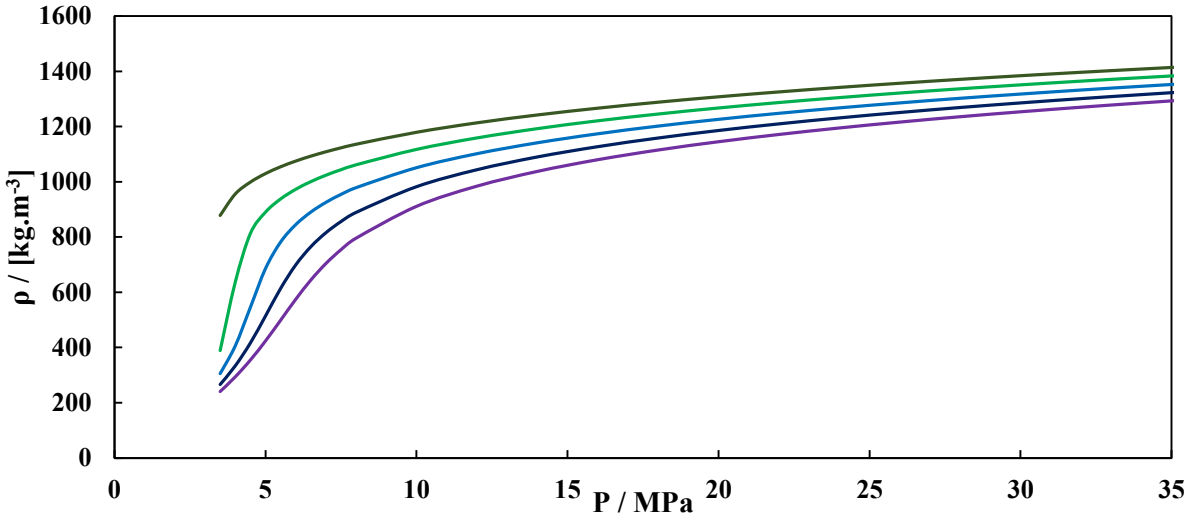

Figure 3.4. Density as a function of pressure for supercritical R-116, calculated by the procedure of Lemmon et al. (2011). Temperature colour scheme: ■, 295 K; ■, 305 K; ■, 315 K; ■, 325 K; ■, 335 K.

No density data could be found for binary systems containing R-116 and the solutes investigated in this study at either sub- or super-critical conditions

Dunlop (1994) reported the dynamic viscosity of R-116 at 298.15 K to be 1.4×10^{-5} Pa·s. Although this measurement was conducted at a temperature above the critical temperature of R-116, the pressure was approximately atmospheric, and the fluid was therefore gaseous, and not a SCF. The viscosities of the sub-critical CO_2, R-23 and R-116 were therefore similar, with the CO_2 having the highest viscosity and the R-116 exhibiting the lowest viscosity. The viscosities of these compounds in their supercritical states could not be estimated from these values.

3.5.3. SOURCES

One of the major sources of R-116 is from the "anode effect" in the Hall electrolytic process for the production of aluminium (Calandra et al., 1982). The off-gases from the Hall electrolytic process are not captured, and approximately 1900 tonnes per year of R-116 are emitted. The off gases from this process have high GWP, but despite this, it is unlikely that capture will be attempted in the foreseeable future, due to the high costs that would be involved.

At present, the major use of R-116 is in the semiconductor manufacturing industry, where it is used as a cleaning and etching gas (Ohno and Ohi, 2003). The R-116 that is manufactured for industrial use

is most commonly produced by fluorination processes, using electrolysis, metal fluorides, or hydrogen fluoride in the presence of a catalyst. For the semiconductor industry, the etching gas is required to be of a very high purity, to ensure high precision etching. There has, of late, however, been a trend to replace R-116 with NF_3, which is a more efficient fluorine source (Muhle et al., 2010). Although not as readily available as other gases, such as CO_2, it is fairly straightforward to obtain a supply of R-116, with a large number of suppliers available.

3.5.4. Emission Mitigation

The standard emission abatement technique used by the semiconductor industry is to recover as much of the PFCs as economical viable, by cryogenic distillation or membrane separation techniques (Tsai et al., 2002). The remainder of the gases are usually destroyed by using high temperature plasmas (Hartz et al., 1998; Namose, 2005). The mitigation of emissions of the R-116 that cannot be recycled in a SCFE process would thus provide serious challenges. Destruction of the R-116 using high temperature plasmas would not be a viable option due to the low expected emission volumes. Capture and recycle using membrane separations would in all likelihood prove a cheaper alternative.

3.5.5. Costs

The high cost of R-116, is mostly due to the lack of demand. The major demand for R-116 is by the semi-conductor industry, where extremely high purity R-116 (greater than 99.999 %) is required. The lack of demand for lower purity R-116 means that it is not supplied. If the demand for lower purity R-116 (approximately 99.5 %) were to increase, this grade would likely be made available at substantially lower prices.

Subramoney (2008) researched the use of R-116 as a solvent for a different separation process, and found that it was approximately 25 times more expensive than CO_2. Beijing Starget Chemicals Co. Ltd. (2015) quoted a price of US$ 10 000 per ton of R-116. Central China Sepcial Gas Co. Ltd. (2015) gave a price of US$ 8 000 per ton. Therefore, the cost that was given by Subramoney appears to be a low estimate. For this study, a price of US$ 10 per kilogram of R-116 is probably a better estimate.

4. MEASUREMENT TECHNIQUES

Development of new SCFE processes requires an understanding of the phase behaviour of the solvents and the solutes at sub-critical, critical and supercritical conditions. Although predictive models allow the behaviour to be approximated, a better understanding of the systems comes from models that are based upon experimentally measured phase equilibrium data.

In this chapter, the types of equilibrium measurements that have been used for obtaining data required by thermodynamic models are first reviewed. Thereafter, the equipment and procedures that have been used to perform the measurements in this study have been summarised. Three experimental apparatus were used to measure the experimental data for this study. Finally, the methods for the estimation of the measurement uncertainties are presented.

4.1. SUPERCRITICAL EQUILIBRIUM MEASUREMENTS

A number of different analytical techniques have been used to investigate the phase behaviour of systems involving a supercritical solvent with the desired solutes. These measurements are necessary for the design of a SCF process plant, as would be the case with any chemical processing plant. Data of a higher accuracy provides improved, more efficient designs, and it is therefore imperative that the measured data be as accurate as possible.

The measurement of data for the design of a SCF process can generally be separated into two classes. In instances where the solute comprises a vast range of components, it would be difficult and extremely time consuming to measure the binary or ternary equilibrium data for each combination, and therefore only the quantity and the composition of the soluble portion, at different process conditions, are analysed. As an alternative, the binary or ternary equilibria data of a select few 'representative' components are measured, and these are then used to estimate the phase behaviour of the entire system (Jiménez-Gallegos et al., 2006).

4.1.1. EXTENSIVE MEASUREMENTS

Extensive measurements refer to measurements in which only the quantity and composition of an extract obtained at a given set of process parameters is investigated. In cases where the solute is a mixture of hundreds, if not thousands of components, such as natural plant extracts, these measurements are most commonly performed.

The aim of extensive measurements is to determine optimal parameters to obtain a particular separation. The main parameters of interest are the temperature, the pressure, and the solvent-to-solute ratio. These measurements are generally performed in transient, batch extraction units, in

which the solute is loaded at the start of the measurements, and the solvent is passed through the cell, stripping the soluble components out, while the insoluble components remain in the cell.

A list of some of the studies that have been undertaken with this type of measurement are provided in Table 4.1.

Table 4.1. Measurements of complex real systems in SCFs (Extensive measurements).

Author	Investigation
Gopalakrishnan and Narayanan (1991)	Investigated the effect that the pressure, temperature, contact time and moisture content of the feed had on the yield and compositional variance of essential oils extracted from cardamom seeds using supercritical CO_2. The authors found that the concentrations of the non-volatiles and the chlorophyll in the extract varied with changes in these operational parameters.
Reverchon et al. (1995)	Both a laboratory scale apparatus and a pilot plant were used to investigate the extraction of lavender essential oils using supercritical CO_2. The plant matter was packed into the pressure vessels, through which the supercritical solvent flowed. Three separators, operating in series, were used to fractionate the product, by varying the temperatures and pressures of the separations. The solvent was recirculated within the pilot plant. The pressure, temperature, extraction time and solvent flow rate were all investigated to determine the optimum operating conditions. The authors showed that identical process conditions on the two apparatus produced extracts with identical chemical compositions.
Ferreira et al. (1999)	An extraction cell was used to investigate the fixed bed extraction of black pepper essential oils by passing supercritical CO_2 through the bed. The highest solubility was obtained at the conditions at which the highest solvent density was achieved. A maximum recovery of 70% of the total oil present was achieved at these conditions.
Al-Marzouqi et al. (2007)	Investigated the use of supercritical CO_2 for the extraction of hydrocarbons from an oil-saturated soil obtained from the Sahel oil field in the United Arab Emirates. The effects that the pressure, temperature and composition of the oil had on the extraction process were investigated. The maximum extraction efficiency for the process was found to be 72.4%. This was at the maximum pressure (30 MPa) and at a temperature of 373 K.

Author	Investigation
Ávila-Chávez et al. (2007)	Used a solvent recirculating 'flow-type' SCFE unit for the study of the extraction of hydrocarbons from sludge collected from the bottom of a crude oil storage tank. The ethane (solvent) was added to the base of the extraction vessel and removed from the top after having passed through the sludge sample. The pressure of this exiting stream was thereafter decreased such that the solute and solvent separated, with the solvent being re-used after re-pressurisation. The extraction pressure was varied between (10 and 17.2) MPa and the temperature between (308 and 338) K. It was found that the supercritical extraction provided a significant upgrade of the liquid, with a recovery of up to 58.5% of the hydrocarbons present.
Parra et al. (2010)	The efficiency of the extraction of fractions from a typical vacuum distillation residue using supercritical n-hexane was investigated at a pilot plant scale. Various fractions were recovered by altering the pressure of the extraction process, while the temperature was maintained at a constant value. The sulphur content of each of the extracted fractions was also investigated.

4.1.2. Representative Measurements

Representative measurements use either solubilities or VLE data for a small number of components in order to investigate the possibility of performing a specific separation. Thermodynamic models are usually fitted to the measured data, enabling the prediction of the phase behaviour for a range of process conditions, as opposed to only at the conditions at which the measurements were performed.

Solubility Measurements

A significant number of authors have reported solubilities in SCF. The solubility refers to the amount of solute that is present in the solvent-rich phase. It is reported alongside the pressure and temperature at which it is measured. Many SCF solubility measurements are actually performed at subcritical conditions, and are only supercritical with respect to the pure solvent. The solubilities both above and below the mixture critical points are referred to as solubilities in SCFs, as the measurements are being undertaken at conditions above the critical point of the pure solvent.

The solubilities above the mixture critical point cannot be correlated with an EOS, as is the case for sub-critical mixtures (Akgün et al., 1999). Some authors have modelled the sub-critical data with EOS models, but for many systems these models provide fairly poor correlation of the data. Several semi-empirical correlations have been developed in an attempt to better describe the supercritical solubilities.

A few of the authors who measured the solubilities in SCFs are described in Table 4.2. Some information on the equipment utilised for the measurements, as well as any modelling or correlation that was performed are also given.

Table 4.2. Solubility measurements of single component solutes in SCFs.

Author	Investigation
Kurnik et al. (1981)	Measured the solubilities of five organic solids in supercritical CO_2 and ethylene. The measurements were undertaken using a single-pass flow-through extraction device within which the solids were contained. These measurements assumed that the SCF was saturated with the solute upon leaving the extraction device, with a number of tests being performed to validate this assumption. A solute-solvent interaction parameter for each system was determined by correlating the PR EOS to the experimental *P-y* data.
Kurnik and Reid (1982)	Investigated the solubilities of organic solids extracted from binary mixtures using supercritical CO_2 and ethylene in a single-pass flow through extraction device. They found that the mass ratios in the solid mixture did not affect the solubilities of the individual components. The PR EOS was used to correlate the experimental data, using binary interaction parameters reported in the previous study. For a number of the systems, no satisfactory correlation of the ternary systems could be achieved.
Dobbs et al. (1986)	Determined the solubility of hexamethylbenzene and phenanthrene in CO_2, using a "microsampling apparatus".
Mitra et al. (1988)	Measured the isothermal solubilities of pure naphthalene and pure dibenzothiophene, as well as the solubilities of a binary mixture of these two components using a batch equilibrium cell. The experimental data was correlated using the SRK and PR EOS. The solubility data was used to calculate the partial molar volumes of the components.
Mukhopadhyay and De (1995)	Investigated the solubilities of three binary mixtures of aromatic chemicals, of similar molecular weights, in supercritical CO_2. A batch equilibrium cell without continous flow was utilised to perform the measurements. One of the pairs of chemicals was a liquid at room temperature, while the other two pairs were solid binary mixtures at room temperature.
Nieuwoudt and Du Rand (2002)	Measured the 'dew point curve' for systems involving CO_2 and n-alkanes, using a variable-volume view cell. The solute mixture in the cell was pressurised isothermally until there was only one phase present in the cell. The pressure was thereafter reduced until the formation of a second phase was observed. This pressure was verified by a number of observations, and was denoted as the 'dew pressure'.

Author	Investigation
Li et al. (2003)	Determined the solubilities of 2-naphthanol and anthracene in supercritical CO_2, with and without the use of co-solvents. The co-solvents that were investigated were acetone, ethanol and cyclohexane. These co-solvents greatly enhanced the solubilities of the solutes. A flow technique, was used in this investigation and no correlation of the data was attempted.
Brandt et al. (2010)	Measured the solubility of palmitic acid in supercritical CO_2 using a view cell. The density of the SCF was measured simultaneously with the solubility measurements in a vibrating tube densitometer. The solubility and density were then correlated using the semi-empirical density-based correlation of Méndez-Santiago and Teja (1999).

VAPOUR-LIQUID EQUILIBRIUM MEASUREMENTS

Other investigations into SCFE have involved the measurement of the VLE of the binary or ternary systems. This VLE data is usually modelled using thermodynamic models. The correlated models are then used to investigate the phase behaviour of the systems at near-critical conditions. A few of the VLE measurement studies that have been conducted are briefly described in Table 4.3.

Table 4.3. VLE measurements for the characterisation of SCFE processes.

Author	Investigation
Huie et al. (1973)	Performed phase equilibrium measurements, investigating the VLE, VLLE and solid-vapour-liquid equilibria (SVLE) of a binary mixture of CO_2 + n-eicosane. The VLLE data of a ternary system of CO_2 + n-decane + n-eicosane were also measured. The authors made the assumptions that the vapour phase was always pure CO_2, and that the solid phase was always pure n-eicosane, which caused inaccuracies in the data.
Chou et al. (1990)	Isothermal VLE was measured for the binary systems of CO_2 + n-decane and CO_2 + tetralin as well as the ternary mixture of CO_2 + n-decane + tetralin at sub-critical pressures. The measurements were performed in a cell with vapour recirculation and sampling capabilities for both the liquid and vapour phases. The sampling was performed through sampling valves which sampled volumes of approximately 30 µl of each phase. The reported experimental data was not correlated to any thermodynamic models.

Author	Investigation
Nagarajan et al. (1990)	Measured the VLE, interfacial tensions and phase densities of a ternary system of CO_2, n-butane and n-decane using a constant overall molar composition. This work was an attempt to develop a basis for the testing of various models for phase equilibria and interfacial tensions. The data measured here was used to test the ability of the models to describe systems involving more than two components. A cell with recirculation of the liquid, which was developed by Hsu et al. (1985), was used for all of the measurements. The fluid in the recirculation loop was sampled to analyse the composition, interfacial tensions and densities. A scaling law was used to estimate the system critical point properties.
Iwai et al. (1996)	Investigated the high-pressure phase equilibrium data for the system of CO_2 and limonene above the critical point of pure CO_2 using a circulation-type cell. The PR EOS with conventional mixing rules with two interaction parameters was used to correlate the experimental data.
Shariati et al. (1998)	Measured the bubble point pressures for mixtures of C_{6+} hydrocarbons in the presence of approximately 25 mole % CO_2. These measurements were performed in the high pressure Cailletet apparatus described by Peters et al. (1993). The bubble point pressures were correlated with the PR EOS.
Scheidgen and Schneider (2000)	Measured high pressure phase equilibrium data for systems involving CO_2, an 1-alkanol with 10 or less carbon atoms and an n-alkane with 16 or less carbon atoms. The measurements were performed using a cell developed by Konrad et al. (1983). Additional measurements were made 'quasi-synthetically', to obtain datum points for the 'near-critical' curves of the binary mixtures. This was possible because the composition of the vapour phase was found to vary only slightly with increases in pressure by the addition of CO_2. The ternary systems was viewed as quasi-binary, because the separation factors were very close to unity around the critical region. The method of Pöhler et al. (1996) was used to perform the 'quasi-synthetic' measurements.
Florusse et al. (2004)	Measured the phase equilibria of binary mixtures of CO_2 with tributyrin, tricaproin and tricaprylin at subcritical conditions using a Cailletet apparatus. The Cailletet apparatus is a variable volume cell without sampling capabilities (i.e. synthetic) (Raeissi and Peters, 2001). This work was performed in order to investigate the effect that the molecular weight of triglycerides had on the phase behaviour. The 'group contribution' (GC) EOS of (Skjold-Jørgensen, 1984) was applied to the data reported for this study.

Author	Investigation
Jiménez-Gallegos et al. (2006)	Studied the VLE for a CO_2 + octane system and a CO_2 + n-decane system in a cell developed by Galicia-Luna et al. (2000), at temperatures above the critical temperature of CO_2. The PR EOS with either the classical mixing rules or the WS mixing rules with the NRTL activity coefficient model was used to correlate the experimental data. It was found that the model using the WS mixing rule gave a better representation of the systems.
Gironi and Maschietti (2008)	Measured the phase equilibria of CO_2 and limonene at temperatures and pressures above the critical point of pure CO_2 in a continuously circulated VLE cell. The data was correlated with the PR EOS using the VDW mixing rules.
Kulik et al. (2008)	Investigated the phase equilibria of CO_2 + pyrrole in a variable-volume view cell, at temperatures and pressures above the critical point of pure CO_2. The variable-volume view cell that was used was developed by Crampon et al. (1999). Liquid-liquid immiscibility was experienced for this system below the critical point of the pure CO_2, but not above it. The data was correlated with the PR EOS combined with the Mathias-Klotz-Prausnitz mixing rule (Mathias et al., 1991).
Sánchez-García et al. (2011)	Studied the isothermal VLE for two ternary systems; CO_2 + n-decane with either n-hexane or n-octane; at temperatures of between 312 and 376 K, using the 'online static-analytic apparatus with a movable ROLSI^{TM} sampler', developed by Galicia-Luna et al. (2000). The authors utilised the temperature independent binary parameters, fitted to the binary systems, to predict the behaviour of the ternary mixtures with the PR EOS. The predicted behaviour was compared with the experimental data.
Mendo-Sánchez et al. (2012)	The apparatus developed by Galicia-Luna et al. (2000), was used to investigate the VLE for ternary and quaternary systems with n-hexane and thiophene alongside CO_2 and ethanol. The data was measured at temperatures above the critical temperature of pure CO_2. The PR EOS with the classical mixing rule was used to correlate the data.

Huie et al. (1973), Nagarajan et al. (1990) and Chou et al. (1990) all measured the ternary VLE for systems involving CO_2 and two n-alkanes. A common thread for all of these authors was the inclusion of n-decane. The n-decane was described by Sánchez-García et al. (2011), as a 'base normal alkane'. This 'base normal alkane' was used as a benchmark, against which the solubility of the other components could be compared.

de Leeuw et al. (1992) and Peters et al. (1992; 1993) investigated real-life multicomponent fractions (which could contain countless components) by using mixtures with a finite, number of components; with each component being well defined. This data was used to determine parameters for use in the

thermodynamic modelling of the model systems. Hiyoshi et al. (2010) used a model hydrocarbon system of tetralin, decalin and tetradecane in their investigation into the separation of aromatic sulphur compounds from hydrocarbons.

An example of the use of the interaction parameters from each of the binary systems constituting the system of interest, to predict the behaviour of the entire system, is given in the work of Araujo et al. (2001). These authors used the PR EOS binary interaction parameters for combinations of the main components present in a multicomponent distillate from a soybean oil deodoriser to predict the VLE of the system. They compared the predicted data to distribution coefficients and selectivities which were found in literature. The authors showed that it was possible to predict the solubilities of the solutes present in the soybean oil distillate by using the PR EOS. This technique was, however, said to be suitable only for the preliminary investigations.

4.2. VLE Equipment Used in Literature

Representative measurements were determined to be the best technique for the characterisation of the performance of supercritical solvents in the petroleum industry for this study. With the measurement of the phase equilibrium of a select number of binary systems, it would be possible to approximate a number of different separation processes. Although solubility measurements are faster and cheaper to perform, they do not provide the same degree of understanding of a process, because the behaviour of the liquid phase is not investigated. VLE measurements, which provide a far more comprehensive characterisation of the system behaviour were therefore preferred for this study.

Complete measurement of the VLE of a binary two phase system requires the measurement of the temperature and the pressure of the system, as well as the analysis of the composition of any liquid and vapour phases present. With VLLE, the analysis of the second liquid phase increases the number of composition analyses required to three. For the measurement of VLE or VLLE data, it is extremely important that the measurements are performed at the point at which equilibrium exists. There exist a large collection of apparatus available for the measurement of high pressure phase equilibrium. With most of the equipment designs that have been proposed over the years, changes are made to existing designs in order to improve the sampling technique, the reliability in reaching equilibrium or the speed at which equilibrium is obtained within the apparatus.

Reviews of the measurement of high pressure VLE data has been undertaken by many authors, and include studies into the equipment used and the data that has been collected. Reviews include the works of McGlashan and Hicks (1978), of Knapp et al. (1982), of Fornari et al. (1990), of Richon and de Loos (1991), of Raal and Mühlbauer (1994), and of Dohrn and Brunner (1995). McGlashan and Hicks

investigated various techniques used for the measurement of binary thermodynamic quantities between 1900 and 1978. Knapp et al. performed a review on high pressure vapour liquid equilibrium measurements from 1900 to 1980, and Fornari et al. reviewed the high pressure fluid phase equilibria measurements that were conducted between 1978 and 1987. Dohrn and Brunner classified and described a number of experimental methods for equilibrium measurements at pressures greater than 10 MPa from between 1988 and 1993. More recent reviews have been conducted by Christov and Dohrn (2002) for the period from 1994 to 1999, Dohrn et al. (2010) for the period of 2000 to 2004 and Fonseca et al. (2011) for the period from 2005 to 2008.

VLE measurements can be grouped into two classes; those using dynamic apparatus and those using static apparatus. In true dynamic apparatus, there is circulation of both the vapour and liquid phases (Knox, 2005). This circulation could be as simple as withdrawal and recirculation of the phases through an equilibrium chamber, or could have greater complexities such as a flow-through device. In such an apparatus, the components are mixed and pass through an equilibrium chamber in a steady-state continuous manner. A number of quasi-dynamic apparatus have also been developed, which allow for the circulation of only one of the phases present, while the other phase remains static (Chou et al., 1990). This type of cell has been classed as a static cell in some reviews. Dynamic equilibrium cells are easier to construct and operate when operating at low to medium pressures, than when operating at high pressures (Weir and de Loos, 2005). Because of the complexities of operating a dynamic cell at high pressure, this is seldom done. A review into various dynamic cells reported in literature for the measurement of VLE was therefore not undertaken for this study.

Static equilibrium apparatus can be divided into static-synthetic and static-analytic designs. With static-analytic apparatus, the compositions of the individual phases in the cell are analysed, whereas with static-synthetic cells, only the loading composition is known. Several of the static designs that have been developed for the measurement of high pressure phase equilibrium data are discussed below in Sections 4.2.1 and 4.2.2.

4.2.1. Static-Synthetic Equilibrium Measurements

The majority of static-synthetic measurement apparatus have a variable-volume cell at the centre of their construction. Most of these variable-volume cells provide a means for the contents of the cell to be observed. This viewing capability could be by means of a small viewing port, or could be due to a large portion of the cell being constructed of a transparent material such as a sapphire crystal. A few variable-volume cells, for which no viewing capabilities are provided, rely on the discontinuities in the isothermal volume-pressure relationship to determine the bubble point of a system. If the cell has viewing capabilities, the phase transition points are normally determined by simple visual observation.

A possibility also exists for VLE data to be measured using a static-synthetic cell. For this type of measurement, however, thermodynamic equations must be relied upon to determine the compositions of the individual phases (Van Ness, 1964).

Some examples of the types of static-synthetic equipment that have been reported in literature are presented in Table 4.4. Included with the description of the equipment are the pressure and temperature ranges at which they can be used.

Table 4.4. Literature examples of static-synthetic measurements.

Author	Description of equipment
Reamer and Sage (1963)	A stainless steel vessel, into which mercury was added for the purpose of varying the cell volume was used. Bubble point data was measured at pressures of up to 18.9 MPa and at temperatures of between (277 and 511) K. The composition of the contents of the cell was determined upon loading. Discontinuities in the isothermal volume-pressure relationship were used to determine the bubble point.
Nasrifar et al. (2003)	A Cailletet equipment, capable of measuring bubble point data at pressures of between (0.35 and 15) MPa and at temperatures of between (250 and 470) K, was used. The Cailletet apparatus consists of a glass capillary tube with mercury as the sealant. The pressure in the cell was controlled hydraulically.
Mutelet et al. (2005)	A stainless steel variable-volume equilibrium cell with a sapphire viewing window, capable of performing measurements at pressures of up to 70 MPa and temperatures of up to 423 K, was used to measure bubble point data. The mass of each of the components that was added into the cell was used to determine the composition of the mixture. A hand-screw was used to move the piston, which changed the cell volume.
Lay (2010)	Used a high pressure variable-volume view cell with a maximum volume of 130 cm^3, a maximum pressure of 70 MPa and a maximum temperature of 473 K to measure bubble point pressures of binary mixtures. Mixing within the cell was performed by using a magnetically coupled stirrer. The viscosity and density of the cell contents were measured with an in-line viscometer and densitometer respectively. The volume of the cell was controlled by a piston. The position of this piston was controlled by a positive displacement pump, which pumped a fluid into the volume above the piston, in order to move it.

Static-synthetic apparatus are not very popular, as it is difficult to load the components into the cell while simultaneously ensuring that no impurities enter the cell. Additionally, the dew and bubble curves must be characterised separately, which results in longer analysis times.

4.2.2. STATIC-ANALYTIC EQUILIBRIUM MEASUREMENTS

Analytical VLE measurements involve the analysis of the individual phases present within the equilibrium cell (Dohrn and Brunner, 1995). This analysis could be either by sampling of the phases and thereafter utilising an external analysis technique, or by using physicochemical methods for the analysis of the compositions of the phases in situ within the cell.

A variety of different static analytic equilibrium apparatus have been used to investigate high pressure VLE. Several of these designs are described below.

Table 4.5. Literature examples of static-analytic measurements.

Author	Description of Equipment
Ohgaki and Katayama (1975)	Utilised a 300 cm^3 stainless steel equilibrium cell with two Pyrex glass disk windows. The maximum operational pressure was 14.8 MPa. Samples of the liquid and vapour phases were obtained through small steel tubes sealed with a ball valve and a needle valve. A magnetically coupled stirrer was used to agitate the cell contents.
Kalra et al. (1978)	Designed a (10 to 175) cm^3 stainless steel variable volume cell consisting of two cylinder-piston end sections and a central windowed section. This cell was capable of performing measurements at pressures of up to 20.7 MPa and at temperatures of between (250 and 393) K. The composition of the phases were analysed by measuring their refractive indices.
Ng and Robinson (1978)	Ng and Robinson's apparatus consisted of a stainless steel equilibrium cell with an internal volume of 150 cm^3, designed with a Pyrex-glass viewing window to enable observation of the phase interface. This apparatus was capable of measurements at temperatures of between 310 and 588 K (100 to 600°F) and pressures of up to 17.2 MPa (2500 psia). The cell contents were agitated by a magnetically coupled stirrer. A liquid sampling valve, based upon the design of Fredenslund et al. (1973) was inserted into the body of the cell for sampling the liquid phase. For sampling of the vapour phase, a vapour sampling valve, designed by Kalra and Robinson (1975), was included.
Li et al. (1981)	Used a windowed stainless steel variable-volume cell with a maximum volume of 600 cm^3. The windows were constructed of quartz glass. Mixing the contents of the cell was achieved by the rocking of the cell in an air bath. Measurements were conducted at temperatures of between (313 and 393) K, and at pressures of up to 12 MPa. Samples of the liquid and vapour phases were obtained through sampling valves.

Author	Description of Equipment
Cotterman (1985)	Chou et al. (1990) described the static-analytic apparatus that was developed by Cotterman (1985). This equipment had an equilibrium section, which included a recirculation line for the vapour phase, and a sampling section. The equilibrium cell had a volume of approximately 100 cm^3. The authors did not provide information about the pressure and temperature range capabilities of this equipment. The phase samples were withdrawn from the equipment into microcell type sampling valves. Once a sample of the fluid was obtained in the microcell, it was transferred to a separate sample analysis facility, where the composition was analysed.
Wagner and Wichterle (1987)	A 65 cm^3 stainless steel cell with two Pyrex glass viewing windows and an internal stirrer was used by Wagner and Wichterle. Capillaries were used for the sampling of both the liquid and vapour phases. This cell had a maximum pressure rating of 9 MPa. It was used to perform measurements at temperatures of between (303 and 323) K.
Traub and Stephan (1990)	Developed a static-analytic apparatus which consisted of a 50 cm^3 high-pressure visual-cell which could be rotated to allow the sampling of any of the phases present within the cell, through a capillary tube. A sample was withdrawn from this capillary tube into a sample loop by opening a needle valve. The contents of the cell were agitated by a magnetically coupled stirrer. Measurements could be conducted at pressures of up to 30 MPa and at temperatures up to 393 K.
Crampon et al. (1999)	Used a high pressure sapphire crystal view cell attached to a stainless steel manual screw pump, which created a variable-volume cell with a volume range of between (4.05 and 14.35) cm^3. A magnetic stirrer was used to agitate the fluid within the cell. Pressures of up to 18 MPa were measured by Crampon et al. The temperatures at which the data was measured were between (313 and 333) K. Sampling of the fluid in both the upper and the lower portions of the cell was possible with three-way micro-valves.
Galicia-Luna et al. (2000)	Developed a static-analytic type apparatus for the fast measurement of VLE at pressures of up to 60 MPa and temperatures of up to 523 K. The stainless steel equilibrium cell had a 40 cm^3 volume. The cell body had two sapphire crystal windows, one on each side, which made the entire height of the inside of the cell visible. Viton 'o'-rings were used between the flanges to seal the cell. A moveable capillary, entering through a flange on the cell, was used to obtain liquid and vapour samples.

Author	Description of Equipment
Valtz et al. (2004)	The equipment developed by Valtz et al. was based on a cell designed by Laugier and Richon (1986). Central to this equipment was a hollow sapphire tube enclosed by stainless steel flanges at either end. The equipment was capable of operating at pressures of up to 8 MPa and temperatures of between (223 and 473) K. Mixing within the 28 cm^3 equilibrium cell was achieved with a stirrer that was magnetically coupled to a variable speed stirrer. Two ROLSI pneumatic capillary samplers were used to sample the vapour and liquid phases.
Yu et al. (2006)	A variable-volume view cell with a maximum volume of 100 cm^3 and a single quartz window was used by Yu et al. This cell was used to perform measurements at pressures and temperatures of up to 200 MPa and 393 K respectively (Lentz and Weber, 1994). A magnetic stirrer was used to agitate the cell contents, and samples of the phases were obtained through a capillary and a needle valve.
Naidoo et al. (2008)	An approximately 200 cm^3 stainless steel, variable-volume equilibrium cell was used by Naidoo et al. A pair of opposing sapphire tube windows enabled the contents of the cell to be viewed. The equilibrium cell was capable of withstanding pressures of up to 12 MPa, and could be used within the temperature range of (250 to 393) K. A magnetically coupled composite impeller was used to agitate the contents of the cell. A 2-position 6-port GC valve was used to obtain samples from various heights within the equilibrium cell.
Tochigi et al. (2010)	A 500 cm^3 static equilibrium cell with a Pyrex glass 'bull's eye' window was used for these measurements. An externally driven agitator was used to stir the cell contents. The cell had a maximum working pressure of 30 MPa and a maximum temperature of 480 K (Sako et al., 1991). The vapour phase was sampled with a metering valve, and the liquid phase was sampled with a magnetic circulating pump and a 3 cm^3 liquid sampler.

For high-pressure phase equilibrium measurements, static-analytic measurements are by far the most common, as they can provide a more complete characterisation of the phase behaviour of a liquid-vapour system, are easier to operate and consume smaller volumes of chemicals than dynamic cells.

Many of the equilibrium cells used in static-analytic apparatus are fairly large in order to negate the effect that drawing a sample from the equilibrium chamber has on the thermodynamic equilibrium of the system (Narasigadu et al., 2013). Of late, with the development of high precision fluid sampling equipment, such as the Rapid-Online-Sampler-Injector (ROLSI^{TM}) of Guilbot et al. (2000b), it has become possible to reduce the size of the equilibrium cell. Details of several of these newer so-called 'microcells' are tabulated in Table 4.6.

Table 4.6. Examples of microcell equilibrium measurement apparatus [a].

Author	V / cm^3	P / MPa	T / K	Sampling Technique
Winkler and Stephan (1997)	50	5.8 [b] to 11.0 [b]	296 [b] to 315 [b]	Needle valves
Baba-Ahmed et al. (1999)	43	0 to 40	77 to 123 [b]	ROLSI™
da Silva et al. (2000)	23	0 to 30	295.2 to 353.2	6-way valve
Galicia-Luna et al. (2000)	40	0 to 60	Up to 523	Moveable capillary tube
Valtz et al. (2004)	28	0 to 8	223 to 473	ROLSI™
Houssin-Agbomson et al. (2010)	12	0 to 10	109.98[a] to 125.63 [b]	ROLSI™

[a] cell volume, V, measureable pressures, P, and temperature ranges, T, and the sampling technique used for the measurements are included

[b] experimental data limits, as the equipment limits are not specified.

4.3. STATIC-ANALYTIC APPARATUS

To minimise the consumption of chemicals, the high pressure, static analytic microcell apparatus that was developed and commisioned by Narasigadu (2011), was employed in this study. This apparatus is currently located at the Thermodynamics Research Unit of the University of KwaZulu-Natal. The sampling of the various phases present within this equilibrium microcell is performed by using a single moveable capillary through a ROLSI™. This enables multiple phases, such as would occur with VLLE, to be sampled, simply by adjusting the height at which the capillary tip is positioned.

4.3.1. EQUIPMENT DESCRIPTION

Central to the static analytic apparatus of Narasigadu (2011) was the equilibrium cell. Adjoining this equilibrium cell was the equipment for the measurement of the temperature, pressure and composition. This apparatus was capable of measuring VLE at temperatures of between (263 and 473) K and pressures of between (0.7 and 15) MPa. The apparatus is depicted in Figure 4.1.

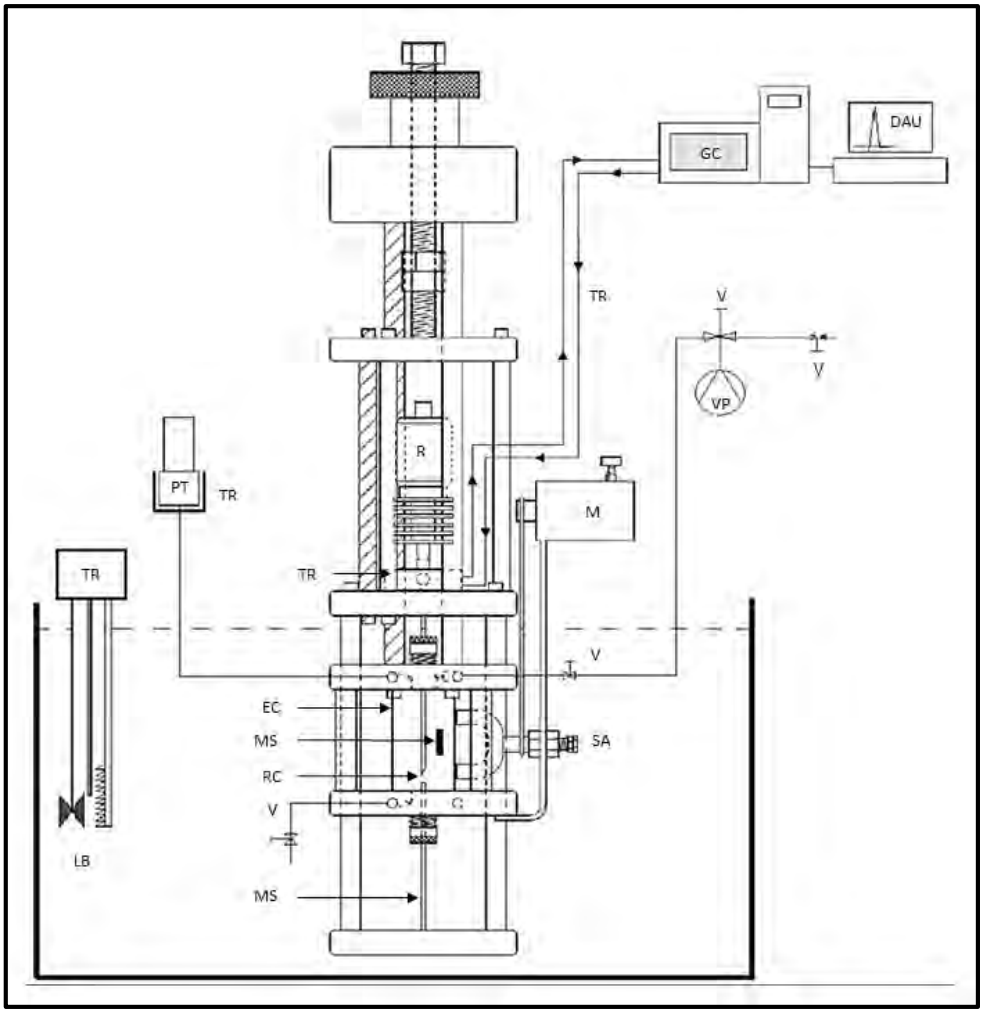

Figure 4.1. Schematic of the static-analytic high-pressure VLE apparatus of Narasigadu et al. (2013). DAU, data acquisition unit; EC, equilibrium cell; GC, gas chromatograph; LB, liquid bath; M, motor; MR, metal rod; MS, magnetic stirrer; PT, pressure transducer; R, moveable ROLSI^{TM}; RC, capillary; SA, stirring assembly; TR, thermal regulation; V, valve; VP, vacuum pump.

EQUILIBRIUM CELL

The equilibrium cell consisted of a cored sapphire crystal tube with dimensions of (OD = 35.60, ID = 17.80, L = 70.00) mm. This tube was purchased from Rayotek Scientific Inc. The sapphire crystal was used because, in addition to providing good visibility of the cell contents from all angles, it was also designed to be capable of withstanding high pressures. Furthermore, sapphire crystal also has good thermal conductivity (Narasigadu, 2011).

The sapphire crystal tube was enclosed at either end with a 316 stainless steel flange with dimensions of (t = 15, D = 110) mm, giving it an approximate internal volume of 18 cm^3. To fix the sapphire tube in place, it was fitted into a slight recess on the flanges. The flanges were held in place by spacer rods (D = 10 mm). Perfluoroelastomer o-rings (ID = 19 mm, AS 568A-116) were used to seal between the sapphire tube and the flanges. These o-rings were placed into grooves machined into the flanges. A

second set of o-rings (ID = 35 mm, AS 568A-126) were placed around the outer diameter of the sapphire tube at either end, to prevent any movement of the tube within the recesses in the flanges.

The compatibilities of the materials of construction and the o-rings with the components that were to be measured were considered. The compatibilities given by several literature sources are listed in Table 4.7.

Table 4.7. Material compatibilities, with components to be measured, for the construction of the static-analytic and the static-synthetic apparatus. E, excellent; S, satisfactory; M, moderate; P, poor; X, no data.

Material	alkanes	aromatics	acetone	CO_2	R-23	R-116
316 stainless steel	E [a]	E [a]	E [a]	E [a]	S [c]	E
viton	E [a]	M [b]	P [a]	M [b]	E [d]	X [d]
nitrile	M [a]	P [a]	P [a]	P [b]	P [d]	X [d]
perfluoroelastomer	E [b]	E [b]	P [b]	M [b]	E [d]	M [d]
Teflon®	E [a]	E [a]	E [a]	E [b]	S [c]	X [d]

[a] Adinco BV (2015)

[b] Graco Inc. (2013)

[c] Air Liquide (2013)

[d] Mykin Inc. (2015)

The perfluoroelastomer o-rings were determined to be the most suitable for the equipment, despite the moderate compatibility with carbon dioxide and with R-116. Teflon® had a better compatibility with the chemicals that were used, but due to it being a stiff plastic, it was not used for o-rings in the equipment.

Access into the cell for loading, discharging, cleaning and sampling, as well as for the pressure measurements was through passages drilled into the top and bottom flanges. The upper flange contained three 6 mm diameter passages, while the lower flange contained two. On the upper flange, the passages were included for:

- Loading of the cell. A 1/8th inch NPT thread was machined into the flange, and a NPT to compression adaptor was fitted. A short section of 1/8th inch OD 316 SS tubing connected this fitting to a 1/8th inch 316 SS ball valve. The diameter of the passage was tapered to 3 mm where it entered the equilibrium cell.
- Pressure measurement. A similar connection format as the cell loading line was used for this line. However, in the place of the ball valve, a section of 1/16th inch 316 SS tubing connected the cell to the pressure transducer.

- Obtaining samples from the cell through a capillary. The design of this port is discussed below.

On the lower flange, the two passages were for:

- Discharge and cleaning of the cell. This passage was connected to a 1/8th inch 316 SS ball valve in exactly the same manner as the loading cell.
- The rod to compensate for the movement of the capillary, which is discussed below.

In addition, 6 mm diameter ports with depths of 30 mm were also drilled into each flange for housing the temperature probes.

The length of tubing section between the flanges and the valves were kept to a minimum in order to minimise the dead volumes within the cell. A short length of 1/16th inch tubing was used to connect the pressure transducer to the equilibrium cell. Narasigadu (2011) estimated the dead volume of the pressure transducer connection to be as much as 0.9 cm^3, although this appears to be an excessive estimate. To reduce this dead volume, a PTFE filler plug was inserted into the gap inside of the ¼ inch pressure transducer connection nut.

Mixing of the contents of the equilibrium cell was achieved with a Teflon® coated bar magnet within it. This stirrer bar was magnetically coupled to a horseshoe magnet outside of the cell. This magnet was driven by a small DC motor. The degree of agitation provided by the internal stirrer was directly proportional to the speed of the external magnet. This speed was controlled by varying the electrical power delivered to the DC motor.

Temperature and Pressure

The temperature of the equilibrium cell was held constant by submersion in a liquid-filled 304 stainless steel bath with a capacity of 30 litres. The bath had glass viewing ports in the front and back walls, with a light source placed at the back window, enabling the contents of the cell to be monitored through the front window. This was useful, as the cell did not have to be removed from the bath for the positioning of the capillary tip; thus preventing any disturbance of the equilibrium within the cell. The temperatures at which measurements were undertaken in this study allowed the use of either an ethylene glycol-water mixture or pure water as the thermal medium within the bath. The temperature of the solution in the bath was controlled by a Grant Instruments Optima TX150 immersion thermostat and circulator with a stability of ± 0.01 K and a uniformity of ± 0.05 K. A chiller unit with a submersible cold-finger was used to provide cooling when operating close to or below the ambient temperature.

Pt100 probes, which were supplied by WIKA Instruments (model REB 1/10 DIN), were inserted into the ports in each flange to monitor the temperature. These probes were calibrated against a WIKA

Instruments CTH 6500 temperature standard probe. For the temperature, *T*, the gradient across the cell was defined as:

$$T_{grad} = T_{upper} - T_{lower} \quad 4.1$$

where the subscript 'upper' denotes the upper flange, and 'lower' denotes the lower flange.

For the duration of the measurements, it was ensured that the temperature gradient across the cell was smaller than 0.05 K, as this was less than the uncertainty of the temperature measurement of each probe. The uncertainties related to the measurement of the temperature are discussed in section 4.6.1.

A (0 to 25) MPa pressure transducer, from WIKA Instruments (model P-10), was used to measure the pressure within the equilibrium cell. This pressure transducer was calibrated against a (0 – 25) MPa MENSOR CPT 6000 standard pressure transmitter. The atmospheric pressure at the time of the measurement was recorded from the internal barometer measurements of a Mensor CPC 3000 Pneumatic High-Speed Pressure Controller. The uncertainties of the pressure measurements are discussed in section 4.6.2.

The pressure transducer was housed in an aluminium heating block, which was maintained at a constant temperature by heating cartridges controlled by a Shinko ACS-13A Series 1/16 DIN Digital Indicating Controller (Shinko DIC). Feedback to the controller was provided by a Pt100 which was embedded into the heating block. A feature of the P-10 pressure transducer is the temperature compensation that is applied to its output signal. For the measurements conducted in this study, the pressure calibrations and the measurements were completed with the pressure transducer heating block held constant at 313 K. This was simply to prevent errors from being introduced into the pressure measurements due to any rapid fluctuations in the ambient temperature during the measurements. Although these fluctuations should be accounted for by the temperature compensation feature, the heating block was included to add redundancy to the pressure measurements.

To prevent any condensation of vapours from occurring within the pressure transducer line, the line was heat traced with nichrome wire in a glass wool sheath. The temperature of the heat tracing was maintained at between (3 and 5) K above the temperature of the measurements by a Shinko DIC, with feedback being supplied by a Pt100 probe.

The analogue data signals from the temperature probes and the pressure transducer were obtained with an Agilent 34970A data acquisition unit. The analogue data signals were digitised by the data acquisition unit, and thereafter logged on a desktop computer via the I/O serial port.

Composition Analysis and Sampling Technique

The apparatus had the capability of sampling the phases present within the equilibrium cell by means of a capillary, which was opened and closed by a ROLSI™. This capillary could be moved up and down within the cell to sample at different locations. The internal diameter of the capillary was suitable for the sampling of fluids of pressures between (0.7 and 50) MPa. The capillary was sealed with a polyphenylene sulfide (PPS) seat inside of the ROLSI™. A solenoid was used to change the position of this seat to open or close the capillary. The size of the sample that was obtained with the ROLSI™ was dependent upon the time for which it was in the 'open' position. This opening time was controlled by a Crouzet TOP948 electronic timer.

Due to the high pressures inside of the cell, any change in the volume of the cell could have affected the equilibrium conditions within the cell. Were the capillary to be moved, to sample a different phase, for example, the entire equilibrium of the cell would change and the different phases would be measured at varied conditions. A compensation rod of the same outer diameter as the capillary was therefore added to the cell, and its movement was coupled to that of the capillary. With the diameter of the compensation rod being the same as the outer diameter as the capillary, the change in the volume of the cell with any movement of the capillary was considered negligible. The pressure within the cell remained almost constant as the position of the capillary was varied.

To allow the movement of the ROLSI™ capillary within the equilibrium cell, it remained detached from the upper flange. The entry port for the ROLSI™ capillary in the top flange was packed with a Teflon® plug sandwiched between two perfluoroelastomer o-rings (ID = 2.6 mm, AS 568A-103). The cell was sealed about the capillary by compression of this arrangement of seals with the tightening of an external nut. An identical arrangement was used to seal between the compensation rod and the lower flange.

The samples of the fluids, taken from the equilibrium cell were analysed with a Shimadzu GC-2010 gas chromatograph (GC). For these measurements, the GC was equipped with a (3m length, 2.1mm ID) column, which contained a 10 wt. % dimethyl silicone elastomer (SE30) liquid phase on a Chromosorb W-HP 80/100 support. This column separated the samples into their various constituents, and a thermal conductivity detector (TCD) was used to elicit responses from the separated components, thus obtaining a compositional analysis of the samples. The flow route of the carrier gas used for the GC analysis was modified for this equipment, such that from the flow controller, it flowed through the ROLSI™ vaporisation chamber then to the column and detector. This enabled it to transport the vaporised sample from the ROLSI™ to the GC.

The vaporisation chamber, inside of the ROLSI™, was situated above the equilibrium cell with the samples flowing directly out of the capillary into this chamber. The flange upon which the vaporisation chamber was fastened, was heated by a heating cartridge. This was to vaporise the liquid samples and to prevent any possible condensation of vapour samples, due to Joule-Thompson cooling effects (Partington, 1949) which would associate with the pressure drops experienced across the capillary. The temperature of the flange was controlled by a Shinko DIC with feedback via a Pt100 probe. The temperature of the flange was varied between (373 and 453) K, as dictated by the volatility of the system being measured. For systems containing lighter components, the flange temperature could be maintained at lower temperatures, but for systems containing heavier components, for example n-undecane, the flange temperature had to be increased to ensure vaporisation of the sample. The repeatability of the measured compositions of the samples was used to monitor the efficiency of the vaporisation chamber.

To prevent condensation of the vaporised samples in the transfer line between the ROLSI™ and the GC column, this line was heat traced with glass-fibre sheathed nichrome wire and thereafter insulated with Fiberfrax. The temperature of the transfer line was maintained at between (373 and 423) K by a Shinko DIC with feedback from a Pt100 probe. As with the flange, the temperature at which the transfer line was maintained was dependent on the system that was being measured.

4.3.2. Experimental Procedure

Prior to the VLE measurements, the integrity of the perfluoroelastomer seal for withstanding pressures of up to 10 MPa was verified. Nitrogen was loaded into the cell and it was then ensured that the pressure inside the cell remained constant over a period of a number of hours. Once this was verified, the equilibrium cell was cleaned with water and then n-hexane, and thereafter subjected to a vacuum (0.2 kPa absolute) overnight. This was to minimise the possibilities of any impurities remaining within the cell.

Degassing

While the cell was still under vacuum, the less volatile component was loaded and a vacuum was drawn for approximately 10 minutes, while the cell remained at room temperature. The pressure within the cell during this degassing was sufficient to cause some of the liquid to boil, and thus varied from component to component. After this degassing of the first component, a small amount of the second component was added into the cell and then removed by drawing a vacuum. The second component was substantially more volatile and this therefore purged the cell, ensuring that no inert gases remained therein.

After this degassing procedure, the cell was cooled to approximately 275 K, and the required volume of the second component was loaded from the cylinder as a liquid. The differences in temperature between the gas cylinder and the cell created a pressure gradient, allowing faster loading of the component into cell. Degassing of the more volatile component in situ entailed the opening of a valve on the loading line to release some of the vapour phase from the cell, and then allowing it to regenerate from the liquid phase. This process was repeated at least five times, but until such a time as the pressure after the vapour phase regeneration was approximately the same as that before purging, or else until no impurities were revealed upon GC analysis of a sample. This technique was only possible due to the large relative volatilities of the systems that were measured.

EQUILIBRIUM

After the loading and degassing were completed, the cell was submerged into the constant temperature bath which was set to the temperature at which measurements were required. The DC motor controlling the stirring within the cell was then activated, and the phases present within the cell were allowed to equilibrate. Equilibrium was assumed to have occurred when the temperature and pressure within the cell remained constant (within the experimental uncertainties at a minimum) for at least 10 minutes.

GC CALIBRATION

The TCD of the Shimadzu GC-2010 GC was calibrated using a direct injection technique. Known numbers of moles of the various components were injected through the GC and the responses elicited from the TCD were used to produce calibration curves. For gases, a 500 µl gas-tight SGE syringe was used to inject known volumes of the gases at known ambient conditions (temperature and pressure) into the GC. The ambient pressure was recorded from the internal barometer of a Mensor CPC 3000 Pneumatic High-Speed Pressure Controller. The number of moles of the gas that was injected was calculated using the ideal gas equation. This was an acceptable assumption because of the moderate temperature and low pressures at which the gases were injected.

A 1.0 µl SGE liquid syringe was used to inject precision volumes of the liquids into the GC. The molar density of the liquids at the ambient temperature was used to calculate the number of moles that were injected. The ambient temperatures were measured with a calibrated glass thermometer. The calculation of the uncertainties in the GC calibration are given in section 4.6.3.

ROLSI™ SAMPLING

Once equilibrium was attained, the ROLSI™ was first purged by liberating a number of samples of the phase to be analysed in quick succession. The compositions of these samples were not analysed,

despite them passing through the GC. For the analysis, repeatability of the composition analysis was verified by applying the criterion that at least 5 subsequent samples should give mole fractions with a range of less than 0.003. Once this criterion was satisfied, the capillary was then moved until the tip was submerged within the next phase to be sampled and the purging and analysis was repeated. This was repeated until compositions of all of the phases present in the cell were known. Before the composition analyses of a vapour phase, as many as 30 purges were required before the repeatability criterion was satisfied.

The ROLSI™ opening times, as controlled by the electronic timer, varied between two-hundredths of a second and two seconds. The opening time was set such that the sample size was suitable for analysis, and the TCD response was within the calibrated values. In addition to the dependency on the opening time, the sample size was also dependent on a number of additional factors, such as the pressure gradient across the capillary, the phase being sampled and the temperature of the ROLSI™ flange. Thus, the opening times differed depending on the phase that was being sampled.

To protect against fractionation of the samples upon sampling, as was discussed by Kalra et al. (1978), the opening time was varied when checking the repeatability of a sample. Kalra et al. discovered that, for systems with high relative volatilities, flash distillation occurred upon sampling. This was thought to be due to the sudden pressure drop, which allowed a greater proportion of the more volatile component to pass through the orifice, and thus gave poorly representative samples. Varying the ROLSI™ opening times allowed any fractionation to be detected, as the composition should have remained the same with any opening time so long as no fractionation occurred. If fractionation occurred, the proportion of the more volatile component that was sampled would increase with any increases in the opening time.

Once temperature, pressure and composition of all of the phases had been recorded for a specific loading, a new composition was obtained by releasing a portion of the more volatile component from the equilibrium cell. The contents of the cell were then allowed to equilibrate and the next data point was measured. The measurements were conducted in this manner of ‘stepping down’ in composition of the more volatile component, rather than the more common ‘stepping up’ in composition because of the nature of the systems. The addition of gas into the system entailed a lengthy delay before equilibrium was obtained, due to the slow absorption of the excess vapours by the liquid phase. In contrast, the regeneration of the vapour phase after releasing a portion of the vapour phase was fairly rapid. It is probable that an improved stirring mechanism would have improved the rate of absorption of the vapours.

4.4. STATIC-SYNTHETIC APPARATUS

No literature data was available for binary systems involving R-23 or R-116. Therefore, in order to validate the measured data from the static-analytic apparatus, a variable-volume static-synthetic apparatus was used to measure bubble pressure data for the (R-23 or R-116) + hydrocarbon systems. This apparatus was also commissioned and located at the Thermodynamics Research Unit of the University of KwaZulu-Natal.

4.4.1. EQUIPMENT DESCRIPTION

The variable-volume cell of Ngema et al. (2014), designed for gas hydrate measurements was modified for use as a static-synthetic cell for the measurement of bubble pressure data. This variable-volume apparatus had a number of similarities to the static-analytic cell of Narasigadu (2011). The apparatus was capable of measuring bubble point data at temperatures of between (278 and 323) K and at pressures of up to 10 MPa. The modified apparatus is depicted in Figure 4.2 below.

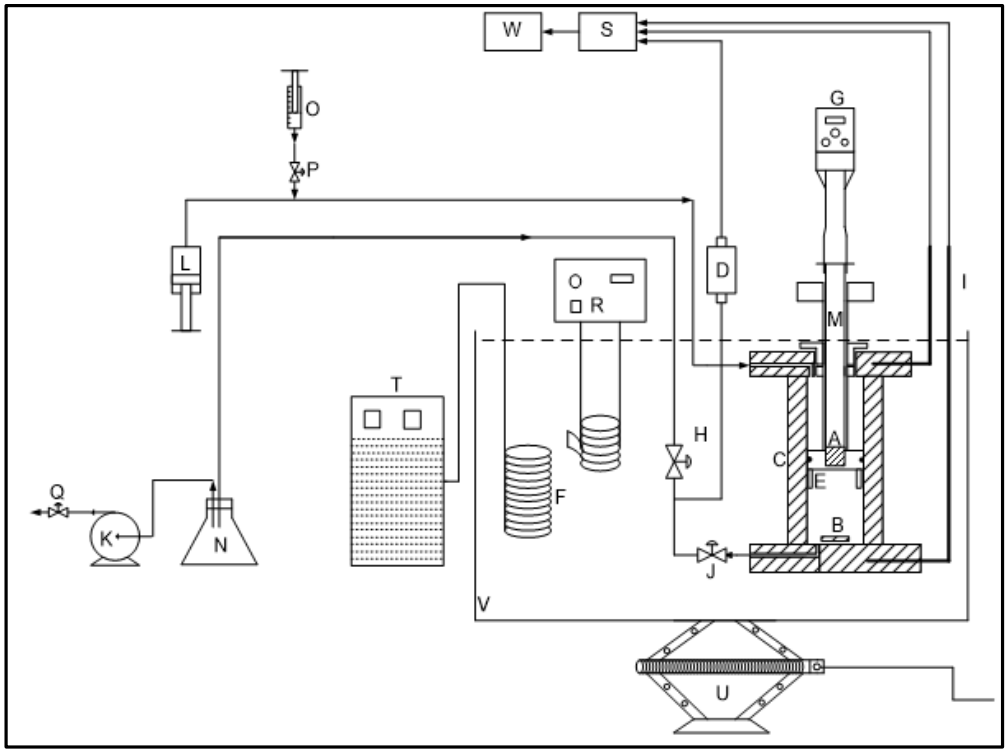

Figure 4.2. Schematic diagram of the modified static-synthetic variable volume apparatus of Ngema et al. (2014): A, rare earth magnet; B, magnetic stirrer bar; C, variable-volume cell; D, WIKA P-10 (0-12) MPa pressure transducer; E, top impeller; F, refrigeration coil; G, Heidolph RZR 2041 overhead stirrer; H, ball valve; I, Pt100 resistance temperature probes; J, cell output (loading or draining and to the pressure transducer); K, vacuum pump; L, WIKA HD 250 hand pump; M, mechanical shaft; N, vacuum flask; O, hydraulic fluid reservoir; P, ball valve; Q, vent to fume hood; R, Grant Instruments Optima TX150 immersion thermostat and circulator; S, Agilent data acquisition unit; T, chiller unit; U, mechanical jack; V, water bath; W, PC.

EQUILIBRIUM CELL

The principal component of the static-synthetic equilibrium cell is the 70 mm long sapphire crystal tube with an inner diameter (ID) of 17.8 mm and an outer diameter (OD) of 35.6 mm, manufactured by Rayotek Scientific. The dimensions of the tube are sufficient to withstand pressures of up to 20 MPa, at temperatures of between (273 and 373) K. The sapphire tube is enclosed on either end by 316 stainless steel flanges. The seal between the sapphire tube and the flanges is created with Viton o-rings (ID = 19 mm, AS 568A-116). The compatibility of the Viton with the hydrocarbons and refrigerants is reviewed in Table 4.7 above in section 4.3.1. As systems containing aromatics were not measured with the variable-volume cell, Viton o-rings could be used for this equipment. Although the performance of Viton o-rings with the refrigerants is only satisfactory, regular replacement of the o-rings was found to be a more viable option than the purchase of the more expensive perfluoroelastomer o-rings.

A port for a piston shaft was machined in the upper flange of the cell. Teflon® packing within this port was used to provide a seal between the shaft and the flange. The piston shaft was constructed from 316 stainless steel, with a composite head attached to the end. This head consisted of a Teflon® cap encircled by two Viton o-rings (ID = 16 mm, thickness = 1.8 mm) which were set into grooves machined into the Teflon® cap. The volume of the cell was determined by the positioning of the piston within the cell but for these measurements the position was not monitored. The position of the piston was altered by changing the pressure of the hydraulic fluid above it. The hydraulic fluid entered above the piston through a passage drilled into the upper flange and its pressure was controlled with a WIKA HD 250 hand pump.

Inside of the piston shaft, a mixing shaft, driven by a Heidolph RZR 2041 overhead stirrer provided mixing capabilities within the cell. At the base of the piston, neodymium magnets (supplied by Supermagnete), attached to the mixing shaft drove the stirrers within the cell by magnetic coupling. The two stirrers within the equilibrium cell; an upper cylindrical PTFE mixer and a lower PTFE paddle mixer; were imbedded with neodymium magnets.

A single passage in the lower flange allowed access into the cell for loading and discharging, as well as to connect the pressure transducer as this reduced the dead volume of the equipment. There remained a substantial dead volume created by the use of a union tee to allow simultaneous connection of the pressure transducer, the feed or discharge line and the vacuum line. The three lines emanating from the union tee were as follows.

- A 1/8th inch line from the union tee to the cell. A ball valve on this line allowed for the removal of the cell for loading.
- A 1/16th inch line from the union tee to the pressure transducer.

- A 1/8th inch line from the union tee to a ball valve, from which a line was connected to a vacuum pump.

The maximum volume of the equilibrium cell, after accounting for the displacements caused by the piston and the mixing system, was approximately 8 cm^3. A 6 mm diameter port with a depth of 30 mm was drilled into each flange for the housing of a Pt100 temperature probe. The probes were held in position by NPT to compression fittings threaded into the ports.

Temperature and Pressure

The two Pt100 temperature probes were supplied by WIKA Instruments (model REB 1/10 DIN). Calibration of these probes was performed against a WIKA Instruments CTH 6500 temperature standard probe. The average of the values measured with the two probes was assumed to be the temperature of the fluid inside of the cell. The temperature gradient within the cell was defined by equation 4.1 in section 4.3. The calculation of the uncertainties in the temperature measurements are discussed in section 4.6.1 below.

The temperature of the variable-volume cell was held constant by submersion in water in a 304 stainless steel bath with a capacity of 40 litres. The temperature of the water within the bath was controlled by a Grant Instruments Optima TX150 immersion thermostat and circulator. Grant Instruments claimed that this temperature controller had a stability of ± 0.01 K and a uniformity of ± 0.05 K. A chiller unit with a submergible cold-finger was used when operating at close to or below the ambient temperature. The 304 stainless steel bath had two glass viewing ports, which allowed a visual search technique to be used in finding the bubble point. The viewing ports allowed the cell to be viewed while being held at a constant temperature.

The pressure within the static-synthetic cell was monitored with a (0 to 12) MPa pressure transducer from WIKA Instruments (model P-10). This pressure transducer was calibrated against a (0 – 25) MPa WIKA Instruments CPT 6000 standard pressure transmitter. The internal barometer of a Mensor CPC 8000 Automated High Pressure Calibrator provided the atmospheric pressure at the time of the measurement. The uncertainties of the pressure measurements are discussed in section 4.6.2.

The pressure transducer for the variable-volume cell was held in an aluminium heating block. The temperature of the heating block was controlled by a Shinko DIC, which regulated the power supplied to two heating cartridges, with feedback from a Pt100 probe. The heating block was maintained at a constant temperature of 313 K for all measurements. This was to prevent the pressure readings from being adversely affected by fluctuations in the ambient air temperature. The portion of the 1/16th inch line from the cell to the pressure transducer that was not submerged in the water bath was wrapped with glass-fibre sheathed nichrome wire heat tracing. The temperature of the heat tracing

was maintained at approximately the same temperature as the water bath by a Shinko DIC. This line contained a liquid at its bubble point during measurements, and therefore could not be heated to temperatures greater than those of the bath without causing boiling to occur within the line. Boiling of the liquid within this line would have led to an unstable pressure profile and would have provided pressures greater than the bubble point pressure.

The analogue data signals from the temperature probes and the pressure transducer were sent to an Agilent 34970A data acquisition unit. After conversion to a digital signal, the data were recorded by the Agilent, and thereafter logged to a desktop computer via one of the I/O ports.

4.4.2. Experimental Procedure

Leak detection was performed for this equipment by pressurisation of the cell with nitrogen to approximately 10 MPa, and thereafter monitoring the pressure and ensuring that this remained constant over several hours. Once the cell had been shown to be free of any leaks at 10 MPa, it was then cleaned with water and thereafter n-hexane, and a vacuum (0.2 kPa absolute) was drawn from the cell for at least 10 hours.

Loading and Degassing

After the degassing of the cell, it was detached from the pressure transducer and vacuum lines with the ball valve between the cell and the union tee closed.

- The mass of the empty cell was measured with a calibrated Ohaus EP Explorer top loading balance (model EP6102).
- The cell was purged using the more volatile component (component 1) a number of times and thereafter filled to approximately atmospheric pressure with this component.
- The mass of the gas used to fill the cell was measured, and thereafter, the desired mass of the less volatile component (component 2) was added into the cell.
- The cell was then cooled with ice water, and component 1 was added into the cell. The cooling of the cell created a temperature gradient (and subsequently a pressure gradient), which expedited the cell loading process.
- After the loading of component 1, the mass of the cell was once again recorded, and from this mass, the mass of component 1 added was calculated.

Component 1 was not degassed for these measurements, as in situ degassing was not possible, because the mass of each component that was added into the cell had to be accurately known. The refrigerants were found to be of a sufficient purity for this stage to be neglected. Degassing of component 2 was performed in a vial prior to loading. For this degassing, a vacuum sufficient to cause the liquid within the vial to begin boiling at ambient temperature, was drawn by a vacuum pump. Care

had to be taken during the loading of the cell with this liquid, to prevent the ingression of air or other inert components. The uncertainties in the determination of the composition for this technique are presented in section 4.6.3.

After loading of the cell, it was reattached to the remainder of the equipment, and a vacuum was drawn within the pressure transmitter line for at least 1 hour. At the same time, the contents of the cell were compressed until only a single liquid phase remained within the cell. After sufficient degassing, the valve to the vacuum line was closed, and the valve between the cell and the pressure transducer was opened, allowing the monophasic liquid to fill the line to the pressure transducer. It was important to keep the contents of the cell as a homogeneous one-phase fluid, as this ensured that the increase in the volume of the cell did not create composition gradients due to flashing of the more volatile component. After this, the cell was submerged into the water bath with the stirrer on, and the contents of the cell were allowed to equilibrate.

VISUAL METHOD

The visual search method for the bubble point pressure entailed observing the behaviour of the fluid within the cell with changes in volume in order to ascertain the isothermal pressure at which the bubble point occurred. In these measurements, the contents of the cell were compressed until such a time as no vapour phase was present. The volume of the cell was then gradually increased until such a time as the first bubble of vapour phase was observed. After allowing the pressure and temperature to stabilise, these values were recorded as the bubble point conditions for the composition present within the cell. This procedure was repeated until at least three repeatable pressure data points were obtained.

With a single cell loading, the bubble point pressure was recorded for a number of different isotherms. In cases where VLLE occurred for the system, the bubble point was taken as the point at which the first bubble of a vapour phase was observed upon reducing the pressure from a pressure at which only the two liquid phases were present in the cell.

4.5. CRITICAL POINT DETERMINATION APPARATUS

With an investigation into alternative solvents for use as supercritical solvents, a logical investigation would be into the mixture critical locus curves of the systems. These mixture critical locus curves would provide useful information as to whether a solution would be a subcritical or SCF at a given set of process conditions. The description of the critical locus curve is also necessary for defining the van Konynenburg and Scott (1980) classification of a mixture. This classification is useful in determining whether any useful phase phenomena will occur with the system. Although several techniques exist for either extrapolation to the critical loci from sub-critical co-existence data or else for calculation of

the critical locus curve from thermodynamic models, experimental data is necessary to verify the curves calculated by using these techniques.

Additionally, mixture critical points are required in order to improve the ability of predictive thermodynamic models to estimate the critical point (Soo et al., 2010). According to Soo et al., it is imperative that more experimental critical point data is reported if the performance of predictive thermodynamic models, such as the SAFT type equations (Chapman et al., 1990), at critical conditions are to be improved.

4.5.1. Literature Survey

Teja and Mendez-Santiago (2005) provided a comprehensive literature survey of the techniques that are currently available for the measurement of mixture critical loci. There are three principal techniques that have been used to determine critical points. These are the static (sealed ampoule) method, the dynamic (flow) method and methods observing the extrema (maxima or minima) of properties of the fluid at the critical point.

Static Method

This method is the oldest method for determination of a critical point as this method describes all of the earliest measurements of critical loci from the 1800s that are described in section 2.1. In this technique, a small mass of a mixture with a known composition is placed into a cell with viewing capabilities, whereafter the cell is sealed and heated. The observance of the disappearance and reappearance of the meniscus (with the associated critical opalescence), as the temperature is increased and decreased, is used to determine the critical temperature and pressure of the mixture.

An important consideration for the static method is the amount of the mixture that is added into the cell. The mass to volume ratio must give a value within 1 to 2 % of the critical density (Teja and Mendez-Santiago, 2005). If this is not done, the fluid within the cell could become a single liquid phase (if the ratio is too low) or a single vapour phase (if the ratio is too high).

Many of the earliest measurements of mixture critical points were for the petroleum industry, and were interested only in the critical temperature of streams consisting of many components (Zeitfuchs, 1926; McKee and Parker, 1928; McKee and Szayna, 1930; Eaton and Porter, 1932). As such, they did not require any external pressure measurement device, and therefore could be sealed completely.

The design of Ambrose and Grant (1957), although it was only used for the measurement of the critical properties of pure components was an improvement, in that it allowed for the measurement of the critical pressure as well as the critical temperature. Mogollon et al. (1982) designed an apparatus for the measurement of the critical temperature of thermally unstable fluids, but this design did not have

capabilities of measuring the critical pressure. A static-synthetic cell was used by Wilson et al. (1995) to measure the critical temperature and pressure of pure components. Difficulties experienced in using static cells for critical point determination include ensuring good mixing of the fluid in the cell, and ensuring good thermal contact between the fluid and the temperature transducer (Teja and Mendez-Santiago, 2005).

Ambrose and Grant (1957) made mention of the disappearance of the meniscus between the vapour and liquid being far more difficult to observe than the reappearance. They suggested the use of the mean of the conditions at which this meniscus disappeared and reappeared as the critical point, rather than using just one or the other.

Dynamic Method

With dynamic cells, the fluid (pure component or mixture) is allowed to flow through the cell, and the critical point is searched for in the same manner as with the static method. This method was first suggested by Roess (1936) to allow the measurement of petroleum fractions without their decomposition. The flow technique was suggested due to the relatively short retention time within the cell, which reduced the degree of decomposition of the fraction. This technique was also used by Teja et al. (1989), where they used the critical opalescence and the disappearance of the meniscus to detect the critical point. After the study of Teja et al., there were a number of similar designs produced, each with a few improvements on the previous equipment. These included the designs of Guilbot et al. (2000a), of Horstmann et al. (2002) and of Soo et al. (2010).

Horstmann et al. make mention of the difficulties that are experienced with dynamic cells when mixtures with large relative volatilities are investigated. A degree of flash distillation occurs within the cell, with the lowest boiling component leaving the cell faster than the other components. This leads to a change in the composition of the fluid. Horstmann et al. suggest increasing the flow rate through the cell to as much as 3 cm^3 per minute (in a 10 cm^3 cell) in order to prevent this from occurring.

Other Methods

Alternative methods for measuring the critical point of a fluid use extrema in the properties of the fluid at the critical point in order to identify the conditions at which they occur. An example is the speed of sound in the fluid, which displays a minimum at the critical point (Chynoweth and Schneider, 1952; Chase et al., 1964; Kozhevnikov et al., 1996). This technique has not always been successful, due to a large attenuation in the speed of sound that is experienced at the critical point. Other properties that have been used to investigate the critical point include the density via NMR (Hayes and Carr, 1977) and the refractive index (Defibaugh et al., 1992; Schmidt and Moldover, 1994)

4.5.2. EQUIPMENT DESCRIPTION

The apparatus for the measurement of the mixture critical loci of binary mixtures presented by Soo et al. (2010), and commisioned at the Centre Thermodynamique des Procédés at Mines ParisTech, was used for this study. This apparatus is depicted in Figure 4.3.

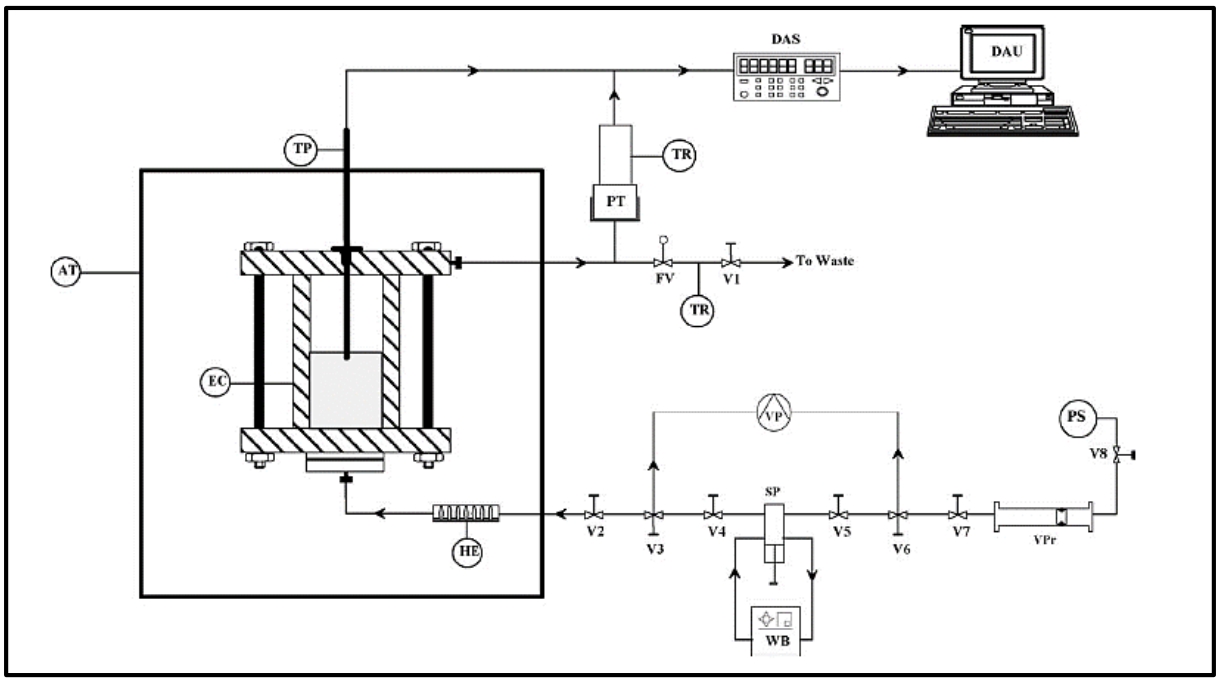

Figure 4.3. The critical point determination apparatus of Soo et al. (2010). AT, air thermostat; DAS, data acquisition system; DAU, data acquisition unit; EC, equilibrium cell; FV, flow control Valve; HE, heat exchanger; PS, pressure source; PT, pressure transducer; SP, syringe pump; TP, platinum resistance temperature probe; TR, temperature regulator; V, valve; VP, vacuum pump; VPr, volumetric press; WB, water bath.

The critical point determination apparatus of Soo et al. is a flow-type (dynamic) apparatus, through which flows a fluid of known composition (synthetic), but by simple modifications can be converted into a static-synthetic apparatus.

DYNAMIC CONFIGURATION

The description of the apparatus when operated as a dynamic-synthetic apparatus is as follows. A fluid of known composition is prepared in the volumetric press, **VPr**, by mixing known masses of the various components. The fluid is then forced into the syringe pump (ISCO 260D), **SP**, by applying pressure to the volumetric press from a pressure source, **PS**. Before this occurs, a vacuum pump, **VP**, is used to pull a vacuum in the syringe pump and the equilibrium cell. The temperature of the syringe pump is controlled by ethanol in a jacket encasing the pump reservoir. This ethanol is circulated from a constant temperature bath, **WB**, ensuring that the desired temperature is maintained.

From the syringe pump, the fluid flows through the heat exchanger, **HE**, into the equilibrium cell, **EC**. The flow rate of the fluid is held constant by the syringe pump. Both the heat exchanger and the equilibrium cell are housed within a France Etuves XU 125 air thermostat, **AT**, which maintains them at the same temperature. The heat exchanger is utilised to ensure that the fluid entering into the equilibrium cell is at the same temperature as the equilibrium cell contents.

The equilibrium cell is constructed of a sapphire tube (12.7 mm ID, 30.03mm length) enclosed on either end with a titanium flange. The internal volume of the cell is approximately 3.8 cm^3. Glass loaded PTFE seals are used to provide a seal between the sapphire tube and the flanges. A light source placed inside of the air thermostat illuminates the contents of the cell sufficiently to allow observation of the critical point. The fluid flowing through the apparatus enters the cell through a port machined into the bottom flange and exits through another in the top flange. A Pt100 temperature probe (Type 5187 A), **TP**, supplied by Tinsley Precision Instruments, is inserted through the top flange and into the cell. The tip of this probe is positioned along the central axis of the tube, 15 mm beyond the centre. Pressure measurement of the cell contents is performed with a Druck PTX 611 pressure transducer, **PT**, with a range of (0 to 16) MPa. The pressure transducer measures the pressure in the exit line from the equilibrium cell. The pressure transducer is maintained at a constant temperature of 373 K by a heating cartridge, which is regulated by a West 6100 PID controller, **TR**. The signals from the temperature probe and the pressure transducer are obtained by an Agilent 34401A data acquisition unit, **DAU**, converted to a digital signal and logged to a PC, **DAS**.

Upon exiting the equilibrium cell, the fluid flowed through a flow control valve, **FV**, supplied by Top Industry, and thereafter a final valve, **V1**, before being vented in a fume hood. These two valves were situated outside of the air thermostat, and therefore required additional temperature regulation. A West 6100 PID controller was used to regulate the temperature of the heat tracing on these valves and the adjoining lines.

STATIC CONFIGURATION

In cases where the relative volatilities of the binary system were too large to prevent distillation of the cell contents, the apparatus had to be operated in a static mode.

With the static mode, the heat exchanger, **HE**, is bypassed. Instead of allowing the fluid to flow through the cell, the cell is filled to approximately half of its volume with the fluid of a known composition, and thereafter the valves on the inlet and outlet lines from the cell, **V1** and **V2**, are closed. The critical point is then searched for in a similar manner as with the dynamic configuration.

4.5.3. Experimental Procedure

With both configurations, the mixture is prepared by the addition of high precision masses of each the required components into the volumetric press. These masses are measured with a Mettler Toledo XP2004S balance (uncertainty of 0.7 mg). The resulting uncertainties in composition are discussed in section 4.6.3. The temperature probe was calibrated between (296.36 and 486.65) K against a 25 Ω Hart Scientific N° 1678 standard, which in turn was calibrated by the Laboratoire National d'Essais (Paris), based on the 1990 International Temperature Scale (ITS 90). The pressure transducer was calibrated, between (0 and 15.5) MPa, against a Druck PACE5000 pressure controller, the calibration of which was verified by Laboratoire National d'Essais (Paris). The uncertainties in the temperature and pressure measurements are provided in section 4.6.1 and section 4.6.2 respectively.

The mixture in the volumetric press is pressurised to approximately 10 MPa, to ensure that only a single phase is present. The valve between the volumetric press and the syringe pump is then opened and the fluid is transferred into the syringe pump, while maintaining the pressure at 10 MPa. The temperature of the syringe pump was maintained at 288 K.

Dynamic Configuration

When operating the apparatus in the dynamic configuration, the flow rate of the fluid was set at a value of between (1 and 10) $cm^3 \cdot min^{-1}$. A vacuum (P < 10 Pa) was drawn in the equilibrium cell and thereafter **V4** was opened. The higher flowrates were used for mixtures of high relative volatility in an attempt to minimise distillation of the components within the equilibrium cell. **V1** was held closed until such time as the liquid level in the equilibrium cell reached the temperature probe. **V1** was then opened, and **FV** was manipulated manually in order to maintain the level of the liquid phase. This manipulation had to occur continuously, especially as the mixture approached the critical point and upon exiting the critical region. Once the liquid level was constant at approximately midway, the temperature of the air thermostat was slowly increased beyond the critical temperature and the conditions at which the meniscus disappeared (and critical opalescence was observed) was noted. The temperature of the air thermostat was thereafter slowly decreased and the conditions at which the meniscus reappeared (with the associated critical opalescence) was again noted. This heating and cooling procedure was repeated until sufficient repeatable points had been recorded.

The rate at which heating and cooling could occur had to be less than 1 K per minute, to prevent larger temperature gradients from occurring within the cell and the heat exchanger.

Static Configuration

With the static configuration, **V1** is not opened, and rather, once the liquid level reaches the midpoint of the cell, the flow rate from the syringe pump is set to zero, and **V4** is closed. Thereafter, a similar

technique is utilised to determine the critical point. The most important difference in the technique being the rate at which the air thermostat is allowed to heat and cool. As there is no mixing within the cell without the flow of the fluid through it, the maximum rate of temperature change that was allowed was reduced to 0.3 K per minute. This was to ensure that no sizeable temperature gradients occurred within the cell. The critical point was taken as the average of the critical points measured for at least five different refills of the contents of the cell.

4.6. Uncertainty Estimation

The National Institute of Standards and Technology (NIST) approach, described by Taylor and Kuyatt (1994) and Taylor et al. (2007), were used to estimate the uncertainties for these measurements. The NIST approach attempts to minimise the selectivity of uncertainty estimation. However, the estimation of the uncertainties of certain facets of a measurement remain dependent upon estimations or previous experiences. The uncertainties reported for this work are reported as combined expanded uncertainties with a coverage factor (*k*) equal to 2. The combined expanded uncertainties were calculated from the combined standard uncertainties by equation 4.2.

$$U_i(\theta) = k\, u(\theta) \tag{4.2}$$

The NIST approach defines two types of uncertainties. These are denoted type A and type B. Type A uncertainties are calculated as the standard uncertainty of a number of random measurements, whereas type B estimates are determined without the availability of sampled data (Castrup, 2004). The type A estimates have a defined distribution about the mean value. With Type B uncertainties, the true value of the data has an equal likelihood of occurring anywhere within the range given by the uncertainty estimate. The calculation of type A and a type B uncertainties are given by equations 4.3 and 4.4 respectively.

$$u_i(\theta) = \frac{\sigma}{\sqrt{N_{rp}}} \tag{4.3}$$

where σ is the standard deviation of the data set and N_{rp} is the number of items in the data set.

$$u_i(\theta) = \frac{b}{\sqrt{3}} \tag{4.4}$$

where *b* is the width of half of the uncertainty interval.

The estimation of the uncertainties for phase equilibrium measurements, and in particular VLE was discussed by Soo (2011). The law of propagation of uncertainties was used to obtain equations for the calculation of the combined uncertainties in temperature, pressure and composition. These equations are presented in the subsequent sections.

4.6.1. Temperature Uncertainties

Equation 4.5 is used to determine the combined standard temperature uncertainty. It is a simple application of the law of the propagation of errors

$$u_c(T) = \pm\sqrt{u_{corr}(T)^2 + u_{std}(T)^2 + u_{grad}(T)^2 + u_{rep}(T)^2 + u_{\Delta}(T)^2} \quad 4.5$$

The various terms within this equation for the various apparatus that were used are provided below. For those uncertainties that are variable, the maximum value was stated. Only those uncertainties that were applicable to the measurements with each apparatus were included in Tables 4.8 to 4.10.

Static-Analytic Equipment

For the static-analytic apparatus, the estimated individual uncertainties and their types are presented in Table 4.8.

Table 4.8. Individual uncertainties, *u*(*T*), for temperature measurement with the static-analytic apparatus

Uncertainty	Type	Symbol	*u*(*T*) / K
Temperature Standard Probe Standard Deviation	B	$u_{std}(T)$	0.012 [a]
Correlation Standard Deviation	B	$u_{corr}(T)$	0.034 [b]
Temperature Gradient	B	$u_{grad}(T)$	< 0.05
Measurement Repeatability	A	$u_{rep}(T)$	< 0.02
Variation in temperature between sampling of vapour and liquid phases	B	$u_{\Delta}(T)$.	< 0.05

[a] According to the calibration certificate supplied by WIKA Instruments.
[b] Calibrated at temperatures of between (268 and 328) K.

Variable-Volume Synthetic Apparatus

The uncertainties for the variable-volume cell are given in Table 4.9.

.

Table 4.9. Individual uncertainties, *u*(*T*), for temperature measurement with the variable-volume apparatus

Uncertainty	Type	Symbol	*u*(*T*) / K
Temperature Standard Probe Standard Deviation	B	$u_{std}(T)$	0.012 [a]
Correlation Standard Deviation	B	$u_{corr}(T)$	0.008 [b]
Temperature Gradient	B	$u_{grad}(T)$	< 0.05
Measurement Repeatability	A	$u_{rep}(T)$	< 0.02

[a] According to the calibration certificate provided by WIKA Instruments.
[b] Calibrated at temperatures of between (283 and 323) K.

CRITICAL POINT DETERMINATION APPARATUS

Table 4.10. Individual uncertainties, *u*(*T*), for temperature measurement with the critical point determination apparatus

Uncertainty	Type	Symbol	*u*(*T*) / K
Temperature Standard Probe Standard Deviation	B	$u_{std}(T)$	0.039 [a]
Correlation Standard Deviation	B	$u_{corr}(T)$	0.02 [b]
Measurement Repeatability	A	$u_{rep}(T)$	< 0.5

[a] According to the calibration certificate provided by Laboratoire National d'Essais.
[b] Calibrated at temperatures of between (296.36 and 486.65) K.

4.6.2. PRESSURE UNCERTAINTIES

The equation for combining the various uncertainties involved in the measurement of the pressure within the equilibrium cells is given by equation 4.6.

$$u_c(P) = \pm\sqrt{u_{corr}(P)^2 + u_{std}(P)^2 + u_{atm}(P)^2 + u_{rep}(P)^2 + u_{\Delta}(P)^2} \quad 4.6$$

For the calculation of the pressure uncertainties, the values used for the various terms with each of the three apparatus are listed in Tables 4.11 to 4.13 below. Any terms for which an uncertainty was not provided was not applicable to the apparatus, and could therefore be assumed to be equal to zero. With all of the uncertainties that varied for each data point, the maximum value was provided.

STATIC-ANALYTIC EQUIPMENT

The individual uncertainties used to calculate the combined uncertainties of the pressure measurements from the static-analytic apparatus are listed in Table 4.11.

.

Table 4.11. Individual uncertainties, *u*(*P*), for pressure measurement with the static-analytic apparatus

Uncertainty	Type	Symbol	*u*(*P*) / MPa
Standard Pressure Transmitter Standard Deviation	B	$u_{std}(P)$	3.6 x 10^{-3} [a]
Correlation Standard Deviation	B	$u_{corr}(P)$	3.0 x 10^{-4} [b]
Atmospheric Pressure Uncertainty	B	$u_{atm}(P)$	6.8 x 10^{-6} [c]
Repeatability of the measurements	A	$u_{rep}(P)$	< 0.002
Variation of the pressure between sampling of liquid and vapour phases	B	$u_{\Delta}(P)$	< 0.005

[a] As provided on the calibration certificate from WIKA Instruments.
[b] Calibrated at pressures of between (0 and 8.5) MPa.
[c] As provided by Mensor.

VARIABLE-VOLUME SYNTHETIC APPARATUS

The constituent uncertainties in pressure for the variable-volume cell are tabulated in Table 4.12.

Table 4.12. Individual uncertainties, *u*(*P*), for pressure measurement on the variable-volume apparatus

Uncertainty	Type	Symbol	*u*(*P*) / MPa
Standard Pressure Transmitter Standard Deviation	B	$u_{std}(P)$	3.6 x 10^{-3} [a]
Correlation Standard Deviation	B	$u_{corr}(P)$	8.3 x 10^{-4} [b]
Atmospheric Pressure Uncertainty	B	$u_{atm}(P)$	3.4 x 10^{-6} [c]
Repeatability of the measurements	A	$u_{rep}(P)$	< 0.002

[a] As provided on the calibration certificate from WIKA Instruments.
[b] Calibrated at pressures of between (0 and 10.5) MPa.
[c] As provided by Mensor.

CRITICAL POINT DETERMINATION APPARATUS

For the critical point determination apparatus, the constituent uncertainties in the measurement of pressure are given in Table 4.13.

Table 4.13. Individual uncertainties, *u*(*P*), for pressure measurement with the critical point determination apparatus

Uncertainty	Type	Symbol	*u*(*P*) / MPa
Standard Pressure Transmitter Standard Deviation	B	$u_{std}(P)$	1.0 x 10^{-3} [a]
Correlation Standard Deviation	B	$u_{corr}(P)$	3.9 x 10^{-4} [b]
Repeatability of the measurements	A	$u_{rep}(P)$	< 0.1

[a] As provided on the calibration certificate from Laboratoire National d'Essais (Paris).
[b] Calibrated at pressures of between (0 and 15.5) MPa.

4.6.3. UNCERTAINTIES IN COMPOSITION

For each of the apparatus, the compositions were determined differently. Therefore, different calculation procedures were required for the estimation of the uncertainties in composition for each of the apparatus.

STATIC-ANALYTIC EQUIPMENT

The calibration technique for composition in the static-analytic cell rendered uncertainty in the composition dependent on a number of variables, including temperature, pressure, volume and density. The variables upon which the uncertainties were dependent are tabulated in Table 4.14. The uncertainty of the composition, $u_c(x_i)$, is dependent upon the uncertainty derived from the repeatability of the measurements, $u_{rep}(x_i)$, and the uncertainty derived from the calibration of the TCD, $u_{calib}(x_i)$.

$$u_c(x_i) = \pm\sqrt{u_{rep}(x_i)^2 + u_{calib}(x_i)^2} \quad 4.7$$

where $u_{calib}(x_i)$ is a function of the uncertainty in the composition of each component, and is dependent upon the uncertainties in the number of moles of each component calculated from the calibration curve.

$$u_{calib}(x_i) = \pm\sqrt{\left[\frac{n_j}{n_i + n_j}u(n_i)\right]^2 + \left[\frac{n_i}{n_i + n_j}u(n_j)\right]^2} \quad 4.8$$

where n_i denotes the number of moles of component *i*. Equation 4.8 applies only for binary systems.

The uncertainty in the number of moles of component *i* is calculated by equation 4.9 for gases and by equation 4.10 for liquids.

$$u(n_i) = \pm\sqrt{u_{corr}(n_i)^2 + u_{ig}(n_i)^2} \quad 4.9$$

$$u(n_i) = \pm\sqrt{u_{corr}(n_i)^2 + u_l(n_i)^2} \quad 4.10$$

$u_{ig}(n_i)$ and $u_\rho(n_i)$ are calculated using the law of propagation of errors by equations 4.11 and 4.12 respectively.

$$u_{ig}(n_i) = n_i\sqrt{\left(\frac{u(P)}{P}\right)^2 + \left(\frac{u(V_g)}{V}\right)^2 + \left(\frac{u(T)}{T}\right)^2} \quad 4.11$$

$$u_\rho(n_i) = n_i\sqrt{\left(\frac{u(\rho)}{\rho}\right)^2 + \left(\frac{u(V_l)}{V}\right)^2} \quad 4.12$$

Table 4.14. Constituent uncertainties for determining the uncertainty in the compositions measured with the static-analytic apparatus

Uncertainty	σ or b	Type	Symbol	$u(n_i)$
Atmospheric Pressure Uncertainty	0.01 bar	B	$u(P)$	0.006 [a]
Volume Uncertainty (SGE gas syringe)	0.01	B	$u(V_g)$	0.006 [b]
Volume Uncertainty (SGE liquid syringe)	0.02	B	$u(V_l)$	0.012 [b]
Temperature Uncertainty	1 K	B	$u(T)$	0.002 [c]
Density Uncertainty	0.007 kg.m^{-3}	B	$u(\rho)$	6 x 10^{-6} [d]
Anton Paar Density Meter Accuracy	0.005 kg.m^{-3}	B	$u_{meas}(\rho)$	
Density Measurement Repeatability	0.01 kg.m^{-3}	A	$u_{rep}(\rho)$	

[a] As stated by Mensor.

[b] As stated by SGE.

[c] Estimated

[d] $u(\rho) = \sqrt{u_{meas}(\rho)^2 + u_{rep}(\rho)^2}$

VARIABLE-VOLUME SYNTHETIC APPARATUS

The combined standard uncertainty in the composition of the fluid within the variable-volume cell was dependent on only the uncertainty of the Ohaus balance and the impurities present in the binary mixture. The combined standard uncertainty for the composition of a binary mixture in the variable-volume cell was calculated by equation 4.13 (Coquelet and Richon, 2007). The individual uncertainties are presented in Table 4.15.

$$u_c(x_i) = x_i x_j \sqrt{\left(\frac{\frac{u(m)}{M_i}}{n_i}\right)^2 + \left(\frac{\frac{u(m)}{m_j}}{n_j}\right)^2 + \left(u_p(x_i)\right)^2 + \left(u_p(x_j)\right)^2} \qquad 4.13$$

where M_i is the molecular mass of component i, n_i is the number of moles of component i, and

$$u(m) = \sqrt{\left(u_{bal}(m)\right)^2 + \left(u_{rep}(m)\right)^2} \qquad 4.14$$

The impurity reported in Table 4.15 was the maximum impurity used in these measurements.

Table 4.15. Constituent uncertainties for the estimation of the overall uncertainty in the composition reported for the variable-volume apparatus

Uncertainty	Type	Symbol	*u*(*m*) / g or *u(x)*
Fraction of impurities in component [a]	B	$u_p(x_i)$	0.01
Uncertainty in balance calibration [b]	B	$u_{bal}(m)$	0.07 [a]
Repeatability [b]	A	$u_{rep}(m)$	0.03

[a] mass fraction

[b] mass

CRITICAL POINT DETERMINATION APPARATUS

The mixture used in the critical point determination apparatus was synthesised in the same manner as the static-synthetic apparatus, and therefore the identical equations were used. The Mettler-Toledo XP2004S mass comparator had a higher precision than the Ohaus balance, thus reducing the uncertainties in the mass.

Table 4.16. Constituent uncertainties for the estimation of the overall uncertainty in the compositions reported for the critical determination apparatus

Uncertainty	Type	Symbol	*u*(*m*) / mg or *u(x)*
Fraction of impurities in component [a]	B	$u_p(x_i)$	0.01
Uncertainty in balance calibration [b, c]	B	$u_{bal}(m)$	0.7
Repeatability [c]	A	$u_{rep}(m)$	0.5

[a] mass fraction

[b] Calibration performed by Mettler Toledo

[c] mass

5. SUPERCRITICAL FLUID EXTRACTION PROCESSES

At present, there are a fair number of active separation processes in which SCFs are used to extract a product from a feed stream. Many of these applications are in the food and pharmaceuticals industries and are operated as batch processes. The accurate design of an SCFE process, as with the design of any chemical process, is important, not only to ensure the construction of an economically viable process, but also to ensure the safe operation of the process.

In order to design a safe and economically viable SCFE process, thermodynamic models, fitted to high precision phase equilibrium data, are required. Once the parameters for the thermodynamic models have been obtained, the process can be simulated using a process engineering simulation package, such as ASPEN Plus. This allows the process to be tuned to give the optimum operating conditions.

5.1. INDUSTRIAL CONDITIONS

The major units of a typical SCFE plant include the extraction vessels, the separation vessels, solvent storage reservoirs, pumps or compressors and heat exchangers (Brunner, 1998). An example of a process flowsheet for a separation using a SCF is given in Figure 5.1.

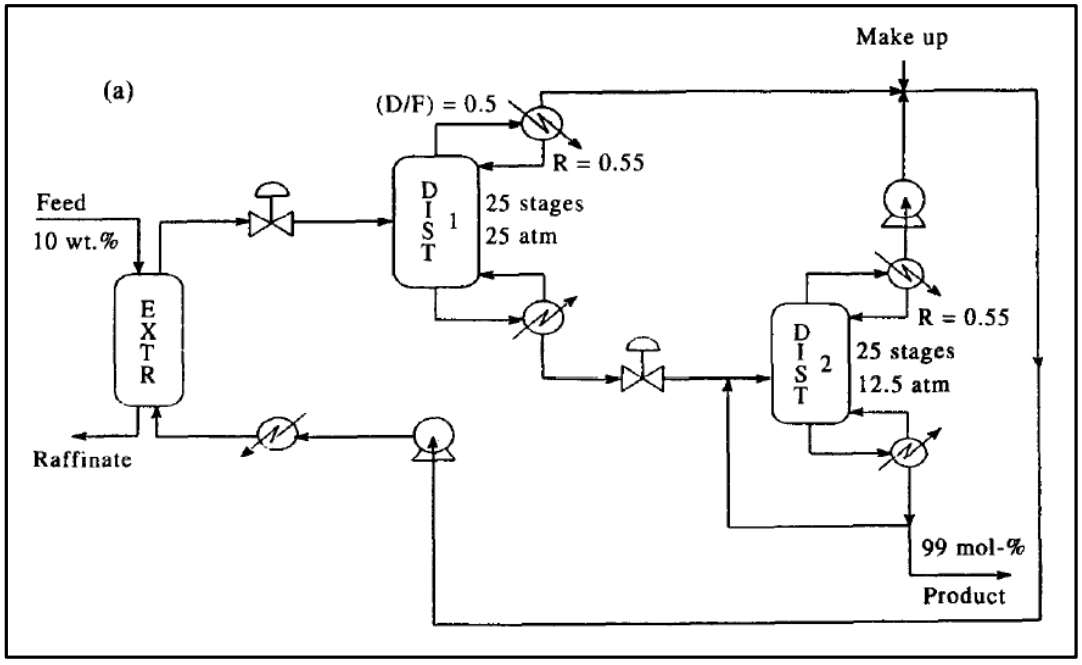

Figure 5.1. Process flowsheet given by Gani et al. (1997) for the separation of a water-ethanol system using supercritical propane.

The process depicted in Figure 5.1 is for the separation of a water-ethanol system, using supercritical propane. The process makes use of fractionation of the extract to obtain products with high purities. Because the feed and the raffinate are liquids, the process can operate continuously, as the liquid

raffinate at the bottom of the extraction vessel allows the pressure to be maintained in the vessel. When the feed or the raffinate is a solid material, the process must be operated batch-wise, as there is no means of maintaining the pressure within the vessel.

Many SCFE processes are operated in batch mode because of this difficulty in maintaining the pressure within the vessel while removing solids. A process was, however, patented by Rice and Singh (1990), in which the extraction of a solid raffinate stream could be performed continuously. This process used a system consisting of a section of piping with a number of valves, which allowed loading at atmospheric pressures, and thereafter pressurisation to the extraction pressure. No mention was made of the loss of solvent due to the frequent de-pressurisation of the solids feed section. A suggested alternative was the use of a screw-type extruder, which would inject the solids into a flowing solvent. The process of Rice and Singh used a cyclone to remove the spent solids from the process, although how this mechanism prevented a loss of solvent (and pressure) was not defined.

Sihvonen et al. (1999) gave a description of a simplified semi-batch SCFE system. An extraction cycle begins with the raw materials being charged into the extraction vessel, which is equipped with temperature and pressure control. The vessel is then pressurised to the operational pressure with the supercritical solvent. The solvent is pressurised by liquid pumps at temperatures at which the solvent is a liquid, and is thereafter heated to create a SCF. From the extraction vessel, the solvent, with the solubilised products, is transferred to the separation vessel, where either the pressure is reduced, or in some cases the temperature is varied. By doing this, the solubility of the product in the solvent is decreased and the product can be separated from the solvent. The solvent is recycled from this vessel to a storage vessel via a series of heat exchangers and pumps. The flow of solvent is continued until such a time as the extraction is completed. The product is recovered from the bottom of the separation vessel as a liquid or a solid, and the spent solids are removed from the extraction vessel after de-pressurisation.

When the feedstock is a liquid, there is no reason as to why the process cannot be operated in a continuous mode, with the raw feed and the solvent both being pumped into a vessel operating with a counter-current flow in a ‘gas extraction’, as was suggested by Brunner (1998).

As of 1998, there were approximately 125 industrial SCFE vessels with volumes of over 0.1 m^3 (Gehrig, 1998). This number has increased in the years since this information was published (Knez et al., 2013). In the USA, a number of large extraction vessels were constructed for the extraction of components from coffee, hops and tobacco. The largest of these vessels had a volume of over 40 m^3. Some of the current extractions processes, alongside the process conditions (pressure and temperature) used, are listed in Table 5.1.

Table 5.1. Applications of SCFE WITH Typical Process Conditions

Application	Pressures	Temperatures
Extraction of seed oils using SC CO_2 (Stahl et al., 1980)	9 to 70 MPa. Higher pressures produced better yields.	313.15 K (40° C)
Extraction of lignin from kraft black liquor with SC CO_2 (Avedesian, 1987)	Above the critical pressure of CO_2 (7.38 MPa).	Above the critical temperature of CO_2 (304.21 K), up to 323.15 K.
Continuous extraction of soybean oil using SC CO_2 (Rice and Singh, 1990)	Pressures up to 82.74 MPa.	Temperatures from (255.37 to 366) K successfully utilised. SC or liquid solvent used.
Extraction of grape seed oil using SC CO_2 (Molero Gómez et al., 1996)	Higher pressures yielded more oil, but the optimal operating pressure was found to be 20 MPa.	Of the temperatures mentioned (283.15, 313.15 and 333.15 K), the best yield was obtained at 313.15 K.
Selective extraction of lipids from solid (lipid and carotenoid containing) substrate using SC CO_2 (Schonemann et al., 2008)	Pressures of between (10.3 and 20.7) MPa preferred	Temperatures of between (308.15 and 353.15) K
Extraction of oil from kenaf seeds using SC CO_2 (Ismail et al., 2014)	Pressures of between (20 and 60) MPa. Different pressures allowed for different products and yields.	Temperature varied from (313.15 to 353.15) K

The name of supercritical fluid extraction is partially misleading, as it infers that the fluid inside of the extraction vessel is always in the supercritical state. Although this may be true in some cases, especially when the extraction of components from solid matrices is being performed, in other cases, especially where some solutes are being stripped from a liquid, this is not the case. The dynamic nature of SCFE is the major contributor to this 'grey' area. The fresh fluid that is entering the extraction vessel is in all likelihood in its supercritical state (above the critical temperature and pressure of the solvent), but as the solutes diffuse into the solvent-rich phase, the conditions of the critical locus vary. This change is usually in the form of an increase in both the critical temperature and pressure. As the critical locus moves, the solvent-rich fluid could exit the vessel in a sub-critical state. This departure of the solvent rich stream from the supercritical state can result in the solvent being present as either a liquid, or a vapour, or as both phases.

Additionally, depending upon the degree to which the fluid in the extraction vessel is mixed, pockets within the vessel could be in the supercritical state whilst others have become sub-critical fluids.

5.2. Process Design

With the availability of cheap imported equipment, many supercritical fluid extraction processes are treated as 'one size fits all' pseudo-design. In this type of design, the process is tailored to fit the equipment, rather than the equipment being selected and designed, based upon the requirements of the process. This pseudo-design trend has been exacerbated by incomplete phase equilibrium data being available, which has resulted in the optimisation of the design being performed by varying the process temperatures and pressures and observing the solubilities and yields at the different conditions.

The pseudo-design trend has drawn concern within both the academic and the industrial communities, as it is believed that such a trend inhibits improvements in supercritical fluid extraction technologies (Beckman, 2004). Without small incremental improvements in the technology from one design to the next, it is unlikely that any radical improvements will be achieved over time. For the complete design of equipment for a SCF process, it is imperative that high precision thermodynamic modelling be available for the binary mixtures that will be present in the solution. The transport properties of the solution, such as densities, diffusivities and viscosities are also very important in order to obtain an accurate design of the process. In general, many of the difficulties encountered in a SCFE process, are due to a lack of understanding of the fundamentals of the process and the systems involved. These fundamentals include the molecular structures and intermolecular interactions. If these fundamentals were better understood, improvements in the process design would likely be achieved.

5.2.1. Extraction Type

In the detailed the design of a counter-current SCFE column by Brunner (1998), it was proposed that the 'gas extraction' technique would enable the separation and extraction of components that have a low volatility and very similar properties, beyond those possible with more conventional techniques such as distillation or liquid-liquid extraction. The temperature of this gas extraction would be decided by the critical temperature of the solvent, rather than by the boiling temperature of the feed. The work of Brunner provides guidelines as to the design of such a 'gas extraction' process, from the initial estimation of the column design, through laboratory separation experiments and to computer process simulations.

A typical SCFE column is best modelled with an extraction column rather than with a distillation column. Many extraction columns can be modelled as a mixer-settler, single-stage vessel. In contrast,

the separation stage is usually modelled as a flash distillation at sub-critical conditions (Gani et al., 1997). If multiple flash vessels are used, this is equivalent to a gas stripping column. The thermodynamic model to be used for the simulation therefore requires an ability to predict the binary LLE in addition to the binary VLE.

5.2.2. Economics

Perrut (2000) reviewed some of the economic aspects behind the construction and operation of a SCFE plant. He established that the cost of a SCF process increased proportionally to the square root of the capacity of the process. Larger process plants, although possibly being more economically feasible, come with their own sets of challenges, most of which are in respect to safety, operation and logistics.

5.3. Process Considerations

Beckman (2004) made mention of a number of different considerations that should be made when performing the design of a SCF extraction process using a process simulation programme, such as Aspen Plus. The purposes of these considerations, which were discussed below are to ensure the economic operation of the process.

5.3.1. Solvent to Solute Ratio

The amount of the supercritical solvent should be minimised, as this reduces the volumes that are flowing through the process (Beckman, 2004). This can be performed by choosing conditions such that the solubility of the solutes is high. It was suggested that these increased solubilities could be obtained by using co-solvents.

5.3.2. Pressure

It is intuitively less energy intensive to operate a process at lower pressures, rather than at higher pressures. There are also safety considerations and increased equipment costs that need be considered with increased pressures. For a typical SCFE process, it is therefore more economical to operate at lower pressures (Beckman, 2004). The suggestion, made by Beckmann, was to make use of a co-solvent, to lower the operating pressure of the separation. Another suggestion was to operate in the subcritical region with liquid-liquid extraction. This, however, negates any advantages to be gained from the improved diffusivities of SCF, while at the same time increasing utility costs due to additional cooling requirements. Alternatives to making these adjustments would be to use a different solvent that exhibits lowered critical pressures. Gani et al. (1997) simulated an extraction at pressures that were significantly higher than the critical pressure of their solvent (n-propane). They found that, at these elevated pressures; pressure fluctuations had no significant effect on the

performance of the extraction. This is not the case at the critical point, where a small pressure fluctuation could have a large effect on the extraction performance.

5.3.3. Temperature

The density of a supercritical fluid is highly adjustable with changes in temperature and pressure in the vicinity of the critical point (Gani et al., 1997; Sihvonen et al., 1999). However, at temperatures further from the critical point, the changes in density that occur with temperature fluctuations are markedly lower. It is therefore important to operate at temperatures near to the critical temperature in order to use these density fluctuations advantageously.

Due to the sensitivity of the separation to even small temperature fluctuations at temperatures close to the critical point, it is imperative that high precision temperature control be provided for a SCF extraction unit. The design of Gani et al. (1997) controlled the extract stream temperature by manipulating the solvent input temperature, and the raffinate stream temperature by means of the feed temperature.

5.3.4. Solvent Recovery

Although the best technique for the recovery of the product from the solvent is to reduce the pressure to near to atmospheric pressure, this is not the optimal solvent recovery technique with regards to the economics of the process (Beckman, 2004). By using this technique, and reducing the mixture to pressures as low as one atmosphere, large amounts of energy would be required to recompress the solvent. This in turn would translate into high energy costs, as well as requiring larger vessels to contain large volumes of the low pressure gas. It is likely to be more economically feasible to reduce the pressure by a relatively small amount, and to recover most, but not all of the solute. The biggest disadvantage to this would be that the solvent would return to the extraction vessel after compression with a small amount of the solute remaining in solution.

There are two main reasons for a loss of solvent (Perrut, 2000). The first occurs in cases where solid feedstocks are used, as the extractor must be de-pressurised prior to the cleaning and replenishment of the feedstock. Most of the solvent present in the extractor can be recycled through the separation vessels, but a certain portion must be vented. The second case of a loss of solvent is due to the solvent being soluble to some extent in the product. As the product is recovered from the process, a portion of the solvent which is soluble in the product is lost from the process. To overcome this, the conditions within the separation and recovery vessel should be tailored to ensure that this loss is minimised.

5.4. SAFETY CONSIDERATIONS

As supercritical processes must operate at elevated pressures, safety is of greatest importance. Careful attention must be paid to each and every aspect, from the design specifications of the equipment to the operating procedures for the process. Due to the large numbers of incidents involving process plants, many of which have led to releases of toxic and/or flammable materials into the atmosphere, greater emphasis has, of late, been placed upon the inherently safe design of process plants (Soares and Coelho, 2012). The impact of an incident is directly related to the chemicals involved, their quantities and the process conditions. Duarte and Duarte (2009) list four classes of hazards that could occur when working with chemicals, and in particular, SCF. These are the chemical hazards, the mechanical hazards, the thermodynamic hazards, and the biological hazards.

Chemical hazards refer to the toxicity of the chemicals involved, as well as the quantities thereof. The solvent embodies the largest portion of the chemical inventory, and as such, it is most important to consider the safety with respect to the use of the solvent. Consideration was given to these factors in section 3.1. The toxicity of the feedstock and products must also be considered in the analysis of the process safety.

SCFE is usually operated at near-ambient conditions, and therefore, the only concerns with process safety are due to the large pressures that are utilised. Both mechanical and thermodynamic hazards are embroiled within the hazards due to high pressures. Any damage to the pressure vessels (mechanical hazard) in a SCFE plant due to over-pressurisation (thermodynamic hazard) could lead to extensive damage of the surrounding infrastructure (Soares and Coelho, 2012). This could be worsened by the occurrence of a 'boiling liquid expanding vapour explosion' (BLEVE), due to the rapid de-pressurisation of the fluids subsequent to the failure of a containment vessel.

The mechanical hazards for the process equipment can be overcome by stringently following the design standards for pressure vessels and ensuring that the required tests and inspections are performed on the equipment (Duarte and Duarte, 2009). In cases where the operation occurs in batch mode, an additional consideration that should be taken into account is the number of pressurisation and de-pressurisation cycles to which the vessel is exposed. According to Duarte and Duarte (2009), a typical vessel life duration is typically in the region of 20 000 cycles.

Above and beyond these design standards, tests and inspections, an additional safety level that should be utilised is the installation of overpressure protection. Means of over-pressurisation protection for the vessels could be in the form of safety relief valves and rupture disks. Generally these pressure relief systems discharge the released fluids directly into the atmosphere. In cases where the solvent is toxic or flammable, this cannot be allowed and additional treatment steps, such as flaring, scrubbing

or a means of containment must be allowed for. If the solvent is of high value, there will be additional incentive for the containment of the released gases, but regardless, a treatment technique must be provided. The biological hazards class referred to by Duarte and Duarte (2009) concerns the effect that any released chemical would have on biological systems. Even carbon dioxide, R-23 and R-116, which are considered to be non-toxic, exhibit biological hazards, as they are asphyxiants, and the accumulation of large volumes of these gases could be potentially fatal. Care must therefore be taken to ensure that accumulation of gases does not occur.

An additional thermodynamic hazard that should be considered is the rapid cooling due to the Joule-Thompson effect when a pressure drop is applied in order to separate the solvent from the products (Duarte and Duarte, 2009). This cooling of the fluid could cause solidification of either the solvent or the solutes, which could plug the process equipment. The design of the sections of a SCFE process where pressure drops occur should be carefully considered. The pressure relief systems must also take this phenomenon into account, as plugging could cause failure of these devices. A possible technique for overcoming the formation of solid plugs is to heat the sections where this is prevalent, or likely to occur (Böhm et al., 1989; York et al., 2004). It would, however, be more advantageous to simply avoid the conditions at which the Joule-Thompson cooling effect occurs.

In addition to the use of design techniques to create an inherently safer process plant, an understanding and awareness of the hazards of the plant, and the procedures in place to minimise these risks, on the part of the operators is also of vital importance.

5.5. ASPEN SIMULATION

Aspen Plus V8.4 (Aspen Technology, 2012) is a process simulation package that can be used to simulate the operation of a process plant. The program utilises models for the properties of the pure and binary components present in the process streams in order to provide a fairly accurate picture of the real operation of the process being simulated. Because the simulation relies on models in performing the necessary calculations, these models must describe the actual system properties to a high degree of accuracy. The models are most often, therefore, fitted to experimental data. For a basic simulation that assumes that the transport properties of the fluid can be neglected, the most important models are those describing the phase behaviour of the binary mixtures of the constituent components. The parameters for many of the more common models, for a large number of binary systems are available within Aspen Plus V8.4. Other parameters must be provided by the user from the fitting of parameters for the thermodynamic models to measured VLE data.

6. RESULTS AND DISCUSSION

The principal aim of this study was to determine whether R-23 or R-116 could replace CO_2 as supercritical solvents in the petroleum industry for the treatment of streams which conventional separation techniques are not capable of treating. The R-23 and R-116 were chosen based upon the screening process explained in Chapter 3. Since little data was available for these components with the selected hydrocarbon solutes, phase equilibrium data were required in order to further the investigation. VLE and VLLE data were measured for the binary systems consisting of combinations of the solvents with the solutes (hydrocarbons or water). In addition, the VLE of some ternary systems were also measured, to provide comparisons of the separations of simplified systems. The data sets for the binary systems were used to regress parameters for thermodynamic models. The ability of these thermodynamic models to describe the binary systems enabled the separation of several systems to be simulated with a process simulation tool. The results from these simulations were thereafter used to evaluate the economics behind the use of three solvent systems.

The results of this study are divided into three sections, first the experimental data, which includes the thermodynamic modelling, secondly, the process simulations of several SCFE processes and thirdly, an economic analysis of these SCFE processes.

6.1. EXPERIMENTAL PHASE EQUILIBRIUM MEASUREMENTS

The experimental measurements were undertaken using the three different apparatuses. These apparatuses are described in sections 4.3 through to 4.5. The data that was collected using all three of these apparatuses is presented, per solvent, and then per system, below. The sub-critical thermodynamic models that are discussed in section 2.5 were fitted to the measured data, and the abilities of the models to describe the systems are briefly discussed. In addition, the methods of Ungerer et al. (2005), and Heidemann and Khalil (1980) for determining the critical loci of binary systems, as discussed in section 2.6, were applied to the systems of interest.

6.1.1. CHEMICAL PURITIES

The chemicals that were used for the measurement of phase equilibrium data for this study are listed in Table 6.1. The purities of the components that were stated by the suppliers were verified by analysis of the peak area fractions from the TCD of the Shimadzu GC 2010 gas chromatograph fitted with the SE30 column. The supplier of each chemical, the purity that was claimed by the supplier and the GC area fractions are reported in Table 6.1. The GC area fraction was the integrated area under the peak corresponding to the chemical of interest as a fraction of the total integrated area under all of the peaks. The GC area fraction was measured for the gases prior to degassing, but for the liquids these

values were measured after degassing. Finally, the critical temperature and pressure of each component is also included in Table 6.1.

Table 6.1. Details of the chemicals used in this study [a].

	Supplier	Stated Purity	GC Area Fraction	T_c / K	P_c / MPa
Carbon dioxide, CO_2	Afrox South Africa	> 0.999 [b]	0.9959	304.26 [f]	7.377 [f]
Trifluoromethane, CHF_3	A-Gas (South Africa) (Pty) Ltd	> 0.999 [b]	0.9996	299.07 [f]	4.836 [f]
Hexafluoroethane, C_2F_6	A-Gas (South Africa) (Pty) Ltd	> 0.999 [b]	0.9999	293.03 [e]	3.013 [d]
n-Hexane, C_6H_{14}	Sigma-Aldrich Co. LLC.	> 0.99 [c]	0.9904	507.35 [f]	3.03 [f]
n-Heptane, C_7H_{16}	Merck Schuchardt OHG	> 0.995 [c]	0.9974	540.3 [f]	2.756 [f]
n-Octane, C_8H_{18}	Merck Schuchardt OHG	> 0.99 [c]	0.9980	568.9 [f]	2.493 [f]
n-Nonane, C_9H_{20}	Merck Schuchardt OHG	> 0.99 [c]	0.9984	594.9 [f]	2.288 [f]
n-Decane, $C_{10}H_{22}$	Sigma-Aldrich Co. LLC.	> 0.99 [c]	0.9964	617.65 [f]	2.104 [f]
n-Undecane, $C_{11}H_{24}$	Merck Schuchardt OHG	> 0.99 [c]	0.9973	638.85 [f]	1.955 [f]
1-Hexene, C_6H_{12}	Merck Schuchardt OHG	> 0.99 [c]	0.9992	504.5 [f]	3.126 [f]
3-Methylpentane, C_6H_{14}	Sigma Aldrich Co. LLC	> 0.99 [c]	0.9980	504.1 [f]	3.206 [f]
Methylcyclohexane, C_7H_{14}	Sigma Aldrich Co. LLC	> 0.996 [c]	0.9989	572.2 [f]	3.471 [f]
Toluene, C_7H_8	Sigma Aldrich Co. LLC	> 0.995 [c]	0.9967	591.79 [f]	4.104 [f]
Water, H_2O	Ultrapure MilliQ [g]		0.9974	647.14 [f]	22.06 [f]

[a] includes the suppliers, stated purities, GC area fractions (mol. basis) and critical properties, T_c and P_c

[b] Volumetric basis

[c] Molar basis

[d] (Kim, 1974)

[e] (Saikawa et al., 1979)

[f] (Lide, 2004)

[g] Produced on site

To further verify the purities of the liquids that were used in this investigation, the densities and refractive indices of each component were measured and compared against literature data. These data sets are presented in several journal paper manuscripts contained in Appendices C to H.

6.1.2. Equipment Calibrations

The calibrations of the pressure transducers and of the temperature probes for the static-analytic apparatus, the static-synthetic apparatus and the critical point determination apparatus are provided in Appendix B.1. The calibration polynomials for the gas chromatograph TCD for each component, which were used for composition analysis for the static-analytic apparatus, are also provided in Appendix B.1.

6.1.3. Vapour Pressures

The vapour pressures of the three gases were measured using the static-analytic apparatus. The experimental data alongside the uncertainties for the measurements, and a comparison to the PR EOS

with the MC alpha function (PR-MC EOS) which was fitted to the vapour pressure data that was available in literature, are given in Appendix C for CO_2 and R-23 and Appendix D for R-116. The literature data were obtained from the work of Meyers and Van Dusen (1932), Duschek et al. (1990), and Suehiro et al. (1996) for CO_2, the work of Hou and Martin (1959), Rasskazov et al. (1975), and Hori et al. (1982) for R-23, and the work of Kim (1974), Kijima et al. (1977), Kleiber (1994), Kao and Miller (2000), Valtz et al. (2007) and Madani et al. (2008) for R-116. The data are presented in Figure 6.1, 6.2 and 6.3 for CO_2, R-23 and R-116 respectively.

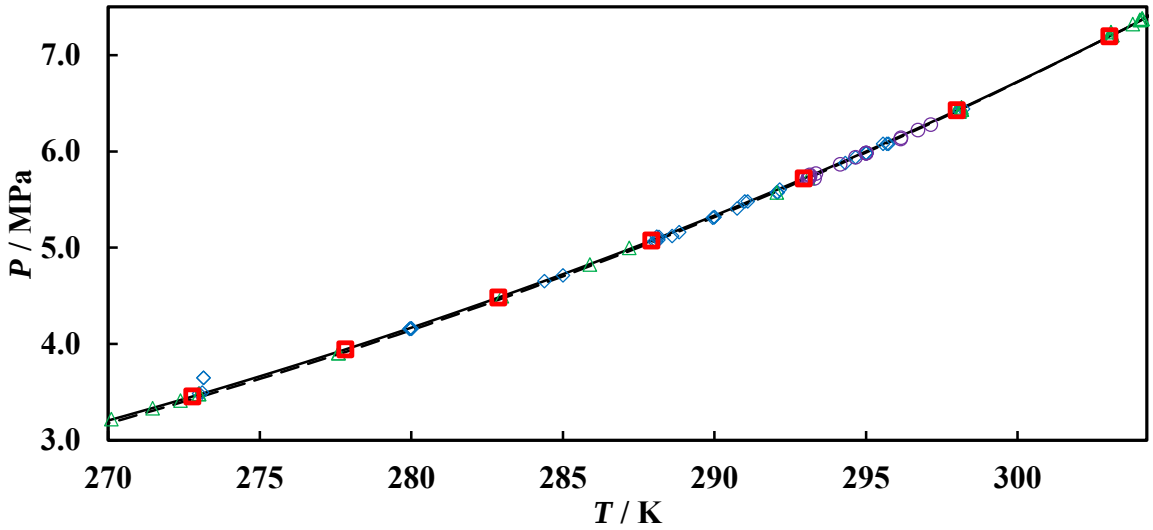

Figure 6.1. Vapour pressure data, *P*, for carbon dioxide between temperatures of *T* = (270 to 304.26) K. □, experimental data; △, Meyers and Van Dusen (1932); ◇, Duschek et al. (1990); ○, Suehiro et al. (1996); ——, PR MC EOS model; - - -, PR EOS model.

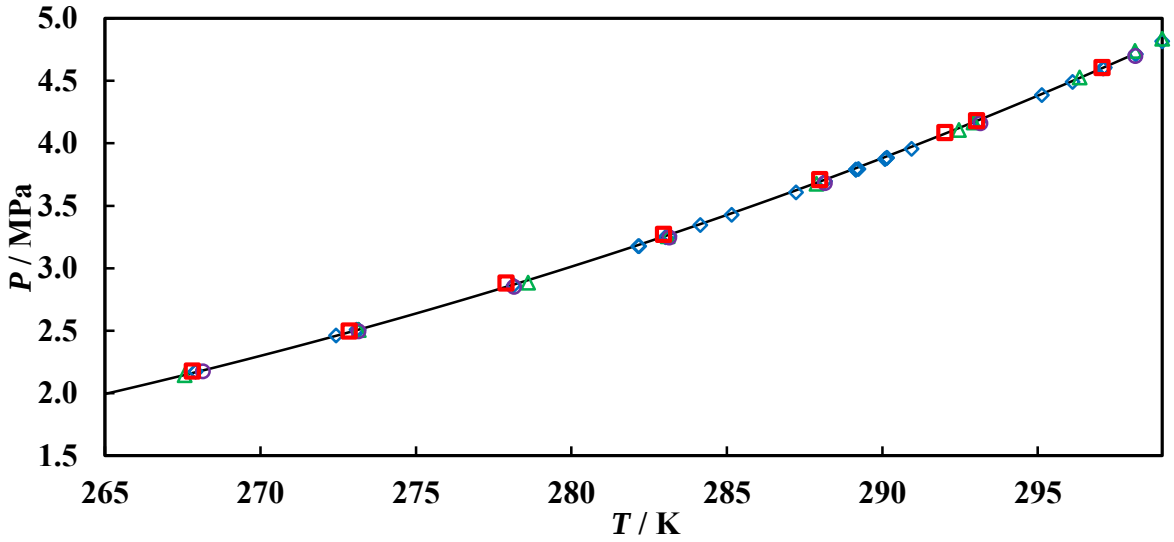

Figure 6.2. Vapour pressure data, *P*, for trifluoromethane between temperatures of *T* = (265 to 299.07) K. □, experimental data; △, Hou and Martin (1959); ○, Rasskazov et al. (1975); ◇, Hori et al. (1982); ——, PR-MC EOS.

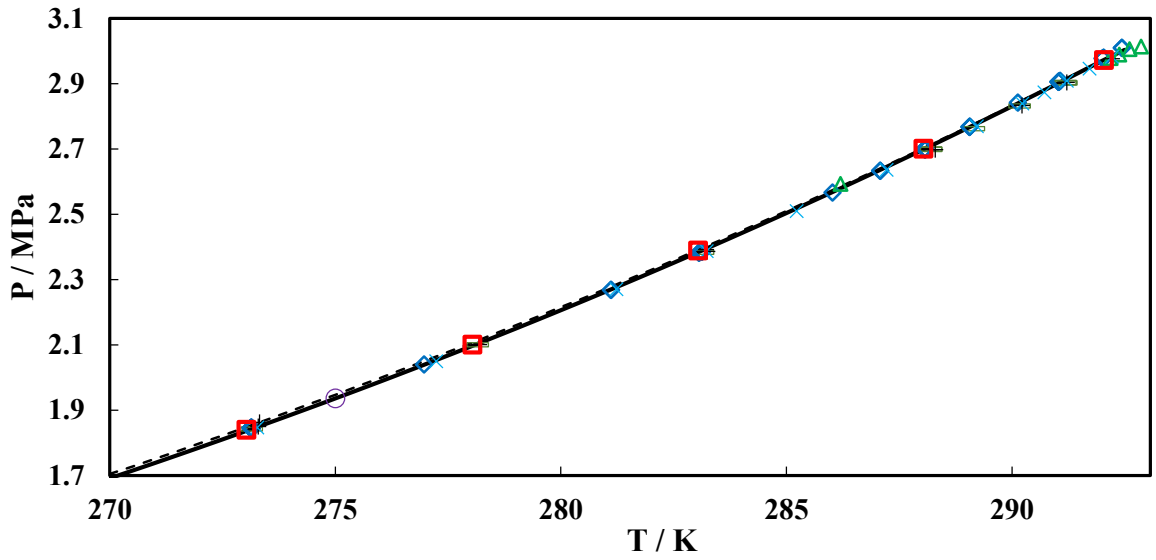

Figure 6.3. Vapour pressure data, *P*, for hexafluoroethane at temperatures of between *T* = (270 to 293.07) K. □, experimental data; △, Kim (1974); ═, Kao and Miller (2000); ○, Kleiber (1994); ◇, Kijima et al. (1977); +, Madani et al. (2008); X, Valtz et al. (2007); ——, PR-MC EOS.

The PR-MC EOS is used to describe the vapour pressures rather than the PR EOS because of the superiority of the fit that is achieved with the addition of the MC alpha function to the EOS. An example of this superiority can be observed with the data presented in Table 6.2. For this comparison, both of the models are fitted to vapour pressure data that were obtained from the work of Kim (1974), Kijima et al. (1977), Kleiber (1994), Kao and Miller (2000), Valtz et al. (2007) and Madani et al. (2008).

Table 6.2. The literature and modelled vapour pressure data, P_{exp}, for hexafluoroethane at temperatures, T, of between (273.06 and 292.07) K.

T / K	P_{exp} / MPa	P_{calcPR} [a] / MPa	(ΔP_{PR} / P_{exp}) [b]	P_{calcMC} [c] / MPa	(ΔP_{MC} / P_{exp}) [d]
273.06	1.839	1.883	-2.42	1.850	-0.60
278.07	2.100	2.136	-1.71	2.108	-0.39
283.07	2.388	2.413	-1.03	2.393	-0.17
288.07	2.701	2.716	-0.57	2.704	-0.15
292.07	2.972	2.977	-0.17	2.974	-0.09

[a] Calculated using the PR EOS, which was fitted to literature data

[b] $\Delta P_{PR} = 100 \cdot (P_{exp} - P_{calcPR})$

[c] Calculated using the PR-MC EOS, which was fitted to literature data

[d] $\Delta P_{MC} = 100 \cdot (P_{exp} - P_{calcMC})$

The MC alpha function parameters are fitted to vapour pressure data that were obtained from literature for all of the components investigated in this study. The literature sources for the components with low volatilities (liquids at ambient temperatures) are presented in Table 6.3.

Table 6.3. Literature sources for vapour pressure data for the compounds used in this study.

Component	Literature sources for vapour pressure data at temperatures of between (260 and 320) K
n-Hexane, C_6H_{14}	Li et al. (1972), Książczak (1986), Książczak and Jan Kosinski (1988), Bich et al. (1992), and Fernández et al. (2010).
n-Heptane, C_7H_{16}	Young (1898), Young (1928), Forziati et al. (1949), Van Ness et al. (1967), Pividal et al. (1992), Lozano et al. (1995), Dahmani et al. (1997), Rhodes et al. (1997) and Negadi et al. (2007).
n-Octane, C_8H_{18}	Young (1900; 1910; 1928), Gracia et al. (1992), Dejoz et al. (1996), Plesnar et al. (1996) and Boukais-Belaribi et al. (2000).
n-Nonane, C_9H_{20}	Young (1928), Schaefer et al. (1958), Wolff et al. (1964), Carruth and Kobayashi (1973), Kolasinska et al. (1982), Paul et al. (1986) and Ahmad et al. (2004).
n-Decane, $C_{10}H_{22}$	Woringer (1900), Reamer and Sage (1963), Wadsö (1966), Carruth and Kobayashi (1973), Brunner (1985), Allemand et al. (1986), Chirico et al. (1989), Belaribi et al. (1991) and Dejoz et al. (1996).
n-Undecane, $C_{11}H_{24}$	Krafft (1882), Young (1928), Kohlraush and Koppl (1934), Letsinger and Traynham (1948), Tilicheev et al. (1951), Wadsö (1966), Marsh et al. (1980) and Schmelzer et al. (1983).
1-Hexene, C_6H_{12}	Forziati et al. (1950), Camin and Rossini (1956), Negadi et al. (1993), Segovia et al. (1998), Segura et al. (2001), Chamorro et al. (2002), Sapei et al. (2006), Negadi et al. (2007) and Marrufo et al. (2009).
3-Methylpentane, C_6H_{14}	Willingham et al. (1945), Funk et al. (1972), Liu and Davison (1981), Berro et al. (1994), Garriga et al. (1994) and Uusi-Kyyny et al. (2001).
Methylcyclohexane, C_7H_{14}	Willingham et al. (1945), Bonhorst et al. (1948), Nicolini and Laffitte (1949), Heady and Cahn (1973), Castellari et al. (1988), Wu et al. (1991), Pividal et al. (1992) and Mokbel et al. (1995).
Toluene, C_7H_8	Kahlbaum (1884), Kahlbaum (1898), Woringer (1900), Willingham et al. (1945), Forziati et al. (1949), Li et al. (1972), Besley (1974), Mokbel et al. (1998) and Negadi et al. (2009).
Water, H_2O	Data was obtained from the NIST ThermoData Engine (2013) provided in Aspen Plus V8.4 (Aspen Technology, 2012).

The MC alpha function parameters were fitted with the PR EOS, to the vapour pressure data, using a least squares regression. These parameters for equation 2.7 are given in Table 6.4. Due to the phase

equilibrium measurements being conducted both above and below the critical points of CO_2, R-23 and R-116, the one parameter form of the MC alpha function was used for these components.

Table 6.4. Mathias-Copeman alpha function parameters (κ_1, κ_2, and κ_3) [a] for the components used in this study.

Component	T / K	κ_1	κ_2	κ_3
Carbon dioxide, CO_2	270.00 – 304.26 [b]	0.694	0 [c]	0 [c]
Trifluoromethane, CHF_3	252.93 – 299.07 [b]	0.776	0 [c]	0 [c]
Hexafluoroethane, C_2F_6	273.10 – 292.90 [b]	0.777	0 [c]	0 [c]
n-Hexane, C_6H_{14}	273.00 – 339.00	0.780	0.212	-0.238
n-Heptane, C_7H_{16}	272.30 – 315.90	0.908	-0.265	0.729
n-Octane, C_8H_{18}	269.90 – 333.80	0.944	-0.022	0.289
n-Nonane, C_9H_{20}	273.15 – 353.13	1.001	-0.009	0.299
n-Decane, $C_{10}H_{22}$	273.15 – 333.15	1.107	-0.330	0.843
n-Undecane, $C_{11}H_{24}$	298.09 – 333.11	0.412	3.965	-7.000
1-Hexene, C_6H_{12}	283.15 – 323.15	0.823	-0.291	0.778
3-Methylpentane, C_6H_{14}	283.10 – 333.15	0.772	-0.076	0.378
Methylcyclohexane, C_7H_{14}	273.15 – 323.13	0.712	0.033	0.193
Toluene, C_7H_8	283.10 – 333.15	0.744	0.063	0.122
Water, H_2O	273.00 – 323.16	0.516	2.232	-3.736

[a] Parameters fitted to literature data (see Table 6.3).

[b] The range extended up to the pure component critical temperature.

[c] Set to zero in this study.

6.1.4. CO_2 SYSTEMS

VLE data are readily available for the binary systems containing CO_2 with the solutes that were of interest in this study. Therefore, the only system containing CO_2 for which VLE data was measured was that with n-hexane. This was measured in order to verify the equipment and the procedures that were utilised. For this system, the VLE data, along with the thermodynamic model, and a comparison to the literature data are presented. For the remaining systems, experimental data were obtained from literature. The VLE data for all of the systems of interest were regressed with the PR-MC + WS/NRTL model.

CO_2 (1) + N-HEXANE (2)

The CO_2 + n-hexane binary system was used to verify the experimental apparatus and technique. The experimental data from this study were compared to data that had previously been reported in literature. This data included the *P-x-y* VLE data of Ohgaki et al. (1976), Wagner and Wichterle (1987), Chen and Chen (1992) and Zhu et al. (2006); the bubble pressure (*P-x*) data of Kaminishi et al. (1987) and Lay et al. (2006; 2010); and the solubilities of hexane in CO_2 (*P-y* data) reported by Wang et al. (2006). The data for the CO_2 (1) + n-hexane (2) system are provided in Appendix D. The *P-x-y* plot of the experimental data is given by Figure 6.4.

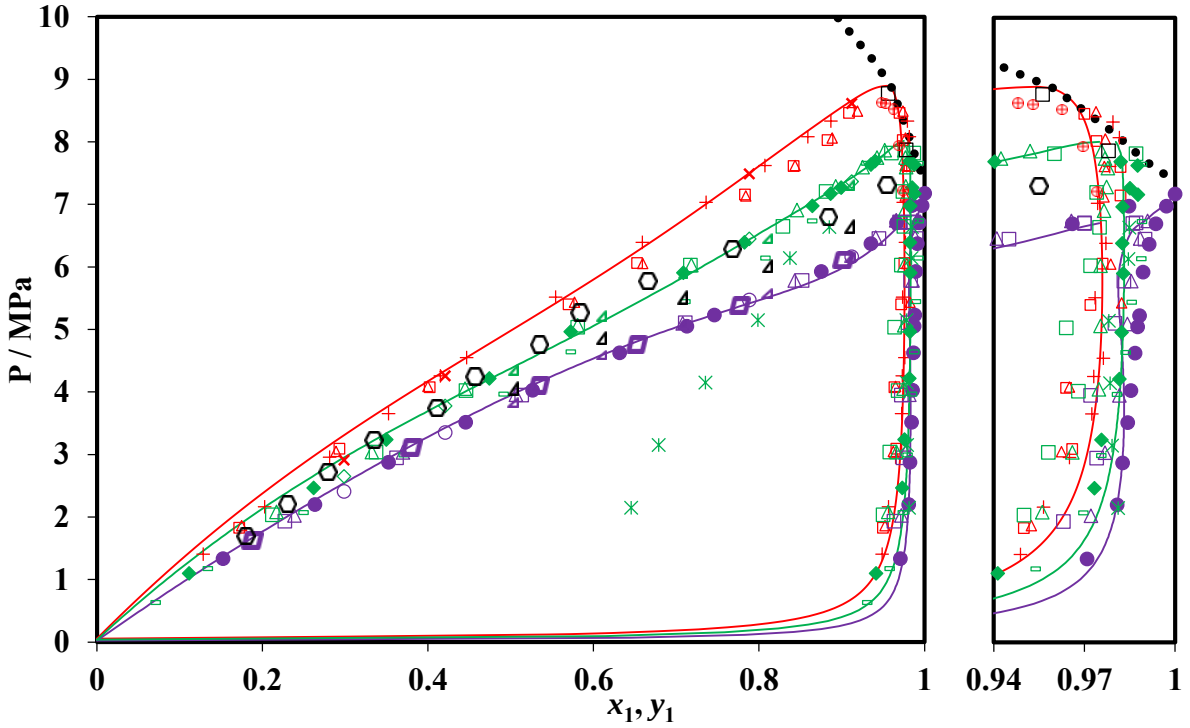

Figure 6.4. Pressure, *P*, liquid phase composition, *x*, and vapour phase composition, *y*, plot for the binary system of carbon dioxide (1) + n-hexane (2) measured with the static-analytic apparatus at temperatures of *T* = ●, 303.09 K; ◆, 313.10 K; ✚, 323.05 K. Pressure, *P*, liquid phase composition, *x*, data measured with the static-synthetic apparatus at temperatures of *T* = ○, 303.2 K; ◇, 313.2 K; X, 323.2 K. Solid lines, PR-MC + WS/NRTL model; ••••, critical loci. □, extrapolated critical points. Literature data of: Wagner and Wichterle (1987), □,303.14 K; □, 313.14 K; □, 323.14 K; Chen and Chen (1992), △, 303.15 K; △, 313.15 K; △, 323.15 K; Ohgaki and Katayama (1976), ⎯, 313.1 K; Kaminishi et al. (1987), ▱, 303.14 K; Lay et al. (2006), ⬡, 308.15 K; Wang et al. (2006), ⊕, 323 K; Zhu et al. (2006), Ж, 313 K; Lay (2010), ◿, 303.15 K; ◿, 308.15 K; ◿, 313.15 K.

The parameters for the thermodynamic models were fitted to the experimental data using a modified Barker's objective function. This objective function sought to minimise the deviations between the experimental and modelled pressures and vapour-phase compositions. Discussions into the thermodynamic modelling and the phase behaviour is given in Appendix C.

The critical loci for the system were extrapolated from the sub-critical VLE data as well as calculated using the PR-MC + WS/NRTL model. The extrapolation was performed using the method of Ungerer et al., whereas the calculation using the model was performed by the technique of Heidemann and Khalil.

Other CO_2 Binary Systems

For the remainder of the binary systems containing CO_2, the parameters for the PR-MC + WS/NRTL model were fitted against data which was reported in literature. These literature sources, for the various systems, are tabulated in Table 6.5.

Table 6.5. Literature data sources for phase equilibrium data of systems containing CO_2.

System	Literature sources for phase equilibrium data
CO_2 + n-heptane	Robinson and Kalra (1976), Kalra et al. (1978), He et al. (1994), Mutelet et al. (2005) and Lay (2010).
CO_2 + n-octane	Chen and Chen (1992), Weng and Lee (1992), Wang et al. (1996), Jiménez-Gallegos et al. (2006), Yu et al. (2006) and Tochigi et al. (2010).
CO_2 + n-nonane	Jennings and Schucker (1996) and Camacho-Camacho et al. (2007).
CO_2 + n-decane	Reamer and Sage (1963), Inomata et al. (1986), Nagarajan and Robinson (1986), Adams et al. (1988), Chou et al. (1990), Iwai et al. (1994), Jennings and Schucker (1996), Shaver et al. (2001) and Jiménez-Gallegos et al. (2006)
CO_2 + n-undecane	Camacho-Camacho et al. (2007).
CO_2 + 1-hexene	Vera and Orbey (1984), Wagner and Wichterle (1987) and Jennings and Teja (1989).
CO_2 + 3-methylpentane	Mutelet et al. (2005).
CO_2 + methylcyclohexane	Ng and Robinson (1979) and Nasrifar et al. (2003).
CO_2 + toluene	Ng and Robinson (1978), Sebastian et al. (1980), Morris and Donohue (1985), Kim et al. (1986), Fink and Hershey (1990), Muhlbauer and Raal (1991), Tochigi et al. (1998), Lay et al. (2006) and Naidoo et al. (2008).
CO_2 + water	King and Coan (1971), Bamberger et al. (2000) and Valtz et al. (2004).

The parameters were regressed using a modified Barker's objective function. This objective function was composed of the residuals of pressure (P) and vapour-phase composition (y). Thus, the model was fitted to the experimental data by fitting these two variables, while assuming that the temperature remained constant and neglecting the liquid-phase composition residuals. The pressure residuals took into account the variations in the bubble curve between the experimental data and the modelled data. This can be observed from the *P-x-y* plots given below, with small deviations between the experimental data and the bubble point curve. The parameters that gave the best fit of the model to the experimental data, along with statistical data for the regressions are presented in Table 6.6.

Table 6.6. Regressed parameters for the PR-MC + WS/NRTL model, for binary systems containing CO_2.

	T / K	k_{12}	τ_{12} / K [a]	τ_{21} / K [a]	ARD [c]		AARD [d]	
					P	*y*	*P*	*y*
CO_2 + n-hexane	*(303.1 to 323.1)*	0.5704	534.24	46.85	0.2	-0.50	1.5	0.62
CO_2 + n-heptane	*(293.15 to 363.15)*	0.6441	581.7	-115.5	-4.0	-0.67	8.7	0.73
CO_2 + n-octane	*(290 to 373.2)*	0.6544	1035.2	-177.9	-0.3	-0.19	5.3	0.37
CO_2 + n-nonane	*(315.12 to 373.28)*	0.6983	934.2	-224.7	-0.4	0.4	4.8	0.53
CO_2 + n-decane	*(277.59 to 377.57)*	0.7388	1068.1	-134.9	-1.7	-0.18	7.0	0.42
CO_2 + n-undecane	*(314.98 to 418.3)*	0.7367	2228.7	6015.4	-1.1	0.58	6.1	0.59
CO_2 + 1-hexene	*(303.14 to 343.13)*	0.5162	-72.9	344.5	0.1	0.63	5.2	1.92
CO_2 + 3-methylpentane	*(293.15 to 283.15)*	0.5864	-549.6	399.4	-2.5	- [e]	10.0	- [e]
CO_2 + methylcyclohexane	*(281.21 to 338.88)*	0.6325	299.1	129.8	-1.0	-0.05	7.3	0.76
CO_2 + toluene	*(293.15 to 393.67)*	0.5537	397.7	-44.5	-3.1	-0.78	8.5	0.92
CO_2 + water	*(297.99 to 372.97)*	0.6127	-587.6	2257.6	11.1	0.45	39.1	0.48

[a] τ_{12}, τ_{21} for the NRTL activity coefficient model

[b] Δu_{12}, Δu_{21} for the UNIQUAC activity coefficient model

[c] average relative deviation, $ARD(\bar{\theta}) = \frac{100}{N_p}\sum_{1}^{N_p}\frac{\bar{\theta}_{exp} - \bar{\theta}_{calc}}{\bar{\theta}_{exp}}$

[d] absolute average relative deviation, $AARD(\bar{\theta}) = \frac{100}{N_p}\sum_{1}^{N_p}\frac{\left|\bar{\theta}_{exp} - \bar{\theta}_{calc}\right|}{\bar{\theta}_{exp}}$

[e] No vapour phase data was available for this system, and therefore deviations were not calculated

For most of the systems, the fits of the model to the experimental data are acceptable, with ARDs of less than $\pm$ 1.5 %. The ARDs for the CO_2 + n-heptane and the CO_2 + water systems highlighted large deviations between the model and the experimental data. The large disagreement between the model and the experimental data for the CO_2 + n-heptane system is possibly due to differences between the data measured by different authors. The large deviations for the CO_2 and water system are due to the marginal mutual solubilities of the two components, which the model was incapable of describing. Only bubble pressure data from a single author was available for the CO_2 + 3-methylpentane system, and this had a notable effect on the quality of the fit of the model for this system. A different model was not used for this system, as the intention was to perform simulations using Aspen Plus, which requires the same model for all of the systems.

6.1.5. R-23 SYSTEMS

The isothermal binary VLE and VLLE measurements were conducted for R-23 with 10 different solutes. This data are collated in six journal manuscripts which have been published in, or are yet to be submitted to peer-reviewed journals (the articles are attached in Appendices C through to H). A summary of the temperature and pressure ranges and the number of isotherms at which this VLE data were measured is provided in Table 6.7 below. The number of data points that were measured for each system are also indicated alongside the appendix in which the the journal manuscript is located.

In addition to the systems indicated in Table 6.7, VLE data were also measured for the system of R-23 and water. The data for this system are given in this section, as it had not yet been collated into a peer reviewed article. Furthermore, critical loci for the systems of R-23 + n-propane and R-23 + n-hexane were also measured and reported in this section.

Table 6.7. Systems containing R-23 measured in this study.

System	*T* / K	*P* / MPa	N_I	N_D	Bubble points	Located in Appendix
R-23 + n-hexane	272.9 to 313.2	1.06 to 5.77	5	50	12	C
R-23 + n-heptane	272.9 to 313.2	1.11 to 5.74	5	49	11	D
R-23 + n-octane	272.9 to 313.2	1.16 to 6.24	5	52	13	E
R-23 + n-nonane	272.9 to 313.2	1.05 to 6.30	5	50	11	F
R-23 + n-decane	272. 9 to 313.3	0.85 to 6.60	4	40	15	F
R-23 + n-undecane	293.1 to 313.3	0.89 to 6.46	3	31	8	F
R-23 + 1-hexene	293.1 to 313.3	0.88 to 5.51	3	37	0	G
R-23 + 3-methylpentane	293.1 to 313.3	0.76 to 5.61	3	38	0	G
R-23 + methylcyclohexane	293.0 to 313.2	0.91 to 6.08	3	33	0	H
R-23 + toluene	293.0 to 313.3	0.83 to 5.70	3	34	0	H

[a] including the temperature, *T*, and pressure, *P*, ranges, the number of isotherms measured, N_I, the number of data points reported, N_D, and the location of the data

The experimental VLE datasets that are referred to in Table 6.7 were regressed using the regression toolbox provided in Aspen Plus V8.4 (Aspen Technology, 2012). The regression was performed by minimising the modified Barker's objective function. The temperature dependent PR-MC + WS/NRTL parameters for each of the binary systems containing R-23 investigated in this study, are tabulated in Table 6.8. Theoretically, these parameters are only applicable within the ranges of the measured data, which are provided alongside the parameters. For the estimation of the critical locus curves, however, these temperature ranges were disregarded.

Table 6.8. Regressed parameters and deviations for the PR-MC + WS/NRTL model, for binary systems containing R-23.

	T / K	k_{12}	τ_{12} / K [a]	τ_{21} / K [a]	ARD [b]		AARD [c]	
					P	*y*	*P*	*y*
R-23 + n-hexane	*303.1 to 323.1*	0.570	634.7	220.9	0.16	-0.50	1.51	0.62
R-23 + n-heptane	*272.9 to 313.2*	0.563	662.1	244.3	2.01	0.63	4.28	1.26
R-23 + n-octane	*272.9 to 313.2*	0.634	650.6	172.5	-0.98	0.10	5.07	0.42
R-23 + n-nonane	*272.9 to 313.2*	0.670	647.0	281.1	-2.73	-0.06	6.06	0.18
R-23 + n-decane	*272.9 to 313.3*	0.608	520.2	626.9	-2.29	0.69	6.75	1.65
R-23 + n-undecane	*293.1 to 313.3*	0.706	620.3	595.8	-7.14	0.10	8.68	0.52
R-23 + 1-hexene	*293.1 to 313.3*	0.558	310.3	495.9	0.48	-0.45	3.18	4.47
R-23 + 3-methylpentane	*293.1 – 313.3*	0.555	469.0	512.6	2.42	1.63	4.34	6.45
R-23 + methylcyclohexane	*293.0 to 313.2*	0.562	313.4	689.1	0.50	-0.58	2.87	1.93
R-23 + toluene	*293.1 to 313.2*	0.462	215.5	435.6	-2.18	-1.12	3.69	1.15
R-23 + water	*293.2 to 313.2*	-0.384	3945.3	1668.9	-17.9	-0.08	23.4	0.28

[a] τ_{12}, τ_{21} for the NRTL activity coefficient model

[b] average relative deviation, $$ARD(\bar{\theta}) = \frac{100}{N_p}\sum_{1}^{N_p}\frac{\bar{\theta}_{exp} - \bar{\theta}_{calc}}{\bar{\theta}_{exp}}$$

[c] absolute average relative deviation, $$AARD(\bar{\theta}) = \frac{100}{N_p}\sum_{1}^{N_p}\frac{\left|\bar{\theta}_{exp} - \bar{\theta}_{calc}\right|}{\bar{\theta}_{exp}}$$

Experimental critical loci data for the R-23 + n-propane and R-23 + n-hexane systems as well as VLE data for the R-23 + water system were measured and are provided in their respective sections below. For the other binary systems, the data and the details thereof are discussed in the paper manuscripts included as Appendices C to H. Only brief overviews of each system, highlighting important observations and possibly useful phenomena are provided below.

R-23 (1) + n-Propane (2)

Several VLE isotherms for the R-23 and n-propane system were measured by Ju et al. (2009). This VLE data was extrapolated using the technique of Ungerer et al. Points along the critical locus curve were then measured with the critical point determination apparatus and were compared to this extrapolated data.

Table 6.9. Critical loci (*T-P-x*) calculated by the method of Ungerer et al. from the VLE data reported by Ju et al. (2009) alongside the critical loci measured using the critical point determination apparatus.

Method of Ungerer et al.			Critical Point Determination Apparatus [a]					
T_c / K	P_c / MPa	$x_{c,1}$	T_c / K	$U(T_c)$ / K	P_c / MPa	$U(P_c)$ / MPa	$x_{c,1}$	$U(x_{c,1})$
303.15	4.75	0.75	369.9	0.10	4.25	0.008	0.000	
313.15	4.98	0.60	364.2	0.58	4.61	0.046	0.071	0.005
			351.9	0.38	5.08	0.026	0.221	0.005
			342.0	0.56	5.32	0.023	0.325	0.004
			342.1	0.36	5.28	0.028	0.326	0.004
			331.3	0.56	5.37	0.054	0.434	0.003
			313.9	0.44	5.07	0.033	0.569	0.003
			311.3	0.54	4.97	0.020	0.624	0.002
			306.5	0.79	4.82	0.028	0.706	0.008

[a] combined expanded uncertainties in the experimental data, *U*, were calculated with a coverage factor of k = 2

RK type models of several different orders, as discussed in section 2.6.4, were fitted to the measured data. These models, alongside the experimental data, which are listed in Table 6.9 are presented in Figures 6.5 and 6.6. The parameters for the different order models as well as the residuals for each model are given in Table 6.10.

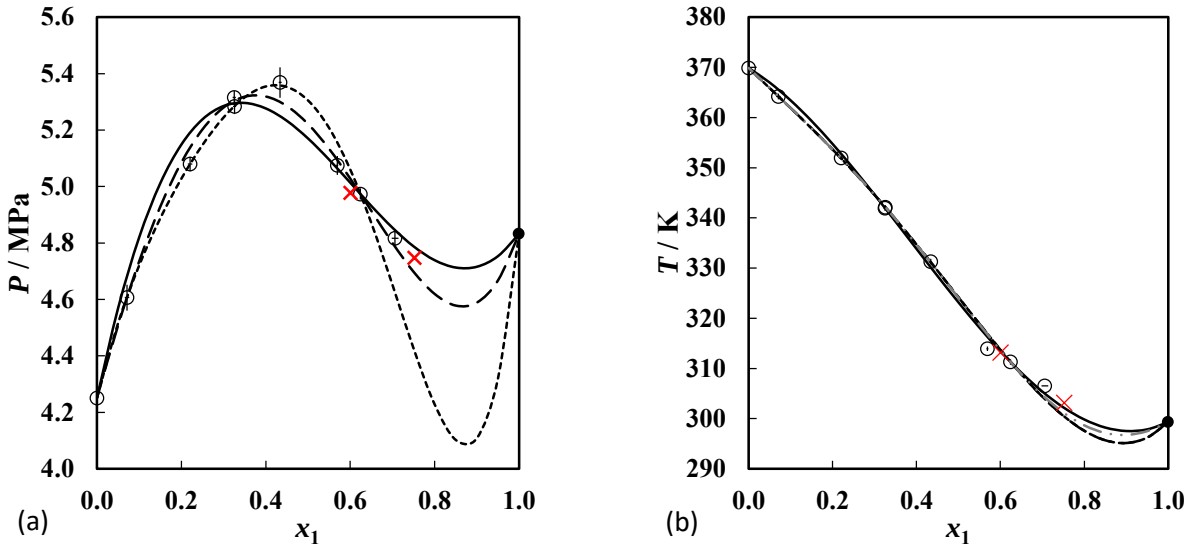

Figure 6.5. (a) *P-x* projection and (b) *T-x* projection of the critical locus curve for the R-23 (1) + n-propane (2) system. ○, critical loci measured with the critical point determination apparatus (uncertainty included as error bars); ×, critical loci extrapolated from the sub-critical coexistence data of Ju et al. (2009); •, R-23 critical point from the NIST ThermoData Engine (2013); ——, 1st order RK correlation; – –, 2nd order RK correlation; · · · ·, 3rd order RK correlation.

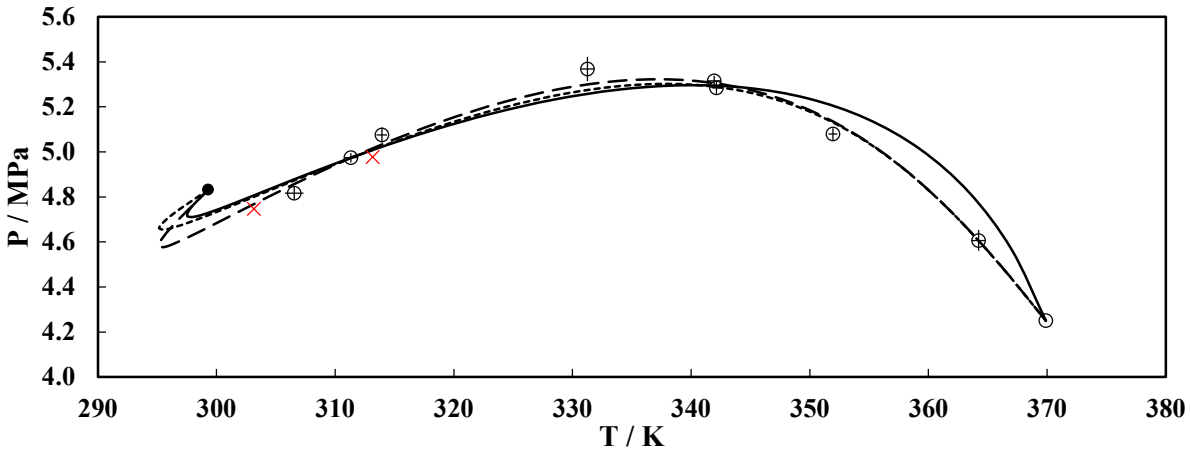

Figure 6.6. *P-T* projection of the critical locus curve for the R-23 (1) + n-propane (2) system. ○, critical loci measured with the critical point determination apparatus (uncertainty included as error bars); ×, critical loci extrapolated from the sub-critical coexistence data of Ju et al. (2009); •, R-23 critical point from the NIST ThermoData Engine (2013); ——, 1st order RK correlation; – –, 2nd order RK correlation; · · · ·, 3rd order RK correlation.

Table 6.10. Parameters for the RK type correlations for the system of R-23 (1) + n-propane (2), describing the critical temperature, T_c, and critical pressure, P_c, as functions of the composition.

RK correlation parameters for $T_c(x_{c,1})$					
	RMS / K [a]	a_1	a_2	a_3	a_4
1st order	2.29	-45.68	-65.50		
2nd order	1.96	-41.69	-71.58	-40.26	
3rd order	1.96	-41.51	-71.33	-40.35	0.24

RK correlation parameters for $P_c(x_{c,1})$					
	RMS / MPa [a]	b_1	b_2	b_3	b_4
1st order	7.43	2.514	-3.947		
2nd order	4.06	2.719	-4.238	-2.157	
3rd order	3.53	2.622	-4.090	-1.347	0.591

[a] root mean square, $RMS(\bar{\theta}) = \frac{1}{N_p}\sqrt{\sum_{1}^{N_p} \bar{\theta}_{N_p}{}^2}$

The inflection of the curves from the RK model for this system indicates the presence of a minimum boiling azeotrope. Extrapolation of the relative volatilities calculated from the data of Ju et al. (2009) further substantiate this observation. However, insufficient VLE data were measured by Ju et al. in the region in which it appeared that the azeotrope occurred to enable further investigations. The data of Ju et al. was regressed with the PR-MC + WS/NRTL model. The regressed parameters are provided alongside the statistics from the regression in Table 6.11. The data and the model are presented in Figure 6.7, alongside the critical locus curve data.

Table 6.11. Regressed parameters for the data for the R-23 (1) + n-propane (2) system measured by Ju et al. (2009).

	T / K	k_{12}	τ_{12} / K [a]	τ_{21} / K [a]	ARD [b]		AARD [c]	
					P	*y*	*P*	*y*
R-23 + n-propane	*283.15 to 313.15*	0.3108	317.6	227.6	-0.04	0.82	0.66	1.32

[a] τ_{12}, τ_{21} for the NRTL activity coefficient model

[b] average relative deviation, $$ARD(\bar{\theta}) = \frac{100}{N_p}\sum_{1}^{N_p}\frac{\bar{\theta}_{exp} - \bar{\theta}_{calc}}{\bar{\theta}_{exp}}$$

[c] absolute average relative deviation, $$AARD(\bar{\theta}) = \frac{100}{N_p}\sum_{1}^{N_p}\frac{\left|\bar{\theta}_{exp} - \bar{\theta}_{calc}\right|}{\bar{\theta}_{exp}}$$

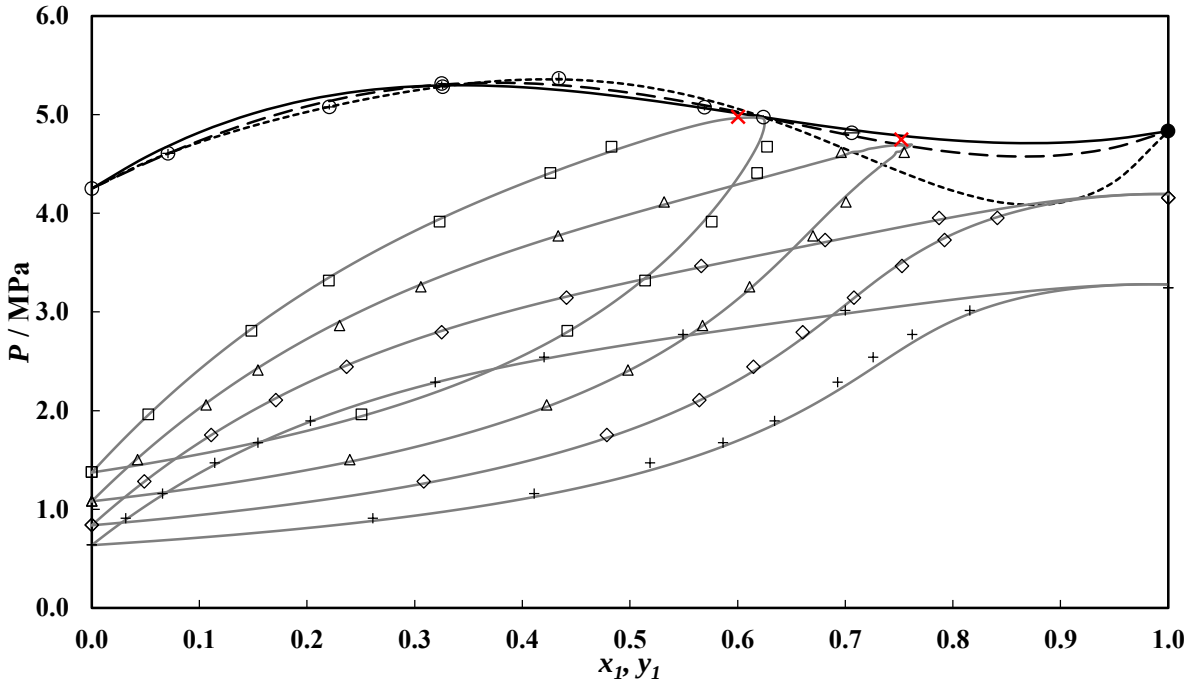

Figure 6.7. *P-x-y* projection for the R-23 (1) + n-propane (2) system. ○, critical loci measured with the critical point determination apparatus (uncertainty included as error bars); ×, critical loci extrapolated from the sub-critical coexistence data of Ju et al. (2009); •, R-23 critical point from the NIST ThermoData Engine (2013). Data reported by Ju et al. (2009): +, 283.15 K; ◊, 293.15 K; Δ, 303.15 K; □, 313.15 K; —, PR-MC + WS/NRTL. — —, 1st order RK correlation; · · · ·, 2nd order RK correlation; – – – –, 3rd order RK correlation.

From Figure 6.7, it would appear that the third order RK correlation best describes the system. This is particularly noticeable when observing the 303.15 K isotherm, for which the dew and bubble point curves of the thermodynamic model converge at almost exactly the same location as their interception with the third order RK correlation. In contrast, the second order RK correlation appears to under-predict the critical pressures as x_1 approaches 1.0. This is due to a lack of flexibility of the curve in conjunction with the attempt of the objective function to minimise the residuals between the curve and the experimental data.

With the presence of an azeotrope in this system, as well as the likelihood of VLLE occurring at lower temperatures, this system is classified as a VKS type II-A system.

R-23 (1) + n-Hexane (2)

Several phase equilibrium data points from a study by Wirths and Schneider (1985) corresponded to the experimental conditions for the R-23 + n-hexane data reported in Appendix C. There was a good agreement between the data set of Wirths and Schneider and that measured in this study, especially when considering the uncertainties in the data. The data for this system is presented in Figure 6.8.

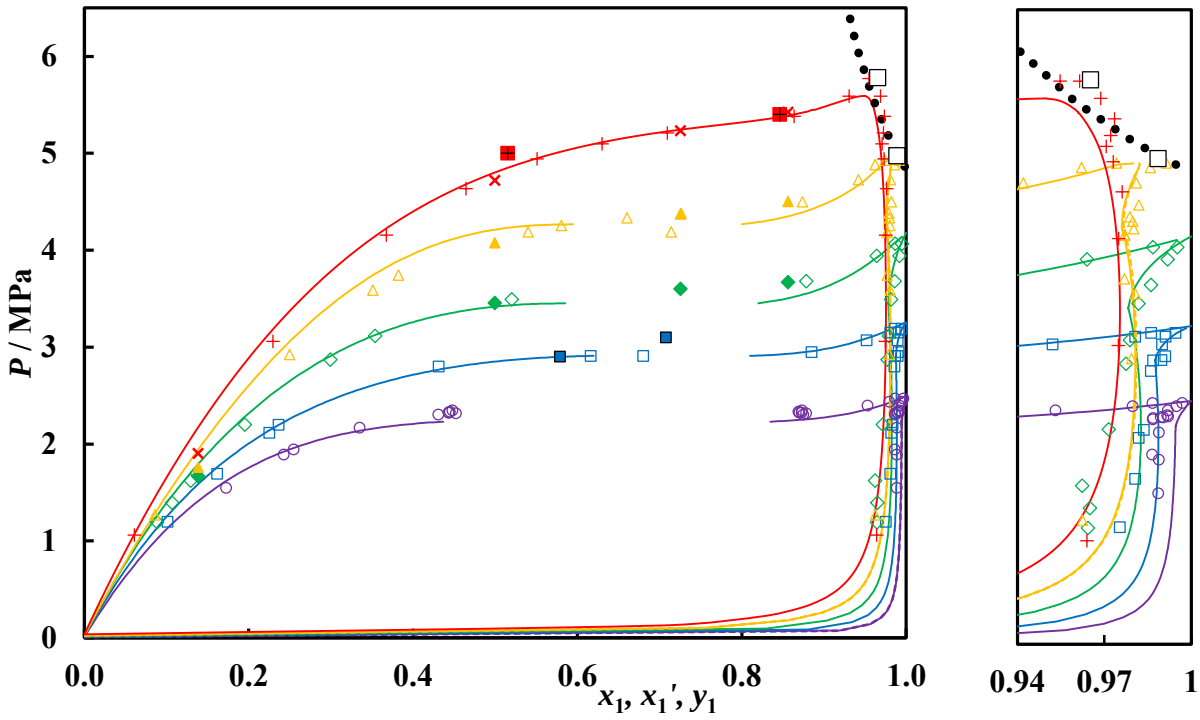

Figure 6.8. *P-x-x'-y* data for the binary system of trifluoromethane (1) + n-hexane (2) measured with the static-analytic apparatus at temperatures of *T* = ○, 272.87 K; □, 282.95 K; ◇, 293.02 K; △, 303.11 K; +, 313.20 K. *P-x* data measured with the static-synthetic apparatus at temperatures of *T* = ◆, 293.02 K; ▲, 303.11 K; X, 313.20 K. The data of Wirths and Schneider (1985), ■, ± 283 K; ✚, ± 313 K. Solid lines, PR-MC + WS/NRTL model; ••••, critical loci. ☐, extrapolated critical points.

This system exhibits a "bird's-beak" phenomenon with a highly acute angle of intersection of the bubble point and dew point curves. According to Rainwater (2001), the angle at which the two curves intersect should approach zero as the temperature approaches the critical temperature. An attempt to verify whether this was the case for this system was made in Appendix C, but the results were inconclusive.

The system exhibited liquid-liquid immiscibility at the lowest isotherm, but with an increase in temperature, the two liquid phases became miscible. The temperature at which this occurs (i.e. an

UCEP with [g + (l_1 = l_2)]), agreed with the data reported by Poot and de Loos (1999). This system is therefore classified as a VKS type II system.

The PR-MC + WS/NRTL model was found to describe the experimental data well, with the average relative deviation (ARD) being less than 2 % for both vapour composition and pressure. The PR-MC EOS with classical mixing rules was also fitted to the experimental data, but it was not able to describe the system with the same precision. The parameters for the PR-MC + WS/NRTL model for R-23 + n-hexane in Table 6.8 were used to calculate the section of the critical locus curve in the region with high R-23 concentrations. The critical loci were also extrapolated from the VLE data for this system at the temperatures of the isotherms. Lastly, a number of critical loci were measured for this system using the critical point determination apparatus. These critical loci are provided in Table 6.12.

Table 6.12. Critical loci (*P-T-x*) data for the R-23 (1) + n-hexane (2) system, calculated by the method of Ungerer et al., calculated by the method of Heidemann and Khalil, using the PR-MC + WS/NRTL model and measured using the critical point determination apparatus.

Method of Ungerer et al.			Method of Heidemann and Khalil			Critical Point Determination Apparatus [a]					
T_c / K	P_c / MPa	$x_{c,1}$	T_c / K	P_c / MPa	$x_{c,1}$	T_c / K	$U(T_c)$ / K	P_c / MPa	$U(P_c)$ / MPa	$x_{c,1}$	$U(x_{c,1})$
303.1	4.975	0.989	301.8	4.982	0.99	503.3	0.92	3.66	0.083	0.111	0.005
313.0	5.782	0.965	303.5	5.150	0.98	486.9	0.68	5.34	0.080	0.320	0.004
			309.0	5.556	0.96	454.3	1.11	7.91	0.091	0.537	0.003
			321.5	6.099	0.94	427.8	0.24	9.18	0.118	0.661	0.002
			333.9	6.821	0.92	383.2	1.04	9.82	0.100	0.773	0.002
			347.4	7.446	0.90	343.0	0.92	7.98	0.038	0.860	0.002
			380.0	9.201	0.85	318.7	0.53	5.95	0.056	0.922	0.002
						310.8	0.30	5.41	0.027	0.944	0.002

[a] combined expanded uncertainties in the experimental data, *U*, were calculated with a coverage factor of k = 2

RK type correlations of various orders (Section 2.6.4) were used to describe the experimental data. The parameters for the RK correlations with terms for different order correlations are tabulated in Table 6.13. The critical loci from the three sources are presented and compared with one another in Figures 6.9 and 6.10.

Table 6.13. Parameters for the RK type correlations for the system of R-23 (1) + n-hexane (2), describing the critical temperature, T_c, and critical pressure, P_c, as functions of the composition, $x_{c,1}$.

RK correlation parameters for T_c ($x_{c,1}$)						
	RMS / K [a]	a_1	a_2	a_3	a_4	a_5
1st order	7.77	231.58	55.46			
2nd order	5.18	235.00	20.28	-124.13		
3rd order	1.71	257.23	91.27	-190.70	-256.13	
4th order	1.61	256.50	94.71	-189.22	-268.95	-9.66
RK correlation parameters for P_c ($x_{c,1}$)						
	RMS / MPa [a]	b_1	b_2	b_3	b_4	b_5
1st order	43.94	14.58	13.86			
2nd order	31.61	14.08	21.34	10.42		
3rd order	22.56	16.22	23.41	-8.82	-23.61	
4th order	9.17	13.64	25.05	20.66	-23.09	-37.50

[a] root mean square, $$RMS(\bar{\theta}) = \frac{1}{N_p}\sqrt{\sum_{1}^{N_p} \bar{\theta}_{N_p}{}^2}$$

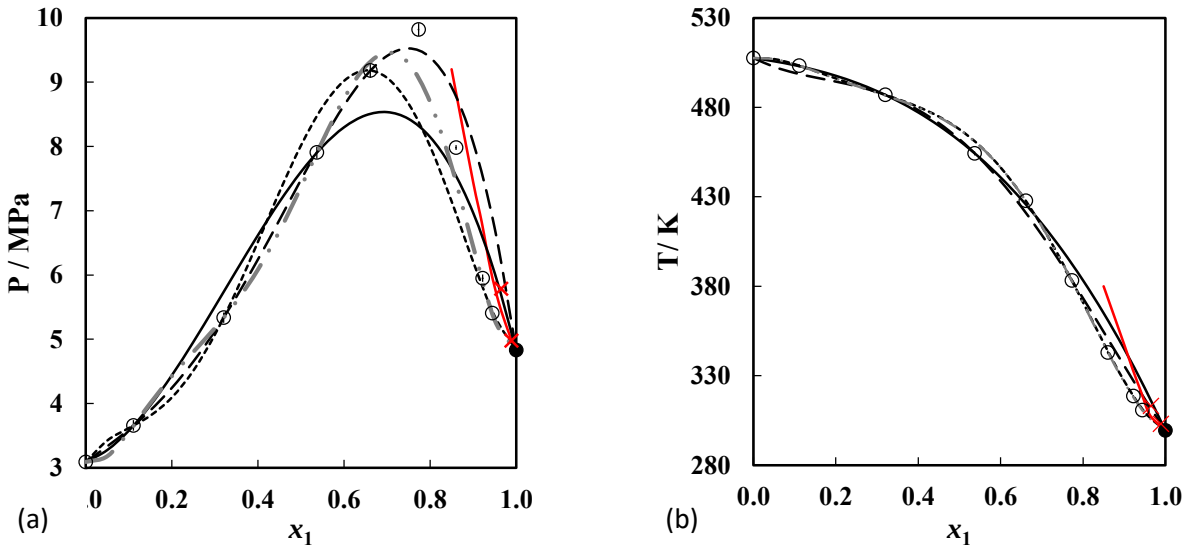

Figure 6.9. (a) *P-x* projection and (b) *T-x* projection of the critical locus curve for the R-23 (1) + n-hexane (2) system. ○, critical loci measured with the critical point determination apparatus (uncertainty included as error bars); ×, critical loci extrapolated from the sub-critical coexistence data; •, R-23 critical point from the NIST ThermoData Engine (2013); ——, calculated critical locus curve by the method of Heidemann and Khalil; —, 1st order RK correlation; – –, 2nd order RK correlation; · · ·, 3rd order RK correlation, – · · – · ·, 4th order RK correlation.

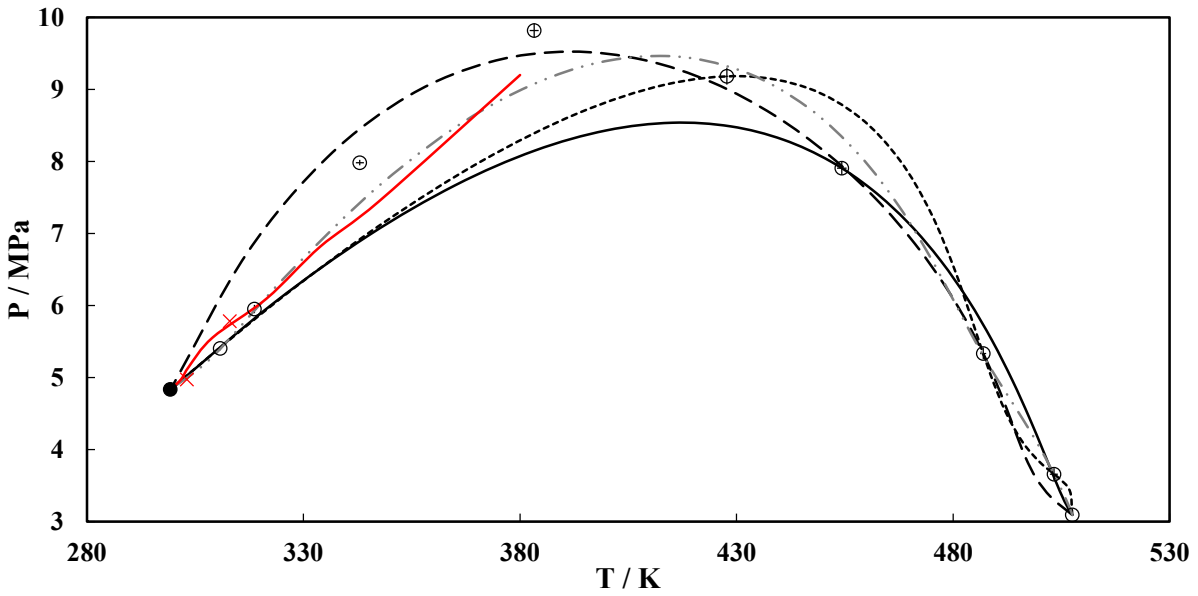

Figure 6.10. *P-T* projection of the critical locus curve for the R-23 (1) + n-hexane (2) system. ○, critical loci measured with the critical point determination apparatus (uncertainty included as error bars); ×, critical loci extrapolated from the sub-critical co-existence data; •, R-23 critical point from the NIST ThermoData Engine (2013); ——, calculated critical locus curve by the method of Heidemann and Khalil; —, 1st order RK correlation; – –, 2nd order RK correlation; · · ·, 3rd order RK correlation, – · · – · ·, 4th order RK correlation.

The RK type correlations are not able to adequately describe the behaviour of the critical locus curve, even when the number of parameters is increased to five. This is possibly due to the complexity of the system. Were the number of parameters used in the correlation increased further, they would possibly describe the system more precisely. This could, however, be at the expense of over-specifying the correlations.

At temperatures close to the temperature range for which the model parameters are fitted, there is a good agreement between the critical loci from all three sources. As the distance from this temperature range increases, the agreement between the critical loci calculated by the method of Heidemann and Khalil and the experimental data is lessened. Without the measurement of the VLE over a wider range of temperatures, it won't be possible to improve the temperature range for which the thermodynamic model can be applied.

There is also a fairly large discrepancy between the extrapolated data and the measured data. This is due to the significant flexibility in the extrapolation technique, which requires a discretion on the part of the user in extrapolating the critical locus. The measured critical loci are obviously the best means of describing the critical locus curve, but also require specialised equipment and are time consuming. Figures 6.9 and 6.10 show that the indirect techniques can provide reasonable estimates of the critical locus curves in cases in which critical loci cannot be directly measured.

R-23 (1) + n-HEPTANE (2)

This system is examined in the manuscript provided in Appendix D. This system also exhibited the "bird's-beak" phenomenon. The data from the static-analytic and the static-synthetic apparatuses agreed with one another, and the PR-MC + WS/NRTL model described the system well. This model was shown to provide a far superior description of the system than the PR-MC EOS. The ARD for pressure was 10.0 % with the PR-MC EOS, but only 2.0 % with the PR-MC + WS/NRTL model. The ARD for the vapour phase composition was 0.6 % with the PR-MC + WS/NRTL model. For this system, the *P-x-y* plot is given by Figure 6.11.

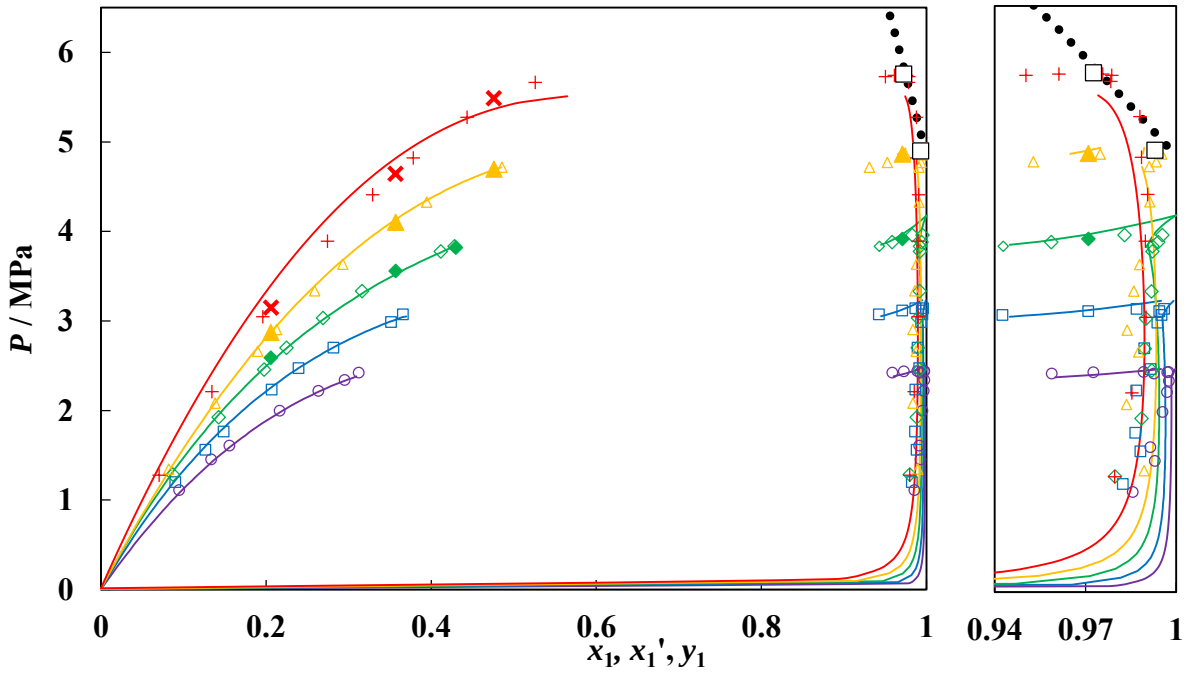

Figure 6.11. *P-x-x'-y* data for the binary system of R-23 (1) + n-heptane (2), measured using a static analytic apparatus, at temperatures of: ○, 272.9 K; □, 283.0 K; ◇, 293.0 K; △, 303.1 K; +, 313.2 K. *P-x* data measured, using a variable volume apparatus, at temperatures of: ◆, 293.0 K; ▲, 303.1 K; X, 313.2 K. Solid lines, PR-MC + WS/NRTL model; □, extrapolated critical loci; ••••, calculated critical locus curve.

In contrast to the R-23 + n-hexane system, for this system, liquid-liquid immiscibility occurs throughout the entire temperature range that was investigated. The compositions of the one liquid phase and the vapour phase appear to be approaching one another with increased temperature. It is therefore assumed that the UCEP occurs at a temperature slightly higher than the maximum temperature (313.2 K). Because the compositions of the one liquid phase and the vapour phase become similar, it is assumed that the UCEP would be of the form, [l_1 + (l_2 = g)]. This agrees with the observations made by Poot and de Loos (1999). Due to the occurrence of the UCEP [l_1 +(l_2 = g)] at a temperature higher

than the critical temperature of the one component (R-23, in this case), and with no apparent discontinuities in the three phase line, this system is classified as a VKS type III system.

For the critical loci, there are several disagreements between the estimated critical loci and the experimental sub-critical phase equilibrium data. These are likely due to the thermodynamic model becoming less accurate as the critical point is approached. The poor description of the system will therefore be inherent within the calculation of the critical locus curve by the method of Heidemann and Khalil.

R-23 (1) + n-Octane (2)

The data for the R-23 + n-octane system are presented in the manuscript given in Appendix E as well as in Figure 6.12. Appendix E also provides a detailed discussion of the experimental data and the modelling.

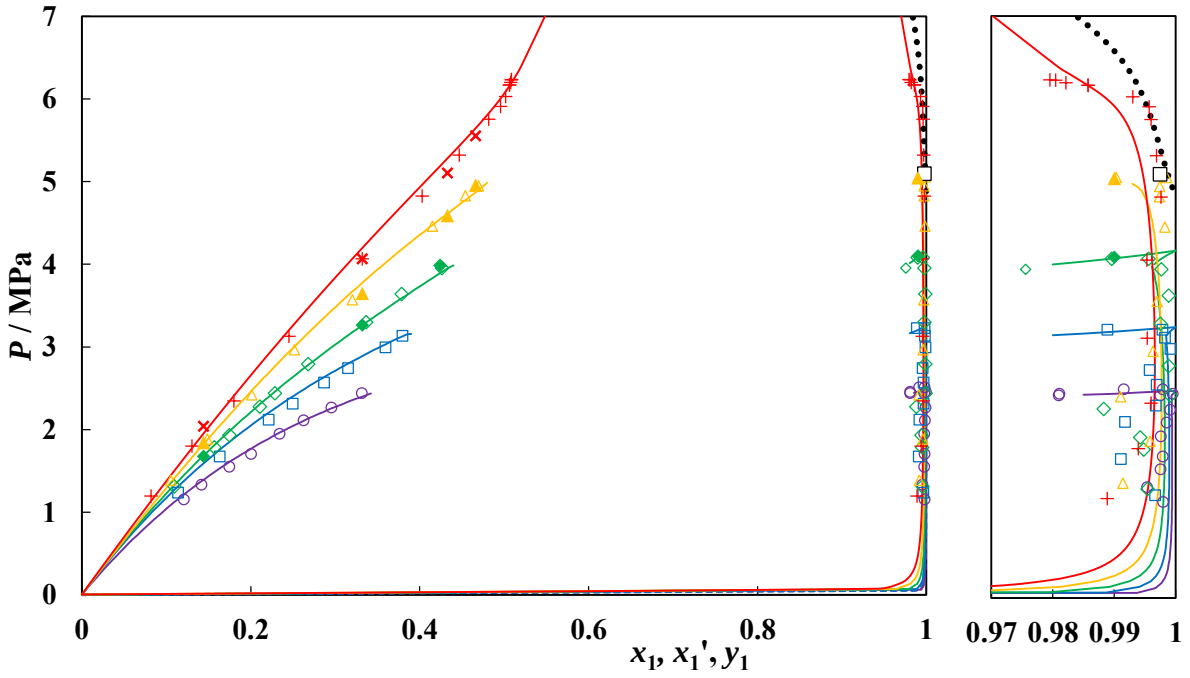

Figure 6.12. *P-x-x'-y* plot of the binary system of R-23 (1) + n-octane (2). Experimental data measured with the static-analytic apparatus at temperatures of *T* = ○, 272.9 K; □, 283.0 K; ◇, 293.0 K; △, 303.1 K; +, 313.2 K. Bubble point data measured using the variable-volume apparatus at temperatures of *T* = ◆, 293.2 K; ▲, 303.2 K; X, 313.2 K. Solid lines, PR-MC + WS/NRTL model; ••••, calculated critical locus curve (Heidemann and Khalil method); □, extrapolated critical points (Ungerer et al. method).

There is good agreement between the two experimental data sets (from the static-analytic and the static-synthetic). The thermodynamic models provide good descriptions of the experimental data, with a pressure ARD of -1.0 % and a vapour phase composition ARD of 0.1 %. The deviations for all of the regressions, described in Appendix E, show that the temperature dependent models are unable

to produce the same degree of correlation of the experimental data as the temperature independent parameters. This lends itself to a small amount of concern, as the temperature dependent parameters are a requirement for the process simulation. On closer examination of the data, it appears that the discrepancies are most exaggerated close to the extrema of the temperature range, with the models providing a good description of the phase behaviour closer to the R-23 critical temperature. This is important, as this is the range within which a SCF process would most likely operate. In addition to the good phase behaviour description, the models are also capable of providing a good description of the liquid-liquid immiscibilities throughout the temperature range.

As with the R-23 + n-heptane system, the R-23 + n-octane system is also classified as a VKS type III system, due to the occurrence of an UCEP [$l_1 + (l_2 = g)$] above the R-23 critical temperature, as well as the apparent continuity of the three phase curve up to the UCEP.

R-23 (1) + n-Nonane (2)

This system is examined in the manuscript given in Appendix F. The experimental data are plotted in Figure 6.13.

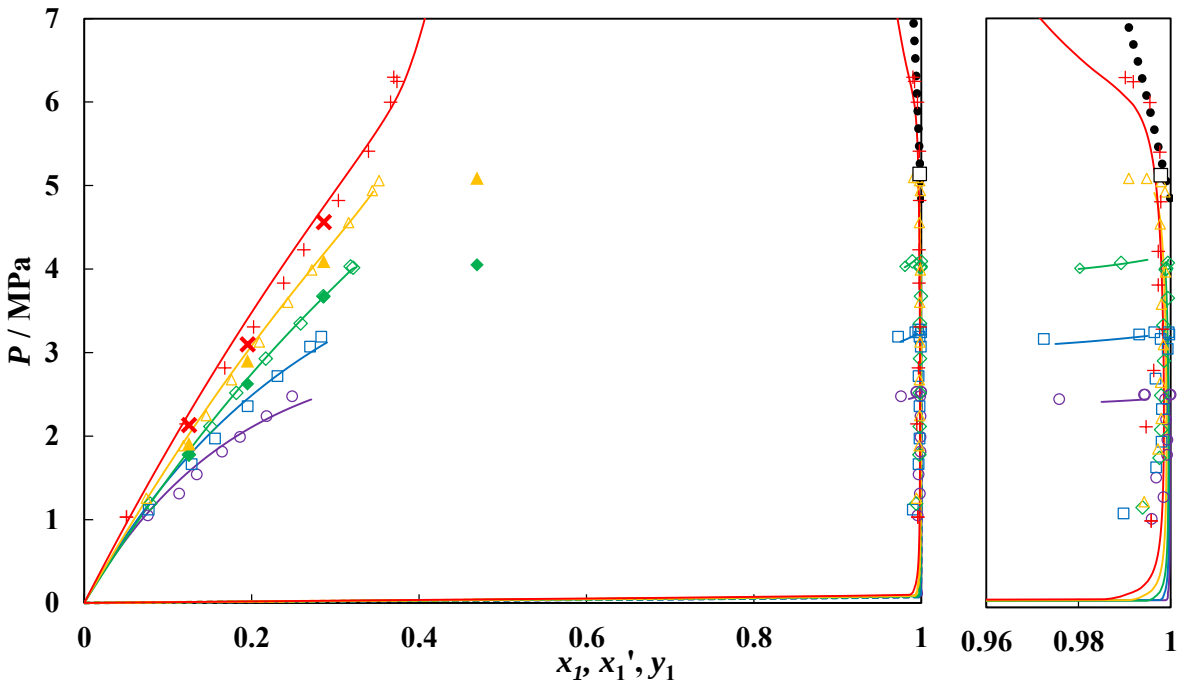

Figure 6.13. ***P-x-x'-y*** **data for the binary system of R-23 (1) + n-nonane (2). Data was measured using a static-analytic apparatus at the temperatures,** T **= ○, 272.9 K; □, 283.0 K; ◇, 293.1 K; △, 303.1 K; +, 313.2 K. Data measured using a variable-volume apparatus at temperatures,** T **= ◆, 293.0 K; ▲, 303.1 K; X, 313.2 K. Solid lines, PR-MC + WS/NRTL model; ☐, mixture critical point (Ungerer et al. method); ••••, mixture critical locus curve (Heidemann and Khalil method).**

The data from the static-analytic and the static-synthetic apparatuses were found to be in agreement. The temperature dependent models did not provide the same accuracy in describing the experimental data as the temperature independent models, with the pressure ARDs mostly being less than 1.0 %, but the pressure ARD for temperature dependent model being 2.7 %. This is likely due to differing trends of the model parameters above and below the R-23 critical temperature. In contrast, the vapour phase ARDs were less than 0.2 % for the temperature dependent and temperature independent models.

The liquid-liquid immiscibilities of the system were fairly well described by the model and the three phase line appeared to disappear below the critical temperature of R-23. Whether another three-phase line appeared at higher temperatures was not observed in this study. If the three phase line does occur at higher temperatures, then this system would be a VKS type IV system.

R-23 (1) + n-Decane (2)

The data for this system and the discussion of the measured data and the model results are also presented in Appendix F. A *P-x-x'-y* plot of the experimental data and the model is presented in Figure 6.14.

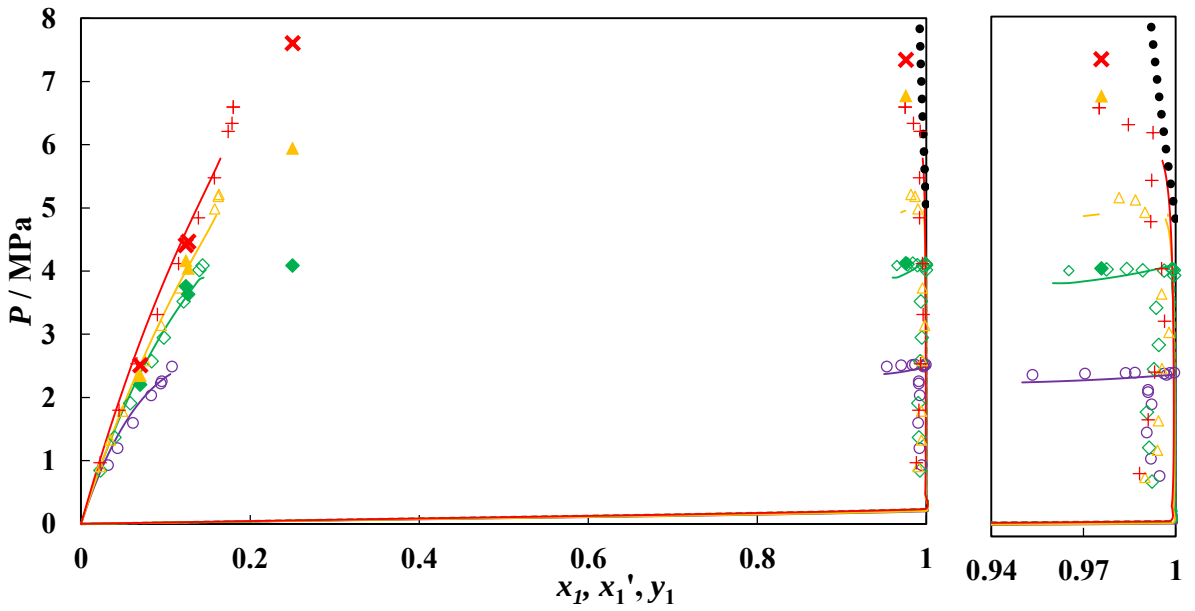

Figure 6.14. *P-x-x'-y* data for the binary system of R-23 (1) + n-decane (2). Data was measured using a static-analytic apparatus at temperatures, *T* = ○, 272.9 K; ◇, 293.1 K; △, 303.1 K; +, 313.3 K. Data measured using a variable-volume apparatus at temperatures of T = ◆, 293.0 K; ▲, 303.1 K; X, 313.2 K Solid lines, PR-MC + WS/NRTL model; ••••, mixture critical locus curve (Heidemann and Khalil method).

The pressure and vapour phase ARDs for the temperature dependent PR-MC + WS/NRTL model for this system are -2.3 % and 0.7 % respectively. The model under-predicts the three-phase pressures

for this system, and is also not capable of accurately describing the location of the UCEP. It does, however, predict a three phase region for the 303.1 K isotherm, despite this not being described by the experimental data. The upper regions of the LLE domes that occur with the (303.1 and 313.2) K isotherms are not investigated in this study. As with the R-23 + n-nonane system, it is suggested that this system be classified as a VKS type IV system.

R-23 (1) + n-Undecane (2)

The data and the model for the R-23 + n-undecane system are given in Appendix F, and plotted in Figure 6.15.

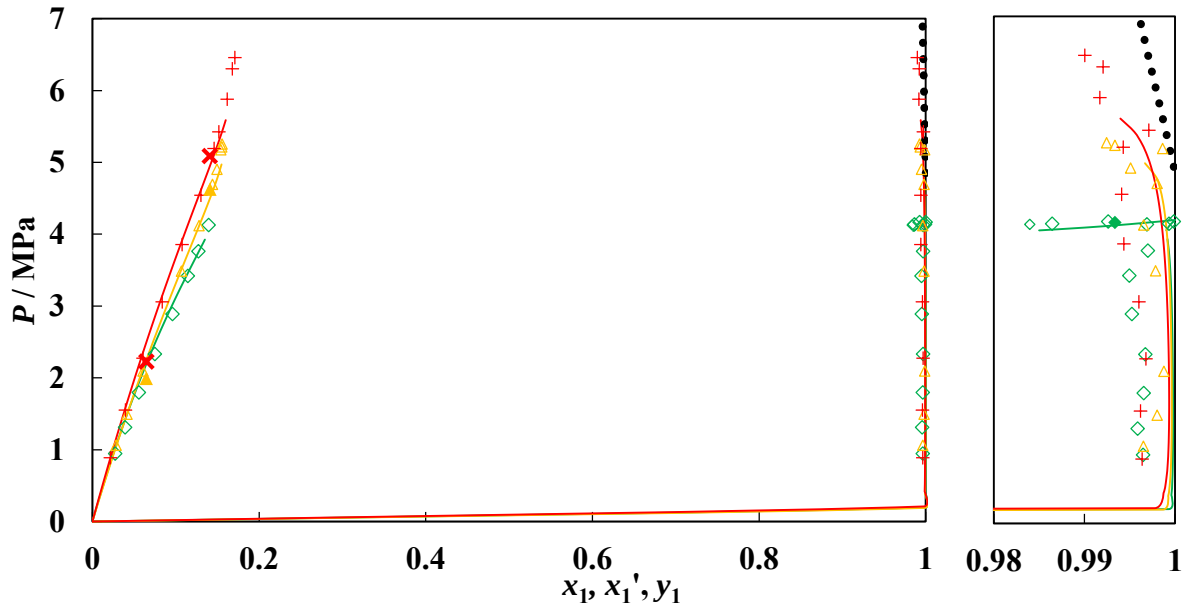

Figure 6.15. *P-x-x'-y* data for the binary system of R-23 (1) + n-undecane (2). Data was measured using a static-analytic apparatus at temperatures of T = ◇, 293.1 K; △, 303.2 K; +, 313.3 K. Data was also measured using a variable-volume apparatus at temperatures of T = ◆, 293.0 K; ▲, 303.1 K; X, 313.2 K. Solid lines, PR-MC + WS/NRTL model; ••••, mixture critical locus curve (Heidemann and Khalil method).

Only three isotherms were measured for this system, as this was the minimum number required to adequately fit temperature dependent parameters, as well as sufficiently covering the range for which data was required. For this system, the large region of immiscibility (three phase region) meant that small changes in composition resulted in fairly large pressure changes. The models accurately predicted the three phase region at 293.0 K, while correctly predicting only two phases at the higher temperatures. The ARDs for pressure and vapour phase composition were -7.0 % and 0.1 % respectively. The ARD for pressure was excessively high, although it is estimated that this was due to poor prediction of the three phase pressures for the system.

It was postulated that this system should also be classified as a VKS type IV system, as it displayed similar characteristics to the R-23 + n-nonane and R-23 + n-decane systems.

R-23 (1) + 1-HEXENE (2)

The manuscript provided in Appendix G provides the data and a discussion on the modelling and the critical locus curve for the R-23 + 1-hexene system. The *P-x-y* plot for this system is given by Figure 6.16.

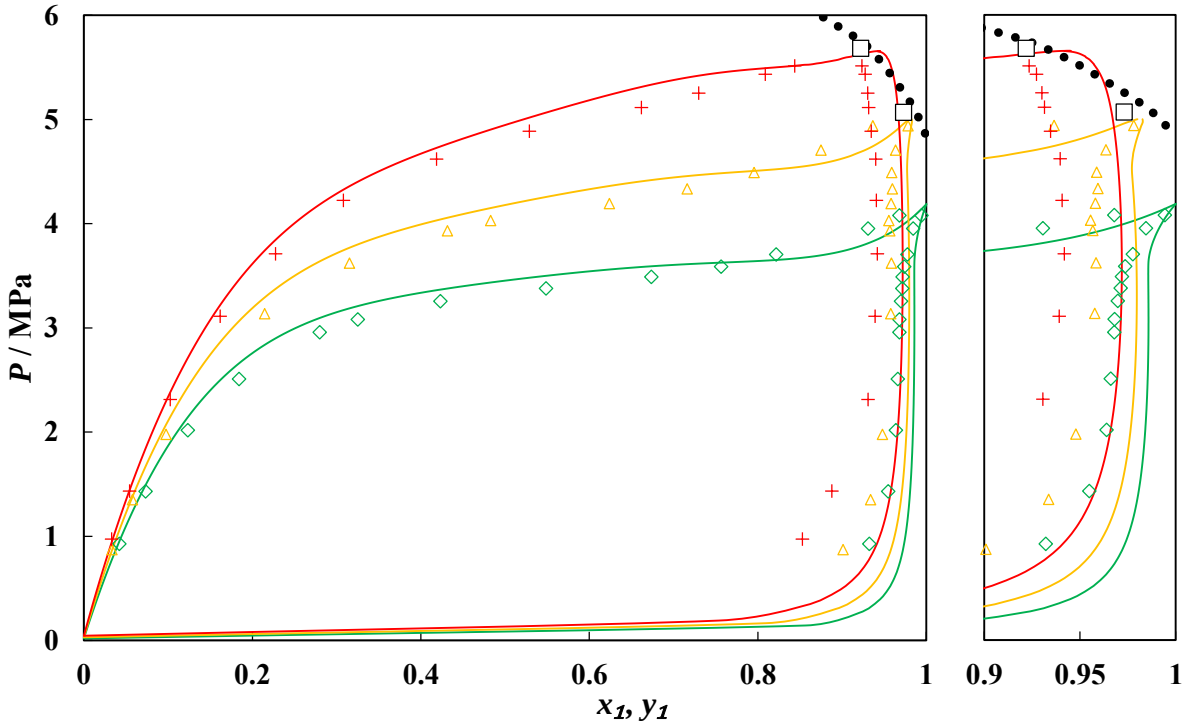

Figure 6.16. *P-x-y* data for the binary system of R-23 (1) + 1-hexene (2). Data measured at temperatures of *T* = ◇, 293.1 K; △, 303.1 K; +, 313.3 K. Solid lines, PR-MC + WS/NRTL model; □, mixture critical point (Ungerer et al. method); ••••, mixture critical locus curve (Heidemann and Khalil method).

This system exhibits the "bird's-beak" phenomenon around the R-23 critical point, but the phenomenon becomes less pronounced and then disappears as the temperature increases above the critical temperature. The thermodynamic models were found to over-estimate the bubble point pressures at compositions of between 0.2 and 0.8, as well as provide a poor description of the vapour phase compositions. ARDs for the pressure and vapour phase composition for this system were less than $\pm$ 0.5 %. Alternatively, however, the AARDs for the model are 3.2 and 4.5 % respectively. These deviations give a more accurate description of the poor fit of the model to the experimental data. The poor fit of the model is possibly due to the intermolecular forces that could come into play because of the double bond present in the 1-hexene molecules.

No liquid-liquid immiscibility was observed for this system in the temperature range that was investigated. Whether LLE would occur at lower temperatures was not investigated. If a three phase region existed at lower temperatures, then this system would be described as a VKS type II system.

R-23 (1) + 3-METHYLPENTANE (2)

The data for the R-23 + 3-methylpentane system are also provided in Appendix H, and are plotted in Figure 6.17.

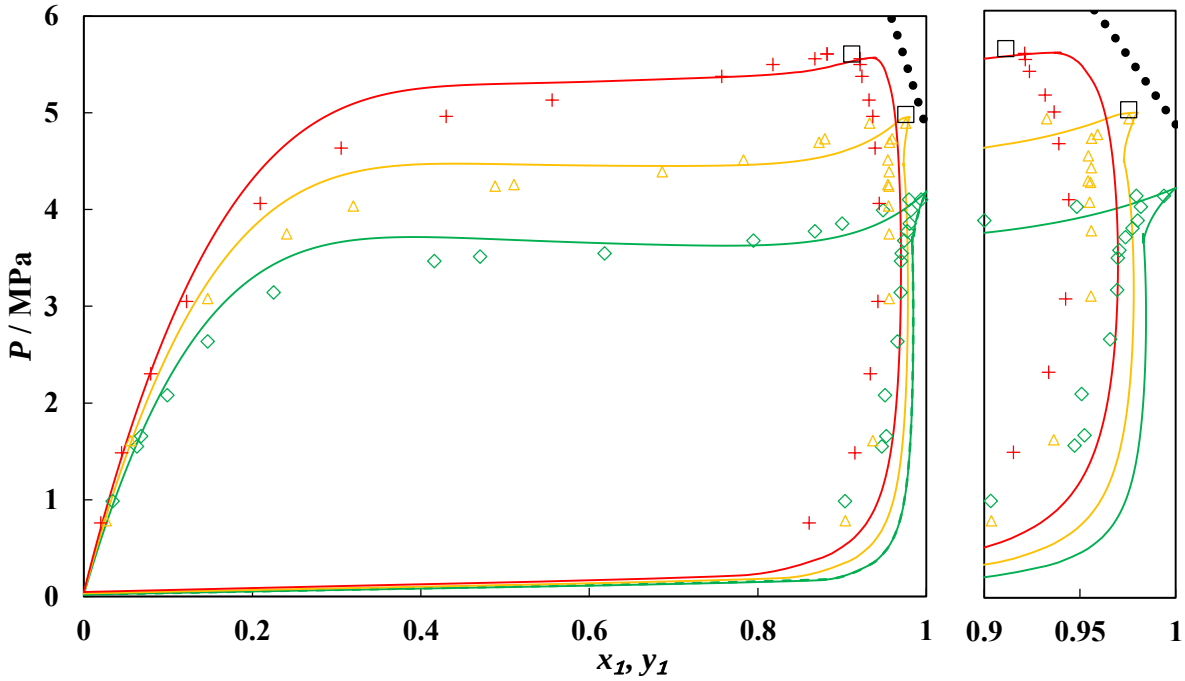

Figure 6.17. *P-x-y* data for the binary system of R-23 (1) + 3-methylpentane (2). Data measured at temperatures of *T* = ◇, 293.1 K; △, 303.2 K; +, 313.3 K. Solid lines, PR-MC + WS/NRTL model; □, mixture critical point (Ungerer et al. method); ••••, mixture critical locus curve (Heidemann and Khalil method).

For this system, the "bird's-beak" phenomenon is once again identified. The thermodynamic models give a poor description of the system, with the pressures being over-predicted in the mid-composition ranges (ARD of 2.4 %), and the composition of the vapour phase being poorly described (ARD of 1.6 %). Significantly, the description of the bubble point curve is improved by replacing the NRTL activity coefficient model with the UNIQUAC activity coefficient model (ARD for pressure of -0.4 %). However, this modification causes the description of the vapour phase composition by the model to deteriorate (ARD for vapour phase composition of -2.8 %).

There are significant discrepancies between the critical loci that were extrapolated using the technique of Ungerer et al. and those calculated based on the thermodynamic model by the method of Heidemann and Khalil. On observation of Figure 6.17, it appears that the calculated values are incorrect, while the values that were extrapolated from the sub-critical data are nearer to the actual critical locus curve. The error in the calculated values is likely due to the poor description of the dew point curve by the model. This poor description of the sub-critical data is then projected to the critical locus curve.

As with the R-23 + 1-hexene model, with no liquid-liquid immiscibilities observed in the temperature range that was studied, the classification of the system according to the VKS scheme cannot be made with complete confidence. Observing the change in the shapes of the isotherms with decrease in temperature leads to a prediction that liquid-liquid immiscibility occurring at lower temperatures. The system is therefore classified as a VKS type II system.

R-23 (1) + METHYLCYCLOHEXANE (2)

For the R-23 + methylcyclohexane (MCH) system (Appendix H and Figure 6.18), there is a large region of liquid-liquid immiscibility observable. The UCEP [l_1 (l_2 = g)] for the system occurs at a temperature only slightly above the R-23 critical temperature. At lower pressures, a liquid phase and a vapour phase are present, but at higher pressures, both of the phases that are present are liquids. The "bird's-beak" phenomenon occurs for this system at temperatures close to the critical temperature of R-23.

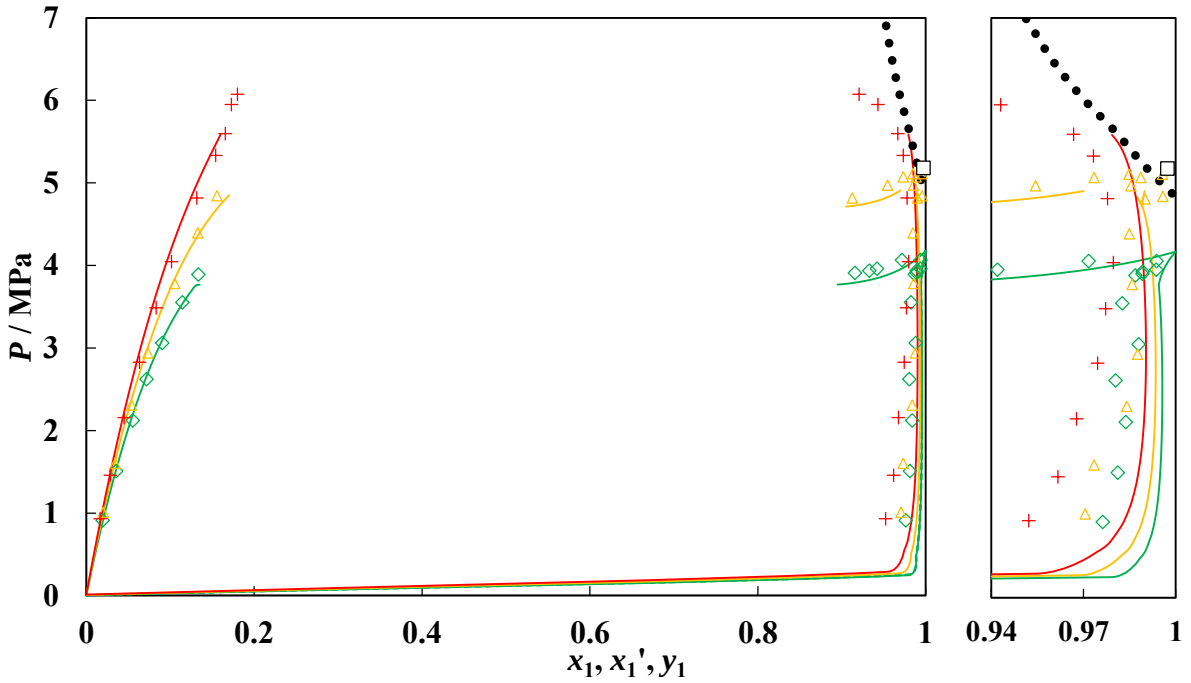

Figure 6.18. *P-x-x'-y* data for the binary system of R-23 (1) + methylcyclohexane (2) at temperatures of ◇, 293.0 K; △, 303.1 K; +, 313.2 K. Solid lines, PR-MC + WS/NRTL model; □, mixture critical locus (Ungerer et al. method); ••••, mixture critical locus curve (Heidemann and Khalil method).

The thermodynamic models were capable of describing the bubble pressure curves fairly accurately, although the dew point curve was not as accurately described. The ARDs for pressure and vapour phase composition are both less than 0.6 %, with the AARDs being less than 3.0 %. The model was able to predict the occurrence of VLLE at (293.0 and 303.1) K, as well as the significant lack of a third phase at 313.2 K. The "bird's beak" phenomenon is well described by the model at 293.0 K, but is not

described at all at a temperature of 303.1 K. There is little difference between the temperature dependent and temperature independent models for this system.

The occurrence of a three phase line (or lack thereof) at low temperatures for this system must be known for complete clarity on the classification of this system according to the VKS scheme. This system is likely one of type III, type IV or type V, with the differentiation between these systems being linked to the occurrence of a LCEP or an UCST.

R-23 (1) + TOLUENE (2)

The manuscript given in Appendix H describes the data that were measured for the R-23 + toluene system. In this Appendix, the thermodynamic modelling is described and the system behaviour is discussed. The data for this system are also plotted in Figure 6.19. For the lower temperature isotherms (293.1 and 303.1) K, the model describes the bubble pressure curve well. For the 313.2 K isotherm, the model is not able to accurately describe the bubble curve. The description of the vapour phase compositions by the model across all of the isotherms is fairly poor, with most of the compositions being over-predicted. The model is, however, capable of predicting the "bird's-beak" behaviour of the system. For this system, the ARDs for pressure and vapour phase composition are 2.2 % and 1.1 % respectively.

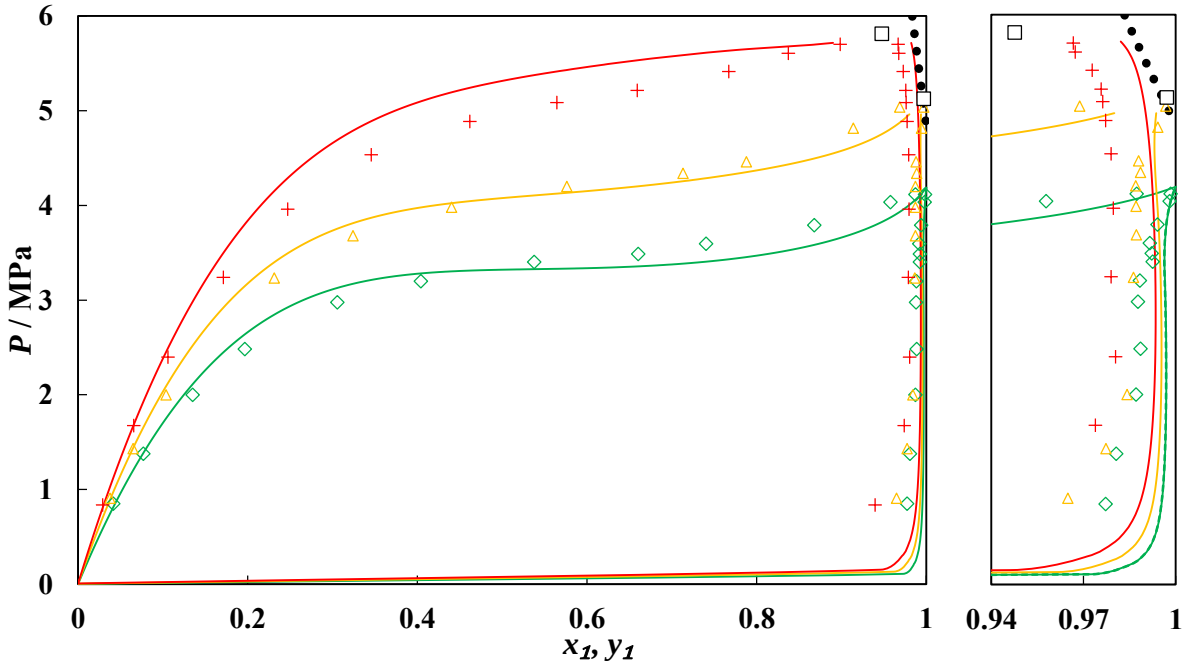

Figure 6.19. *P-x-y* data for the binary system of R-23 (1) + toluene (2) at temperatures of ◇, 293.1 K; △, 303.1 K; +, 313.2 K. Solid lines, PR-MC + WS/NRTL model; □, mixture critical loci (Ungerer et al. method); ••••, mixture critical locus curve (Heidemann and Khalil method).

In the same manner as with the classification of the R-23 + MCH system, the information that is available for the R-23 + toluene system is not sufficient to determine its classification type according to the VKS scheme. It is likely that this system is a VKS type III system, but the possibility also exists that it is a type IV or type V system. Further information for the system is required before this can be accurately determined.

R-23 (1) + WATER (2)

The R-23 + water system exhibited low mutual solubilities, and therefore, due to the narrow composition ranges of the bubble and dew curves, only a limited number of data points were measured per isotherm. The VLE and VLLE data, measured with the static-analytic apparatus are presented in Table 6.14. The model was not capable of predicting the pressures of the system, with an ARD for the pressure of 18.0 % in comparison to an ARD for the vapour phase composition of 0.1 %.

Table 6.14. Experimental *P*-x_1-x_1'-*y* data for the binary system of R-23 (1) + water (2) at temperatures of *T* = (293.15 to 313.15) K.

T / K	*U*(*T*) / K	*P* / MPa	*U*(*P*) / MPa	x_1	*U*(x_1) [a]	x_1'	*U*(x_1') [a]	y_1	*U*(y_1) [a]
293.15	0.04	1.632	0.006	0.001	0.0006			0.996	0.0016
293.16	0.04	2.720	0.006	0.004	0.0012			0.997	0.0016
293.16	0.04	3.598	0.009	0.004	0.0007			0.998	0.0012
293.16	0.04	4.143	0.005	0.006	0.0012	0.997	0.0013	0.998	0.0019
303.16	0.04	1.825	0.008	0.002	0.0011			0.992	0.0011
303.15	0.04	3.081	0.007	0.002	0.0018			0.995	0.0004
303.15	0.04	4.081	0.009	0.003	0.0014			0.997	0.0011
303.14	0.04	5.207	0.004	0.004	0.0018			0.998	0.0008
303.15	0.04	5.269	0.004	0.006	0.0024			0.996	0.0015
303.16	0.04	5.480	0.011	0.004	0.0016			0.997	0.0006
313.15	0.05	1.630	0.009	0.002	0.0025			0.996	0.0011
313.16	0.05	2.648	0.005	0.002	0.0016			0.996	0.0002
313.15	0.05	4.312	0.008	0.004	0.0013			0.998	0.0007
313.15	0.05	5.708	0.005	0.005	0.0005			0.999	0.0005
313.14	0.06	6.756	0.009	0.006	0.0010			0.999	0.0012

[a] combined expanded uncertainties in the experimental data, *U*, were calculated with a coverage factor of k = 2

The phase equilibria data were used to regress model parameters for the system, which are provided in Table 6.8. Due to the low mutual solubilities, which are of a similar magnitude to the uncertainties, the statistical data that are presented for the regression show a poor ability of the model to accurately describe the data. In order to observe the models and the experimental data on a *P*-*x*-*y* plot (Figure 6.20), the composition axis requires significant magnification. This magnification exaggerates the deviations between the data and the model.

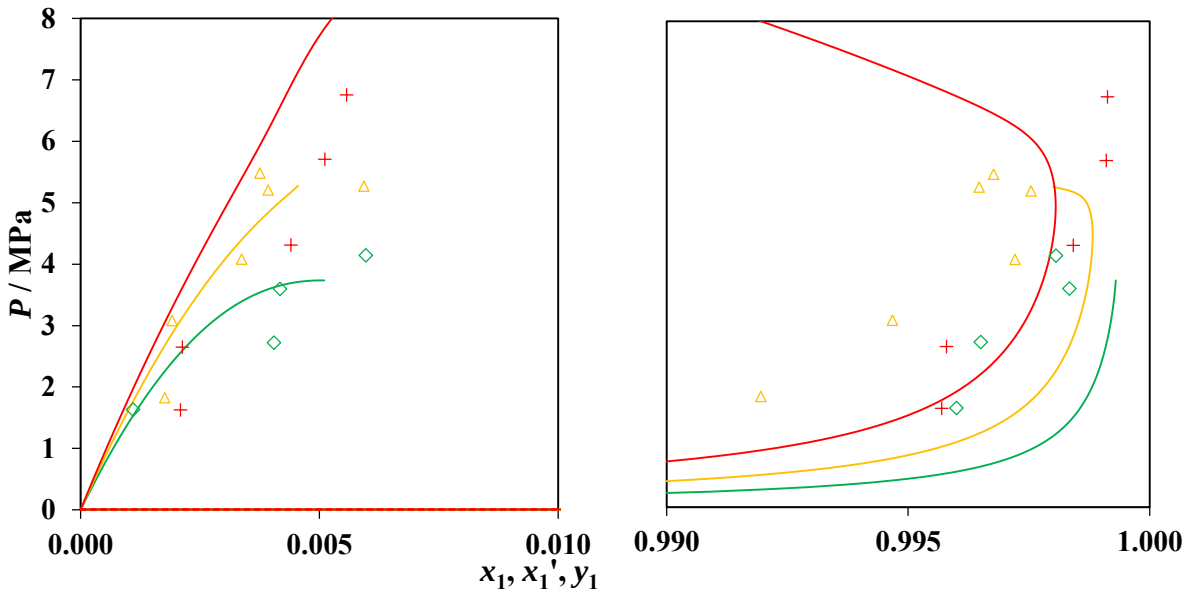

Figure 6.20. ***P*-x_1-x_1'-*y*** **data for the binary system of R-23 (1) + water (2) at temperatures of ◇, 293.15 K; △, 303.15 K; +, 313.15 K. Solid lines, PR-MC + WS/NRTL model.**

The model does not describe the presence of three phases at 293.15 K. Two liquid phases were observed experimentally, but for all intents and purposes, the compositions of the one liquid phase and the vapour phase were identical, meaning that this experimental VLLE will not be observable on Figure 6.20. The temperature dependence of this system is, however, evident in Figure 6.20.

It is likely that the UCEP for this system occurred at a temperature very close to 293.15 K, and therefore below the critical temperature of R-23. This system is therefore probably either a VKS type II or VKS type IV system. Knowing whether another three phase region occurs at higher temperatures would enable the system classification to be better distinguished.

6.1.6. R-116 Systems

The summaries of the measurements of binary phase equilibrium data for seven systems, which were undertaken in this investigation, are presented in Table 6.15. For two of these systems, R-116 + n-heptane and R-116 + n-octane, the bubble pressure data was measured using a static-synthetic apparatus in addition to the data measured with the static-analytic apparatus, in order to validate it.

Table 6.15. Systems containing R-116 measured in this study

System	*T* / K	*P* / MPa	N_I	N_D	N_B	Located in Appendix
R-116 + n-heptane	293.0 to 313.2	0.81 to 4.08	3	36	10	A.2.
R-116 + n-octane	293.1 to 313.1	0.86 to 4.27	3	33	10	A.3.
R-116 + n-decane	293.1 to 313.2	0.90 to 5.44	3	27	0	A.4.
R-116 + 1-hexene	293.1 to 313.2	0.85 to 3.75	3	37	0	A.5.
R-116 + 3-methylpentane	293.1 to 313.1	0.90 to 3.79	3	36	0	A.5.
R-116 + methylcyclohexane	293.1 to 313.2	0.91 to 4.22	3	35	0	A.6.
R-116 + toluene	293.1 to 313.1	1.00 to 4.61	3	20	0	A.6.

[a] including the temperature, *T*, and pressure, *P*, ranges, the number of isotherms measured, N_I, the number of complete data points reported, N_D, the number of bubble points reported, N_B, and the appendix in which the peer reviewed paper is located.

In addition to the data for the seven binary systems listed in Table 6.15, VLE data for several other systems of interest were also reported in literature. VLE data for the R-116 + n-propane system was reported by Ramjugernath et al. (2009), and phase equilibrium data was measured by Ramjugernath et al. (2015) for the R-116 + n-hexane system. A few data points for the R-116 + water system are also presented in this section.

Table 6.16. Regressed parameters for the PR-MC + WS/NRTL model, for binary systems containing R-116.

	T / K	k_{12}	τ_{12} / K [a]	τ_{21} / K [a]	ARD [b]		AARD [c]	
					P	*y*	*P*	*y*
R-116 + n-hexane	*288.2 to 296.2*	0.374	307.3	383.5	-0.03	0.01	1.46	0.38
R-116 + n-heptane	*293.0 to 313.2*	0.479	160.3	788.8	0.99	0.94	2.68	3.93
R-116 + n-octane	*293.0 to 313.2*	0.496	227.6	735.9	1.05	-1.26	2.46	1.37
R-116 + n-decane	*293.1 to 313.2*	0.559	332.8	536.2	-1.80	-0.25	6.99	0.76
R-116 + 1-hexene	*293.1 to 313.1*	0.391	242.1	444.2	-1.03	0.26	1.74	0.38
R-116 + 3-methylpentane	*293.1 to 313.1*	0.356	258.6	415.3	0.51	0.45	2.68	0.62
R-116 + methylcyclohexane	*293.1 to 313.1*	0.411	202.4	656.1	0.30	-0.29	4.84	1.46
R-116 + toluene	*293.1 to 313.1*	0.721	-20.50	1001.1	-3.62	-1.15	6.76	1.15
R-116 + water	*293.2 to 313.2*	1.319	1618.7	2136.0	-12.1	0.43	18.1	0.47

[a] τ_{12}, τ_{21} for the NRTL activity coefficient model

[b] average relative deviation, $$ARD(\bar{\theta}) = \frac{100}{N_p}\sum_{1}^{N_p}\frac{\bar{\theta}_{exp} - \bar{\theta}_{calc}}{\bar{\theta}_{exp}}$$

[c] absolute average relative deviation, $$AARD(\bar{\theta}) = \frac{100}{N_p}\sum_{1}^{N_p}\frac{\left|\bar{\theta}_{exp} - \bar{\theta}_{calc}\right|}{\bar{\theta}_{exp}}$$

The parameters for the PR-MC + WS/NRTL models that were fitted to the data for the nine binary systems are tabulated in Table 6.16. The temperature ranges over which the models were regressed, as well as the statistical data for each of the regressions are included in the table.

Although in some cases, the deviations of the models from the experimental data appear to be fairly large, a single model was necessary for all of the systems, in order for a process simulation to be performed. The PR-MC + WS/NRTL model was therefore used in this study, as it provided a fairly good fit of the experimental data across the entire spectrum of systems studied.

Brief summaries of the data and the models for each of the R-116 systems that were investigated are presented below. The data sets, as well as more detailed discussions of the data and the modelling for each of the systems are presented in several journal manuscripts, which are included in Appendices D to H.

R-116 (1) + n-Propane (2)

The VLE isotherms reported by Ramjugernath et al. (2009) were extrapolated by the method of Ungerer et al. up to the critical loci. These extrapolated critical loci were then compared to the critical loci that were measured with the critical point determination apparatus. Both the extrapolated and the measured critical loci are presented in Table 6.17.

Table 6.17. Critical loci (*T-P-x*) for the R-116 + n-propane system.

Method of Ungerer et al. [a]			Critical Point Determination Apparatus [b]					
T_c / K	P_c / MPa	$x_{c,1}$	T_c / K	$U(T_c)$ / K	P_c / MPa	$U(P_c)$ / MPa	$x_{c,1}$	$U(x_{c,1})$
296.23	3.14	0.81	369.89	0.10	4.251	0.008	0	-
308.21	3.46	0.58	361.98	0.29	4.314	0.029	0.071	0.005
323.19	3.85	0.40	348.24	0.12	4.262	0.038	0.179	0.005
			338.71	0.31	4.164	0.012	0.259	0.004
			323.44	0.21	3.852	0.019	0.411	0.003
			313.33	0.24	3.608	0.017	0.521	0.003
			298.50	0.22	3.171	0.012	0.752	0.002

[a] based upon the experimental data reported by Rumjugernath et al. (2009).

[b] combined expanded uncertainties in the experimental data, *U*, were calculated with a coverage factor of k = 2

To obtain a critical locus curve from the critical loci that were measured, RK type correlations were fitted to the experimental data, relating the temperature or the pressure to the composition. The number of parameters used for the correlations were increased until significant reductions in the root mean squares (RMS) of the deviations between the experimental and correlation could no longer be achieved by the addition of further parameters. An increase in the number of parameters corresponds to an increase in the order of the correlation. The parameters for the correlations are presented in Table 6.18.

Table 6.18. Parameters for the RK type correlations for the system of R-116 (1) + n-propane (2), describing the critical temperature, T_c, and critical pressure, P_c, as functions of the composition, $x_{c,1}$.

RK correlation parameters for $T_c(x_{c,1})$					
	RMS / K [a]	a_1	a_2	a_3	a_4
1st order	0.47	-64.71	-17.16		
2nd order	0.41	-65.53	-16.24	3.16	
3rd order	0.31	-65.83	-8.80	1.13	-22.94
RK correlation parameters for $P_c(x_{c,1})$					
	RMS / MPa [a]	b_1	b_2	b_3	b_4
1st order	1.99	0.044	-2.338		
2nd order	0.43	0.028	-2.133	3.162	
3rd order	0.31	0.030	-2.022	0.433	-0.281

[a] root mean square, $RMS(\bar{\theta}) = \frac{1}{N_p}\sqrt{\sum_{1}^{N_p} \bar{\theta}_{N_p}{}^2}$

The experimental data, the extrapolated data and the various RK type curves are plotted in Figure 6.21 and 6.22. There was a small improvement in the correlation of the experimental data by increasing the number of parameters used in the correlation from two to three. No significant improvement was achieved upon the addition of a fourth parameter to the correlation. The *T-x* projection of the critical locus curve was well described by the 1st order (2 parameter) RK correlation, whereas the *P-x* projection was well described by the 2nd order (3 parameter) RK correlation.

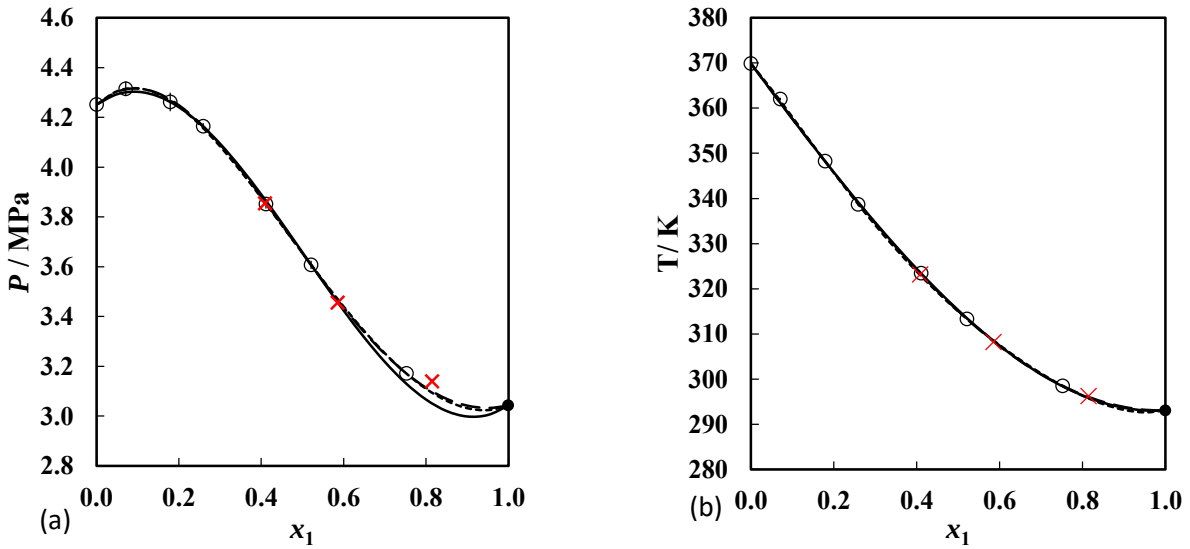

Figure 6.21. (a) *P-x* projection and (b) *T-x* projection of the critical locus curve for the R-116 (1) + n-propane (2) system. ○, critical loci measured with the critical point determination apparatus (uncertainty included as error bars); ×, critical loci extrapolated from the sub-critical coexistence data of Ramjugernath et al. (2009); •, R-23 critical point from the NIST ThermoData Engine (2013); ——, 1st order RK correlation; – –, 2nd order RK correlation; · · · ·, 3rd order RK correlation.

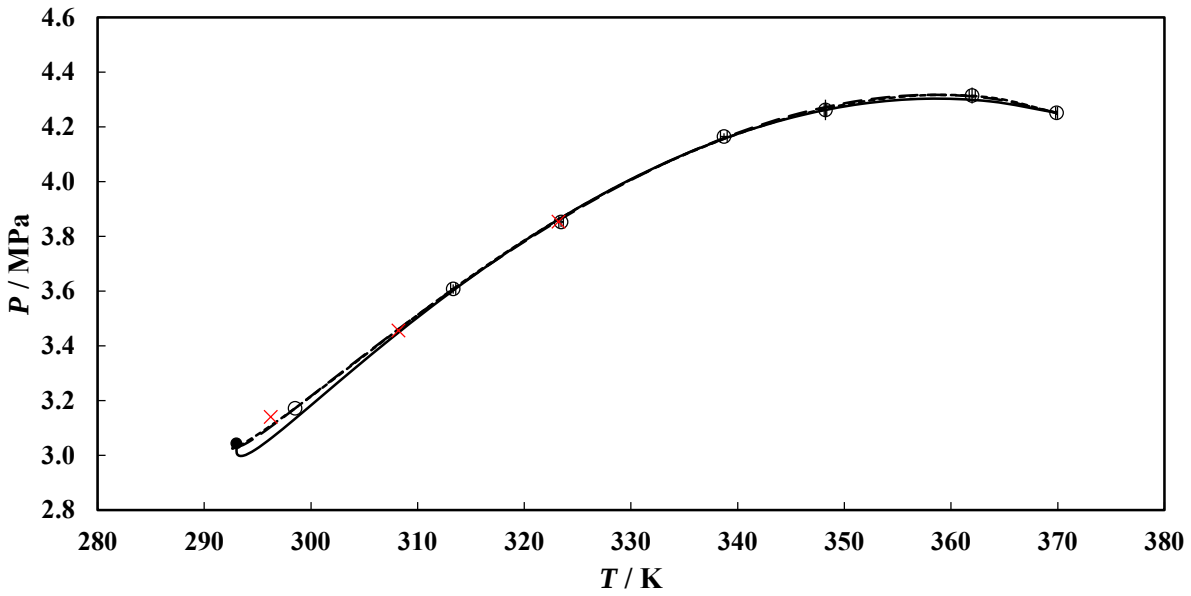

Figure 6.22. ***P-T*** **projection of the critical locus curve for the R-116 (1) + n-propane (2) system. ○, critical loci measured with the critical point determination apparatus (uncertainty included as error bars); ×, critical loci extrapolated from the sub-critical coexistence data of Ramjugernath et al. (2009); •, R-23 critical point from the NIST ThermoData Engine (2013); ——, 1st order RK correlation; – –, 2nd order RK correlation; · · · ·, 3rd order RK correlation.**

The critical loci that were extrapolated from the data reported by Ramjugernath et al. (2009) are in good agreement with the correlations that were fitted to the experimental data. Additionally, an experimentally measured point coincided almost exactly with an extrapolated point, verifying the ability of the method of Ungerer et al. to extrapolate the critical loci of a system from sub-critical experimental data.

Ramjugernath et al. observed a positive azeotrope at temperatures below the critical temperature of R-116 for this system. This azeotrope corresponds to the inflection of the critical locus curves projected by the higher order RK type correlations. There is no three phase line observable in the vicinity of the critical curve for this system, and it is therefore classified as a type II-A VKS system.

R-116 (1) + n-HEPTANE (2)

The R-116 + n-heptane system, which is presented in Appendix D as well as in Figure 6.23, exhibits a three phase region for approximately eighty percent of the composition range at temperatures of T = (293.0 and 303.1) K.

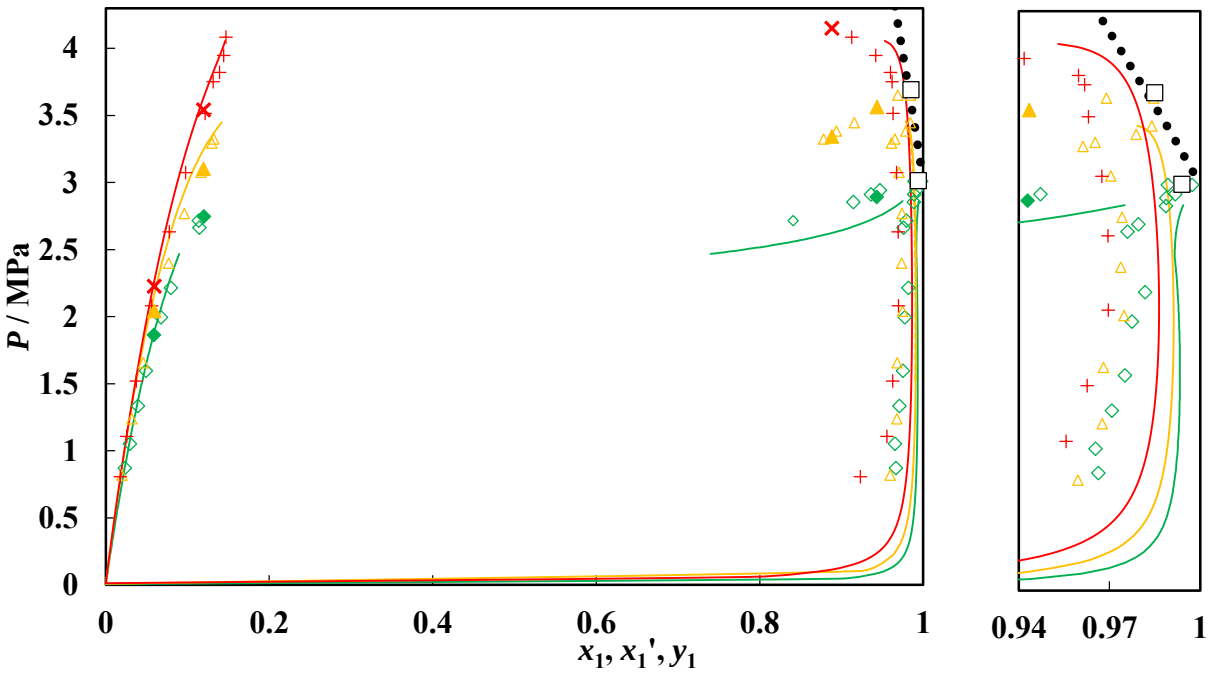

Figure 6.23. *P-x-x'-y* data for the binary system of R-116 (1) + n-heptane (2) measured using a static analytic apparatus, at temperatures of: ◇, 293.0 K; △, 303.1 K; +, 313.2 K. *P-x* data measured, using a variable volume apparatus, at temperatures of: ◆, 293.0 K; ▲, 303.1 K; X, 313.2 K. Solid lines, PR-MC + WS/NRTL model; □, extrapolated critical points; ••••, calculated critical locus curve.

With the UCEP occurring at a temperature of between (303.1 and 313.2) K, the 313.2 K isotherm did not exhibit VLLE, but rather, the VLE at lower pressures became LLE at higher temperatures (with only two phases present throughout). The models under-predicted the three phase pressure at 293.0 K. At 303.1 K, the PR-MC + WS/NRTL model did not describe the occurrence of VLLE. The ARDs for the temperature dependent model were less than 1.0 % for both pressure and vapour phase composition. Thus, apart from a poor ability of the model to predict liquid-liquid immiscibility, the model described the system well.

From the experimental data, it appears that the system exhibits the "bird's-beak" phenomenon, with the bubble and dew point curves of the lower temperature isotherms intersecting one another at a very acute angle. The regressed thermodynamic models did not, however, describe this phenomenon for any of the isotherms. Due to the position of the UCEP, as well as the behaviour of the three phase line, this system was classified as a type III VKS system.

R-116 (1) + n-Octane (2)

The R-116 + n-octane system was presented in Appendix E as well as in the *P-x-x'-y* plot in Figure 6.24. The bubble pressure data confirmed the validity of the data measured using the static-analytic apparatus. The region in which liquid-liquid immiscibility occurred increased from 80 % of the composition range for the R-116 + n-heptane system to approximately 90 % of the composition range for the R-116 + n-octane system.

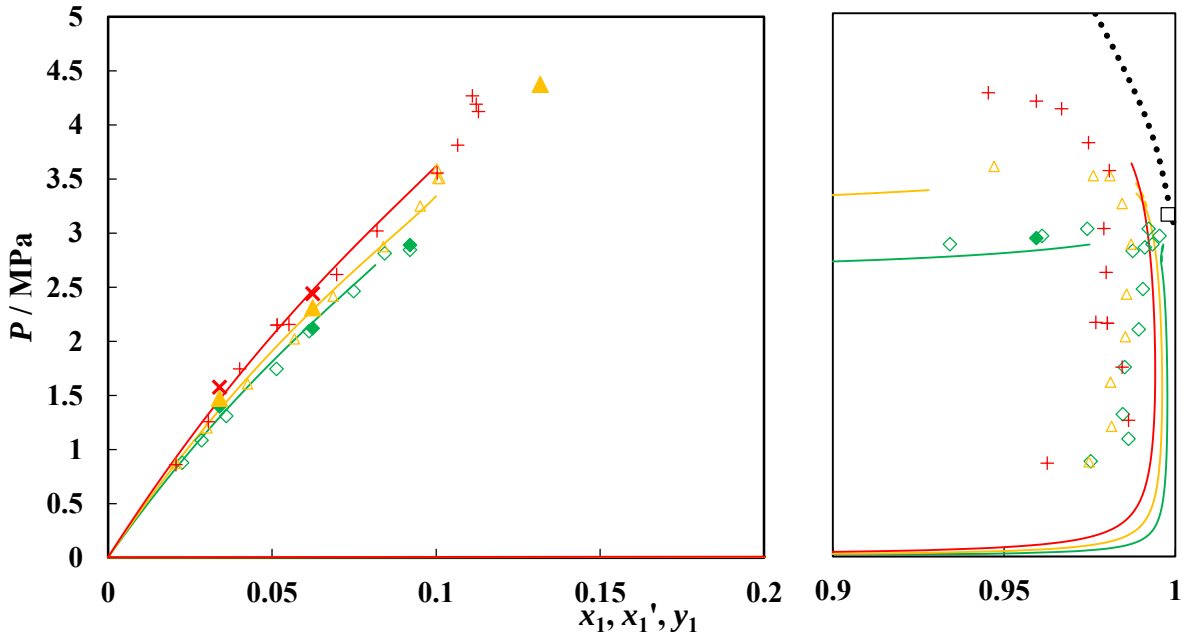

Figure 6.24. *P-x-x'-y* plot of the binary system of R-116 (1) + n-octane (2). Experimental data measured using the static-analytic apparatus at temperatures of *T* = ◇, 293.1 K; △, 303.1 K; +, 313.1 K. Experimental bubble point data measured using the variable-volume apparatus at temperatures of *T* = ◆, 293.0 K; ▲, 303.1 K; X, 313.2 K. Solid lines, PR-MC + WS/NRTL model; ••••, calculated critical locus curve (Heidemann and Khalil method); □ , extrapolated critical point (Ungerer et al. method).

The thermodynamic model provides a good description of most of the experimental data, although substantial deviations occur between the experimental and modelled three-phase region. The model under-predicts the solubility of the n-octane in the R-116 and over-predicts the solubility of the R-116 in the n-octane. The ARDs for the system are 1.1 % and -1.3 % for pressure and vapour phase composition respectively. This system is classified as a VKS type III system, based on the location of the UCEP and the behaviour of the three phase line.

As with the R-23 + n-alkane systems, an increase in the n-alkane chain length resulted in the temperature independent model giving a better description of the experimental data than the temperature dependent model. Despite this, the deviations of the temperature dependent model from the experimental data remained small, with an ARD of less than 3 % for pressure and less than 2

% for vapour phase composition. This good model description was probably due to all three isotherms being measured at temperatures above the critical temperature of R-116. This negated the effect of vastly different model parameters above and below the R-116 critical temperature, and enabled the linear temperature dependency of the model to provide a reasonable fit of the data.

R-116 (1) + n-Decane (2)

The experimental data and the thermodynamic model for the R-116 + n-decane system are examined in Appendix F. The *P-x-x'-y* data for this system was plotted in Figure 6.25.

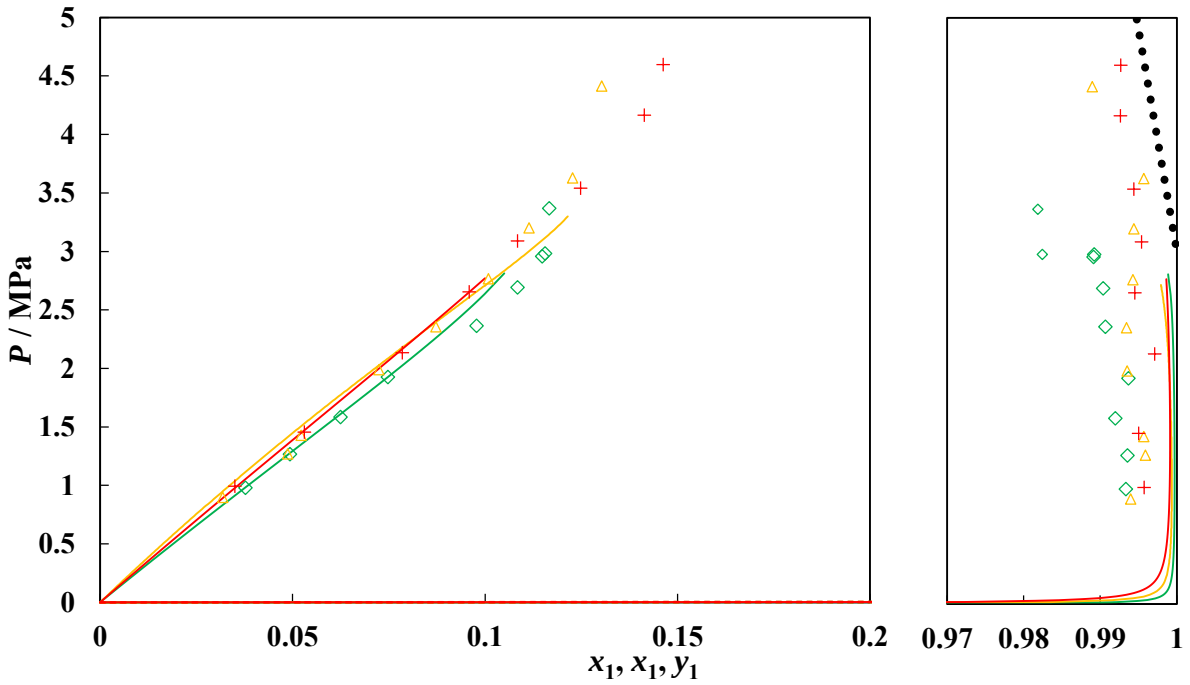

Figure 6.25. *P-x-x'-y* data for the binary system of R-116 (1) + n-decane (2). Data was measured using the static-analytic apparatus at temperatures of T = ◇, 293.1 K; △, 303.1 K; +, 313.2 K. Solid lines, PR-MC + WS/NRTL model; ••••, mixture critical locus curve (Heidemann and Khalil method).

The trend of an increase in the size of the region of immiscibility below the UCEP with increased n-alkane chain length is also observed for this system. Interestingly, however, for this system at a constant pressure above 3.5 MPa, the solubility of the R-116 in the n-decane is proportional to the temperature. This differs from for the R-116 systems containing the shorter chain length n-alkanes, in which at a constant pressure, the solubility of the R-116 in the n-alkane is inversely proportional to the temperature. The description of the bubble curve by the model is good, but for the dew curve, there is a discrepancy between the model and the experimental data, throughout the pressure range, with a maximum deviation of 1.0 %. The ARDs for pressure and vapour phase composition for this system are -1.8 and -0.3 % respectively.

The 293.0 K isotherm exhibits VLLE, but remarkably, the concentration of R-23 in the second liquid phase is greater than in the vapour phase. Thus the situation arises in which the vapour phase has a composition intermediate to the compositions of the two liquid phases. The thermodynamic model is not able to describe any three phase region for this system, let alone describe this peculiar phenomenon.

The three phase line for this system disappears at a temperature below the critical temperature of R-116, thereby indicating that the system be either a VKS type II or a VKS type IV system. The presence of liquid-liquid critical loci disqualifies the type II system, meaning that this system is most likely a type IV system.

R-116 (1) + 1-HEXENE (2)

The experimental data and the thermodynamic model for the R-116 + 1-hexene system are discussed in Appendix G. A plot of the *P-x-x'-y* data is given in Figure 6.26 below.

This system exhibits a three-phase region at (293.1 and 303.1) K, with the UCEP occurring at a temperature of between (303.1 and 313.1) K. The thermodynamic model provides a good fit for most of the experimental data, with the exception being the region close to the critical locus curve for both 303.1 and 313.1 K. The ARDs for the regression of the thermodynamic model for this system are -1.0 and 0.3 % respectively for pressure and vapour phase composition.

At all of the measured temperatures, the experimental data exhibits behaviour akin to the "bird's-beak" phenomenon with an inflection of the dew curve towards the critical loci. The model is not, however, capable of describing this behaviour at 313.1 K. Peculiarly, the calculated critical curve, which is dependent upon the model, appears to allow for the inflection of the dew curve. The disparity between the two may be due to the different convergence criteria used in the regression procedure (using Aspen Plus) and in the critical locus calculation procedure (using Matlab). The three phase region that occurs for this system ends at a temperature above the critical temperature of R-116. This system is therefore a VKS type III system.

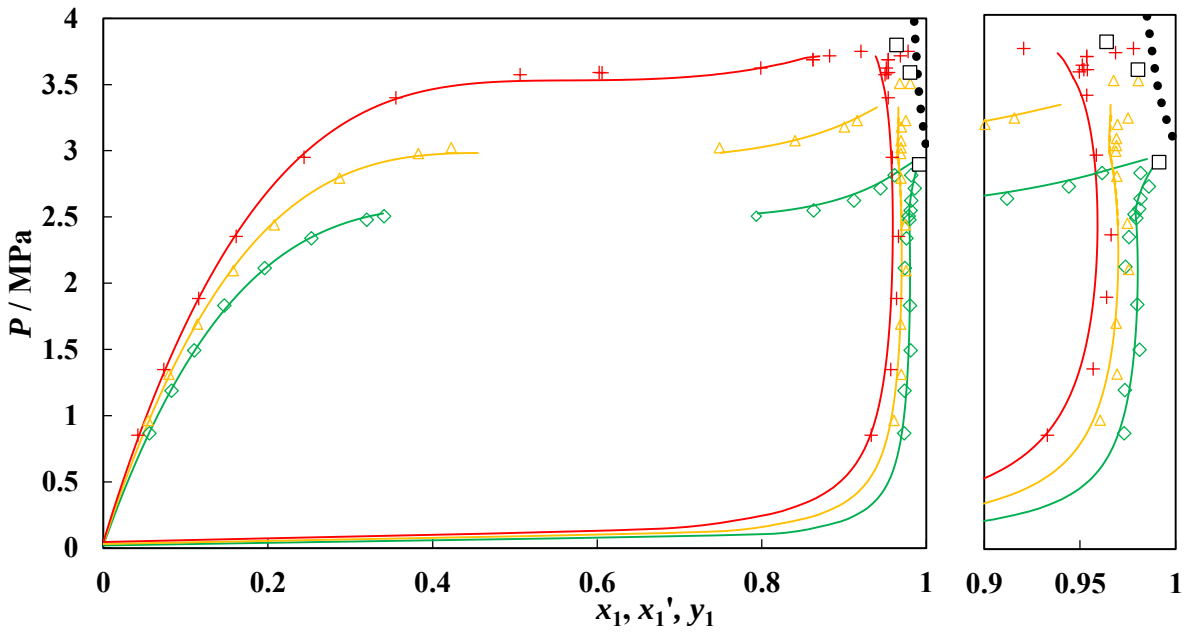

Figure 6.26. ***P-x-x'-y*** **data for the binary system of R-116 (1) + 1-hexene (2). Data measured at temperatures of T = ◇, 293.1 K; △, 303.1 K; +, 313.1 K. Solid lines, PR-MC + WS/NRTL model; □, mixture critical point (Ungerer et al. method); ••••, mixture critical locus curve (Heidemann and Khalil method).**

R-116 (1) + 3-METHYLPENTANE (2)

Appendix G contains the experimental data and the thermodynamic modelling of the R-116 + 3-methylpentane system, as well as a discussion thereof. A *P-x-y* plot of the data is given in Figure 6.27.

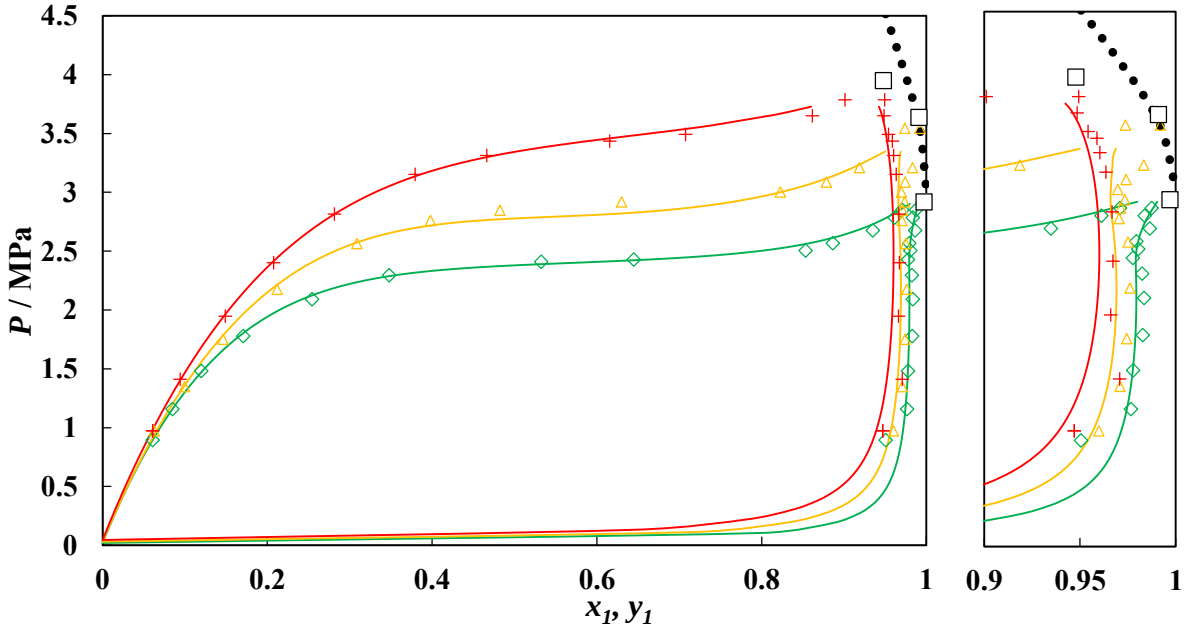

Figure 6.27. ***P-x-y*** **data for the binary system of R-116 (1) + 3-methylpentane (2). Data was measured at temperatures of T = ◇, 293.1 K; △, 303.1 K; +, 313.1 K. Solid lines, PR-MC + WS/NRTL model; □, mixture critical point (Ungerer et al. method); ••••, mixture critical locus curve (Heidemann and Khalil method).**

Within the temperature range that was studied, the system remains a two phase system. The thermodynamic model is able to provide a good description of the experimental data, with ARDs from the regression, for both pressure and vapour phase composition of 0.5 %. There is a slight discrepancy between the model and the experimental data for the dew curve at higher temperatures, but this is not as marked as with some of the other systems that are presented in this study. The model is not able to accurately describe the "bird's-beak" phenomenon that occurs close to the critical locus curve for this system. This is possibly due to the poor convergence of the model calculations close to the critical point.

With no three phase line occurring in the critical region, this system is classified as a simple type II system.

R-116 (1) + METHYLCYCLOHEXANE (2)

The unlike polarities of the R-116 and the MCH molecules are suspected to play a part in the large miscibility gap that occurred with this system. The experimental data and thermodynamic models for this system are included in the manuscript in Appendix H. A *P-x-x'-y* plot for the system is given in Figure 6.28.

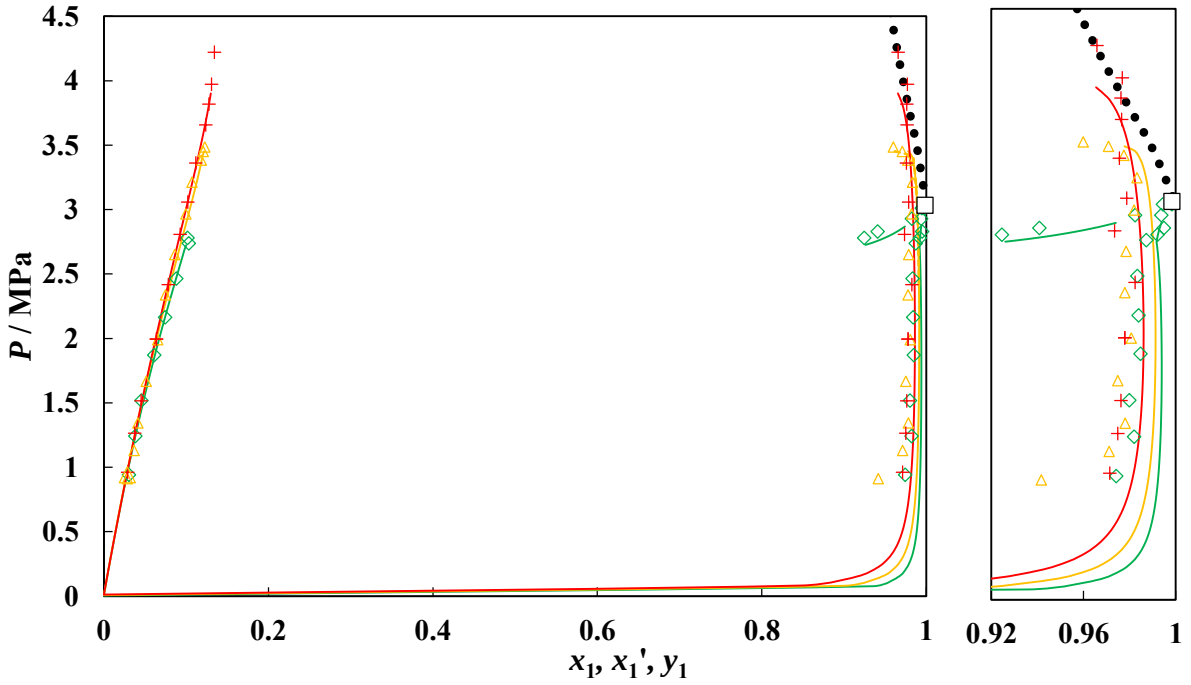

Figure 6.28. *P-x-x'-y* data for the binary system of R-116 (1) + methylcyclohexane (2) at temperatures of ◇, 293.1 K; △, 303.1 K; +, 313.1 K. Solid lines, PR-MC + WS/NRTL model; □, mixture critical locus (Ungerer et al. method); ••••, mixture critical locus curve (Heidemann and Khalil method).

The UCEP of the three phase line ends at a temperature of between (293.1 and 303.1) K, which is slightly higher than the critical temperature of R-116. At 293.1 K, the system exhibits the "bird's-beak"

phenomenon, but this is not observed for the other isotherms. The thermodynamic model is capable of providing an accurate description of this system, although there are several disparities between the experimental and modelled vapour phase compositions, particularly at low pressures. The ARDs for pressure and vapour phase composition for this system were both less than 0.3 %, although the AARD were substantially higher at 4.8 and 1.5 % for pressure and vapour phase composition respectively.

The calculated critical locus curve does not agree with the experimental data at 313.1 K, although this is most likely due to the poor description of the experimental data by the model close to the critical locus at 313.1 K. This system is most likely a VKS type III system, although, without information about the behaviour of the three phase curve at sub-critical conditions and the behaviour of the critical locus curve emanating from the MCH critical point, the type IV and type V systems cannot be ruled out.

R-116 (1) + TOLUENE (2)

The measured data and the thermodynamic modelling for the R-116 + toluene system are also presented in Appendix H. The *P-x-x'-y* data for the system are plotted in Figure 6.29.

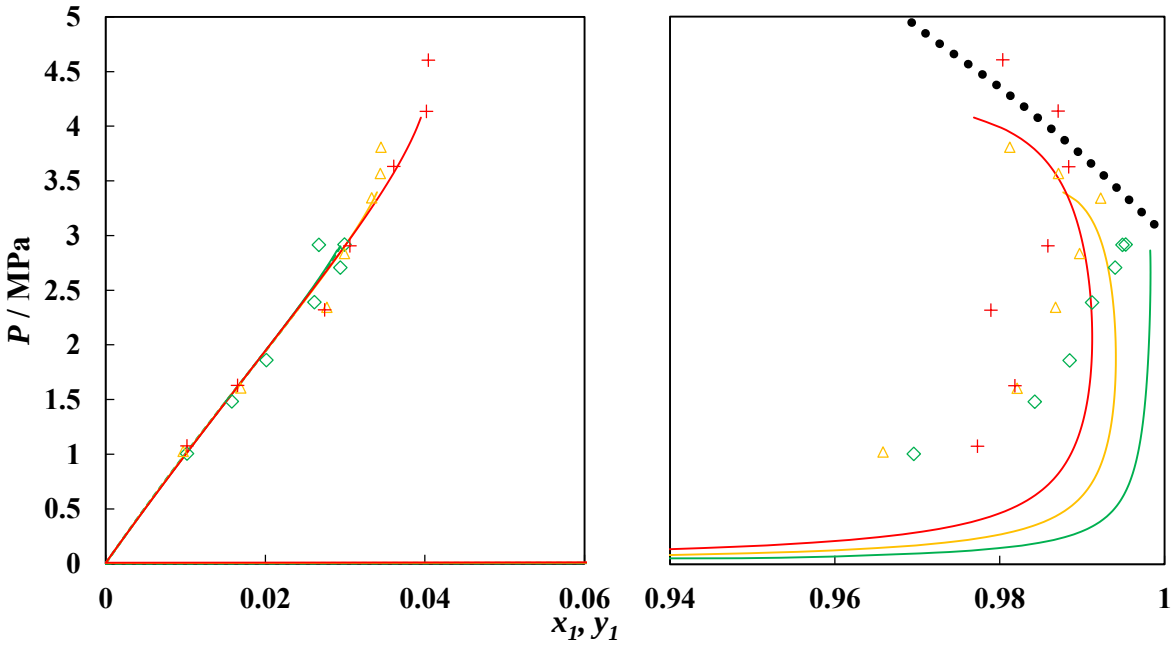

Figure 6.29. *P-x-y* data for the binary system of R-116 (1) + toluene (2) at temperatures of ◇, 293.1 K; △, 303.1 K; +, 313.1 K. Solid lines, PR-MC + WS/NRTL model; ••••, mixture critical locus curve (Heidemann and Khalil method).

The R-116 and the toluene have low mutual solubilities over the temperature range that was investigated. A three phase region is observed at the lower end of this temperature range, but the compositions of one liquid phase and the vapour phase are essentially identical when the uncertainties are taken into consideration. The thermodynamic models are able to describe the system fairly accurately, although there remain discrepancies between the modelled and the

experimental vapour phase compositions, especially at low pressures. The ARDs for pressure and vapour phase composition were -3.6 % and -1.2 % respectively. These values are fairly substantial, and are probably due to the large solubility gap for this system. Although the deviations are substantial, the magnification of the plot of the data in Figure 6.29 also exaggerates the errors between the model and the experimental data, with the largest deviation (at low pressures) only approximately 2 %. From observation of both the experimental data and the model, it appears that the bubble pressure (i.e. the solubility of the R-116 in the toluene at a given pressure) remains approximately constant with changes in the temperature.

No critical loci were extrapolated from the experimental data, and it is therefore not possible to comment on the validity of the calculated critical locus curve, apart from mentioning that several of the sub-critical coexistence data at 313.1 K occurred in the supposed supercritical region. As with the R-116 + MCH system, this system is likely a type III system, although the type IV and type V classifications cannot be overlooked.

R-116 (1) + WATER (2)

The mutual solubilities of R-116 and water are even less than those of R-23 and water. This is presumably due to no dipole or quadrupole moment of the R-116 molecules. Three isotherms, each describing three co-existence points were measured for this system. The data are provided in Table 6.19, alongside the uncertainties in the measured variables.

Table 6.19. Experimental *P-x-x'-y* data for the binary system of R-116 (1) + water (2) at temperatures of *T* = (293.2 to 313.2) K.

T / K	*U*(*T*) / K	*P* / MPa	*U*(*P*) / MPa	x_1 (x10^5)	$U(x_1)$ (x10^5) [a]	x_1'	$U(x_1')$ [a]	y_1	$U(y_1)$ [a]
293.14	0.04	0.933	0.004	3.8	4.2			0.9992	0.0003
293.14	0.04	2.315	0.006	1.5	2.1			0.9993	0.0008
293.13	0.04	3.064	0.004	6.2	2.1	0.9996	0.0004	0.9996	0.0004
303.15	0.04	1.238	0.004	1.1	2.2			0.9991	0.0005
303.15	0.04	2.709	0.005	3.9	3.4			0.9994	0.0007
303.14	0.04	3.749	0.006	6.3	3.7			0.9992	0.0010
313.13	0.04	1.424	0.004	0.9	1.4			0.9985	0.0007
313.13	0.04	2.752	0.006	0.8	1.3			0.9991	0.0008
313.14	0.05	4.482	0.007	1.1	1.2			0.9993	0.0005

[a] combined expanded uncertainties in the experimental data, *U*, were calculated with a coverage factor of k = 2

The mole fraction of R-116 present in the water rich liquid phase is so miniscule that the corresponding uncertainties are of the same order of magnitude as the reported data. These low solubilities resulted in large relative deviations in the regression of the data with the PR-MC + WS/NRTL model. The regressed parameters, as well as the ARD and the AARD between the model and the data are provided

in Table 6.16. The ARD and the AARD for the vapour phase composition were found to be comparatively small. This is most likely due to the higher solubilities of water in the R-116 rich phases than the solubilities of the R-116 in the water-rich phase.

The *P-x-x'-y* plot depicting the model and the experimental data is presented in Figure 6.30 below. The composition axis was substantially magnified in these plots, in order to enable the experimental data points to be distinguishable from one another. This resulted in the magnification of the scatter of the experimental data.

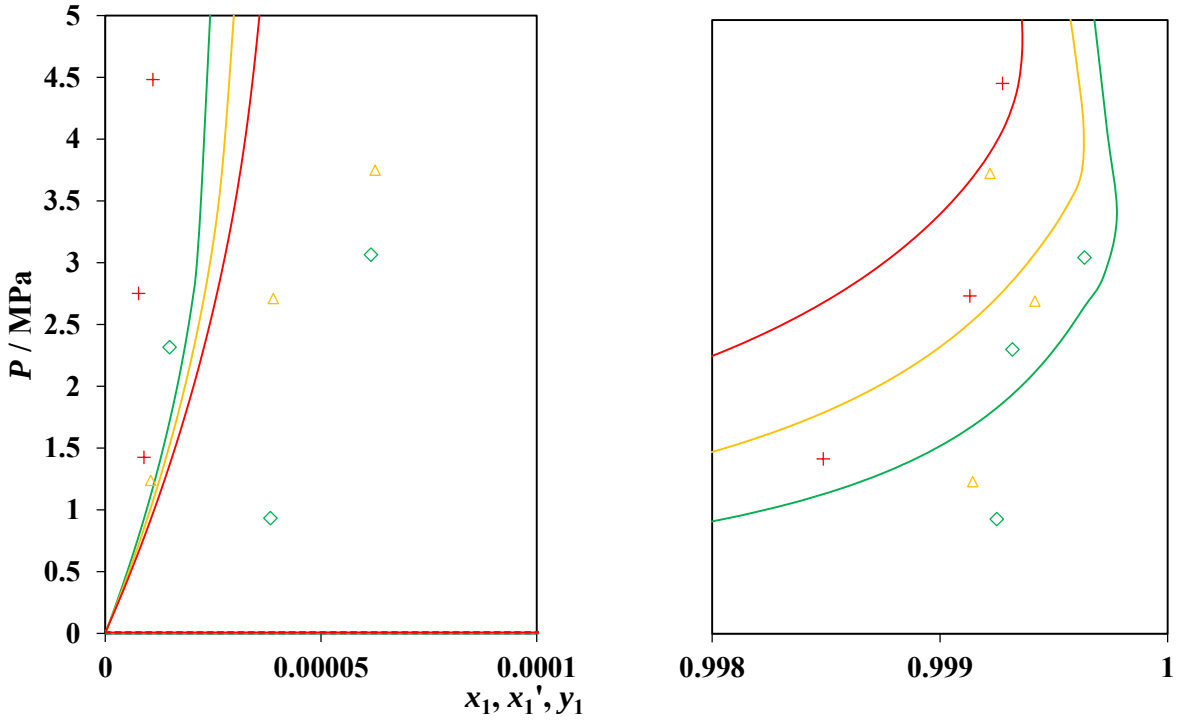

Figure 6.30. *P-x-x'-y* data for the binary system of R-116 (1) + water (2) at temperatures of ◇, 293.15 K; △, 303.15 K; +, 313.15 K. Solid lines, PR-MC + WS/NRTL model.

The thermodynamic models do not predict the occurrence of a three phase region at 293.15 K. This is probably due to the two phases having essentially identical composition profiles. The temperature dependence of the model shows that an increase in the temperature will result in an increase in the mutual solubilities of the two components. However, observation of the experimental bubble point data indicates that the opposite holds true. If considering an isobaric case, the experimental data suggests that an increase in the temperature would result in less R-116 being present in the water-rich phase. The presence of a VLLE point at slightly above the R-116 critical temperature indicates that this system is a VKS type III system.

6.1.7. TERNARY SYSTEMS

To experimentally investigate the separation factors that would be possible with different solvents, the ternary phase equilibrium data for several systems were measured. Ternary VLE data have been previously measured for the systems of CO_2 + n-hexane + n-decane and CO_2 + n-octane + n-decane by Sánchez-García et al. (2011). This data was used to calculate separation factors for n-hexane over n-decane and n-octane over n-decane, using CO_2 as a separation agent. Ternary systems with the CO_2 replaced by the R-23 and the R-116 were therefore also measured in order to compare the abilities of the three solvents to perform the separation of n-hexane or n-octane from n-decane.

SOLVENT (1) + N-HEXANE (2) + N-DECANE (3)

Ternary VLE measurements with either R-23 or R-116 as the solvent were conducted in the static-analytic apparatus. From the ternary data, the separation factor, $S_{i,j}^{k}$ for R-23 and R-116 was calculated (equation 6.1).

$$S_{i,j}^{k} = K_i/K_j \qquad 6.1$$

where $K_i = x_i/y_i$ in a solution with component *k* as the solvent and x_i and y_i are the liquid and vapour fractions of component '*i*'.

The calculated separation factors with R-23 and R-116 as solvents were then compared to those reported by Sànchez-Garcìa et al. with CO_2 as the solvent. The measured ternary data for the systems of (R-23 or R-116) + n-hexane + n-decane are provided in Table 6.20 and 6.21. The selectivities of the solvents for n-hexane over n-decane for each of the measured data points are included in these tables.

For each of the isotherms, there is a transition from VLE to LLE at a certain pressure. The solubilities of the solutes were considerably higher in the liquid solvents than in the solvents in their vapour form. The transition from a liquid to a vapour would correspond with an increase in the solvent density. This observation therefore corresponds to previously reported observations of increases in solubilities with increased densities. At the point of transition, the selectivities of the solvents for n-hexane over n-decane also appeared to increase, with the solvents preferring n-hexane to n-decane. This transition was more noticeable with R-23 than with R-116. There was no dramatic increase in the solubilities of the components in CO_2. This is possibly because the solvent-rich phase remained in the same phase for all of the pressures reported by Sánchez-García et al. (2011).

Table 6.20. Experimental phase equilibrium data [a] for the ternary system of R-23 (1) + n-hexane (2) + n-decane (3) at temperatures of *T* = (303.15 and 313.15) K.

T / K	*U*(*T*) / K	*P* / MPa	*U*(*P*) / MPa	x_2	$U(x_2)$	x_3	$U(x_3)$	y_2	$U(y_2)$	y_3	$U(y_3)$	$S_{23,1}$
303.14	0.06	4.301	0.006	0.421	0.003	0.193	0.006	0.0024	0.0005	0.0007	0.0004	1.71
303.13	0.06	4.690	0.007	0.382	0.008	0.122	0.004	0.0025	0.0006	0.0004	0.0009	1.98
303.14	0.06	4.762	0.005	0.378	0.006	0.128	0.008	0.0024	0.0007	0.0005	0.0007	1.70
303.14	0.06	4.820	0.007	0.365	0.007	0.180	0.010	0.0639	0.0021	0.0088	0.0026	3.60
303.14	0.06	5.161	0.009	0.364	0.005	0.175	0.006	0.0676	0.0030	0.0090	0.0035	3.59
303.14	0.07	5.604	0.007	0.360	0.005	0.170	0.007	0.0787	0.0025	0.0096	0.0031	3.88
303.12	0.06	6.151	0.009	0.353	0.006	0.171	0.004	0.0700	0.0042	0.0103	0.0038	3.28
313.15	0.07	4.689	0.006	0.462	0.005	0.235	0.006	0.0055	0.0012	0.0006	0.0009	4.70
313.16	0.07	5.556	0.007	0.402	0.010	0.206	0.007	0.0116	0.0011	0.0020	0.0012	2.98
313.17	0.07	6.213	0.007	0.364	0.006	0.217	0.003	0.0176	0.0011	0.0061	0.0015	1.72
313.16	0.06	6.369	0.007	0.340	0.010	0.265	0.006	0.0641	0.0013	0.0120	0.0009	4.16
313.15	0.08	6.737	0.009	0.337	0.007	0.260	0.007	0.0702	0.0015	0.0148	0.0031	3.66
313.14	0.08	7.245	0.006	0.335	0.008	0.254	0.009	0.0781	0.0019	0.0184	0.0027	3.23
313.15	0.07	7.976	0.005	0.322	0.008	0.265	0.008	0.0810	0.0036	0.0234	0.0032	2.84
313.14	0.07	8.967	0.006	0.315	0.009	0.260	0.004	0.0850	0.0027	0.0260	0.0021	2.71

[a] Pressure, *P*, the liquid phase compositions, x_2 and x_3, and the vapour phase compositions, y_2 and y_3, are reported, along with their corresponding combined expanded uncertainties, *U*, calculated with k = 2.

Table 6.21. Experimental phase equilibrium data [a] for the ternary system of R-116 (1) + n-hexane (2) + n-decane (3) at temperatures of *T* = (303.15 and 313.20) K.

T / K	*U*(*T*) / K	*P* / MPa	*U*(*P*) / MPa	x_2	$U(x_2)$	x_3	$U(x_3)$	y_2	$U(y_2)$	y_3	$U(y_3)$	$S_{23,1}$
303.15	0.07	2.983	0.008	0.372	0.005	0.469	0.007	0.0156	0.0008	0.0117	0.0006	1.69
303.14	0.07	3.481	0.005	0.358	0.009	0.470	0.004	0.0103	0.0009	0.0052	0.0008	2.60
303.15	0.07	3.566	0.006	0.302	0.006	0.516	0.006	0.0141	0.0007	0.0069	0.0007	3.47
303.15	0.07	3.609	0.005	0.345	0.007	0.485	0.007	0.0134	0.0006	0.0056	0.0009	3.36
303.15	0.06	4.121	0.007	0.275	0.009	0.560	0.007	0.0201	0.0024	0.0159	0.0027	2.56
303.15	0.06	4.642	0.008	0.329	0.005	0.494	0.007	0.0346	0.0019	0.0238	0.0018	2.18
303.16	0.06	5.042	0.006	0.331	0.008	0.481	0.006	0.0349	0.0018	0.0155	0.0021	3.25
303.15	0.06	6.191	0.004	0.330	0.005	0.502	0.008	0.0376	0.0021	0.0143	0.0019	4.00
313.21	0.07	4.044	0.009	0.330	0.006	0.485	0.005	0.0146	0.0006	0.0078	0.0007	2.76
313.22	0.07	4.317	0.009	0.351	0.008	0.476	0.007	0.0146	0.0009	0.0034	0.0009	5.75
313.23	0.08	4.322	0.005	0.310	0.008	0.497	0.008	0.0136	0.0009	0.0077	0.0006	2.83
313.24	0.07	4.494	0.007	0.317	0.006	0.495	0.005	0.0209	0.0007	0.0109	0.0010	2.98
313.23	0.07	4.580	0.007	0.343	0.007	0.489	0.006	0.0213	0.0023	0.0108	0.0023	2.81
313.23	0.07	4.938	0.007	0.307	0.005	0.497	0.005	0.0257	0.0017	0.0126	0.0018	3.30
313.21	0.08	5.938	0.009	0.323	0.006	0.498	0.005	0.0281	0.0019	0.0126	0.0023	3.42

[a] Pressure, *P*, the liquid phase compositions, x_2 and x_3, and the vapour phase compositions, y_2 and y_3, are reported, along with their corresponding combined expanded uncertainties, *U*, calculated with k = 2.

The solubilities of the n-hexane and n-decane in the ternary mixtures with either CO_2, R-23 or R-116 are plotted on against the pressure in Figure 6.31 and 6.12 for 303.15 and 313.2 K respectively.

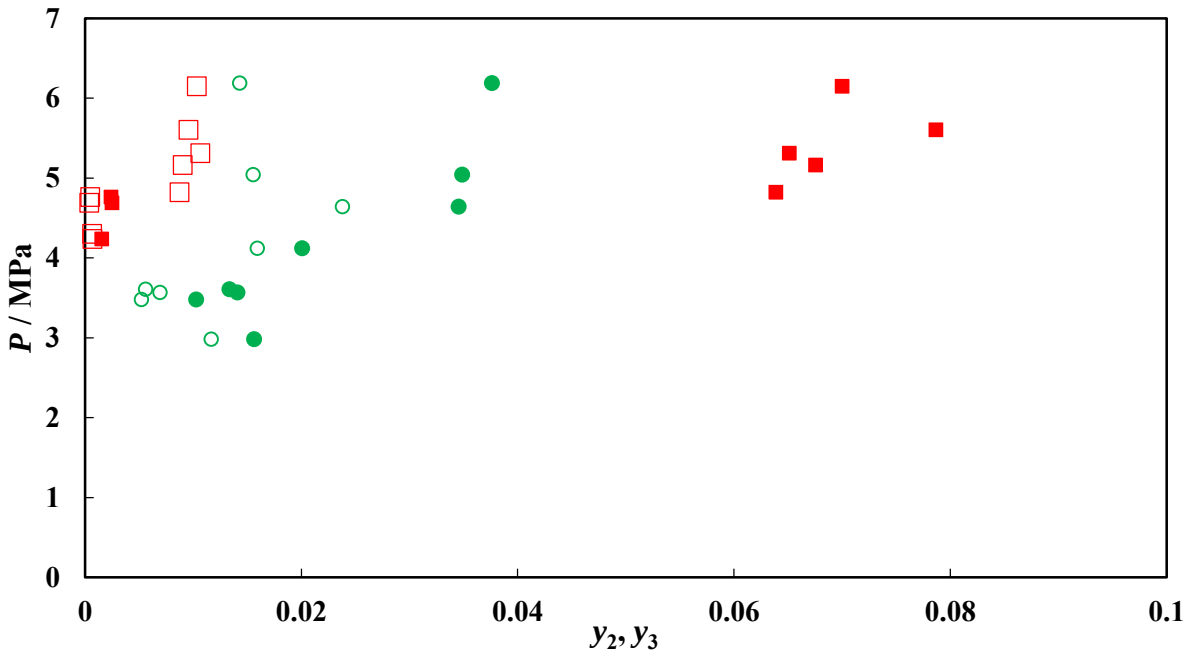

Figure 6.31. Solubilities of n-hexane and n-decane in ternary mixtures with R-23 or R-116 at 303.15 K. ■, n-hexane in R-23; □, n-decane in R-23; ●, n-hexane in R-116; ○, n-decane in R-116.

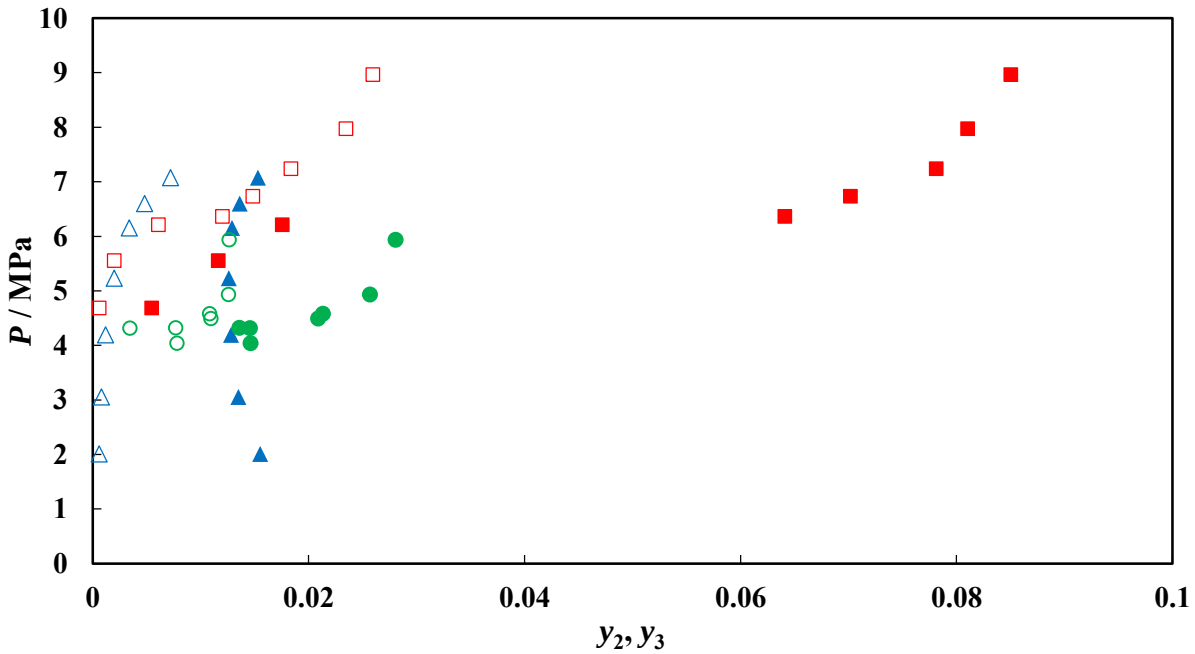

Figure 6.32. Solubilities of n-hexane and n-decane in ternary mixtures with CO_2, R-23 or R-116 at 313.2 K. ▲, n-hexane in CO_2 (Sánchez-García et al., 2011); △, n-decane in CO_2 (Sánchez-García et al., 2011), ■, n-hexane in R-23; □, n-decane in R-23; ●, n-hexane in R-116; ○, n-decane in R-116.

The solubilities of the n-hexane and the n-decane in liquid R-23 are far superior to the solubilities in the CO_2 and the R-116 at similar pressures. The solubilities of the solutes in the R-23 vapour are, however, very similar, and in some cases, less than those in the CO_2. With these results, the solubilities are also dependent upon the fraction of the solvent present in the solution. This lends to a degree of

scatter of the results, which is particularly noticeable with R-116. The increase in the scatter of the R-116 data could possibly be due to the high densities of R-116. Small changes in the composition of the R-116 rich phase can lead to substantial changes in the phase density, because of the large differences in density between R-116 and the solutes. These changes in density will likely then affect the solubilities in this phase.

The solubilities in the vapour phase remain to a great extent dependent upon the composition of the liquid phase. Examining the selectivities of the solvents for n-hexane over n-decane therefore provides a better indication of the performance of each of the solvents. These selectivities are plotted against the pressure of the system in Figure 6.33.

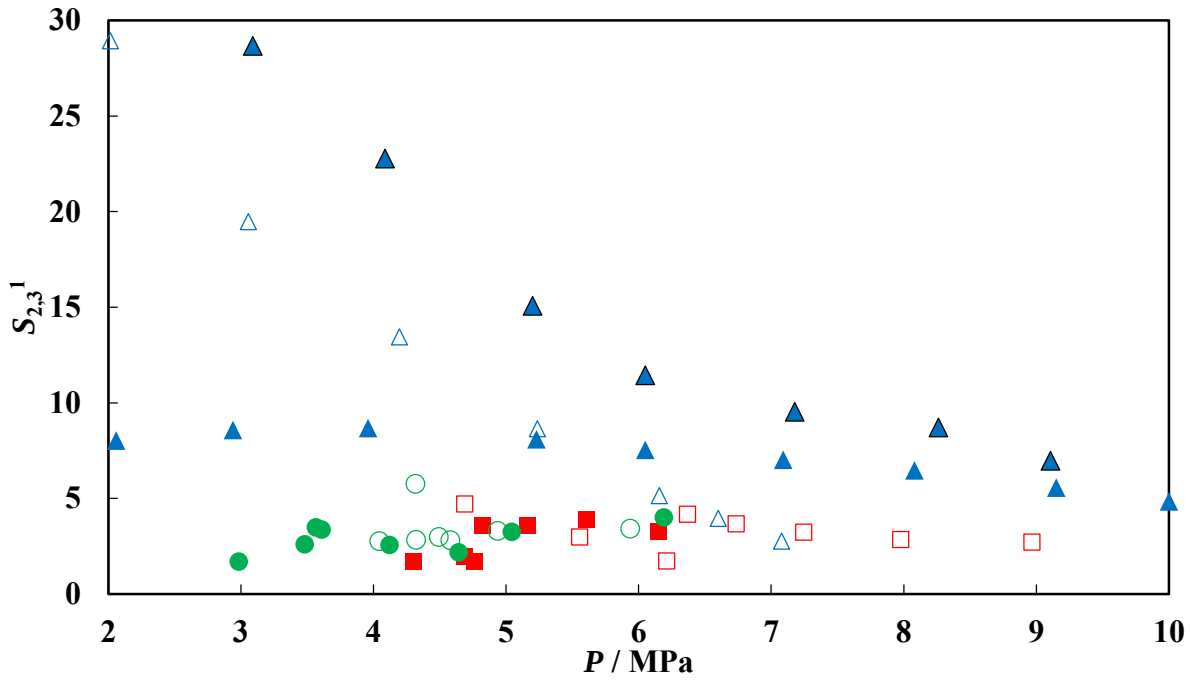

Figure 6.33. Selectivities of CO_2, R-23 or R-116 (1) for n-hexane (2) over n-decane (3) in ternary mixtures. △, $S_{2,3}^{CO2}$ at 312.89 K (Sánchez-García et al., 2011); ▲, $S_{2,3}^{CO2}$ at 342.5 K (Sánchez-García et al., 2011); ▲, $S_{2,3}^{CO2}$ at 376.2 K (Sánchez-García et al., 2011); ■, $S_{2,3}^{R-23}$ at 303.15 K; □, $S_{2,3}^{R-23}$ at 313.2 K; ●, $S_{2,3}^{R-116}$ at 303.15 K; ○, $S_{2,3}^{R-116}$ at 313.2 K.

The selectivities with R-23 are lower than those with CO_2 at low pressures. At higher pressures and similar temperatures, the R-23 exhibits higher selectivities for the n-hexane over n-decane than the CO_2. This, in addition to the substantially higher solubilities, makes the R-23 a better solvent than the CO_2 for separating n-hexane from n-decane. The R-116 exhibits similar selectivities to the R-23, although the solubilities of the solutes in R-116 are markedly lower.

Interestingly, the data reported by Sánchez-García et al. (2011) followed a decaying logarithmic trend with increase in temperature, whereas the data that was measured in this study remained fairly

independent of pressure. This could, however, simply be due to the composition of the solute feed mixtures added to the system. The data for the selectivity of R-23 for n-hexane over n-decane shows the most distinguishable trends. The selectivity decreases slowly with increased pressure up to the pressure at which the transition from VLE to LLE occurs. At this pressure, there was a step increase in the selectivity, and thereafter, another slow decrease with increasing pressure.

SOLVENT (1) + N-OCTANE (2) + N-DECANE (3)

The phase equilibrium of the ternary systems of (R-23 or R-116) with n-octane and n-decane were also measured with the static-analytic apparatus. From this data, the selectivities of the R-23 and the R-116 for the n-octane over n-decane are calculated (by equation 6.1) and compared to the data reported by Sánchez-García et al. (2011) for the selectivities of CO_2. The measured ternary data are reported in Table 6.22 for the (R-23 + n-octane + n-decane) system and in Figure 6.23 for the (R-116 + n-octane + n-decane) system. The solubilities at 303.15 K and at 313.15 K are plotted in Figure 6.34 and Figure 6.35 respectively. The selectivities are plotted against the system pressure for all three solvents at various temperatures in Figure 6.36.

Table 6.22. Experimental phase equilibrium data [a] for the ternary system of R-23 (1) + n-octane (2) + n-decane (3) at temperatures of T = (303.13 and 313.16) K.

T /K	$U(T)$ /K	P /MPa	$U(P)$ /MPa	x_2	$U(x_2)$	x_3	$U(x_3)$	y_2	$U(y_2)$	y_3	$U(y_3)$	$S_{23,1}$
303.15	0.05	3.066	0.007	0.485	0.006	0.313	0.007	0.0048	0.0008	0.0015	0.0007	2.06
303.13	0.05	3.946	0.010	0.454	0.007	0.287	0.008	0.0021	0.0010	0.0006	0.0010	2.25
303.15	0.05	5.064	0.006	0.406	0.005	0.264	0.007	0.0250	0.0018	0.0099	0.0018	1.64
303.14	0.06	5.088	0.007	0.406	0.004	0.256	0.006	0.0289	0.0026	0.0101	0.0030	1.80
303.14	0.05	6.339	0.006	0.391	0.006	0.266	0.004	0.0247	0.0018	0.0074	0.0027	2.27
303.14	0.05	8.111	0.008	0.385	0.006	0.274	0.005	0.0268	0.0018	0.0107	0.0021	1.78
303.13	0.06	9.576	0.011	0.383	0.004	0.265	0.006	0.0285	0.0030	0.0126	0.0021	1.56
313.16	0.06	3.250	0.005	0.497	0.004	0.302	0.009	0.0022	0.0008	0.0010	0.0010	1.29
313.15	0.06	3.564	0.008	0.454	0.006	0.357	0.005	0.0046	0.0009	0.0031	0.0006	1.18
313.15	0.07	4.427	0.005	0.431	0.007	0.331	0.008	0.0058	0.0005	0.0026	0.0007	1.74
313.14	0.07	5.103	0.005	0.407	0.005	0.310	0.005	0.0075	0.0007	0.0034	0.0007	1.69
313.15	0.07	6.048	0.007	0.377	0.006	0.301	0.007	0.0147	0.0015	0.0042	0.0023	2.78
313.15	0.06	6.936	0.007	0.370	0.006	0.286	0.007	0.0160	0.0022	0.0049	0.0028	2.52
313.15	0.06	8.649	0.009	0.361	0.004	0.264	0.006	0.0290	0.0022	0.0125	0.0024	1.69
313.16	0.07	10.131	0.010	0.355	0.005	0.245	0.004	0.0314	0.0018	0.0134	0.0016	1.61

[a] Pressure, P, the liquid phase compositions, x_2 and x_3, and the vapour phase compositions, y_2 and y_3, are reported, along with their corresponding combined expanded uncertainties, U, calculated with k = 2.

Table 6.23. Experimental phase equilibrium data [a] for the ternary system of R-116 (1) + n-octane (2) + n-decane (3) at temperatures of T = (303.13 and 313.16) K.

T /K	$U(T)$ /K	P /MPa	$U(P)$ /MPa	x_2	$U(x_2)$	x_3	$U(x_3)$	y_2	$U(y_2)$	y_3	$U(y_3)$	$S_{23,1}$
303.14	0.06	3.809	0.006	0.354	0.008	0.493	0.006	0.0030	0.0007	0.0069	0.0009	0.62
303.13	0.06	4.089	0.007	0.336	0.006	0.498	0.007	0.0064	0.0009	0.0110	0.0008	0.86
303.14	0.05	4.168	0.004	0.351	0.007	0.493	0.008	0.0050	0.0010	0.0083	0.0009	0.84
303.14	0.06	4.884	0.008	0.348	0.004	0.493	0.007	0.0057	0.0005	0.0084	0.0005	0.95
303.13	0.06	5.785	0.010	0.337	0.006	0.494	0.004	0.0102	0.0013	0.0082	0.0016	1.81
313.16	0.06	4.144	0.009	0.494	0.008	0.308	0.005	0.0087	0.0008	0.0083	0.0010	0.65
313.14	0.07	4.760	0.007	0.336	0.006	0.488	0.007	0.0056	0.0009	0.0097	0.0007	0.83
313.16	0.06	5.001	0.008	0.502	0.005	0.302	0.005	0.0059	0.0007	0.0058	0.0005	0.61
313.14	0.06	5.049	0.005	0.342	0.005	0.490	0.006	0.0059	0.0008	0.0060	0.0007	1.40
313.16	0.06	5.744	0.007	0.498	0.008	0.288	0.005	0.0090	0.0012	0.0089	0.0013	0.59
313.16	0.06	6.416	0.011	0.506	0.005	0.304	0.005	0.0135	0.0011	0.0072	0.0012	1.13

[a] Pressure, P, the liquid phase compositions, x_2 and x_3, and the vapour phase compositions, y_2 and y_3, are reported, along with their corresponding combined expanded uncertainties, U, calculated with k = 2.

Once again with these systems, above the pressure at which the transition from VLE to LLE occurred, there was a substantial increase in the solubilities of the solutes. This increase was more drastic with R-23 as the solvent. A cross-over effect is observed with the R-116 system, as the n-decane has a higher solubility than the n-octane at lower pressures, but as the pressure increases, the n-octane becomes more soluble than the n-decane in the R-116. This cross-over effect was not as pronounced at 313.15 K as at 303.15 K.

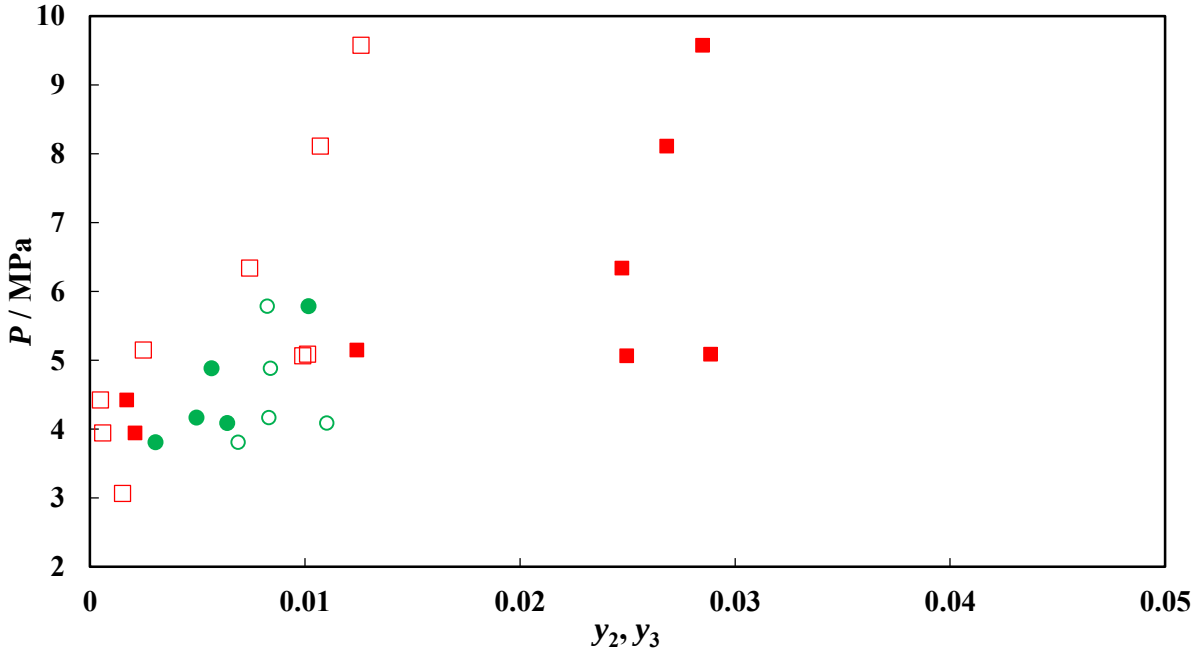

Figure 6.34. Solubilities of n-octane and n-decane in ternary mixtures with R-23 or R-116 at 303.15 K. ■, n-octane in R-23; □, n-decane in R-23; ●, n-octane in R-116; ○, n-decane in R-116.

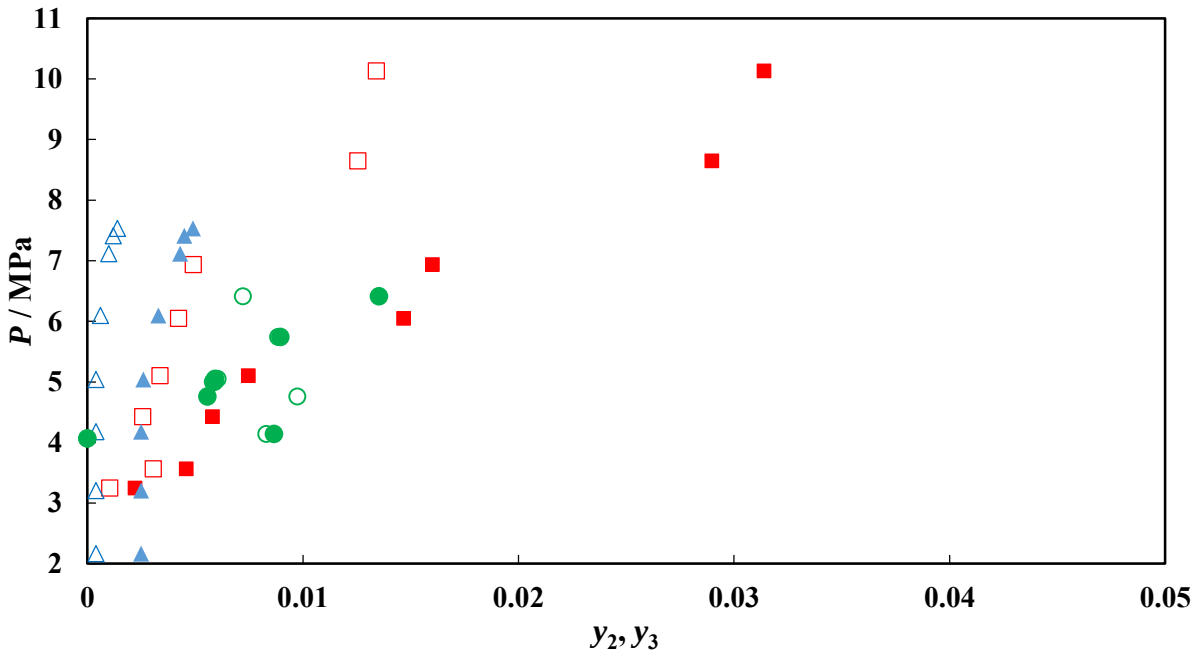

Figure 6.35. Solubilities of n-octane and n-decane in ternary mixtures with CO_2, R-23 or R-116 at approximately 313 K. ▲, n-octane in CO_2 (Sánchez-García et al., 2011); △, n-decane in CO_2 (Sánchez-García et al., 2011), ■, n-octane in R-23; □, n-decane in R-23; ●, n-octane in R-116; ○, n-decane in R-116.

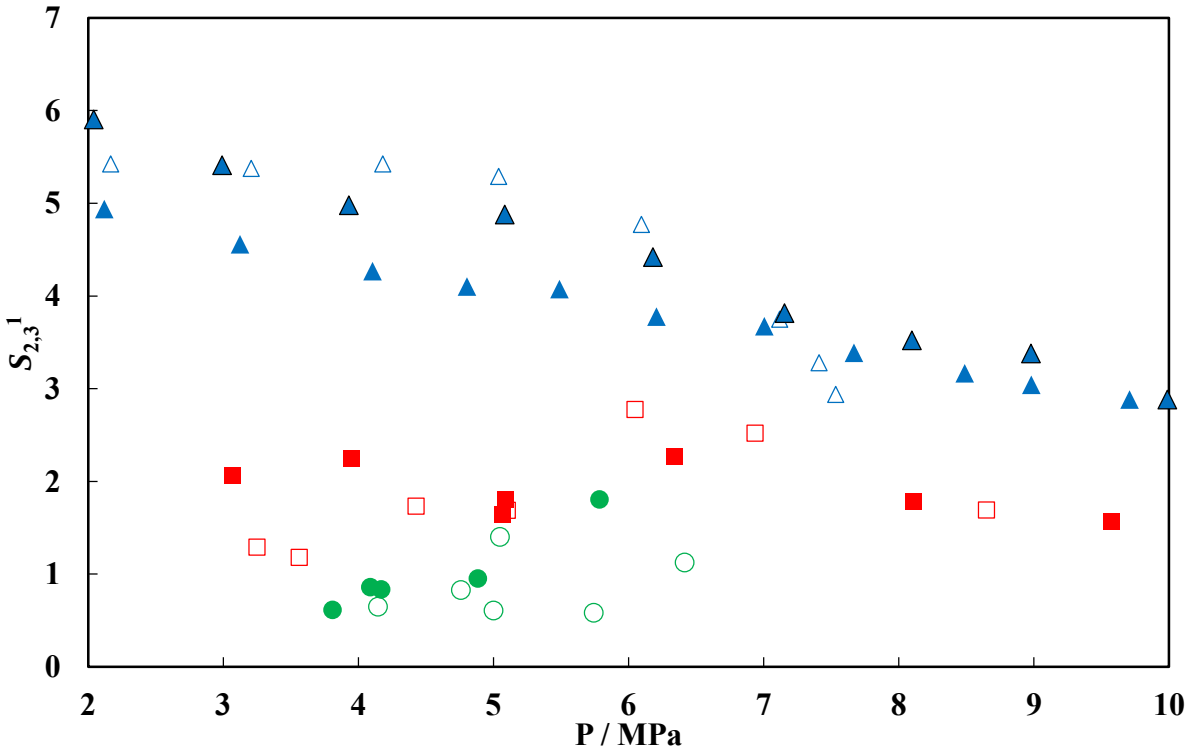

Figure 6.36. Selectivities of CO_2, R-23 or R-116 (1) for n-octane (2) over n-decane (3) in a ternary mixtures. △, $S_{2,3}^{CO2}$ at 312.89 K (Sánchez-García et al., 2011); ▲, $S_{2,3}^{CO2}$ at 342.5 K (Sánchez-García et al., 2011); ▲, $S_{2,3}^{CO2}$ at 376.2 K (Sánchez-García et al., 2011); ■, $S_{2,3}^{R\text{-}23}$ at 303.15 K; □, $S_{2,3}^{R\text{-}23}$ at 313.2 K; ●, $S_{2,3}^{R\text{-}116}$ at 303.15 K; ○, $S_{2,3}^{R\text{-}116}$ at 313.2 K.

The crossover effect can also be observed in Figure 6.36, where the selectivities of R-116 for n-octane over n-decane are less than one at lower pressures, but increase above one at higher pressures. The selectivities of either R-23 or R-116 from this ternary system are markedly lower than those of CO_2. The solubilities of the solutes in the R-23, in particular, were still significantly larger than those in CO_2, especially at elevated pressures. The solubilities of the solutes in the R-116 were also higher than those in the CO_2, but not to the same extent as in the R-23.

If the aim of using a solvent was to separate the n-octane from the n-decane, then CO_2 would be the recommended solvent (of the three investigated here). However, if the aim was to extract both the n-octane and the n-decane using a supercritical solvent, then the R-23 would be a better option because lower solvent flow rates would be required to extract the solutes. Thus, for this study, where the aim was to extract the hydrocarbons from a solution or a solid, the R-23 appeared to be a more efficient solvent, chiefly due to the higher solubilities achievable.

6.1.8. Model Parameters

Moradinia and Teja (1986) reported that systems containing odd- and even-numbered n-alkanes exhibited different behaviour trends. The NRTL parameters from the PR-MC + WS/NRTL model were therefore plotted against their carbon chain lengths for the n-alkanes in each of the three solvents in Figures 6.37 to 6.39.

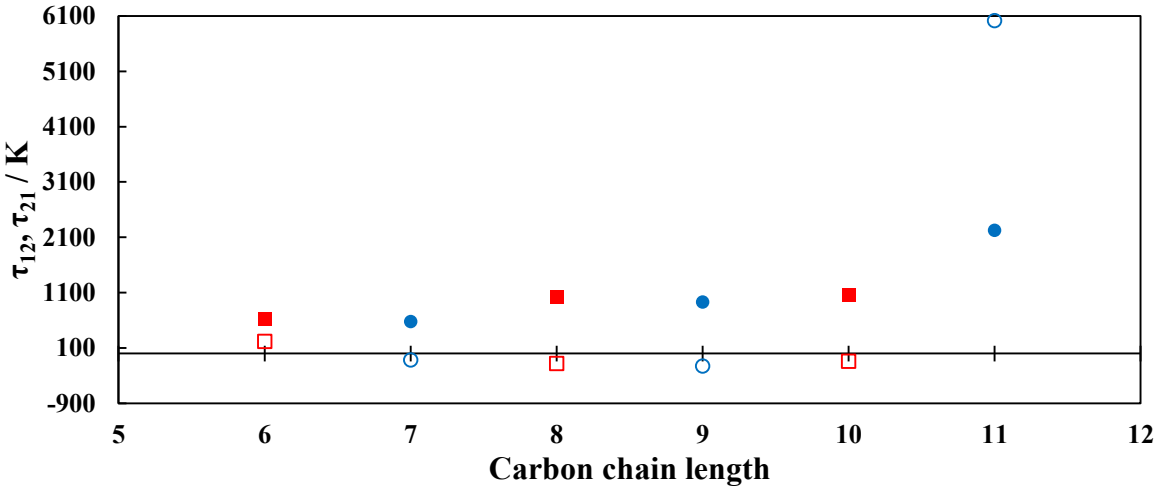

Figure 6.37. NRTL parameters, τ_{12} and τ_{21} for CO_2 (1) + n-alkanes (2) from n-hexane through to n-undecane, plotted against the carbon chain length of the n-alkanes. ■, τ_{12} for C_6, C_8 & C_{10}; ●, τ_{12} for C_7, C_9 & C_{11}; □, τ_{21} for C_6, C_8 & C_{10}; ○, τ_{21} for C_7, C_9 & C_{11}.

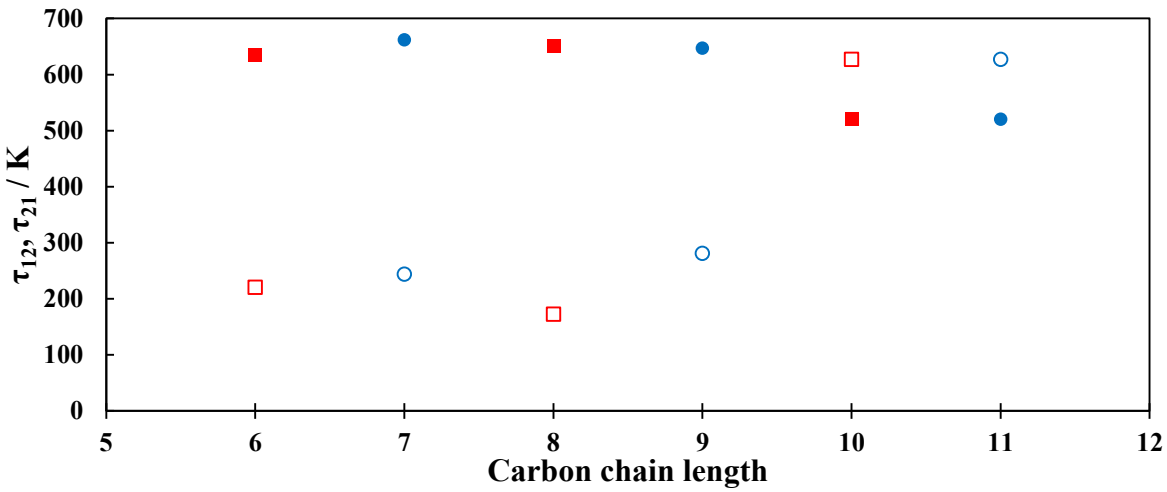

Figure 6.38. NRTL parameters, τ_{12} and τ_{21} for R-23 (1) + n-alkanes (2) from n-hexane through to n-undecane, plotted against the carbon chain length of the n-alkanes. ■, τ_{12} for C_6, C_8 & C_{10}; ●, τ_{12} for C_7, C_9 & C_{11}; □, τ_{21} for C_6, C_8 & C_{10}; ○, τ_{21} for C_7, C_9 & C_{11}.

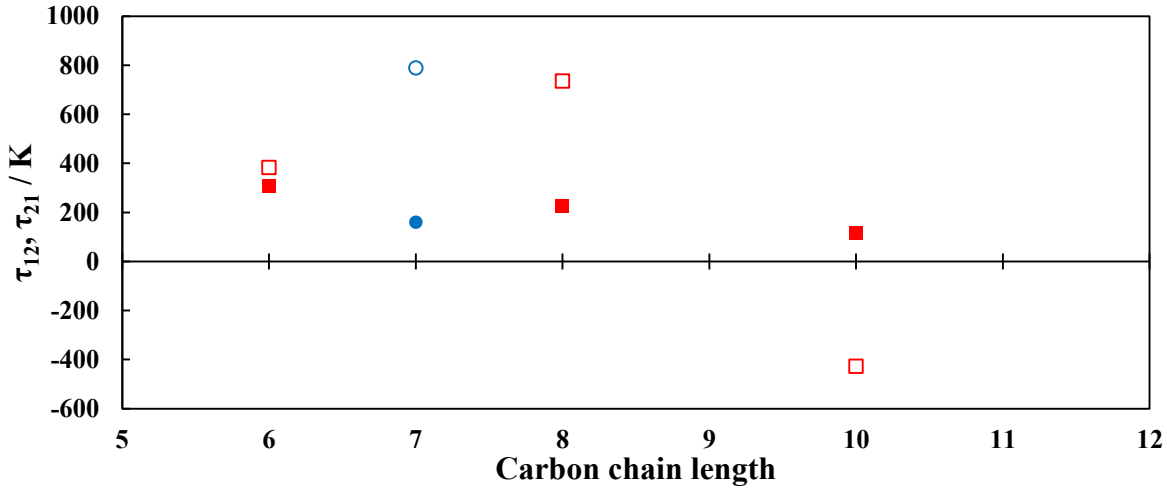

Figure 6.39. NRTL parameters, τ_{12} and τ_{21} for R-116 (1) + n-alkanes (2) from n-hexane through to n-undecane, plotted against the carbon chain length of the n-alkanes. ■, τ_{12} for C_6, C_8 & C_{10}; ●, τ_{12} for C_7; □, τ_{21} for C_6, C_8 & C_{10}; ○, τ_{21} for C_7.

Different trends for the odd- and even-numbered n-alkanes were easily discernible with the NRTL parameters for the CO_2 systems (Figure 6.37). There also appeared to be different trends between odd- and even- numbered n-alkanes in the R-23 systems, particularly with carbon chain lengths of less than 10 (Figure 6.38). With the C_{10} and C_{11} n-alkanes, there was a fairly significant change in the trends of the parameters. An insufficient number of systems containing R-116 + odd-numbered n-alkanes were measured for any conclusions to be ascertained (Figure 6.39).

6.2. PROCESS SIMULATION

By investigating simple ternary systems involving two hydrocarbons and each of the solvents (R-23, R-116 and CO_2), it was shown that the possibility existed that R-23 and R-116 could be used in extraction processes to give greater extraction efficiency than if CO_2 were used as the solvent.

To further the investigation into the ability of these solvents to perform separations that would be useful in the petroleum industry, simulations were undertaken, where the extraction of slightly more complex systems were investigated. Four different 'model' systems were separated using process simulations. Each 'model' system was used to describe a possible extraction problem from the petroleum industry. The aim of the separation was to provide a split between the water fraction and the hydrocarbon fraction. These simple separations could ideally also be performed by mechanical means, due to the presence of hydrocarbon- and water-rich phases. For these simulations, it was assumed that, the presence of solid particles and emulsions within the systems, such as would occur in real situations in the petroleum industry would prevent mechanical separation. A solvent was therefore required to enable this separation. Examples of several of these situations were discussed in Chapter 1, and include oil sludge, oil sands and contaminated soil. The compositions of the four model systems are given in Table 6.24, alongside the possible applications which each model system would approximate.

Table 6.24. Compositions (mass fractions) of the model systems for which separation of the petroleum fraction from the water fraction using supercritical solvents was simulated.

Component	System 1	System 2	System 3	System 4
n-hexane	0.1	0.1	0.09	0.1
n-heptane	0	0.1	0.1	0
n-octane	0.3	0	0.17	0
n-nonane	0	0	0.1	0
n-decane	0.2	0	0.05	0
1-hexene	0	0.1	0	0.1
3-methylpentane	0	0.1	0.05	0
methylcyclohexane	0	0.1	0.04	0.2
toluene	0	0.1	0	0.2
water	0.4	0.4	0.4	0.4
Similar 'real' applications	Oil sludge, oil sands and contaminated soils	Soils contaminated with gasolines	Oil sludge, oil sands and contaminated soils	Separation of B-T-X streams from water

The compositions of these model systems are based on the approximate compositions described by Da Silva et al. (2012). According to Da Silva et al., water comprises between (30 and 90) wt. % of sludge, with between (5 and 60) wt. % being petroleum fractions. Of the petroleum fraction, between (40 and 60) wt. % is saturated hydrocarbons, and between (25 and 40) wt. % is aromatic hydrocarbons.

The remainder usually comprises resins and asphaltenes. A mass fraction of 0.4 for water was set for all of the systems, in order to enable easier comparisons between the systems. System 1 was a very simple system, used to approximate the optimal parameters for a separation, while system 2 contained only the more volatile components, and could approximate a gasoline stream. System 3 was the most comprehensive system which gave the closest approximation of an oil sludge. System 4 was included to investigate the potential of the solvents for the recovery of BTX fractions from water.

6.2.1. EXTRACTION

A basic Aspen Plus flowsheet, using only mixers and flash vessels was used to model the extraction stage of the separation process. This simplified extraction is presented in Figure 6.40. Although the use of a distillation column to perform a type of extractive distillation would undoubtedly have resulted in improved results, a flash vessel had to be used, due to the solid content that was assumed to exist in the feed. These solids would have resulted in fouling of any distillation column internals.

A simple, single stage extraction vessel, with the feed mixing with the solvent and thereafter a separation of the phases occurring, would be easier to operate and maintain. After mixing, the fluid present in the vessel would be allowed to separate, with the extract withdrawn from close to the top of the vessel, and the raffinate withdrawn from close to the bottom of the vessel. A three phase flash vessel was used in the simulation because at certain pressures and temperatures, the solvent-rich phase was a vapour and at other conditions, it was a liquid. The liquid and vapour solvent-rich phases were combined upon exiting the flash vessel, and the resulting stream was used in the analysis of the system performance.

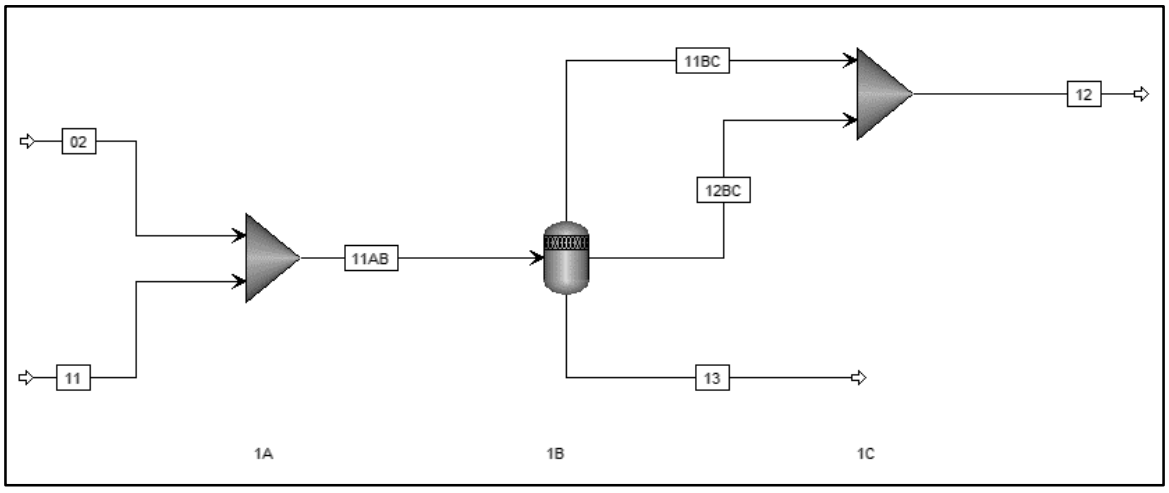

Figure 6.40. Aspen Plus flowsheet for a simplified extraction using SCFs. Vessels: 1A, mixer; 1B, three-phase flash vessel; 1C, mixer. Streams: 02, solvent feed; 11, model system feed; 11AB mixed feed to flash vessel; 11BC, solvent rich vapour extract; 12BC, solvent rich liquid extract; 12, extract; 13, raffinate.

As a departure point for this investigation, the initial aim of the simulation was to optimise the extraction process conditions (temperature and pressure) and the solvent to feed ratio, within reasonable limits, to maximise the recovery and purity of the hydrocarbon fraction for each solvent and each model system. In addition to investigating the CO_2, R-23 and R-116 solvent performances, the performance of a solvent blend containing R-23 (1) and R-116 (2) was also investigated. The conditions at which the maximum recovery and purity were obtained for each system with the 4 mixtures are presented in Table 6.25.

Table 6.25. Optimal conditions for the recovery of a high purity hydrocarbon stream from four model systems using CO_2, R-23, R-116 and a R-23 + R-116 mixture as SCF solvents.

System	T / K	P / MPa	Solvent/Feed[a]	x_{R23} [a]	Recovery [a]	Purity [a]
			Model system 1			
CO_2	313.2	14.52	30.00		0.491	0.685
R-23	300.2	11.20	2.50		0.996	0.991
R-116	295.2	11.20	3.80		0.998	0.996
R-23 + R-116	300.6	4.80	1.47	0.466	0.997	0.996
			Model system 2			
CO_2	314.9	9.19	39.13		0.510	0.876
R-23	300.1	12.00	2.28		0.998	0.988
R-116	295.3	4.80	3.60		0.999	0.998
R-23 + R-116	298.8	4.80	1.48	0.471	0.999	0.996
			Model system 3			
CO_2	308.7	8.00	21.86		0.078	0.811
R-23	299.2	12.00	9.20		0.924	0.990
R-116	295.2	4.80	3.80		0.978	0.998
R-23 + R-116	298.8	4.80	1.48	0.454	0.924	0.997
			Model System 4			
CO_2	311.0	9.53	22.11		0.478	0.868
R-23	299.2	10.00	2.00		0.997	0.978
R-116	295.2	4.80	3.60		0.999	0.998
R-23 + R-116	298.8	4.80	1.48	0.454	0.998	0.996

[a] mass basis

Based upon the optimum results for each solvent + model system combination, the CO_2 was shown to perform substantially worse than the R-23, the R-116 or the R-23 + R-116 mixture. The optimum temperatures for all of the solvents were in proximity to room temperature, and the best separations were all obtained within the pressure range of (4.8 to 14.5) MPa. When using the fluorinated solvents, however, the solvent to feed ratios were substantially reduced from when using CO_2. The fractional recovery of the hydrocarbons, and the purity of the extract were substantially improved when using the fluorinated solvents. With a single stage extraction, CO_2 exhibited a very poor performance. The fluorinated hydrocarbon solvents all had similar performances, with investigations in the solvent recovery and the economic analysis with the various solvents necessary to select the best solvent.

Due to the substantially lower costs of using CO_2 as a solvent, an investigation into the performance of a CO_2 with the addition of R-23 as a polar co-solvent was also undertaken using the Aspen Plus

simulation tool. This solvent mixture was expected to allow the use of the cheap CO_2, while improving the efficiency by the addition of the polar R-23. However, the addition of small amounts of R-23 did not have the desired effect of improving the extraction efficiency. In actual fact, the R-23 further inhibited the ability of the CO_2 to separate the hydrocarbons from the water. This can be observed from the sensitivity of the extraction of the hydrocarbons from system 1 to the composition of the solvent, as is given in Figure 6.41.

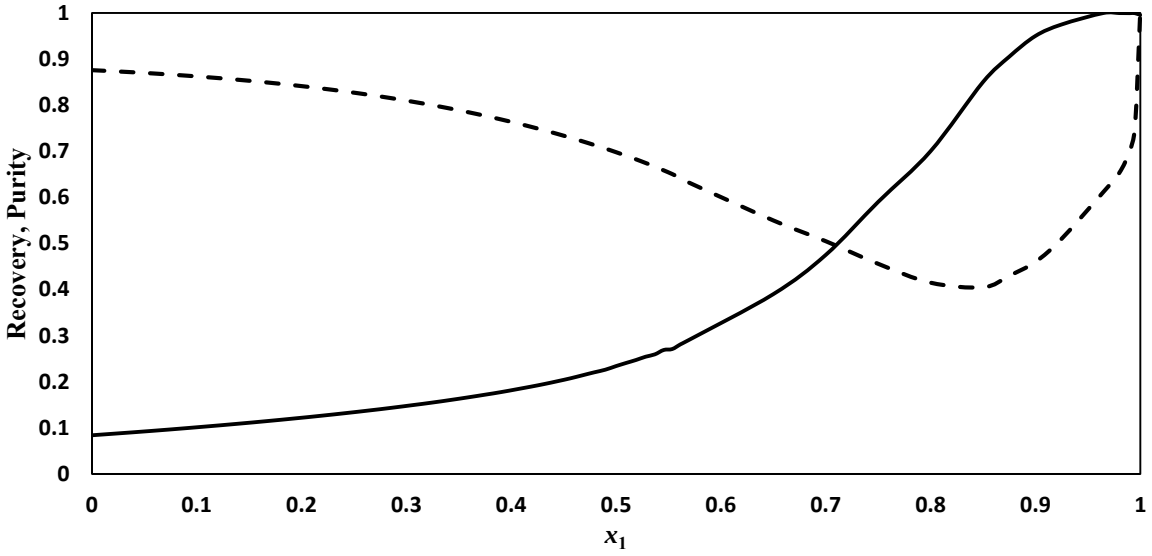

Figure 6.41. Sensitivity of the separation of the hydrocarbons from water from model system 1 using a R-23 (1) + CO_2 (2) mixture at 300 K, 11.2 MPa and a solvent to feed ratio of 8.5. - - - -, recovery of the hydrocarbons as the extract; ——, purity of the hydrocarbons in the extract.

The only compositions at which good recoveries and purities were achievable with the R-23 + CO_2 solvent was with high R-23 concentrations. This contradicted the original aim of the investigation, as it was hoped that addition of a small amount of R-23 to a CO_2 rich solvent would give a good separation. Due to the poor performance of this solvent mixture in the initial investigation, further studies into this mixture were not performed.

With the remaining four solvents, CO_2, R-23, R-116 and R-23 + R-116, sensitivities of the recovery and purity to one-dimensional disturbances of the extraction conditions were investigated. The sensitivity of the recovery and the purity to variations in each variable was investigated while the remaining variables were held constant. The sensitivity plots for these analyses are presented in Appendix B.2.

With CO_2 as a solvent, it was found that the recoveries and purities were affected to a greater extent by the pressure and the solvent-to-feed ratio than by the temperature of the extraction. Below a given threshold pressure and solvent to feed ratio, no separation occurred, with the exit stream having

the same composition as the feed. Above this threshold, however, the dependency of the extraction performance was similar for all three variables.

When investigating the performance of R-23 as a solvent, it was observed that for model systems 1, 2 and 3, the recovery and purity remained greater than 0.9 at all conditions. With model system 4, however, there was a maximum temperature and solvent to feed ratio and a minimum pressure, beyond which, no separation was effected. With R-116 as the solvent, this was not observed, and the recovery and purity remained greater than 0.9 for all conditions that were investigated. The use of R-116 as the solvent gave the highest recoveries of hydrocarbons and the highest purities of the extract.

With the R-23 + R-116 solvent mixture, the fraction of R-23 in the mixture that provided the best recovery and purity was investigated alongside the optimal temperature, pressure and solvent to feed ratio. The recoveries and purities from the extraction stage decreased as the fraction of R-23 in the solvent mixture increased. In contrast to this, when a search for the optimum conditions was performed by varying all four of the variables simultaneously, the best separation for all of the systems was found to occur at a R-23 mole fraction of approximately 0.46 ($\pm$0.02).

The solubilities of water in each of the systems played an important role in determining the optimum solvent flow rates. Due to the lower solubilities of water in R-116 than in R-23, a higher R-116 flow rate could be used, allowing improved recoveries and purities of the hydrocarbons, while at the same time, operating at lower pressures. The slight dependencies of the recoveries and purities upon the solvent flow rate with the R-116 would mean that the optimum flow rate would most likely eventually be selected based upon economic criteria.

6.2.2. Process Design

The extraction of the hydrocarbons from the water did not, however, provide a complete picture of this separation. In order to make this separation technique viable, a means of recovery of the solvent from the extract was required. To ensure that large amounts of energy would not be expended on cooling and recompression of the recovered solvent, a technique that separated the solvent from the extract at high pressures was preferred. Additionally, due to the high GWP of the fluorinated hydrocarbon solvents, ideally, no solvent should be vented or allowed to escape into the atmosphere. Any low pressure solvent that would be too expensive to recompress would have to be incinerated in the same manner as the R-23 produced as a by-product of R-22 manufacture is destroyed.

Rather than having a series of flash vessels, each at a lower pressure than the previous, for the solvent recovery, it was proposed that a stripping column be used to separate the solvent from the extract. The use of a column for the solvent recovery produced a recycled solvent stream with a substantially higher outlet pressure than would be the case with flash vessels. The major drawback in the use of

such a column would be the additional heating requirements for the reboiler at the base of the column. The proposed process flow diagram for the entire separation is given by Figure 6.42. The feed to the proposed process would be sourced from oil sludge collection facilities, such as vacuum suckers and run-off collection facilities. This feed would likely require dehydration by conventional water removal techniques, such as evaporation or decanting, to reduce the flowrate of feed into the process.

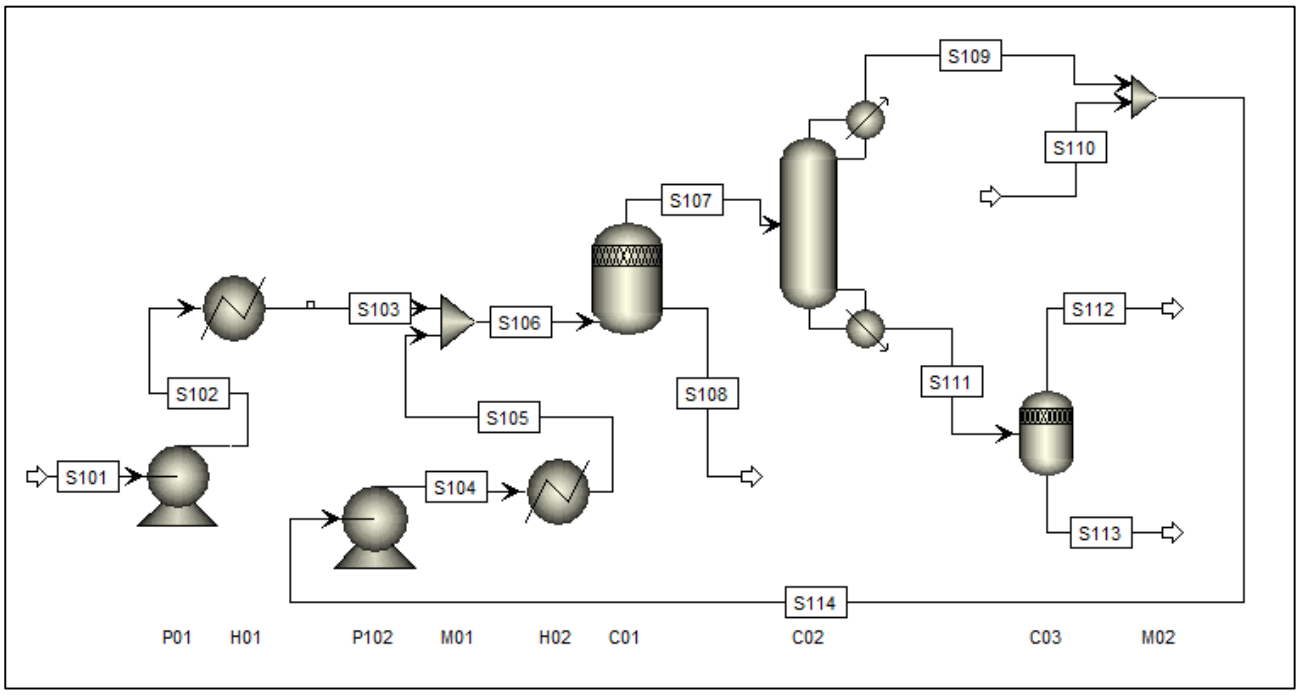

Figure 6.42. Aspen Plus process flow diagram for the proposed SCFE process, using either R-23, R-116 or a mixture of the two as the solvent. C01, extraction vessel; C02, stripping column; C03, product flash vessel; H01, heat exchanger; H02, heat exchanger; M01, feed mixer; M02, recycled solvent and makeup solvent mixer; P01, liquid pump; P02, liquid pump.

The feed (S101) is pumped by a liquid pump (P01) to the extraction vessel (C01). The temperature of the stream exiting this pump (S102) is heated to the correct temperature by a heat exchanger (H01), with the stream leaving the heat exchanger (S103) at the temperature and pressure of the extraction. The feed would then be mixed (M01) with the solvent (S105) prior to entering the extraction vessel (S106). The process conditions of the solvent (S114) are adjusted by a liquid pump (P102) and a heat exchanger (H02), which heats the solvent above the critical temperature. The extract from C01 exits from close to the top of the vessel (S107) and enters the solvent recovery column (C02) just above the bottom tray. In the column, the solvent moves upwards through the column, being stripped of the remaining extract, which exits from the reboiler (S111). This hydrocarbon-rich stream is sent to a further flash vessel (C03), which operates at ambient pressure, in which the solvent remaining in the extract (S112) is separated from the product (S113). If this process were to be used in a petroleum

refinery, the product stream, depending on the composition would be mixed into the feed for the crude distillation column. The distillate (S109), which comprises mainly the solvent, with residual amounts of the more volatile components, is mixed (M02) with a make-up stream (S110) and is returned to the extraction vessel (S114). The raffinate from CO1 could possibly require further treatment prior to disposal. This stream would contain only residual concentrations of hydrocarbons, and would therefore be substantially less hazardous than the oil sludge feed. The volume would also be substantially reduced.

This process could be operated with batch extractions or as a continuous system. The biggest downfall with performing the separation in batches would be the loss of solvent due to the depressurisation of the extraction vessel. Zizovic et al. (2005) estimated that solvent losses due to depressurisation when using CO_2, were as much as 0.5 kg solvent per kilogram of extract. These losses are substantial when using the fluorinated solvents, due to their much higher costs. In addition, all of the solvents from the depressurisation would need to be captured or destroyed, due to their high GWPs. A further consideration would be the operation of the stripping column, which could be operated more efficiently with a continuous process.

Although four different model systems were investigated for each solvent in Section 6.2.1, the design of the solvent recovery section was limited to a single model system for each solvent. The optimisation of the process for each of the sixteen solvent-system combinations was purposeless, as the aim was simply to show that the solvent could be successfully decoupled from the solutes, without losing large amounts of solvent. The separation of the solvent from the extract was found to be most difficult with the more volatile solutes. For this reason, the most volatile of the model systems was chosen for the simulation of the solvent recovery section. If the components that were present in model system 2 (n-hexane, 1-hexene and 3-methylpentane, in particular) could be separated successfully from the solvents, the less volatile components would also be separated easily at the given conditions.

Simulations of three solvent stripping columns were therefore performed; one each with R-23, R-116 and the R-23 + R-116 mixture as the solvent. Optimisation of each simulation was undertaken by varying the operational pressure, the reflux ratio, and the number of theoretical stages required. The optimal performance of the column was described by high solvent recovery (low losses), high recovered solvent and product stream purities and subcritical condenser temperatures. The performance of the column with changes in the distillate rate was also investigated. It was, however, found that, for all of the solvents, the best performance occurred when the distillate flow rate was the same as the feed rate of solvent to the extraction vessel. Thus, the distillate to feed ratios remained approximately the same as the solvent-to-feed ratios given in Table 6.25.

The desire for high solvent recovery was due to the high solvent costs, as well as the high GWPs of the solvents. Therefore, the aim was to recover as much of the solvent as possible at high pressure. After this recovery, any solvent captured at a low pressure would have to be treated, to prevent emission into the atmosphere. Alternatively, depending on the incineration costs, recompression of the low pressure solvent could also be investigated. In order to recover as much solvent as possible, it was not possible to completely separate the product from the recycled solvent, and a fraction of the more volatile components was present in the solvent upon return to the extraction stage. It was desired to minimise the return of product to the extraction vessel; and thus the requirement of a high recovered solvent purity. The fluid present in the condenser of the stripping column could not be supercritical, due to the problems that would occur with pressure control and the return of a reflux to the column without a liquid phase. The temperature of the condenser was therefore required to be below the critical temperature of the mixture present in the condenser.

The optimised parameters, as well as some of the important results from the stripping column are provided in Table 6.26.

Table 6.26. Optimised parameters and results for the recovery of the solvent using a stripping column, with R-23, R-116 and a R-23 + R-116 mixture as solvents.

Solvent	R-23	R-116	R-23 + R-116
$P_{condenser}$ / MPa	3.5	2.0	2.3
Number of theoretical stages	5	5	5
$T_{condenser}$ / K	301.87	299.49	294.51
$Q_{condenser}$ / 100 kg feed / [kW/kg]	-13.614	-20.149	-9.061
$T_{reboiler}$ / K	417.52	435.26	467.42
$Q_{reboiler}$ / 100 kg feed / [kW/kg]	25.984	33.402	18.869
R_{reflux} [kg / kg]	0.3	0.3	0.25
$\dot{m}_{S108}$ / $\dot{m}_{S101}$ (distillate [kg] / feed [kg])	2.28	3.60	1.47
$\dot{m}_{S110}$ / $\dot{m}_{S101}$ (product [kg] / feed [kg])	0.597	0.602	0.605
R-23 lost / $\dot{m}_{S101}$ [kg / kg]	0.0094	-	0.0039
R-116 lost / $\dot{m}_{S101}$ [kg / kg]	-	0.0095	0.0061
Solvent lost / Hydrocarbons recovered [kg / kg]	0.0158	0.0160	0.0166
$\dot{m}_{hc,S112}$ / $\dot{m}_{hc,S101}$ (hydrocarbon recovery) [kg / kg]	0.985	0.988	0.994
$x_{hc,S112}$ (mass purity of product)	0.989	0.984	0.986
$x_{refrig,S108}$ (mass purity of recovered solvent)	0.974	0.986	0.984

The pressure in the condenser, $P_{condenser}$, was highest for R-23 and lowest for R-116. Based upon the binary *P-x-y* data, this was to be expected, with the maximum pressures of systems containing R-116 being substantially lower than those containing R-23. The number of theoretical trays that would be required to perform the separation had to be a trade-off between the purity of the extract and the cost of the column on one hand and the recovery of the product and the solvent on the other. A

column with 5 theoretical stages was found to provide a reasonable balance between the two for all of the systems.

Although the temperatures of the condenser with each of the solvents were between (294.5 and 302) K, the temperature of the reboiler was found to differ fairly substantially. The temperature of the reboiler when using the R-23 + R-116 mixture as the solvent was almost 470 K. The reflux rate and the amount of solvent that was used for each separation played an important factor in the required heat duties for the condenser and the reboiler. Thus, the column with R-116 as the solvent required substantially higher heat duties, due to the higher R-116 flow rates. This also resulted in higher reflux rates. The gains in recovery and purity in the extraction stage by using high R-116 flow rates were therefore negated by the higher energy requirements for solvent recovery.

The product to feed ratio that is presented in Table 6.26 is partially inflated by the presence of small residual amounts of water and the solvent in the product. The R-23 + R-116 mixture appeared to be the easiest solvent to recover, based on the results that are provided in Table 6.26. Most importantly, the loss of solvent to hydrocarbon recovery ratio was only 1.6 to 1.7 % for all of the solvents. The R-23 + R-116 mixture exhibited a marginally better hydrocarbon recovery than the pure solvents. The purities of the solvent and the product are very similar for all three solvent systems.

The sensitivities of the purity and the recovery of the hydrocarbons, the solvent losses and the condenser and reboiler temperatures on changes to the column pressure, the number of stages, the reflux ratio and the distillate to feed ratio are presented in Appendix B.3. The sensitivities with R-23 as a solvent are given in Figures B.20, B.21 and B.22. Those for R-116 as the solvent are given in Figures B.23, B.24 and B.25. For the mixed solvent, the sensitivities are presented in Figures B.26, B.27 and B.28. The pressure of operation of the stripping column appeared to have the greatest effect on the column performance. Thus, good pressure regulation would be required for the column. The column performance was found to be least sensitive to the number of theoretical stages. To save on capital expenditure, it would therefore be possible to retrofit an unused column for this separation, as the number of stages available in the column is not crucial to its operation.

Although higher reflux ratios generally yielded improved product purities and reduced solvent losses, the cost of increasing the reflux ratio was an increase in the energy requirements of the condenser. This was not, however, a cost to the entire process, as all of the distillate would require cooling prior to re-pressurisation. This is due to the pumps requiring a sub-cooled liquid feed, to prevent cavitation from occurring within the pump due to the heat generated by the compression of the liquid.

6.3. ECONOMIC ANALYSIS

A study was undertaken at the Argonne National Laboratory in the USA in the late 1990's into the treatment of wastes from oil sand processing. Approximate prices per cubic meter of waste processed from this study were provided by Shariaty-Niassar et al. (2009). These prices are provided in Table 6.27, alongside values corrected with a 2.4% year on year average inflation rate for the United States of America (Zizovic et al., 2005).

Table 6.27. Approximate prices per cubic metre for processing oil sand wastes in the United States of America in 1998, and in 2015.

Disposal Method	Cost (1998) / US$·m^{-3}	Cost (2015) [a] / US$·m^{-3}
Land farming	35.00 to 85.00	52.40 to 127.20
Landfill	15.00 to 22.00	22.50 to 32.90
Evaporation (only for certain waste streams)	15.00 to 20.00	22.50 to 29.90
Depleted reservoir storage	42.00 to 70.00	62.90 to 104.80
Salt cavern storage	13.00 to 40.00	19.50 to 59.90

[a] calculated with an average yearly inflation of 2.4 %

A report published by the Dincer et al. (2015) estimated that, for the treatment of Saudi Aramco's oil sludge, a unit with an operating capacity of between (2 and 3) m^3 would be required. This large processing volume is due to the large production volumes of crude oil in Saudi Arabia. For a single refinery, the throughput would be substantially lowered. The estimate of van Oudenhoven et al. (1995) would in all likelihood be a better estimate of processing requirements. If this estimate is used, the processing requirements would be 0.6 m^3 per hour. Not all of this volume would require chemical treatment, and a portion could probably be separated by centrifugation or decanting. If it is estimated that half of the sludge can be treated in this manner, approximately 0.3 m^3 of sludge must be processed by solvent extraction per hour. The sludge was estimated to have a density of 825 kg·m^{-3}.

Three product streams would be produced by this process. Of these streams, two would be waste streams, and the third would be the recovered hydrocarbon stream. One waste stream would be the water and solids from which the hydrocarbons are extracted. Depending on the extent to which the hydrocarbons have been removed, it may be possible for this aqueous slurry to be filtered, the water to be sent to the waste water treatment, and the greatly reduced volume of solids sent to landfill. There is the possibility that the solids present in the sludge contain small concentrations of toxic heavy metals. If this is the case, then especial care must be given in the handling and disposal of the solids. The other waste stream would be a low pressure refrigerant rich stream. This stream would require incineration or the refrigerants would need to be captured, to prevent their emission into the atmosphere. In an oil refinery, there is the possibility that this stream could be incinerated in the flare, with little additional costs.

A number of assumptions and values were required for the calculation of the cost of using SCFE to treat oil sludge. These assumptions are listed in Table 6.28.

Table 6.28. Assumptions for the economic analysis.

Variable	Unit	Value
Cost of R-23 [a]	$ / kg	2.4
Cost of R-116 [b]	$ / kg	10
Labour cost [c]	$ / hr	1.46
Electricity cost [d]	$ / kVA	0.0563
Working hours	hr	24
Working days per year	d	300
Maintenance costs [e]	% of CAPEX	2

[a] see Chapter 3.4.5

[b] see Chapter 3.5.5

[c] labour costs were low due to the assumed instalment of the plant on an existing refinery

[d] R0.7662/kVA (Eskom Holdings SOC Ltd, 2014) at R13.60 per US$ (South African Reserve Bank, 2015)

[e] Shariaty-Niassar et al. (2009)

Due to the costs of alternative oil sludge processing techniques being provided in US$ prices, these calculations were also undertaken in terms of US$ prices. Most of the data that was found was already given in US$ prices, and therefore there was no purpose in converting these values to South African Rands for the calculation, and thereafter converting the costs back to US$ for comparison.

6.3.1. INCOME

The recovery of hydrocarbons from oil sludge, using SCFE, would not generate an explicit income, but would rather return the hydrocarbons to the refinery for processing. The recovered hydrocarbon stream was assumed to have a similar value to a 40° API crude oil, which would have a density of 825 kg/m^3. The worth of this stream was estimated to be equivalent to an approximate average Brent Crude Oil price of $50 per bbl. Thus, the savings from recovering the hydrocarbons from the oil sludge was estimated to be $0.26 per kilogram of recovered product. The savings that could be achieved by recovering the hydrocarbon fraction from the oil sludge using SCFE are presented in Table 6.29 for each solvent system.

Table 6.29. Achievable savings by the recovery of the hydrocarbon fraction from the oil sludge.

	Units	R-23	R-116	R-23 + R-116
Oil sludge feed	kg.yr^{-1}	1 782 000	1 782 000	1 782 000
Hydrocarbon fraction		0.6	0.6	0.6
Recovery		0.985	0.988	0.994
Hydrocarbons recovered	kg.yr^{-1}	1 053 162	1 056 370	1 062 785
Savings achieved	$.yr^{-1}	273 248	274 080	275 745

The savings that could be achieved were very similar for all of the solvents, due to the high recoveries that could be achieved with all three of the fluorinated solvent systems.

6.3.2. EXPENDITURE

The advantage in the integration of a new process within an existing processing plant, such as an oil refinery, is the existing availability of utilities such as steam and cooling water. The scale at which these utilities are utilised on a refinery translate into lower costs for their use in a new process. Medium pressure steam (MPS) could be used to provide the heating requirements of the reboiler in the solvent stripping column. The heating value of a MPS stream is given in Table 6.30.

Table 6.30. Medium pressure steam heating value on an oil refinery.

Heating	Properties	Reference
Pressure	13 bar (g)	Dincer et al. (2015)
Temperature	468.19 K	Smith et al. (2005)
Latent heat of condensation	1957.73 kJ/kg	Smith et al. (2005)
Cost on oil refinery	$9.66 / ton	Ocic (2008)
Heating value	202.664 MJ / $	

Some of the cooling requirements for the SCFE plant could be satisfied with cooling water, although the majority of the cooling would have to be performed using refrigeration, due to the temperatures being below ambient temperatures. Due to this requirement, the case was considered in which all of the cooling requirements for the process were provided by refrigeration. The determination of the cost of cooling was therefore calculated based upon the ability of the refrigeration unit to utilise electrical energy to drive the cooling effect. The costs in the operation of a refrigeration unit rise from the energy requirements for the compression of the refrigerant and for driving the heat loss from the heat sink. In many cases, the heat sink is cooled by air, which is blown over the condenser by large fans. Alternatively, cooling water could be used to cool the condenser. The efficiencies that could be expected of a refrigeration unit, and which were used to estimate the electricity costs for cooling are provided in Table 6.31.

Table 6.31. Efficiencies

Refrigeration	Value	Reference
Compressor isentropic efficiency	0.80	Gong et al. (2006)
Carnot efficiency	0.60	Sinnott (2009)
Overall refrigeration efficiency	0.48	
Pump efficiencies	0.2957	Aspen Technology (2012)
Power factor (3 phase motors)	0.9	

The operating costs for the SCFE plant for treating oil sludge are listed in Table 6.32. Due to the lower solvent flow rates required when using the R-23 + R-16 solvent mixture, the energy requirements for this process would be lower, thereby reducing the operating costs. The labour costs that are given are fairly low, as the process would be integrated into an existing refinery, which would be highly automated and controlled from a central control room. It was estimated that only one additional

employee would be required for the operation of the SCFE process. The maintenance costs for the process were estimated to be 2% of the CAPEX per annum (Shariaty-Niassar et al., 2009).

Table 6.32. Estimated costs for the operation of a SCFE plant for the treatment of oil sludge with R-23, R-116 or a R-23 + R-116 mixture.

	Units	R-23	R-116	R-23 + R-116
Cooling requirements	kW	-76.220	-100.126	-49.228
Heating requirements	kW	64.310	82.960	48.569
Pumping requirements	kW	11.086	1.586	1.309
Electrical requirements	kW	47.671	49.647	24.939
R-23 losses	$kg.yr^{-1}$	16 750.8		6 949.8
R-23 makeup	$\$.yr^{-1}$	40 201.92		16 679.52
R-116 losses	$kg.yr^{-1}$		16 929	10 870.2
R-116 makeup	$\$.yr^{-1}$		40 629.60	26 088.48
Heating Costs	$\$.yr^{-1}$	8 225.07	10 610.23	6 211.85
Electricity costs	$\$.yr^{-1}$	21 485.68	22 376.20	11 239.97
Labour costs	$\$.yr^{-1}$	10 504.20	10 504.20	10 504.20
Maintenance costs [a]	$\$.yr^{-1}$	13 800.74	13 973.47	10 684.14
TOTAL	**$\$.yr^{-1}$**	**94 217.61**	**98 093.70**	**81 408.16**

[a] estimated to be 2 % of the CAPEX (see section 6.3.3),

6.3.3. CAPEX

The capital expenditure for the construction of a SCFE plant by far dominates the economic analysis for such a plant. Shariaty-Niassar et al. (2009) estimate that between (70 and 85) % of the costs of operating a SCFE plant result from the initial investment costs. A good estimation of the price of constructing the plant is therefore a necessity in the analysis of the economic feasibility of the process. Perrut and Clavier (2003) investigated the costs of a large number of SCF processes, and correlated a dimensionless price index to the extraction volume and the design flow rate. Perrut and Clavier produced an equation shown in equation 6.2.

$$PI = A(10\, V_T \dot{m}_{solvent})^{0.24} \qquad 6.3$$

where *PI* is the price index, *A* is the a fitted variable, V_T is the total extraction volume, and $\dot{m}_{solvent}$ is the flowrate of the solvent in the process.

del Valle et al. (2005) investigated the applicability of equation 6.3 to the costs that were reported in literature for several large scale industrial SCF processes. They converted the costs for each of the examined processes to values in US$ for plants with 400 bar pressure ratings. In their correlations, they neglected the factor of 10 included by Perrut and Clavier in the equation. They found that the value of *A* varied between (40 000 and 80 000) US$. If the factor of 10 included by Perrut and Clavier is added to the comparison of del Valle et al., the value of *A* was found to vary between (237 000 and 462 000) US$.

The use of a solvent stripping column in the proposed design would likely advocate the use of the higher end of the range of values for *A*. Both the maximum and the minimum values were used in the calculation of the CAPEX. The volume of the extraction vessel was required for the calculation of the cost of the construction of the SCFE plant. The estimates of the sizing of the extraction vessel, as well as the flow rates and the maximum and minimum cost estimates for each of the three solvents are provided in Table 6.33.

Table 6.33. CAPEX for a SCFE plant using different solvents to separate hydrocarbons from an oil sludge.

		R-23	R-116	R-23 + R-116
Solvent flowrate	$kg.hr^{-1}$	564	891	364
Total flowrate	$kg.hr^{-1}$	812	1139	611
Density [a]	$kg.m^{-3}$	1007	2526	1391
Total flowrate	$m^3.hr^{-1}$	0.806	0.451	0.439
Extraction vessel retention time	hr	0.093	0.111	0.091
Extraction vessel size	m^3	0.075	0.05	0.04
Max SCFE plant construction cost	US$	10 351 000	10 480 000	8 013 000
Min SCFE plant construction cost	US$	5 310 000	5 376 000	4 111 000
Max yearly SCFE CAPEX cost over lifetime	$US\$.yr^{-1}$	690 037	698 673	534 207
Min yearly SCFE CAPEX cost over lifetime	$US\$.yr^{-1}$	353 980	358 410	274 041

[a] Value estimated by the process simulation (Aspen Plus V8.4)

[b] plant lifetime estimated to be 15 years

The lower flow rates with the R-23 + R-116 solvent mixture, which result in a smaller extraction vessel being required, reduced the estimated plant construction costs by 20 % when compared to those for R-23 and R-116 when using the correlation proposed by Perrut and Clavier.

6.3.4. SCFE Treatment Costs

The summary of the costs for the treatment of the oil sludge with a SCFE process using either R-23, R-116 or a blend of the two is presented in Table 6.34. The CAPEX as a fraction of the total costs for the process, based on both the minimum and the maximum CAPEX values, shows that for this process, the estimated values were towards the higher end of the expected range. This is possibly due to other costs being lower, because the process would be constructed within an existing facility.

Table 6.34. Pricing of the SCFE plant operation with each of the solvents

		R-23	R-116	R-23 + R-116
Max yearly SCFE CAPEX cost over lifetime	US$.yr^{-1}	690 037	698 673	534 207
Max CAPEX as a fraction of total costs		0.880	0.877	0.868
Min yearly SCFE CAPEX cost over lifetime	US$.yr^{-1}	353 980	358 410	274 041
Min CAPEX as a fraction of total costs		0.802	0.797	0.782
Operational costs for SCFE plant	US$.yr^{-1}	94 218	98 094	81 408
Savings achieved	US$.yr^{-1}	-273 248	-274 080	-275 745
Max yearly costs for operating SCFE plant	US$.yr^{-1}	511 007	522 687	339 870
Max costs per m^3 of sludge	**US$.m^{-3}**	**236.58**	**241.98**	**157.35**
Min yearly costs for operating SCFE plant	US$.yr^{-1}	168 228	175 618	74 501
Min costs per m^3 of sludge	**US$.m^{-3}**	**77.88**	**81.30**	**34.49**

The costs of using a SCFE process to treat the oil sludge in an oil refinery outweigh the savings achieved by recovering the hydrocarbons. This is mainly due to the high CAPEX costs that were estimated. In the calculation of the CAPEX for a SCFE plant, the maximum and minimum parameters that were fitted to data given by del Valle et al. (2005) were used. Due to the large variance in these parameters, there was a large difference in the range of estimated CAPEX costs.

Upon comparison of the costs of treating the oil sludge with a SCFE to those given in Table 6.27, it is obvious that with the high CAPEX costs, the process is inhibitively expensive in comparison to other treatment techniques. If, however, the CAPEX costs are at the lower end of the estimated range, the process will become very competitive with the existing oil sludge disposal techniques.

The costs of operating a processing facility for oil sludge were expected to outweigh the possible savings that were generated. However, the main purpose of such a plant would be to reduce hazardous waste output of the crude oil processing facility, be it an oil refinery or a crude oil production and transportation facility. By removing the majority of the hydrocarbons from the oil sludge, the remaining portion of the oil sludge will be considered non-flammable, thus greatly reducing the hazardous nature of this waste. The removal of the hydrocarbon fraction will also mean that the separation of the solids from the water would also be simplified.

The use of a supercritical R-23 + R-116 solvent mixture to treat waste streams from the petroleum industry has the lowest costs of the solvents that were investigated. This is mainly due to the reduced flowrates that are required when using this mixture. If the flowrates of the other solvents were also reduced, they would likely have similar costs. Unfortunately, however, reducing the flow rates of R-23 or R-116 would also result in reduced recoveries and product purities.

7. CONCLUSIONS

There are a number of difficult separation problems in the petroleum industry for which SCFE may provide a feasible separation technique. The use of SCFs as solvents provide significant advantages over more conventional solvents, in that they exhibit improved extraction capabilities, as well as being substantially easier to separate from the extracted components. SCFs are used in a wide range of chemical processes, but only in a few cases within the petroleum industry. CO_2 is by far the most common fluid used as a SCF solvent, but its weakness lies in the low solubilities of more polar and larger molecular weight components therein. In order to improve the ability of SCFE to extract these components, either co-solvents can be added to the CO_2, or alternatively, the CO_2 can be replaced with alternative, more polar solvents.

The global phase diagram classifications of van Konynenburg and Scott are useful in approximating how a system will behave throughout the critical region. For a system to be categorised according to this classification technique, some information on the behaviour of the system is required. The most common techniques for describing fluid phase behaviour in the critical regions are either through the extrapolation of sub-critical co-existence data, or else through the use of calculation techniques, which are based upon thermodynamic models fitted to the sub-critical co-existence data. Measurements of phase equilibrium data in the critical region, such as measurement of the critical loci, are extremely difficult, and not many of these measurements have been performed. Thus, the sub-critical co-existence data is of great importance for description of the phase behaviour of a system in the critical region.

R-23 and R-116 were selected as two possible solvents for replacing CO_2 as supercritical solvents, based upon their properties. There have been a significant number of measurements into the phase equilibria of systems involving carbon dioxide. However, not much phase equilibrium data have been measured for systems involving R-23 and R-116. Several solutes were therefore chosen with which binary systems with the R-23 and the R-116 were measured. The densities and viscosities of pure CO_2, R-23 and R-116, as well as mixtures containing these components were investigated, as solubility has been shown to be a function of the density of the solvent. Additionally, the availability, costs and environmental impacts of each of the solvents were considered. It was shown that although the R-23 and R-116 had higher GWPs and costs, they remained feasible as replacements for SC CO_2.

Three experimental apparatuses were used to measure the phase equilibrium data for this study. These were a static-analytic high pressure apparatus, used for *P-x-y* measurements; a static-synthetic variable-volume apparatus used for bubble pressure measurements; and a critical point

determination apparatus, used to measure the critical loci of several binary systems. The uncertainties in the measurements of the variables (*P, T, x*) from each of these apparatuses were estimated according to the NIST approach, and using a coverage factor of $k = 2$. Uncertainties were calculated for each equilibrium measurement, rather than a standard uncertainty being estimated for each variable. This was because the uncertainties were dependent upon the repeatability of the measurements, which varied from system to system and variable to variable.

The experimental phase equilibrium data that was measured with the static-analytic apparatus was compared with the bubble point data measured with the static-synthetic apparatus. There was good agreement between the data from the static-analytic apparatus and the data from the static-synthetic apparatus for all of the systems that were measured. The experimental data was found to be fairly accurately described by the PR-MC + WS/NRTL thermodynamic model, which was used to describe all of the systems. A single thermodynamic model was used for all the systems, as this enabled the simulation of SCFE processes. The model provided an excellent fit for most of the systems, with average relative deviations between the experimental data and the modelled data of less than 2.0 % for both temperature and vapour phase composition. However, for other systems, there was a fairly large disparity between the modelled and the experimental data, with average relative deviations of as much as 20 %. This was particularly true for the systems that contained water.

The phase equilibrium data were extrapolated to the critical loci, and the extrapolated critical loci were then compared to locus curves calculated using the thermodynamic model. For most of the systems, there was a fair agreement between the calculated and extrapolated loci. Any deviations that occurred were most probably due to the poor description of the sub-critical data by the model. To verify the ability of the extrapolation or calculation procedures to accurately determine the critical locus curves of the systems, several locus curves were compared with data measured using the critical point determination apparatus. The extrapolation procedure was found to provide estimates of the critical loci that were closer to the experimental data than the calculation based on the thermodynamic models.

The thermodynamic models, fitted to the systems involving CO_2, R-23 and R-116, were used to perform simulations of the separation of water from several hydrocarbon mixtures. R-23, R-116, as well as a mixture of R-23 and R-116, were all found to give substantially better separations of the systems than the CO_2. The abilities to recover the R-23 and R-116 were important for this separation, both in an economic and an environmental aspect. A stripping column with 5 theoretical stages was therefore simulated for the recovery of the solvent from the hydrocarbons. This separation was simulated at high pressures of between (2 and 5) MPa. The stripping column ensured that the recovery of the solvents was very high, whilst at the same time preventing excessive carry-over of the

hydrocarbons back to the extraction vessel. An economic analysis of the processes showed that the separation of an oil sludge using these alternative solvents would be economically competitive processes, when compared with other oil sludge treatment techniques that are currently used. The R-23 + R-116 mixture was shown to be particularly competitive, with high hydrocarbon recoveries (99.4 %), high extract purities (98.4 %), and low solvent losses (1.0 %). The capital expenditure for the construction of a SCFE process to treat oil sludges was found to be the greatest contributor to the costs, with between 75 and 90 % of the costs being derived from capital expenditure. This is likely due to the high pressures at which an SCFE process must operate.

8. REFERENCES

1. Abbott, M.M., Van Ness, H.C. (1975). Vapour-liquid equilibrium: Part II. Data reduction with precise expressions for G^E. AIChE J., **21**(1), pp. 62-71.
2. Abbott, M.M. (1979). Cubic Equations of State: An Interpretive Review. Equations of State in Engineering and Research, American Chemical Society. **182**, pp. 47-70.
3. Abrams, D.S. and Prausnitz, J.M. (1975). "Statistical thermodynamics of liquid mixtures: A new expression for the excess Gibbs energy of partly or completely miscible systems." AIChE J. **21**(1), pp. 116-128.
4. Acda, M.N., Morrell, J.J. and Levien, K.L. (1996). "Decay resistance of composites following supercritical fluid impregnation with tebuconazole " Material und Organismen **30**(4), pp. 293-300.
5. Adachi, Y. and Sugie, H. (1986). "A new mixing rule-modified conventional mixing rule." Fluid Phase Equilibr. **28**(2), pp. 103-118.
6. Adams, W.R., Zollweg, J.A., Streett, W.B. and Rizvi, S.S.H. (1988). "New apparatus for measurement of supercritical fluid-liquid phase equilibria." AIChE J. **34**, pp. 1387-1391.
7. Adinco BV (2015). "Chemical Resistance Chart." Retrieved 28 April, 2015, from http://www.adinco.nl/site/media/downloads/instrumenten/Chemische%20bestendigheidslijst.pdf.
8. Adrian, T., Oprescu, S. and Maurer, G. (1997). "Experimental investigation of the multiphase high-pressure equilibria of carbon dioxide + water + (1-propanol)." Fluid Phase Equilib. **132**(1–2), pp. 187-203.
9. Ahmad, S., Giesen, R. and Lucas, K. (2004). "Vapor−Liquid Equilibrium Studies for Systems Containing n-Butylisocyanate at Temperatures between 323.15 K and 371.15 K." J. Chem. Eng. Data **49**(4), pp. 826-831.
10. Air Liquide (2013). "Gas Encyclopedia - Trifluoromethane." Retrieved 28 April 2015, from http://encyclopedia.airliquide.com/Encyclopedia.asp?GasID=66.
11. Aizpiri, A.G., Rey, A., Davila, J., Rubio, R.G., Zollweg, J.A. and Streett, W.B. (1991). "Experimental and theoretical study of the equation of state of trifluoromethane in the near-critical region." J. Phys. Chem. **95**(8), pp. 3351-3357.
12. Akgün, M., Akgün, N.A. and Dinçer, S. (1999). "Phase behaviour of essential oil components in supercritical carbon dioxide." J. Supercrit. Fluids **15**(2), pp. 117-125.
13. Alexandrou, N. and Pawliszyn, J. (1989). "Supercritical fluid extraction for the rapid determination of polychlorinated dibenzo-p-dioxins and dibenzofurans in municipal incinerator fly ash." Anal. Chem. **61**(24), pp. 2770-2776.
14. Allemand, N., Jose, J. and Merlin, J.C. (1986). "Mesure des pressions de vapeur d'hydrocarbures C10 A C18 n-alcanes et n-alkylbenzenes dans le domaine 3-1000 Pascal." Thermochim. Acta **105**, pp. 79-90.
15. Al-Marzouqi, A.H., Zekri, A.Y., Jobe, B. and Dowaidar, A. (2007). "Supercritical fluid extraction for the determination of optimum oil recovery conditions." J. Petrol. Sci. Eng. **55**(1-2), pp. 37-47.

16. Alonso, E., Cantero, F.J., García, J. and Cocero, M.J. (2002). "Scale-up for a process of supercritical extraction with adsorption of solute onto active carbon. Application to soil remediation." J. Supercrit. Fluids **24**(2), pp. 123-135.
17. Altgelt, K.H. and Boduszynski, M.M. (1994). Composition and Analysis of Heavy Petroleum Fractions, Marcel Dekker.
18. Alwani, Z. and Schneider, G.M. (1969). Berich. Bunsen. Gesell. **73**, pp. 294-301.
19. Ambrose, D. and Grant, D.G. (1957). "The critical temperatures of some hydrocarbons and pyridine bases." T. Faraday Soc. **53**(0), pp. 771-778.
20. Ambrose, D. and Tsonopoulos, C. (1995). "Vapor-Liquid Critical Properties of Elements and Compounds. 2. Normal Alkanes." J. Chem. Eng. Data **40**(3), pp. 531-546.
21. Anastas, P.T. and Warner, J.C. (1998). Green Chemistry Theory and Practice. New York, NY, Oxford University Press.
22. Anderson, T.F. and Prausnitz, J.M. (1978). "Application of the UNIQUAC Equation to Calculation of Multicomponent Phase Equilibria. 1. Vapor-Liquid Equilibria." Ind. Eng. Chem. Proc. Des. Dev. **17**(4), pp. 552-561.
23. Andrews, T. (1869). "The Bakerian Lecture: On the Continuity of the Gaseous and Liquid States of Matter." Philos. Trans. R. Soc. London, Ser. A **159**, pp. 575-590.
24. Anitescu, G. and Tavlarides, L.L. (2006). "Supercritical extraction of contaminants from soils and sediments." J. Supercrit. Fluids **38**(2), pp. 167-180.
25. Araujo, M.E., Machado, N.T., Angela, M. and Meireles, M. (2001). "Modeling the phase equilibrium of soybean oil deodorizer distillates + supercritical carbon dioxide using the Peng - Robinson EOS." Ind. Eng. Chem. Res. **40**(4), pp. 1239-1243.
26. Arora, H.S., Cantor, R.R. and Nemeth, J.C. (1982). "Land treatment: A viable and successful method of treating petroleum industry wastes." Environ. Int. **7**(4), pp. 285-291.
27. Aspen Technology (2012) Aspen Plus V8.4. Bedford, MA, USA
28. ASTM Committee D-2 (1949). The Significance of Tests of Petroleum Products: A Report, American Society for Testing Materials.
29. Avedesian, M.M. (1987). Apparatus and method involving supercritical fluid extraction, **US Patent 4714591**
30. Ávila-Chávez, M.A. and Trejo, A. (2010). "Remediation of soils contaminated with total petroleum hydrocarbons and polycyclic aromatic hydrocarbons: Extraction with supercritical ethane." Ind. Eng. Chem. Res. **49**(7), pp. 3342-3348.
31. Baba-Ahmed, A., Guilbot, P. and Richon, D. (1999). "New equipment using a static analytic method for the study of vapour–liquid equilibria at temperatures down to 77 K." Fluid Phase Equilibr. **166**(2), pp. 225-236.
32. Bamberger, A., Sieder, G. and Maurer, G. (2000). "High-pressure (vapor+liquid) equilibrium in binary mixtures of (carbon dioxide+water or acetic acid) at temperatures from 313 to 353 K." J. Supercrit. Fluids **17**(2), pp. 97-110.
33. Barker, J.A. (1953). Determination of Activity Coefficients from Total Pressure Measurements, Aust. J. Chem. 6, pp. 207-210.

34. Barnabas, I.J., Dean, J.R., Tomlinson, W.R. and Owen, S.P. (1995). "Experimental Design Approach for the Extraction of Polycyclic Aromatic Hydrocarbons from Soil Using Supercritical Carbon Dioxide." Anal. Chem. **67**(13), pp. 2064-2069.
35. Bartle, K.D., Clifford, A.A., Hawthorne, S.B., Langenfeld, J.J., Miller, D.J. and Robinson, R. (1990). "A model for dynamic extraction using a supercritical fluid." J.Supercrit. Fluids **3**(3), pp. 143-149.
36. Basta, N. and McQueen, S. (1985). Supercritical Fluids: Still Seeking Acceptance. Chem. Eng. - New York, pp. 14-17
37. Beckman, E.J. (2004). "Supercritical and near-critical CO2 in green chemical synthesis and processing." J. Supercrit. Fluids **28**(2–3), pp. 121-191.
38. Beijing Starget Chemicals Co. Ltd. (2015). Hexafluoroethane gas. Beijing,
39. Belaribi, B.F., Ait-Kaci, A. and Jose, J. (1991). Liquid vapor equilibrium. Decane-1-hexyne system. Int. DATA Ser., Sel. Data Mixtures, Ser. A. **1**, pp. 74-76
40. Berche, B., Henkel, M. and Kenna, R. (2009). "Critical phenomena: 150 years since Cagniard de la Tour." J. Phys. Studies **13**, pp. 3201.
41. Berger, T.A. (1995). Packed Column SFC. Letchworth, UK, Royal Society of Chemistry.
42. Berger, T.A. (1997). "Separation of polar solutes by packed column supercritical fluid chromatography." J. Chromatogr. A **785**(1–2), pp. 3-33.
43. Berro, C., Laichoubi, F. and Rauzy, E. (1994). "Isothermal (vapour + liquid) equilibria and excess volumes of (3-methylpentane + heptane), of (3-methylpentane + octane), and of (toluene + octane)." J. Chem. Thermodyn. **26**(8), pp. 863–869.
44. Besley, L.M. (1974). "Vapour pressure of toluence from 273.15 to 298.15 K." J. Chem. Thermodyn. **6**(6), pp. 577–580.
45. Biceroglu, O. (1994). "Rendering oily waste land treatable or usable." **US Patent 5288391 A**
46. Bich, E., Lober, T. and Millat, J. (1992). "Quasi-isochoric P-ϱ-T measurements, 2nd virial coefficient and vapor pressure of n-hexane." Fluid Phase Equilibr. **75**, pp. 149-161.
47. Bogatu, C., Vîlcu, R., Geana, D., Duta, A., Poot, W. and De Loos, T.W. (2009). "High pressure phase behaviour of the system R23 + phenylpropane. Experimental results and modeling liquid-vapour equilibrium." Rev. Roum. Chim. **54**(5), pp. 343-349.
48. Bogatu, C., Geană, D., Vîlcu, R., Duţă, A., Poot, W. and de Loos, T.W. (2010a). "Fluid phase equilibria in the binary system trifluoromethane+1-phenyloctane." Fluid Phase Equilibr. **295**(2), pp. 186-193.
49. Bogatu, C., Vilcu, R., Duta, A., Straver, E. and De Loos, T.W. (2010b). "Vapour-liquid, liquid-liquid and vapour-liquid-liquid equilibria in the system of trifluoromethane + (2-methylpropyl)benzene." Rev. Chim.-Bucharest **61**(8), pp. 767-769.
50. Bogatu, C., Geană, D., Duţă, A., Poot, W. and De Loos, T.W. (2011). "Fluid-phase equilibria in the binary system trifluoromethane + 1-phenyltetradecane." Ind. Eng. Chem. Res. **50**(1), pp. 213-220.
51. Böhm, F., Heinisch, R., Peter, S. and Weidner, E. (1989). Design, Construction, and Operation of a Multipurpose Plant for Commercial Supercritical Gas Extraction. Supercritical Fluid Science and Technology, American Chemical Society. **406**, pp. 499-510.

52. Bonhorst, C.W., Althouse, P.M. and Triebold, H.O. (1948). "Esters of Naturally Occurring Fatty Acids - Physical Properties of Methyl, Propyl, and Isopropyl Esters of C6 to C18 Saturated Fatty Acids." Ind. Eng. Chem. **40**(12), pp. 2379-2384.
53. Boston, J.F. and Mathias, P.M. (1980). Phase Equilibria in a Third-Generation Process Simulator. 2nd International Conference on Phase Equilibria and Fluid Properties in the Chemical Process Industries, West Berlin.
54. Bott, T.R. (1980). "Supercritical Gas Extraction." Chem. Ind. (London) **6**, pp. 228-232.
55. Boukais-Belaribi, G., Belaribi, B.F., Ait-Kaci, A. and Jose, J. (2000). "Thermodynamics of n-octane+hexynes binary mixtures." Fluid Phase Equilibr. **167**(1), pp. 83-97.
56. Brady, B.O., Kao, C.P.C., Dooley, K.M., Knopf, F.C. and Gambrell, R.P. (1987). "Supercritical extraction of toxic organics from soils." Ind. Eng. Chem. Res. **26**(2), pp. 261-268.
57. Brandt, L., Elizalde-Solis, O., Galicia-Luna, L.A. and Gmehling, J. (2010). "Solubility and density measurements of palmitic acid in supercritical carbon dioxide + alcohol mixtures." Fluid Phase Equilibr. **289**(1), pp. 72-79.
58. Brennecke, J.F. and Chateauneuf, J.E. (1999). "Homogeneous Organic Reactions as Mechanistic Probes in Supercritical Fluids." Chemical Reviews **99**(2), pp. 433-452.
59. Brignole, E.A. and Pereda, S. (2013). Phase Equilibrium Engineering, Elsevier Science.
60. Brogle, H. (1982). "CO_2 as a solvent: its properties and applications." Chem. Ind. (London) **19**(385-390).
61. Brough, S.A., Riley, S.H., McGrady, G.S., Tanhawiriyakul, S., Romero-Zeron, L. and Willson, C.D. (2010). "Low temperature extraction and upgrading of oil sands and bitumen in supercritical fluid mixtures." Chem. Commun. **46**(27), pp. 4923-4925.
62. Brunner, E. (1985). "Solubility of hydrogen in 10 organic solvents at 298.15, 323.15, and 373.15 K." J. Chem. Eng. Data **30**(3), pp. 269-273.
63. Brunner, G. and Peter, S. (1981). "On the State of Development in the Extraction with Compressed Gases." Chem. Ing. Tech **53**(7), pp. 529-542.
64. Brunner, G. (1983). "Selectivity of supercritical compounds and entrainers with respect to model substances." Fluid Phase Equilib. **10**(2-3), pp. 289-298.
65. Brunner, G. (1998). "Industrial process development: Countercurrent multistage gas extraction (SFE) processes." J. Supercrit. Fluids **13**(1–3), pp. 283-301.
66. Burford, M.D., Hawthorne, S.B. and Miller, D.J. (1993). "Extraction rates of spiked versus native PAHs from heterogeneous environmental samples using supercritical fluid extraction and sonication in methylene chloride." Anal. Chem. **65**(11), pp. 1497-1505.
67. Businelli, D., Massaccesi, L., Said-Pullicino, D. and Gigliotti, G. (2009). "Long-term distribution, mobility and plant availability of compost-derived heavy metals in a landfill covering soil." Sci. Total Environ. **407**(4), pp. 1426-1435.
68. Cabañas, A., Zong, Y. and Watkins, J.J. (2003). Chemical Fluid Deposition of Metals from Supercritical Fluids. 6th International Symposium on Supercritical Fluids. Versailles, France, International Society for the Advancement of Supercritical Fluids,

69. Cagniard de la Tour, C. (1822). "Exposé de quelques résultats obtenu par l'action combinée de la chaleur et de la compression sur certain liquids, tels que l'eau, l'alcool, l'éther sulfurique et l'essence de pétrole rectifiée." Ann. Chim. Phys. **21**, pp. 127-132.
70. Calandra, A.J., Castellano, C.E., Ferro, C.M. and Cobo, O. (1982). Experimental and Theoretical Analysis of the Anode Effects in Industrial Cells. Washington, USA, Metallurgical Society of America.
71. Calm, J.M. and Hourahan, G.C. (2007). "Refrigerant Data Update." Heating-Piping-Air Cond. **79**(1), pp. 50-64.
72. Camacho-Camacho, L.E., Galicia-Luna, L.A., Elizalde-Solis, O. and Martínez-Ramírez, Z. (2007). "New isothermal vapor–liquid equilibria for the CO2+n-nonane, and CO2+n-undecane systems." Fluid Phase Equilibr. **259**(1), pp. 45-50.
73. Camin, D.L. and Rossini, F.D. (1956). "Physical Properties of the 17 Isomeric Hexenes.of the API Research Series." J. Phys. Chem. **60**(10), pp. 1446-1451.
74. Carbognani, L., Orea, M. and Fonseca, M. (1999). "Complex nature of separated solid phases from crude oils." Energ. Fuels **13**(2), pp. 351-358.
75. Carbognani, L., Contreras, E., Guimerans, R., León, O., Flores, E. and Moya, S. (2001). "Physicochemical characterization of crudes and solids deposits as a guide for crude production optimization." Visión tecnológica **8**(1), pp. 111-122.
76. Carruth, G.F. and Kobayashi, R. (1973). "Vapor pressure of normal paraffins ethane through n-decane from their triple points to about 10 mm mercury." J. Chem. Eng. Data **18**(2), pp. 115-126.
77. Carty, D.T., Iliff, R.J., Kong, S.B., Latham, J.R. and Mitchell, J.D. (1992). "Liquid/supercritical cleaning with decreased polymer damage." **US Patent 5370742 A**
78. Castellari, C., Francesconi, R. and Comelli, F. (1988). "Vapor-liquid equilibrium, excess gibbs energy and excess enthalpy of 1,3-dioxolane-methylcyclohexane at T = 313.15 K." Can. J. Chem. Eng. **66**(1), pp. 131-135.
79. Castrup, H. (2004). Selecting and Applying Error Distributions in Uncertainty Analysis. 2004 Measurement Science Conference, Anaheim, CA, USA.
80. Central China Sepcial Gas Co. Ltd. (2015). Hexafluoroethane gas. Hunan, China,
81. Chamorro, C.R., Segovia, J.J., Martín, M.a.C. and Villamañán, M.A. (2002). "Vapor–liquid equilibrium of octane-enhancing additives in gasolines: 4. Total pressure data and GE for ternary mixtures containing isopropyl ether or benzene and n-heptane + 1-hexene at 313.15 K." Fluid Phase Equilibr. **193**(1-2), pp. 289-301.
82. Chapman, W.G., Gubbins, K.E., Jackson, G. and Radosz, M. (1990). "New reference equation of state for associating liquids." Ind. Eng. Chem. Res. **29**(8), pp. 1709-1721.
83. Charoensombut-Amon, T. and Kobayashi, R. (1986). "Application of the Wilson—Wegner expansion to represent vapor—liquid equilibrium surfaces of binary and ternary systems from the critical locus to the vapor pressure of the heavier component." Fluid Phase Equilibr. **31**(1), pp. 23-34.
84. Charpentier, B.A. and Sevenants, M.R., Eds. (1988). Supercritical Fluid Extraction and Chromatography: Techniques and Applications. Am. Chem. Soc. Symp. Ser., American Chemical Society.

85. Chase, C.E., Williamson, R.C. and Tisza, L. (1964). "Ultrasonic Propagation Near the Critical Point in Helium." Phys. Ref. Lett. **13**(15), pp. 467-469.
86. Chen, D. and Chen, W. (1992). "Phase equilibria of n-hexane and n-octane in critical carbon dioxide." Huaxue Gongcheng **20**, pp. 66-69.
87. Chen, L., Zhang, X.-R. and Jiang, B. (2014). "Effects of Heater Orientations on the Natural Circulation and Heat Transfer in a Supercritical CO2 Rectangular Loop." J. Heat Transf. **136**(5), pp. 052501-052501.
88. Cheng, K.-W., Tang, M. and Chen, Y.-P. (2002). "Solubilities of benzoin, propyl 4-hydroxybenzoate and mandelic acid in supercritical carbon dioxide." Fluid Phase Equilibr. **201**(1), pp. 79-96.
89. Chezter, T.L. and Pinkston, J.D. (2004). "Supercritical fluid and unified chromatography." Anal. Chem. **76**(16), pp. 4606-4613.
90. Chirico, R.D., Nguyen, A., Steele, W.V., Strube, M.M. and Tsonopoulos, C. (1989). "The vapor pressure of n-alkanes revisited. New high-precision vapor pressure data on n-decane, n-eicosane, and n-octacosane." J. Chem. Eng. Data **34**(2), pp. 149-156.
91. Chordia, L. (2008). 8th International Symposium on Supercritical Chromatography and Extraction, St Louis, MO.
92. Chou, G.F., Forbert, R.R. and Prausnitz, J.M. (1990). "High-pressure vapor-liquid equilibria for CO2/n-decane, CO2/tetralin, and CO2/n-decane/tetralin at 71.1 and 104.4°C." J. Chem. Eng. Data **35**(1), pp. 26-29.
93. Chou, G.F., Forbert, R.R. and Prausnitz, J.M. (1990). "High-pressure vapor-liquid equilibria for CO2/n-decane, CO2/tetralin, and CO2/n-decane/tetralin at 71.1 and 104.4°C." J. Chem. Eng. Data **35**(1), pp. 26-29.
94. Chrastil, J. (1982). "Solubility of solids and liquids in supercritical gases." J. Phys. Chem. **86**(15), pp. 3016-3021.
95. Christofi, N. and Ivshina, I.B. (2002). "Microbial surfactants and their use in field studies of soil remediation." J. Appl. Microbiol. **93**(6), pp. 915-929.
96. Christofi, N., Ivshina, I.B., Kuyukina, M.S. and Philp, J.C. (1998). Biological treatment of crude oil contaminated soil in Russia. Contaminated Land and Groundwater: Future Directions. Lerner, D. N. and Walton, N. R. G. London, Geological Society, pp. 45-51.
97. Christov, M. and Dohrn, R. (2002). "High-pressure fluid phase equilibria: Experimental methods and systems investigated (1994-1999)." Fluid Phase Equilibr. **202**(1), pp. 153-218.
98. Chueh, P.L. and Prausnitz, J.M. (1967). "Vapor-liquid equilibria at high pressures: Calculation of critical temperatures, volumes, and pressures of nonpolar mixtures." AIChE J. **13**(6), pp. 1107-1113.
99. Chynoweth, A.G. and Schneider, W.G. (1952). "Ultrasonic Propagation in Xenon in the Region of Its Critical Temperature." J. Chem. Phys. **20**(11), pp. 1777-1783.
100. Cookson, L.J., Qader, A., Creffield, J.W. and Scown, D.K. (2009). "Treatment of timber with permethrin in supercritical carbon dioxide to control termites." J. Supercrit. Fluids **49**(2), pp. 203-208.

101. Coquelet, C., Chareton, A., Valtz, A., Baba-Ahmed, A. and Richon, D. (2003). "Vapor−Liquid Equilibrium Data for the Azeotropic Difluoromethane + Propane System at Temperatures from 294.83 to 343.26 K and Pressures up to 5.4 MPa." J. Chem. Eng. Data **48**(2), pp. 317-323.
102. Coquelet, C. and Richon, D. (2007). "Needs of thermodynamic properties measurements and modeling in the frame of new regulations on refrigerants " J. Zhejiang Univ.-Sc. A **8**(5), pp. 724-733.
103. Corbin, D.R. and Shiflett, M.B. (2015). "Capture of Trifluoromethane Using Molecular Sieves.", **World Patent 20150087869** 26 March 2015
104. Cotterman, R.L. (1985). Phase equilibria for systems containing very many components, development and application of continuous thermodynamics. Berkely, CA, University of California,. **Ph.D. Dissertation**,
105. Couillard, D., Tran, F.T. and Tyagi, R.D. (1991). "Process for the in situ restoration of oil-contaminated soils." J. Environ. Manage. **32**(1), pp. 19-34.
106. Crampon, C., Charbit, G. and Neau, E. (1999). "High-pressure apparatus for phase equilibria studies: Solubility of fatty acid esters in supercritical CO2." J. Supercrit. Fluids **16**(1), pp. 11-20.
107. Crause, J.C. and Nieuwoudt, I. (2003). "Paraffin wax fractionation: State of the art vs. supercritical fluid fractionation." J. Supercrit. Fluids **27**(1), pp. 39-54.
108. Cunningham, S.D., Berti, W.R. and Huang, J.W. (1995). "Phytoremediation of contaminated soils." Trends Biotechnol. **13**(9), pp. 393-397.
109. Curie, P. (1891). "Quelques remarques relatives á l'équation réduite de Van der Waals." Arch. Sci. Phys. Nat. **xxvi**(3e), pp. 13.
110. Da Silva, L.J., Alves, F.C. and De França, F.P. (2012). "A review of the technological solutions for the treatment of oily sludges from petroleum refineries." Waste Manage. Res. **30**(10), pp. 1016-1030.
111. da Silva, M.V., Barbosa, D., Ferreira, P.O. and Mendonça, J. (2000). "High pressure phase equilibrium data for the systems carbon dioxide/ethyl acetate and carbon dioxide/isoamyl acetate at 295.2, 303.2 and 313.2 K." Fluid Phase Equilibr. **175**(1–2), pp. 19-33.
112. Dahmani, A., Kaci, A.A. and Jose, J. (1997). "Vapour pressures and excess functions of 1,4-dimethylpiperazine + n-heptane, or cyclohexane measurement and prediction." Fluid Phase Equilibr. **134**(1–2), pp. 255-265.
113. Dankers, J., Groenenboom, M., Scholtis, L.H.A. and van der Heiden, C. (1993). "High-speed supercritical fluid extraction method for routine measurement of polycyclic aromatic hydrocarbons in environmental soils with dichloromethane as a static modifier." J. Chromatogr. A **641**(2), pp. 357-362.
114. de Filippi, R. and Markiewicz, J. (1991). "Propane extraction treats refinery wastes to BDAT standards." Oil Gas J. **89**(36), pp. 52-54.
115. de Leeuw, V.V., de Loos, T.W., Kooijman, H.A. and de Swaan Arons, J. (1992). "The experimental determination and modelling of VLE for binary subsystems of the quaterhary system N2 + CH4 + C4H10 + C14H30 up to 1000 bar and 440 K." Fluid Phase Equilibr. **73**(3), pp. 285-321.
116. Debenedetti, P.G., Tom, J.W., Sang-Do, Y. and Gio-Bin, L. (1993). "Application of supercritical fluids for the production of sustained delivery devices." J. Control. Release **24**(1–3), pp. 27-44.

117. Defibaugh, D.R., Gillis, K.A., Moldover, M.R., Morrison, G. and Schmidt, J.W. (1992). "Thermodynamic properties of CHF2-O-CHF2, bis(difluoromethyl) ether." Fluid Phase Equilibr. **81**, pp. 285-305.
118. Dejoz, A., González-Alfaro, V., Miguel, P.J. and Vázquez, M.I. (1996). "Isobaric Vapor−Liquid Equilibria for Binary Systems Composed of Octane, Decane, and Dodecane at 20 kPa." J. Chem. Eng. Data **41**(1), pp. 93-96.
119. del Valle, J.M., de la Fuente, J.C. and Cardarelli, D.A. (2005). "Contributions to supercritical extraction of vegetable substrates in Latin America." J. Food Eng. **67**(1–2), pp. 35-57.
120. Deschênes, L., Lafrance, P., Villeneuve, J.P. and Samson, R. (1995). "The effect of an anionic surfactant on the mobilization and biodegradation of PAHs in a creosote-contaminated soil." Hydrolog. Sci. J. **40**(4), pp. 471-484.
121. DeSimone, J.M., Maury, E.E., Menceloglu, Y.Z., McClain, J.B., Romack, T.J. and Combes, J.R. (1994). "Dispersion Polymerizations in Supercritical Carbon Dioxide." Science **265**(5170), pp. 356-359.
122. DeSimone, J.M. and Tumas, W. (2003). Green Chemistry Using Liquid and Supercritical Carbon Dioxide. New York, NY, Oxford University Press.
123. Dincer, I., Colpan, C.O., Kizilkan, O. and Ezan, M.A. (2015). Progress in Clean Energy, Volume 1: Analysis and Modeling, Springer International Publishing.
124. Dobbs, J.M., Wong, J.M. and Johnston, K.P. (1986). "Nonpolar co-solvents for solubility enhancement in supercritical fluid carbon dioxide." J. Chem. Eng. Data **31**(3), pp. 303-308.
125. Dohrn, R. and Brunner, G. (1995). "High-pressure fluid-phase equilibria: Experimental methods and systems investigated (1988-1993)." Fluid Phase Equilibr. **106**(1-2), pp. 213-282.
126. Dohrn, R., Peper, S. and Fonseca, J.M.S. (2010). "High-pressure fluid-phase equilibria: Experimental methods and systems investigated (2000-2004)." Fluid Phase Equilibr. **288**(1-2), pp. 1-54.
127. Duarte, A.R.C., Coimbra, P., De Sousa, H.C. and Duarte, C.M.M. (2004). "Solubility of flurbiprofen in supercritical carbon dioxide." J. Chem. Eng. Data **49**(3), pp. 449-452.
128. Duarte, A.R.C. and Duarte, C.M.M. (2009). Current Trends of Supercritical Fluid Technology in Pharmaceutical, Nutraceutical and Food Processing Industries, Bentham Science Publishers.
129. Dunlop, P.J. (1994). "Viscosities of a series of gaseous fluorocarbons at 25 °C." J. Phys. Chem. **100**(4), pp. 3149-3151.
130. DuPont (2015). "DuPont Fluoropolymers Made with Supercritical CO2 Polymerization Technology." Retrieved 12 March 2015, 2015, from http://www2.dupont.com/Teflon_Industrial/en_US/products/supercritical_co2.html.
131. Duschek, W., Kleinrahm, R. and Wagner, W. (1990). "Measurement and correlation of the (pressure, density, temperature) relation of carbon dioxide II. Saturated-liquid and saturated-vapour densities and the vapour pressure along the entire coexistence curve." J. Chem. Thermodyn. **22**(9), pp. 841-864.
132. Dymond, J. and Hildebrand, J.H. (1967). "Apparatus for Accurate, Rapid Determinations of Solubility of Gases in Liquids." Ind. Eng. Chem. Fundam. **6**(1), pp. 130-131.

133. Eaton, G.L. and Porter, C.A. (1932). "Critical Temperatures of Petroleum Oils." Ind. Eng. Chem. **24**(7), pp. 819-822.
134. Eckert-Tilotta, S.E., Hawthorne, S.B. and Miller, D.J. (1993). "Supercritical fluid extraction with carbon dioxide for the determination of total petroleum hydrocarbons in soil." Fuel **72**(7), pp. 1015-1023.
135. El Ahmar, E., Valtz, A., Naidoo, P., Coquelet, C. and Ramjugernath, D. (2011). "Isothermal Vapor−Liquid Equilibrium Data for the Perfluorobutane (R610) + Ethane System at Temperatures from (263 to 353) K." J. Chem. Eng. Data **56**(5), pp. 1918-1924.
136. El Bagouri, I.H., ElNawawy, A.S., Abdal, M., Al-Daher, R. and Khalafawi, M.S. (1994). "Mobility of oil and other sludge constituents during oily sludge treatment by landfarming." Resour Conserv. Recy. **11**(1-4), pp. 93-100.
137. Elektorowicz, M. and Habibi, S. (2005). "Sustainable waste management: Recovery of fuels from petroleum sludge." Can. J. Civil Eng. **32**(1), pp. 164-169.
138. Elektorowicz, M., Habibi, S. and Chifrina, R. (2006). "Effect of electrical potential on the electro-demulsification of oily sludge." J. Colloid Interf. Sci. **295**(2), pp. 535-541.
139. Elliott, J.R. and Daubert, T.E. (1987). "Evaluation of an equation of state method for calculating the critical properties of mixtures." Ind. Eng. Chem. Res. **26**(8), pp. 1686-1691.
140. Emery, A.P., Chesler, S.N. and MacCrehan, W.A. (1992). "Recovery of diesel fuel from clays by supercritical fluid extraction-gas chromatography." J. Chromatogr. **606**(2), pp. 221-228.
141. Enick, R., Holder, G.D. and Morsi, B.I. (1985). "Critical and three phase behavior in the carbon dioxide/tridecane system." Fluid Phase Equilibr. **22**(2), pp. 209-224.
142. Erkey, C. (2000). "Supercritical carbon dioxide extraction of metals from aqueous solutions: a review." J. Supercrit. Fluids **17**, pp. 259-287.
143. Eskom Holdings SOC Ltd (2014) Eskom Tariff & Charges Booklet 2014/15.
144. Espinosa, S., Diaz, S. and Brignole, E.A. (2002). "Thermodynamic Modeling and Process Optimization of Supercritical Fluid Fractionation of Fish Oil Fatty Acid Ethyl Esters." Ind. Eng. Chem. Res. **41**(6), pp. 1516-1527.
145. Essel, J.T., Cortopassi, A.C., Kuo, K.K., Leh, C.G. and Adair, J.H. (2012). "Formation and characterization of nano-sized RDX particles produced using the RESS-AS process." Propell. Explos. Pyrot. **37**(6), pp. 699-706.
146. Falatko, D.M. (1991). Effects of biologically reduced surfactants on the mobility and biodegradability of petroleum hydrocarbons. Blackburg, VA, USA, Virginia Polytechnic Institute and State University. **MS Thesis**,
147. Fall, D.J. and Luks, K.D. (1985). "Liquid-liquid-vapor phase equilibria of the binary system carbon dioxide + n-tridecane." J. Chem. Eng. Data **30**(3), pp. 276-279.
148. Fernández, L., Pérez, E., Ortega, J., Canosa, J. and Wisniak, J. (2010). "Measurements of the Excess Properties and Vapor-Liquid Equilibria at 101.32 kPa for Mixtures of Ethyl Ethanoate + Alkanes (from C_5 to C_{10})." J. Chem. Eng. Data **55**, pp. 5519-5533.

149. Ferreira, S.R.S., Nikolov, Z.L., Doraiswamy, L.K., Meireles, M.A.A. and Petenate, A.J. (1999). "Supercritical fluid extraction of black pepper (Piper nigrun L.) essential oil." J. Supercrit. Fluids **14**(3), pp. 235-245.
150. Fink, S.D. and Hershey, H.C. (1990). "Modeling the vapor-liquid equilibria of 1,1,1-trichloroethane + carbon dioxide and toluene + carbon dioxide at 308, 323, and 353 K." Ind. Eng. Chem. Res. **29**(2), pp. 295-306.
151. Finke, A., McDermott, K., Smith, L.C., Sonnenberg, S. and Zhuang, Z.J. (2003). "Fragrance compositions for CO2 dry cleaning process." World Patent, **WO2003010381 A1**, February 6th, 2003
152. Florusse, L.J., Fornari, T., Bottini, S.B. and Peters, C.J. (2004). "Phase behavior of carbon dioxide-low-molecular weight triglycerides binary systems: measurements and thermodynamic modeling." J. Supercrit. Fluids **31**(2), pp. 123-132.
153. Fonseca, J.M.S., Dohrn, R. and Peper, S. (2011). "High-pressure fluid-phase equilibria: Experimental methods and systems investigated (2005-2008)." Fluid Phase Equilibr. **300**(1-2), pp. 1-69.
154. Fornari, R.E., Alessi, P. and Kikic, I. (1990). "High pressure fluid phase equilibria: experimental methods and systems investigated (1978-1987)." Fluid Phase Equilibr. **57**(1-2), pp. 1-33.
155. Forster, P., Ramaswamy, V., Artaxo, P., Berntsen, T., Betts, R., Fahey, D.W., Haywood, J., Lean, J., Lowe, D.C., Myhre, G., Nganga, J., Prinn, R., Raga, G., Schulz, M. and Van Dorland, R. (2007). Changes in Atmospheric Constituents and in Radiative Forcing. Climate Change 2007: The Physical Science Basis. Contribution of Working Group I to the Fourth Assessment Report of the Intergovernmental Panel on Climate Change. Solomon, S., Qin, D., Manning, M., Chen, Z., Marquis, M., Averyt, K. B., Tignor, M. and Miller, H. L. Cambridge, United Kingdom and New York, NY, USA, Cambridge University Press,
156. Forziati, A.F., Norris, W.R. and Rossini, F.D. (1949). "Vapor pressures and boiling points of sixty API-NBS hydrocarbons." J. Res. Nat. Bur. Stand. **43**(6), pp. 555-564.
157. Forziati, A.F., Camin, D.L. and Rossini, F.D. (1950). "Density, refractive index, boiling point, and vapor pressure of eight monoolefin (1-alkene), six pentadiene, and two cyclomonoolefin hydrocarbons." J. Res. Nat. Bur. Stand. **45**(5), pp. 406-410.
158. Fredenslund, A., Mollerup, J. and Christiansen, L.J. (1973). "An apparatus for accurate determinations of vapour-liquid equilibrium properties and gas PVT properties." Cryogenics **13**(7), pp. 414-419.
159. Funk, E.W., Chai, F.-C. and Prausnitz, J.M. (1972). "Thermodynamic properties of binary liquid mixtures containing aromatic and saturated hydrocarbons." J. Chem. Eng. Data **17**(1), pp. 24-27.
160. Galicia-Luna, L.A., Ortega-Rodriguez, A. and Richon, D. (2000). "New apparatus for the fast determination of high-pressure vapor-liquid equilibria of mixtures and of accurate critical pressures." J. Chem. Eng. Data **45**(2), pp. 265-271.
161. Gallagher, P.M., Krukonis, V.J. and Coffey, M.P. (1995). "Gas anti-solvent recrystallization and application for the separation and subsequent processing of RDX and HMX." **US Patent 5389263**
162. Gani, R., Hytoft, G. and Jaksland, C. (1997). "Design and analysis of supercritical extraction processes." Appl. Therm. Eng. **17**(8–10), pp. 889-899.

163. García-González, J., Molina, M.J., Rodríguez, F. and Mirada, F. (2001). "Solubilities of Phenol and Pyrocatechol in Supercritical Carbon Dioxide." J. Chem. Eng. Data **46**(4), pp. 918-921.
164. García-Sánchez, F., Ruiz-Cortina, J.L., Lira-Galeana, C. and Ponce-Ramírez, L. (1992). "Critical point calculations for oil reservoir fluid systems using the SPHCT equation of state." Fluid Phase Equilib. **81**(0), pp. 39-84.
165. Garriga, R., Sanchez, F., Perez, P., Valero, J. and Gracia, M. (1994). "Vapor pressures at several temperatures and excess functions at 298.15 K of n-butanol + 2-methylpentane, and + 3-methylpentane." Fluid Phase Equilibr. **101**, pp. 227-236.
166. Gearhart, J.A. and Garwin, L. (1976). "ROSE Process Improves Residual Feed." Hydrocarb. Process. **55**(5), pp. 125-128.
167. Gearhart, J.A. and Nelson, S.R. (1983). ROSE Process Offers Energy Savings for Solvent Extraction. Fifth Industrial Energy Technology Conference, Housto, TX.
168. Gehrig, M. (1998). Extraction of Natural Material with Carbon Dioxide: Current Applications. Supercritical Fluids II - Fundamentals and Applications. Kemer, Turkey, NATO Scientific Affairs Division,
169. Gibbs, J.W. and Bumstead, H.A. (1906). Scientific Papers of J. Willard Gibbs: Thermodynamics, Longmans, Green and Company.
170. Gironi, F. and Maschietti, M. (2008). "Continuous countercurrent deterpenation of lemon essential oil by means of supercritical carbon dioxide: Experimental data and process modelling." Chem. Eng. Sci. **63**(3), pp. 651-661.
171. Giusti, L. (2009). "A review of waste management practices and their impact on human health." Waste Manage. **29**(8), pp. 2227-2239.
172. Global Industry Analysts Inc. (2014). Polytetrafluoroethylene (PTFE): A Global Strategic Business Report. San Jose, CA, USA, Global Industry Analysts Inc., pp. 191
173. Goldfarb, D.o.L. and Corti, H.R. (2000). "Electrochemistry in supercritical trifluoromethane." Electrochem. Commun. **2**(9), pp. 663-670.
174. Gong, Y., Carstens, N.A., Driscoll, M.J. and Matthews, I.A. (2006). Analysis of Radial Compressor Options for Supercritical CO2 Power Conversion Cycles Cambridge, MA, MIT Gas Turbine Laboratory of the Department of Aeronautics and Astronautics,
175. Gopal, E.S.R. (2000). Critical Opalescence. Resonance. Bangalore, India, Springer. **5**, pp. 37-45
176. Gopalakrishnan, N. and Narayanan, C.S. (1991). "Supercritical carbon dioxide extraction of cardamom." J. Agr. Food Chem. **39**(11), pp. 1976-1978.
177. Government of Alberta (2014). "Oil Sands - Facts and Statistics." Retrieved 19 March 2015, from http://www.energy.alberta.ca/OilSands/791.asp.
178. Gracia, M., Sánchez, F., Pérez, P., Valero, J. and Losa, C.G. (1992). "Vapour pressures of {x C4H9OH + (1−x) C8H18}(l) at temperatures between 283.16 K and 323.18 K." J. Chem. Thermodyn. **24**(8), pp. 843-849.
179. Graco Inc. (2013). "Chemical Compatibility Guide." Retrieved 28 April 2015, from http://www.graco.com/content/dam/graco/ipd/literature/misc/chemical-compatibility-guide/Graco_ChemCompGuideEN-B.pdf.

180. Griffiths, R.B. (1974). "Thermodynamic model for tricritical points in ternary and quaternary fluid mixtures." J. Chem. Phys. **60**(1), pp. 195-206.
181. Guigard, S.E. and Stiver, W.H. (1998). "A Density-Dependent Solute Solubility Parameter for Correlating Solubilities in Supercritical Fluids." Ind. Eng. Chem. Res. **37**(9), pp. 3786-3792.
182. Guilbot, P., Théveneau, P., Baba-Ahmed, A., Horstmann, S., Fischer, K. and Richon, D. (2000a). "Vapor–liquid equilibrium data and critical points for the system H2S+COS. Extension of the PSRK group contribution equation of state." Fluid Phase Equilibr. **170**(2), pp. 193-202.
183. Guilbot, P., Valtz, A., Legendre, H. and Richon, D. (2000b). "Rapid On-line Sampler Injector: a Reliable Tool for HT-HP Sampling and On-Line GC Analysis." Analusis **28**, pp. 426-431.
184. Güngören, T., Sağlam, M., Yüksel, M., Madenoğlu, H., Işler, R., Metecan, I.H., Özkan, A.R. and Ballice, L. (2007). "Near-critical and supercritical fluid extraction of industrial sewage sludge." Ind. Eng. Chem. Res. **46**(4), pp. 1051-1057.
185. Haghbakhsh, R., Hayer, H., Saidi, M., Keshtkari, S. and Esmaeilzadeh, F. (2013). "Density estimation of pure carbon dioxide at supercritical region and estimation solubility of solid compounds in supercritical carbon dioxide: Correlation approach based on sensitivity analysis." Fluid Phase Equilibr. **342**, pp. 31-41.
186. Hannay, J.B. and Hogarth, J. (1879). "On the Solubility of Solids in Gases." Proc. R. Soc. London Ser. A **30**, pp. 178-188.
187. Hansen, H.K., Rasmussen, P., Fredenslund, A., Schiller, M. and Gmehling, J. (1991). "Vapor-liquid equilibria by UNIFAC group contribution. 5. Revision and extension." Ind. Eng. Chem. Res. **30**(10), pp. 2352-2355.
188. Härröd, M., Macher, M.B., van den Hark, S. and Møller, P. (2001). 9.3 Hydrogenation under supercritical single-phase conditions. Industrial Chemistry Library. Bertucco, A. and Vetter, G., Elsevier. **Volume 9**, pp. 496-508.
189. Hartz, C.L., Bevan, J.W., Jackson, M.W. and Wofford, B.A. (1998). "Innovative Surface Wave Plasma Reactor Technique for PFC Abatement." Environ. Sci. Technol. **32**(5), pp. 682-687.
190. Hartzell, K. and Guigard, S.E. (2012). The Use of Supercritical Carbon Dioxide and Modifiers for the Enhanced Separation of Bitumen from Athabasca Oil Sand. International Symposium on Supercritical Fluids 2012, San Francisco, CA, USA, International Society for Advancement of Supercritical Fluids.
191. Hastings, D.R. and Hendricks, J.A. (1995). "Method & apparatus for spraying a liquid coating containing supercritical fluid or liquified gas." European Patent, **EP0421796 B1**, 9 Aug 1995
192. Hawthorne, S.B. (1990). "Analytical-Scale Supercritical Fluid Extraction." Anal. Chem. **62**(11), pp. 633A-642A.
193. Hawthorne, S.B., Langenfeld, J.J., Miller, D.J. and Burford, M.D. (1992). "Comparison of supercritical chlorodifluoromethane, nitrous oxide, and carbon dioxide for the extraction of polychlorinated biphenyls and polycyclic aromatic hydrocarbons." Anal. Chem. **64**(14), pp. 1614-1622.
194. Hayes, C.E. and Carr, H.Y. (1977). "NMR Measurement of the Liquid-Vapor Critical Exponents Beta and Beta 1." Phys. Rev. Lett. **39**(24), pp. 1558-1561.

195. He, Y., Luo, Z., Ma, S. and Hu, Y. (1994). "Measuring Phase Equilibria of Carbon Dioxide-n-Heptane System by Stoichiometry." Huadong Huagong Xueyuan Xuebao **20**(1), pp. 79-84.
196. Heady, R.B. and Cahn, J.W. (1973). "Experimental test of classical nucleation theory in a liquid-liquid miscibility gap system." J. Chem. Phys. **58**(3), pp. 896-910.
197. Heidarzadeh, N., Gitipour, S. and Abdoli, M.A. (2010). "Characterization of oily sludge from a Tehran oil refinery." Waste Manage. Res. **28**(10), pp. 921-927.
198. Heidemann, R.A. and Khalil, A.M. (1980). "The calculation of critical points." AIChE J. **26**(5), pp. 769-779.
199. Hejazi, R.F. and Husain, T. (2004). Oily sludge degradation study under arid conditions using landfarm and bioreactor technologies, Calgary, Alta.
200. Helfgen, B., Türk, M. and Schaber, K. (2003). "Hydrodynamic and aerosol modelling of the rapid expansion of supercritical solutions (RESS-process)." J. Supercrit. Fluids **26**(3), pp. 225-242.
201. Hernández, E.J., Reglero, G. and Fornari, T. (2011). "Correlating the solubility of supercritical gases in high-molecular weight substances using a density-dependent equation." AIChE J. **57**(3), pp. 765-771.
202. Hernández-Garduza, O., García-Sánchez, F. and Neau, E. (2001). "Generalization of composition-dependent mixing rules for multicomponent systems: Prediction of vapor-liquid and liquid-liquid equilibria." Chem. Eng. J. **84**(3), pp. 283-294.
203. Hicks, C.P. and Young, C.L. (1975). "The gas-liquid critical properties of binary mixtures." Chem. Rev. **75**(2), pp. 119-175.
204. Hillmann, R. and Bächmann, K. (1995). "Extraction of pesticides using supercritical trifluoromethane and carbon dioxide." J. Chromatogr. A **695**(1), pp. 149-154.
205. Hiyoshi, N., Murakami, Y., Yamaguchi, A., Sato, O., Rode, C.V. and Shirai, M. (2010). "Purification of hydrocarbons from aromatic sulfur compounds by supercritical carbon dioxide extraction." J. Supercrit. Fluids **55**(1), pp. 122-127.
206. Ho, C.u.-S. and Shih, S.-M. (1992). "Co(OH)2/fly ash sorbents for SO2 removal." Ind. Eng. Chem. Res. **31**(4), pp. 1130-1135.
207. Hojjati, M., Yamini, Y., Khajeh, M. and Vatanara, A. (2007). "Solubility of some statin drugs in supercritical carbon dioxide and representing the solute solubility data with several density-based correlations." J. Supercrit. Fluids **41**(2), pp. 187-194.
208. Hori, K., Okazaki, S., Uematsu, M. and Watanabe, K. (1982). An Experimental Study of Thermodynamic Properties of Trifluoromethane. 8th Symp. Thermophys. Prop., Gaithersburg, ASME.
209. Horstmann, S., Fischer, K. and Gmehling, J. (2002). "Measurement and calculation of critical points for binary and ternary mixtures." AIChE J. **48**(10), pp. 2350-2356.
210. Hou, Y.C. and Martin, J.J. (1959). "Physical and thermodynamic properties of trifluoromethane." AIChE J. **5**(1), pp. 125-129.
211. Houssin-Agbomson, D., Coquelet, C., Richon, D. and Arpentinier, P. (2010). "Equipment using a "static-analytic" method for solubility measurements in potentially hazardous binary mixtures under cryogenic temperatures." Cryogenics **50**(4), pp. 248-256.

212. Hoy, K.L. (1991). "Unicarb System for Spray Coatings — A Contribution to Pollution Prevention." Eur. Polym. Paint Colour J. **181**, pp. 438-442.
213. Hoy, K.L., Lee, C. and Nielsen, K.A. (1992). "Liquid spray application of coatings with supercritical fluids as diluents and spraying from an orifice." US Patent, **US108799 A**.
214. Hsu, J.J.C., Nagarajan, N. and Robinson, R.L. (1985). "Equilibrium phase compositions, phase densities, and interfacial tensions for carbon dioxide + hydrocarbon systems. 1. Carbon dioxide + n-butane." J. Chem. Eng. Data **30**(4), pp. 485-491.
215. Hubert, P. and Vitzthum, O.G. (1978). "Fluid Extraction of Hops, Spices, and Tobacco with Supercritical Gases." Angew. Chem. Int. Edit. **17**(10), pp. 710-715.
216. Huie, N.C., Luks, K.D. and Kohn, J.P. (1973). "Phase-equilibria behavior of systems carbon dioxide-n-eicosane and carbon dioxide-n-decane-n-eicosane." J. Chem. Eng. Data **18**(3), pp. 311-313.
217. Ichikawa, T. (2007). "Electrical demulsification of oil-in-water emulsion." Colloid. Surface. A **302**(1–3), pp. 581-586.
218. IHS Inc. (2015). Chemical Economics Handbook: Carbon Dioxide. HIS Inc., Denver, CO, USA,
219. Inomata, H., Tuchiya, K., Arai, K. and Saito, S. (1986). "Measurement of vapor-liquid equilibria at elevated temperatures and pressures using a flow type apparatus." J. Chem. Eng. Jpn. **19**, pp. 386.
220. Ismail, M., Chan, K.W. and Ghafar, S.A. (2014). Supercritical fluid extraction process of kenaf seeds, US Patent, **US 8829214.**
221. Ivshina, I.B., Kuyukina, M.S., Philp, J.C. and Christofi, N. (1998). "Oil desorption from mineral and organic materials using biosurfactant complexes produced by Rhodococcus species." World J. Microb. Biot. **14**(5), pp. 711-717.
222. Iwai, Y., Margerum, M.R. and Lu, B.C.Y. (1988). "A new three-parameter cubic equation of state for polar fluids and fluid mixtures." Fluid Phase Equilibr. **42**(0), pp. 21-41.
223. Iwai, Y., Hosotani, N., Morotomi, T., Koga, Y. and Arai, Y. (1994). "High-Pressure Vapor-Liquid Equilibria for Carbon Dioxide + Linalool." J. Chem. Eng. Data **39**(4), pp. 900-902.
224. Iwai, Y., Morotomi, T., Sakamoto, K., Koga, Y. and Arai, Y. (1996). "High-Pressure Vapor–Liquid Equilibria for Carbon Dioxide + Limonene." J. Chem. Eng. Data **41**(5), pp. 951-952.
225. Jauna, P.B. and Henshaw, A. (2005). Biodegradation at a land-farming site at 14,000 feet in the high bolivian altiplano, Miami Beach, FL.
226. Jennings, D.W. and Schucker, R.C. (1996). "Comparison of High-Pressure Vapor–Liquid Equilibria of Mixtures of CO2 or Propane with Nonane and C9 Alkylbenzenes." J. Chem. Eng. Data **41**(4), pp. 831-838.
227. Jennings, D.W. and Teja, A.S. (1989). "Vapor-liquid equilibria in the carbon dioxide-1-hexene and carbon dioxide-1-hexyne systems." J. Chem. Eng. Data **34**(3), pp. 305-309.
228. Jiménez-Gallegos, R., Galicia-Luna, L.A. and Elizalde-Solis, O. (2006). "Experimental vapor-liquid equilibria for the carbon dioxide + octane and carbon dioxide + decane systems." J. Chem. Eng. Data **51**(5), pp. 1624-1628.
229. Jing, G., Luan, M. and Chen, T. (2011). "Prospects for development of oily sludge treatment." Chem. Tech. Fuels Oil. **47**(4), pp. 312-326.

230. Johnston, K.P., Peck, D.G. and Kim, S. (1989). "Modeling supercritical mixtures: how predictive is it?" Ind. Eng. Chem. Res. **28**(8), pp. 1115-1125.
231. Jonas, J. and Lamb, D.M. (1987). Transport and Intermolecular Interactions in Compressed Supercritical Fluids. Supercritical Fluids: Chemical and Engineering Principles and Applications. Squires, T. G. and Paulaitis, M. E. Chicago, American Chemical Society, pp. 15-28.
232. Ju, M., Yun, Y., Shin, M.S. and Kim, H. (2009). "(Vapour&liquid) equilibria of the {trifluoromethane (HFC-23)&propane} and {trifluoromethane (HFC-23)&n-butane} systems." J. Chem. Thermodyn. **41**(12), pp. 1339-1342.
233. Ju, M., Yun, Y., Shin, M.S. and Kim, H. (2009). "(Vapour&liquid) equilibria of the {trifluoromethane (HFC-23)&propane} and {trifluoromethane (HFC-23)&n-butane} systems." J. Chem. Thermodyn. **41**(12), pp. 1339-1342.
234. Jung, J. and Perrut, M. (2001). "Particle design using supercritical fluids: Literature and patent survey." J. Supercrit. Fluids **20**(3), pp. 179-219.
235. Kahlbaum, G.W.A. (1884). "Ueber die Abhängigkeit der Siedetemperatur vom Luftdruck." Ber. Dtsch. Chem. Ges. **17**(1), pp. 1245-1262.
236. Kahlbaum, G.W.A. (1898). "Studies on Vapor Pressure Measurements: II." Z. Phys. Chem.-Stoch. Ve. **26**(577-658).
237. Kalra, H. and Robinson, D.B. (1975). "An apparatus for the simultaneous measurement of equilibrium phase composition and refractive index data at low temperatures and high pressures." Cryogenics **15**(7), pp. 409-412.
238. Kalra, H., Kubota, H., Robinson, D.B. and Ng, H.-J. (1978). "Equilibrium phase properties of the carbon dioxide-n-heptane system." J. Chem. Eng. Data **23**(4), pp. 317-321.
239. Kam, E.K.T. (2001). Assessment of sludges and tank bottoms treatment processes. The 8th International Petroleum Environmental Conference. Houston, Texas, Integrated Petroleum Environmental Consortium,
240. Kaminishi, G.I., Yokoyama, C. and Shinji, T. (1987). "Vapor pressures of binary mixtures of carbon dioxide with benzene, n-hexane and cyclohexane up to 7 MPa." Fluid Phase Equilibr. **34**(1), pp. 83-99.
241. Kamiya, M., Muroki, K. and Uematsu, M. (1995). "(P, ρ, T) measurements on trifluoromethane in the supercritical region at temperatures from 310 K to 350 K." J. Chem. Thermodyn. **27**(4), pp. 337-345.
242. Kang, S.M., Cho, M.W., Kim, K.M., Kang, D.Y., Koo, W.M., Kim, K.H., Park, J.Y. and Lee, S.S. (2012). "Cyproconazole impregnation into wood using sub- and supercritical carbon dioxide." Wood Sci. Technol. **46**(4), pp. 643-656.
243. Kao, C.-P.C. and Miller, R.N. (2000). "Vapor Pressures of Hexafluoroethane and Octafluorocyclobutane." J. Chem. Eng. Data **45**(2), pp. 295-297.
244. KBR Technology Inc. (2007). Residuum Oil Supercritical Extraction (ROSE™). http://www.kbr.com/Newsroom/Publications/Brochures/Residuum-Oil-Supercritical-Extraction-ROSE.pdf,
245. Kemmere, M.F. and Meyer, T. (2005). Supercritical Carbon Dioxide: in Polymer Reaction Engineering. Weinheim, FRG, Wiley-VCH Verlag GmbH & Co. KGaA.

246. Kijima, J., Saikawa, K., Watanabe, K., Oguchi, K. and Tanishita, I. (1977). Experimental study of thermodynamic properties of hexafluoroethane (R116). Proc. Symp. Thermophys. Prop., 7th, New York, ASME.
247. Kim, C.H., Vimalchand, P. and Donohue, M.D. (1986). "Vapor-liquid equilibria for binary mixtures of carbon dioxide with benzene, toluene and p-xylene." Fluid Phase Equilibr. **31**(3), pp. 299-311.
248. Kim, J., Min, B.K., Kim, J.D., Park, J.M. and Jang, W. (2011). "Fabrication method for quantum dot sensitized solar cell using supercritical fluid or subcritical fluid and quatum dot sensitized solar cell prepared thereby." US Provisional Patent, **US 20110303269**
249. Kim, K.Y. (1974). Calorimetric studies on argon and hexafluoroethane and a generalized correlation of maxima in isobaric heat capacity, **PhD Thesis**, University of Michigan, USA
250. Kim, S.W., Kim, K.D. and Moon, D.J. (2013). "Shape controlled synthesis of nanostructured magnesium oxide particles in supercritical carbon dioxide with ethanol cosolvent." Mater. Res. Bull. **48**(8), pp. 2817-2823.
251. King, A.D. and Coan, C.R. (1971). "Solubility of water in compressed carbon dioxide, nitrous oxide, and ethane. Evidence for hydration of carbon dioxide and nitrous oxide in the gas phase." J. Am. Chem. Soc. **93**(8), pp. 1857-1862.
252. King, A.D. and Coan, C.R. (1971). "Solubility of water in compressed carbon dioxide, nitrous oxide, and ethane. Evidence for hydration of carbon dioxide and nitrous oxide in the gas phase." J. Am. Chem. Soc. **93**(8), pp. 1857-1862.
253. King, J.W. (2014). "Modern Supercritical Fluid Technology for Food Applications." Annual Review of Food Science and Technology **5**(1), pp. 215-238.
254. Kleiber, M. (1994). "Vapor-liquid equilibria of binary refrigerant mixtures containing propylene or R134a." Fluid Phase Equilib. **92**, pp. 149-194.
255. Knapp, H. and Dechema (1982). Vapor-liquid equilibria for mixtures of low-boiling substances, DECHEMA.
256. Knez, Z. and Weidner, E. (2003). "Particles formation and particle design using supercritical fluids." Curr. Opin.Solid St. M. **7**(4–5), pp. 353-361.
257. Knez, Ž., Škerget, M. and KnezHrnčič, M. (2013). 1 - Principles of supercritical fluid extraction and applications in the food, beverage and nutraceutical industries. Separation, Extraction and Concentration Processes in the Food, Beverage and Nutraceutical Industries. Rizvi, S. S. H. Chicago, USA, Woodhead Publishing, pp. 3-38.
258. Knox, D.E. (2005). "Solubilities in Supercritical Fluids." Pure Appl. Chem. **77**(3), pp. 513-530.
259. Kohlraush, K.W.F. and Koppl, F. (1934). Z. Phys. Chem. B-Chem. E. **26**, pp. 209.
260. Kolář, P. and Kojima, K. (1996). "Prediction of critical points in multicomponent systems using the PSRK group contribution equation of state." Fluid Phase Equilib. **118**(2), pp. 175-200.
261. Kolasinska, G., Goral, M. and Giza, J. (1982). "Vapor-Liquid Equilibrium and Excess Gibbs Free Energy in Binary Systems of Acetone with Aliphatic and Aromatic Hydrocarbons." Z. Phys. Chem.-Leipzig **263**, pp. 151.

262. Konrad, R., Swaid, I. and Schneider, G.M. (1983). "High-pressure phase studies on fluid mixtures of low-volatile organic substances with supercritical carbon dioxide." Fluid Phase Equilibr. **10**(2-3), pp. 307-314.
263. Kordikowski, A. and Schneider, G.M. (1993). "Fluid phase equilibria of binary and ternary mixtures of supercritical carbon dioxide with low-volatility organic substances up to 100 MPa and 393 K." Fluid Phase Equilibr. **90**(1), pp. 149-162.
264. Kostecki, P. (1999). Assessments And Remediation Of Oil Contaminated Soils. London, UK, Taylor & Francis.
265. Kotlyar, L.S., Sparks, B.D., Woods, J.R. and Ripmeester, J.A. (1990). "Supercritical fluid extraction of bitumen free solids separated from Athabasca oil sand feed and hot water process tailings pond sludge." Fuel Sci. Techn. Int. **8**(8), pp. 871-879.
266. Kozhevnikov, V., Arnold, D., Grodzinskii, E. and Naurzakov, S. (1996). "Phase transitions and critical phenomena in mercury fluid probed by sound." Fluid Phase Equilibr. **125**(1–2), pp. 149-157.
267. Krafft, F. (1882). "Ueber neunzehn höhere Normalparaffine Cn H2n + 2 und ein einfaches Volumgesetz für den tropfbar flüssigen Zustand. I." Ber. Dtsch. Chem. Ges. **15**(2), pp. 1687-1711.
268. Kreglewski, A. and Kay, W.B. (1969). "The critical constants of conformal mixtures." J. Phys. Chem. **73**(10), pp. 3359-3366.
269. Kriipsalu, M., Marques, M. and Maastik, A. (2008). "Characterization of oily sludge from a wastewater treatment plant flocculation-flotation unit in a petroleum refinery and its treatment implications." J. Mater. Cycles Waste **10**(1), pp. 79-86.
270. Książczak, A. (1986). "Solid—liquid equilibrium and the structure of solutions of highly polar aromatic compounds." Fluid Phase Equilibr. **28**(1), pp. 57-72.
271. Ksiązczak, A. and Jan Kosinski, J. (1988). "Solid-liquid-vapour equilibrium of binary systems." Fluid Phase Equilibr. **42**, pp. 241-259.
272. Kulik, B., Kruse, S. and Pelto, J. (2008). "High pressure phase equilibrium studies of the pyrrole–carbon dioxide binary system." J. Supercrit. Fluids **47**(2), pp. 135-139.
273. Kurnik, R.T., Holla, S.J. and Reid, R.C. (1981). "Solubility of solids in supercritical carbon dioxide and ethylene." J. Chem. Eng. Data **26**(1), pp. 47-51.
274. Kurnik, R.T. and Reid, R.C. (1982). "Solubility of solid mixtures in supercritical fluids." Fluid Phase Equilibr. **8**(1), pp. 93-105.
275. Laitinen, A. and Jäntti, M. (1996). "Solubility of 6-Caprolactam in Supercritical Carbon Dioxide." J. Chem. Eng. Data **41**(6), pp. 1418-1420.
276. Langevin, D., Poteau, S., Hénaut, I. and Argillier, J.F. (2004). "Crude oil emulsion properties and their application to heavy oil transportation." Oil Gas Sci. Technol. **59**(5), pp. 511-521.
277. Laugier, S. and Richon, D. (1986). "New Apparatus to Perform Fast Determinations of Mixture Vapour-Liquid Equilibria up to 10 MPa and 423 K." Rev. Sci. Instrum. **57**, pp. 469-472.
278. Lavanchy, F., Fourcade, E., de Koeijer, E., Wijers, J., Meyer, T. and Keurentjes, J.T.F. (2006). Transport Properties of Supercritical Carbon Dioxide. Supercritical Carbon Dioxide, Wiley-VCH Verlag GmbH & Co. KGaA, pp. 37-54.

279. Lay, E.N., Taghikhani, V. and Ghotbi, C. (2006). "Measurement and Correlation of CO2 Solubility in the Systems of CO2 + Toluene, CO2 + Benzene, and CO2 + n-Hexane at Near-Critical and Supercritical Conditions." J. Chem. Eng. Data **51**(6), pp. 2197-2200.
280. Lay, E.N. (2010). "Measurement and Correlation of Bubble Point Pressure in (CO2 + C6H6), (CO2 + CH3C6H5), (CO2 + C6H14), and (CO2 + C7H16) at Temperatures from (293.15 to 313.15) K." J. Chem. Eng. Data **55**(1), pp. 223-227.
281. Lemmon, E.W., McLinden, M.O. and Friend, D.G. (2011). Thermophysical Properties of Fluid Systems. NIST Chemistry WebBook, NIST Standard Reference Database Number 69. Linstrom, P. J. and Mallard, W. G. Gaithersburg MD, National Institute of Standards and Technology.
282. Lentz, H. and Weber, M. (1994). "P, V, T, x values of the gas-liquid phase equilibria in the binary system methane-ammonia at high pressures." Fluid Phase Equilibr. **93**(0), pp. 363-368.
283. Lester, E., Blood, P., Denyer, J., Giddings, D., Azzopardi, B. and Poliakoff, M. (2006). "Reaction engineering: The supercritical water hydrothermal synthesis of nano-particles." J. Supercrit. Fluids **37**(2), pp. 209-214.
284. Letsinger, R.L. and Traynham, J.G. (1948). "The Reaction of Allylsodium with 2-Bromoöctane." J. Am. Chem. Soc. **70**(10), pp. 3342-3344.
285. Li, C.C. (1971). "Critical temperature estimation for simple mixtures." Can. J. Chem. Eng. **49**(5), pp. 709-710.
286. Li, I.P.C., Wong, Y.-W., Chang, S.-D. and Lu, B.C.Y. (1972). "Vapor-liquid equilibriums in systems n-hexane-benzene and n-pentane-toluene." J. Chem. Eng. Data **17**(4), pp. 492-498.
287. Li, Q., Zhang, Z., Zhong, C., Liu, Y. and Zhou, Q. (2003). "Solubility of solid solutes in supercritical carbon dioxide with and without cosolvents." Fluid Phase Equilibr. **207**(1–2), pp. 183-192.
288. Li, Y.-H., Dillard, K.H. and Robinson, R.L. (1981). "Vapor-liquid phase equilibrium for carbon dioxide-n-hexane at 40, 80, and 120 degree C." J. Chem. Eng. Data **26**(1), pp. 53-55.
289. Lide, D.R. (2004). CRC Handbook of Chemistry and Physics 2004-2005. Boca Raton, USA, CRC Press LLC.
290. Lira, C.T. (1988). Physical Chemistry of Supercritical Fluids. Supercritical Fluid Extraction and Chromatography, American Chemical Society. **366**, pp. 1-25.
291. Liu, E.K. and Davison, R.R. (1981). "Vapor-liquid equilibriums for the binary systems n-octane with 2-methylpentane, 3-methylpentane, and 2,4-dimethylpentane." J. Chem. Eng. Data **26**(1), pp. 85-88.
292. Low, R.E. and Sharratt, A.P. (2015). Compositions comprising 1,1 -difluoroethene (r-1132a), World Patent, **WO 2015015188 A1.**
293. Lozano, L.M., Montero, E.A., Martín, M.C. and Villamañán, M.A. (1995). "Vapor-liquid equilibria of binary mixtures containing methyl tert-butyl ether (MTBE) and/or substitution hydrocarbons at 298.15 K and 313.15 K." Fluid Phase Equilibr. **110**(1–2), pp. 219-230.
294. Machida, H., Takesue, M. and Smith Jr, R.L. (2011). "Green chemical processes with supercritical fluids: Properties, materials, separations and energy." J. Supercrit. Fluids **60**(0), pp. 2-15.

295. Madani, H., Valtz, A., Coquelet, C., Meniai, A.H. and Richon, D. (2008). "Vapour-Liquid Equilibrium Data for the (Hexafluoroethane + 1,1,1,2-Tetrafluoroethane) System at Temperatures from 263 to 353 K and Pressures up to 4.16 MPa." Fluid Phase Equilibr. **268**, pp. 68-73.
296. Mamane, Y., Miller, J.L. and Dzubay, T.G. (1986). "Characterization of individual fly ash particles emitted from coal- and oil-fired power plants." Atmos. Environ. A.-Gen **20**(11), pp. 2125-2135.
297. Marrufo, B., Aucejo, A., Sanchotello, M. and Loras, S. (2009). "Isobaric vapor–liquid equilibrium for binary mixtures of 1-hexene + n-hexane and cyclohexane + cyclohexene at 30, 60 and 101.3 kPa." Fluid Phase Equilibr. **279**(1), pp. 11-16.
298. Marsh, K.N., Ott, J.B. and Richards, A.E. (1980). "Excess enthalpies, excess volumes, and excess Gibbs free energies for (n-hexane + n-undecane) at 298.15 and 308.15 K." J. Chem. Thermodyn. **12**(9), pp. 897-902.
299. Martin, J.J. (1979). "Cubic Equations of State-Which?" Ind. Eng. Chem. Fundam. **18**(2), pp. 81-97.
300. Martinez, J.L. (2007). Supercritical Fluid Extraction of Nutraceuticals and Bioactive Compounds. Boca Raton, USA, CRC Press.
301. Mathias, P.M. and Copeman, T.W. (1983). "Extension of the Peng-Robinson Equation of State to Complex Mixtures: Evaluation of the Various Forms of the Local Composition Concept." Fluid Phase Equilibr. **13**, pp. 91-108.
302. Mathias, P.M., Klotz, H.C. and Prausnitz, J.M. (1991). "Equation-of-State mixing rules for multicomponent mixtures: the problem of invariance." Fluid Phase Equilibr. **67**(C), pp. 31-44.
303. McCulloch, A. (2004). Incineration of HFC-23 Waste Streams for Abatement of Emissions from HCFC-22 Production: A Review of Scientific, Technical and Economic Aspects, United Nations Framework Convention on Climate Change.
304. McDermott, W., Subawalla, H., Johnson, A., Schwarz, A. and Ockovic, R. (2008). "Processing of semiconductor components with dense processing fluids." US Provisional Patent, **US 2008 0004194.**
305. McGlashan, M.L. and Hicks, C.P. (1978). A bibliography of thermodynamic quantities for binary fluid mixtures. Chemical Thermodynamics: Volume 2, The Royal Society of Chemistry. **2**, pp. 275-538.
306. McHardy, J. and Sawan, S.P. (1998). Supercritical Fluid Cleaning. Westwood, NJ, Noyes.
307. McHugh, M.A. and Krukonis, V.J. (1986). Supercritical Fluid Extraction Principles and Practice. Stoneham, MA, Butterworths.
308. McKee, R.H. and Parker, H.H. (1928). "Critical Temperatures and Oil Cracking1,2." Ind. Eng. Chem. **20**(11), pp. 1169-1172.
309. McKee, R.H. and Szayna, A. (1930). "Cracking of Hydrocarbons at Temperatures Higher than Critical Temperatures." Ind. Eng. Chem. **22**(9), pp. 953-956.
310. Melhem, G.A., Saini, R. and Goodwin, B.M. (1989). "A modified Peng-Robinson equation of state." Fluid Phase Equilibr. **47**(2–3), pp. 189-237.
311. Méndez-Santiago, J. and Teja, A.S. (1999). "The solubility of solids in supercritical fluids." Fluid Phase Equilibr. **158-160**, pp. 501-510.

312. Mendo-Sánchez, R.P., Sánchez-García, C., Galicia-Luna, L.A. and Elizalde-Solis, O. (2012). "Vapor-liquid equilibrium for the ternary carbon dioxide+ethanol+n-hexane and quaternary carbon dioxide+ethanol+n-hexane+thiophene systems." Fluid Phase Equilibr. **315**, pp. 40-45.
313. Mendoza, R. and Portal, R. (2000). "Landfarming of petroleum wastes in a cold dry climate of Tierra del Fuego. Effect on soil and vegetation." Ciencia del Suelo **18**(1), pp. 36-43.
314. Meyers, C.H. and Van Dusen, M.S. (1932). "The Vapour Pressure of Liquid and Solid Carbon Dioxide." Bur. Stand. J. Res. **10**, pp. 381-412.
315. Michelsen, M.L. and Heidemann, R.A. (1981). "Calculation of critical points from cubic two-constant equations of state." AIChE J. **27**(3), pp. 521-523.
316. Michelsen, M.L. (1984). "Calculation of critical points and phase boundaries in the critical region." Fluid Phase Equilibr. **16**(1), pp. 57-76.
317. Michelsen, M.L. and Kistenmacher, H. (1990). "On composition-dependent interaction coefficeints." Fluid Phase Equilibr. **58**(1-2), pp. 229-230.
318. Michelsen, T.C. and Boyce, C.P. (1993). "Cleanup standards for petroleum hydrocarbons. Part 1. Review of methods and recent developments." J. Soil Contam. **2**(2), pp. 109-124.
319. Miguel, A.A.F., Ferreira, A.G.M. and Fonseca, I.M.A. (2000). "Solubilities of some new refrigerants in water." Fluid Phase Equilibr. **173**(1), pp. 97-107.
320. Miller, D.J., Hawthorne, S.B., Clifford, A.A. and Zhu, S. (1996). "Solubility of Polycyclic Aromatic Hydrocarbons in Supercritical Carbon Dioxide from 313 K to 523 K and Pressures from 100 bar to 450 bar." J. Chem. Eng. Data **41**(4), pp. 779-786.
321. Miller, J.D. and Misra, M. (1982). "Hot water process development for Utah tar sands." Fuel Process. Technol. **6**(1), pp. 27-59.
322. Miller, K.W. (1968). "Solubility of fluorocarbon gases in cyclohexane." J. Phys. Chem. **72**(6), pp. 2248-2249.
323. Mitra, S., Chen, J.W. and Viswanath, D.S. (1988). "Solubility and partial molar volumes of heavy aromatic hydrocarbons in super critical carbon dioxide." J. Chem. Eng. Data **33**(1), pp. 35-37.
324. Mogollon, E., Kay, W.B. and Teja, A.S. (1982). "Modified sealed-tube method for the determination of critical temperature." Ind. Eng. Chem. Fundam. **21**(2), pp. 173-175.
325. Mokbel, I., Rauzy, E., Loiseleur, H., Berro, C. and Jose, J. (1995). "Vapor pressures of 12 alkylcyclohexanes, cyclopentane, butylcyclopentane and trans-decahydronaphthalene down to 0.5 Pa. Experimental results, correlation and prediction by an equation of state." Fluid Phase Equilibr. **108**(1-2), pp. 103–120.
326. Mokbel, I., Rauzy, E., Meille, J.P. and Jose, J. (1998). "Low vapor pressures of 12 aromatic hydrocarbons. Experimental and calculated data using a group contribution method." Fluid Phase Equilibr. **147**, pp. 271-284.
327. Molero Gómez, A., Pereyra López, C. and Martinez de la Ossa, E. (1996). "Recovery of grape seed oil by liquid and supercritical carbon dioxide extraction: a comparison with conventional solvent extraction." Chem. Eng. J. Bioch. Eng. **61**(3), pp. 227-231.
328. Mollerup, J. (1981). "A note on excess Gibbs energy models, equations of state and the local composition concept." Fluid Phase Equilibr. **7**(2), pp. 121-138.

329. Mollerup, J.M. and Michelsen, M.L. (1992). "Calculation of thermodynamic equilibrium properties." Fluid Phase Equilibr. **74**(C), pp. 1-15.
330. Montero, G.A., Giorgio, T.D. and Schnelle, K.B. (1996). "Scale-up and economic analysis for the design of supercritical fluid extraction equipment for remediation of soil." Environmental Progress **15**(2), pp. 112-121.
331. Moradinia, I. and Teja Amyn, S. (1987). Solubilities of Five Solid n-Alkanes in Supercritical Ethane. Supercritical Fluids: Chemical and Engineering Principles and Applications. Squires, T. G. and Paulaitis, M. E. Chicago, American Chemical Society, pp. 130-137.
332. Moradinia, I. and Teja, A.S. (1986). "Solubilities of solid n-octacosane, n-triacontane and n-dotriacontane in supercritical ethane." Fluid Phase Equilibr. **28**(2), pp. 199-209.
333. Morris, W.O. and Donohue, M.D. (1985). "Vapor-liquid equilibria in mixtures containing carbon dioxide, toluene, and 1-methylnaphthalene." J. Chem. Eng. Data **30**(3), pp. 259-263.
334. Muhlbauer, A.L. and Raal, J.D. (1991). "Measurement and thermodynamic interpretation of high-pressure vapour-liquid equilibria in the toluene + CO2 system." Fluid Phase Equilibr. **64**, pp. 213-236.
335. Muhle, J., Ganesan, A.L., Miller, B.R., Salameh, P.K., Harth, C.M., Greally, B.R., Rigby, M., Porter, L.W., Steele, L.P., Trudinger, C.M., Krummel, P.B., O'Doherty, S., Fraser, P.J., Simmonds, P.G., Prinn, R.G. and Weiss, R.F. (2010). "Perfluorocarbons in the global atmosphere: tetrafluoromethane, hexafluoroethane, and octafluoropropane." Atmos. Chem. Phys. **10**, pp. 5145-5164.
336. Muin, M. and Tsunoda, K. (2003). "Preservative treatment of wood-based composites with 3-iodo-2-propynyl butylcarbamate using supercritical carbon dioxide impregnation." J. Wood Sci. **49**(5), pp. 430-436.
337. Mukhopadhyay, M. and De, S.K. (1995). "Fluid phase behavior of close molecular weight fine chemicals with supercritical carbon dioxide." J. Chem. Eng. Data **40**(4), pp. 909-913.
338. Mulligan, C.N., Yong, R.N. and Gibbs, B.F. (2001). "Surfactant-enhanced remediation of contaminated soil: a review." Eng. Geol. **60**(1–4), pp. 371-380.
339. Musser, B.J. and Kilpatrick, P.K. (1998). "Molecular characterization of wax isolated from a variety of crude oils." Energ. Fuels **12**(4), pp. 715-725.
340. Mutelet, F., Vitu, S., Privat, R. and Jaubert, J.-N. (2005). "Solubility of CO2 in branched alkanes in order to extend the PPR78 model (Predictive 1978, Peng–Robinson EOS with temperature-dependent kij calculated through a group contribution method) to such systems." Fluid Phase Equilibr. **238**(2), pp. 157-168.
341. Mykin Inc. (2015). "Rubber Chemical Resistance Chart." Retrieved 28 April 2015, from http://mykin.com/rubber-chemical-resistance-chart-6.
342. Nagarajan, N. and Robinson, R.L. (1986). "Equilibrium phase compositions, phase densities, and interfacial tensions for carbon dioxide + hydrocarbon systems. 2. Carbon dioxide + n-decane." J. Chem. Eng. Data **31**(2), pp. 168-171.
343. Nagarajan, N., Gasem, K.A.M. and Robinson, R.L. (1990). "Equilibrium phase compositions, phase densities, and interfacial tensions for carbon dioxide + hydrocarbon systems. 6. Carbon dioxide + n-butane + n-decane." J. Chem. Eng. Data **35**(3), pp. 228-231.

344. Naidoo, P., Ramjugernath, D. and Raal, J.D. (2008). "A new high-pressure vapour–liquid equilibrium apparatus." Fluid Phase Equilibr. **269**(1–2), pp. 104-112.
345. Namose, I. (2005). "Method of processing PFC and apparatus for processing PFC." US Patent, **US6838011**.
346. Narasigadu, C. (2011). Design of a Static Micro-Cell for Phase Equilibrium Measurements: Measurements and Modelling, University of KwaZulu-Natal. **PhD Thesis**,
347. Narasigadu, C., Naidoo, P., Coquelet, C., Richon, D. and Ramjugernath, D. (2013). "A novel static analytical apparatus for phase equilibrium measurements." Fluid Phase Equilibr. **338**, pp. 188-196.
348. Nasrifar, K., Mooijer-van den Heuvel, M.M., Peters, C.J., Ayatollahi, S. and Moshfeghian, M. (2003). "Measurements and modeling of bubble points in binary carbon dioxide systems with tetrahydropyran and methylcyclohexane." Fluid Phase Equilibr. **204**(1), pp. 1-14.
349. Nasrifar, K., Mooijer-van den Heuvel, M.M. and Peters, C.J. (2008). "Experimental Determination and Modeling of Bubble and Dew Points in the System CO2 + CHF3." J. Chem. Eng. Data **53**(10), pp. 2328-2332.
350. National Fire Protection Asociation (2012). NFPA 704: Standard System for the Identification of the Hazards of Materials for Emergency Response, NFPA. **NFPA 704**,
351. Negadi, L., Blondel, A., Mokbel, I., Ait-Kaci, A. and Jose, J. (1993). "Liquid-vapor equilibria, excess Gibbs energies, and excess volumes of dimethyl carbonate + heptane, 1-hexene, cyclohexane, or benzene." Int. Data Ser., Sel. Data Mixtures Ser. A **21**, pp. 169-194.
352. Negadi, L., Belabbaci, A., Ait Kaci, A. and Jose, J. (2007). "Isothermal Vapor−Liquid Equilibria and Excess Enthalpies of (Propyl Ethanoate + Heptane), (Propyl Ethanoate + Cyclohexane), and (Propyl Ethanoate + 1-Hexene)." J. Chem. Eng. Data **52**(1), pp. 47-55.
353. Negadi, L., Mokbel, I., Negadi, A., Kaci, A.A., Jose, J. and Gmehling, J. (2009). "Isothermal Vapor−Liquid Equilibria and Excess Enthalpy Data for the Binary System (Butyric Acid + Toluene)." J. Chem. Eng. Data **54**(7), pp. 2045-2048.
354. Ng, H.-J. and Robinson, D.B. (1978). "Equilibrium-phase properties of the toluene-carbon dioxide system." J. Chem. Eng. Data **23**(4), pp. 325-327.
355. Ng, H.-J. and Robinson, D.B. (1979). "The equilibrium phase properties of selected naphthenic binary systems: Carbon dioxide-methylcyclohexane, hydrogen sulfide-methylcyclohexane." Fluid Phase Equilibr. **2**(4), pp. 283-292.
356. Ngema, P.T., Nelson, W.M., Naidoo, P., Ramjugemath, D. and Richon, D. (2014). "Isothermal method for hydrate studies using a transparent variable volume cell." Rev. Sci. Instrum. **85**, pp. 045123.
357. Nicolini, E. and Laffitte, P.C. (1949). "Vapor Pressure of Some Pure Organic Liquids." R. Hebd. Seances Acad. Sci. **229**, pp. 757-759.
358. Nieuwoudt, I. (1996). "The fractionation of high molecular weight alkane mixtures with supercritical fluids." Process Technol. Proc. **12**, pp. 283-290.
359. Nieuwoudt, I. and Du Rand, M. (2002). "Measurement of phase equilibria of supercritical carbon dioxide and paraffins." J. Supercrit. Fluids **22**(3), pp. 185-199.

360. NIST ThermoData Engine (2013). NIST ThermoData Engine 103b: Pure Compounds, Binary Mixtures, and Chemical Reactions. Thermodynamics Research Centre. Boulder, CO, USA,
361. Ocic, O. (2008). Oil Refineries in the 21st Century: Energy Efficient, Cost Effective, Environmentally Benign, Wiley.
362. O'Connell, J.P. and Haile, J.M. (2005). Thermodynamics: Fundamentals for Applications, Cambridge University Press.
363. Ohgaki, K. and Katayama, T. (1975). "Isothermal vapor-liquid equilibriums for systems ethyl ether-carbon dioxide and methyl acetate-carbon dioxide at high pressures." J. Chem. Eng. Data **20**(3), pp. 264-267.
364. Ohgaki, K. and Katayama, T. (1976). "Isothermal vapor-liquid equilibrium data for binary systems containing carbon dioxide at high pressures: methanol-carbon dioxide, n-hexane-carbon dioxide, and benzene-carbon dioxide systems." J. Chem. Eng. Data **21**(1), pp. 53-55.
365. Ohgaki, K., Umezono, S. and Katayama, T. (1990). "Pressure-density-temperature (P-p-T) relations of CHF3, N2O, and C3H6 in the critical region." J. Supercrit. Fluids **3**(2), pp. 78-84.
366. Ohno, H. and Ohi, T. (2003). "Production and Use of Hexafluoroethane." World Patent, **WO 2003 014047**,
367. Oonk, H.A.J. and Tamarit, J.K.L. (2005). Condensed Phases of Organic Materials: Solid-Liquid and Solid-Solid Equilibrium. Measurement of the Thermodynamic Properties of Multiple Phases. Weir, R. D. and de Loos, T. W. Amsterdam, The Netherlands, Elsevier.
368. Osman, K., Coquelet, C. and Ramjugernath, D. (2012). "Absorption Data and Modeling of Carbon Dioxide in Aqueous Blends of Bis(2-hydroxyethyl)methylamine (MDEA) and 2,2-Iminodiethanol (DEA): 25 % MDEA + 25 % DEA and 30 % MDEA + 20 % DEA." J. Chem. Eng. Data **57**(5), pp. 1607-1620.
369. Palmer, M.V. and Ting, S.S.T. (1995). "Applications for supercritical fluid technology in food processing." Food Chem. **52**(4), pp. 345-352.
370. Panagiotopoulos, A.Z. and Reid, R.C. (1986). New Mixing Rule for Cubic Equations of State for Highly Polar, Asymmetric Systems. Equations of State, American Chemical Society. **300**, pp. 571-582.
371. Park, S.J., Kwak, T.Y. and Mansoori, G.A. (1987). "Statistical mechanical description of supercritical fluid extraction and retrograde condensation." Int. J. Thermophys. **8**(4), pp. 449-471.
372. Parra, M.J., León, A.Y. and Hoyos, L.J. (2010). "Separation of fractions from vacuum residue by supercritical extraction." CT&F - Ciencia, Tecnologia & Futuro **4**(2), pp. 83-90.
373. Parsons Brinckerhoff (2011) Accelerating the uptake of CCS: Industrial use of captured carbon dioxide.
374. Partington, J.R. (1949). Fundamental Principles. The Properties of Gases. London, UK, Longmans, Green and Co.
375. Patel, N.C. and Teja, A.S. (1982). "A new cubic equation of state for fluids and fluid mixtures." Chem. Eng. Sci. **37**(3), pp. 463-473.
376. Paul, H.-I., Krug, J. and Knapp, H. (1986). "Measurements of VLE, hE and vE for binary mixtures of n-alkanes with n-alkylbenzenes." Thermochim. Acta **108**, pp. 9-27.

377. Peng, D.Y. and Robinson, D.B. (1976). "A New Two-Constant Equation of State." Ind. Eng. Chem. Fundam. **15**, pp. 59-64.
378. Perrut, M. (2000). "Supercritical Fluid Applications: Industrial Developments and Economic Issues." Ind. Eng. Chem. Res. **39**(12), pp. 4531-4535.
379. Perrut, M. (2010). Supercritical Fluid technology impact on environment. 12th European Meeting on Supercritical Fluids. Graz, Austria, International Society for Advancement of Supercritical Fluids,
380. Perrut, M. and Clavier, J.-Y. (2003). "Supercritical Fluid Formulation: Process Choice and Scale-up." Ind. Eng. Chem. Res. **42**(25), pp. 6375-6383.
381. Peter, S. and Brunner, G. (1978). "The Separation of Nonvolatile Substances by Means of Compressed Gases in Countercurrent Processes." Angew. Chem. Int. Edit. **17**(10), pp. 746-750.
382. Peters, C.J., de Roo, J.L. and de Swaan Arons, J. (1992). "Measurements and calculations of phase equilibria in binary mixtures of propane + tetratriacontane." Fluid Phase Equilibr. **72**, pp. 251-266.
383. Peters, C.J., de Roo, J.L. and de Swaan Arons, J. (1993). "Phase equilibria in binary mixtures of propane and hexacontane." Fluid Phase Equilibr. **85**, pp. 301-312.
384. Petkovic, L.M., Ginosar, D.M. and Burch, K.C. (2005). "Supercritical fluid removal of hydrocarbons adsorbed on wide-pore zeolite catalysts." J. Catal. **234**(2), pp. 328-339.
385. Pfeiffer, J.P. and Saal, R.N.J. (1940). "Asphaltic bitumen as colloid system." J. Phys. Chem. **44**(2), pp. 139-149.
386. Pividal, K.A., Sterner, C., Sandler, S.I. and Orbey, H. (1992). "Vapor-liquid equilibrium from infinite dilution activity coefficients: measurement and prediction of oxygenated fuel additives with alkanes." Fluid Phase Equilibr. **72**, pp. 227-250.
387. Plesnar, Z., Fu, Y.-H., Sandler, S.I. and Orbey, H. (1996). "Vapor−Liquid Equilibrium of the Acetic Acid + Octane Binary System at 323.15 K and 343.15 K." J. Chem. Eng. Data **41**(4), pp. 799-801.
388. Pöhler, H., Scheidgen, A.L. and Schneider, G.M. (1996). "Fluid phase equilibria of binary and ternary mixtures of supercritical carbon dioxide with a 1-alkanol and an n-alkane up to 100 MPa and 393 K - Cosolvency effect and miscibility windows (Part II)." Fluid Phase Equilibr. **115**(1-2), pp. 165-177.
389. Poliakoff, M., George, M.W., Howdle, S.M., Bagratashvili, V.N., Han, B.X. and Yan, H.K. (1999). "Supercritical fluids: Clean solvents for green chemistry " Chinese J. Chem. **17**(3), pp. 212-222.
390. Polishuk, I., Wisniak, J. and Segura, H. (1999). "Prediction of the critical locus in binary mixtures using equation of state: I. Cubic equations of state, classical mixing rules, mixtures of methane–alkanes." Fluid Phase Equilibr. **164**(1), pp. 13-47.
391. Polishuk, I., Wisniak, J. and Segura, H. (2003). "Simultaneous prediction of the critical and sub-critical phase behavior in mixtures using equations of state II. Carbon dioxide-heavy n-alkanes." Chem. Eng. Sci. **58**(12), pp. 2529-2550.
392. Poot, W. and de Loos, W. (1999). "Liquid-liquid-vapour equilibria in binary and quasi-binary systems of CHF3 with n-alkanes, phenylalkanes and alkanols." Phys. Chem. Chem. Phys. **1**(18), pp. 4293-4297.

393. Prausnitz, J.M., Lichtenthaler, R.N. and Gomes de Azevedo, E. (1999). Molecular Thermodynamics of Fluid-Phase Equilibria. 3rd Edition, Upper Saddle River, NJ, Pearson Education.
394. Raal, J.D. and Mühlbauer, A.L. (1994). "The Measurement of High Pressure Vapour-Liquid-Equilibria: Part I: Dynamic Methods." Developments in Chemical Engineering and Mineral Processing **2**(2-3), pp. 69-87.
395. Raal, J.D. and Mühlbauer, A.L. (1998). Phase Equilibria: Measurement & Computation. Bristol, PA, Taylor & Francis.
396. Raeissi, S. and Peters, C.J. (2001). "Bubble-point pressures of the binary system carbon dioxide + linalool." J. Supercrit. Fluids **20**(3), pp. 221-228.
397. Rainwater, J.C. (2001). "An asymptotic expression for the critical-region "bird's beak" isotherm and adjacent isotherms on the vapor-liquid phase diagram of a simple binary mixture." Fluid Phase Equilibr. **183-184**, pp. 41-51.
398. Ramírez, E., Mayorga, M.J., Cuevas, D. and Recasens, F. (2011). "Fatty oil hydrogenation in supercritical solvents: Process design and safety issues." J. Supercrit. Fluids **57**(2), pp. 143-154.
399. Ramjugernath, D., Valtz, A., Coquelet, C. and Richon, D. (2009). "Isothermal Vapor−Liquid Equilibrium Data for the Hexafluoroethane (R116) + Propane System at Temperatures from (263 to 323) K." J. Chem. Eng. Data **54**(4), pp. 1292-1296.
400. Ramjugernath, D., Valtz, A., Richon, D., Williams-Wynn, M.D. and Coquelet, C. (2015a). "Isothermal Vapor-Liquid Equilibrium Data for the Hexafluoroethane (R116) + n-Pentane and n-Hexane Systems at Temperatures from (288 to 296) K." J. Chem. Eng. Data **unpublished**.
401. Ramjugernath, D., Valtz, A., Richon, D., Williams-Wynn, M.D. and Coquelet, C. (2015b). "Isothermal Vapour-Liquid Equilibrium Data for the Hexafluoroethane (R116) + n-Butane System at Temperatures from (273 to 323) K." J. Chem. Eng. Data, **unpublished**.
402. Ramsey, E., Sun, Q., Zhang, Z., Zhang, C. and Gou, W. (2009). "Mini-Review: Green sustainable processes using supercritical fluid carbon dioxide." J. Environ. Sci. **21**(6), pp. 720-726.
403. Randall, L.G. (1982). "Introductory Remarks." Separ. Sci. Technol. **17**(1), pp. v-v.
404. Rasskazov, D.S., Petrov, E.K., Spiridonov, G.A. and Ushmajkin, E.R. (1975). "Investigation of P-V-T Data of Freon 31." Teplofiz. Svoistva Veshchestv Mater. **8**, pp. 4-16.
405. Reamer, H.H. and Sage, B.H. (1963). "Phase Equilibria in Hydrocarbon Systems. Volumetric and Phase Behavior of the n-Decane-CO2 System." J. Chem. Eng. Data **8**(4), pp. 508-513.
406. Redlich, O. and Kister, A.T. (1948). "Algebraic Representation of Thermodynamic Properties and the Classification of Solutions." Ind. Eng. Chem. **40**(2), pp. 345-348.
407. Redlich, O. and Kwong, J.N.S. (1949). "On the Thermodynamics of Solutions. V. An Equation of State. Fugacities of Gaseous Solutions." Chem. Rev. **44**(1), pp. 233-244.
408. Redlich, O., Kister, A.T. and Turnquist, C.E. (1952). "Thermodynamics of solutions. Analysis of vapor-liquid equilibria." Chem. Eng. Prog. Symp. Ser. No. 2 **48**, pp. 49-61.
409. Renon, H. and Prausnitz, J.M. (1968). "Local Compositions in Thermodynamic Excess Functions for Liquid Mixtures." AIChE J. **14**, pp. 135-144.
410. Reverchon, E., Della Porta, G. and Senatore, F. (1995). "Supercritical CO2 extraction and fractionation of lavender essential oil and waxes." J. Agr. Food Chem. **43**(6), pp. 1654-1658.

411. Reverchon, E. and Cardea, S. (2004). "Formation of cellulose acetate membranes using a supercritical fluid assisted process." J. Membrane Sci. **240**(1-2), pp. 187-195.
412. Rhodes, J.M., Bhethanabotla, V.R. and Campbell, S.W. (1997). "Total Vapor Pressure Measurements for Heptane + 1-Pentanol, + 2-Pentanol, + 3-Pentanol, + 2-Methyl-1-butanol, + 2-Methyl-2-butanol, + 3-Methyl-1-butanol, and + 3-Methyl-2-butanol at 313.15 K." J. Chem. Eng. Data **42**(4), pp. 731-734.
413. Rice, W.K. and Singh, L. (1990). Dynamic supercritical fluid extraction system, US Patent 4898673,
414. Richon, D. and de Loos, T.W. (2005). Vapour-Liquid Equilibrium at High Pressure. Measurement of the Thermodynamic Properties of Multiple Phases. Weir, R. D. and de Loos, T. W. Amsterdam, The Netherlands, Elsevier.
415. Rizvi, S.S.H., Daniels, J.A., Benado, A.L. and Zollweg, J.A. (1986). "Supercritical fluid extraction: Operating principles and food applications." Food Technol.-Chicago **40**(7), pp. 57-64.
416. Robinson, D.B. and Kalra, H. (1976). "The Equilibrium Phase Properties of Selected Binary Systems: n-Heptane-Hydrogen Sulfide, n-Heptane-Carbon Dioxide, iso-Butane-Nitrogen." NGPA RR-18.
417. Roess, L.C. (1936). "Determination of critical temperature and pressure of petroleum fractions by a flow method." J. I. Petrol. **22**, pp. 665-705.
418. Rose, J.L., Svrcek, W.Y., Monnery, W.D. and Chong, K. (2000). "Fractionation of Peace River Bitumen Using Supercritical Ethane and Carbon Dioxide." Ind. Eng. Chem. Res. **39**(10), pp. 3875-3883.
419. Roth, H., Peters-Gerth, P. and Lucas, K. (1992). "Experimental vapor-liquid equilibria in the systems R 22-R 23, R 22-CO2, CS2-R 22, R 23-CO2, CS2-R 23 and their correlation by equations of state." Fluid Phase Equilibr. **73**(1–2), pp. 147-166.
420. Rozzi, N.L. and Singh, R.K. (2002). "Supercritical Fluids and the Food Industry." Compr. Rev. Food Sci. F. **1**(1), pp. 33-44.
421. Sadus, R.J. (1992). "Predicting the Gas-Liquid Critical Properties of Binary Mixtures: An Alternative to Conventional Mixing Rules." Berich. Bunsen. Gesell. **96**(10), pp. 1454-1459.
422. Saikawa, K., Kijima, J., Uematsu, M. and Watanabe, K. (1979). "Determination of the critical temperature and density of hexafluoroethane." J. Chem. Eng. Data **24**(3), pp. 165-167.
423. Saito, M. (2013). "History of supercritical fluid chromatography: Instrumental development." J. Biosci. Bioeng. **115**(6), pp. 590-599.
424. Sako, T., Sugeta, T., Nakazawa, N., Okubo, T., Sato, M., Taguchi, T. and Hiaki, T. (1991). "Phase equilibrium study of extraction and concentration of furfural produced in reactor using supercritical carbon dioxide." J. Chem. Eng. Jpn. **24**(4), pp. 449-455.
425. Samedova, F.I., Kasumova, A.M., Rashidova, S.Y. and Bakhshesh, G.R. (2011). "Dehydration and desalination of oils using supercritical carbon dioxide." Russ. J. Phys. Chem. B **5**(7), pp. 1076-1079.
426. Sánchez-García, C., Vázquez-Hernández, K.E., Galicia-Luna, L.A. and Elizalde-Solis, O. (2011). "Vapor-liquid equilibrium measurements for the ternary systems of CO2 + n-hexane + n-decane and CO2 + n-octane + n-decane." Ind. Eng. Chem. Res. **50**(21), pp. 12254-12258.
427. Sandarusi, J.A., Kidnay, A.J. and Yesavage, V.F. (1986). "Compilation of parameters for a polar fluid Soave-Redlich-Kwong equation of state." Ind. Eng. Chem. Proc. Des. Dev. **25**(4), pp. 957-963.

428. Sankaran, S., Pandey, S. and Sumathy, K. (1998). "Experimental investigation on waste heat recovery by refinery oil sludge incineration using fluidised-bed technique." J. Environ. Sci. Heal. A **33**(5), pp. 829-845.
429. Sapei, E., Zaytseva, A., Uusi-Kyyny, P., Keskinen, K.I. and Aittamaa, J. (2006). "Vapor−Liquid Equilibrium for Binary System of Thiophene + n-Hexane at (338.15 and 323.15) K and Thiophene + 1-Hexene at (333.15 and 323.15) K." J. Chem. Eng. Data **51**(6), pp. 2203-2208.
430. Savage, P.E., Gopalan, S., Mizan, T.I., Martino, C.J. and Brock, E.E. (1995). "Reactions at supercritical conditions: Applications and fundamentals." AIChE J. **41**(7), pp. 1723-1778.
431. Schaefer, K., Rall, W. and Wirth-Lindemann, F.C. (1958). "Thermodynamic experiments on the systems acetone + n-heptane and acetone + n-nonane." Z. Phys. Chem. **14**, pp. 197-207.
432. Scheidgen, A.L. and Schneider, G.M. (2000). "Fluid phase equilibria of (carbon dioxide + a 1-alkanol + an alkane) up to 100 MPa and T = 393 K: Cosolvency effect, miscibility windows, and holes in the critical surface." J. Chem. Thermodyn. **32**(9), pp. 1183-1201.
433. Scheidgen, A.L. and Schneider, G.M. (2000). "Fluid phase equilibria of (carbon dioxide + a 1-alkanol + an alkane) up to 100 MPa and T = 393 K: Cosolvency effect, miscibility windows, and holes in the critical surface." J. Chem. Thermodyn. **32**(9), pp. 1183-1201.
434. Schmelzer, J., Lieberwirth, I., Krug, M. and Pfestorf, R. (1983). "Vapour-liquid equilibria and heats of mixing in alkane-alcohol(1) systems. I. Vapour-liquid equilibria in 1-alcohol-undecane systems." Fluid Phase Equilibr. **11**(2), pp. 187–200.
435. Schmidt, J.W. and Moldover, M.R. (1994). "Alternative refrigerants difluoromethane and pentafluoroethane: critical temperature, refractive index, surface tension, and estimates of liquid, vapor, and critical densities." J. Chem. Eng. Data **39**(1), pp. 39-44.
436. Schmidt, P.F. (1986). Why Treat Your Fuel Oil. New York, Industrial Press.
437. Schneider, G.M. (1978). "Physicochemical Principles of Extraction with Supercritical Gases." Angew. Chem. Int. Edit. **17**(10), pp. 716-727.
438. Scholander, P.F. (1947). "Analyser for Accurate Estimation of Respiratory Gases in One-Half Cubic Centimeter Samples." J. Biol. Chem. **167**, pp. 235-250.
439. Schonemann, H., Gudinas, A., Williams, K., Wetmore, P. and Krukonis, V. (2008). Method for extraction and concentration of carotenoids using supercritical fluids, US Patent 7329789,
440. Schultz, W.G. and Randall, J.M. (1970). "Liquid carbon dioxide for selective aroma extraction." Food Technol.-Chicago **24**, pp. 1282-1286.
441. Schwartzentruber, J., Renon, H. and Watanasiri, S. (1990). "K-values for Non-Ideal Systems:An Easier Way." Chem. Eng., pp. 118-124.
442. Schwarz, C.E. (2001). The Phase Equilibria of Alkanes and Supercritical Fluids. Chemical Engineering, University of Stellenbosch. **Master of Science in Engineering**,
443. Schwarz, C.E. and Knoetze, J.H. (2007). "Phase equilibria of high molecular mass 1-alcohols in supercritical propane." Fluid Phase Equilibr. **258**(1), pp. 51-57.
444. Schwarz, C.E., Bonthuys, G.J.K., Knoetze, J.H. and Burger, A.J. (2008). "The influence of functional end groups on the high-pressure phase equilibria of long chain molecules in supercritical propane." J. Supercrit. Fluids **46**(3), pp. 233-237.

445. Schwarz, C.E., Zamudio, M. and Knoetze, J.H. (2011). "Phase equilibria of long-chain carboxylic acids in supercritical Propane." J. Chem. Eng. Data **56**(4), pp. 1116-1124.
446. Sebastian, H.M., Simnick, J.J., Lin, H.-M. and Chao, K.-C. (1980). "Gas-liquid equilibrium in mixtures of carbon dioxide + toluene and carbon dioxide + m-xylene." J. Chem. Eng. Data **25**(3), pp. 246-248.
447. Segovia, J.J., Martín, M.C., Chamorro, C.R. and Villamañán, M.A. (1998). "Vapor−Liquid Equilibrium of Ternary Mixtures Containing Methyl tert-Butyl Ether and/or Substitution Hydrocarbons. Methyl tert-Butyl Ether + Heptane + Cyclohexane and Methyl tert-Butyl Ether + Cyclohexane + 1-Hexene at 313.15 K." J. Chem. Eng. Data **43**(6), pp. 1021-1026.
448. Segura, H., Lam, E., Reich, R. and Wisniak, J. (2001). "Isobaric Phase Equilibria in the Binary Systems Ethyl 1,1-Dimethylethyl Ether + 1-hexene and + Cyclohexene at 94.00 kPa." Phys. Chem. Liq. **39**(1), pp. 43-54.
449. Senger Elsbernd, C.L. (2001). "Stabilized carbon dioxide fluid composition and use thereof." US Patent, **US6235701 B1**.
450. Shariati, A., Peters, C.J. and Moshfeghian, M. (1998). "Bubble point pressures of some selected carbon dioxide + synthetic C6+ mixtures." J. Chem. Eng. Data **43**(5), pp. 785-788.
451. Shariaty-Niassar, M., Aminzadeh, B., Azadi, P. and Soltanali, S. (2009). "Economic Evaluation of Herb Extraction Using Supercritical Fluid." Chem. Ind. Chem. Eng. Q. **15**(3), pp. 143-148.
452. Shaver, R.D., Robinson Jr, R.L. and Gasem, K.A.M. (2001). "An automated apparatus for equilibrium phase compositions, densities, and interfacial tensions: data for carbon dioxide + decane." Fluid Phase Equilibr. **179**(1–2), pp. 43-66.
453. Sheng, Y.J., Chen, P.C., Chen, Y.P. and Wong, D.S.H. (1992). "Calculations of solubilities of aromatic compounds in supercritical carbon dioxide." Ind. Eng. Chem. Res. **31**(3), pp. 967-973.
454. Shie, J.L., Chen, Y.H., Chang, C.Y., Lin, J.P., Lee, D.J. and Wu, C.H. (2002). "Thermal pyrolysis of poly(vinyl alcohol) and its major products." Energ. Fuels **16**(1), pp. 109-118.
455. Shie, J.L., Lin, J.P., Chang, C.Y., Wu, C.H., Lee, D.J., Chang, C.F. and Chen, Y.H. (2004). "Oxidative thermal treatment of oil sludge at low heating rates." Energ. Fuels **18**(5), pp. 1272-1281.
456. Shieh, Y.T. and Liu, K.H. (2004). "Conformational changes of poly(ethylene oxide) in poly(ethylene oxide)/poly(methyl methacrylate) blends by supercritical carbon dioxide." J. Polym. Sci. Pol. Phys. **42**(13), pp. 2479-2489.
457. Shiflett, M.B. and Sandier, S.I. (1998). "Modeling fluorocarbon vapor-liquid equilibria using the Wong-Sandler model." Fluid Phase Equilibr. **147**(1-2), pp. 145-162.
458. Sihvonen, M., Järvenpää, E., Hietaniemi, V. and Huopalahti, R. (1999). "Advances in supercritical carbon dioxide technologies." Trends Food Sci. Tech. **10**(6–7), pp. 217-222.
459. Silva, C.S.O., Fonseca, I.M.A. and Lobo, L.Q. (1997). "Solubility of methyl fluoride in some alcohols." Fluid Phase Equilibr. **135**(1), pp. 137-144.
460. Singh, H., Lucien, F.P. and Foster, N.R. (2000). "Critical Properties for Binary Mixtures of Ethane Containing Low Concentrations of n-Alkane." J. Chem. Eng. Data **45**(1), pp. 131-135.
461. Sinnott, R.K. (2009). Chemical Engineering Design: SI edition. Amsterdam, The Netherlands, Elsevier Science.

462. Skjold-Jørgensen, S. (1984). "Gas solubility calculations. II. Application of a new group-contribution equation of state." Fluid Phase Equilibr. **16**(3), pp. 317-351.
463. Smith, J.M., Van Ness, H.C. and Abbott, M.M. (2005). Introduction to Chemical Engineering Thermodynamics. New York, NY, Mcgraw-Hill.
464. Soares, V.B. and Coelho, G.L.V. (2012). "Safety study of an experimental apparatus for extraction with supercritical CO2." Braz. J. Chem. Eng. **29**, pp. 677-682.
465. Soave, G. (1972). "Equilibrium constants from a modified Redlich-Kwong equation of state." Chem. Eng. Sci. **27**(6), pp. 1197-1203.
466. Soave, G., Barolo, M. and Bertucco, A. (1993). "Estimation of high-pressure fugacity coefficients of pure gaseous fluids by a modified SRK equation of state." Fluid Phase Equilibr. **91**(1), pp. 87-100.
467. Soo, C.-B. (2011). Experimental Thermodynamic Measurements of Biofuel-related Associating Compounds and Modeling using the PC-SAFT Equation of State. Centre Énergétique et Procédés - Laboratoire CEP/TEP. Fontainebleau, France, l'École Nationale Supérieure des Mines de Paris. **PhD Thesis**,
468. Soo, C.-B., Théveneau, P., Coquelet, C., Ramjugernath, D. and Richon, D. (2010). "Determination of critical properties of pure and multi-component mixtures using a "dynamic–synthetic" apparatus." J. Supercrit. Fluids **55**(2), pp. 545-553.
469. Sousa, M., Melo, M.J., Casimiro, T. and Aguiar-Ricardo, A. (2007). "The art of CO2 for art conservation: A green approach to antique textile cleaning." Green Chem. **9**(9), pp. 943-947.
470. South African Reserve Bank (2015). "Important Rates." Retrieved 10 September 2015, 2015, from https://www.resbank.co.za/Pages/default.aspx.
471. Spencer, C.F., Daubert, T.E. and Danner, R.P. (1973). "A critical review of correlations for the critical properties of defined mixtures." AIChE J. **19**(3), pp. 522-527.
472. Squires, T.G. and Paulaitis, M.E., Eds. (1987). Supercritical Fluids: Chemical Engineering Principles and Applications. Am. Chem. Soc. Symp. Ser.
473. SRI Consulting (2010). Chemical Economics Handbook 2010. Stanford, CA, USA, SRI International,
474. Stahl, E., Quirin, K.W. and Gerard, D. (1988). Dense gases for extraction and refining. Berlin, Germany, Springer-Verlag.
475. Stahl, E., Schuetz, E. and Mangold, H.K. (1980). "Extraction of seed oils with liquid and supercritical carbon dioxide." J. Agr. Food Chem. **28**(6), pp. 1153-1157.
476. Stephan, K. and Lucas, K. (1979). Viscosity of dense fluids, Plenum Press.
477. Stockfleth, R. and Dohrn, R. (1998). "An algorithm for calculating critical points in multicomponents mixtures." Fluid Phase Equilibr. **45**, pp. 43-52.
478. Stryjek, R. and Vera, J.H. (1986). "Vapor-liquid equilibrium of hydrochloric acid solutions with the PRSV equation of state." Fluid Phase Equilibr. **25**(3), pp. 279-290.
479. Subramanian, M. and Hanson, F.V. (1998). "Supercritical fluid extraction of bitumens from Utah oil sands." Fuel Process. Technol. **55**(1), pp. 35-53.

480. Subramoney, S.C. (2008). The Separation of Hexafluoropropylene and Hexafluoropropylene Oxide Using Toluene and a Novel Solvent. School of Chemical Engineering. Durban, South Africa, University of KwaZulu-Natal. **MSc. Eng. Dissertation**,
481. Suehiro, Y., Nakajima, M., Yamada, K. and Uematsu, M. (1996). "Critical parameters of {x CO2+ (1 −x) CHF3} for x = (1.0000, 0.7496, 0.5013, and 0.2522)." J. Chem. Thermodyn. **28**(10), pp. 1153-1164.
482. Sztukowski, D.M. and Yarranton, H.W. (2005). "Oilfield solids and water-in-oil emulsion stability." J. Colloid Interf. Sci. **285**(2), pp. 821-833.
483. Tabernero, A., Martín del Valle, E.M. and Galán, M.A. (2012). "Supercritical fluids for pharmaceutical particle engineering: Methods, basic fundamentals and modelling." Chemical Engineering and Processing: Process Intensification **60**(0), pp. 9-25.
484. Taiwo, E.A. and Otolorin, J.A. (2009). "Oil recovery from petroleum sludge by solvent extraction." Pet. Sci. Technol. **27**(8), pp. 836-844.
485. Taylor, B.N. and Kuyatt, C.E. (1994). "Guidelines for Evaluating and Expressing the Uncertainty of NIST Measurement Results." NIST Technical Note **1297**.
486. Taylor, B.N., Mohr, P.J. and Douma, M. (2007). The NIST Reference on constants, units, and uncertainty.
487. Taylor, L.T. (2009). "Supercritical fluid chromatography for the 21st century." J. Supercrit. Fluids **47**(3), pp. 566-573.
488. Taylor, S.L. and King, J.W. (1994). Supercritical Fluid Extraction of Organochlorine Pesticides Using Trifluoromethane. Food Quality and Safety Research - National Centre for Agricultural Utilisation Research. Peoria, Il,
489. Teja, A.S. and Eckert, C.A. (2000). "Commentary on supercritical fluids: Research and applications." Ind. Eng. Chem. Res. **39**(12), pp. 4442-4444.
490. Teja, A.S. and Mendez-Santiago, J. (2005). Critical Parameters. Measurement of the Thermodynamic Properties of Multiple Phases. Weir, R. D. and de Loos, T. W. Amsterdam, The Netherlands, Elsevier B.V. **VII**.
491. Teja, A.S., Gude, M. and Rosenthal, D.J. (1989). "Novel methods for the measurement of the critical properties of thermally unstable fluids." Fluid Phase Equilibr. **52**, pp. 193-200.
492. Tester, J.W., A. Marrone, P., DiPippo, M.M., Sako, K., Reagan, M.T., Arias, T. and Peters, W.A. (1998). "Chemical reactions and phase equilibria of model halocarbons and salts in sub- and supercritical water (200–300 bar, 100–600°C)." J. Supercrit. Fluids **13**(1–3), pp. 225-240.
493. Thompson, D.N., Ginosar, D.M. and Coates, K. (2001). Abstr. Pap. Am. Chem. Soc. **222**, pp. U466.
494. Tilicheev, M.D., Peshkov, V.P. and Yuganova, S.A. (1951). "Cryoscopic Constants and Transition Temperatures of Normal Alkanes." Zh. Obshch. Khim. **21**(1229-1237).
495. Tochigi, K., Hasegawa, K., Asano, N. and Kojima, K. (1998). "Vapor-liquid equilibria for the carbon dioxide + pentane and carbon dioxide + toluene systems." J. Chem. Eng. Data **43**(6), pp. 954-956.
496. Tochigi, K., Namae, T., Suga, T., Matsuda, H., Kurihara, K., dos Ramos, M.C. and McCabe, C. (2010). "Measurement and prediction of high-pressure vapor–liquid equilibria for binary mixtures of

carbon dioxide&n-octane, methanol, ethanol, and perfluorohexane." J. Supercrit. Fluids **55**(2), pp. 682-689.

497. Todd, D.B. and Elgin, J.C. (1955). "Phase Equilibria in Systems with Ethylene Above its Critical Temperature." AIChE J. **1**(1), pp. 20 - 27.
498. Tom, J.W. and Debenedetti, P.G. (1991). "Particle formation with supercritical fluids—a review." J. Aerosol Sci. **22**(5), pp. 555-584.
499. Tomasko, D.L., Han, X., Liu, D. and Gao, W. (2003). "Supercritical fluid applications in polymer nanocomposites." Curr. Opin. Solid St. M. **7**(4-5), pp. 407-412.
500. Topsøe, H., Egeberg, R.G. and Knudsen, K.G. (1996). "Future Challenges of Hydrotreating Catalyst Technology." Prepr. Pap. Am. Chem. Soc., Div. Fuel Chem. **49**(2), pp. 568-569.
501. Toribio, L., Del Nozal, M.J., Bernal, J.L., Jiménez, J.J. and Alonso, C. (2004). "Chiral separation of some triazole pesticides by supercritical fluid chromatography." J. Chromatogr. A **1046**(1-2), pp. 249-253.
502. Traub, P. and Stephan, K. (1990). "High-pressure phase equilibria of the system CO2—water—acetone measured with a new apparatus." Chem. Eng. Sci. **45**(3), pp. 751-758.
503. Trowbridge, T.D. and Holcombe, T.C. (1995). "Refinery sludge treatment/hazardous waste minimization via dehydration and solvent extraction." J. Air Waste Manage. **45**(10), pp. 782-788.
504. Tsai, W.-T., Chen, H.-P. and Hsien, W.-Y. (2002). "A review of uses, environmental hazards and recovery/recycle technologies of perfluorocarbons (PFCs) emissions from the semiconductor manufacturing processes." J. Loss Prevent. Proc. **15**(2), pp. 65-75.
505. Türk, M. (2009). "Manufacture of submicron drug particles with enhanced dissolution behaviour by rapid expansion processes." J. Supercrit. Fluids **47**(3), pp. 537-545.
506. Twu, C.H., Bluck, D., Cunningham, J.R. and Coon, J.E. (1991). "A Cubic Equation of State with a New Alpha Function and a New Mixing Rule." Fluid Phase Equilibr. **69**, pp. 33-50.
507. Twu, C.H., Coon, J.E. and Cunningham, J.R. (1992). "A New Cubic Equation of State." Fluid Phase Equilibr. **75**, pp. 65-79.
508. UNEP (2003). Handbook for the International Treaties for the Protection of the Ozone Layer The Vienna Convention (1985) The Montreal Protocol (1987). Nairobi, Kenya, UNEP.
509. Ungerer, P., Tavitian, B. and Boutin, A. (2005). Applications of molecular simulation in the oil and gas industry- Monte Carlo methods, IFP Publications.
510. United Nations Framework Convention on Climate Change (1997). Report of the Conference of the Parties on its Third Session, held at Kyoto, from 1 to 11 December 1997. Bonn, Germany, pp. 7-30
511. Uusi-Kyyny, P., Pokki, J.-P., Aittamaa, J. and Liukkonen, S. (2001). "Vapor−Liquid Equilibrium for the Binary Systems of 3-Methylpentane + 2-Methyl-2-propanol at 331 K and + 2-Butanol at 331 K." J. Chem. Eng. Data **46**(3), pp. 754-758.
512. Valtz, A., Chapoy, A., Coquelet, C., Paricaud, P. and Richon, D. (2004). "Vapour–liquid equilibria in the carbon dioxide–water system, measurement and modelling from 278.2 to 318.2 K." Fluid Phase Equilibr. **226**(0), pp. 333-344.

513. Valtz, A., Coquelet, C. and Richon, D. (2007). "Vapor-liquid equilibrium data for the hexafluoroethane + carbon dioxide system at temperatures from 253 to 297 K and pressures up to 6.5 MPa." Fluid Phase Equilibr. **258**(2), pp. 179-185.
514. van Konynenburg, P.H. and Scott, R.L. (1980). "Critical Lines and Phase Equilibria in Binary Van Der Waals Mixtures." Philos. Trans. R. Soc. London, Ser. A **298**, pp. 495-540.
515. Van Ness, H.C. (1964). Classical Thermodynamics of Non-Electrolyte Solutions, Pergamon.
516. Van Ness, H.C., Soczek, C.A., Peloquin, G.L. and Machado, R.L. (1967). "Thermodynamic excess properties of three alcohol-hydrocarbon systems." J. Chem. Eng. Data **12**(2), pp. 217-224.
517. van Oudenhoven, J.A.C.M., Cooper, G.R. and Cricchi, G. (1995). Oil refinery waste disposal methods, quantities and costs 1993 : survey. Brussels, CONCAWE.
518. Vera, J.H. and Orbey, H. (1984). "Binary vapor-liquid equilibria of carbon dioxide with 2-methyl-1-pentene, 1-hexene, 1-heptene, and m-xylene at 303.15, 323.15, and 343.15 K." J. Chem. Eng. Data **29**(3), pp. 269-272.
519. Vesovic, V., Wakeham, W.A., Olchowy, G.A., Sengers, J.V., Watson, J.T.R. and Millat, J. (1990). "The Transport Properties of Carbon Dioxide." J. Phys. Chem. Ref. Data **19**(3), pp. 763-808.
520. Wadsö, I. (1966). "A Heat of Vaporisation Calorimeter for Work at 25C and for Small Amounts of Substances." Acta Chem. Scand. **20**, pp. 536-543.
521. Wagner, Z. and Wichterle, I. (1987). "High-pressure vapour-liquid equilibrium in systems containing carbon dioxide, 1-hexene, and n-hexane." Fluid Phase Equilibr. **33**(1-2), pp. 109-123.
522. Walas, S.M. (1985). Phase Equilibria in Chemical Engineering. Oxford, Butterworth-Heinemann.
523. Wang, B., He, J., Sun, D., Zhang, R. and Han, B. (2006). "Solubility of chlorobutane, ethyl methacrylate and trifluoroethyl acrylate in supercritical carbon dioxide." Fluid Phase Equilibr. **239**(1), pp. 63-68.
524. Wang, H. and Prins, R. (2009). "Hydrodesulfurization of dibenzothiophene, 4,6-dimethyldibenzothiophene, and their hydrogenated intermediates over Ni–MoS2/γ-Al2O3." J. Catal. **264**(1), pp. 31-43.
525. Wang, J., Yin, J., Ge, L., Shao, J. and Zheng, J. (2010). "Characterization of oil sludges from two oil fields in china." Energ. Fuels **24**(2), pp. 973-978.
526. Wang, L.S., Lang, Z.X. and Guo, T.M. (1996). "Measurement and correlation of the diffusion coefficients of carbon dioxide in liquid hydrocarbons under elevated pressures." Fluid Phase Equilibr. **117**(1–2), pp. 364-372.
527. Watkins, J.J., Brown, G.D., Pollard, M.A., Ramachandrarao, V.S. and Russell, T.P. (2000). Phase Transitions in Polymer Blends and Block Copolymers Induced by Selective Dilation with Supercritical CO2. Supercritical Fluids. Kiran, E., Debenedetti, P. and Peters, C., Springer Netherlands. **366**, pp. 277-289.
528. Weng, W.L. and Lee, M.J. (1992). "Vapor-liquid equilibrium of the octane/carbon dioxide, octane/ethane, and octane/ethylene systems." J. Chem. Eng. Data **37**(2), pp. 213-215.
529. Widom, B. (1973). "Tricritical points in three- and four-component fluid mixtures." J. Phys. Chem. **77**(18), pp. 2196-2200.

530. Wiebe, R. and Gaddy, V.L. (1940). "The Solubility of Carbon Dioxide in Water at Various Temperatures from 12 to 40° C and at Pressures to 500 atmospheres. Critical Phenomena*." J. Am. Chem. Soc. **62**(4), pp. 815-817.
531. Willingham, C.B., Taylor, W.J., Pignocco, J.M. and Rossini, F.D. (1945). "Vapor Pressures and Boiling Points of Some Paraffin, Alkylcyclopentane, Alkylcyclohexane and Alkylbenzene Hydrocarbons." J. Res. Nat. Bur. Stand. **35**, pp. 219.
532. Wilson, G.M. (1964). "Vapor-Liquid Equilibrium. XI. A New Expression for the Excess Free Energy of Mixing." J. Am. Chem. Soc. **86**(2), pp. 127-130.
533. Wilson, L.C., Wilding, W.V., Wilson, H.L. and Wilson, G.M. (1995). "Critical Point Measurements by a New Flow Method and a Traditional Static Method." J. Chem. Eng. Data **40**(4), pp. 765-768.
534. Wilson, S.C. and Jones, K.C. (1993). "Bioremediation of soil contaminated with polynuclear aromatic hydrocarbons (PAHs): A review." Environ. Pollut. **81**(3), pp. 229-249.
535. Winkler, S. and Stephan, K. (1997). "Fluid multiphase behavior in ternary mixtures of CO2, H2O and 1-butanol." Fluid Phase Equilibr. **137**(1–2), pp. 247-263.
536. Wirths, M. and Schneider, G.M. (1985). "High-pressure phase studies on fluid binary mixtures of hydrocarbons with tetrafluoromethane and trifluoromethane between 273 and 630 K and up to 250 MPa." Fluid Phase Equilibr. **21**(3), pp. 257-278.
537. Wolff, H., Höpfner, A. and Höpfner, H.M. (1964). "Die Assoziation von Methyl-, Äthyl- und n-Propylamin in gesättigten aliphatischen Kohlenwasserstoffen (nach Dampfdruckmessungen)." Ber. Bunsen. Phys. Chem. **68**(4), pp. 410-417.
538. Wong, D.S.H. and Sandler, S.I. (1992). "Theoretically Correct Mixing Rule for Cubic Equations of State." AIChE J. **38**, pp. 671-680.
539. Woringer, B. (1900). "Vapor Pressures of a Series of Benzene Derivatives." Z. Phys. Chem.-Stoch. Ve. **34**, pp. 257.
540. Worthy, W. (1981). Supercritical Fluids Offer Improved Separations. Chem. Eng. News, American Chemical Society. **59**, pp. 16-17
541. Wu, H.S., Pividal, K.A. and Sandler, S.I. (1991). "Vapor-liquid equilibria of hydrocarbons and fuel oxygenates." J. Chem. Eng. Data **36**(4), pp. 418-421.
542. Wypych, G. (2001). Handbook of solvents. Ontario, Canada, ChemTec Publishing.
543. Yan, N., Kurbis, C. and Masliyah, J.H. (1997). "Continuous Demulsification of Solids-Stabilized Oil-in-Water Emulsions by the Addition of Fresh Oil." Ind. Eng. Chem. Res. **36**(7), pp. 2634-2640.
544. Yang, X. and Kilpatrick, P. (2005). "Asphaltenes and waxes do not interact synergistically and coprecipitate in solid organic deposits." Energ. Fuels **19**(4), pp. 1360-1375.
545. York, P., Kompella, U.B. and Shekunov, B.Y. (2004). Supercritical Fluid Technology for Drug Product Development. London, UK, Taylor & Francis.
546. Young, S. (1898). "LXX.-The vapour pressures, specific volumes, and critical constants of normal heptane." J. Chem. Soc. Trans. **73**, pp. 675-681.
547. Young, S. (1900). "Vapor Pressures, Specific Volumes, and Critical Constants of Normal Octane." J. Chem. Soc. **77**, pp. 1145.

548. Young, S. (1910). "The Internal Heat of Vaporization constants of thirty pure substances." Sci. Proc. R. Dublin Soc. **12**, pp. 374-443.
549. Young, S. (1928). "On the Boiling Points of the Normal Paraffins at Different Pressures." Proc. Roy. Irish Acad. B **38**, pp. 65-92.
550. Yu, J., Wang, S. and Tian, Y. (2006). "Experimental determination and calculation of thermodynamic properties of CO2 & octane to high temperatures and high pressures." Fluid Phase Equilibr. **246**(1–2), pp. 6-14.
551. Zabaloy, M.S., Vasquez, V.R. and Macedo, E.A. (2005). "Viscosity of pure supercritical fluids." J. Supercrit. Fluids **36**(2), pp. 106-117.
552. Zamudio, M., Schwarz, C.E. and Knoetze, J.H. (2011). "Phase equilibria of branched isomers of C 10-alcohols and C 10-alkanes in supercritical ethane." J. Supercrit. Fluids **59**, pp. 14-26.
553. Zeitfuchs, E.H. (1926). "Specific heats, heats of vaporization, and critical temperatures of California petroleum oils." Ind. Eng. Chem. **18**(1), pp. 79-82.
554. Zhang, Y., Gong, M., Zhu, H. and Wu, J. (2006). "Vapor-liquid equilibrium data for the ethane + trifluoromethane system at temperatures from (188.31 to 243.76) K." J. Chem. Eng. Data **51**(4), pp. 1411-1414.
555. Zhang, Y., Gong, M.Q., Zhu, H.B. and Wu, J.F. (2005). "Vapour-Liquid Equilibrium Measurements for Ethane + Hexafluoroethane System over a Temperature Range from (199.64 to 242.93) K." J. Chem. Eng. Data **50**, pp. 2074-2076.
556. Zhang, Y., Zhao, H., Shi, Q., Chung, K.H., Zhao, S. and Xu, C. (2011). "Molecular investigation of crude oil sludge from an electric dehydrator." Energ. Fuels **25**(7), pp. 3116-3124.
557. Zhu, R., Hoshi, T., Muroga, Y., Hagiwara, T., Yano, S. and Sawaguchi, T. (2013). "Microstructure and mechanical properties of a polyethylene/ polydimethylsiloxane composite prepared using supercritical carbon dioxide." J. Appl. Polym. Sci. **127**(5), pp. 3388-3394.
558. Zhu, R., Yu, J., Xu, W., Liu, Z. and Tian, Y.-L. (2006). "High pressure vapor liquid equilibrium of carbon dioxide + hexane system." Huagong Xuebao **57**(10), pp. 2270.
559. Zizovic, I., Stamenić, M., Orlović, A. and Skala, D. (2005). "Supercritical carbon dioxide essential oil extraction of Lamiaceae family species: Mathematical modelling on the micro-scale and process optimization." Chem. Eng. Sci. **60**(23), pp. 6747-6756.
560. Zosel, K. (1978). "Separation with Supercritical Gases: Practical Applications." Angew. Chem. Int. Edit. **17**(10), pp. 702-709.
561. Zubaidy, E.A.H. and Abouelnasr, D.M. (2010). "Fuel recovery from waste oily sludge using solvent extraction." Process Saf. Environ. **88**(5), pp. 318-326.
562. Zuo, Y.-X. and Guo, T.-M. (1991). "Extension of the Patel-Teja equation of state to the prediction of the solubility of natural gas in formation water." Chem. Eng. Sci. **46**(12), pp. 3251-3258.

A. Additional Information from Literature

A.1. Oil Sludge Treatment Techniques

More detailed descriptions of some of the oil sludge treatment techniques given in Section 1.1.1.3. are provided in this appendix.

A.1.1. Centrifugation

Centrifugation allows for the separation of a gaseous phase, an aqueous phase and an oily phase from the oil sludge (Da Silva et al., 2012). This process is fairly clean, and has relatively low costs. Conditioners, such as potassium alum, are often added to the sludge to improve the de-waterability (Jing et al., 2011)

A.1.2. Electro-Demulsification

Elektorowicz et al. (2006) investigated the use of an electric potential gradient to demulsify an oily sludge by removing the fine particles which were absorbed at the droplet surface. These particles were believed to 'act as a barrier to prevent droplet coalescence' (Yan et al., 1997). It was found that the method investigated by Elektorowicz et al. was successful; producing a separation of a solid phase and a water and hydrocarbon mixture.

Electorowicz et al. claimed that the costs of using electro-demulsification were lower than other 'conventional remediation techniques'.

A.1.3. Extraction

The use of solvents for the extraction of valuable products from oily sludge is by far the most investigated and used treatment technique. The solvent is most commonly used as a liquid, in solvent extraction, but there are also reports of investigations into the use of SCFs.

There have been a number of authors who have investigated the use of solvent extraction for the recovery of valuable products from oily sludges. Table A.1 lists some examples of investigations into the use of solvent extraction with liquids for the recovery of valuable products from oil sludges. The recovery of the oil from the sludge was generally found to be between 50 and 90%.

Table A.1. Examples of the use of solvent extraction for recovery of valuable products from oil sludges.

Authors	Investigation
Couillard et al. (1991)	Utilised pressurised hot water and air flotation to separate heavy oils from the bottoms sludges of crude oil storage tanks after pre-treatment with a wetting agent (Na_2SiO_3). The heavy oil recovery was found to be 82%.
Biceroglu (1994)	Utilised a low value, 'light cat. heating oil' or 'heavy cat. naptha' product stream from the refinery to extract oils from the refinery sludge. The product from this extraction was then blended with the crude for reprocessing. The viscous oil recovery using this process was claimed to be 90%.
Trowbridge and Holcombe (1995)	Utilised a 'narrow-cut refinery hydrocarbon stream' with a boiling point of approximately 475 K to extract the indigenous oil from dehydrated sludge. Centrifugation was then used to separate the solids from the solvent. The solids therefore contained very small amounts of liquid. The recovery of the oils from the feed was claimed to be 99%.
de Filippi and Markiewicz (1991)	Utilised liquid propane in a solvent extraction process to treat hazardous refinery wastes. A full scale unit was constructed for a refinery in Port Arthur, Texas, United States of America. The solvent/solute mixture was fed back to the refinery for reprocessing.
Taiwo and Otolorin (2009)	Studied the use of solvent extraction, with either hexane or xylene as the solvent, to recover oil from sludge recovered from storage tanks in the Niger delta. The use of hexane as the solvent produced better recoveries of the aromatic hydrocarbons, while the use of xylene recovered more aliphatic hydrocarbons. The total hydrocarbon recovery was found to be approximately 65%.
Zubaidy and Abouelnasr (2010)	Utilised different sludge to solvent ratios with methyl ethyl ketone and LPG condensate to recover oil from oily sludge. The solvent/solute mixture was recovered from the solids by filtration. The solvent was recovered by distillation, and the bottoms oil from the solvent recovery was used as a low quality diesel fuel.

One of the major difficulties experienced with solvent extraction using liquid solvents is the recovery of the solvent after extraction. In many cases; such as the processes of Biceroglu (1994), Trowbridge and Holcombe (1995) and de Filippi and Markiewicz (1991); the solvent is simply re-processed in the refinery along with the extracts, blending it into the feed to the crude distillation column. The increased feed rate to the crude distillation column would increase the column load, the energy consumption for heating and cooling, and possibly the optimum sizing of the column.

SCFE of the oil sludges was proposed by Ávila-Chávez et al. (2007) as a technique that would overcome the problem of separating the recovered hydrocarbons from the solvent. With supercritical solvents, the separation of the solutes from the solute is simply a matter of altering either of the temperature or the pressure in such a manner as to force the solvent out of the supercritical state.

Ávila-Chávez and co-workers investigated the use of supercritical ethane for the extraction of hydrocarbons from the crude oil tank bottom sludge at pressures of between (10 and 17.2) MPa and temperatures of between (308 and 338) K. The recovered hydrocarbons were found to be mostly saturated hydrocarbons. Only small fraction of the polar compounds present in the oil sludge were recovered. The supercritical ethane was also found to extract some of the metals present in the untreated sludge. It was found that the recovery of the hydrocarbons from the oil sludge was increased by increasing the pressure at a constant temperature, but decreased by increasing the temperature at a constant pressure.

The use of SCFs for the recovery of valuable components from refinery sludge as with the general use of SCFs provides an advantage of being highly tuneable.

A.1.4. INCINERATION

Incineration of the oil sludges is a simple way of volume reduction, but it offers no product recovery (Da Silva et al., 2012). The products from incineration are often polluting, with the gaseous products often requiring treatment and the fly ash containing heavy metals and other toxic components (Giusti, 2009).

The heavy metal content in the ash is, however, dependent upon the heavy metal content in the oil sludge. For waste volume reduction purposes, Sankaran et al. (1998) performed tests with the fluidised bed incineration of an oil sludge from an oil refinery in South India. Their tests included waste heat recovery through the production of steam. After incorporating cyclonic separators and alkali venturi scrubbers, it was found by analysis of the flue gas, the fly ash and the scrubber sludge, that this method was an effective means of treating the refinery sludge. No analysis of the heavy metal content of the oil sludge was performed and it was therefore possible that the low heavy metal content in the waste products was due to low heavy metal content in the feedstock.

A.1.5. LANDFILL

Technically speaking, landfill disposal of oil sludges is merely a disposal technique, and not a treatment technique. The oil sludge is deposited into ‘cells’ with sealed bases to prevent the permeation of the sludge into the underground water. The oil sludge is allowed to decompose in these cells, producing gas and a dark, foul-smelling liquid (Da Silva et al., 2012). This is the most economical technique for the disposal of oil sludge (Businelli et al., 2009), but has been banned in a number of countries (Kriipsalu et al., 2008). Elsewhere, it is used only when there is no other viable reuse or recycling technologies available.

A.1.6. LAND FARMING

Land farming is a fairly diverse, environmentally attractive method for the disposal and decomposition of refinery and oil field sludges (Arora et al., 1982; ElBagouri et al., 1994; Hejazi and Husain, 2004). It has been used successfully in a vast number of different climates, from locations at high altitudes, such as the Bolivian Antiplano (Jauna and Henshaw, 2005), to the cold and dry Tierra del Fuego in Argentina (Mendoza and Portal, 2000), to the deserts of Saudi Arabia (Hejazi and Husain, 2004) and Kuwait (ElBagouri et al., 1994).

The oily sludge is added to the top layer of soil in small amounts (approximately 3 w/w%) (Mendoza and Portal, 2000). The micro-organisms that are present in the soil degrade the oil and other organic compounds, producing mainly CO_2, water and some other environmentally friendly by-products (Arora et al., 1982). It was found that there was no migration of harmful components present in the oily sludge, with these being adsorbed or decomposed in the upper soil levels. Mendoza and Portal (2000) found that the risk of contamination of the groundwater was relatively low.

Factors that were found to increase the rate of degradation of the oily sludge included soil dampening, fertilisation and aeration through tilling (Hejazi and Husain, 2004; Da Silva et al., 2012).

The disposal of oily wastes by land-farming is by far the most economical option, but it requires the availability of large tracts of unused land, and is therefore only viable in climates in which agriculture is not viable. This is most likely the reason that it has only been investigated in areas that receive very little rainfall.

A.1.7. PYROLYSIS

Shie et al. (2002) proposed the use of pyrolysis for the conversion of oil sludges into useful synthesis products such as light hydrocarbons. In pyrolysis, the oil sludge is heated, in the absence of air, to produce light hydrocarbons, which can be used as synthesis gases (Jing et al., 2011). The volume of waste remaining after this conversion is greatly reduced, while the products can be used as a valuable feedstock for other processes. In order to improve the composition and amount of product that can be produced, Shie and co-workers investigated the addition of “inexpensive and non-harmful additives”.

The fly ash from the pyrolysis must be disposed of responsibility, as if not correctly treated, it could lead to environmental problems such as air pollution and the release of heavy metals into the atmosphere (Mamane et al., 1986). Uses of the fly ash include the manufacture of zeolites (Shie et al., 2004) and use as a sorbent in the place of hydrated lime (Ho and Shih, 1992).

A.2. CONTAMINATED SOIL TREATMENT TECHNIQUES

Further discussions on the treatment techniques that have been proposed for soils that have been contaminated with petroleum components as discussed in section 1.1.2.2 are provided here.

A.2.1. BIODEGRADATION

In biodegradation, the natural biological degradation of the contaminants that are present in the environment is used to remediate the soil. The existing microorganisms are usually supplemented in order to enhance the rate of degradation (Deschênes et al., 1995; Christofi et al., 1998). Other methods of enhancing the biodegradation are the increased aeration of the contaminated environment and nutrient addition (Ivshina et al., 1998).

Important parameters when performing biodegradation of a contaminated soil include pH levels, water availability, redox potential, oxygen availability and the temperature of the soil (Christofi and Ivshina, 2002).

A.2.2. EXCAVATION AND LANDFILL

This is the simplest and quickest remediation technique, although the costs are generally a lot higher (Cunningham et al., 1995). This technique simply involves the removal of the contaminated soil, disposal of this soil in a landfill site, and replacement with soils sourced elsewhere. Disposing of the contaminated soil in a landfill site is simply a means of 'hiding' the problem, and could give rise to contamination of ground water, etc. It is therefore not utilised unless there is an urgent need for the removal of contaminated soils.

A.2.3. INCINERATION

In incineration, the soil is exposed to a naked flame at high temperatures, resulting in spontaneous combustion of any of the organic material present in the soil. This process is fairly energy intensive, and therefore impractical when large volumes of contaminated soil must be processed. Incineration is also not widely used for the treatment of contaminated soils due to air pollution concerns (Anitescu and Tavlarides, 2006).

A.2.4. LIQUID EXTRACTION

In liquid extraction, the contaminated soil is washed with a liquid solvent, usually in large mixer-settler vessels. Filtration and drying then has to be used to remove the solvent from the cleaned soil. A small amount of solvent will still, however, remain in the pores of the soils, and this is of concern (Anitescu and Tavlarides, 2006). The use of liquid extraction for the remediation of contaminated soils is therefore not of great popularity. Liquid extraction also requires a process to recover the

contaminants from the solvent, to enable the solvent to be re-used. These regeneration processes often make liquid extraction expensive. Another disadvantage is the large volumes of the solvents that are required on-site (Hawthorne et al., 1992).

A.2.5. PHYTOREMEDIATION

Phytoremediation is not a new technology, although its use in decontaminating soils and removing atmospheric pollutants has not yet been fully investigated (Cunningham et al., 1995). In phytoremediation, soil conditions and vegetative cover are manipulated in order to reduce the environmental hazard, to decontaminate the soil or to remove a contaminant from the soil completely. Phytoremediation is generally slower than physico-chemical remediation techniques but it is cheaper as a whole.

A.2.6. SOIL WASHING OR FLUSHING

Cationic, anionic or non-ionic surfactants (SURFace ACTive AgeNTS) in an aqueous solution are added to the contaminated soil (Mulligan et al., 2001; Christofi and Ivshina, 2002). These surfactants improve the solubility of the petroleum contaminants in water, or decrease the interfacial tensions between the organic and aqueous phases, allowing the organics to be withdrawn with an aqueous phase (Falatko, 1991). The liquid is removed from the soil through wells which are drilled into the ground, and the recovery of the surfactants is vital for both economic and environmental reasons (Mulligan et al., 2001).

The safety and toxicity of many of the surfactants that are used cannot be guaranteed. The surfactants are also often expensive and this technique is therefore often not cost effective.

A.2.7. SUPERCRITICAL EXTRACTION

There have been a number of investigations into the use of SCFs for the extraction of hydrocarbons from different natural matrices. Some authors utilised 'spiked' matrices to perform their investigations, whereas others, claiming that these artificially polluted matrices exhibited different characteristics to real systems (Hawthorne et al., 1992; Burford et al., 1993), only used samples from areas in which leaks and spillages had occurred. The investigations using both spiked and real matrices are listed in A.2.

Table A.2. Authors who have used SCFE for contaminated soils.

Authors	Investigation
Emery et al. (1992)	Investigated the use of supercritical CO_2 for the recovery of diesel from spiked clays. It was found that the recovery was greater than 75% in all of the investigated conditions.
Hawthorne et al. (1992)	Investigated the use of N_2O and $CHClF_2$ (R-22) for extraction of polycyclic aromatic hydrocarbons (PAHs) from soil matrices. They found that the increased dipole moments of these molecules led to higher extraction efficiencies for the higher molecular weight PAHs. The recoveries that were obtained using R-22 compared favourably with the recoveries obtained when using CO_2.
Burford et al. (1993)	Studied the extraction of PAHs from samples taken from petroleum waste sludge, urban air particulate matter and railroad bed soil. Supercritical CO_2 extraction, with and without a methanol co-solvent, and sonication with methylene chloride was used. Burford et al. found that the extraction rates of the spiked PAHs were substantially higher than the extraction rates of the native PAHs.
Dankers et al. (1993)	Modified the supercritical CO_2 extraction of PAHs from polluted soil samples to increase the speed and efficiency of the process by adding dichloromethane as co-solvent. Recoveries of spiked samples were found to be very near to 100%.
Eckert-Tilotta et al. (1993)	Investigated the extraction of total petroleum hydrocarbons (TPH) from both spiked and polluted natural soils using supercritical CO_2 extraction. The results were found to be similar to the results obtained during extraction with Freon-113 in a Soxhlet apparatus, except when kerosene and gasoline were extracted.
Montero et al. (1996)	Presented a bench-top study into the remediation of soild contaminated with naphthalene and 1,2,4 trimethyl benzene. Their study investigated the effect of changes in solvent flow-rate and SCF densities. The scale-up of the process to be useful industrially was investigated. The economic analysis of the process for these two contaminants was performed, showing that the process would be feasible on an industrial scale.
Subramanian and Hanson (1998)	Studied the extraction of four different bitumens from oil sand deposits using supercritical propane as the solvent. The products were found to be substantially upgraded from the bitumens, and were substantially more volatile. Most of the asphaltene content was not extracted from the oil sands. This was supposed to be due to the differing polarities of the asphaltenes and the solvent.

Authors	Investigation
Alonso et al. (2002)	Investigated the use of supercritical CO_2 for the decontamination of a soil contaminated with gasoil. Any pollutants present in the extract were then adsorbed upon activated carbon. Operational parameters, such as temperature, soil particle sizes, and solvent to soil ratios were investigated.
Al-Marzouqi et al. (2007)	Extracted oil from an oil-saturated soil, obtained from the Sahel oil field, using supercritical CO_2. A wide range of temperatures and pressures were investigated and the extraction efficiency was found to increase with increased pressure, and decrease with increased temperature. The maximum efficiency was found to be 72.4%.

Quantitative extractions from environmental matrices show that SCFs that are capable of interacting with or altering the matrix to enhance the speed of solvation of the 'trapped' solutes into the bulk SCF, as well as solvating the 'free' hydrocarbons, are necessary (Hawthorne, 1990; Hawthorne et al., 1992). These interactions are enhanced by the polarity of the SCF (Alexandrou and Pawliszyn, 1989; Bartle et al., 1990), meaning that the interactions of CO_2, which is non-polar, are very limited (Hawthorne et al., 1992).

A.3. Industrial Applications of SCF

More detailed descriptions of several industrial applications of SCF than those that are described in Section 1.3 are provided in this section.

A.3.1. Analytical Applications

The foremost analytical application of SCFs is in supercritical chromatography (Teja and Eckert, 2000; Chezter and Pinkston, 2004). The first prototypes of supercritical fluid chromatography (SFC) instruments were developed in the 1960's (Taylor, 2009), but at the same time, high pressure liquid chromatography (HPLC) was developed, and was preferred to SFC (Saito, 2013). From the 1990's and onwards, SFC gained traction for the separation and analysis of chiral compounds, which conventional low pressure chromatography and HPLC was not able to perform (Berger, 1997; Toribio et al., 2004). Modern SFC can be considered an extension of HPLC (Taylor, 2009), as many of the solvent characteristics are not unique to SFC, but are present irrespective of whether the mobile fluid is a gas, a liquid or a SCF (Berger, 1995). The advantages of using SFC include the ability to separate chiral components, and the high through-puts; however, the major drawback remains the poor performance in the analysis of polar components (Taylor, 2009). The use of a more polar mobile phase, by either the addition of polar modifiers to CO_2, or replacement of CO_2 with a more polar compound, are two options to overcome this drawback.

Another application of SCFs in analysis is in the extraction of select components during sample preparation (Teja and Eckert, 2000; Saito, 2013).

A.3.2. Dry Cleaning

At least three patents in which a SCF is utilised to dry clean fabric have been registered (Carty et al., 1992; Senger Elsbernd, 2001; Finke et al., 2003). McHardy and Sawan (1998) published a book describing the use of SCFs for cleaning applications. Sousa et al. (2007) found that supercritical CO_2 could be used successfully to clean antique textiles without damaging them or causing them to lose material.

A.3.3. Painting and Dying

The UNICARB process, developed by Hoy et al. (1992), at the Union Carbide Chemicals and Plastics Technology Corporation, uses supercritical CO_2 to reduce the viscosities of coatings to allow them to be applied by spraying (Hoy, 1991). Hastings and Hendricks (1995) patented a method and apparatus for spraying the fluid containing a SCF or a liquefied gas, as difficulties arose with the original apparatus utilised by Hoy and co-workers.

SCFs have also been used as a solvent for the dyeing of fabrics, as the fabrics can be dried rapidly after the dyes have been added to the fabric. Additionally, there is little wastage of the dye, because the unused dyes can be easily recovered from the solvent, simply by reducing the pressure. The use of SCFs reduces the waste of water, which is the conventional solvent used in dying processes.

A.3.4. Particle Production

SCFs have been used in the formation of particles with particular properties, such as uniform size, high porosities or specific morphology (Tom and Debenedetti, 1991; Jung and Perrut, 2001; Knez and Weidner, 2003; Tabernero et al., 2012), as well as in the formation of particles free from residual solvents (Debenedetti et al., 1993). The SCFs are used to dissolve solids and are then spray-dried to give particles with a controlled shape (Essel et al., 2012; Kim et al., 2013). Hakuta et al. showed that the morphology of particles could be finely controlled by changing the temperature and pressure of the SCF in which the crystallisation occurred. Pharmaceutical companies have also investigated a number of processes for the manufacture of improved "drug delivery systems", such as the manufacture of nano-particulate drugs, encapsulation of drugs and coating of tablets and beads (Perrut, 2000). These investigations have been in order to improve the delivery and release of the drugs upon administration (Türk, 2009).

One of the simplest techniques in the manufacture of small, mono-dispersed particles with SCFs is the "rapid expansion of supercritical solutions" (RESS) process (Jung and Perrut, 2001). This process forms particles by spraying a supercritical solution saturated with the substrate through very fine nozzles. The biggest drawback of this process is the limited suitability, as only substrates with a reasonable solubility in the solvent of choice can be used. In the case of CO_2, this limits the product to compounds that have a low polarity. This drawback could be overcome by altering the supercritical solvent. The addition of liquid co-solvents is not possible for RESS, as it would somehow have to be removed from the resulting powder. Therefore the only possible alterations to the solvent could be to use a gaseous co-solvent, or to replace CO_2 with a more polar solvent.

Another application of SCFs in particle production is as an 'anti-solvent', wherein the SCF is added to a liquid solvent, causing dissolved substrates to precipitate (Jung and Perrut, 2001). Rather than use RESS, in which a supercritical solution, saturated with the substrate, is sprayed through a nozzle to produce the particles, it is also possible to spray a solution of the melted or liquid suspended substrate, saturated with the SCF through a nozzle to produce solid particles. This method is called the "particles from gas-saturated solutions/suspensions" or PGSS method (Jung and Perrut, 2001). The advantage of this method is that the substrates need not be highly soluble in the solvent, although it would be required that the SCF be soluble in the substrate.

A.3.5. Polymer Manufacture

SCFs are used to replace conventional solvents in polymerisation applications, as they allow a better control of the properties of the polymers, by altering the properties of the structures at a nano-scale (Teja and Eckert, 2000; Tomasko et al., 2003). The polymer molecules that are formed when using SCFs as the solvent have a very narrow molecular weight distribution and a high degree of polymerisation is achievable (DeSimone et al., 1994). It has also been shown that the properties of the polymer, such as the glass transition temperature and the viscosity, differ when in solution with the SCF (Watkins et al., 2000). This allows for new prospects for the polymer use, due to different processing and modification capabilities.

These additional processing techniques allow the production of films, coatings, foams, block co-polymers and porous structures. One example of an industrial process that makes use of this technology is that licenced by the University of North Carolina at Chapel Hill, where supercritical CO_2 replaces water as the solvent for the manufacture of fluoropolymers (DuPont, 2015). An extensive overview of polymerisation in SCFs, including guidance into current polymer research applications was given by Kemmere and Meyer (2005). It is recommended that, should further information be required, this publication be consulted.

SCFs have also been used to allow synthesis of different polymers and to foam existing polymers to make them microporous. Reverchon and Cardea (2004) formed microporous cellulose acetate membranes, while Shieh and Liu (2004) were able to cause conformational changes to polymers by altering the amount of SCF that was added in the polymerisation stages. Zhu et al. (2013) were able to produce a composite of two polymers that are, under normal conditions immiscible, by using supercritical CO_2.

A.3.6. Preservative Infusion

Due to the high diffusivity of the SCF as well as the high sensitivity of solute solubilities to changes in pressure and temperature, SCF can be used to infuse preservatives and biocides into wood (Acda et al., 1996; Muin and Tsunoda, 2003; Cookson et al., 2009; Kang et al., 2012). A fair amount of research has been conducted into this method of applying these chemicals to the wood, as it makes it possible to not only coat the exterior of the wood, but the biocides are able to enter the wood structure, and ensure that no pests are able to survive within the wood and cause damage internally.

A.3.7. Reaction Medium

A number of reviews into the use of supercritical CO_2 and supercritical water, as reaction mediums, have been undertaken by authors such as Savage and co-workers (1995), Tester et al. (1998) and

Brennecke and Chateauneuf (1999). The use of a SCF as a reaction medium takes advantage of improved mass transfer, which in turn improves the reaction rates, the selectivity and the yield (Teja and Eckert, 2000). An additional enhancement of reaction rates in SCFs is due to the increased molecular densities, which causes more frequent solvent-solute collisions (Ramsey et al., 2009). The simplicity at which the subsequent separation of products from the reaction medium can be performed is also advantageous, although this depends on the medium that is used for the process.

The two main SCF chemical reaction media that have been investigated are CO_2 and water (Machida et al., 2011). The use of water in its supercritical state requires extremely elevated temperatures and pressures in comparison to the use of CO_2 (Lester et al., 2006). It also requires the precursors for the reaction to be water soluble. There has also been research conducted into the use of a SCF to reduce the viscosities of ionic liquids used as a reaction media (Machida et al., 2011). The reduced viscosities that can be obtained by the addition of the SCF enable better reaction rates and yields.

In catalytic reactions, SCFs have been shown to drastically increase the speed at which the reaction occurs, due to the ability of the solvent to transfer the reactants within the pores of the catalyst (Härröd et al., 2001). SCFs are particularly useful for homogeneous catalysis, as they simplify the separation of the products. There have also been reports that the use of supercritical CO_2 extends the lifespan of the catalysts, as it eliminates the 'coking' problems, and thereby reduces catalyst deactivation (Ramsey et al., 2009). Petkovic and co-workers (2005) tested the ability of SCFs to re-generate different catalysts that had been deactivated by coking, as was claimed by Thompson et al. (2001). They found that there was only a partial re-activation of certain zeolite catalysts.

B. ADDITIONAL RESULTS

B.1. CALIBRATION DATA

PRESSURE CALIBRATIONS

The calibrations of the pressure transducers for the static-analytic and static-synthetic apparatuses were discussed in Appendices C through to H. The residuals for the calibration of these transducers are given in Figure B.1 and B.2.

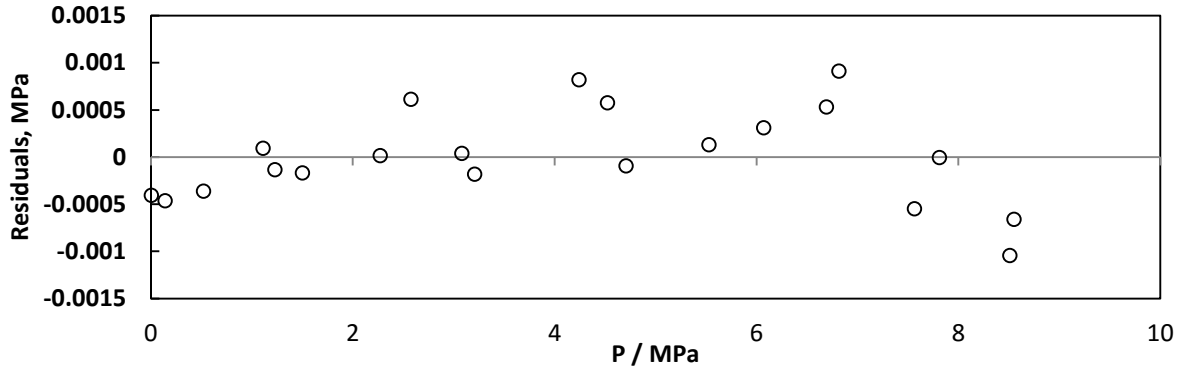

Figure B.1. Pressure residuals for the calibration of the (0 to 25) MPa pressure transducer for the static-analytic cell at pressures of between (0 and 8.5) MPa.

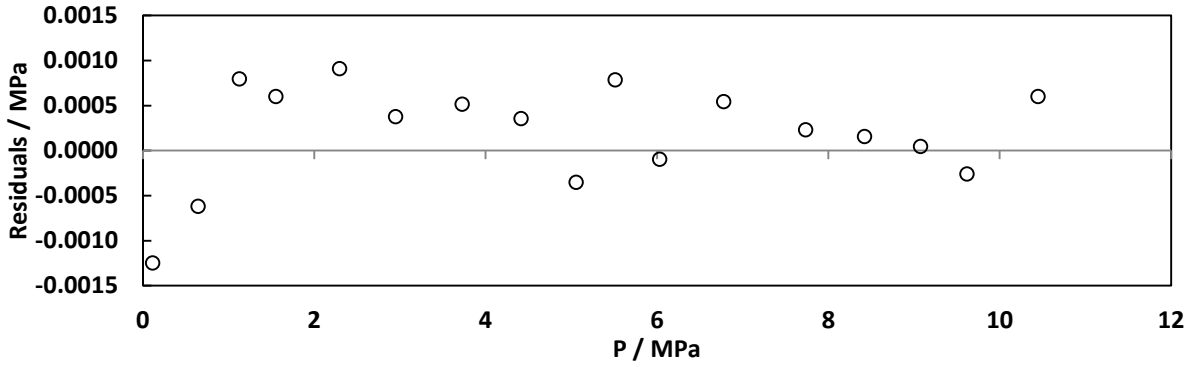

Figure B.2. Pressure residuals for the calibration of the (0 to 16) MPa pressure transducer for the static-synthetic cell at pressures of between (0 and 10.5) MPa.

The pressure calibration for the (0 to 16) MPa pressure transducer for the critical point determination apparatus was calibrated in two sections; a first order polynomial between (0 and 6.5) MPa and a second order polynomial between (6.5 and 16) MPa. The residuals for this calibration are presented in Figure B.3.

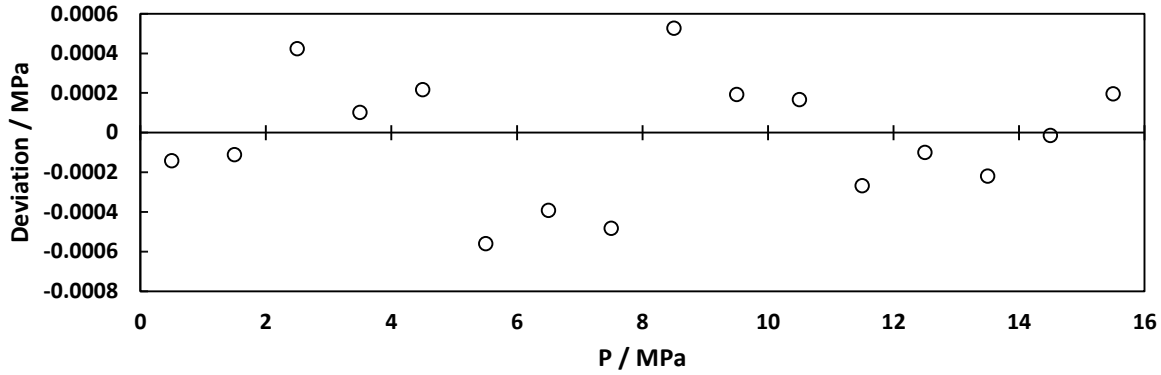

Figure B.3. Pressure residuals for the calibration of the (0 to 16) MPa pressure transducer for the critical point determination apparatus at pressures of between (0 and 15.5) MPa.

The parameters for the polynomials, as well as the uncertainties in the pressure derived from the calibration are presented in Table B.1. These parameters are for the calculation of the actual pressure using equation B.1,

$$P_{actual} = a\,P_{meas}{}^{2} + b\,P_{meas} + c \qquad \text{B.1}$$

where P_{actual} is the real pressure, a, b and c are the fitted parameters, and P_{meas} is the pressure reported by the transducer.

Table B.1. Pressure transducer calibration curves and the uncertainty in the pressure derived from the calibrations.

Apparatus	P / MPa	a × 10^5	b	c	$u(P) \times 10^4$ / MPa
Static-analytic	0 to 8.5	0	0.9997	-0.0331	5.2
Static-synthetic	0 to 10.5	0	1.0003	-0.0874	14.4
Critical point	0 to 6.5	0	0.9968	0.0033	3.9
	6.5 to 15.5	-1.515	1.0017	-0.2708	3.5

TEMPERATURE CALIBRATIONS

The temperature calibrations for the static-analytic and the static-synthetic apparatus are described in each of the manuscripts constituting Appendices C through to H. The parameters for the calibration polynomials for equation B.2, as well as the uncertainties derived from the calibrations are given in Table B.2

$$T_{actual} = a\,T_{meas}{}^{2} + b\,T_{meas} + c \qquad \text{B.2}$$

where T_{actual} is the real temperature (in °C), a, b and c are the fitted parameters, and T_{meas} is the temperature reported from the probe (in °C).

Table B.2. Parameters for the Pt100 temperature probe calibration polynomials and the uncertainty in the temperature derived from these calibrations.

Apparatus	T / K	a × 10^5	b	c	u(T) / K
Static-analytic	267.47 to 372.93	-10.22	1.0131	-1.2328	0.062
		-8.849	1.0106	-1.1183	0.051
Static-synthetic	272.49 to 323.32	0	1.0011	-1.3676	0.015
		0	0.9975	-1.6665	0.007
Critical Point	296.36 to 486.65	0	0.9931	-0.0733	0.039

GAS CHROMATOGRAPH CALIBRATIONS

First and second order polynomial calibration curves were fitted to the calibration data for the gas chromatograph (GC). The parameters for the polynomials are provided in Table B.3. The parameters are for equation B.3.

$$n_i = a\,A^2 + b\,A + c \qquad \text{B.3}$$

where n_i is the number of moles, a, b and c are the fitted parameters, and A is the area under the response curve from the GC.

Table B.3. Parameters for the calibration polynomials for the gas chromatograph, alongside the uncertainty in the calibration.

	a × 10^{23}	b × 10^{13}	c × 10^{7}	$u(n_i) \times 10^7$ / mol
Carbon dioxide, CO_2	0	6.88	2.72	1.19
	6.71	1172	1.18	1.16
Trifluoromethane, CHF_3	0	1.19	4.77	0.54
	-5.13	1.30	0	1.68
Hexafluoroethane, C_2F_6	0	1.81	3.21	1.59
	-1.31	1.98	0	0.62
n-Hexane, C_6H_{14}	0	1.18	-0.010	0.14
	6.79	1.16	0	0.14
n-Heptane, C_7H_{16}	0	0.765	-1.26	0.15
	-75.4	3.09	0	0.23
n-Octane, C_8H_{18}	0	0.416	0.272	0.15
	-0.414	0.424	0	0.16
n-Nonane, C_9H_{20}	0	0.394	0.273	0.19
	-0.421	0.402	0	0.21
n-Decane, $C_{10}H_{22}$	0	2.12	0.393	0.07
	-14.5	2.18	0	0.20
n-Undecane, $C_{11}H_{24}$	0	1.68	0.194	0.12
	-5.14	1.70	0	0.15
1-Hexene, C_6H_{12}	0	2.96	0.713	0.20
	-33.2	3.07	0	0.27
3-Methylpentane, C_6H_{14}	0	2.28	-0.045	0.16
	4.08	2.26	0	0.15
Methylcyclohexane, C_7H_{14}	0	2.35	5.25	2.48
	-38.9	2.71	0	0.44
Toluene, C_7H_8	0	3.36	0.415	0.33
	-18.1	3.42	0	0.35
Water, H_2O	0	4.92	5.58	3.45
	-268	5.91	0	1.37

B.2. SENSITIVITIES OF EXTRACTION STAGE

CO_2 WITH SYSTEM 1

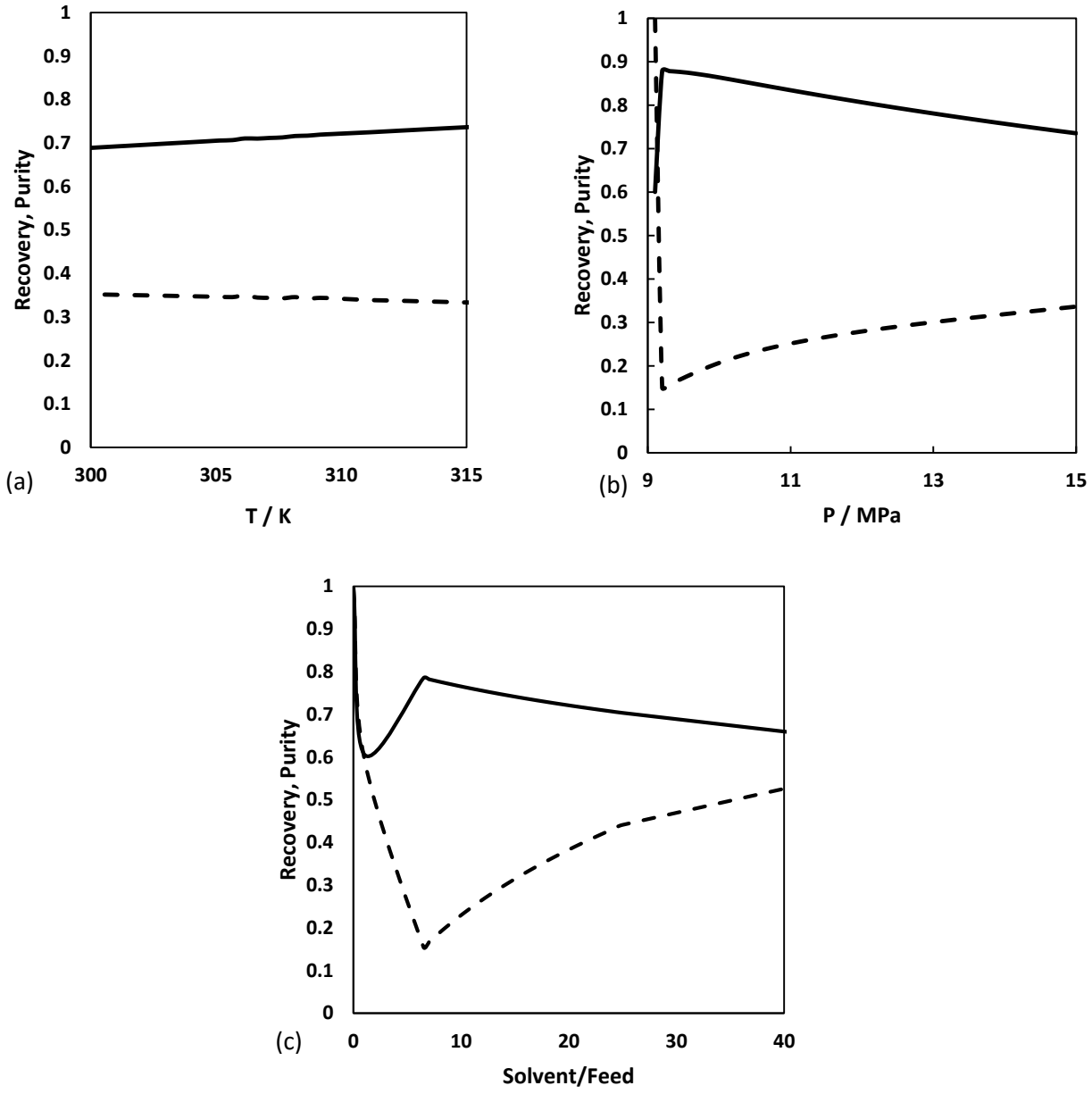

Figure B.4. Sensitivity of the extraction of the hydrocarbons from system 1 using CO_2, to variations in (a) temperature, (b) pressure, and (c) solvent to feed ratio. - - - -, recovery of hydrocarbons; ————, purity of extract.

CO_2 WITH SYSTEM 2

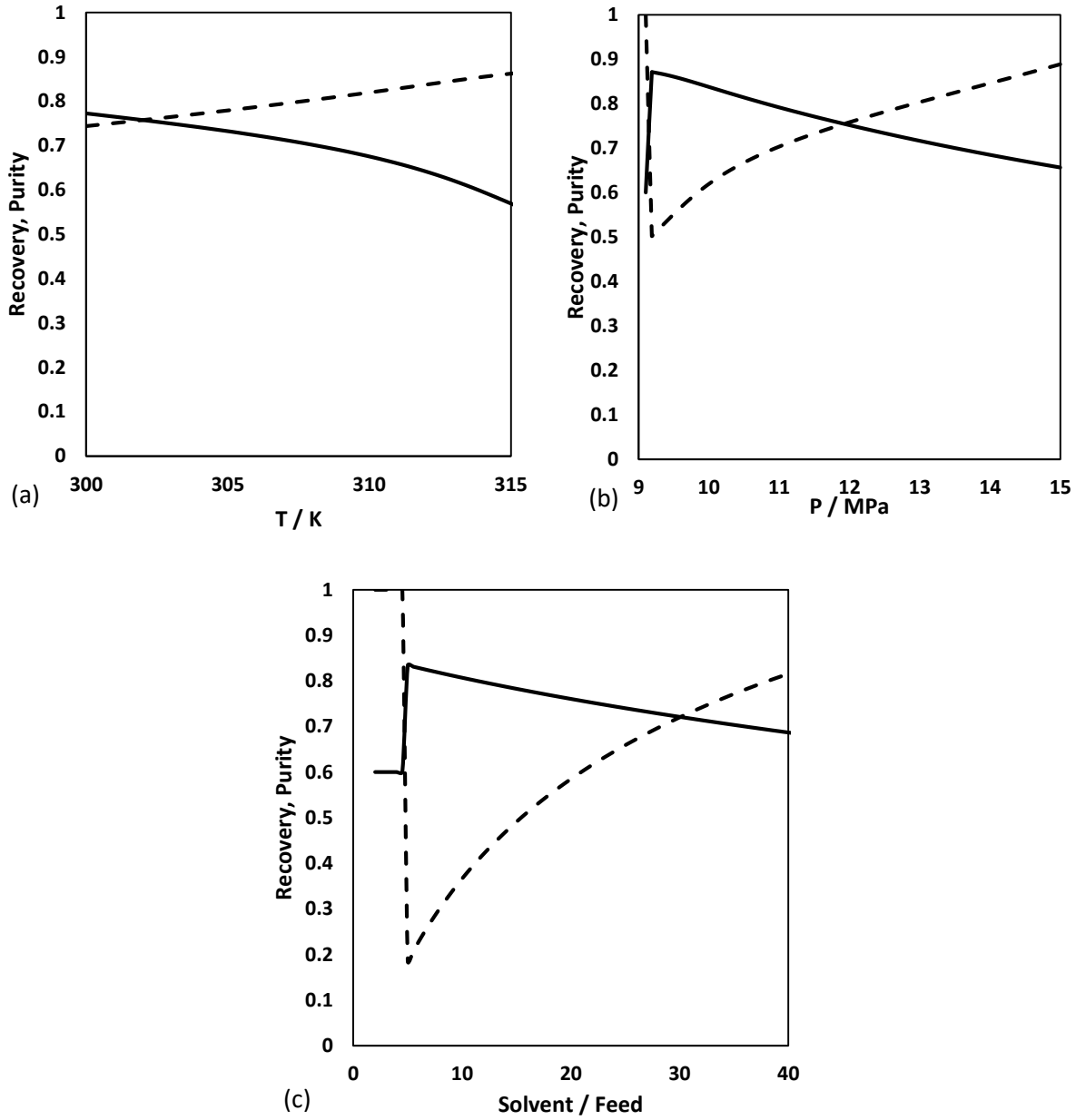

Figure B.5. Sensitivity of the extraction of the hydrocarbons from system 2 using CO_2, to variations in (a) temperature, (b) pressure, and (c) solvent to feed ratio. - - - -, recovery of hydrocarbons; ————, purity of extract.

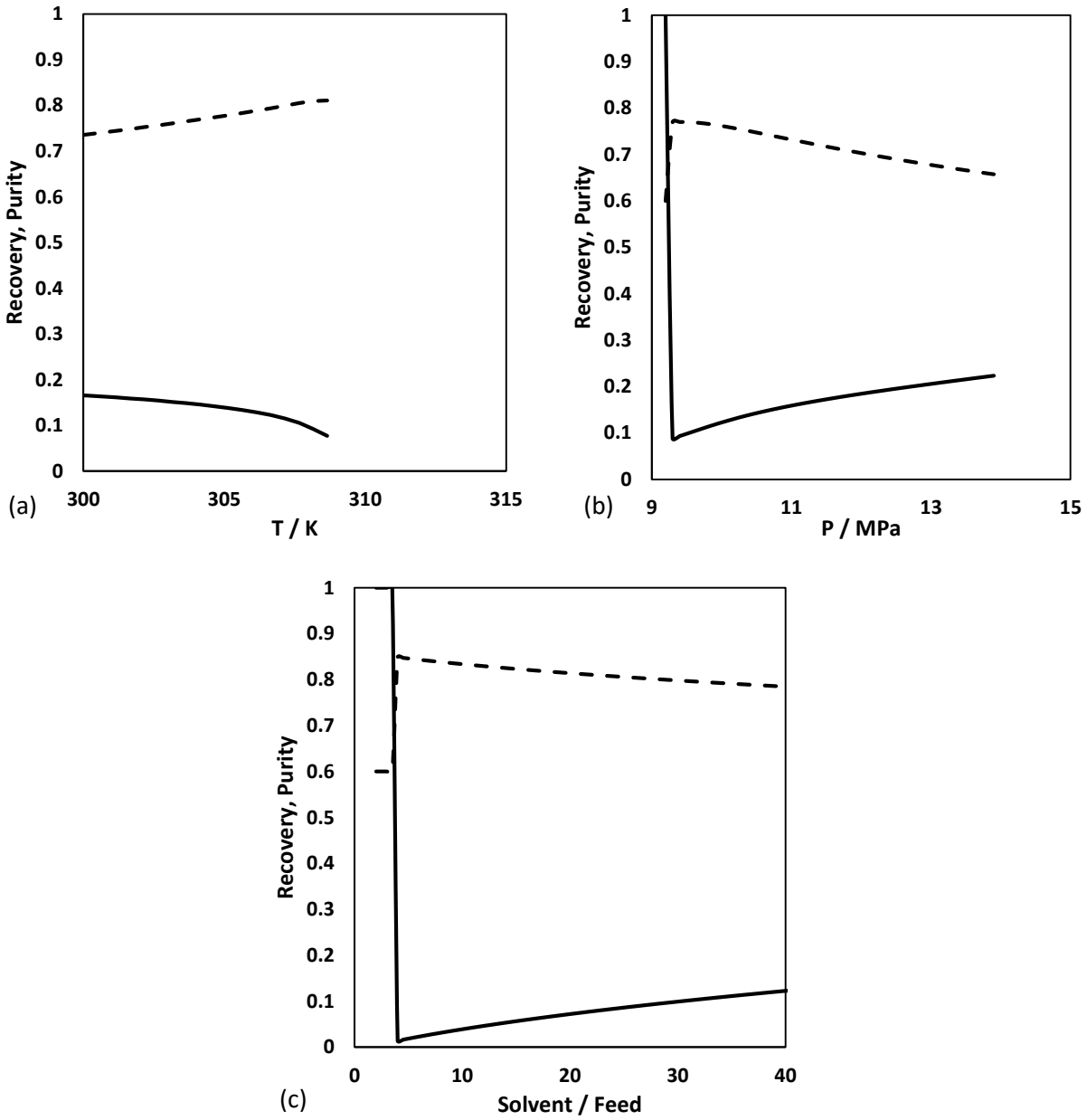

Figure B.6. Sensitivity of the extraction of the hydrocarbons from system 3 using CO_2, to variations in (a) temperature, (b) pressure, and (c) solvent to feed ratio. - - - -, recovery of hydrocarbons; ————, purity of extract.

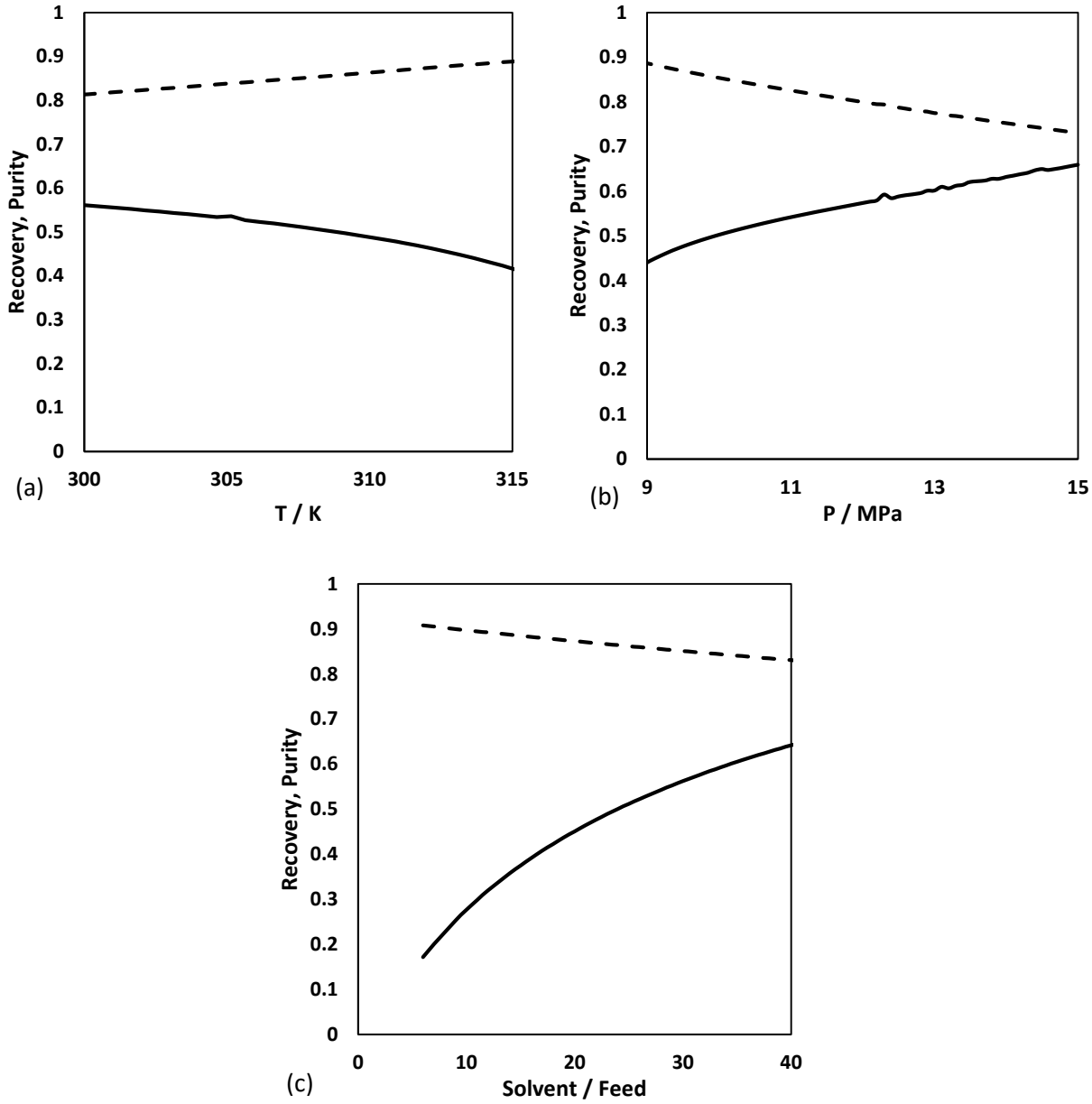

Figure B.7. Sensitivity of the extraction of the hydrocarbons from system 4 using CO_2, to variations in (a) temperature, (b) pressure, and (c) solvent to feed ratio. - - - -, recovery of hydrocarbons; ————, purity of extract.

R-23 WITH SYSTEM 1

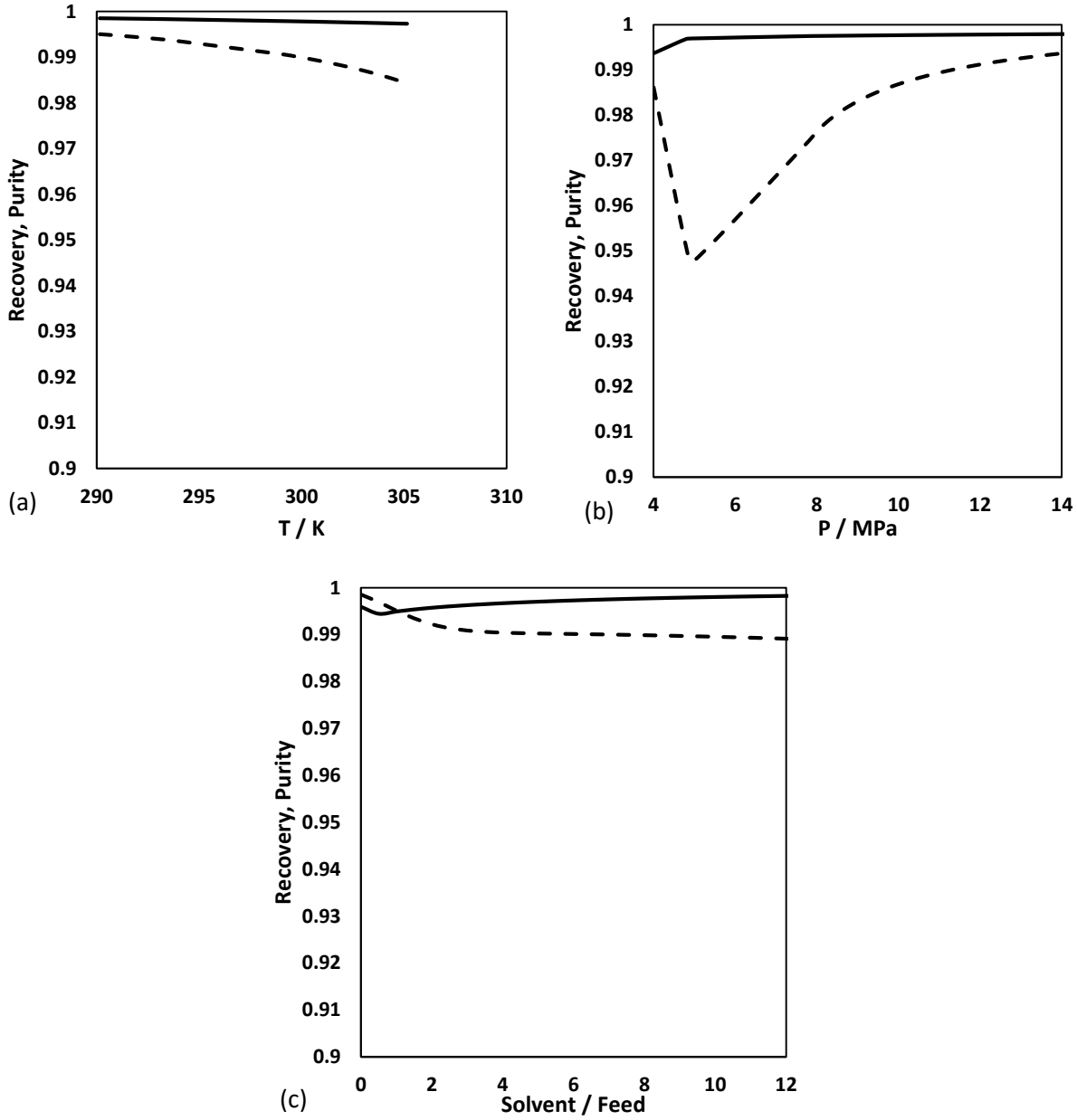

Figure B.8. Sensitivity of the extraction of the hydrocarbons from system 1 using R-23, to variations in (a) temperature, (b) pressure, and (c) solvent to feed ratio. - - - -, recovery of hydrocarbons; ————, purity of extract.

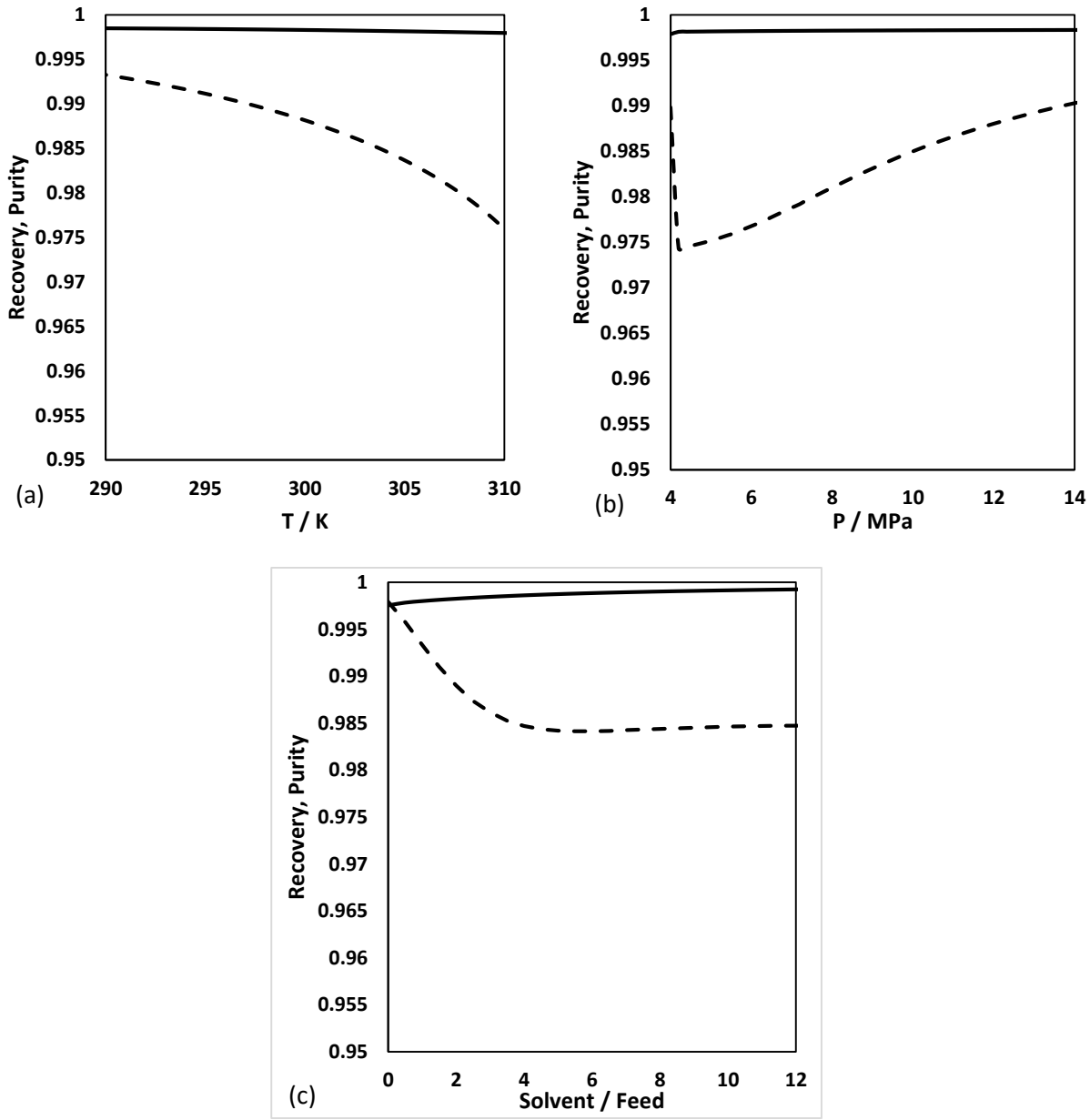

Figure B.9. Sensitivity of the extraction of the hydrocarbons from system 2 using R-23, to variations in (a) temperature, (b) pressure, and (c) solvent to feed ratio. - - - -, recovery of hydrocarbons; ————, purity of extract.

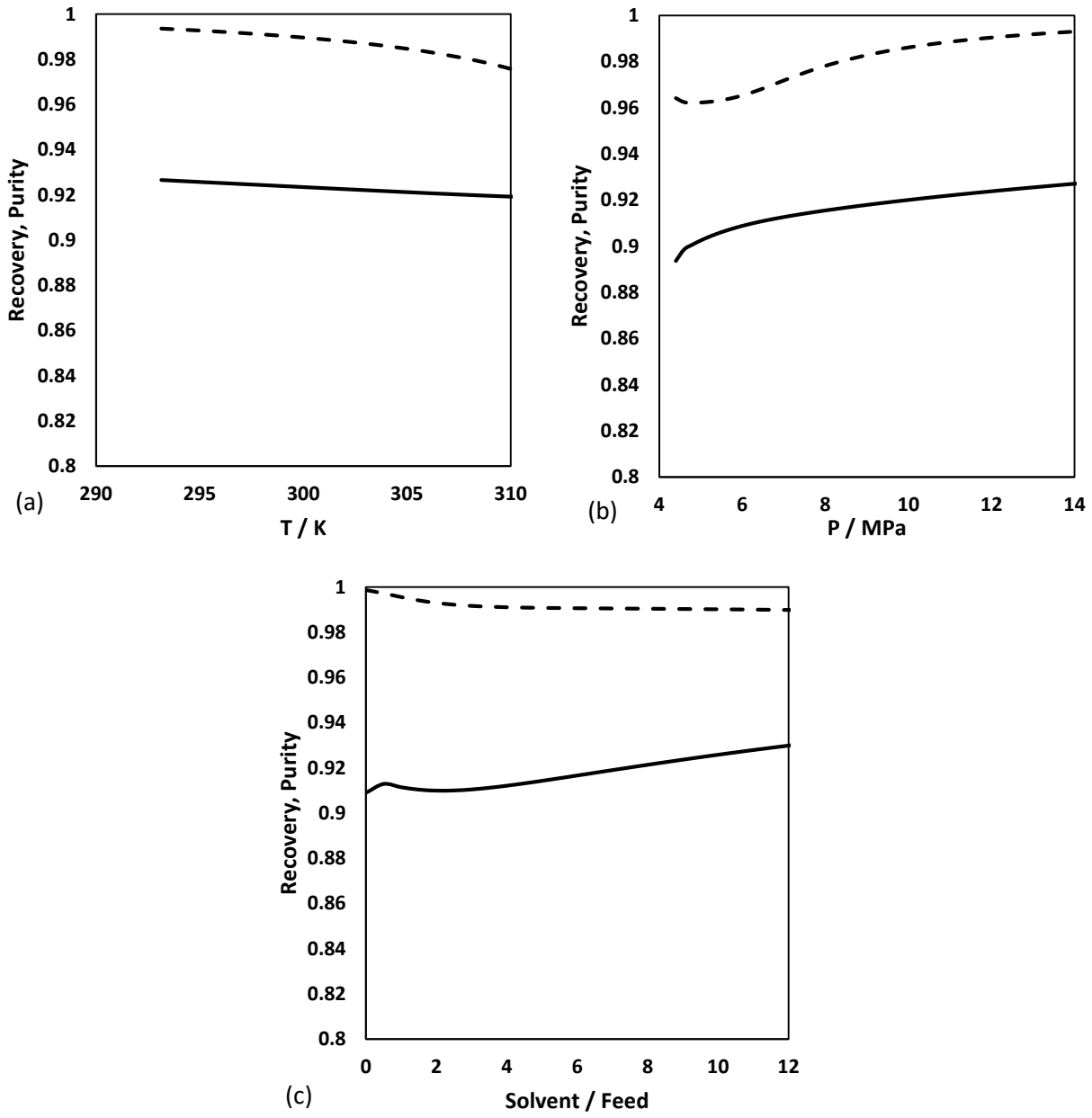

Figure B.10. Sensitivity of the extraction of the hydrocarbons from system 3 using R-23, to variations in (a) temperature, (b) pressure, and (c) solvent to feed ratio. - - - -, recovery of hydrocarbons; ————, purity of extract.

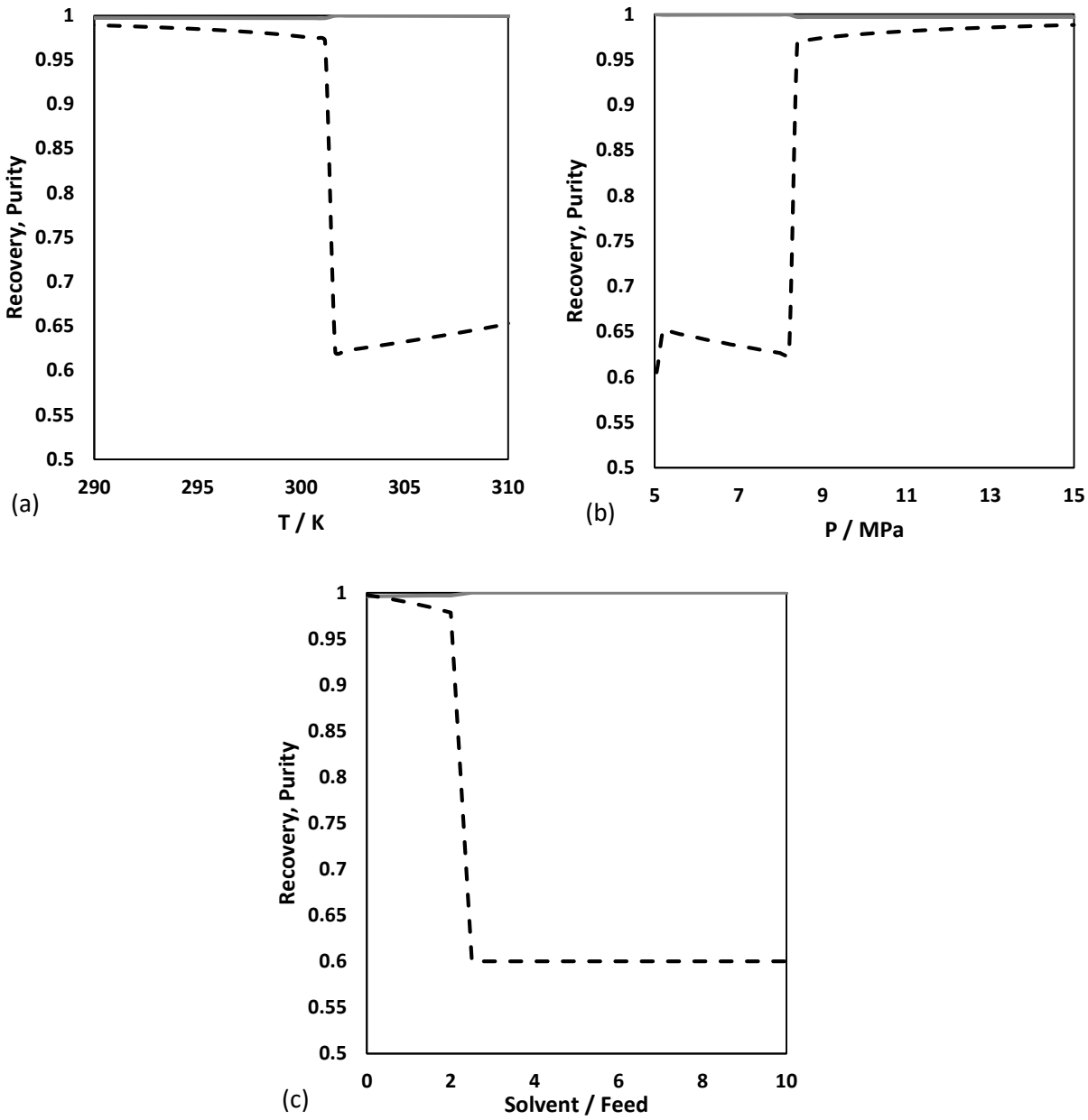

Figure B.11. Sensitivity of the extraction of the hydrocarbons from system 4 using R-23, to variations in (a) temperature, (b) pressure, and (c) solvent to feed ratio. - - - -, recovery of hydrocarbons; ————, purity of extract.

R-116 WITH SYSTEM 1

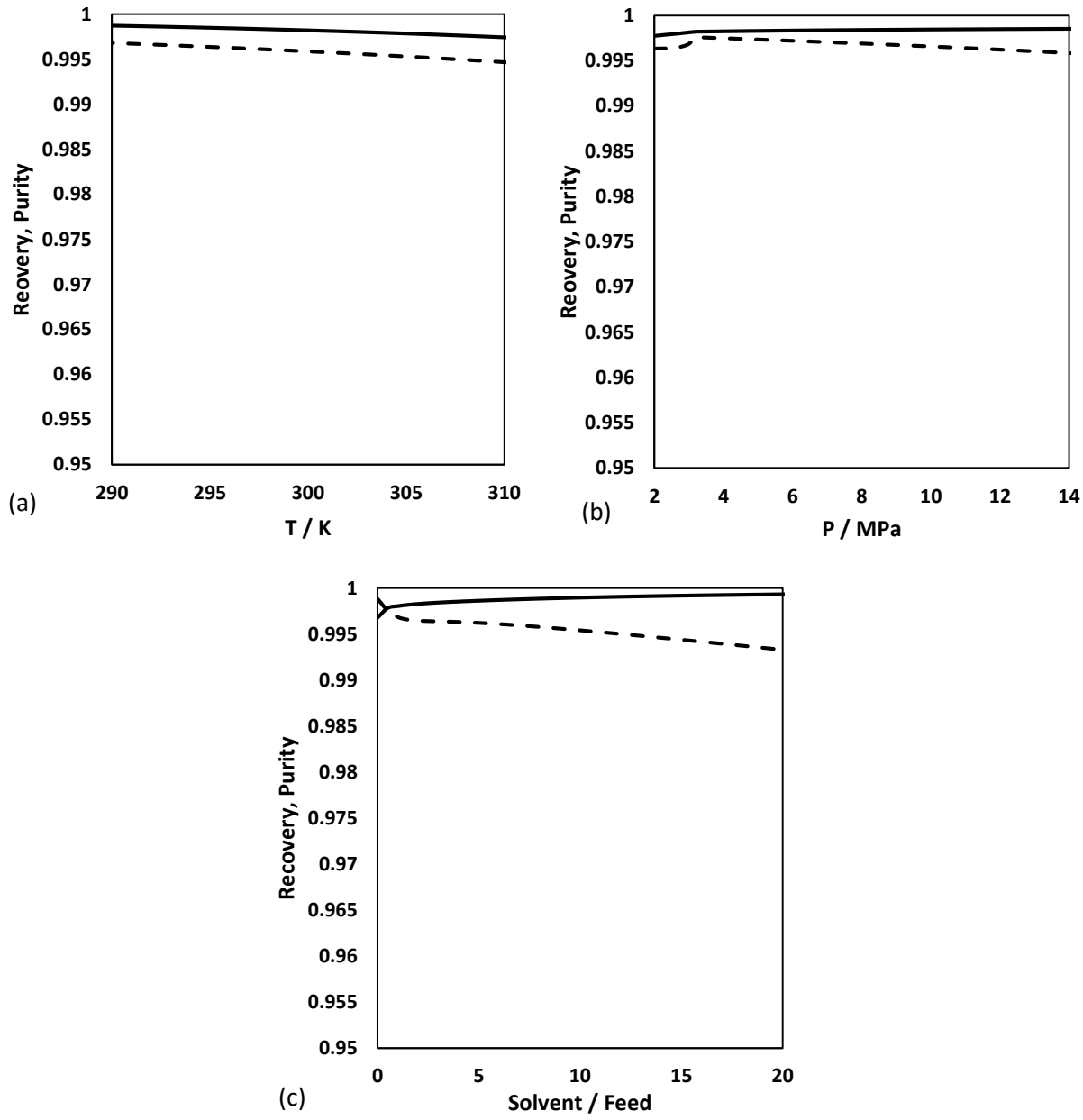

Figure B.12. Sensitivity of the extraction of the hydrocarbons from system 1 using R-116, to variations in (a) temperature, (b) pressure, and (c) solvent to feed ratio. - - - -, recovery of hydrocarbons; ————, purity of extract.

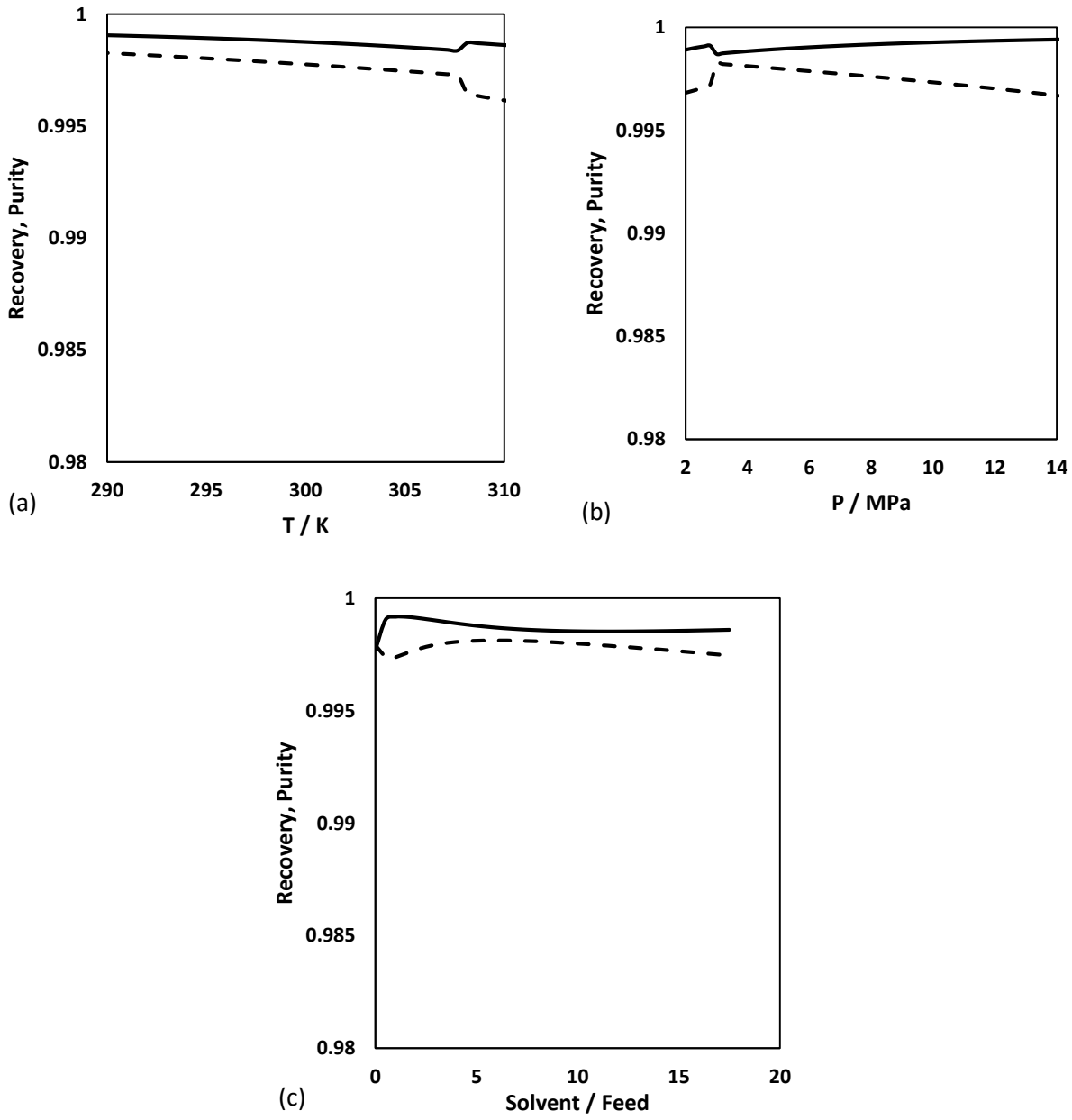

Figure B.13. Sensitivity of the extraction of the hydrocarbons from system 2 using R-116, to variations in (a) temperature, (b) pressure, and (c) solvent to feed ratio. - - - -, recovery of hydrocarbons; ————, purity of extract.

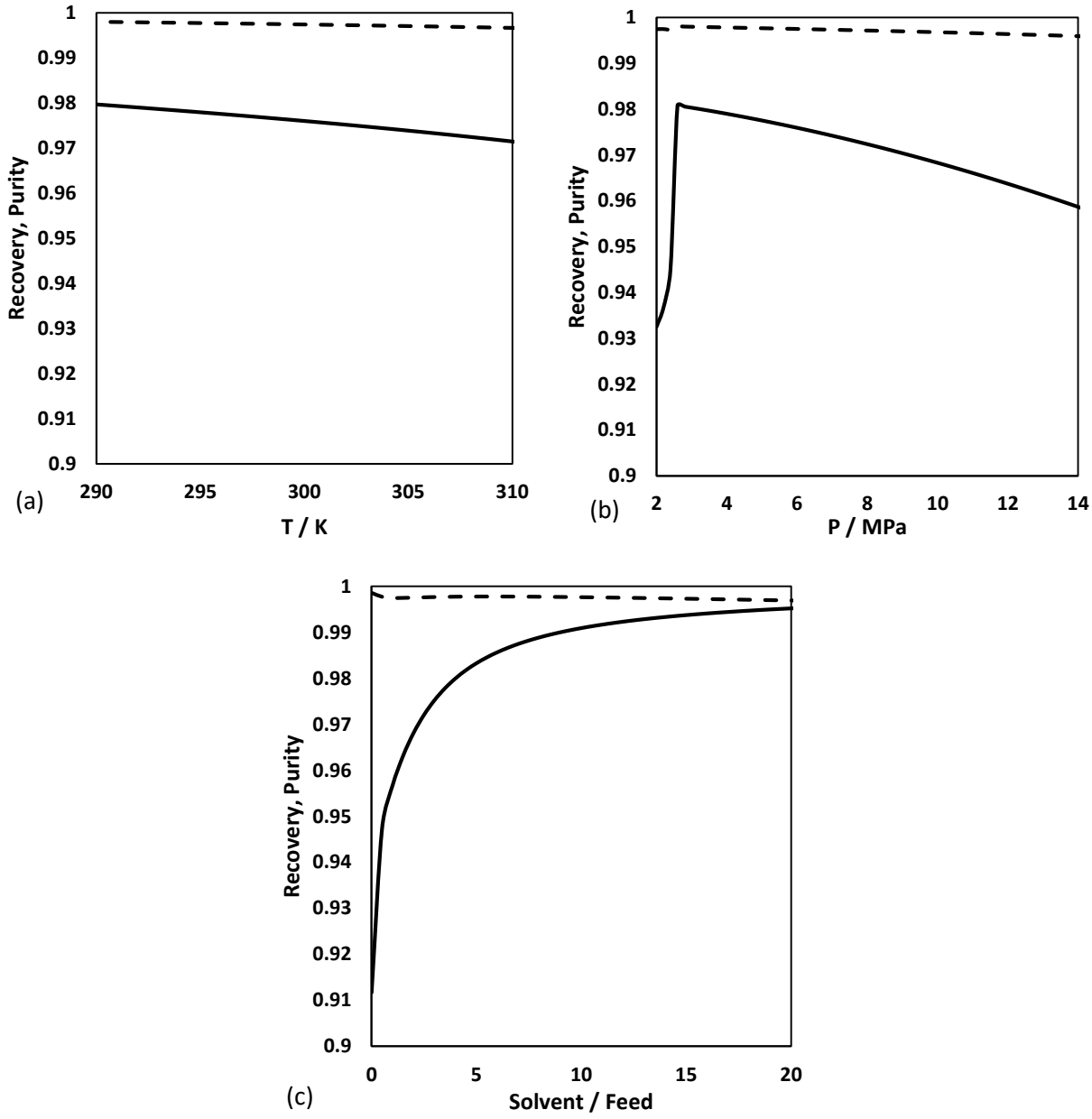

Figure B.14. Sensitivity of the extraction of the hydrocarbons from system 3 using R-116, to variations in (a) temperature, (b) pressure, and (c) solvent to feed ratio. - - - -, recovery of hydrocarbons; ————, purity of extract.

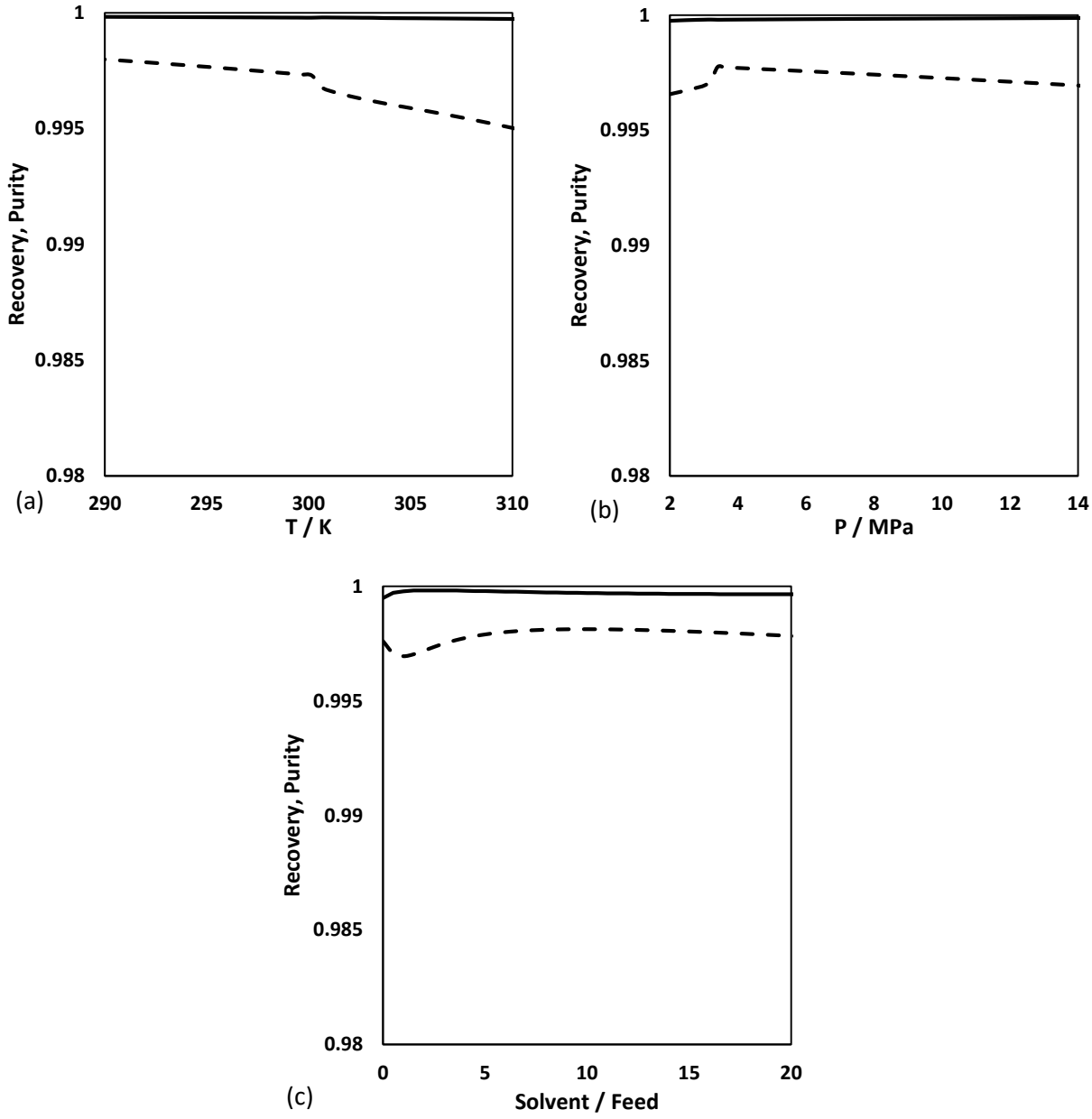

Figure B.15. Sensitivity of the extraction of the hydrocarbons from system 4 using R-116, to variations in (a) temperature, (b) pressure, and (c) solvent to feed ratio. - - - -, recovery of hydrocarbons; ————, purity of extract.

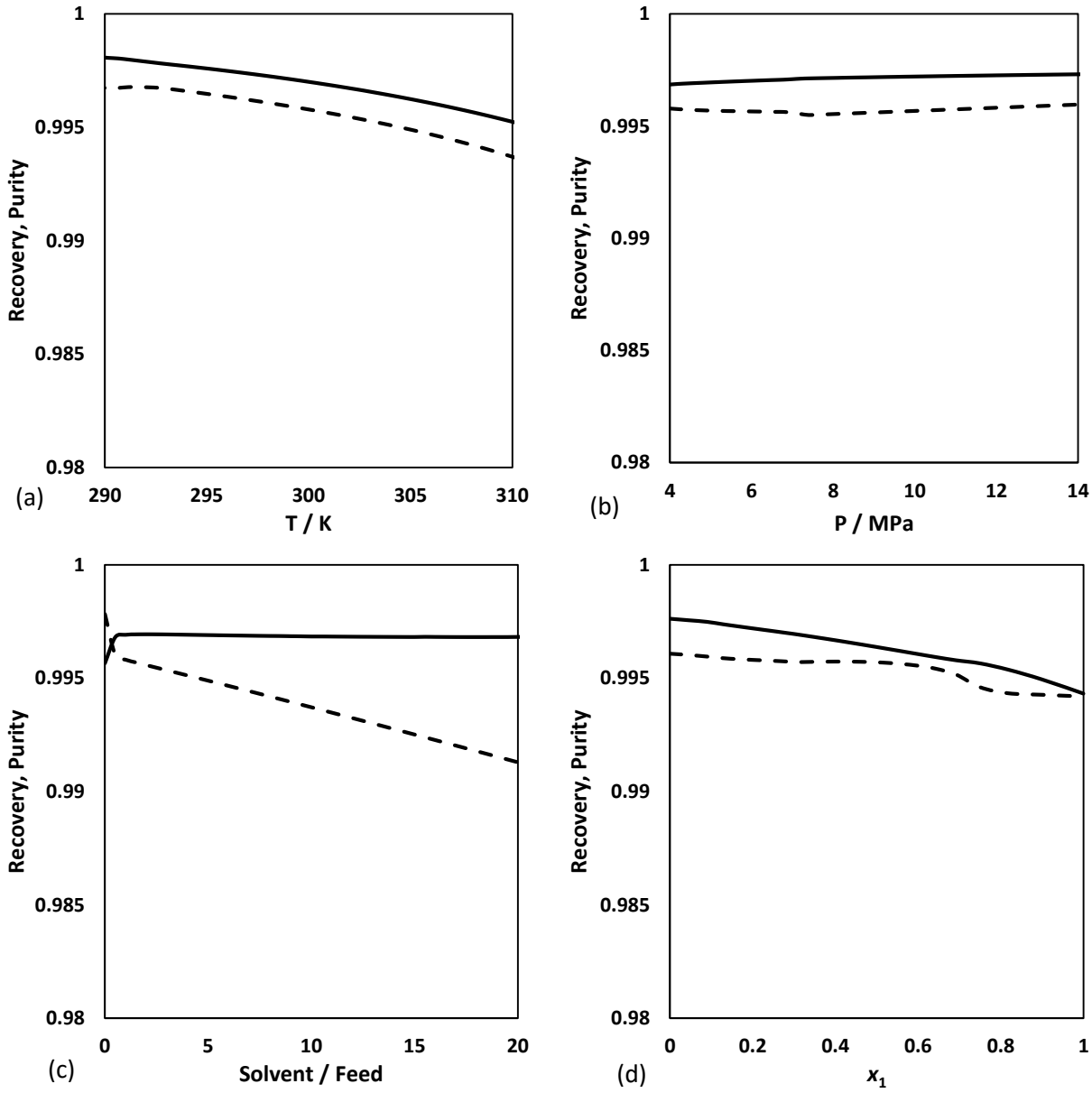

Figure B.16. Sensitivity of the extraction of the hydrocarbons from system 1 using R-23 (1) + R-116 (2) mixtures, to variations in (a) temperature, (b) pressure, and (c) solvent to feed ratio. - - - -, recovery of hydrocarbons; ———, purity of extract, (d) mole fraction of R-23.

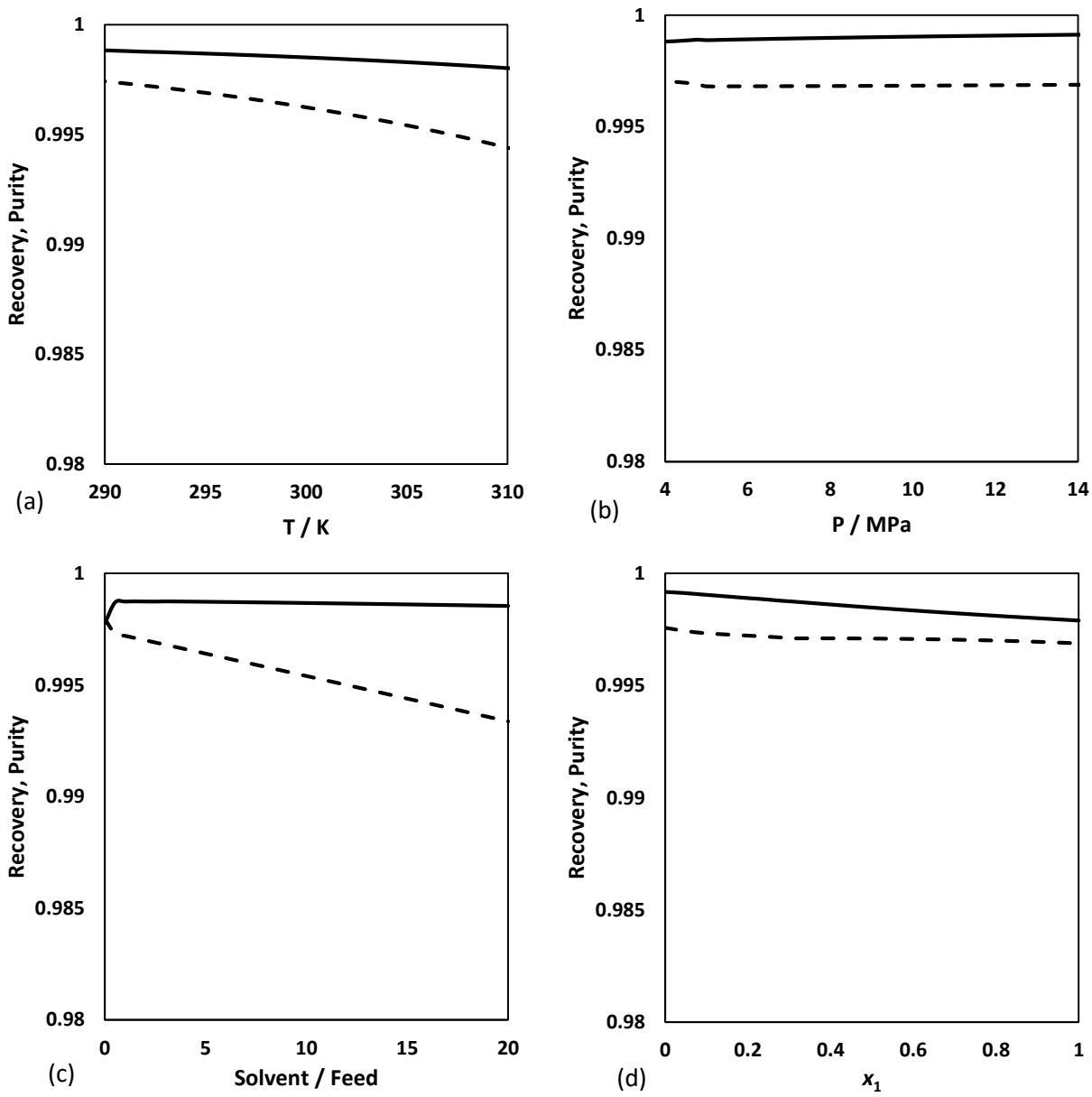

Figure B.17. Sensitivity of the extraction of the hydrocarbons from system 2 using R-23 (1) + R-116 (2) mixtures, to variations in (a) temperature, (b) pressure, and (c) solvent to feed ratio. - - - -, recovery of hydrocarbons; ———, purity of extract, (d) mole fraction of R-23.

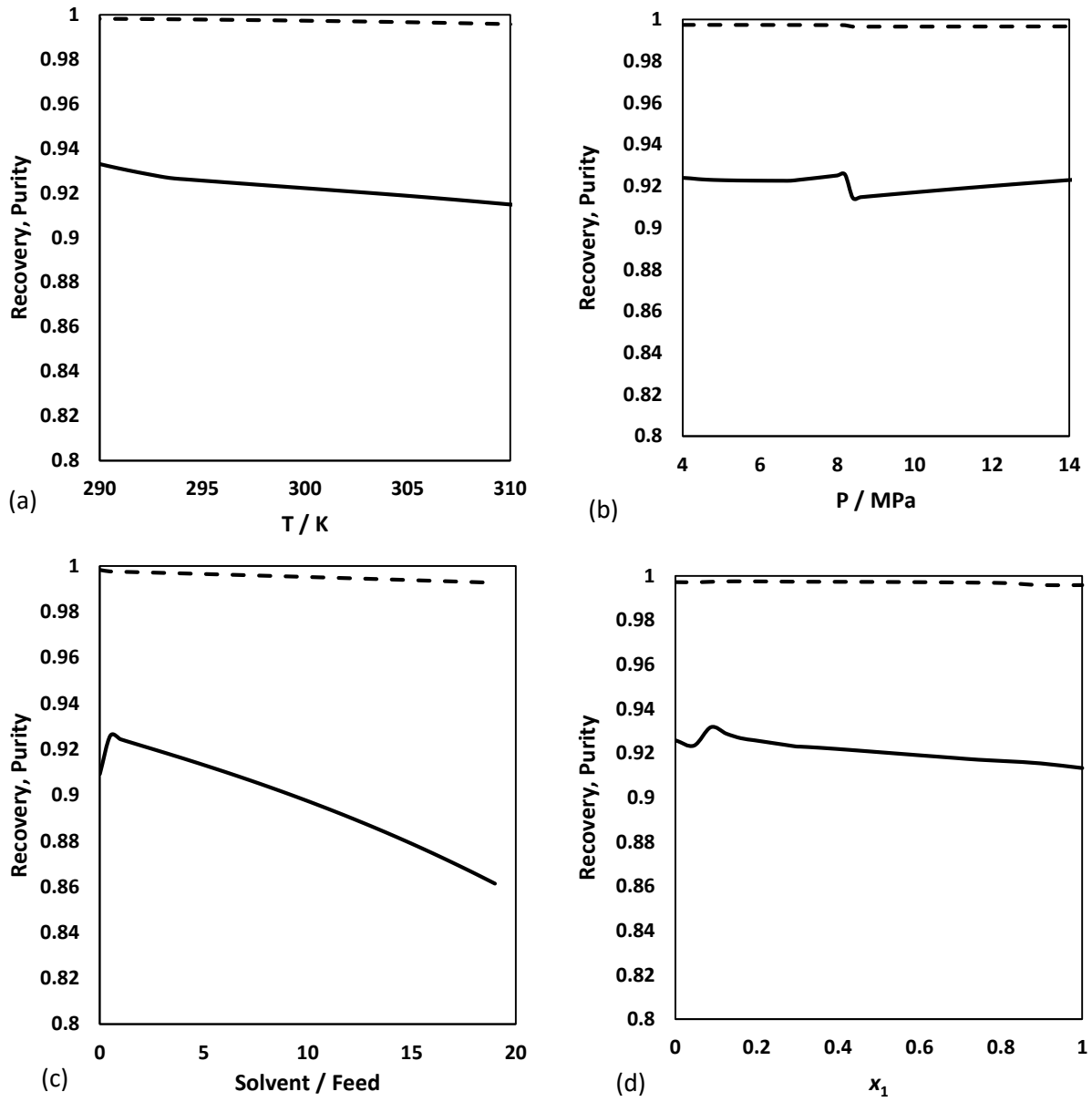

Figure B.18. Sensitivity of the extraction of the hydrocarbons from system 3 using R-23 (1) + R-116 (2) mixtures, to variations in (a) temperature, (b) pressure, and (c) solvent to feed ratio. - - - -, recovery of hydrocarbons; ———, purity of extract, (d) mole fraction of R-23.

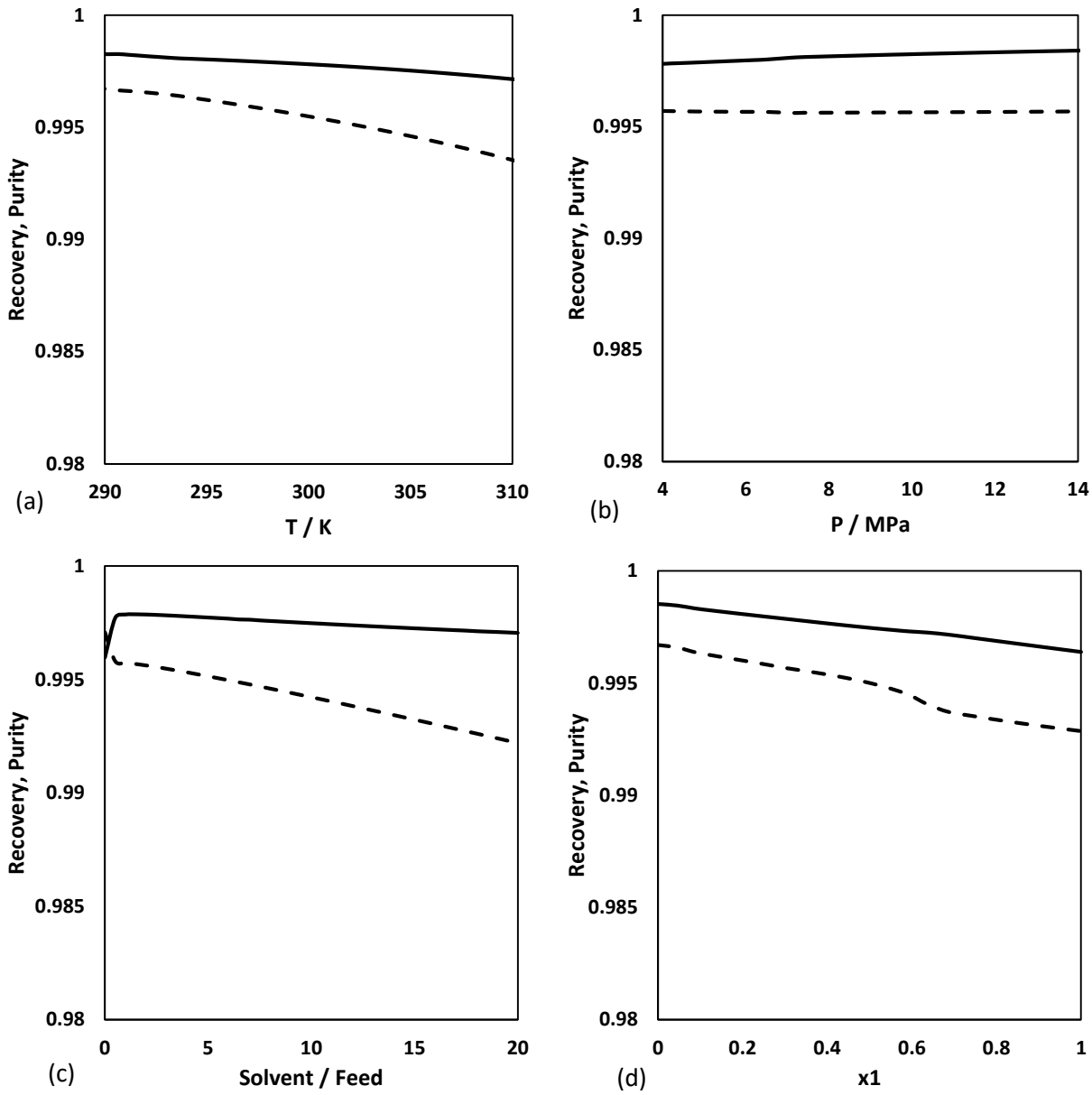

Figure B.19. Sensitivity of the extraction of the hydrocarbons from system 4 using R-23 (1) + R-116 (2) mixtures, to variations in (a) temperature, (b) pressure, and (c) solvent to feed ratio, (d) mole fraction of R-23. - - - -, recovery of hydrocarbons; ———, purity of extract.

B.3. SENSITIVITY OF SOLVENT RECOVERY

R-23 SOLVENT

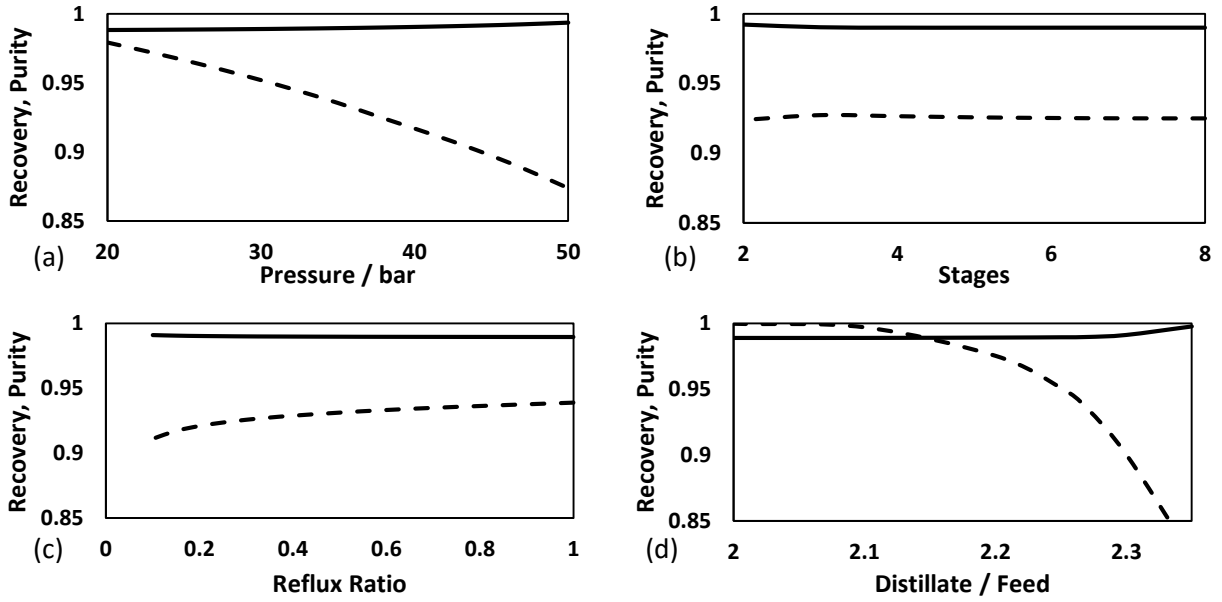

Figure B.20. Sensitivity of the product to variations in the solvent recovery column design parameters; (a) condenser pressure, (b) number of theoretical stages, (c) reflux ratio, (d) distillate to feed ratio. - - - -, recovery of hydrocarbons; ——, purity of product.

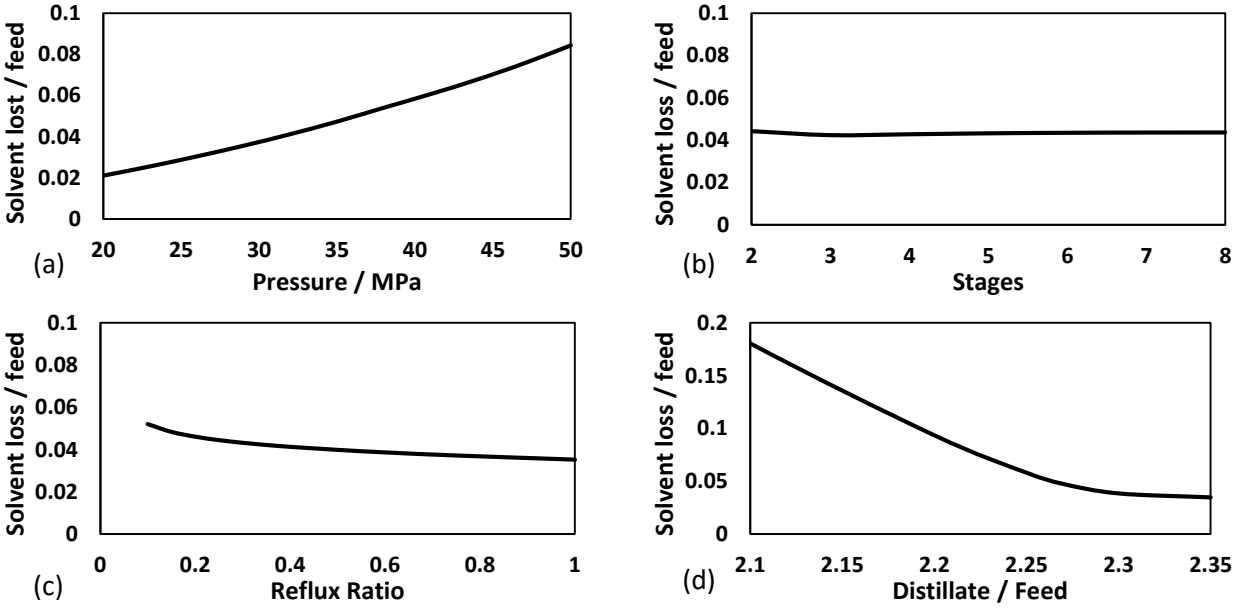

Figure B.21. Sensitivity of the loss of solvent to variations in the solvent recovery column design parameters; (a) condenser pressure, (b) number of theoretical stages, (c) reflux ratio, (d) distillate to feed ratio.

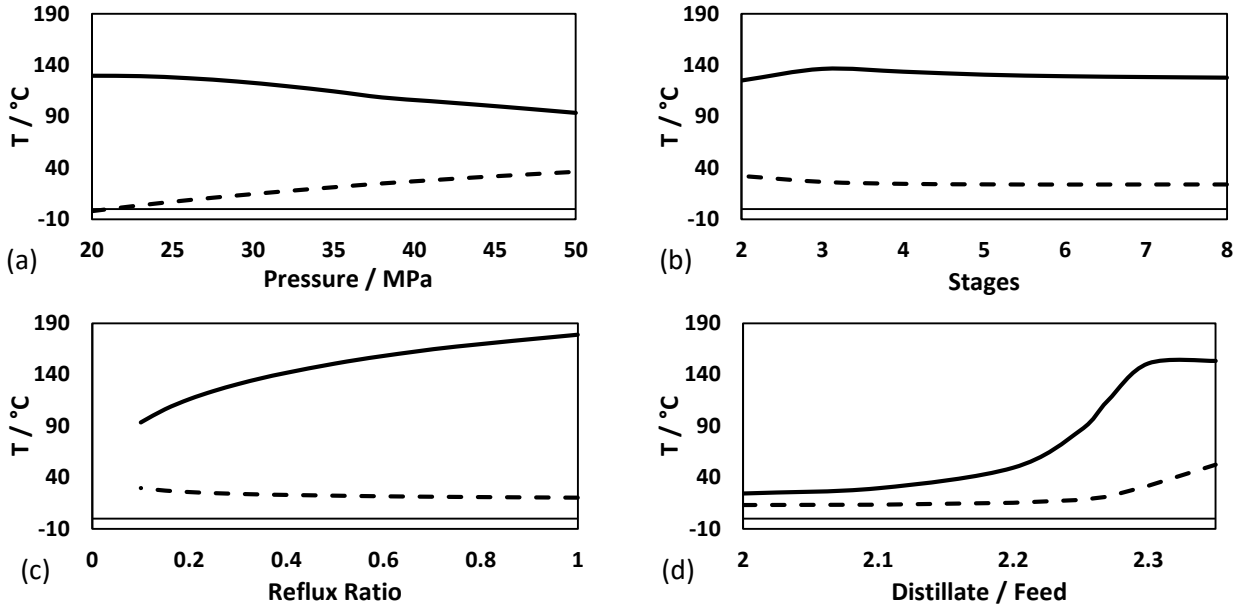

Figure B.22. Sensitivity of the condenser and reboiler temperatures to variations in the solvent recovery column design parameters; (a) condenser pressure, (b) number of theoretical stages, (c) reflux ratio, (d) distillate to feed ratio. - - - -, condenser temperature; ——, reboiler temperature.

R-116 SOLVENT

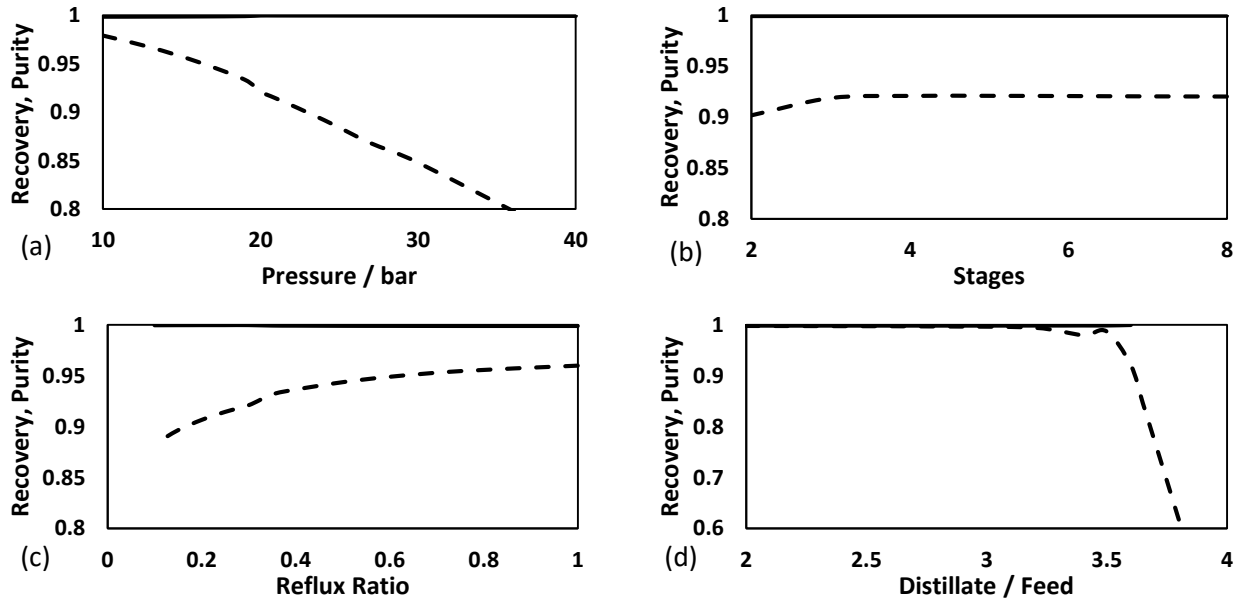

Figure B.23. Sensitivity of the product to variations in the solvent recovery column design parameters; (a) condenser pressure, (b) number of theoretical stages, (c) reflux ratio, (d) distillate to feed ratio. - - - -, recovery of hydrocarbons; ——, purity of product.

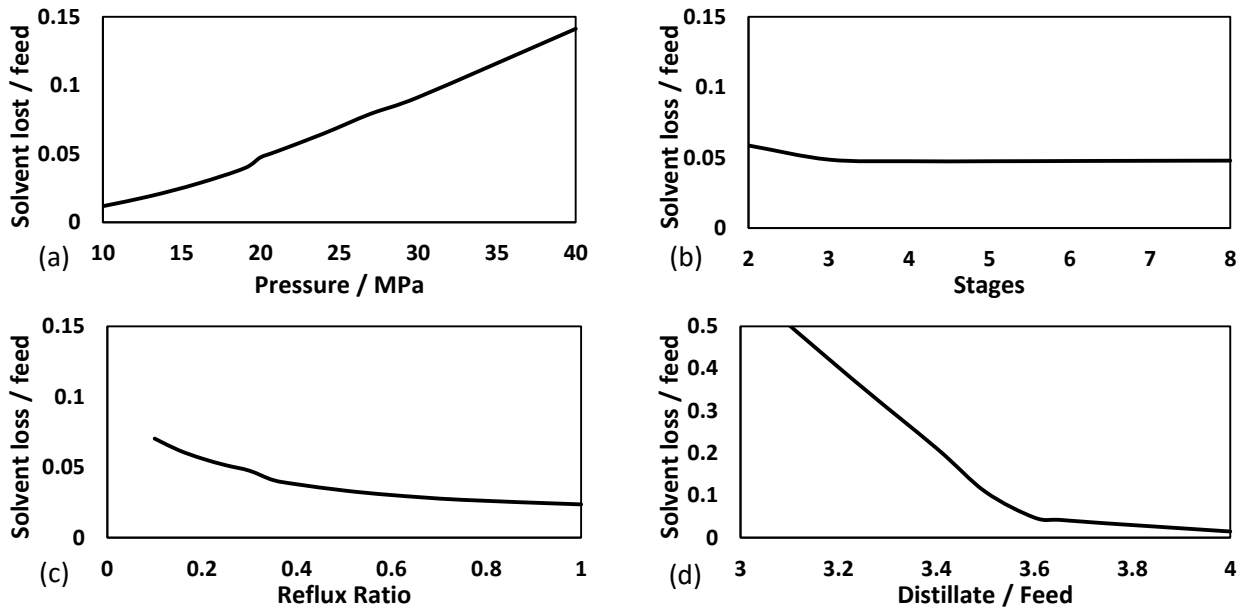

Figure B.24. Sensitivity of the loss of solvent to variations in the solvent recovery column design parameters; (a) condenser pressure, (b) number of theoretical stages, (c) reflux ratio, (d) distillate to feed ratio.

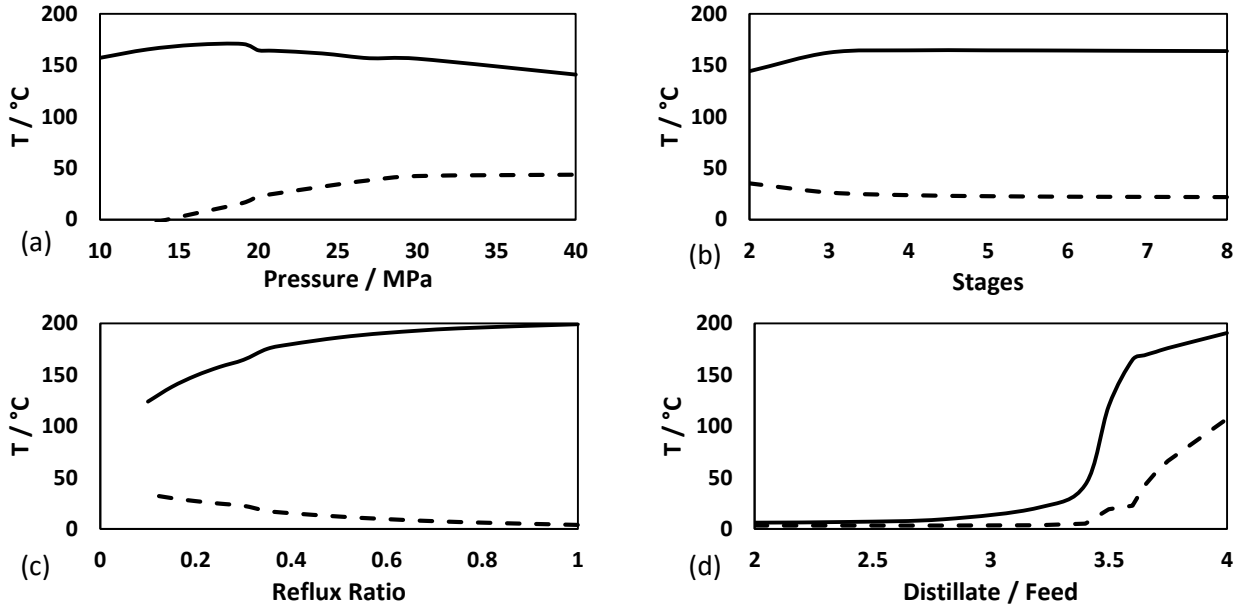

Figure B.25. Sensitivity of the condenser and reboiler temperatures to variations in the solvent recovery column design parameters; (a) condenser pressure, (b) number of theoretical stages, (c) reflux ratio, (d) distillate to feed ratio. - - - -, condenser temperature; ——, reboiler temperature.

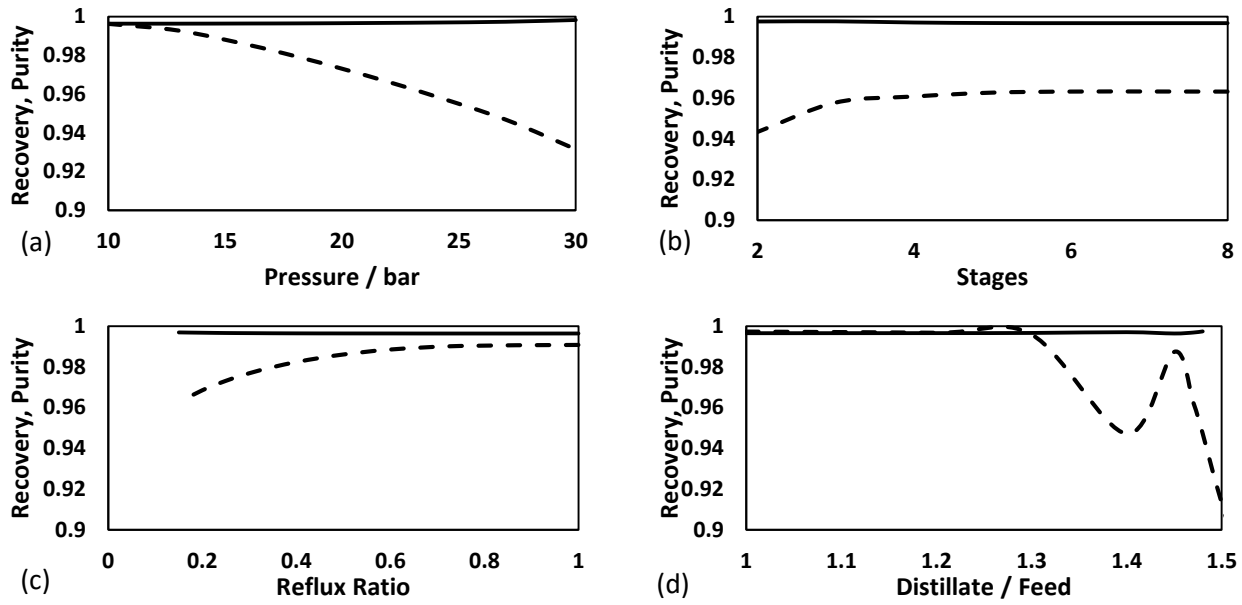

Figure B.26. Sensitivity of the product to variations in the solvent recovery column design parameters; (a) condenser pressure, (b) number of theoretical stages, (c) reflux ratio, (d) distillate to feed ratio. - - - -, recovery of hydrocarbons; ——, purity of product.

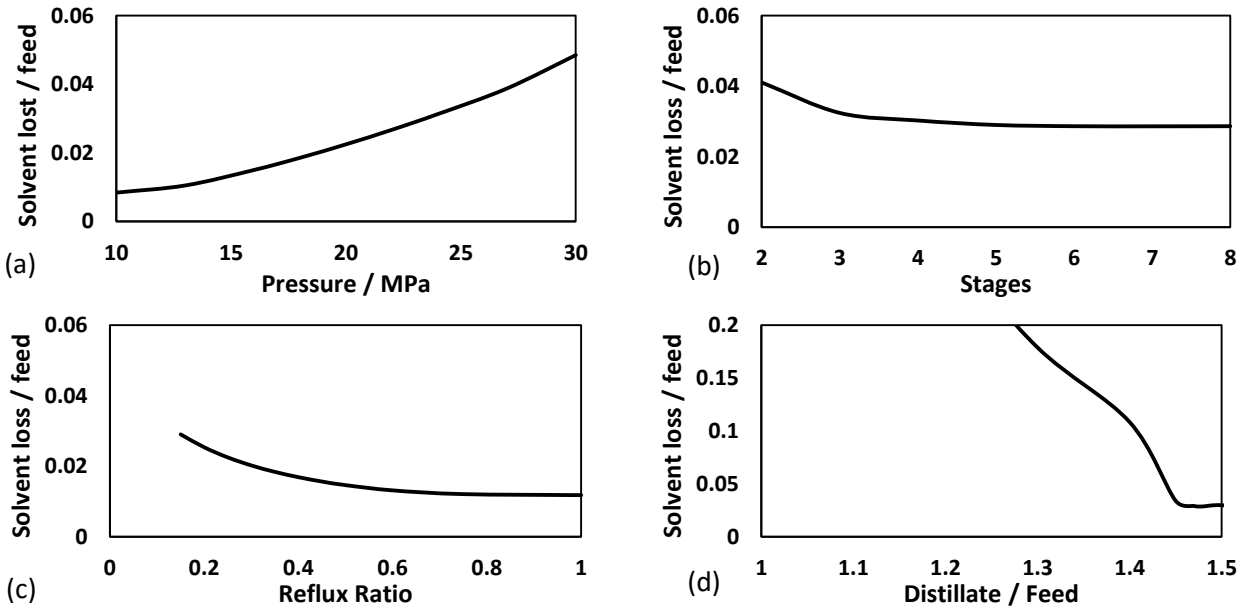

Figure B.27. Sensitivity of the loss of solvent to variations in the solvent recovery column design parameters; (a) condenser pressure, (b) number of theoretical stages, (c) reflux ratio, (d) distillate to feed ratio.

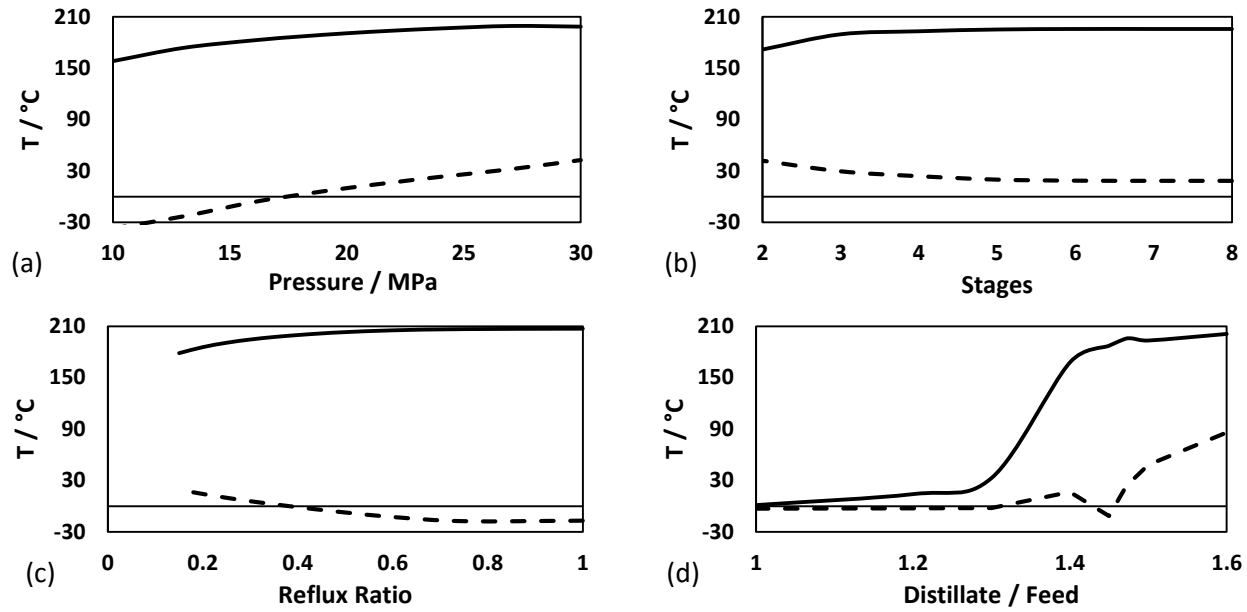

Figure B.28. Sensitivity of the condenser and reboiler temperatures to variations in the solvent recovery column design parameters; (a) condenser pressure, (b) number of theoretical stages, (c) reflux ratio, (d) distillate to feed ratio. - - - -, condenser temperature; ——, reboiler temperature.

Appendix C

J. Chem. Thermodynamics 94 (2016) 31–42

Contents lists available at ScienceDirect

J. Chem. Thermodynamics

journal homepage: www.elsevier.com/locate/jct

Isothermal (vapour + liquid) equilibrium data for binary systems of (n-hexane + CO_2 or CHF_3)

Mark D. Williams-Wynn, Paramespri Naidoo, Deresh Ramjugernath *

Thermodynamics Research Unit, School of Engineering, University of KwaZulu-Natal, Howard College Campus, Durban, South Africa

ARTICLE INFO

Article history:
Received 4 May 2015
Received in revised form 7 October 2015
Accepted 9 October 2015
Available online 19 October 2015

Keywords:
VLE
Static-analytic
Carbon dioxide
Trifluoromethane
n-Hexane

ABSTRACT

The (vapour + liquid) equilibrium (VLE) was measured for the (carbon dioxide + n-hexane) binary system at temperatures between T = (303.1 and 323.1) K. In addition, VLE and (vapour + liquid + liquid) equilibria (VLLE) were determined for the (trifluoromethane + n-hexane) binary system at temperatures between T = (272.9 and 313.3) K and pressures in the range of P = (1.0 to 5.7) MPa. Measurements were undertaken in a static-analytic apparatus, with verification of experimental values undertaken using a static-synthetic equilibrium cell to measure bubble point pressures at several compositions.

The phase equilibrium results were modelled with the Peng–Robinson equation of state with the Mathias–Copeman alpha function, coupled with the Wong–Sandler mixing rules. Regression of the data was performed with the NRTL and the UNIQUAC activity coefficient models with the Wong–Sandler mixing rules, and the performance of the models was compared. Critical loci for both systems were estimated, using the calculation procedures of Ungerer *et al.* and Heidemann and Khalil.

For the (trifluoromethane + n-hexane) system, liquid–liquid immiscibility was experienced at the lowest temperature measured (T = 272.9 K). At higher temperatures, no immiscibility was visible during the measurements; however, the models continued to predict a miscibility gap.

1. Introduction

While conventional distillation may be the simpler and preferred method for most separation and purification problems, it is not always the best or most economical technique available [1]. At times, alternative separation techniques, such as liquid–liquid extraction or extractive distillation, can provide a better separation. Some of the main disadvantages of the current extraction techniques, however, include the high viscosities and the high toxicities of the solvents [2]. In liquid–liquid extraction and extractive distillation, the same characteristics that make the solvent useful (the solubilities and capacities), make the solute recovery difficult [3].

The nature of supercritical solvents means that their viscosities are substantially lower than those of liquids and the dispersion is greater, due to the reduced surface tension [2]. These phenomena lead to improved efficiency in the solute mass transfer into the solvent phase with supercritical fluid extraction. The separation of the supercritical solvent from the solutes can usually be achieved simply by employing a reduction in pressure.

Supercritical fluid (SCF) extraction can be performed at near ambient temperatures resulting in it being a more attractive option for the separation of heat sensitive systems [4,5]. The temperature of operation is, however, dependent upon the (solvent + solute) mixture critical temperature. It is therefore lucrative to utilise a solvent that has a critical temperature that is in close proximity to the ambient temperature.

Safety and economic considerations, are the two most important factors, amongst many, which must be considered when selecting a solvent for a SCF process [6]. For the safety requirements, the solvent must be non-toxic and non-flammable, and with regards to economics, it should be cheap and readily available. A vast amount of research has been conducted into supercritical fluid extraction processes, with the majority of these investigations using carbon dioxide (CO_2) as the solvent. This is due to good availability of CO_2, and because it fulfils safety requirements [6,7]. Short-chained n-alkanes have, on occasion, also been investigated as supercritical solvents, but not to the extent that CO_2 has been investigated and used [8–16]. There has not been a substantial amount of interest in replacements for carbon dioxide in supercritical fluid extraction processes, despite the recurrent requirement of polar co-solvent additions for assistance with the extractions [17,18].

* Corresponding author. Tel.: +27 31 2603128; fax: +27 31 2601118.
E-mail address: ramjuger@ukzn.ac.za (D. Ramjugernath).

http://dx.doi.org/10.1016/j.jct.2015.10.009
0021-9614/

To avoid the need to use a co-solvent in the extraction process, the use of a polar solvent is proposed. This will simplify the downstream solvent recovery processes. Trifluoromethane (R-23, CHF_3) is a possible alternative supercritical solvent that fulfils all of the aforementioned criteria; including a low critical pressure and a critical temperature that is in close proximity to ambient temperature (see table 1).

The variety of components that are present in a 'real' petroleum stream are countless, rendering it impossible to individually measure and model the phase behaviour of each binary system present in the stream, in addition to the binary mixtures containing the solvent with each individual component. To approximate the behaviour of such a petroleum stream, the use of a 'model' petroleum stream has been proposed [19]. The binary phase equilibrium data measurements can then be conducted for the finite number of components in the model stream. This information provides an approximation and estimation as to the solvent performance with the 'real' stream. The design of a separation process would rely heavily on these measured binary equilibrium data [20].

Wirths and Schneider [21] conducted an investigation into the high pressure phase equilibria of several hydrocarbons with R-23, however, only *P*–*T*–*x* isopleths were reported due to the equipment being of the static-synthetic type. Poot and de Loos [22] measured the (vapour + liquid + liquid) equilibrium (VLLE) pressure for R-23 and hexane at temperatures between T = (253.76 and 281.78) K. They determined that the upper critical end point (UCE), at which the liquid immiscibility disappears, occurred at a temperature of T = 281.78 K. They did not, however, investigate the phase equilibria further than the VLLE pressures. The bubble point pressures at a number of temperatures and compositions for systems involving R23 and several phenyl-alkanes were measured by Bogatu *et al.* [23–25].

The phase equilibrium data for the systems containing R-23 with an *n*-alkane series were therefore measured with the intent of determining the performance of trifluoromethane as a solvent for the extraction of petroleum components by supercritical fluid extraction. The data for the binary system of (R-23 + *n*-hexane) are presented alongside the data for the (CO_2 + *n*-hexane) system.

2. Experimental

2.1. Materials

Carbon dioxide (CO_2, CAS Number 124-38-9) used in these measurements was purchased from Afrox South Africa. Trifluoromethane (CHF_3, R-23, CAS Number 75-46-7) was obtained from A-Gas (South Africa) (Pty) Ltd, and *n*-hexane (C_6H_{14}, CAS Number 110-54-3) was obtained from Sigma–Aldrich. Afrox South Africa also supplied the helium (Baseline 5.0), which was used for the gas chromatography analysis.

The stated purities, GC area percentages (mole basis), and the critical properties of the gases and *n*-hexane are listed in table 1. For *n*-hexane, the refractive index and density measured in this work, as well as values obtained from literature, are given in table 2. The refractive index was measured with an Atago RX7000 refractometer with an estimated uncertainty in the refractive index of $\pm 1 \cdot 10^{-4}$ and an estimated uncertainty in temperature of 0.01 K. The *n*-hexane density was measured with an Anton Paar DMA 5000 densimeter with uncertainties in the density and the temperature of 0.05 kg · m^{-3} and 0.05 K respectively.

Degassing of the *n*-hexane was performed *in-situ* in the equilibrium cell, by drawing a vacuum in the cell with a vacuum pump (0.2 kPa absolute for 10 min), after loading the liquid. Due to the large differences in volatilities of the components in the binary mixtures, degassing of the carbon dioxide or trifluoromethane could also be performed in the equilibrium cell. This was undertaken by repeatedly releasing some of the vapour phase that formed in the equilibrium cell, and thereafter allowing it to regenerate from the liquid. There were no 'heavier' components observed in the chemicals when analysing the purities with the gas chromatograph, and for this reason, no other purification techniques were employed.

2.2. Experimental apparatus

2.2.1. Static-analytic apparatus

A static-analytic type equilibrium cell, designed by Narasigadu *et al.* [26], was used to measure the (vapour + liquid) equilibrium and (vapour + liquid + liquid) equilibrium phase data. This apparatus has been used previously for a number of phase equilibrium data measurements, and is well documented [27,28].

TABLE 2
The refractive index, R^I, and density, ρ, of *n*-hexane at a temperature of T = 298.15 K.

T/K	R^I (lit.)	R^I (exp.)[h]	ρ (lit.)/kg · m^{-3}	ρ (exp.)[i]/kg · m^{-3}
298.15	1.3723[a]	1.3724	655.1[a]	655.241
	1.37242[b]		655.3[b]	
	1.37226[c]		655.07[e]	
	1.37236[d]		655.28[f]	
	1.3721[g]			

[a] [79].
[b] [80].
[c] [81].
[d] [82].
[e] [83].
[f] [84].
[g] [85].
[h] $u(T)$ = 0.01 K, $u(R^I) = 1 \cdot 10^{-4}$.
[i] $u(T)$ = 0.05 K, $u(\rho)$ = 0.05 kg · m^{-3}.

TABLE 1
The suppliers, stated purities, GC area fractions and critical properties (T_c, P_c) of the chemicals used in this study.

	Carbon dioxide	Trifluoromethane	*n*-Hexane
Supplier	Afrox South Africa	A-Gas (South Africa) (Pty) Ltd	Sigma–Aldrich
Stated purity	>0.999[a]	>0.999[a]	>0.99[b]
GC peak area fraction (mole)	0.9959	0.9996	0.9904
T_c/K[c]	304.26	299.07	507.35
P_c/MPa[c]	7.377	4.836	3.03

[a] Volumetric basis.
[b] Mass basis.
[c] [78].

The equipment comprises a sapphire crystal tube, enclosed at each end by a stainless steel flange, and has an internal volume of approximately 18 cm^3. It is equipped with a single moveable ROLSI™ for sampling of both the vapour and liquid phases. In this study, the composition analysis was performed with a Shimadzu GC-2010 gas chromatograph (GC), which was equipped with a thermal conductivity detector (TCD) and fitted with a (3 m length, 2.1 mm ID) column packed with a 10 wt.% dimethyl silicone elastomer (SE30) liquid phase supported on Chromosorb W-HP 80/100.

The temperature of the equilibrium cell is monitored using two Pt100 probes supplied by WIKA Instruments (model REB 1/10 DIN). The cell is maintained at a constant temperature by submersion in a 30 litre stainless steel bath filled with an ethylene glycol and water solution. The temperature of the bath is controlled by a Grant Instruments Optima TX150 immersion thermostat and circulator. The stability of the temperature controller is stated as ±0.01 K and the uniformity as ±0.05 K by the manufacturer.

The pressure in the equilibrium cell is measured with a (0 to 25) MPa P-10 pressure transducer purchased from WIKA Instruments. Atmospheric pressure is obtained from a Mensor CPC 3000 Pneumatic High-Speed Pressure Controller installed with an internal barometer. The maximum uncertainty in the atmospheric pressure from the CPC 3000 is 0.01 kPa (0.02% of full range).

2.2.2. Static-synthetic apparatus

A static-synthetic variable volume apparatus, modified from the design of Ngema *et al.* [29] (see figure 1), was used to verify the validity of the values measured with the static-analytic cell. Isothermal bubble pressure (P–x) data were recorded at specific compositions and compared to the P–x–y data collected from the static-analytic apparatus.

The variable volume cell is constructed in a similar manner to the cell of Narasigadu *et al.* [26]. It consists of a sapphire crystal tube (manufactured by Rayotek Scientific) enclosed on either end by 316 stainless steel flanges. Nitrile o-rings are compressed between the sapphire tube and the flanges to seal the cell. The 70 mm long sapphire tube has inner and outer diameters of 17.8 mm and 35.6 mm respectively. These dimensions are such that it can withstand pressures of at least 20 MPa at temperatures of T = (273 to 373) K.

A moveable 316 stainless steel piston passes through the top flange. The position of the piston (and consequently the volume of the cell) is altered by changing the pressure of the hydraulic fluid above it with a WIKA HD 250 hand pump. To provide a seal between the piston and the cell wall, as well as to prevent the mixing of the hydraulic fluid and the mixture being investigated, two nitrile o-rings are set in grooves encircling the piston head. Stirring of the cell contents is accomplished with an upper cylindrical PTFE (polytetrafluoroethylene) mixer and a lower PTFE mixer paddle. These mixers are both magnetically coupled with Neodymium magnets, obtained from Supermagnete, Germany, which are embedded into the PTFE. The magnets are magnetically coupled to a stirring shaft inside the piston, which is driven by a Heidolph RZR 2041 overhead stirrer. The cell has a maximum internal volume of approximately 8 cm^3, after accounting for the displacement caused by the piston and the top and bottom mixers.

The cell temperature is measured using two Pt100 thermometer probes, supplied by WIKA Instruments (model REB 1/10 DIN). In a similar manner to the static-analytic cell, one probe is inserted into a well drilled into the top flange, and the other into a well in the bottom flange. The temperature of the cell is kept constant by immersion in a stainless steel water bath. The temperature of the water in the bath is controlled by a Grant Instruments Optima TX150 immersion thermostat and circulator, identical to that used for the static-analytic cell. The water bath has two viewing windows, which allows observation of the contents of the cell, even with the cell submerged.

The pressure inside the cell is measured with a (0 to 12) MPa P-10 pressure transducer purchased from WIKA. This pressure transducer is housed in a heated aluminium block, maintained at

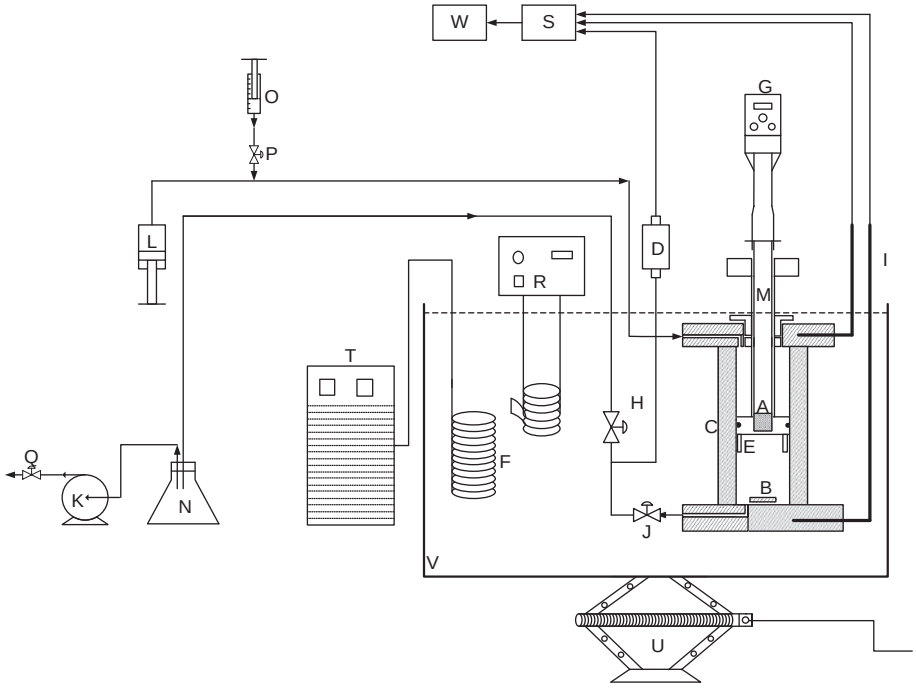

FIGURE 1. Schematic diagram of the modified static-synthetic variable volume apparatus of Ngema *et al.* [29]: A, Rare earth magnet; B, magnetic stirrer bar; C, variable volume cell; D, WIKA P-10 (0 to 12) MPa pressure transducer; E, top impeller; F, refrigeration coil; G, Heidolph RZR 2041 overhead stirrer; H, ball valve; I, Pt-100 resistance temperature probes; J, cell output (loading or draining and to the pressure transducer); K, vacuum pump; L, WIKA HD 250 hand pump; M, mechanical shaft; N, vacuum flask; O, hydraulic fluid reservoir; P, ball valve; Q, vent to fume hood; R, Grant Instruments Optima TX150 immersion thermostat and circulator; S, Agilent data acquisition unit; T, chiller unit; U, mechanical jack; V, water bath; W, computer.

T = 313 K, which prevents any external temperature fluctuations from adversely affecting the pressure measurement. The portion of the transfer line from the cell to the pressure transducer that is not submerged in the water bath is heated to the bath temperature with nichrome wire heat tracing. The atmospheric pressure is obtained from a Mensor CPC 8000 Automated High Pressure Calibrator fitted with a barometric reference. The barometric reference on this device has a maximum uncertainty of 0.005 kPa (0.01% of full range).

The analogue data signals from the thermometer probes and the pressure transmitter on the static-synthetic apparatus are recorded by an Agilent 34970A data acquisition unit, and are logged in real-time on a desktop computer via the I/O port.

2.3. Calibrations

The two Pt100 resistance thermometer probes from each apparatus were calibrated against a WIKA Instruments CTH 6500 temperature standard probe (maximum uncertainty of 0.02 K). The maximum error from the correlations of the temperature calibrations between T = (273.15 and 323.15) K, for each of the four probes was 0.06 K. The (0 to 25) MPa pressure transducer from the static-analytic apparatus and the (0 to 12) MPa pressure transducer from the static-synthetic apparatus were both calibrated against a (0 to 25) MPa WIKA Instruments CPT 6000 standard pressure transmitter (linearity of $\leqslant$0.025% of the span). This standard pressure transducer had a maximum uncertainty of 6.2 kPa. The standard deviation from the calibration of the (0 to 25) MPa pressure transducer was 0.5 kPa. The calibration of the (0 to 12) MPa pressure transducer had a standard deviation of 1.5 kPa.

The thermal conductivity detector of the gas chromatograph (GC) was calibrated using the direct injection technique. Known volumes of the gases (using a 500 μL gas-tight SGE syringe) and *n*-hexane (using a 1.0 μL SGE liquid syringe) were injected into the GC, and a calibration curve was used to relate the resultant output peaks from the detector to the number of moles of the species injected. For the gases, the ideal gas equation was used to determine the number of moles injected; with the volume, the pressure and the temperature all measured variables. For the liquid, the number of moles that was injected was calculated from the volume by using the liquid density (see table 2).

The standard deviations resulting from the calibration correlations for CO_2 and R-23 were $1 \cdot 10^{-7}$ moles and $6 \cdot 10^{-8}$ moles respectively. For the *n*-hexane, the standard deviation resulting from the correlation was $3 \cdot 10^{-8}$ moles.

2.4. Experimental procedure

2.4.1. Static-analytic apparatus

The experimental procedure that was followed in this study is similar to that detailed by Nandi *et al.* [28]. One notable addition to the technique was the flushing of the ROLSI™ prior to the composition analysis of the vapour phase. To flush the capillary of the ROLSI™, a large number of samples (approximately 30 to 40) were made in quick succession (30 s intervals) until such time as the peaks became uniform in size and shape. This flushing procedure was more important for the vapour phase than for the liquid phase, with the liquid phase requiring less than 10 flushes before the peaks became uniform.

The flange upon which the ROLSI™ was seated was heated to T = 393 K for these measurements. The transfer line from the flow controller of the gas chromatograph, to the ROLSI™ and from the ROLSI™ to the injection port of the gas chromatograph was held at a constant temperature of T = 373 K.

2.4.2. Static-synthetic apparatus

The cell was cleaned to remove any contaminants from the cell. The cell was then subjected to vacuum overnight (0.2 kPa absolute) to remove any volatile components adsorbed onto the Teflon stirrers or the nitrile o-rings. A valve, placed between the cell and the pressure transducer, was then closed and the empty, dry cell (sans the pressure transducer and thermometer probes) was weighed with an Ohaus EP Explorer top loading balance (model EP6102). This mass balance was calibrated by Trilab Support and was certified to have an uncertainty of measurement of 0.07 g. The required volume of degassed liquid was added into the cell, and the cell was once again weighed.

The cell was then cooled and the required amount of carbon dioxide or trifluoromethane was added into the cell as a liquid. The mass of the cell was recorded, and the line to the pressure transducer was reconnected. The portion of lines between the closed valve and the pressure transducer was evacuated for at least half an hour, to remove any air present. The contents of the cell were then compressed such that only a single phase existed, and thereafter, the valve between the cell and the pressure transducer was opened. The criterion that only a single fluid phase be present in the cell when this valve was opened was applied to ensure that there would be no composition gradient in the line between the cell and the pressure transducer.

Once the thermometer probes, the pressure transducer and the mixing mechanisms had been reconnected, the cell was submerged in the water bath, and the temperature was allowed to equilibrate. The volume of the cell was then varied until the bubble point of the fluid was observed. In this case, the bubble point was taken to be the point at which the first bubble of a vapour phase appeared in the cell upon increasing the cell volume. The pressure at which this bubble appeared was recorded as the bubble pressure. The repeatability of the measured data was tested by repeating the measurement at least three times. The measurements were performed at a number of temperatures before the cell contents were changed for a different composition and the loading and experimental procedure were repeated.

2.5. Data treatment

The uncertainties of the measurements were estimated with the methods outlined by the National Institute of Standards and Technology (NIST) [30,31]. The combined expanded uncertainties for the temperature, pressure and composition were estimated for all of the reported VLE data. A coverage factor, k = 2, was used for evaluation of the combined expanded uncertainties reported in this work.

The data regression tool available within Aspen Plus V8.0 [32] was used to model the experimental (vapour + liquid) equilibrium data. The modelled parameters were fitted with the Modified Barker's objective function, which minimised the residuals for the pressure and the vapour composition, at a constant temperature.

The isothermal binary phase equilibrium data sets were regressed using the PR EOS with the MC alpha function and the Wong–Sandler (WS) mixing rule [33]. The parameters for the Mathias Copeman (MC) alpha function [34] modification to the Peng–Robinson equation of state (PR EOS) [35], were obtained by adjusting the parameters to fit the model to experimental and literature vapour pressure data. The binary phase equilibrium results were modelled using either the Non-Random Two-Liquid (NRTL) activity coefficient model [36] or the Universal Quasi-Chemical (UNIQUAC) activity coefficient model [37] within the WS mixing rule.

The statistical qualities utilised to evaluate how well the models fitted to the experimental values were the average relative deviation (ARD) and the absolute average relative deviation (AARD).

The ARD is calculated by equation (1) and the AARD is calculated by equation (2).

$$ARD(\overline{\theta}) = \frac{100}{N_p}\sum_{1}^{N_p}\frac{\overline{\theta}_{exp} - \overline{\theta}_{calc}}{\overline{\theta}_{exp}}, \quad (1)$$

$$AARD(\overline{\theta}) = \frac{100}{N_p}\sum_{1}^{N_p}\frac{|\overline{\theta}_{exp} - \overline{\theta}_{calc}|}{\overline{\theta}_{exp}}, \quad (2)$$

where $\overline{\theta}$ is the quantity being measured (P, y_1, etc.), the subscripts 'exp' and 'calc' denote the experimental value and the value calculated with the model respectively, and N_p is the number of data points.

El Ahmar *et al.* [38] showed that it was possible to use the indirect extended scaling laws of Ungerer *et al.* [39] to extrapolate experimental VLE data up to the mixture critical points at the given temperatures. This method was therefore used to estimate the mixture critical loci at the temperatures at which the experimental data was available.

Castier and Sandler [40] showed that the calculation procedure of Heidemann and Khalil [41] coupled with the PR + WS/NRTL thermodynamic model predicted the shapes of critical loci for several highly non-ideal systems fairly accurately. They did, however, make a note that the predictions were found to be sensitive to the values of the parameters used. Stockfleth and Dohrn [42] proposed the use of numerical differentiation for the determination of the first and second order partial derivatives in the procedure of Heidemann and Khalil. This negated the requirement of determining the analytic partial derivatives for the fugacity terms in the thermodynamic model.

In some cases, such as in Aspen Plus [32], the independent variables for the calculation of the fugacity are the temperature and pressure, rather than the temperature and molar volume. Stockfleth and Dohrn showed that the calculation procedure could be altered to allow for this change in the independent variables, although this alteration did have an effect on the "efficiency and reliability of the algorithm". The advantage of making this alteration, however, is the ease at which a different thermodynamic model can be used. The calculation procedure of Stockfleth and Dohrn with a four point finite difference scheme was used to estimate the critical loci for both (CO_2 + *n*-hexane) and (R-23 + *n*-hexane).

3. Results and discussion

The vapour pressures for carbon dioxide and trifluoromethane were measured with the static-analytic apparatus, and compared to previously measured experimental data obtained from Meyers and van Dusen [43], Duschek *et al.* [44], and Suehiro *et al.* [45] for CO_2, and from Hou and Martin [46], Rasskazov *et al.* [47], Hori *et al.* [48], Timoshenko *et al.* [49], Ohgaki *et al.* [50] and Ju *et al.* [51] for R-23. The adjustable parameters for the MC alpha function within the modified PR EOS were obtained by fitting the model to both the experimental and literature pure component vapour pressures. The model was also used to provide a comparison between the experimental vapour pressures from this work, and the data from literature. In addition to the PR MC EOS, the original PR EOS was also used to predict the vapour pressure of pure CO_2. At lower temperatures (further away from the critical temperature), the PR EOS did not provide as good a fit of the experimental data as the PR MC EOS. This was expected, as the PR EOS contains no adjustable parameters, and depends only on the critical properties of the pure component.

The experimental vapour pressures for CO_2 along with the data calculated from the PR MC EOS model are presented in table 3. Also included in this table are the expanded uncertainties in both the experimental temperature and pressure readings and the deviations between the experimental and modelled values. The experimental vapour pressures as well as the literature vapour pressures and the vapour pressure curves calculated with the PR EOS with and without the MC alpha function are plotted in figure 2 for carbon dioxide. The measured vapour pressure data points and the vapour pressure calculated with the PR MC EOS model are plotted in figure 3 for trifluoromethane. The experimental data sets for both CO_2 and R-23 give a fair description of the literature values, with some deviations larger than the measurement uncertainties.

Because of the different temperatures at which the measurement of the data sets was conducted, it was not possible for a direct comparison between the individual sets. The experimental values were therefore compared to those calculated from a PR MC EOS model which was fitted to the literature data. Any deviations between the model and the literature values were projected as deviations between the literature and the experimental values.

TABLE 3
Vapour pressure, P, for carbon dioxide and trifluoromethane at temperatures between T = (267.81 and 303.03) K, with associated combined expanded uncertainties, U, calculated with the coverage factor, k = 2.

T/K	$U(T)$/K	P_{exp}[a]/MPa	$U(P_{exp})$/MPa	P_{calc}[b]/MPa	$(100 \cdot \Delta P/P_{exp})$[c]
			Carbon dioxide (CO_2)		
272.78	0.07	3.476	0.007	3.455	0.58
277.83	0.07	3.958	0.007	3.944	0.34
282.87	0.08	4.487	0.007	4.483	0.10
287.92	0.07	5.069	0.007	5.074	−0.10
292.95	0.07	5.705	0.007	5.719	−0.25
297.99	0.07	6.404	0.007	6.426	−0.33
303.03	0.07	7.176	0.007	7.194	−0.25
			Trifluoromethane (CHF_3)		
267.81	0.07	2.176	0.007	2.162	0.64
272.86	0.07	2.497	0.007	2.489	0.31
277.90	0.07	2.881	0.007	2.852	1.00
282.96	0.07	3.269	0.007	3.254	0.02
287.99	0.07	3.707	0.007	3.695	0.32
292.02	0.07	4.084	0.007	4.079	0.12
293.04	0.07	4.180	0.007	4.181	−0.42
297.07	0.07	4.605	0.007	4.608	−0.06

[a] Vapour pressures measured with the static-analytic cell.
[b] Vapour pressures were calculated from the PR EOS with the MC alpha function fitted to the literature data of Meyers and van Dusen [43], Duschek *et al.* [44], and Suehiro *et al.* [45] for CO_2, and that of Hou and Martin [46], Rasskazov *et al.* [47], Hori *et al.* [48], Timoshenko *et al.* [49], Ohgaki *et al.* [50] and Ju *et al.* [51] for R-23.
[c] $\Delta P = P_{exp} - P_{calc}$.

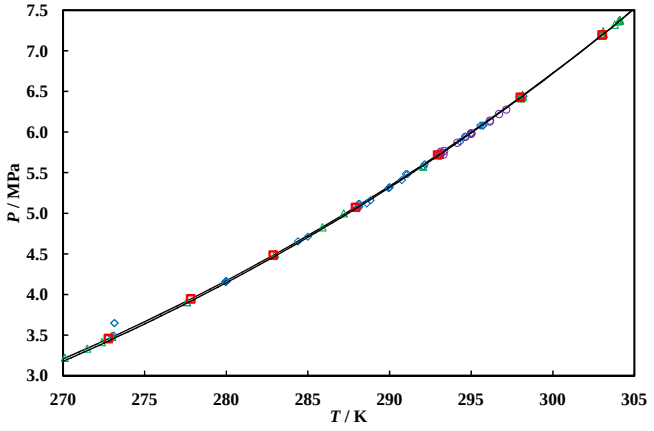

FIGURE 2. Vapour pressures, P, for carbon dioxide at temperatures between T = (270 and 304.26) K □, experimental values; △, Meyers and Van Dusen [43]; ◇, Duschek *et al.* [44]; ○, Suehiro *et al.* [45]; —, PR MC EOS model; - - -, PR EOS model.

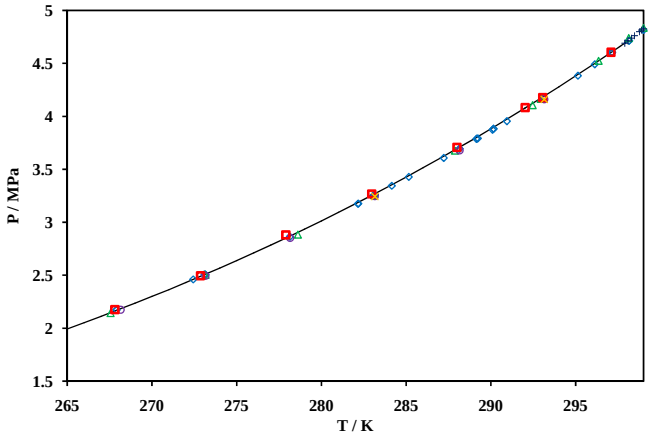

FIGURE 3. Vapour pressure, P, for trifluoromethane between temperatures of T = (265 and 299.07) K. □, experimental values; △, Hou and Martin [46]; ○, Rasskazov *et al.* [47]; ◇, Hori *et al.* [48]; ▬, Timoshenko *et al.* [49]; +, Ohgaki *et al.* [50]; x, Ju *et al.* [51] —, PR MC EOS.

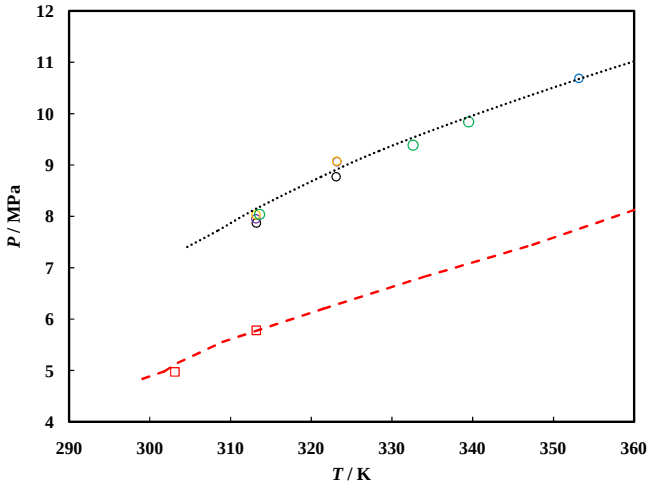

FIGURE 5. T–P projection of the binary mixture critical locus curves for (CO_2 + n-hexane) and (R-23 + n-hexane) between temperatures of T = (290 and 360) K. (CO_2 + n-hexane) literature values: ○, Li *et al.* [76]; ○, Chen and Chen [59] (extrapolated); ○, Wagner and Wichterle [58] (extrapolated); ○, Choi and Yeo [77]. This work: ○, extrapolated (CO_2 + n-hexane) critical loci; □, extrapolated (R-23 + n-hexane) critical loci; ·····, calculated (CO_2 + n-hexane) critical loci; ····, calculated (R-23 + n-hexane) critical loci. All of the "extrapolations" were performed by the procedure of Ungerer *et al.* [39]. All of the "calculations" of critical loci were performed by the procedure of Heidemann and Khalil [41].

Certain experimental vapour pressure values for R-23 did not agree with the vapour pressures calculated from the PR-MC EOS fitted to the results from several literature sources [46–51]. These deviations can be clearly observed in figure 4. Figure 4 gives a plot of the deviations of the literature data from the predicted values from this curve, as well as the deviations between the experimental and the predicted values. The differences between the values of the measurements and those of the literature were most likely due to impurities in the components used in these measurements, although great care was taken in ensuring their removal from the cell, with a substantial amount of degassing performed.

Vapour pressures for n-hexane were obtained from the works of Li *et al.* [52], Ksiązczak [53], Ksiązczak and Kosinski [54], Bich *et al.* [55], and Fernández *et al.* [56] and the parameters for the MC alpha function in the PR EOS for n-hexane were fitted to these values. The κ_i parameters for each of the three components, CO_2, R-23 and n-hexane, are given in table 4.

The experimental P–x–y results for the system of (carbon dioxide + n-hexane) at temperatures between (303.08 and 323.05) K, measured with the static-analytic apparatus, are listed in table 5, along with the combined expanded uncertainties for temperature, pressure and vapour and liquid compositions. The ($P + x + x' + y$) phase equilibrium data for the (R-23 + n-hexane) system at temperatures of between (272.85 and 313.21) K, measured with the static-analytic apparatus, are presented in table 6. These values are also presented with the associated combined expanded uncertainties for temperature, pressure and vapour and liquid compositions. The experimental VLE values determined using the static-analytic apparatus are presented in figure 6 for (CO_2 + n-hexane) and in figure 7 for (R-23 + n-hexane).

Ohgaki *et al.* [57], Wagner and Wichterle [58], Chen and Chen [59] and Zhu *et al.* [60] measured P–x–y VLE for the (carbon dioxide + n-hexane) system. Kaminishi *et al.* [61] and Lay *et al.* [62,63] reported bubble pressure P–x measurements, while Wang *et al.*

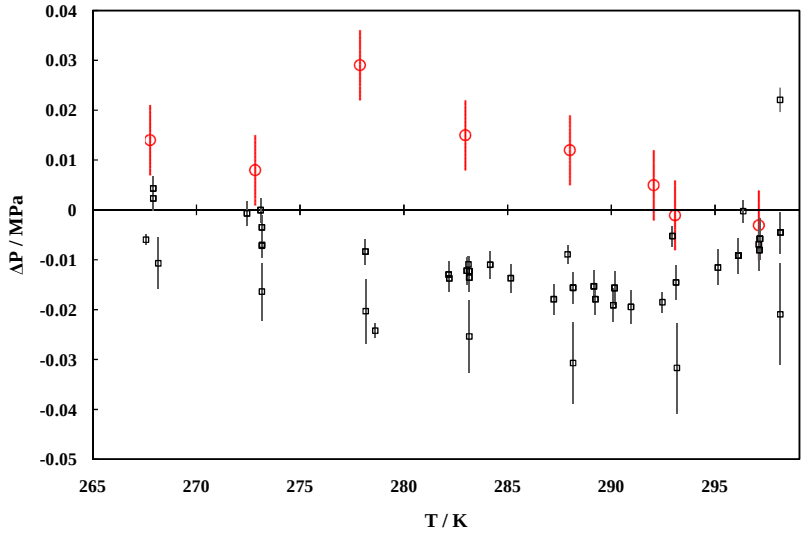

FIGURE 4. Plot of the deviations of literature and experimental vapour pressures as a function of temperature for R-23 from the PR-MC EOS between T = (265 and 299.07) K. ○, experimental; □, literature [46–51]. Error bars denote the uncertainty of the data where they have been reported.

TABLE 4
The Mathias–Copeman alpha function parameters, κ_i, for carbon dioxide, trifluoromethane and *n*-hexane, fitted to experimental and literature values within given temperature ranges, *T*.

Component	*T*/K	κ_1	κ_2	κ_3
Carbon dioxide	270–304.26[a]	0.694	0[b]	0[b]
Trifluoromethane	252.93–299.07[a]	0.776	0[b]	0[b]
n-Hexane[c]	273–339	0.780	0.212	−0.238

[a] The range extended up to the pure component critical temperature.
[b] Set to zero in this study.
[c] Vapour pressures obtained from references [52–56].

TABLE 5
Experimental *P*–*x*–*y* values with combined expanded uncertainties, *U*, calculated with the coverage factor, $k = 2$, for the binary system {carbon dioxide (1) + *n*-hexane (2)} at temperatures of between $T = (303.08$ and $323.07)$ K. Pressures, *P*, liquid phase compositions, *x*, and vapour phase compositions, *y*, are reported for each isotherm.

T/K	*U*(*T*)/K	*P*/MPa	*U*(*P*)/MPa	x_1	$U(x_1)$	y_1	$U(y_1)$
303.08	0.07	2.201	0.008	0.254	0.006	0.9772	0.0011
303.08	0.07	2.873	0.008	0.338	0.007	0.9774	0.0008
303.09	0.07	3.516	0.009	0.435	0.007	0.9804	0.0011
303.09	0.07	4.029	0.011	0.517	0.008	0.9813	0.0007
303.09	0.07	4.628	0.008	0.624	0.009	0.9821	0.0008
303.10	0.07	5.051	0.008	0.709	0.006	0.9835	0.0005
303.10	0.07	5.228	0.007	0.741	0.006	0.9835	0.0005
303.10	0.07	5.929	0.007	0.874	0.004	0.9854	0.0005
303.10	0.07	6.374	0.007	0.935	0.003	0.9877	0.0004
303.09	0.07	6.703	0.007	0.966	0.001	0.9901	0.0003
303.10	0.07	6.982	0.007	0.985	0.001	0.9928	0.0003
313.11	0.07	1.100	0.007	0.111	0.003	0.9413	0.0025
313.13	0.07	2.466	0.008	0.262	0.006	0.9733	0.0015
313.11	0.08	3.241	0.008	0.350	0.006	0.9757	0.0013
313.12	0.08	4.216	0.009	0.474	0.008	0.9815	0.0007
313.11	0.07	4.965	0.010	0.572	0.007	0.9823	0.0007
313.12	0.07	5.907	0.009	0.708	0.006	0.9828	0.0006
313.13	0.07	6.391	0.008	0.782	0.005	0.9825	0.0006
313.10	0.07	6.974	0.008	0.864	0.003	0.9826	0.0006
313.11	0.07	7.170	0.008	0.886	0.003	0.9876	0.0005
313.11	0.07	7.269	0.009	0.899	0.003	0.9850	0.0009
313.11	0.07	7.636	0.009	0.935	0.002	0.9876	0.0005
313.12	0.07	7.694	0.007	0.940	0.002	0.9820	0.0006
323.05	0.07	1.405	0.007	0.128	0.003	0.9489	0.0018
323.06	0.07	2.166	0.007	0.202	0.004	0.9564	0.0020
323.04	0.08	2.957	0.008	0.281	0.006	0.9650	0.0019
323.07	0.07	3.656	0.008	0.352	0.006	0.9724	0.0012
323.03	0.08	4.257	0.010	0.415	0.007	0.9731	0.0009
323.06	0.07	4.551	0.009	0.447	0.007	0.9762	0.0008
323.05	0.07	5.516	0.011	0.554	0.007	0.9735	0.0016
323.05	0.07	6.391	0.013	0.659	0.006	0.9771	0.0007
323.05	0.07	7.031	0.008	0.736	0.006	0.9744	0.0008
323.04	0.07	7.621	0.009	0.807	0.005	0.9784	0.0007
323.03	0.07	8.083	0.010	0.859	0.004	0.9816	0.0007
323.05	0.07	8.334	0.008	0.887	0.003	0.9794	0.0007

[64] reported solubilities of hexane in CO_2 (*P*–*y* data). The experimental values and those from all of these authors are plotted in figure 6. The values that were reported by Zhu *et al.* do not agree with those from the other authors, and therefore appear to be erroneous. There is a good comparison among the remaining data sets at $T = (303.1$ and $313.1)$ K. However, at $T = 323.0$ K and at carbon dioxide compositions of between (0.5 and 0.9) mol fraction, the deviation between the data sets increases. These deviations are larger than the uncertainties of the measurements. A possible cause of the experimental pressures being higher than the literature values would be the presence of inert gases (such as air) in the system, however with the degassing method performed, this is unlikely since the elevated pressures occurred at a single temperature, and only for a portion of this isotherm.

The bubble point values, measured with the static-synthetic apparatus were therefore used to validate the data from the static-analytic apparatus, and these data sets are presented in table 7 for the (carbon dioxide + *n*-hexane) system and in table 8 for the (trifluoromethane + *n*-hexane) system. The data are also included in figures 6 and 7. There is good agreement between the bubble points and the those measured using the static-analytic apparatus, especially at the higher pressures.

Four data points from the work of Wirths and Schneider [21] (see table 9) could be compared to the reported isotherms. These data points are plotted on figure 7. Wirths and Schneider reported the pressures and temperatures at which a single homogeneous phase occurs for a given composition, with most of their results being for (liquid + liquid) equilibrium (LLE). The LLE of the system was not measured in this study, and therefore most of the data of Wirths and Schneider was not useful for comparison. The results of Wirths and Schneider also had a high degree of randomness to them, with neither isothermal nor isobaric measurements being performed. The point of homogeneity for each composition was curiously measured at any arbitrary temperature. This further reduced the number of values that could be compared to the data reported here. The values determined in this study compare fairly well with the few comparable data points of Wirths and Schneider, especially when taking into account the high uncertainties reported by Wirths and Schneider. They reported $u(P)$ of 1 MPa, and $u(T)$ of between $T = (0.3$ and $0.7)$ K.

The system of (R-23 + *n*-hexane) was hypothesised to have a "bird's beak" isotherm at the critical temperature of R-23, because the bubble curves and dew curves were observed to create very sharp points as they approached the pure component vapour pressure below the critical temperature and as they approached the mixture critical point above the critical temperature [65]. The VLE behaviour at the critical temperature of R-23 was predicted using temperature dependent parameters for the {PRMCWS + (NRTL)} model, and this is plotted in figure 7. It was not possible, however, to confirm from this prediction that at this temperature, the slopes of the bubble curve and the dew curve were equal at the critical point.

There were two liquid phases present at $T = 272.85$ K. However, at higher temperatures, only a single liquid phase was present. This confirms that an upper critical end point (UCEP) occurred for this system within the temperature range being investigated, as reported by Poot and de Loos [22]. This UCEP occurred where the locus of liquid–liquid critical points intercepted the VLLE curve [66]. The pressure of the (vapour + liquid + liquid) equilibria at $T = 272.85$ K was very similar to the pressure at $T = 273.41$ K reported by Poot and de Loos in their study. The temperatures at which the measurements were undertaken differed slightly, consequently preventing any direct comparison. The (R-23 + *n*-hexane) system contained a gas–liquid critical locus with no azeotropes alongside of a second critical line ending at the UCEP, and is therefore categorised as a type II system in the classification system of van Konynenburg and Scott [67].

The PR EOS with the MC alpha function and the WS mixing rules, incorporating either the NRTL activity coefficient model or the UNIQUAC activity coefficient model, was fitted to each individual isotherm independently (temperature independent parameters), as well as to all of the isotherms concurrently (temperature dependent parameters). These models have been used previously to describe the phase equilibria of systems containing hydrocarbons and refrigerants, where they were found to provide good correlation [27,68–70]. The regressed temperature dependent and temperature independent parameters for the models are listed in tables 9 and 10 for the (CO_2 + *n*-hexane) and the (R-23 + *n*-hexane) systems respectively. There is a good fit of the modelled data to the experimental values, with the ARD being less than 2% for both vapour composition and pressure. There was very little difference between the ARD and the AARD of the two different models.

TABLE 6
Experimental P–x^{I}–x^{II}–y values with combined expanded uncertainties, U, calculated with the coverage factor, $k = 2$, for the binary system {trifluoromethane (1) + n-hexane (2)} at temperatures of between $T = (272.86$ and $313.21)$ K. Pressures, P, liquid phase compositions, x^{I} and x^{II}, and vapour phase compositions, y, are reported for each isotherm.

T/K	$U(T)$/K	P/MPa	$U(P)$/MPa	x_1^{I}	$U(x_1^{I})$	x_1^{II}	$U(x_1^{II})$	y_1	$U(y_1)$
272.86	0.07	1.545	0.010	0.173	0.004			0.9886	0.0006
272.85	0.08	1.891	0.010	0.243	0.005			0.9888	0.0008
272.86	0.07	1.943	0.011	0.255	0.005			0.9865	0.0004
272.87	0.08	2.167	0.009	0.335	0.006			0.9889	0.0008
272.87	0.06	2.324	0.006	0.444	0.006	0.873	0.003	0.9896	0.0006
272.87	0.07	2.396	0.007	0.953	0.002			0.9919	0.0011
272.87	0.07	2.436	0.007	0.980	0.001			0.9949	0.0007
272.86	0.07	2.469	0.007	0.987	0.001			0.9970	0.0005
282.95	0.07	1.197	0.011	0.101	0.003			0.9754	0.0012
282.95	0.07	1.693	0.010	0.162	0.004			0.9807	0.0007
282.94	0.08	2.114	0.011	0.225	0.005			0.9819	0.0007
282.95	0.07	2.196	0.008	0.237	0.005			0.9837	0.0011
282.96	0.07	2.798	0.009	0.432	0.008			0.9861	0.0005
282.96	0.07	2.906	0.007	0.616	0.007			0.9868	0.0007
282.95	0.07	2.908	0.007	0.680	0.007			0.9898	0.0008
282.96	0.07	2.948	0.007	0.885	0.003			0.9911	0.0003
282.96	0.07	3.071	0.007	0.952	0.002			0.9900	0.0006
282.95	0.07	3.149	0.007	0.981	0.001			0.9911	0.0015
282.95	0.07	3.189	0.007	0.986	0.001			0.9946	0.0003
293.03	0.07	1.192	0.007	0.088	0.002			0.9644	0.0029
293.02	0.07	1.395	0.008	0.107	0.003			0.9650	0.0015
293.02	0.07	1.623	0.009	0.130	0.003			0.9624	0.0011
293.00	0.07	2.201	0.008	0.195	0.005			0.9715	0.0012
293.03	0.07	2.872	0.012	0.299	0.006			0.9775	0.0009
293.02	0.07	3.116	0.012	0.354	0.007			0.9789	0.0008
293.03	0.07	3.491	0.008	0.520	0.007			0.9818	0.0009
293.02	0.07	3.681	0.007	0.879	0.003			0.9861	0.0010
293.02	0.07	3.943	0.007	0.964	0.001			0.9918	0.0009
293.03	0.07	4.065	0.007	0.987	0.001			0.9951	0.0005
303.10	0.07	1.270	0.010	0.086	0.002			0.9625	0.0022
303.11	0.07	2.925	0.010	0.250	0.005			0.9793	0.0012
303.11	0.07	3.589	0.011	0.351	0.007			0.9807	0.0011
303.11	0.08	3.744	0.010	0.382	0.007			0.9770	0.0013
303.09	0.08	4.256	0.010	0.580	0.007			0.9801	0.0007
303.11	0.07	4.333	0.007	0.660	0.007			0.9798	0.0012
303.10	0.07	4.380	0.008	0.726	0.006			0.9788	0.0007
303.12	0.07	4.500	0.007	0.874	0.003			0.9820	0.0012
303.11	0.07	4.726	0.007	0.942	0.002			0.9810	0.0008
303.12	0.07	4.884	0.007	0.962	0.001			0.9859	0.0006
303.11	0.07	4.929	0.007	0.974	0.001			0.9914	0.0003
313.21	0.08	1.060	0.007	0.061	0.002			0.9640	0.0016
313.20	0.09	3.059	0.009	0.230	0.005			0.9748	0.0010
313.19	0.09	4.156	0.011	0.367	0.007			0.9749	0.0011
313.19	0.09	4.634	0.010	0.464	0.007			0.9762	0.0008
313.19	0.09	4.942	0.011	0.551	0.007			0.9730	0.0008
313.20	0.07	5.099	0.010	0.630	0.007			0.9706	0.0009
313.20	0.08	5.209	0.008	0.710	0.006			0.9722	0.0009
313.20	0.08	5.381	0.007	0.864	0.003			0.9735	0.0012
313.21	0.08	5.590	0.009	0.931	0.002			0.9688	0.0012
313.20	0.08	5.770	0.009	0.955	0.001			0.9615	0.0015

Wagner and Wichterle [58] used the Grabowski and Daubert [71] modification to the Soave–Redlich–Kwong EOS [72] and the Peng–Robinson EOS [35] with the classical mixing rules for the correlation of their experimental results. Thus both of their models consisted of a single adjustable parameter. The parameter for each model was fitted with a maximum likelihood objective function. However, the difficulty with the use of the maximum likelihood function is the relatively large deviation between the experimental and the estimated temperatures that is allowed. This deviation is masked in their evaluation of the mean absolute temperature deviations for the regression, due to the magnitude of the absolute temperature relative to the temperature deviations. Wagner and Wichterle allowed deviations of up to 0.24 K between the experimental and the estimated temperatures.

A single parameter PR EOS model with the classical mixing rules was also fitted to the experimental values from this study using a modified Barker objective function (P and y) in order to compare the correlation of a model with a single adjustable parameter to one with three adjustable parameters. The binary interaction parameter for the classical mixing rules within the PR EOS is also included in table 11 along with the statistics for this regression. Although the ARD and AARD for the vapour composition using the PR EOS with the classical mixing rules are similar to those of the more complex models, the description of the bubble curve pressures are fairly poor, as can be observed on figure 6. The inclusion of the WS mixing rule with an activity coefficient model improves the agreement between the experimental and predicted bubble point pressures.

The thermodynamic model parameters for the (CO_2 + n-hexane) system and the (R-23 + n-hexane) system are plotted in figures 8 and 9 respectively. In mixtures where the conditions are such that at least one component is supercritical, k_{ij} is often considered to be

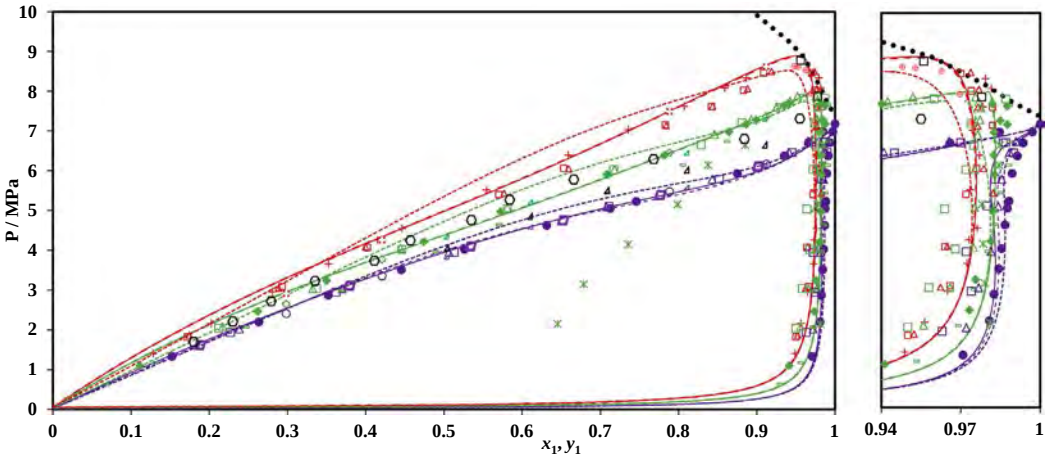

FIGURE 6. Pressure, P, liquid phase composition, x, and vapour phase composition, y, plot for the binary system of {carbon dioxide (1) + n-hexane (2)} measured with the static-analytic apparatus at temperatures of T = ●, 303.09 K; T = ◆, 313.10 K; T = +, 323.05 K. Pressure, P, liquid phase composition, x, data measured with the static-synthetic apparatus at temperatures of T = ○, 303.2 K; T = ◇, 313.2 K; T = X, 323.2 K. Solid lines, PRMC + WS/(NRTL) model; dashed line, PRMC + WS/(NRTL) model; dotted line, PR model; ····, critical loci. ■, extrapolated critical points. Literature data of: Wagner and Wichterle [58], T = □, 303.14 K; T = □, 313.14 K; T = □, 323.14 K; Chen and Chen [59], T = △, 303.15 K; T = △, 313.15 K; T = △, 323.15 K; Ohgaki *et al.* [57], T = ▬, 313.1 K; Kaminishi *et al.* [61], T = ▱, 303.14 K; Lay *et al.* [62], T = ⬡, 308.15 K; Wang *et al.* [64], T = ⊕, 323 K; Zhu *et al.* [60], T = ж, 313 K; Lay *et al.* [63], T = ◿, 303.15 K; T = ◭, 308.15 K; T = ◿, 313.15 K.

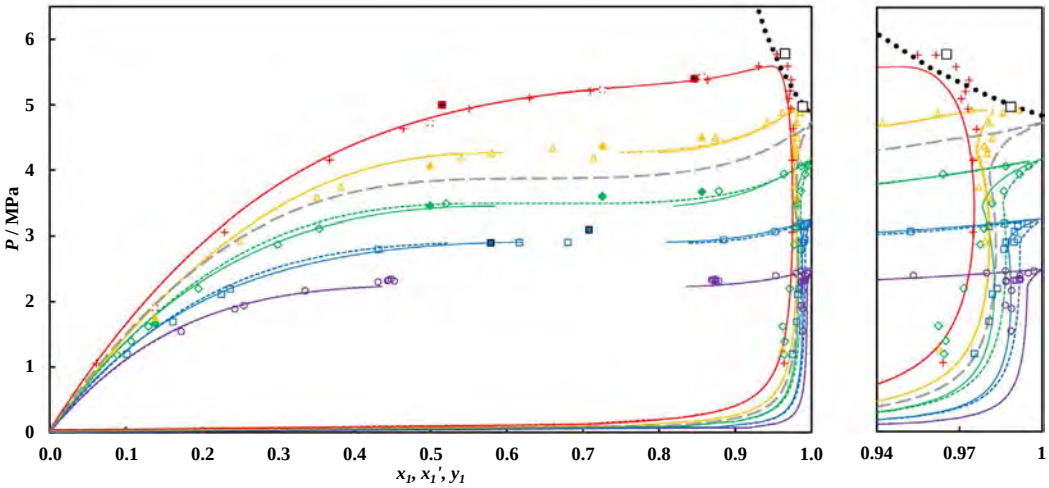

FIGURE 7. P–x–x'–y data for the binary system of {trifluoromethane (1) + n-hexane (2)} determined using the static-analytic apparatus at temperatures of T = ○, 272.87 K; T = □, 282.95 K; T = ◇, 293.02 K; T = △, 303.11 K; T = +, 313.20 K. P–x values determined with the static-synthetic apparatus at temperatures of T = ◆, 293.02 K; T = ▲, 303.11 K; T = X, 313.20 K. The results of Wirths and Schneider [21], T = ■, ±283 K; T = ■, ±313 K. Solid lines, (PR MC + WS/NRTL) model; dotted line, (PR MC + WS/UNIQUAC) model; dashed line, predicted VLE at R-23 critical temperature using the (PR MC + WS/NRTL) model; ····, critical loci. □, extrapolated critical points. The plot includes the pressure, P, liquid phase composition, x/x', and vapour phase composition, y, relationship.

TABLE 7
Experimental bubble point P–x values with combined expanded uncertainties, U, calculated with the coverage factor, k = 2, for the binary system {carbon dioxide (1) + n-hexane (2)} at temperatures of between T = (303.09 and 323.26) K. The pressure, P, and liquid phase composition, x, are reported.

T/K	$U(T)$/K	P/MPa	$U(P)$/MPa	x_1	$U(x_1)$
303.18	0.03	2.411	0.012	0.2983	0.0008
303.09	0.03	3.353	0.012	0.4208	0.0003
303.20	0.03	5.473	0.015	0.7884	0.0001
303.20	0.03	6.164	0.015	0.9121	0.0002
313.21	0.03	2.650	0.017	0.2983	0.0008
313.18	0.03	3.777	0.020	0.4208	0.0003
313.23	0.03	6.451	0.013	0.7884	0.0001
313.22	0.03	7.365	0.008	0.9121	0.0002
323.21	0.04	2.913	0.012	0.2983	0.0008
323.19	0.04	4.259	0.018	0.4208	0.0003
323.26	0.04	7.486	0.011	0.7884	0.0001
323.25	0.04	8.617	0.009	0.9121	0.0002

TABLE 8
Experimental bubble point P–x values with combined expanded uncertainties, U, calculated with the coverage factor, k = 2, for the binary system {trifluoromethane (1) + n-hexane (2)} at temperatures of between T = (293.14 and 313.23) K. The pressure, P, and liquid phase composition, x, are reported.

T/K	$U(T)$/K	P/MPa	$U(P)$/MPa	x_1	$U(x_1)$
293.17	0.03	1.6692	0.011	0.1383	0.0010
293.15	0.03	3.4569	0.008	0.4993	0.0003
293.14	0.03	3.6003	0.007	0.7255	0.0002
293.16	0.03	3.6710	0.005	0.8562	0.0002
303.16	0.05	1.7610	0.008	0.1383	0.0010
303.17	0.03	4.0757	0.009	0.4993	0.0003
303.13	0.03	4.3736	0.005	0.7255	0.0002
303.18	0.03	4.5038	0.005	0.8562	0.0002
313.17	0.06	1.9043	0.005	0.1383	0.0010
313.21	0.04	4.7213	0.010	0.4993	0.0003
313.16	0.06	5.2332	0.006	0.7255	0.0002
313.23	0.05	5.4251	0.008	0.8562	0.0002

TABLE 9
P–T–x values for the two phase envelope of the {R-23 (1) + *n*-hexane (2)} system at temperatures similar to the isothermal temperatures reported in this study. These four data points were extracted from the larger data set that was reported by Wirths and Schneider [21].

T/K	*P*/MPa	x_1
282.3	2.90	0.579
283.6	3.10	0.708
312.99	5.00	0.515
313.79	5.40	0.846

temperature dependent [73–75]. Because this was the case in this study, the k_{ij} terms were treated as temperature dependent along with the activity coefficient model parameters. From figures 8 and 9, it can be observed that the parameters follow two separate trends, one below and one above the critical temperature of the pure component. This phenomenon was more obvious with the parameters for the activity coefficient models than it was with the binary interaction parameters.

There is a good fit of both models (NRTL and UNIQUAC) to the experimental values, although both models predicted that the UCEP occurs at higher temperatures than were measured. This was, however, due to the minor experimental pressure changes with changes in the R-23 liquid phase composition between 0.5 and 0.85.

The critical loci extrapolated directly from the measured VLE data by the method of Ungerer *et al.* [39], as well as the critical locus curve estimated using the PR-MC + WS/NRTL temperature dependent parameters by the method of Heidemann and Khalil [41] are included in table 12, as well as in figures 6 and 7. The *T-P* projections of the critical loci for both (CO_2 + *n*-hexane) and (R-23 + *n*-hexane) are presented in figure 5. It can be observed that the calculation procedure of Heidemann and Khalil provided a good prediction of the experimental critical locus curve, and there was little deviation between this curve and the experimental values [58,59,76,77]. Not all of these literature data sets contained mixture critical point values, and in these cases, the VLE data were extrapolated to the critical point using the procedure of Ungerer *et al.* [39].

TABLE 10
For the system {CO_2 (1) + *n*-hexane (2)}, the temperature independent and temperature dependent parameters for the PR model (k_{12}), the (PRMC + WS/NRTL) model (k_{12} and τ_{ij}) and the (PRMC + WS/UNIQUAC) model (k_{12} and Δu_{ij}), with regression statistics. The ARD and the AARD for the pressure, *P*, and vapour phase composition, *y*, are reported for each temperature, *T*, or temperature range.

T/K	k_{12}	τ_{12}/K[a]||Δu_{12}[b]/J · mol^{-1}	τ_{21}/K[a]||Δu_{21}[b]/J · mol^{-1}	ARD[c]		AARD[d]	
				P	*y*	*P*	*y*
			PR				
(303.1 to 323.1)	0.1310	–	–	−0.50	−0.15	3.85	0.62
			PRMC + WS/NRTL				
303.1	0.4479	2072.0	105.87	0.48	0.02	0.84	0.28
313.1	0.5746	449.92	91.10	0.01	−0.55	1.38	0.59
323.1	0.5774	438.68	85.97	0.07	−0.54	1.77	0.76
(303.1 to 323.1)	0.5704	534.24	46.85	0.16	−0.50	1.51	0.62
			PRMC + WS/UNIQUAC				
303.1	0.4794	2926.7	1256.7	0.69	−0.17	1.37	0.23
313.1	0.5713	−3.49	3417.6	0.06	−0.52	1.32	0.57
323.1	0.5753	−91.82	3503.7	0.09	−0.52	1.68	0.76
(303.1 to 323.1)	0.5656	223.30	3118.5	0.21	−0.47	1.48	0.60

[a] τ_{12}, τ_{21} for the NRTL activity coefficient model.
[b] Δu_{12}, Δu_{21} for the UNIQUAC activity coefficient model.
[c] Absolute average deviation, $ARD(\overline{\theta}) = \frac{100}{N_p}\sum_1^{N_p}|\overline{\theta}_{exp} - \overline{\theta}_{calc}|$.
[d] Absolute average relative deviation, $AARD(\overline{\theta}) = \frac{100}{N_p}\sum_1^{N_p}\frac{|\overline{\theta}_{exp}-\overline{\theta}_{calc}|}{\overline{\theta}_{exp}}$.

TABLE 11
For the system {trifluoromethane (1) + *n*-hexane (2)}, the temperature independent and temperature dependent parameters for the PR model (k_{12}), the (PRMC + WS/NRTL) model (k_{12} and τ_{ij}) and the (PRMC + WS/UNIQUAC) model (k_{12} and Δu_{ij}), with regression statistics. The ARD and the AARD for the pressure, *P*, and vapour phase composition, *y*, are reported for each temperature, *T*, or temperature range.

T/K	k_{12}	τ_{12}/K[a]||Δu_{12}[b]/J · mol^{-1}	τ_{21}/K[a]||Δu_{21}[b]/J · mol^{-1}	ARD		AARD	
				P	*y*	*P*	*y*
			NRTL				
272.9	0.3972	1 745.6	441.9	0.22	−0.71	1.12	0.71
283.0	0.3788	1 773.9	398.9	0.25	−0.97	0.72	0.97
293.0	0.3569	1 684.4	361.1	0.75	−1.81	0.87	1.88
303.1	0.4905	754.4	192.1	1.01	−0.98	2.12	1.07
313.2	0.5348	505.8	235.9	0.39	−0.63	1.07	0.67
(272.9 to 313.2)	0.4973	657.9	248.9	0.77	−0.18	0.77	0.18
			UNIQUAC				
272.9	0.5301	178.0	3415.0	1.16	−0.90	1.71	0.90
283.0	0.5425	164.3	3284.7	0.45	−1.30	0.94	1.30
293.0	0.5056	427.8	3049.2	0.33	−2.28	1.25	2.28
303.1	0.4982	597.0	2757.0	0.78	−1.00	1.96	1.09
313.2	0.5345	7.1	3313.3	0.38	−0.62	1.07	0.67
(272.9 to 313.2)	0.5135	356.3	3079.3	0.75	−0.36	0.75	0.36

[a] τ_{12}, τ_{21} for the NRTL activity coefficient model.
[b] Δu_{12}, Δu_{21} for the UNIQUAC activity coefficient model.

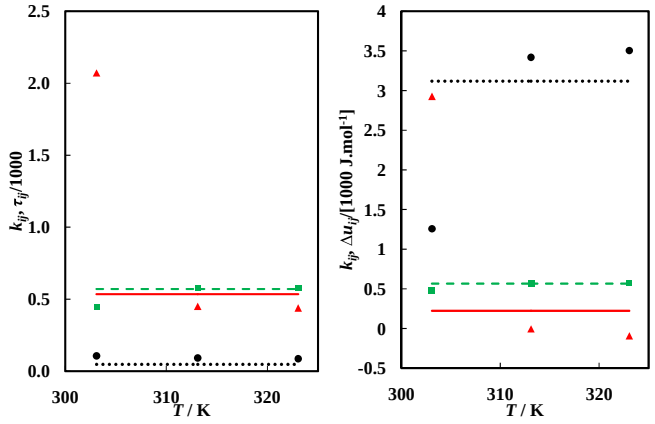

FIGURE 8. PR MC + WS/(NTRL or UNIQUAC) model parameters for the {carbon dioxide (1) + *n*-hexane (2)} binary system at temperatures between T = (303.1 to 323.05) K. The symbols represent temperature independent parameters, and lines represent temperature dependent parameters. *Left*: (NRTL) ■ / ···, k_{12}, WS binary interaction parameter; ● / ·····, τ_{12}; ▲ / —, τ_{21}. *Right*: (UNIQUAC) ■ / ···, k_{12}, WS binary interaction parameter; ● / ·····, Δu_{12}; ▲ / —, Δu_{21}.

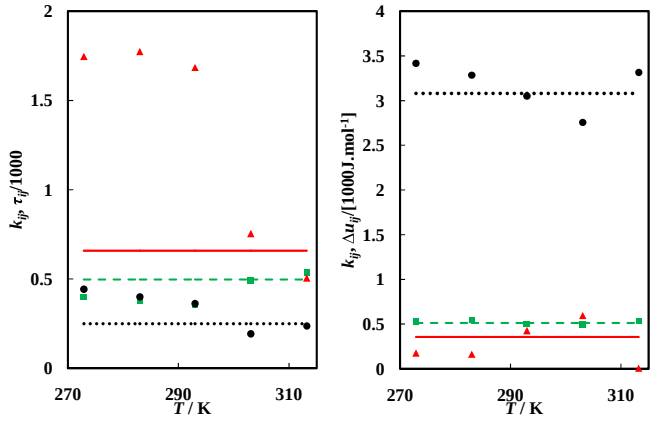

FIGURE 9. PR MC + WS/(NTRL or UNIQUAC) model parameters for the {trifluoromethane (1) + *n*-hexane (2)} binary system at temperatures between T = (272.9 to 313.2) K. The symbols represent temperature independent parameters, and lines represent temperature dependent parameters. *Left*: (NRTL) ■ / ···, k_{12}, WS binary interaction parameter; ● / ·····, τ_{12}; ▲ / —, τ_{21}. *Right*: (UNIQUAC) ■ / ···, k_{12}, WS binary interaction parameter; ● / ·····, Δu_{12}; ▲ / —, Δu_{21}.

For the (CO_2 + *n*-hexane) system, the extrapolated critical loci had lower pressures than the calculated critical loci. It is suspected that this was due to the "bird's beak" phenomenon, which occurred in this system. The sudden inflection in the dew point curve (referred to as the "bird's beak" phenomenon) meant that the extrapolated *P*-*y* curve did not provide a good description of the system near to the critical point. In figure 6, it can be observed that several measured data points occurred outside of the supposed heterogeneous phase envelope. This can be attributed to the difficulty for the thermodynamic model to describe accurately the system at near critical conditions. This poor performance is one of the known drawbacks to using cubic equations of state [40].

For the (R-23 + *n*-hexane) system, the extrapolated critical loci appear to be better estimations than the critical loci calculated by the method of Heidemann and Khalil. The pressures of the critical loci calculated from the thermodynamic models appear to be too low. This under-prediction of the pressure is, however, simply inherited from the thermodynamic models, which also under-predicted the pressure at near critical conditions.

TABLE 12
Critical loci extrapolated from experimental data by the method of Ungerer *et al.* [39], and estimated from thermodynamic models by the method of Heidemann and Khalil [41] for {CO_2 (1) + *n*-hexane (2)} and {trifluoromethane (1) + *n*-hexane (2)}. The reported critical loci include the critical temperature, T_c, the critical pressure, P_c, and the critical mixture composition of component 1, $x_{c,1}$.

Method of Ungerer *et al.*			Method of Heidemann and Khalil		
T_c	P_c	$x_{c,1}$	T_c	P_c	$x_{c,1}$
		CO_2 (1) + n-hexane (2)			
313.2	7.870	0.978	308.3	7.714	0.99
323.0	8.774	0.956	313.2	8.150	0.98
			321.2	8.866	0.96
			328.3	9.271	0.94
			339.1	9.910	0.90
			353.7	10.702	0.85
			369.6	11.492	0.80
		R-23 (1) + n-hexane (2)			
303.1	4.975	0.989	301.8	4.982	0.99
313.0	5.782	0.965	303.5	5.150	0.98
			309.0	5.556	0.96
			321.5	6.099	0.94
			333.9	6.821	0.92
			347.4	7.446	0.90
			380.0	9.201	0.85

4. Conclusions

Isothermal VLE data are presented for the binary (carbon dioxide + *n*-hexane) system at temperatures of between T = (303.08 and 323.05) K, and for the binary system of (trifluoromethane + *n*-hexane) at temperatures of between (272.85 and 313.21) K. The values were determined using both a static-analytic apparatus and a variable-volume static-synthetic apparatus. The results for the various isotherms were correlated both individually and simultaneously, using the Peng–Robinson equation of state with the Mathias–Copeman alpha function, coupled with either the NRTL or the UNIQUAC activity coefficient model, via the Wong–Sandler mixing rule. For the (carbon dioxide + *n*-hexane) system, there is a good agreement between the experimental values and those found in the literature, and the modelled data points fitted the experimental values well. An upper critical end point is observed for the (R-23 + *n*-hexane) system, and it was classified as a van Konynenburg and Scott type II mixture. The models generally provided good correlation of the VLE data for the (R-23 + *n*-hexane) system, although the UCEP prediction is fairly poor. The critical locus curve that was calculated depended upon the performance of the thermodynamic models in the region near to the critical point. Therefore, at temperatures at which the models performed poorly, there were larger discrepancies between the calculated and extrapolated mixture critical points.

Acknowledgements

This work is based upon research supported by the South African Research Chairs Initiative of the Department of Science and Technology and the National Research Foundation.

References

[1] T.M. Letcher, Thermodynamics, Solubility and Environmental Issues, Elsevier Science, 2007.
[2] C. Erkey, J. Supercrit. Fluids 17 (2000) 259–287.
[3] M. Perrut, Ind. Eng. Chem. Res. 39 (12) (2000) 4531–4535.
[4] I. Nieuwoudt, Process Technol. Proc. (1996) 283–290.
[5] G. Wypych, Handbook of Solvents, ChemTec Publishing, 2001.
[6] Y.J. Sheng, P.C. Chen, Y.P. Chen, D.S.H. Wong, Ind. Eng. Chem. Res. 31 (3) (1992) 967–973.
[7] M.A. McHugh, V.J. Krukonis, Supercritical Fluid Extraction Principles and Practice, Butterworths, Stoneham, MA, 1986.

[8] I. Moradinia, S. TejaAmyn, in: T.G. Squires, M.E. Paulaitis (Eds.), Supercritical Fluids: Chemical and Engineering Principles and Applications, American Chemical Society, Chicago, 1987, pp. 130–137.
[9] M.A. Ávila-Chávez, A. Trejo, Ind. Eng. Chem. Res. 49 (7) (2010) 3342–3348.
[10] M.A. Ávila-Chávez, R. Eustaquio-Rincón, J. Reza, A. Trejo, Sep. Sci. Technology 42 (10) (2007) 2327–2345.
[11] C.J. Peters, J.L. de Roo, J. De Swaan Arons, Fluid Phase Equilib. 72 (1992) 251–266.
[12] C.E. Schwarz, J.H. Knoetze, Fluid Phase Equilib. 258 (1) (2007) 51–57.
[13] C.E. Schwarz, M. Zamudio, J.H. Knoetze, J. Chem. Eng. Data 56 (4) (2011) 1116–1124.
[14] C.E. Schwarz, A.J. De Villiers, C.B. McClune, G.J.K. Bonthuys, A.J. Burger, J.H. Knoetze, J. Supercrit. Fluids 55 (2) (2010) 554–565.
[15] M. Zamudio, C.E. Schwarz, J.H. Knoetze, J. Supercrit. Fluids 59 (2011) 14–26.
[16] D.E. Knox, Pure Appl. Chem. 77 (3) (2005) 513–530.
[17] J.M. Dobbs, J.M. Wong, K.P. Johnston, J. Chem. Eng. Data 31 (3) (1986) 303–308.
[18] A. Kordikowski, G.M. Schneider, Fluid Phase Equilib. 90 (1) (1993) 149–162.
[19] R. Jiménez-Gallegos, L.A. Galicia-Luna, O. Elizalde-Solis, J. Chem. Eng. Data 51 (5) (2006) 1624–1628.
[20] G.F. Chou, R.R. Forbert, J.M. Prausnitz, J. Chem. Eng. Data 35 (1) (1990) 26–29.
[21] M. Wirths, G.M. Schneider, Fluid Phase Equilib. 21 (3) (1985) 257–278.
[22] W. Poot, W. de Loos, Phys. Chem. Chem. Phys. 1 (18) (1999) 4293–4297.
[23] C. Bogatu, D. Geană, R. Vîlcu, A. Duță, W. Poot, T.W. de Loos, Fluid Phase Equilib. 295 (2) (2010) 186–193.
[24] C. Bogatu, R. Vîlcu, D. Geana, A. Duta, W. Poot, T.W. De Loos, Rev. Roum. Chim. 54 (5) (2009) 343–349.
[25] C. Bogatu, D. Geană, A. Duță, W. Poot, T.W. De Loos, Ind. Eng. Chem. Res. 50 (1) (2011) 213–220.
[26] C. Narasigadu, P. Naidoo, C. Coquelet, D. Richon, D. Ramjugernath, Fluid Phase Equilib. 338 (2013) 188–196.
[27] A. Köster, P. Nandi, T. Windmann, D. Ramjugernath, J. Vrabec, Fluid Phase Equilib. 336 (2012) 104–112.
[28] P. Nandi, S. Moodley, D. Ramjugernath, Fluid Phase Equilib. 344 (2013) 84–91.
[29] P.T. Ngema, W.M. Nelson, P. Naidoo, D. Ramjugernath, D. Richon, Rev. Sci. Instrum. 85 (2014) 045123.
[30] B.N. Taylor, C.E. Kuyatt, Guidelines for Evaluating and Expressing the Uncertainty of NIST Measurement Results, NIST Technical Note 1994, 1297.
[31] B.N. Taylor, P.J. Mohr, M. Douma, The NIST Reference on Constants, Units, and Uncertainty, 2007.
[32] Aspen Technology Aspen Plus V8.4, 2012.
[33] D.S.H. Wong, S.I. Sandler, AIChE J. 38 (1992) 671–680.
[34] P.M. Mathias, T.W. Copeman, Fluid Phase Equilib. 13 (1983) 91–108.
[35] D.Y. Peng, D.B. Robinson, Ind. Eng. Chem. Fundam. 15 (1976) 59–64.
[36] H. Renon, J.M. Prausnitz, AIChE J. 14 (1968) 135–144.
[37] D.S. Abrams, J.M. Prausnitz, AIChE J. 21 (1) (1975) 116–128.
[38] E. El Ahmar, A. Valtz, P. Naidoo, C. Coquelet, D. Ramjugernath, J. Chem. Eng. Data 56 (5) (2011) 1918–1924.
[39] P. Ungerer, B. Tavitian, A. Boutin, Applications of Molecular Simulation in the Oil and Gas Industry – Monte Carlo methods, 2005.
[40] M. Castier, S.I. Sandler, Chem. Eng. Sci. 52 (20) (1997) 3579–3588.
[41] R.A. Heidemann, A.M. Khalil, AIChE J. 26 (5) (1980) 769–779.
[42] R. Stockfleth, R. Dohrn, Fluid Phase Equilib. 45 (1998) 43–52.
[43] C.H. Meyers, M.S. Van Dusen, Refrig. Eng. 13 (1932) 180. vol. 10, 1932, pp. 381–412.
[44] W. Duschek, R. Kleinrahm, W. Wagner, J. Chem. Thermodyn. 22 (9) (1990) 841–864.
[45] Y. Suehiro, M. Nakajima, K. Yamada, M. Uematsu, J. Chem. Thermodyn. 28 (10) (1996) 1153–1164.
[46] Y.C. Hou, J.J. Martin, AIChE J. 5 (1) (1959) 125–129.
[47] D.S. Rasskazov, E.K. Petrov, G.A. Spiridonov, E.R. Ushmajkin, Teplofiz. Svoistva Veshchestv Mater. 8 (1975) 4–16.
[48] K. Hori, S. Okazaki, M. Uematsu, K. Watanabe, in: Proc. Symp. Thermophys. Prop., ASME, Gaithersburg, 1982.
[49] N.I. Timoshenko, E.P. Kholodov, A.L. Yamnov, T.A. Tatarinova, in: V.A. Rabinovich (Ed.), Teplofiz. Svoistva Veshchestv Mater., Standards Publ., Moskow, 1975, pp. 17–39.
[50] K. Ohgaki, S. Umezono, T. Katayama, J. Supercrit. Fluids 3 (2) (1990) 78–84.
[51] M. Ju, Y. Yun, M.S. Shin, H. Kim, J. Chem. Thermodyn. 41 (12) (2009) 1339–1342.
[52] I.P.C. Li, Y.-W. Wong, S.-D. Chang, B.C.Y. Lu, J. Chem. Eng. Data 17 (4) (1972) 492–498.
[53] A. Ksiązczak, Fluid Phase Equilib. 28 (1) (1986) 57–72.
[54] A. Ksiązczak, J. Jan Kosinski, Fluid Phase Equilib. 42 (1988) 241–259.
[55] E. Bich, T. Lober, J. Millat, Fluid Phase Equilib. 75 (1992) 149–161.
[56] L. Fernández, E. Pérez, J. Ortega, J. Canosa, J. Wisniak, J. Chem. Eng. Data 55 (2010) 5519–5533.
[57] K. Ohgaki, T. Katayama, J. Chem. Eng. Data 21 (1) (1976) 53–55.
[58] Z. Wagner, I. Wichterle, Fluid Phase Equilib. 33 (1–2) (1987) 109–123.
[59] D. Chen, W. Chen, Huaxue Gongcheng 20 (1992) 66–69.
[60] R. Zhu, J. Yu, W. Xu, Z. Liu, Y.-L. Tian, Huagong Xuebao 57 (10) (2006) 2270.
[61] G.I. Kaminishi, C. Yokoyama, T. Shinji, Fluid Phase Equilib. 34 (1) (1987) 83–99.
[62] E.N. Lay, V. Taghikhani, C. Ghotbi, J. Chem. Eng. Data 51 (6) (2006) 2197–2200.
[63] E.N. Lay, J. Chem. Eng. Data 55 (1) (2010) 223–227.
[64] B. Wang, J. He, D. Sun, R. Zhang, B. Han, Fluid Phase Equilib. 239 (1) (2006) 63–68.
[65] J.C. Rainwater, Fluid Phase Equilib. 183–184 (2001) 41–51.
[66] J.P. O'Connell, J.M. Haile, Thermodynamics: Fundamentals for Applications, Cambridge University Press, 2005.
[67] P.H. van Konynenburg, R.L. Scott, Philos. Trans. R. Soc. 298 (1980) 495–540.
[68] D. Ramjugernath, A. Valtz, C. Coquelet, D. Richon, J. Chem. Eng. Data 54 (4) (2009) 1292–1296.
[69] D. Ramjugernath, A. Valtz, D. Richon, M.D. Williams-Wynn, C. Coquelet, J. Chem. Eng. Data, 2015, submitted for publication.
[70] A. Valtz, C. Coquelet, A. Baba-Ahmed, D. Richon, Fluid Phase Equilib. 207 (2003) 53–67.
[71] M.S. Graboski, T.E. Daubert, Ind. Eng. Chem. Proc. Des. Dev. 17 (4) (1978) 443–448.
[72] G. Soave, Chem. Eng. Sci. 27 (6) (1972) 1197–1203.
[73] J.-N. Jaubert, F. Mutelet, Fluid Phase Equilib. 224 (2) (2004) 285–304.
[74] A.R.H. Goodwin, J.V. Sengers, C.J. Peters, Applied Thermodynamics of Fluids, Royal Society of Chemistry, RSC Publishing, 2010.
[75] M.B. Oliveira, A.J. Queimada, J.A.P. Coutinho, J. Supercrit. Fluids 52 (3) (2010) 241–248.
[76] Y.-H. Li, K.H. Dillard, R.L. Robinson, J. Chem. Eng. Data 26 (1) (1981) 53–55.
[77] E.-J. Choi, S.-D. Yeo, J. Chem. Eng. Data 43 (5) (1998) 714–716.
[78] D.R. Lide, CRC Handbook of Chemistry and Physics 2004–2005: A Ready-Reference Book of Chemical and Physical Data, CRC Press LLC, 2004.
[79] A. Blanco, A. Gayol, D. Gómez-Díaz, J.M. Navaza, J Phys. Chem. Liq. 51 (3) (2013) 404–413.
[80] E. Mascato, L. Mosteiro, M.M. Piñeiro, J. García, T.P. Iglesias, J.L. Legido, J. Chem. Thermodyn. 33 (9) (2001) 1081–1096.
[81] J.A. Riddick, W.B. Bunger, T.K. Sakano, Organic Solvents: Physical Properties and Methods of Purification Techniques of Chemistry, fourth ed., Wiley, New York, 1986.
[82] G.C. Benson, Int. Data Ser., Ser. A 4 (1986) 273.
[83] A. Aucejo, M.C. Burguet, R. Munoz, J.L. Marques, J. Chem. Eng. Data 40 (1) (1995) 141–147.
[84] M.M. Mato, J. Balseiro, J. Salgado, E. Jiménez, J.L. Legido, M.M. Piñeiro, M.I. Paz Andrade, J. Chem. Eng. Data 47 (1) (2001) 4–7.
[85] G.H. Eduljee, A.P. Boyes, J. Chem. Eng. Data 25 (3) (1980) 249–252.

JCT 15-305

APPENDIX D

Isothermal vapour-liquid equilibrium data for binary systems of n-heptane + (CHF_3 or C_2F_6)

Mark D. Williams-Wynn [a], Paramespri Naidoo [a] and Deresh Ramjugernath [a,*]

[a] Thermodynamics Research Unit, School of Engineering, University of KwaZulu-Natal, Howard College Campus, Durban, South Africa

ARTICLE INFO

Keywords:
VLE;
static-analytic,
variable-volume,
trifluoromethane,
hexafluoroethane,
n-heptane

ABSTRACT

Isothermal vapour-liquid equilibrium data for two binary systems; trifluoromethane and n-heptane at temperatures of between (272.9 and 313.2) K, and hexafluoroethane and n-heptane at temperatures of between (293.0 and 313.2); were measured with a static-analytic apparatus. Bubble pressures at temperatures of between (293.0 and 313.2) K, at several compositions, were also measured with a variable-volume static-synthetic apparatus. VLLE was found to occur for certain isotherms with both of the systems. The PR EOS, with the MC alpha function, combined with either the classical mixing rule or the WS mixing rule, was used to correlate the experimental data. Either the NRTL or the UNIQUAC activity coefficient model was used within the WS mixing rule.

The indirect extended scaling laws of Ungerer et al. were used to extrapolate critical loci from the experimental coexistence data, and the calculation procedure of Heidemann and Khalil was employed to calculate the mixture critical locus curves at temperatures near to the refrigerant critical temperatures. At lower temperatures on the mixture critical curve, gas-liquid critical points occurred, whereas, at higher temperatures, the critical points occurred along a liquid-liquid locus curve. The two systems were categorised according to the van Konynenburg and Scott classification.

1. Introduction

Interest in the use of supercritical fluid extraction (SCFE) to provide a solution for difficult separation problems has drastically increased over the last couple of decades [1-3]. The most commonly used solvent for use in these SCFE processes is carbon dioxide, as it fulfils almost all of the requirements for a supercritical solvent [3-5]. However, the principal drawback in the use of supercritical carbon dioxide as the solvent in an extraction process is the low dielectric constant and low polarity of the CO_2 [3, 5].

The simplest method to overcome the low polarity of the carbon dioxide is by the addition of co-solvents (modifiers), thereby increasing the solvating power of the solvent for the solutes of interest [3, 6]. These co-solvents are most commonly liquids at ambient conditions. Their addition to the separation results in complications in the downstream product recovery processes, as a separation of two liquid streams must then be performed. It is therefore of interest to discover whether there are any alternative polar gases that it could realistically replace the use of carbon dioxide and a co-solvent in extraction processes. A few refrigerants (chlorofluorocarbons, hydrofluorocarbons and perfluorocarbons) exhibiting some of the characteristics essential for supercritical fluid solvents (suitable critical point, non-flammable, etc.) were therefore chosen [7].

The production and utilisation of chlorofluorocarbons has been banned by the Montreal Protocol [8] and therefore R-13 (monochlorotrifluoromethane), was not considered in this study. The remaining hydrofluorocarbons and perfluorocarbons that were likely candidates for supercritical solvents include trifluoromethane (R-23), hexafluoroethane (R-116), and difluoro-1,1-ethylene (R-1132a). The R-1132a was not investigated as it is a category 1 carcinogen [9]. Of the possible two remaining gases, the use of R-23 is likely to be advantageous, as the trifluoromethane molecules are highly polar.

A further reason behind this investigation into the performance of fluorinated hydrocarbons as supercritical solvents extends from a drive within South Africa to develop new technologies that make use of either fluorine in its pure form, or else chemicals that contain fluorine as a part of their molecules [10]. The field of fluorine chemistry is of interest in South Africa because of the large reserves of acid grade fluorspar available. Only 5 percent of the fluorspar that is mined in South Africa is processed locally, while the majority is exported as crude fluorspar. It is therefore desirable that novel uses for fluorinated compounds be developed, in order to expand the South African fluorine industry.

As a continuation of the study of high pressure phase equilibria data for the evaluation of the performance of alternatives to carbon dioxide in supercritical fluid extraction processes, the isothermal phase equilibria for the systems of trifluoromethane (1) + n-heptane (2) and hexafluoroethane (1) + n-heptane (2) were measured. The measurements were conducted with a 'static-analytic type' phase equilibrium apparatus, and were verified by measuring bubble point data with a 'static-synthetic' variable volume apparatus. Five isotherms were measured for the trifluoromethane (1) and n-heptane (2) system at temperatures of between (272.9 and 313.2) K, and three isotherms were measured for the hexafluoroethane (1) and n-heptane (2) system at temperatures of between (293.0 and 313.2) K.

2. Experimental

2.1. Materials.

The trifluoromethane (CHF_3, CAS Number 75-46-7) and the hexafluoroethane (C_2F_6, CAS Number 76-16-4) were obtained from A-Gas (South Africa) (Pty) Ltd. The n-heptane (C7H16, CAS Number 142-82-5) was obtained from Merck KGaA. The helium (Baseline 5.0) for the gas chromatograph was purchased from Afrox South Africa.

The stated purities, peak area fractions from GC analysis, as well as

Table 1.
The suppliers, stated purities, GC area fractions and critical properties (T_c, P_c) of the trifluoromethane, hexafluoroethane and n-heptane used in these measurements.

	Trifluoro-methane, CHF_3	Hexafluoro-etharne, C_2F_6	n-Heptane, C_7H_{16}
Supplier	A-Gas (South Africa) (Pty) Ltd	A-Gas (South Africa) (Pty) Ltd	Merck KGaA
Stated Purity	> 0.999 [a]	> 0.999 [a]	> 0.995 [b]
GC Peak Area Fraction (mole)	0.9996	0.9999	0.9974
T_c / K	299.07 [c]	293.03 [d]	540.3 [c]
P_c / MPa	4.836 [c]	3.013 [e]	2.756 [c]

[a] Volumetric basis
[b] Mass basis
[c] [7]
[d] [12]
[e] [11]

the literature pure component critical properties for the trifluoromethane [7], hexafluoroethane [11, 12] and n-heptane [7] are listed in Table 1. The refractive indices and densities reported in literature [13-20], as well as those measured in this study, are provided in Table 2. The refractive indices were measured with an Atago RX7000 refractometer. This refractometer had uncertainties in refractive index and in temperature of $\pm 1\times10^{-4}$ and 0.01 K respectively. The liquid densities were measured with an Anton Paar DMA 5000 density meter. The DMA 5000 had uncertainties in density and in temperature of 0.005 kg.m^{-3} and 0.05 K respectively.

All of the components were degassed in situ after being loaded into the cell. The n-heptane was loaded first, and was degassed by drawing a vacuum within the cell for approximately 10 minutes. The vacuum pump used to pull this vacuum was capable of reducing the pressure to 0.2 kPa absolute. Thereafter, subsequent to the addition of the more volatile refrigerant, degassing was once again performed by releasing a small purge of the vapour phase from within the cell and then allowing this to regenerate. This purge procedure was repeated a number of times; usually until the pressure returned to the same value after the vapour phase was regenerated. No 'heavier' impurities were detected during the GC analysis of the pure components, and therefore these degassing procedures were deemed to provide sufficient purification of the chemicals for this study.

Table 2.
The refractive indices, R^I, and densities, ρ, of n-heptane at temperatures of T = (293.15 to 300.40) K. Data obtained by experimental measurement (exp.) is compared with data from literature (lit.).

T / K	R^I (lit.)	R^I (exp.) [i]	ρ (lit.) / [kg/m^3]	ρ (exp.) [j] / [kg/m^3]
293.15	1.38807 [a]	1.3878	683.66 [f] 683.82 [g]	683.770
295.15				681.605
297.15				679.910
298.15	1.38581 [a] 1.3857 [b] 1.3855 [d] 1.3851 [f]	1.3852	679.3 [b] 679.4 [c] 679.5 [e] 679.4 [h]	679.050
300.40				677.145

[a] [13]
[b] [16]
[c] [18]
[d] [14]
[e] [15]
[f] [17]
[g] [19]
[h] [20]
[i] combined uncertainties, $u(T) = 0.01$ K, $u(R^I) = 3\times10^{-4}$
[j] combined uncertainties, $u(T) = 0.05$ K, $u(\rho) = 0.045$ kg.m^{-3}

2.2. Experimental Apparatus.

A static analytic high pressure equilibrium apparatus, described in detail by Narasigadu et al. [21], was used to measure vapour-liquid equilibrium (VLE) and vapour-liquid-liquid equilibrium (VLLE) data for the two refrigerant-hydrocarbon systems. A variable volume high pressure equilibrium apparatus, described in a previous paper [22], was used to measure the bubble pressures of these systems as a means of data verification.

Both the equilibrium cell used in the apparatus of Narasigadu et al. and that described by Williams-Wynn et al. are constructed of sapphire crystal tubes, enclosed on both ends with stainless steel flanges. The temperatures of each of the cells are monitored by two Pt100 probes (model REB 1/10 DIN), supplied by WIKA Instruments, which are inserted into wells drilled into both the top and bottom flanges.

The static analytic cell is equipped with a moveable ROLSI TM which allows samples to be taken from any level within the cell. The composition of these samples is analysed with a Shimadzu GC-2010 gas chromatograph fitted with a thermal conductivity detector (TCD). A 3 m long SE30 column (10 % dimethyl silicone elastomer liquid phase supported on Chromosorb W-HP 80/100) is used to separate the components. The pressure inside of the cell is measured with a (0 to 25) MPa P-10 pressure transducer, which was purchased from WIKA Instruments. The atmospheric pressure is monitored using the internal barometer of a Mensor CPC 3000 Pneumatic High-Speed Pressure Controller, with an uncertainty of 0.01 kPa (0.02% of full range).

The volume within the variable volume cell is varied by moving a piston vertically within the cell. This movement is induced by varying the pressure of a hydraulic fluid above the piston with a WIKA HD 250 hand pump. The pressure below the piston in the variable volume cell is measured using a (0 – 12) MPa P-10 pressure transducer, supplied by WIKA Instruments. The atmospheric pressure obtained from the barometer of a Mensor CPC 8000 Automated High Pressure Calibrator is used for the bubble pressure measurements. The maximum uncertainty for this barometer is 0.005 kPa (0.01% of full range).

2.3. Calibrations.

A CTH 6500 temperature standard probe, supplied and certified by WIKA Instruments, was used to calibrate the two Pt100 probes from each apparatus. The standard probe had a maximum uncertainty of 0.02 K and the maximum error from the calibrations performed at temperatures of between (273.15 and 323.15) K was 0.06 K. The pressure transducers from the two apparatuses were calibrated against a (0 to 25) MPa CPT 6000 standard pressure transmitter with an uncertainty of less than 6.2 KPa. The standard deviation of the calibration of the (0 to 25) MPa transducer from the static analytic apparatus was 0.5 kPa, and that of the (0 to 12) MPa transducer for the variable volume apparatus was 1.5 kPa.

Several known volumes of the gases and of the n-heptane; injected into the GC with a 500 µl gas-tight SGE syringe and a 1.0 µl SGE liquid syringe respectively; were used to calibrate the TCD. The number of moles injected; calculated from the gas volume, using the ideal gas equation, and from the liquid volume using the liquid density; was related to the areas under the corresponding GC peaks. The uncertainties in the number of moles of R-23 and R-116 from the calibration were 6.1×10^{-8} moles and 6.3×10^{-8} moles respectively. The uncertainty in the

number of moles of n-heptane from the calibration was 2.3×10^{-8} moles.

2.4. Experimental Procedure.

The experimental procedures followed for the measurement of the phase equilibrium data with both the static analytic apparatus and the variable volume apparatus are identical to those described by Williams-Wynn and co-workers [22].

In the discussions of Kalra et al. [23], mention was made of a 'flashing' phenomenon when measuring systems with large relative volatilities, such as heavier hydrocarbons with gases. This phenomenon was also noted by Brunner et al. [24]. Kalra and co-workers measured binary VLE data for the CO_2 + n-heptane system using a variable volume equilibrium cell with micro-metering valves for the sampling of the vapour and liquid phases [25]. According to their study, this 'flashing' phenomenon occurred due to the large pressure gradient across the micro-metering valves, and caused the concentration of the more volatile component to be superficially higher in the liquid phase sample than in the cell. Their reasoning for this phenomenon was that the sample undergoes a 'flash distillation' due to the sudden drop in pressure of the sample, allowing a higher proportion of the more volatile component to pass through the orifice than that present in the cell. To avoid this problem the opening time of the ROLSITM was kept to a minimum. Additionally, the opening time was varied to check the repeatability of the measurements with different sample sizes. In analysing the composition of several different sample sizes, it was possible to confirm that the 'flash distillation' phenomenon did not adversely affect the measurements.

2.5. Data Treatment.

The guidelines for the estimation of uncertainties in measurement results that were published by the National Institute of Standards and Technology (NIST) were used to estimate the uncertainties for this study [26, 27]. The combined expanded uncertainties, evaluated with a coverage factor, k, equal to 2, were reported for pressure, temperature and composition for all of the data points

The Peng-Robinson equation of state (PR EOS) [28], modified with the Mathias-Copeman (MC) alpha function [29], was used to model the experimental data; firstly with the classical mixing rule, and thereafter with the Wong-Sandler (WS) mixing rule [30]. The fit of the models, containing either the Non-Random Two-Liquid (NRTL) activity coefficient model [31] or the Universal Quasi-Chemical (UNIQUAC) activity coefficient model [32] within the WS mixing rule, were compared to one another.

The data regression tool within Aspen Plus V8.0 [33] was used to regress the experimental data from this study, using a modified Barker's objective function. Using this objective function, the residuals of the pressure and of the vapour phase composition were minimised in the search for the best model fit. The parameters for the MC alpha function for each pure component were regressed from vapour pressure data.

$$MRD(\theta) = \frac{100}{N_p}\sum_{1}^{N_p}\frac{\theta_{exp} - \theta_{calc}}{\theta_{exp}} \qquad \text{Eqn. 1}$$

$$AARD(\theta) = \frac{100}{N_p}\sum_{1}^{N_p}\frac{|\theta_{exp} - \theta_{calc}|}{\theta_{exp}} \qquad \text{Eqn. 2}$$

where θ_{exp} denotes the experimental measurand and θ_{calc} denotes the value calculated from the model. N_p is the number of data points in the set.

The coefficients for second and third terms of the Mathias-Copeman alpha function, κ_1 and κ_2, were neglected for components with low critical temperatures, as above the critical temperature, the second and third parameters become trivial, and the model must rely on the first MC parameter [29].

The statistics used to evaluate the performance of the models were the average relative deviation (ARD) and the average absolute relative deviation (AARD). The ARD and AARD were calculated for the pressure and vapour phase composition using Equations 1 and 2.

The indirect extended scaling laws of Ungerer et al. [34] were used to extrapolate from the experimental VLE data to the mixture critical points for the isotherms at temperatures above the solvent critical temperature. This was shown to be possible by El Ahmar and co-workers [35]. In addition to this, the mixture critical locus curves were evaluated, using the thermodynamic models, with the procedure of Heidemann and Khalil [36]. This procedure determines the stability limit for a mixture of known composition, by minimising the determinant of two simultaneous non-linear equations, which are functions of the intensive variables of the critical phase. The elements of the matrix for which the determinant is minimised, through varying the temperature, can be calculated using equation 3.

$$q_{ij} = n_T\left(\partial\, lnf_i/\partial\, n_j\right) \qquad \text{Eqn. 3}$$

However, Heidemann and Khalil altered this equation in such a manner as to ensure that convergence occurred at the higher of the possible temperature limits. This was to overcome the occurrence of multiple temperature stability limits at identical compositions. The equation used to calculate the individual elements of the matrix was therefore altered to the form given in equation 4.

$$q_{ij} = (T/100)\, n_T\left(\partial\, lnf_i/\partial\, n_j\right) \qquad \text{Eqn. 4}$$

The calculation procedure, described by Stockfleth and Dohrn [37], was used to calculate the critical locus curve, making use of a central finite difference approximation for the partial derivatives of the fugacity in Equation 4. Further to this, the critical temperature and pressure were defined as the independent variables, as opposed to the standard classification of the critical temperature and volume as the independent variables. This change in independent variables allowed the use of the existing MATLAB® code of Moodley [38] to calculate the fugacity from the thermodynamic models.

3. Results and discussion

The experimental vapour pressures of hexafluoroethane, measured using the static analytic apparatus, were compared to data obtained from literature [11, 39-43], through the use of equation of state models. Although there have been other authors who have reported on the vapour pressures of R-116, these literature sources were those in which data was reported in the temperature range examined in this study. The PR MC EOS was firstly fitted only to the literature data, in order to obtain a curve describing the saturated pressures for R-116. The experimental data was then compared to the data calculated with the model. There was a good agreement between the experimental data from this study and the PR MC EOS model fitted to the literature data. The PR EOS with the standard alpha function was also used to predict the vapour pressures of R-116. The PR EOS provided good predictions of the vapour pressure at temperatures closer to the critical point, but the prediction deteriorated at temperatures further from the critical point. This is presumably due to the use of the pure component critical properties

Table 3.
The experimental and modelled vapour pressure data, P_{exp}, for hexafluoroethane at temperatures, T, of between (273.06 and 292.07) K. Data calculated using the original PR EOS, P_{calcPR}, and the PR EOS, modified with the MC alpha function, P_{calcMC}, were both compared to the literature data.

T [a] / K	P_{exp} [b] / MPa	P_{calcPR} [c] / MPa	$(\Delta P_{PR} / P_{exp})$ [d]	P_{calcMC} [e] / MPa	$(\Delta P_{MC} / P_{exp})$ [f]
273.06	1.839	1.883	-2.42	1.850	-0.60
278.07	2.100	2.136	-1.71	2.108	-0.39
283.07	2.388	2.413	-1.03	2.393	-0.17
288.07	2.701	2.716	-0.57	2.704	-0.15
292.07	2.972	2.977	-0.17	2.974	-0.09

[a] $U(T) = 0.07$ K (coverage factor, $k = 2$)
[b] $U(P_{exp}) = 0.004$ MPa (coverage factor, $k = 2$)
[c] Calculated using the PR EOS
[d] $\Delta P_{PR} = 100 \cdot (P_{exp} - P_{calcPR})$
[e] Calculated using the PR MC EOS with the single adjustable parameter in the MC alpha function fitted to literature data [11, 39-43]
[f] $\Delta P_{MC} = 100 \cdot (P_{exp} - P_{calcMC})$

within the equation of state as the reference point. At temperatures further from this reference point, the model would therefore not perform as well and deviations between the measured data and the predicted data would increase.

Both of the modelled data sets (PR and PR MC) for R-116 are plotted on Figure 1, along with the literature data and the experimental data. The deviations between the data that was measured in this study and both the PR EOS and the PR EOS with the MC alpha function are provided in Table 3. The deviations between the data and the fitted model are presented in Figure 2, showing the good agreement of the experimental and literature data. The PR model data are independent of all experimental data other than the pure component critical properties, and will therefore not provide as good a description of the experimental data. Since the PR MC EOS model provided a better representation of the vapour pressures for R-116, this model was then fitted to both the literature and experimental data to obtain a new MC parameter. This new MC parameter was used for the regression of the binary data.

Literature data [22, 44-46] was used to obtain the single MC alpha function parameter for trifluoromethane. The three adjustable Mathias-Copeman alpha function parameters for n-heptane were fitted to vapour pressure data that was reported in literature [47-55]. The regressed MC alpha function parameters for the three pure components, and the temperature ranges for which they are applicable, are given in Table 4.

Table 4.
The Mathias-Copeman alpha function parameters, κ_i, for carbon dioxide, trifluoromethane and n-hexane, fitted to experimental and literature data within given temperature ranges, T.

Component	T / K	κ_1	κ_2	κ_3
Trifluoromethane	252.93 - 299.07 [a]	0.776	0 [b]	0 [b]
Hexafluoroethane	273.1 - 292.9 [a]	0.777	0 [b]	0 [b]
n-Heptane [c]	272.3 - 315.9	0.908	-0.265	0.729

[a] Critical temperature of the component [7, 12]
[b] Set to zero for this study.

The *P-x-x-y* data for the system of R-23 (1) and n-heptane (2) at temperatures of between (272.9 and 313.2) K are reported in Table 5. The combined expanded uncertainties in temperature, pressure and composition are reported alongside of the experimental data. Liquid-liquid immiscibility was experienced for this system for the entire temperature range investigated. Three different thermodynamic models were fitted to the experimental data. The first model was the PR EOS with classical mixing rules, and the second and third models consisted of

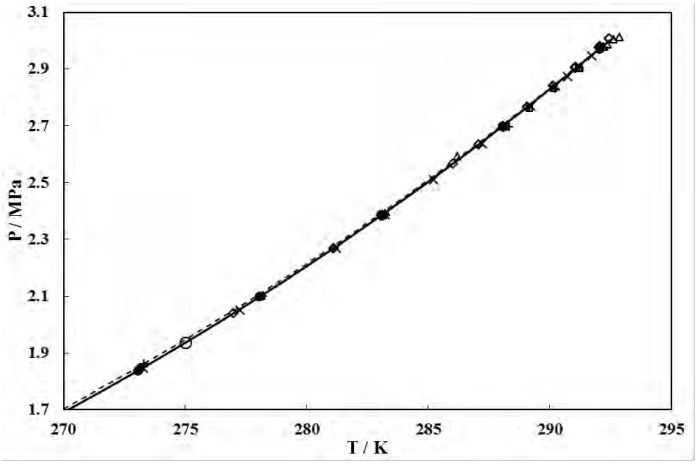

Fig. 1. Vapour pressure data for hexafluoroethane between (270 and 293.07) K. Literature data of: △ Kim [11]; □, Kao and Miller [41]; ○, Kleiber [40]; ◇, Kijima et al. [39]; +, Madania et al. [43]; and x, Valtz et al. [42]; ●, experimental data; ——, PR-MC model; - - -, PR model. model.

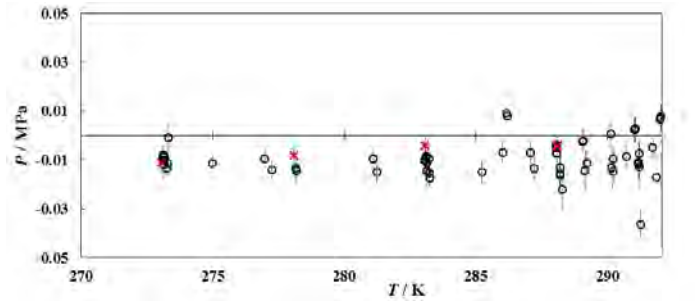

Fig. 2. Deviations of vapour pressure, P, data from the fitted PR EOS with the MC alpha function, at temperatures of between T = (270 and 293.07) K. The combined expanded uncertainties for the data are included on the plot as error bars. ×, experimental data from this study; ○, literature data [11, 39-43].

the PR EOS with the MC alpha function and the WS mixing rule, with either the NRTL activity coefficient model or the UNIQUAC activity coefficient model. All three of these models are plotted against the experimental data for this system in Figure 3.

The *P-x-x-y* data for the R-116 (1) and n-heptane (2) system at temperatures of between (293.0 and 313.2) K are reported with corresponding combined expanded uncertainties in Table 6. This system also exhibited a liquid-liquid immiscibility window, which was observable with both the (293.0 and 303.1) K isotherms. No VLLE occurred at 313.2 K. At lower pressures, it appeared that a vapour phase and a liquid phase were present within the cell, whereas at higher pressures both of the phases present in the cell appeared to be liquids. The pressure at which this transition from VLE to liquid-liquid equilibrium (LLE) occurred could not be accurately determined by visual observation. Two models are fitted to the experimental data and are plotted alongside the experimental data on Figure 4. Both models consist of the PR EOS with the MC alpha function and the WS mixing rules, but contain either the NRTL activity coefficient model or the UNIQUAC activity coefficient model. The PR MC EOS model with classical mixing rule is also fitted to the experimental data, but these curves are not plotted on Figure 3, due to the very poor description of the system behaviour.

Table 7 and 8 contain the experimental bubble pressure data measured using the variable volume cell. These measurements were performed in order to verify the *P-x-x-y* data measured with the static-analytic apparatus. The bubble pressure data for R-23 and n-heptane, listed in Table 7, are also plotted on Figure 3. The bubble pressure data and the VLE data agreed with one another very closely. For R-116 and

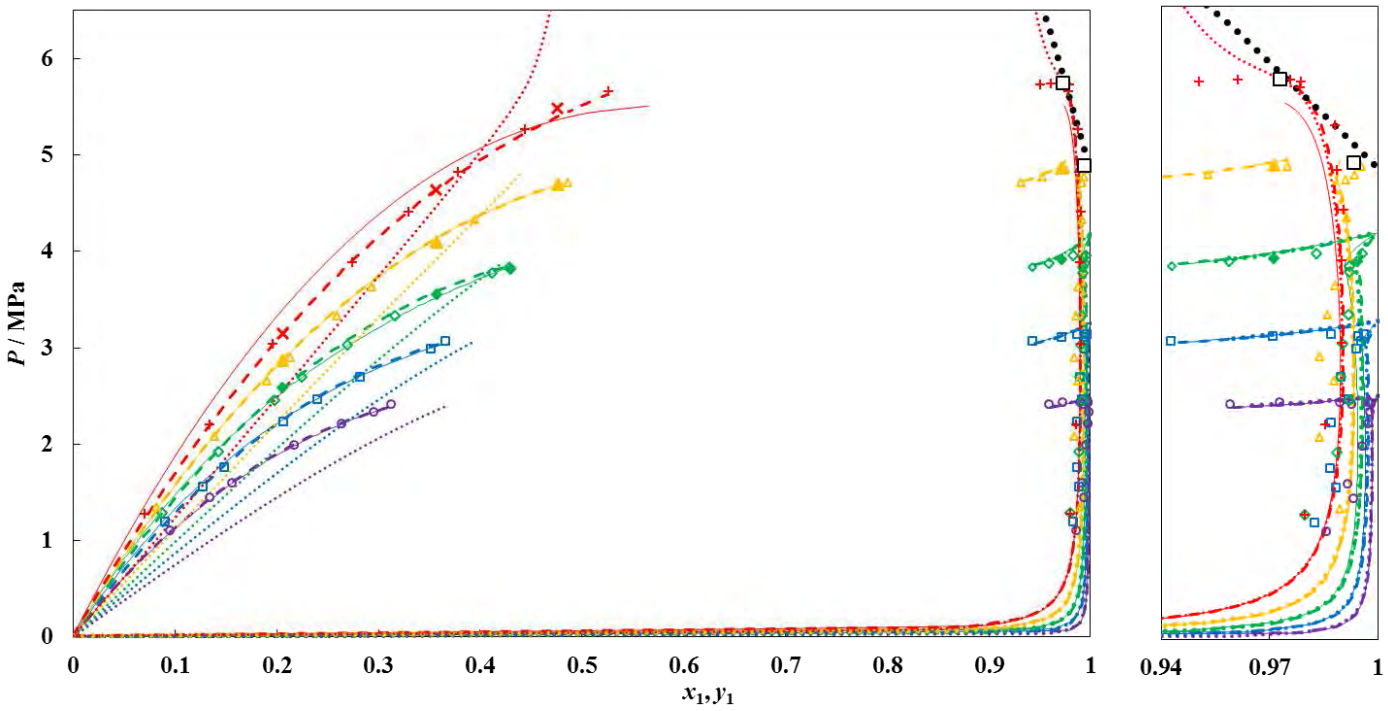

Fig. 3. *P-x-x-y* data for the binary system of trifluoromethane (1) + n-heptane (2), measured using a static analytic apparatus, at temperatures of: ○, 272.9 K; □, 283.0 K; ◇, 293.0 K; △, 303.1 K; +, 313.2 K. *P-x* data measured, using a variable volume apparatus, at temperatures of: ◆, 293.0 K; ▲, 303.1 K; X, 313.2 K. Solid lines, PRMC WS + (NRTL) model; dashed lines, PRMC WS + (UNIQUAC) model; dotted lines, PR EOS model; □, extrapolated critical loci; ••••, calculated critical locus curve.

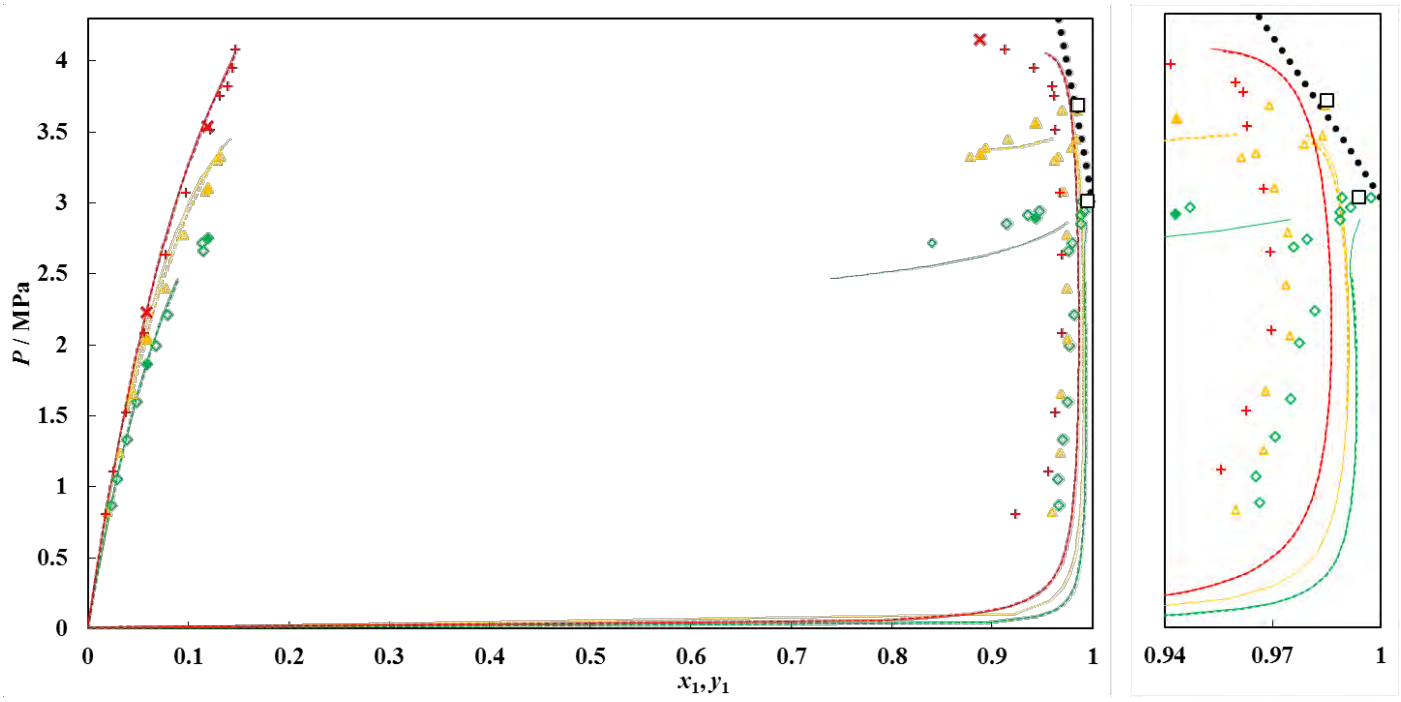

Fig. 4. *P-x-x-y* data for the binary system of hexafluoroethane (1) + n-heptane (2) measured using a static analytic apparatus, at temperatures of: ◇, 293.0 K; △, 303.1 K; +, 313.2 K. *P-x* data measured, using a variable volume apparatus, at temperatures of: ◆, 293.0 K; ▲, 303.1 K; X, 313.2 K. Solid lines, PRMC WS + (NRTL) model; dashed line, PRMC WS + (UNIQUAC) model; □, extrapolated critical points; ••••, calculated critical locus curve.

n-heptane, the bubble pressure data that are reported in Table 8 are plotted alongside the experimental data measured with the static-analytic apparatus on Figure 4. There was a good agreement between the two data sets.

The parameters of the three thermodynamic models for (R-23 and n-heptane) are given in Table 9 and those for (R-116 and n-heptane) are given in Table 10. The ARD and the AARD for pressure and vapour phase composition are also included in these tables. The statistics of the regression for the PR MC EOS model with classical mixing rules give a picture of a poor fit of the model. This is confirmed by observing the plot of the PR MC EOS model on Figure 3. The fit of the PR MC EOS model to the experimental data for R-116 and n-heptane was even worse than that of the R-23 and n-heptane, and it was therefore not included in Figure 4.

The fit of the other two models were very similar, with neither model providing an obviously superior fit to the experimental data. However, at 313.2 K, the PR MC + WS/UNIQUAC model provided a markedly better description of the R-23 + n-heptane experimental data than the PR MC + WS/NRTL model. This can be observed from the statistical analysis as well as by observing the plotted data (Figure 2).

Table 5.
Experimental P-x_1^I-x_1^{II}-y_1 data, with combined expanded uncertainties, U, calculated with a coverage factor of $k = 2$, for the binary system of R-23 (1) + n-heptane (2) at temperatures, T = (272.9 to 313.2) K.

T / K	U (T) / K	P/ MPa	U(P) / MPa	x_1^I	U (x_1^I)	x_1^{II}	U (x_1^{II})	y_1	U(y_1)
272.89	0.06	1.108	0.009	0.095	0.004			0.986	0.0019
272.88	0.08	1.453	0.010	0.134	0.003			0.993	0.0027
272.88	0.06	1.604	0.008	0.156	0.005			0.992	0.0020
272.87	0.08	1.994	0.010	0.217	0.005			0.996	0.0020
272.89	0.09	2.215	0.009	0.264	0.005			0.997	0.0008
272.88	0.08	2.338	0.006	0.295	0.005			0.998	0.0005
272.88	0.09	2.428	0.004	0.312	0.003	0.959	0.006	0.995	0.0021
272.87	0.09	2.436	0.004	0.973	0.004			0.997	0.0005
272.88	0.09	2.440	0.004	0.989	0.001			0.998	0.0001
282.96	0.08	1.198	0.008	0.090	0.003			0.983	0.0018
282.95	0.08	1.559	0.004	0.127	0.004			0.988	0.0015
282.96	0.08	1.763	0.008	0.149	0.004			0.987	0.0005
282.96	0.08	2.232	0.008	0.207	0.005			0.987	0.0016
282.96	0.09	2.471	0.007	0.239	0.006			0.992	0.0031
282.95	0.08	2.701	0.009	0.282	0.006			0.990	0.0011
282.98	0.08	2.986	0.009	0.352	0.007			0.994	0.0007
282.97	0.08	3.063	0.005	0.366	0.007	0.943	0.003	0.995	0.0008
282.96	0.08	3.114	0.004	0.971	0.003			0.995	0.0016
282.96	0.08	3.138	0.004	0.987	0.002			0.996	0.0012
293.03	0.07	1.283	0.009	0.087	0.004			0.980	0.0023
293.04	0.07	1.923	0.004	0.143	0.005			0.989	0.0029
293.04	0.07	2.456	0.007	0.198	0.005			0.992	0.0008
293.04	0.07	2.698	0.006	0.225	0.006			0.990	0.0018
293.03	0.07	3.032	0.007	0.269	0.006			0.990	0.0017
293.06	0.07	3.333	0.007	0.316	0.006			0.992	0.0014
293.04	0.07	3.775	0.006	0.412	0.007			0.992	0.0021
293.04	0.07	3.833	0.005	0.429	0.007	0.943	0.003	0.992	0.0014
293.02	0.07	3.879	0.004	0.959	0.003			0.994	0.0009
293.04	0.07	3.959	0.004	0.983	0.002			0.996	0.0006
303.10	0.08	1.344	0.010	0.082	0.004			0.989	0.0016
303.11	0.08	2.081	0.009	0.139	0.004			0.984	0.0020
303.11	0.08	2.661	0.010	0.190	0.006			0.988	0.0008
303.12	0.08	2.902	0.008	0.213	0.005			0.984	0.0018
303.10	0.08	3.336	0.007	0.259	0.006			0.986	0.0014
303.11	0.08	3.632	0.005	0.293	0.006			0.988	0.0015
303.11	0.08	4.327	0.008	0.395	0.008			0.991	0.0006
303.12	0.08	4.716	0.005	0.486	0.008	0.931	0.003	0.991	0.0016
303.11	0.08	4.771	0.004	0.953	0.003			0.994	0.0010
303.12	0.08	4.857	0.004	0.975	0.002			0.995	0.0005
313.21	0.08	1.278	0.005	0.071	0.002			0.980	0.0020
313.21	0.09	2.208	0.007	0.134	0.004			0.985	0.0018
313.20	0.09	3.044	0.006	0.196	0.005			0.990	0.0019
313.20	0.09	3.889	0.010	0.274	0.006			0.990	0.0021
313.20	0.09	4.410	0.006	0.329	0.006			0.991	0.0010
313.20	0.10	4.821	0.004	0.378	0.008			0.989	0.0016
313.20	0.09	5.273	0.010	0.444	0.007			0.988	0.0014
313.20	0.10	5.663	0.006	0.526	0.008			0.978	0.0009
313.19	0.08	5.728	0.008	0.542	0.007	0.950	0.004	0.979	0.0014
313.20	0.08	5.742	0.010	0.961	0.002			0.976	0.0017

Table 6.
Experimental P-x_1^I-x_1^{II}-y_1- data, with combined expanded uncertainties, U, calculated with a coverage factor of $k = 2$, for the binary system of R-116 (1) + n-heptane (2) for temperatures, T = (293.0 to 313.2) K.

T / K	U(T) /K	P/ MPa	U(P)/ MPa	x_1^I	U (x_1^I)	x_1^{II}	U (x_1^{II})	y_1	U(y_1)
293.04	0.07	0.872	0.005	0.023	0.001			0.966	0.002
293.03	0.07	1.054	0.005	0.029	0.002			0.965	0.002
293.03	0.07	1.335	0.006	0.039	0.002			0.971	0.003
293.05	0.07	1.597	0.005	0.049	0.002			0.975	0.003
293.05	0.07	1.996	0.007	0.068	0.003			0.977	0.002
293.04	0.07	2.214	0.009	0.080	0.002			0.982	0.002
293.04	0.07	2.664	0.005	0.115	0.004			0.976	0.003
293.04	0.07	2.717	0.005	0.114	0.003	0.841	0.004	0.980	0.002
293.05	0.08	2.854	0.004	0.915	0.003			0.989	0.002
293.05	0.08	2.912	0.003	0.936	0.003			0.989	0.002
293.05	0.07	2.942	0.006	0.947	0.002			0.992	0.002
293.05	0.07	3.011	0.005	0.989	0.001			0.997	0.001
303.11	0.05	0.820	0.004	0.020	0.001			0.960	0.002
303.11	0.06	1.239	0.006	0.032	0.001			0.968	0.002
303.11	0.05	1.657	0.009	0.046	0.001			0.968	0.002
303.11	0.05	2.040	0.007	0.061	0.002			0.975	0.002
303.11	0.05	2.399	0.011	0.077	0.003			0.974	0.003
303.10	0.05	2.770	0.004	0.096	0.003			0.974	0.002
303.10	0.05	3.077	0.006	0.117	0.003			0.971	0.002
303.12	0.05	3.295	0.008	0.130	0.004			0.961	0.002
303.12	0.07	3.325	0.004	0.132	0.004	0.878	0.004	0.965	0.001
303.14	0.06	3.385	0.006	0.894	0.007			0.979	0.003
303.13	0.06	3.448	0.004	0.916	0.003			0.984	0.001
303.13	0.05	3.653	0.006	0.969	0.002			0.985	0.001
313.22	0.04	0.807	0.006	0.018	0.001			0.923	0.003
313.22	0.04	1.108	0.006	0.025	0.001			0.956	0.002
313.22	0.04	1.521	0.005	0.037	0.002			0.963	0.002
313.21	0.05	2.082	0.005	0.056	0.002			0.970	0.002
313.21	0.04	2.632	0.006	0.078	0.004			0.970	0.003
313.23	0.05	3.074	0.006	0.098	0.004			0.968	0.003
313.23	0.04	3.517	0.004	0.121	0.004			0.963	0.008
313.23	0.04	3.753	0.006	0.131	0.005			0.962	0.002
313.22	0.05	3.822	0.011	0.139	0.004			0.960	0.002
313.23	0.05	3.948	0.006	0.144	0.004			0.942	0.003
313.22	0.05	4.084	0.005	0.147	0.002			0.913	0.001

Table 7.
Experimental bubble point P-x_1 data, with combined expanded uncertainties, U, calculated with a coverage factor, $k = 2$, for the binary system of R-23 (1) + n-heptane (2) at temperatures, T = (293.2 to 313.2) K.

T / K	U(T) / K	P / MPa	U(P) / MPa	x_1	U(x_1)
293.20	0.03	2.586	0.006	0.206	0.0004
293.17	0.04	3.557	0.008	0.357	0.0002
293.17	0.03	3.820	0.004	0.430	0.0002
293.17	0.03	3.915	0.005	0.971	0.0017
303.21	0.03	2.870	0.007	0.206	0.0004
303.18	0.04	4.101	0.008	0.357	0.0002
303.18	0.04	4.695	0.005	0.476	0.0005
303.19	0.03	4.864	0.005	0.971	0.0017
313.23	0.03	3.149	0.008	0.206	0.0004
313.21	0.04	4.642	0.007	0.357	0.0002
313.23	0.03	5.486	0.004	0.476	0.0002

The models, using either the NRTL or the UNIQUAC activity coefficient models, were regressed to each individual isotherm with temperature independent parameters, as well as to the entire system data set with temperature dependent parameters. The temperature dependent and temperature independent parameters for R-23 + n-heptane are plotted in Figure 5, and for R-116 + n-heptane in Figure 6. There was a better correlation of the models fitted to each isotherm individually than those fitted with temperature dependent parameters. From Figure 5, the different trends of the parameters, both above and below the critical temperature of the pure refrigerant, can be observed. For the model containing the NRTL activity coefficient model, there was a substantial difference in the trends of these parameters. The differing trends are likely the reason for the better fit of the models to the experimental data when regressed for each isotherm individually. The model containing the UNIQUAC activity coefficient model does not; however, appear to suffer from this phenomenon of differing trends above and below the critical temperature.

Table 8.
Experimental bubble point P-x_1 data, with combined expanded uncertainties, U, calculated with a coverage factor, $k = 2$, for the binary system of R-116 (1) + n-heptane (2) at temperatures of between T = (293.0 to 313.2) K.

T / K	U(T) / K	P / MPa	U(P) / MPa	x_1	U(x_1)
293.04	0.03	1.864	0.005	0.059	0.0002
293.04	0.03	2.748	0.004	0.120	0.0002
293.03	0.03	2.894	0.004	0.943	0.0077
303.22	0.04	2.044	0.005	0.059	0.0002
303.06	0.04	3.105	0.005	0.120	0.0002
303.14	0.03	3.344	0.004	0.888	0.0017
303.15	0.03	3.565	0.004	0.943	0.0077
313.17	0.03	2.227	0.006	0.059	0.0002
313.18	0.04	3.542	0.005	0.120	0.0002
313.17	0.04	4.151 [a]	0.006	0.888	0.0017

[a] liquid-liquid equilibrium miscibility pressure

From the experimental VLE data at temperatures greater than the critical temperature of the more volatile component, the critical point loci were extrapolated by the method of Ungerer et al. [34]. These extrapolated critical loci are included on Figure 3 and 3 for the R-23 + n-heptane and R-116 + n-heptane systems respectively. The "bird's-beak" behaviour of some of the isotherms reduced the number of data points that could be used to extrapolate to the mixture critical point for each isotherm, and the accuracy of this method was therefore diminished. The Ungerer et al. method could also not be applied in cases where liquid-liquid critical points occurred [56]. Liquid-liquid critical points occurred at temperatures above the upper critical end point (UCEP), which, for both of these systems, occurred at a temperature of between 303.1 and 313.2 K.

Table 9.
For the system of R-23 (1) + n-heptane (2), the temperature independent and temperature dependent parameters for the PR model (k_{12}), the PRMC + WS/NRTL model (k_{12} and τ_{ij}) and the PRMC + WS/UNIQUAC model (k_{12} and Δu_{ij}), with regression statistics. The ARD and the AARD for the pressure, P, and vapour phase composition, y, are reported for each temperature, T, or temperature range.

T / K	k_{12}	τ_{12} / K [a] || Δu_{12} [b] / J·mol^{-1}	τ_{21} / K [a] || Δu_{21} [b] / J·mol^{-1}	ARD [c]		AARD [d]	
				P	y	P	y
PR-MC							
(272.9 – 313.2)	0.190	-	-	10.88	-0.17	12.33	0.53
PR-MC + WS/NRTL							
272.9	0.488	1569.8	386.13	1.75	-0.26	1.82	0.33
283.0	0.476	1690.1	365.18	-0.34	-0.50	0.74	0.51
293.0	0.471	1960.3	376.22	-0.38	-0.20	0.74	0.42
303.1	0.588	639.94	211.32	-0.32	-0.24	0.69	0.44
313.2	0.591	606.63	196.01	1.10	-0.04	1.16	0.23
(272.9 – 313.2)	0.563	662.07	244.25	2.01	0.63	4.28	1.26
PR-MC + WS/UNIQUAC							
272.9	0.610	255.26	3289.9	1.41	-0.47	1.50	0.47
283.0	0.595	255.21	3260.9	0.46	-0.58	0.76	0.58
293.0	0.602	122.93	3339.6	-0.62	-0.44	0.95	0.44
303.1	0.587	145.43	3284.4	-0.25	-0.16	0.73	0.45
313.2	0.589	47.20	3334.7	0.83	0.09	0.90	0.30
(272.9 – 313.2)	0.580	33.24	3552.2	1.64	0.58	3.62	1.22

[a] τ_{12}, τ_{21} for the NRTL activity coefficient model
[b] Δu_{12}, Δu_{21} for the UNIQUAC activity coefficient model

[c] average relative deviation, $$ARD(\theta) = \frac{100}{N_p}\sum_{1}^{N_p}\frac{\theta_{exp} - \theta_{calc}}{\theta_{exp}}$$

[d] absolute average relative deviation, $$AARD(\bar{\theta}) = \frac{100}{N_p}\sum_{1}^{N_p}\frac{|\bar{\theta}_{exp} - \bar{\theta}_{calc}|}{\bar{\theta}_{exp}}$$

The critical locus curves for both systems were also calculated, at refrigerant compositions of between 0.85 and 1.0, from the temperature dependent model parameters. These critical locus curves are also plotted on the corresponding P-x-y plot (either Figure 3 or 3). Both the extrapolated critical loci and the calculated critical locus curves are reported in Table 11. The critical locus curves agree very closely with the models from which they were determined. Unfortunately there are discrepancies between the experimental data and these thermodynamic models, and this translates into discrepancies between the critical locus curves and the experimental data. Examples of these discrepancies can be observed on both Figure 2 and Figure 3. Several of the experimentally measured vapour phase points occur slightly outside of the calculated heterogeneous subcritical region, meaning that the calculated pressure for the critical locus curve was in fact too low. Despite these deficiencies, the calculation does still provide a useful estimation of the critical locus curve, with the deficiencies being due to the fit of the thermodynamic model rather than due to the calculation procedure.

The R-23 + n-heptane system exhibited a gas-liquid critical line from the R-23 critical point to an UCEP, as well as a liquid-liquid critical line beyond the UCEP. The range in which the experimental study was undertaken did not allow the critical line moving from the critical point of n-heptane to be characterised. However, based on the first two critical lines, and the fact that there does not appear to be a discontinuity in the three phase line, this system can be classified as a van Konynenburg and Scott [57] type III system. The same characteristics were present for the R-116 + n-heptane system, although the gas-liquid critical line between the critical point of R-116 and the UCEP comprised a very short section. The R-116 + n-heptane system was therefore also classified as a van Konynenburg and Scott type III system.

4. Conclusions

The VLE and VLLE for the system of trifluoromethane (1) + n-heptane (2) was measured with a static-analytic phase equilibrium apparatus at temperatures of between (272.9 and 313.2) K. This equipment was also used to measure the VLE and VLLE for the hexafluoroethane (1) + n-heptane (2) at temperatures of between (293.0 and 313. 2) K. Bubble pressure data was measured for both systems with a variable volume phase equilibrium apparatus at temperatures of between (293.0

Table 10.
For the system of hexafluoroethane (1) + n-heptane (2), the temperature independent and temperature dependent parameters for the PRMC + WS/NRTL model (k_{12} and τ_{ij}) and the PRMC + WS/UNIQUAC model (k_{12} and Δu_{ij}), with regression statistics. The ARD and the AARD for the pressure, P, and vapour phase composition, y, are reported for each temperature, T, or temperature range.

T / K	k_{12}	τ_{12} / K [a] || Δu_{12} [b] / J·mol^{-1}	τ_{21} / K [a] || Δu_{21} [b] / J·mol^{-1}	ARD		AARD	
				P	y	P	y
PRMC							
(293.0 – 313.2)	0.270	-	-	-16.14	8.28	38.63	11.02
PRMC + WS/NRTL							
293.0	0.430	190.16	795.16	1.32	0.03	2.95	2.19
303.1	0.492	130.11	822.02	-1.75	-0.32	3.53	1.71
313.2	0.480	141.20	822.84	-1.08	-1.63	2.38	2.22
(293.0 – 313.2)	0.479	160.25	788.84	0.99	0.94	2.68	3.93
PRMC + WS/UNIQUAC							
293.0	0.447	1058.8	-4199.9	1.29	-1.30	2.50	1.31
303.1	0.498	1173.9	-4329.9	0.26	-0.87	1.61	1.16
313.2	0.482	1182.7	-4366.5	-0.91	-2.12	2.19	2.69
(293.0 – 313.2)	0.493	1115.1	-4176.1	1.21	-1.33	3.85	1.51

[a] τ_{12}, τ_{21} for the NRTL activity coefficient model
[b] Δu_{12}, Δu_{21} for the UNIQUAC activity coefficient model

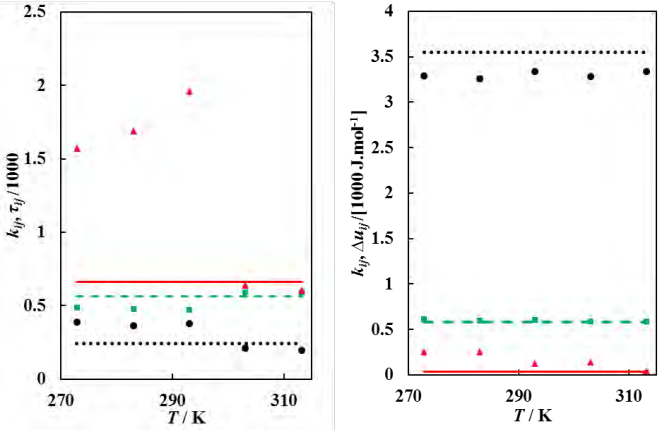

Fig. 5. The PRMC WS + (NTRL/UNIQUAC) parameters for the trifluoromethane (1) + n-heptane (2) binary system. Symbols represent parameters regressed independently for each isotherm, while lines represent parameters regressed for all isotherms simultaneously. *Left*: (NRTL) ■/- - -, k_{12}; ●/·····, τ_{12}; ▲/——, τ_{21}. *Right*: (UNIQUAC) ■/- - -, k_{12}; ●/·····, Δu_{12}; ▲/——, Δu_{21}.

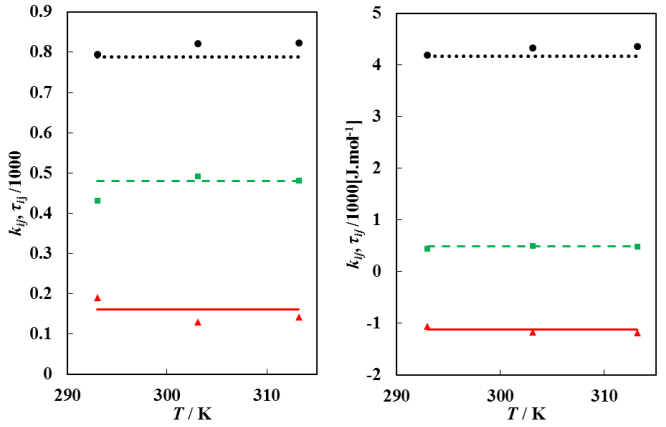

Fig. 6. The PRMC WS + (NTRL/UNIQUAC) parameters for the hexafluoroethane (1) + n-heptane (2) binary system. Symbols represent parameters regressed independently for each isotherm, while lines represent parameters regressed for all isotherms simultaneously. *Left*: (NRTL) ■/- - -, k_{12}; ●/·····, τ_{12}; ▲/——, τ_{21}. *Right*: (UNIQUAC) ■/- - -, k_{12}; ●/·····, Δu_{12}; ▲/——, Δu_{21}.

and 313.2) K. This bubble pressure data verified the accuracy of the VLE data measured with the static-analytic apparatus.

The PR MC EOS with classical mixing rules was used to model the system, but this model did not provide a good description of the system. The VLLE pressures and compositions description was found to be poor. The PR EOS with the MC alpha function modification along with the WS mixing rule was therefore used to model the system. The NRTL and the UNIQUAC activity coefficient models were both used within the WS mixing rule, with the UNIQUAC model slightly outperforming the NRTL model.

Critical loci were extrapolated from the experimental data by the method of Ungerer and co-workers for all measured temperatures at which vapour-liquid critical loci occurred. Additionally, the critical locus curves were calculated from the thermodynamic models. These curves were affected by the inferior performance of the thermodynamic models at near-critical conditions. The critical locus curves remained good approximations of the mixture critical loci despite these limitations. Based upon their characteristics within the investigated temperature ranges, both systems were estimated to be van Konynenburg and Scott type IV systems.

Table 11.
Critical loci (T_c-P_c-x_c data) extrapolated from experimental data by the method of Ungerer et al. [34], and calculated from thermodynamic models by the method of Heidemann and Khalil [36].

Method of Ungerer et al.			Method of Heidemann and Khalil		
T_c	P_c	$x_{c,1}$	T_c	P_c	$x_{c,1}$
R-23 (1) + n-heptane (2)					
303.1	4.90	0.993	302.1	5.21	0.99
313.2	5.76	0.973	317.5	6.28	0.96
			340.0	7.22	0.93
			369.3	8.41	0.90
			434.6	10.21	0.85
R-116 (1) + n-heptane (2)					
293.1	3.02	0.994	300.0	3.41	0.99
303.1	3.69	0.985	313.5	4.51	0.96
			333.3	5.45	0.93
			368.7	6.75	0.90
			427.0	8.71	0.85

Acknowledgements

This work is based upon research supported by the South African Research Chairs Initiative of the Department of Science and Technology and the National Research Foundation.

References

[1] Knox, D.E. Solubilities in Supercritical Fluids. Pure Appl. Chem. 2005, 77 (3), 513-530.

[2] Kiran, E.; Brunner, G.; Smith Jr, R.L. The 20th anniversary of the Journal of Supercritical Fluids–A special issue on future directions in supercritical fluid science and technology. J. Supercritical Fluids 2009, 47 (3), 333-335.

[3] Herrero, M.; Mendiola, J.A.; Cifuentes, A.; Ibáñez, E. Supercritical fluid extraction: Recent advances and applications. J. Chromatography A 2010, 1217 (16), 2495-2511.

[4] Sheng, Y.J.; Chen, P.C.; Chen, Y.P.; Wong, D.S.H. Calculations of solubilities of aromatic compounds in supercritical carbon dioxide. Ind. Eng. Chem. Res. 1992, 31 (3), 967-973.

[5] Beckman, E.J. Supercritical and near-critical CO2 in green chemical synthesis and processing. J. Supercrit. Fluids 2004, 28 (2–3), 121-191.

[6] Kordikowski, A.; Schneider, G.M. Fluid phase equilibria of binary and ternary mixtures of supercritical carbon dioxide with low-volatility organic substances up to 100 MPa and 393 K. Fluid Phase Equilib. 1993, 90 (1), 149-162.

[7] Lide, D.R., CRC Handbook of Chemistry and Physics 2004-2005, CRC Press LLC: Boca Raton, USA, 2004.

[8] The Montreal Protocol On Substances That Deplete The Ozone Layer, Ozone Secretariat, U.N.E.P., Editor 2008, United Nations Environment Programme: Montreal, Canada.

[9] National Fire Protection Association Safety Data Sheet, Halocarbon R1132a (1,1 Difluoroethylene). 1997.

[10] Mangena, M., Fluorochemical Expansion Initiative Launch, Department of Science and Technology, Editor 2009: Pretoria, South Africa.

[11] Kim, K.Y., 1974. Calorimetric studies on argon and hexafluoroethane and a generalized correlation of maxima in isobaric heat capacity, Thesis, University of Michigan,

[12] Saikawa, K.; Kijima, J.; Uematsu, M.; Watanabe, K. Determination of the critical temperature and density of hexafluoroethane. J. Chem. Eng. Data 1979, 24 (3), 165-167.

[13] O'Brien, R.N.; Quon, D. Refractive index of some alcohols and saturated hydrocarbons at 6328 A. J. Chem. Eng. Data 1968, 13 (4), 517-517.

[14] Ortega, J.; Matos, J.S. Mater. Chem. Phys. 1986, 15, 415.

[15] Garcia, I.; Cobos, J.C.; Gonzalez, J.A.; Casanova, C.; Cocero, M.J. Thermodynamics of binary mixtures containing organic carbonates. 1. Excess enthalpies of dimethyl carbonate + hydrocarbons or + tetrachloromethane. J. Chem. Eng. Data 1988, 33 (4), 423.

[16] Aminabhavi, T.M.; Aralaguppi, M.I.; Bindu, G.; Khinnavar, R.S. Densities, Shear Viscosities, Refractive Indices, and Speeds of Sound of Bis(2-methoxyethyl) Ether with Hexane, Heptane, Octane, and 2,2,4-Trimethylpentane in the Temperature Interval 298.15-318.15 K. J. Chem. Eng. Data 1994, 39 (3), 522-528.

[17] Aucejo, A.; Burguet, M.C.; Munoz, R.; Marques, J.L. Densities, Viscosities, and Refractive Indices of Some n-Alkane Binary Liquid Systems at 298.15 K. J. Chem. Eng. Data 1995, 40 (1), 141-147.

[18] Aminabhavi, T.M.; Patil, V.B.; Aralaguppi, M.I.; Phayde, H.T.S. Density, Viscosity, and Refractive Index of the Binary Mixtures of Cyclohexane with Hexane, Heptane, Octane, Nonane, and Decane at (298.15, 303.15, and 308.15) K. J. Chem. Eng. Data 1996, 41 (3), 521-525.

[19] Chorążewski, M. Thermophysical and Acoustical Properties of the Binary Mixtures 1,2-Dibromoethane + Heptane within the Temperature Range from 293.15 K to 313.15 K. J. Chem. Eng. Data 2006, 52 (1), 154-163.

[20] Blanco, A.; Gayol, A.; Gómez-Díaz, D.; Navaza, J.M. Density, speed of sound, refractive index and derivatives properties of the binary mixture n-hexane + n-heptane (or n-octane or n-nonane), T = 288.15 - 313.15 K. J. Phys. Chem. Liq. 2013, 51 (3), 404-413.

[21] Narasigadu, C.; Naidoo, P.; Coquelet, C.; Richon, D.; Ramjugernath, D. A novel static analytical apparatus for phase equilibrium measurements. Fluid Phase Equilibr. 2013, 338, 188-196.

[22] Williams-Wynn, M.D.; Naidoo, P.; Ramjugemath, D. 1. Isothermal vapour-liquid equilibrium data for the binary systems of (CO2 + n-hexane) and (CHF3 + n-hexane). J. Chem. Thermodyn. 2015, unpublished.

[23] Kalra, H.; Kubota, H.; Robinson, D.B.; Ng, H.-J. Equilibrium phase properties of the carbon dioxide-n-heptane system. J. Chem. Eng. Data 1978, 23 (4), 317-321.

[24] Brunner, G.; Teich, J.; Dohrn, R. Phase equilibria in systems containing hydrogen, carbon dioxide, water and hydrocarbons. Fluid Phase Equilib. 1994, 100, 253-268.

[25] Besserer, G.J.; Robinson, D.B. Equilibrium-phase properties of isobutane-carbon dioxide system. J. Chem. Eng. Data 1973, 18 (3), 298-301.

[26] Taylor, B.N.; Kuyatt, C.E. Guidelines for Evaluating and Expressing the Uncertainty of NIST Measurement Results. NIST Technical Note 1994, 1297.

[27] Taylor, B.N.; Mohr, P.J.; Douma, M., The NIST Reference on constants, units, and uncertainty, 2007.

[28] Peng, D.Y.; Robinson, D.B. A New Two-Constant Equation of State. Ind. Eng. Chem. Fundam. 1976, 15, 59-64.

[29] Mathias, P.M.; Copeman, T.W. Extension of the Peng-Robinson Equation of State to Complex Mixtures: Evaluation of the Various Forms of the Local Composition Concept. Fluid Phase Equilib. 1983, 13, 91-108.

[30] Wong, D.S.H.; Sandler, S.I. Theoretically Correct Mixing Rule for Cubic Equations of State. AIChE J. 1992, 38, 671-680.

[31] Renon, H.; Prausnitz, J.M. Local Compositions in Thermodynamic Excess Functions for Liquid Mixtures. AIChE J. 1968, 14, 135-144.

[32] Abrams, D.S.; Prausnitz, J.M. Statistical thermodynamics of liquid mixtures: A new expression for the excess Gibbs energy of partly or completely miscible systems. AIChE J. 1975, 21 (1), 116-128.

[33] Aspen Technology Aspen Plus V8.4. 2012.

[34] Ungerer, P.; Tavitian, B.; Boutin, A., Applications of molecular simulation in the oil and gas industry- Monte Carlo methods, IFP Publications, 2005.

[35] El Ahmar, E.; Valtz, A.; Naidoo, P.; Coquelet, C.; Ramjugernath, D. Isothermal Vapor−Liquid Equilibrium Data for the Perfluorobutane (R610) + Ethane System at Temperatures from (263 to 353) K. J. Chem. Eng. Data 2011, 56 (5), 1918-1924.

[36] Heidemann, R.A.; Khalil, A.M. The calculation of critical points. AIChE J. 1980, 26 (5), 769-779.

[37] Stockfleth, R.; Dohrn, R. An algorithm for calculating critical points in multicomponents mixtures. Fluid Phase Equilibr. 1998, 45, 43-52.

[38] Moodley, K., 2002. High-pressure Vapour-liquid Equilibrium Studies at Low Temperatures, Ph.D Thesis, University of Natal,

[39] Kijima, J.; Saikawa, K.; Watanabe, K.; Oguchi, K.; Tanishita, I. Experimental study of thermodynamic properties of hexafluoroethane (R116) 1977. New York: ASME.

[40] Kleiber, M. Vapor-liquid equilibria of binary refrigerant mixtures containing propylene or R134a. Fluid Phase Equilib. 1994, 92, 149-194.

[41] Kao, C.-P.C.; Miller, R.N. Vapor Pressures of Hexafluoroethane and Octafluorocyclobutane. J. Chem. Eng. Data 2000, 45 (2), 295-297.

[42] Valtz, A.; Coquelet, C.; Richon, D. Vapor-liquid equilibrium data for the hexafluoroethane + carbon dioxide system at temperatures from 253 to 297 K and pressures up to 6.5 MPa. Fluid Phase Equilibr. 2007, 258 (2), 179-185.

[43] Madani, H.; Valtz, A.; Coquelet, C.; Meniai, A.H.; Richon, D. Vapour-Liquid Equilibrium Data for the (Hexafluoroethane + 1,1,1,2-Tetrafluoroethane) System at Temperatures from 263 to 353 K and Pressures up to 4.16 MPa. Fluid Phase Equilibr. 2008, 268, 68-73.

[44] Hou, Y.C.; Martin, J.J. Physical and thermodynamic properties of trifluoromethane. AIChE J. 1959, 5 (1), 125-129.

[45] Rasskazov, D.S.; Petrov, E.K.; Spiridonov, G.A.; Ushmajkin, E.R. Investigation of P-V-T Data of Freon 31. Teplofiz. Svoistva Veshchestv Mater. 1975, 8, 4-16.

[46] Hori, K.; Okazaki, S.; Uematsu, M.; Watanabe, K. An Experimental Study of Thermodynamic Properties of Trifluoromethane. Proc. Symp. Thermophys. Prop. 1982. Gaithersburg: ASME.

[47] Young, S. LXX.-The vapour pressures, specific volumes, and critical constants of normal heptane. J. Chem. Soc. Trans. 1898, 73, 675-681.

[48] Young, S. On the Boiling Points of the Normal Paraffins at Different Pressures. Proc. Roy. Irish Acad. B 1928, 38, 65-92.

[49] Forziati, A.F.; Norris, W.R.; Rossini, F.D. Vapor pressures and boiling points of sixty API-NBS hydrocarbons. J. Res. Nat. Bur. Stand. 1949, 43 (6), 555-564.

[50] Van Ness, H.C.; Soczek, C.A.; Peloquin, G.L.; Machado, R.L. Thermodynamic excess properties of three alcohol-hydrocarbon systems. J. Chem. Eng. Data 1967, 12 (2), 217-224.

[51] Pividal, K.A.; Sterner, C.; Sandler, S.I.; Orbey, H. Vapor-liquid equilibrium from infinite dilution activity coefficients: measurement and prediction of oxygenated fuel additives with alkanes. Fluid Phase Equilibr. 1992, 72, 227-250.

[52] Lozano, L.M.; Montero, E.A.; Martín, M.C.; Villamañán, M.A. Vapor-liquid equilibria of binary mixtures containing methyl tert-butyl ether (MTBE) and/or substitution hydrocarbons at 298.15 K and 313.15 K. Fluid Phase Equilibr. 1995, 110 (1–2), 219-230.

[53] Dahmani, A.; Kaci, A.A.; Jose, J. Vapour pressures and excess functions of 1,4-dimethylpiperazine + n-heptane, or cyclohexane measurement and prediction. Fluid Phase Equilibr. 1997, 134 (1–2), 255-265.

[54] Rhodes, J.M.; Bhethanabotla, V.R.; Campbell, S.W. Total Vapor Pressure Measurements for Heptane + 1-Pentanol, + 2-Pentanol, + 3-Pentanol, + 2-Methyl-1-butanol, + 2-Methyl-2-butanol, + 3-Methyl-1-butanol, and + 3-Methyl-2-butanol at 313.15 K. J. Chem. Eng. Data 1997, 42 (4), 731-734.

[55] Negadi, L.; Belabbaci, A.; Ait Kaci, A.; Jose, J. Isothermal Vapor−Liquid Equilibria and Excess Enthalpies of (Propyl Ethanoate + Heptane), (Propyl Ethanoate + Cyclohexane), and (Propyl Ethanoate + 1-Hexene). J. Chem. Eng. Data 2007, 52 (1), 47-55.

[56] O'Connell, J.P.; Haile, J.M., Thermodynamics: Fundamentals for Applications, Cambridge University Press, 2005.

[57] van Konynenburg, P.H.; Scott, R.L. Critical Lines and Phase Equilibria in Binary Van Der Waals Mixtures. Philos. Trans. R. Soc. London, Ser. A 1980, 298, 495-540.

APPENDIX E

Isothermal vapour-liquid equilibrium data for the binary systems of (CHF_3 or C_2F_6) and n-octane

Mark D. Williams-Wynn [a], Paramespri Naidoo [a] and Deresh Ramjugernath [a,*]

[a] Thermodynamics Research Unit, School of Engineering, University of KwaZulu-Natal, Howard College Campus, Durban, South Africa

The isothermal P-x-y and P-x-x-y phase equilibrium data for the systems of trifluoromethane or hexafluoroethane with n-octane were measured using a static-analytic type apparatus. Five isotherms between (272.9 and 313.2) K were measured for the trifluoromethane + n-octane system, and three isotherms at temperatures between (293.0 and 313.2) K were measured for the hexafluoroethane + n-octane system. Bubble pressure data for both systems at temperatures of between (293.0 and 313.2) K were measured with a variable-volume static-synthetic apparatus. The PR EOS with the MC alpha function, coupled with the WS mixing rule was used to model the experimental data. Both the NRTL and the UNIQUAC activity coefficient models were used to model the excess Gibbs energy term within the WS mixing rule, and the performances of these two thermodynamic models were compared. The temperature dependency of the thermodynamic model parameters were investigated at the temperatures for which data was measured. The indirect extended scaling law technique of Ungerer et al. and the critical locus curve calculation procedure of Heidemann and Khalil were used to estimate mixture critical points for the systems. The two binary systems were categorised according to the van Konynenburg and Scott classification system .

Introduction

The use of supercritical fluids as solvents offers many advantages over the use of conventional liquid solvents. These advantages pertain to the fluid properties; such as improved diffusivities and lower viscosities [1-2]; and to improvements in the processes, such as attaining better solvent recovery [3] and requiring reduced operational temperatures [4].

There are two common methods for the characterisation of the performance of a supercritical fluid for use as a solvent. The first method is to perform 'extensive measurements', with which the optimal operational conditions for the desired extraction can be obtained [5]. This type of investigation is often used for the extraction of natural products, as these products often contain a large matrix of components, for which the large number of individual binary phase equilibrium measurements required for characterisation would be prohibitive. In the second characterisation method, a small selection of components that approximate the behaviour of the system are defined, and the phase equilibrium of binary systems involving these components are investigated [6-7]. The investigations of the phase equilibria can range from solubility measurements [8-9] to vapour-liquid equilibrium (VLE) and solid-liquid equilibrium (SLE) measurements [10-11].

The method of 'representative measurements' has an advantage over the 'extensive measurements' in that thermodynamic models can be fitted to the phase equilibrium data, which then allows the prediction of the phase equilibria for a range of process conditions. The thermodynamic models also make it possible to optimise the process by performing multiple process simulations with different conditions. The most commonly utilised model systems contain species from the homogeneous n-alkane series [10, 12-13]. It was therefore decided to measure the phase behaviour of the same n-alkane solutes in the solvents of interest in this study, trifluoromethane (R-23, fluoroform, CHF_3) and hexafluoroethane (R-116, perfluoroethane, C_2H_6). A number of binary systems involving trifluoromethane, hexafluoroethane and n-alkanes have been investigated in previous studies [14-17]. The experimental data for the systems of R-23 + n-octane (C_8H_{18}) and R-116 + n-octane measured in this study is therefore a continuation of the 'representative measurements' for the characterisation of R-23 and R-116 as supercritical solvents.

In addition to the use of the thermodynamic models to predict the phase equilibria, within the range over which the experimental data was measured, the experimental data can also be used to tune predictive models for similar systems or different temperature ranges. There are a substantial number of predictive thermodynamic models that have been developed over the years, but for better accuracy of the predictions by these models, experimental data is required to tune the model parameters. The predictive models that are available range from the group contribution methods such as the UNIQUAC Functional-group Activity Coefficients (UNIFAC) [18] and the Predictive Soave-Redlich-Kwong (PSRK) [19] models to newer COSMO-based methods [20], such as the COSMO-SAC method [21].

The measurement of the VLE data for these two systems therefore has an additional purpose, in that it can provide experimental data for systems containing hydrofluorocarbons (HFCs) and perfluorocarbons (PFCs), with which parameters for the predictive models can be tuned.

Experimental

Materials. The n-octane (C_8H_{20}, CAS Number 111-65-9) used in these measurements was obtained from Merck Schuchardt OHG. Trifluoromethane (CHF_3, CAS Number 75-46-7) and hexafluoroethane (C_2F_6, CAS Number 76-16-4) were obtained from A-Gas (South Africa) (Pty) Ltd. Helium gas (Baseline 5.0) for the gas chromatograph was purchased from Afrox South Africa.

The purities of the n-octane, R-23 and R-116 were verified using GC peak area analysis. Table 1 lists the measured GC peak area fractions for the three components. Also tabulated in Table 1 are the suppliers of the chemicals, the purities given by the suppliers and the pure component critical properties, which were obtained from literature [22-24]. For the n-octane, the refractive indices and the densities were measured for further verification of the purity. The refractive indices at 293.15 K and 298.15 K were measured with an Atago RX7000 refractometer,

Table 1.
The suppliers, stated purities, GC area fractions and critical properties (T_c, P_c) of the pure components used in these measurements.

	Trifluoromethane	Hexafluoroethane	n-Octane
	CHF_3	C_2F_6	C_8H_{18}
Supplier	A-Gas (South Africa) (Pty) Ltd	A-Gas (South Africa) (Pty) Ltd	Merck Schuchardt OHG
Stated Purity	> 0.999 [d]	> 0.999 [d]	> 0.99 [e]
GC Area Fraction	0.9996	0.9999	0.9980
T_c / K	299.07 [a]	293.03 [b]	568.9 [a]
P_c / MPa	4.836 [a]	3.013 [c]	2.493 [a]

[a] Reference 24
[b] Reference 22
[c] Reference 23
[d] Volumetric basis
[e] Mass basis

certified to have uncertainties in refractive index and in temperature of ± 1 x 10^{-4} and 0.01 K respectively. The measured data were compared with data obtained from literature [25-27] in Table 2. The densities, at temperatures of between 293.15 K and 299.45 K were measured with an Anton Paar DMA 5000 density meter. The uncertainty in the measured density was 0.04 kg.m^{-3} with a temperature uncertainty was 0.05 K. The measured densities are reported alongside the literature data [26, 28-32] in Table 3.

After the addition of the components into the cell, degassing was performed, ensuring that no light impurities remained within the equilibrium cell. The n-octane was first added into the cell, under vacuum, with the vacuum pump continuing to pull a vacuum from the cell for a further 10 minutes after loading. The vacuum pump that is utilised for degassing is capable of creating a vacuum pressure of down to 0.2 kPa absolute. The pressure within the cell during the degassing was found to be sufficiently low to cause the n-octane to boil at room temperature. After the degassing of the n-octane, the cell was cooled and the refrigerant was added to the cell as a liquid. The mixture in the cell was then degassed again; this time by purging the vapours present within the cell, and allowing them to be re-generated from the liquid phase. This procedure was repeated a number of times until there was negligible difference between the cell pressure before purging and after the vapour phase had regenerated. Unfortunately, with this degassing technique, it is not possible to remove any of the less volatile impurities from the system. The GC analysis of the pure components did not detect any of these less volatile components, however, and this was therefore not problematic in this study.

Table 2.
The literature and measured refractive indices (R^I) of n-octane at T = 293.15 K and T = 298.15 K.

T / K	R^I (literature)	R^I (measured) [d]
293.15	1.39778 [a]	1.3978
298.15	1.39574 [a]	1.3953
	1.39505 [a]	
	1.3951 [b]	
	1.3951 [c]	

[a] 25
[b] 27
[c] 26
[d] $u(T)$ = 0.01 K, $u(R^I) = 1\times10^{-4}$

Table 3.
The literature and measured densities (ρ) of n-octane at temperatures of between T = (293.15 and 299.45) K .

T / K	ρ (literature) / [kg/m^3]	ρ (measured) [g] / [kg/m^3]
293.15	702.56 [a]	702.694
	702.5 [b]	
	702.6 [c]	
	702.76 [d]	
295.15		700.592
297.15		698.977
298.15	698.53 [a]	698.264
	698.5 [c]	
	698.5 [f]	
	698.29 [g]	
299.45		697.128

[a] 28
[b] 30
[c] 31
[d] 32
[e] 26
[f] 29
[g] $u(T)$ = 0.05 K, $u(\rho)$ = 0.05 kg·m^{-3}

Experimental Apparatus. Measurement of the VLE and vapour-liquid-liquid equilibrium (VLLE) data was undertaken with a static-analytic high-pressure equilibrium apparatus which was developed by Narasigadu et al. [33]. A variable-volume static-synthetic high pressure apparatus, described in a preceding paper by Williams-Wynn et al. [16] was used to measure the bubble point pressures for both of the systems at several known compositions. This bubble point data was used to verify the data measured with the static-analytic equilibrium apparatus.

The construction of both equilibrium apparatuses has been dealt with in detail in the previous papers [16, 33]. Pt100 probes, obtained from WIKA Instruments (model REB 1/10 DIN), were used to monitor the temperatures of the cells. The pressure within the static-analytic and static-synthetic cells were monitored with a (0 to 25) MPa P-10 pressure transducer and a (0 – 12) MPa P-10 pressure transducer respectively. Both of these transducers were purchased from WIKA Instruments. The atmospheric pressure was measured with the internal barometer of a Mensor CPC 3000 Pneumatic High-Speed Pressure Controller in the case of the static-analytic apparatus and the internal barometer of a Mensor CPC 8000 Automated High Pressure Calibrator in the case of the static-synthetic apparatus. The maximum uncertainties for these barometers were 0.01 kPa (0.02% of full range) and 0.005 kPa (0.01% of full range) respectively.

Calibrations. The two Pt100 temperature probes from each apparatus were calibrated against a CTH 6500 temperature standard probe, which was also purchased from WIKA Instruments. This standard probe was certified by WIKA Instruments to have a maximum temperature uncertainty of 0.02 K. The Pt100 probes were calibrated between T = (268.15 and 323.15) K and the uncertainties in the calibrations were both 0.06 K.

The two P-10 pressure transducers were calibrated against a (0 to 25) MPa CPT 6000 standard pressure transmitter. This standard pressure transmitter was verified by WIKA Instruments to have an uncertainty of less than 6.2 KPa for its full range. For the calibration of the (0 to 25) MPa transducer, the standard deviation was 0.5 kPa, and for the calibration of the (0 to 12) MPa transducer, the standard deviation was 1.5 kPa.

To calibrate the TCD of the gas chromatograph, various known volumes of the n-octane, the trifluoromethane and the hexafluoroethane were injected individually through the gas chromatograph to elicit a response (peak) from the GC. The number of moles of each component was then calculated from the volume injected and calibrated against the peak areas obtained from the TCD. The number of moles was related to the volume of gas by the ideal gas EOS and the volume of n-octane via the liquid molar density. A 500 µl gas-tight SGE syringe was used to

inject the two refrigerants into the GC; while for the n-octane, a 1.0 µl SGE liquid syringe was used.

The uncertainties in the number of moles of R-23 and R-116 from the calibration were 1.68×10^{-7} moles and 2.1×10^{-8} moles respectively. The uncertainty in the number of moles of n-heptane from the calibration was 1.63×10^{-7} moles .

Experimental Procedure. The experimental procedure followed for the measurement of the vapour-liquid and vapour-liquid-liquid equilibrium data has been described in detail in a number of preceding papers [16-17, 34].

Data Treatment. Uncertainties in the measured data were estimated using the guidelines of the National Institute of Standards and Technology (NIST) [35-36]. The combined expanded uncertainties in pressure, temperature and composition were reported for all measured data points. A coverage factor, *k*, equal to 2, was used to calculate these combined expanded uncertainties from the combined standard uncertainties.

The experimental data for both the R-23 (1) + n-octane (2) system and the R-116 (1) + n-octane (2) system was modelled with the Peng-Robinson equation of state (PR EOS) [37] modified with the Mathias-Copeman (MC) alpha function [38]. The MC alpha function parameters were regressed from vapour pressure data. For the refrigerants, only a single MC parameter was fitted to the data, as the second and third terms of the function become trivial at temperatures above the critical temperature of the pure component.

For systems containing a hydrocarbon and a refrigerant, Williams-Wynn and co-workers [16] showed that a simple thermodynamic model, containing only a cubic equation of state with classical mixing rules, did not adequately describe the behaviour of the bubble curve. In further discussions [17], on the modelling of R-23 + n-heptane, they showed that this simple thermodynamic model was also not capable of providing an accurate prediction of the pressure and compositions of the VLLE region for a given isotherm. The models that were used to describe the phase equilibrium data in this study required the capability to describe the VLLE of the system. The Wong-Sandler (WS) mixing rule [39] alone was therefore used in this work, as it provided a substantially better fit for the R-23 (1) + n-heptane (2) and the R-116 + n-heptane systems investigated by Williams-Wynn et al. [17].

The performance of two different liquid activity coefficient models within the WS mixing rule was investigated. The two activity coefficient models that were investigated were the Non-Random Two-Liquid (NRTL) activity coefficient model [40] and the Universal Quasi-Chemical (UNIQUAC) activity coefficient model [41]. Another possible activity coefficient model, proposed by Wilson [42] was not investigated, because of its inability to model the occurrence of liquid-liquid equilibria in the system.

Aspen Plus V8.0 [43] was used to regress the models to the experimental data. A modified Barker's objective function, which minimised the residuals of the pressure and the vapour phase composition, was used to search for the optimal model parameters. The quality of the fit of the models to the experimental data was evaluated statistically using the average relative deviation (ARD) and the average absolute relative deviation (AARD) between the experimental data and the data calculated with the regressed parameters in the thermodynamic models. Equations 1 and 2 were used to calculate the ARD and the AARD for the pressure and vapour phase composition respectively.

$$ARD(\theta) = \frac{100}{N_p}\sum_{1}^{N_p}\frac{\theta_{exp}-\theta_{calc}}{\theta_{exp}} \quad (1)$$

$$AARD(\theta) = \frac{100}{N_p}\sum_{1}^{N_p}\frac{\left|\theta_{exp}-\theta_{calc}\right|}{\theta_{exp}} \quad (2)$$

where θ_{exp} denotes the experimental data points and θ_{calc} denotes the modelled data points. The number of data points in the set is denoted N_p.

For those isotherms with vapour-liquid critical points, the indirect extended scaling laws of Ungerer et al. [44-45] were applied in order to estimate the mixture critical loci. These extended scaling laws could not, however, be used in cases where the critical point occurred in the liquid-liquid regime. The calculation procedure of Ungerer et al. was shown to provide fairly accurate estimates of the mixture critical points by El Ahmar al. [45]. A disadvantage of this technique is the ability to solely obtain a mixture critical point at the exact temperatures at which there is isothermal sub-critical VLE data available. It is therefore difficult to present a critical locus curve using this method, as multiple VLE isotherms must be measured.

The procedure of Heidemann and Khalil [46] was therefore also used in order to calculate the critical loci of the mixtures at molar compositions of between 0.9 and 1.0. These calculations required the thermodynamic models that were fitted to the experimental sub-critical phase equilibria data. Because this calculation method relies on the thermodynamic model rather than on the experimental data, it has the ability to estimate of the mixture critical point at any given temperature within a reasonable range of the temperatures at which the model parameters were regressed. The calculation procedure that was suggested by Stockfleth and Dohrn [47], using the equations that were developed by Heidemann and Khalil [46], was used to calculate estimates of the critical locus curve for both R-23 + n-octane and R-116 + n-octane. A central finite difference method approximation of the partial derivatives of the fugacity with respect to the number of moles was used in this calculation procedure. The alteration of the calculation procedure suggested by Stockfleth and Dohrn for cases in which *T* and *P* are required to be the independent variables was used .

Results and discussion

The parameters for the MC alpha function for n-octane were obtained by the regression of n-octane vapour pressure data which was obtained from the works of Boukais-Belaribi et al. [48], Dejoz and coworkers [49], Gracia et al. [50], Plesnar et al. [51] and Young [52-54]. Literature data was used to obtain the MC alpha function parameters for R-23 [16, 55-57], and for R-116 [17, 23, 58-61]. Table 4 provides the regressed MC alpha function parameters for n-octane, trifluoromethane and hexafluoroethane.

Table 4.
The Mathias-Copeman alpha function parameters (κ_i) for trifluoromethane, hexafluoroethane and n-octane fitted within the given temperature (*T*) ranges.

	T / K	κ_1	κ_2	κ_3
Trifluoromethane	252.93 – 299.07 [a]	0.776	0 [d]	0 [d]
Hexafluoroethane	273.1 – 293.0 [b]	0.777	0 [d]	0 [d]
n-Octane	269.9 – 333.8 [c]	0.944	-0.022	0.289

[a] Reference 16
[b] Reference 17
[c] Regressed to literature data [48-54]
[d] Set to zero for this study.

Table 5.
Experimental P-x_1^{I}-x_1^{II}-y_1 data with combined expanded uncertainties (U) for the binary system of R-23 (1) + n-octane (2) at temperatures of T = (272.9 to 313.2) K. The uncertainties were calculated with k = 2.

T / K	U (T)/ K	P/ MPa	U (P)/ MPa	x_1^{I}	U (x_1^{I})	x_1^{II}	U (x_1^{II})	y_1	U(y_1)
272.88	0.08	1.156	0.004	0.121	0.004			0.9980	0.0033
272.90	0.08	1.332	0.004	0.142	0.004			0.9953	0.0017
272.89	0.09	1.550	0.006	0.175	0.005			0.9975	0.0013
272.90	0.08	1.703	0.004	0.201	0.005			0.9979	0.0004
272.89	0.09	1.947	0.008	0.234	0.007			0.9976	0.0002
272.88	0.08	2.110	0.004	0.263	0.006			0.9985	0.0010
272.89	0.08	2.265	0.005	0.296	0.006			0.9991	0.0003
272.89	0.09	2.440	0.005	0.332	0.007	0.981	0.002	0.9975	0.0023
272.89	0.09	2.458	0.004	0.981	0.002			0.9995	0.0008
272.88	0.08	2.512	0.004	0.992	0.002			0.9979	0.0002
282.96	0.08	1.236	0.005	0.114	0.004			0.9966	0.0030
282.97	0.08	1.672	0.006	0.164	0.005			0.9910	0.0013
282.98	0.08	2.118	0.007	0.222	0.006			0.9918	0.0017
282.96	0.08	2.314	0.009	0.250	0.006			0.9967	0.0016
282.97	0.08	2.566	0.009	0.287	0.006			0.9969	0.0011
282.97	0.08	2.743	0.008	0.315	0.006			0.9957	0.0016
282.97	0.08	2.996	0.008	0.360	0.007			0.9991	0.0004
282.97	0.08	3.133	0.007	0.380	0.007	0.979	0.002	0.9983	0.0006
282.96	0.07	3.227	0.004	0.989	0.002			0.9979	0.0009
293.04	0.07	1.313	0.006	0.109	0.003			0.9954	0.0012
293.05	0.07	1.786	0.006	0.157	0.004			0.9948	0.0013
293.06	0.08	1.935	0.004	0.175	0.005			0.9942	0.0023
293.05	0.07	2.277	0.010	0.211	0.005			0.9883	0.0025
293.06	0.07	2.439	0.008	0.228	0.006			0.9991	0.0005
293.03	0.08	2.794	0.008	0.268	0.006			0.9988	0.0004
293.04	0.07	3.301	0.009	0.337	0.007			0.9975	0.0009
293.05	0.07	3.640	0.008	0.378	0.007			0.9988	0.0007
293.05	0.07	3.957	0.007	0.426	0.007	0.976	0.002	0.9977	0.0010
293.04	0.07	4.083	0.004	0.990	0.002			0.9956	0.0012
303.11	0.08	1.385	0.006	0.105	0.004			0.9914	0.0010
303.12	0.07	1.888	0.007	0.149	0.004			0.9958	0.0019
303.13	0.07	2.422	0.009	0.201	0.005			0.9910	0.0017
303.11	0.08	2.968	0.008	0.252	0.006			0.9963	0.0006
303.12	0.08	3.571	0.007	0.320	0.007			0.9969	0.0008
303.13	0.08	4.464	0.008	0.415	0.007			0.9982	0.0009
303.13	0.07	4.830	0.008	0.454	0.008			0.9973	0.0006
303.13	0.08	4.953	0.008	0.470	0.007	0.980	0.002	0.9974	0.0010
303.12	0.08	5.061	0.005	0.990	0.002			0.9985	0.0003
313.20	0.08	1.197	0.005	0.082	0.005			0.9888	0.0029
313.20	0.08	1.800	0.006	0.131	0.005			0.9939	0.0023
313.21	0.08	2.347	0.006	0.180	0.006			0.9960	0.0014
313.21	0.08	3.129	0.007	0.245	0.005			0.9953	0.0014
313.21	0.08	4.068	0.004	0.332	0.007			0.9953	0.0018
313.21	0.08	4.826	0.004	0.403	0.008			0.9976	0.0007
313.21	0.08	5.322	0.011	0.447	0.007			0.9969	0.0007
313.22	0.08	5.757	0.004	0.482	0.008			0.9959	0.0005
313.21	0.08	5.913	0.012	0.496	0.007			0.9957	0.0011
313.22	0.08	6.032	0.011	0.502	0.007			0.9930	0.0007
313.22	0.08	6.171	0.006	0.506	0.008			0.9857	0.0011
313.21	0.08	6.201	0.009	0.508	0.007			0.9821	0.0008
313.20	0.08	6.232	0.004	0.509	0.007			0.9805	0.0014
313.23	0.08	6.237	0.012	0.509	0.008			0.9795	0.0015

The P-x-x-y data for the system of R-23 and n-octane, measured with the static-analytic apparatus, at temperatures of between T = (273.9 and 313.2) K, are tabulated in Table 5, and are plotted in Figure 1. The estimated uncertainties for the data, calculated according to the NIST guidelines, were also tabulated in Table 5. For the verification of the data measured with the static-analytic apparatus, bubble pressure data was measured with the variable-volume apparatus. This data is reported in Table 7, and is also plotted in Figure 1, providing a comparison between the two data sets. Figure 1 displays the favourable agreement between the bubble pressure data and the data measured with the static-analytic apparatus.

Table 6.
Experimental P-x_1^{I}-x_1^{II}-y_1 data with combined expanded uncertainties (U) for the binary system of R-116 (1) + n-octane (2) for temperatures of T = (293.1 to 313.1) K. The combined expanded uncertainties were calculated with k = 2.

T / K	U (T)/ K	P/ MPa	U(P)/ MPa	x_1^{I}	U (x_1^{I})	x_1^{II}	U(x_1^{II})	y_1	U(y_1)
293.11	0.09	0.877	0.004	0.023	0.002			0.9753	0.0022
293.11	0.10	1.084	0.006	0.029	0.002			0.9864	0.0011
293.11	0.09	1.311	0.006	0.036	0.001			0.9847	0.0024
293.11	0.09	1.745	0.007	0.051	0.002			0.9852	0.0022
293.10	0.08	2.092	0.008	0.061	0.003			0.9894	0.0019
293.12	0.09	2.464	0.008	0.075	0.003			0.9906	0.0020
293.12	0.09	2.814	0.004	0.084	0.003			0.9876	0.0021
293.11	0.08	2.846	0.004	0.092	0.003	0.919	0.0031	0.9912	0.0012
293.11	0.09	2.876	0.004	0.934	0.002			0.9934	0.0003
293.10	0.09	2.952	0.004	0.961	0.002			0.9954	0.0012
293.11	0.09	3.019	0.008	0.974	0.001			0.9922	0.0011
303.11	0.05	0.873	0.004	0.021	0.001			0.9748	0.0022
303.11	0.07	1.201	0.006	0.030	0.001			0.9814	0.0014
303.11	0.06	1.605	0.005	0.043	0.002			0.9812	0.0029
303.11	0.06	2.024	0.007	0.057	0.003			0.9855	0.0017
303.11	0.06	2.418	0.006	0.069	0.003			0.9858	0.0025
303.11	0.06	2.875	0.004	0.084	0.004			0.9871	0.0012
303.11	0.06	3.251	0.008	0.095	0.003			0.9845	0.0021
303.11	0.06	3.506	0.004	0.1005	0.003			0.9761	0.0022
303.12	0.06	3.506	0.009	0.1011	0.003			0.9809	0.0022
303.12	0.07	3.593	0.004	0.1012	0.003			0.9471	0.0025
313.13	0.05	0.860	0.004	0.021	0.003			0.9626	0.0015
313.13	0.05	1.256	0.005	0.031	0.002			0.9864	0.0021
313.13	0.05	1.744	0.006	0.040	0.003			0.9845	0.0009
313.13	0.05	2.149	0.004	0.052	0.002			0.9802	0.0023
313.13	0.05	2.157	0.004	0.055	0.004			0.9768	0.0021
313.14	0.06	2.617	0.005	0.070	0.003			0.9798	0.0021
313.14	0.06	3.019	0.005	0.082	0.002			0.9791	0.0025
313.14	0.05	3.555	0.004	0.100	0.003			0.9808	0.0016
313.12	0.04	3.812	0.005	0.107	0.003			0.9747	0.0015
313.13	0.04	4.124	0.006	0.1130	0.004			0.9668	0.0019
313.13	0.06	4.193	0.008	0.1122	0.004			0.9595	0.0022
313.13	0.05	4.269	0.004	0.1113	0.004			0.9454	0.0029

Table 7.
Experimental bubble point P-x_1 data with combined expanded uncertainties (U) for the binary system of R-23 (1) and n-octane (2) at temperatures of T = (293.1 to 313.2) K. The combined expanded uncertainties were calculated with k = 2.

T / K	U(T) / K	P / MPa	U(P) / MPa	x_1	U(x_1)
293.15	0.03	1.678	0.007	0.144	0.002
293.15	0.03	3.267	0.007	0.332	0.001
293.16	0.03	3.989	0.005	0.424	0.001
293.16	0.03	4.102	0.007	0.990	0.003
303.16	0.03	1.845	0.005	0.144	0.002
303.16	0.04	3.650	0.007	0.332	0.001
303.17	0.03	4.589	0.008	0.433	0.001
303.19	0.03	4.958	0.004	0.466	0.001
303.16	0.04	5.048	0.007	0.990	0.003
313.19	0.04	2.041	0.007	0.144	0.002
313.19	0.04	4.068	0.010	0.332	0.001
313.20	0.04	5.104	0.006	0.433	0.001
313.21	0.04	5.553	0.006	0.466	0.001

For the R-116 + n-octane system, P-x-x-y data was measured at temperatures of between (293.0 and 313.2) K using a static-analytic phase equilibrium apparatus. The measured data is tabulated in Table 6, along with the corresponding combined expanded uncertainty estimates. Bubble pressure data for this system, measured with a variable-volume

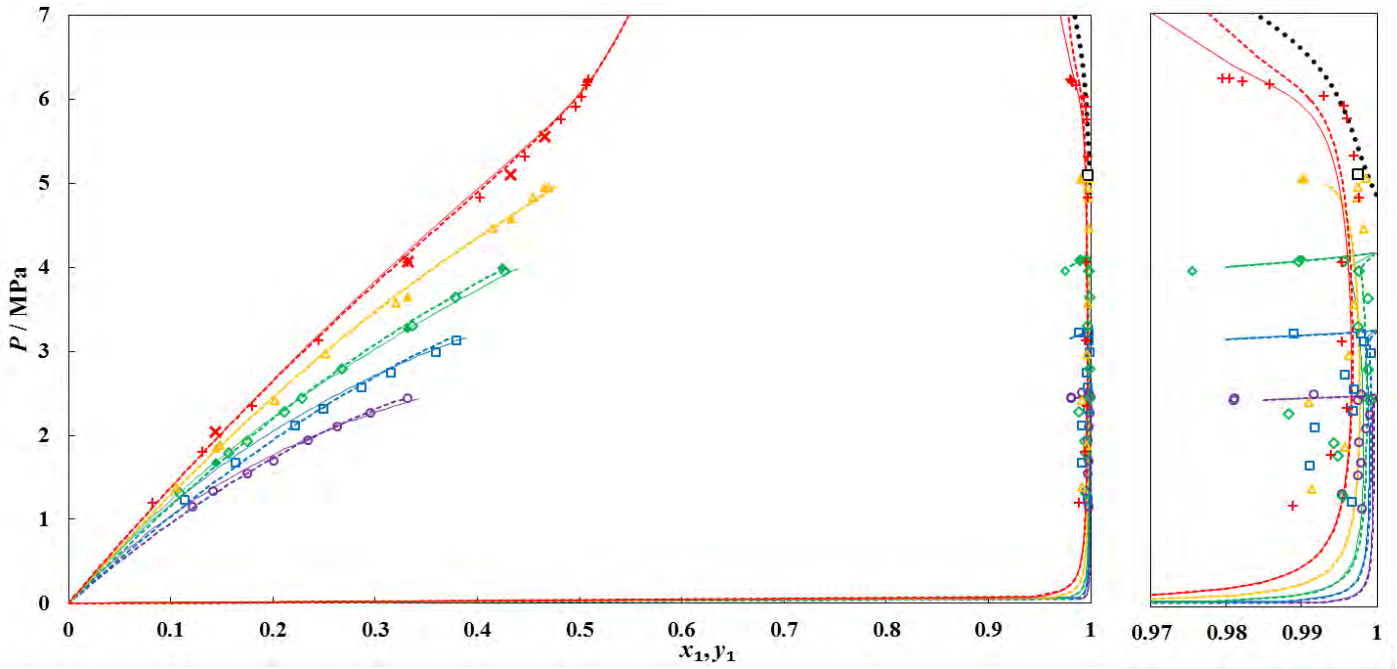

Figure 1. P-x_1^{I}-x_1^{II}-y_1 plot for the binary system of R-23 (1) + n-octane (2). Experimental data measured with the static-analytic apparatus at temperatures of T = ○, 272.9 K; □, 283.0 K; ◇, 293.0 K; △, 303.1 K; +, 313.2 K. Bubble point data measured using the variable-volume apparatus at temperatures of T = ◆, 293.2 K; ▲, 303.2 K; X, 313.2 K. Modelled data: solid lines, PR MC + WS/NRTL model; dashed lines, PRMC + WS/UNIQUAC model; ••••, calculated critical locus curve (Heidemann and Khalil); □, extrapolated critical points (Ungerer et al.) .

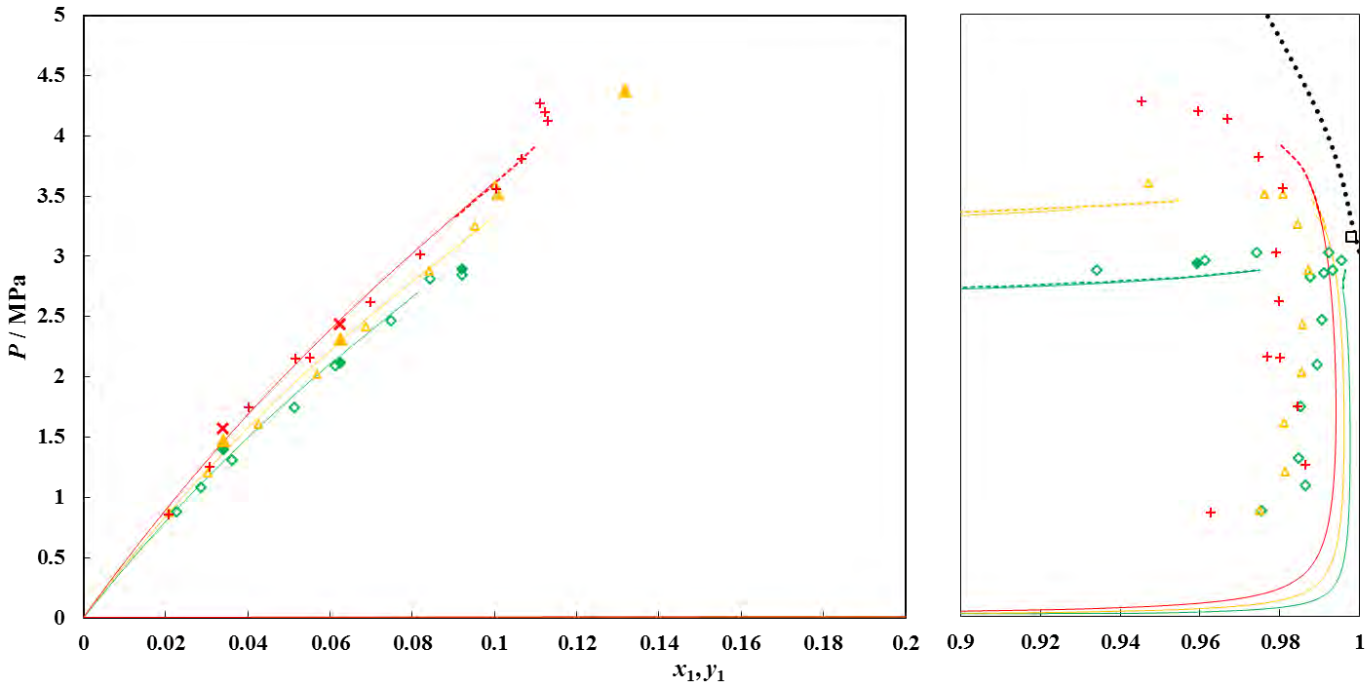

Figure 2. P-x_1^{I}-x_1^{II}-y_1 plot of the binary system of R-116 (1) + n-octane (2). Experimental data from the static-analytic apparatus at temperatures of T = ◇, 293.1 K; △, 303.1 K; +, 313.1 K. Experimental bubble point data measured using the variable-volume apparatus at temperatures of T = ◆, 293.0 K; ▲, 303.1 K; X, 313.2 K. Modelled data: solid lines, PRMC + WS/NRTL model; dashed lines, PRMC + WS/UNIQUAC model; ••••, calculated critical locus curve (Heidemann and Khalil); □, extrapolated critical point (Ungerer et al.) .

Table 8.

Experimental bubble point P-x_1 data with combined expanded uncertainties (U) for the binary system of R-116 (1) and n-octane (2) at temperatures of T = (293.0 to 313.2) K. The combined expanded uncertainties were calculated with k = 2 .

T/K	$U(T)$/K	P/MPa	U(P)/MPa	x_1	U(x_1)
293.04	0.03	1.399	0.005	0.034	0.001
293.05	0.03	2.121	0.004	0.062	0.001
293.04	0.03	2.891	0.005	0.132	0.001
293.04	0.03	2.932	0.004	0.959	0.008
303.04	0.03	1.474	0.004	0.034	0.001
303.17	0.03	2.309	0.004	0.062	0.001
303.14	0.03	4.376	0.004	0.132	0.001
313.16	0.03	1.575	0.004	0.034	0.001
313.20	0.03	2.439	0.004	0.062	0.001
313.17	0.04	5.598	0.004	0.132	0.001

apparatus, is tabulated in Table 8. The uncertainty estimates for the bubble pressure data are reported alongside the data. The P-x-x-y data and the bubble pressure data is plotted in Figure 2. The bubble pressure data for the R-116 + n-octane system agreed with the data from the static -analytic apparatus.

The PR EOS, with the MC alpha function, and coupled with the WS mixing rule with either the NRTL or the UNIQUAC activity coefficient model was fitted to the experimental data. The modelled data for each system were included on the respective P-x-y plots. For both models, temperature dependent parameters were fitted to the entire data set for each system, while temperature independent parameters were fitted to

each isothermal data set individually. The model parameters for the R-23 + n-octane system are presented in Table 9, and those for the R-116 + n-octane system in Table 10. The statistical data for the regression of the thermodynamic models to the experimental data sets are also included in Table 9 and 10. From observation of the *P-x-y* plots and the statistical data, the models provide a good description of the systems.

The temperature independent parameters for R-23 and n-octane had AARDs for pressure that were lower than 2.0 %, and for vapour phase composition that were less than 0.5 %. The temperature dependent models did not provide the same degree of correlation. The simple linear temperature dependency of the parameters for the thermodynamic models did not appear to be capable of accurately modelling the system. This is especially noticeable with the correlation of the equilibrium pressures. The poor correlation of the temperature dependency of the system was masked when observing the vapour phase compositions, because of the small changes in vapour phase solubility with large changes in temperature or pressure. The description of the temperature dependency was marginally improved when using the UNIQUAC activity coefficient model, as compared to using the NRTL activity coefficient model. However, the temperature independent models provided a better correlation than either of the temperature dependent models.

The R-116 + n-octane system was also described better by the temperature independent models than by the temperature dependent versions of the thermodynamic model. With the NRTL activity coefficient model and the R-116 + n-octane system, the correlation of the data was fair, with AARDs of less than 3 % for pressure, and of less than 2 % for vapour phase composition. For this system, the temperature independent UNIQUAC model provided a better correlation of the experimental data than the NRTL model. The temperature dependent parameters, on the other hand, provided a worsened correlation of the experimental data. The models described the R-23 + n-octane system better than the R-116 + n-octane system. It was postulated that this was due to the greater non-idealities of the R-116 system. The region of immiscibility for the R-116 + n-octane system covered a greater range of molar compositions (0.13 to 0.93) than the region of immiscibility for the R-23 + n-octane system (0.50 to 0.97).

The temperature dependent and the temperature independent parameters for the R-23 + n-octane system are plotted in Figure 3, and those of the R-116 + n-octane system are plotted in Figure 4. The curves on Figure 3 exhibit two very different trends for the temperature independent parameters, above and below the critical temperature of R-23. The large differences in the value of τ_{21} above and below the critical temperature are probably the reason behind the poor correlation of the experimental data with the temperature dependent model. The large changes in this parameter are possibly due to the experimental data exhibiting "birds-beak" behaviour 62 only below the critical temperature of R-23. At temperatures above this point, the models were therefore not forced to model the "bird's beak" behaviour, allowing vastly different parameter values.

For the R-116 + n-octane system, all three isotherms were above the critical temperature of R-116. This meant that the temperature dependent models were not affected by the phenomenon of different parameter trends above and below the critical temperature. Thus the poor performance of the temperature dependent models was not only due to the modelling of the system above and below the pure refrigerant critical point simultaneously, and there was a deficiency in the manner in which the temperature dependence was modelled. This deficiency was most likely linked to the simple linear temperature dependency of the model.

For the R-23 + n-octane system, an upper critical end point (UCEP) occurred at a temperature of between T = (303.1 and 313.2) K, as the 303.1 K isotherm exhibited VLLE, whereas for the 313.2 K isotherm, no immiscibility was observed. At this temperature and at higher pressures, however, both phases present within the cell were liquids.

The method of Ungerer and co-workers 44 was used to extrapolate from the measured VLE data, to estimate the mixture critical loci at the temperatures of the measured isotherms. Only one extrapolation was possible for each system, due to the occurrence of liquid-liquid critical loci at the higher temperatures. The extrapolated critical points are included in Figures 1 and 2, and the values are reported in Table 11. For a more complete critical locus curve estimation, an alternative method was required.

Table 9.

The PRMC + WS/NRTL (k_{12} and τ_{ij}) and the PRMC + WS/UNIQUAC model parameters (k_{12} and Δu_{ij}) for the system of R-23 (1) + n-octane (2). Both the temperature dependent and the temperature independent parameters were fitted to the experimental data. The ARD and AARD for the pressure (P) and vapour phase compositions (y) are also tabulated.

T / K	k_{12}	τ_{12} / K [a] || Δu_{12} [b] / J·mol^{-1}	τ_{21} / K [a] || Δu_{21} [b] / J·mol^{-1}	ARD [c] P	ARD [c] y	AARD [d] P	AARD [d] y
PRMC + WS/NRTL							
272.9	0.554	1724.0	340.0	-0.92	-0.11	1.65	0.15
283.0	0.553	1868.0	312.6	-1.79	-0.21	1.94	0.28
293.0	0.543	2063.1	283.5	-0.34	-0.14	0.78	0.31
303.1	0.636	738.5	91.0	0.69	-0.07	1.66	0.24
313.2	0.653	675.2	60.2	-0.36	-0.05	1.59	0.31
(272.9 to 313.2)	0.634	6 50.6	172.5	-0.98	0.10	5.07	0.42
PRMC + WS/UNIQUAC							
272.9	0.652	-481.2	-2765.7	0.39	-0.18	0.91	0.18
283.0	0.647	-556.5	-2556.1	-0.12	-0.27	1.74	0.27
293.0	0.643	-370.0	-2696.6	-0.31	-0.16	1.01	0.24
303.1	0.639	-230.4	-2802.4	-0.09	0.18	1.16	0.36
313.2	0.669	95.1	-2976.0	-0.37	-0.18	1.40	0.39
(272.9 to 313.2)	0.597	-418.2	-2866.7	0.04	0.53	3.75	0.82

[a] τ_{12}, τ_{21} for the NRTL activity coefficient model
[b] Δu_{12}, Δu_{21} for the UNIQUAC activity coefficient model

[c] average relative deviation, $$ARD(\theta) = \frac{100}{N_p}\sum_{1}^{N_p}\frac{\theta_{exp} - \theta_{calc}}{\theta_{exp}}$$

[d] absolute average relative deviation, $$AARD(\bar{\theta}) = \frac{100}{N_p}\sum_{1}^{N_p}\frac{|\bar{\theta}_{exp} - \bar{\theta}_{calc}|}{\bar{\theta}_{exp}}$$

Table 10.

The PRMC + WS/NRTL (k_{12} and τ_{ij}) and the PRMC + WS/UNIQUAC model parameters (k_{12} and Δu_{ij}) for the system of R-116 (1) + n-octane (2). Both the temperature dependent and the temperature independent parameters were fitted to the experimental data. The ARD and AARD for the pressure (P) and vapour phase compositions (y) are also tabulated.

T / K	k_{12}	τ_{12} / K [a] || Δu_{12} [b] / J·mol^{-1}	τ_{21} / K [a] || Δu_{21} [b] / J·mol^{-1}	ARD P	ARD y	AARD P	AARD y
PRMC + WS/NRTL							
293.0	0.483	239.2	748.4	0.14	-0.37	1.87	1.09
303.1	0.466	216.5	765.6	0.22	-0.17	2.51	2.03
313.2	0.471	205.7	773.7	0.67	-0.94	2.92	1.32
(293.0 to 313.2)	0.496	227.6	735.9	1.05	-1.26	2.46	1.37
PRMC + WS/UNIQUAC							
293.0	0.493	1059.7	-4188.8	-0.13	-0.79	1.85	0.79
303.1	0.476	1138.9	-4316.2	0.26	-0.87	1.61	1.16
313.2	0.474	1202.2	-4427.7	0.40	-1.21	2.78	1.28
(293.0 to 313.2)	0.527	1203.8	-4401.7	-2.88	-1.37	4.18	1.37

[a] τ_{12}, τ_{21} for the NRTL activity coefficient model
[b] Δu_{12}, Δu_{21} for the UNIQUAC activity coefficient model

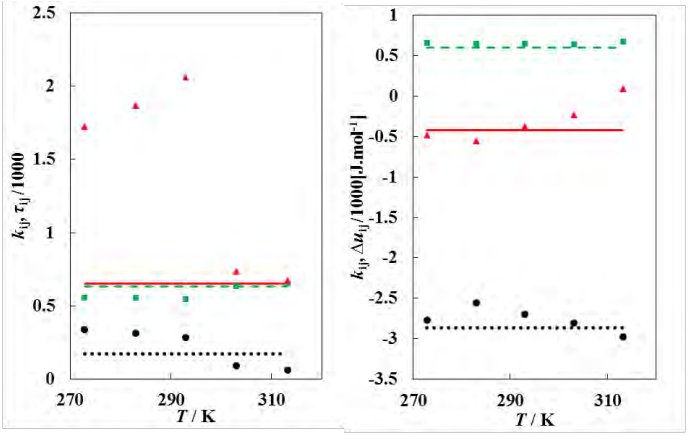

Figure 3. Fitted binary interaction parameters (k_{ij}, τ_{ij}, and Δu_{ij}) for the R-23 (1) + n-octane (2) binary system. Left: (PRMC + WS/NRTL model): /- - -, k_{12}; /·····, τ_{12}; /——, τ_{21}. Right: (PRMC + WS/UNIQUAC model): /- - -, k_{12}; /·····, Δu_{12}; /——, Δu_{21}. The symbols represent the parameters that were regressed independently of temperature and the lines represent the parameters obtained while regressing the model as temperature dependent.

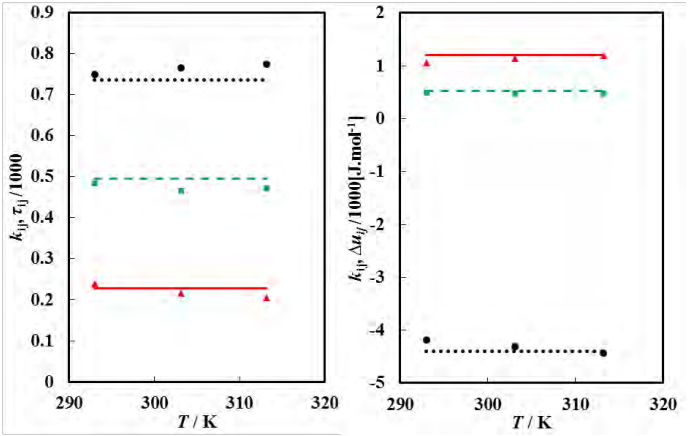

Figure 4. Fitted binary interaction parameters (k_{ij}, τ_{ij}, and Δu_{ij}) for the R-116 (1) + n-octane (2) binary system. Left: (PRMC + WS/NRTL model): /- - -, k_{12}; /·····, τ_{12}; /——, τ_{21}. Right: (PRMC + WS/UNIQUAC model): /- - -, k_{12}; /·····, Δu_{12}; /——, Δu_{21}. The symbols represent the parameters that were regressed independently of temperature and the lines represent the parameters obtained while regressing the model as temperature dependent.

The calculation procedure of Heidemann and Khalil [46], was used to estimate the critical locus curves for both R-23 + n-octane and R-116 + n-octane. These curves are included in Figure 1 for R-23 + n-octane and in Figure 2 for R-116 + n-octane. Several of the calculated values on the critical locus curves are tabulated in Table 11. The critical locus curves were only calculated at R23 or R-116 compositions of between 0.9 and 1.0 for a number of reasons. The first reason was the limit in the temperature range of the data to which the models were fitted. This limit would have led to the possibility of inaccurate critical locus curves, especially when taking into account the poor performance of the temperature dependent thermodynamic models. The second reason was the possibility that at some composition, there could be a case of no critical loci occurring. At certain compositions, the calculation procedure suggested by Stockfleth and Dohrn [47] was unable to converge to a critical temperature, indicating that a case of no critical points was a possibility. The phenomenon of regions with no critical points has been discussed previously by both Peng and Robinson [37] and by Heidemann and Khalil [46].

The critical locus curve for the R-23 + n-octane system fits the experimental data with a fairly good accuracy, especially considering that it is based upon the temperature dependent model, which can be at best

Table 11.
Critical loci (T_c, P_c, $x_{c,1}$) extrapolated from experimental data by the method of Ungerer et al. [44], and estimated from the fitted thermodynamic models by the method of Heidemann and Khalil [46].

Method of Ungerer et al.			Method of Heidemann and Khalil		
T_c	P_c	$x_{c,1}$	T_c	P_c	$x_{c,1}$
		R-23 (1) + n-octane (2)			
303.1	5.10	0.994	313.9	6.58	0.99
			333.8	8.21	0.96
			358.2	9.81	0.93
			379.5	10.80	0.90
		R-116 (1) + n-octane (2)			
293.1	3.15	0.998	308.8	4.15	0.99
			327.6	5.95	0.96
			352.8	7.50	0.93
			384.5	9.02	0.90

described as giving a mediocre fit of the experimental data. The critical locus curve for the R-116 + n-octane system, in contrast, does not accurately fit the experimental data or the phase equilibrium curves of the temperature independent parameters. With this system, a number of experimental co-existence points occur outside of the two phase envelope bordered by the critical locus curve.

Based upon the data available from this study, it is projected that the R-23 + n-octane system is a van Konynenburg and Scott type III system 63. A (gas-liquid) critical line existed between the R-23 critical point and the UCEP, which occurred somewhere between (303.1 and 313.2) K. Thereafter, a liquid-liquid critical line occurred between the UCEP and an arbitrary 'critical point at infinite pressure'. For this system, any composition between those of the LCEP and the critical end point at infinite pressure would not reveal a mixture critical point. Conversely, the possibility exists for the system to exhibit two critical locus curves in certain composition ranges.

The R-116 + n-octane system was also classified as a type III van Konynenburg and Scott system. It exhibited characteristics unique to type III systems, such as a critical locus curve between C_1 and the UCEP, and a (liquid-liquid) critical locus curve emanating from the UCEP to a critical point at infinite pressure. For this system, the third critical curve between C_2 and the LCEP was once again not investigated .

Conclusions

The VLE and VLLE data for the systems of R-23 (1) + n-octane (2) and R-116 (1) + n-octane (2) were measured at temperatures of between T = (272.9 and 313.2) K and T = (293.0 and 313.2) K respectively. The data was measured using a static-analytic apparatus and a variable volume, static-synthetic apparatus. Both of the systems exhibited the "bird's-beak" phenomenon at temperatures near to the critical temperature of the more volatile component. Uncertainties in the reported data were calculated according the NIST guidelines. The PR EOS, modified with the MC alpha function and using the WS mixing rule was fitted to the experimental data. The NRTL and the UNIQUAC activity coefficient models were used within the WS mixing rule.

Temperature independent parameters, fitted to each isotherm, provided better correlation of the experimental data than the temperature dependent models, which were fitted across all of the isotherms. This was especially the case with the R-23 + n-octane system. The poor correlation using the temperature dependent models was due, in part, to the large differences between the model parameters fitted above and

below the critical temperature. Despite this, the thermodynamic models adequately described the phase equilibrium of these systems. Critical loci were extrapolated using the method of Ungerer et al., and the critical locus curve was calculated by the method of Heidemann and Khalil, in conjunction with the temperature dependent thermodynamic model. The calculated critical locus curve for the system containing R-23 appeared to approximate the mixture critical loci fairly closely; however that of the R-116 + n-octane system did not appear to provide the same degree of accuracy. Both the R-23 + n-octane and the R-116 + n-octane systems were judged to be van Konynenburg and Scott type IV systems, due to the characteristics that they exhibited within the temperature ranges that were investigated .

Acknowledgements

This work is based upon research supported by the South African Research Chairs Initiative of the Department of Science and Technology and National Research Foundation. The authors would like to thank the NRF Focus Area Programme and the NRF Thuthuka Programme .

Literature Cited

1. Rizvi, S. S. H.; Benado, A. L.; Zollweg, J. A.; Daniels, J. A. Food Technol. 1986, 40 (6), 55-65.
2. Erkey, C. J. Supercritical Fluids 2000, 17, 259-287.
3. Palmer, M. V.; Ting, S. S. T. Food Chem. 1995, 52 (4), 345-352.
4. Wypych, G. Handbook of solvents. ChemTec Publishing: 2001.
5. Reverchon, E.; Della Porta, G.; Senatore, F. J. Agric. Food Chem. 1995, 43 (6), 1654-1658.
6. de Leeuw, V. V.; de Loos, T. W.; Kooijman, H. A.; de Swaan Arons, J. Fluid Phase Equilib. 1992, 73 (3), 285-321.
7. Peters, C. J.; de Roo, J. L.; de Swaan Arons, J. Fluid Phase Equilib. 1992, 72, 251-266.
8. Kurnik, R. T.; Holla, S. J.; Reid, R. C. J. Chem. Eng. Data 1981, 26 (1), 47-51.
9. Dobbs, J. M.; Wong, J. M.; Johnston, K. P. J. Chem. Eng. Data 1986, 31 (3), 303-308.
10. Huie, N. C.; Luks, K. D.; Kohn, J. P. J. Chem. Eng. Data 1973, 18 (3), 311-313.
11. Scheidgen, A. L.; Schneider, G. M. J. Chem. Thermodyn. 2000, 32 (9), 1183-1201.
12. Nagarajan, N.; Gasem, K. A. M.; Robinson, R. L. J. Chem. Eng. Data 1990, 35 (3), 228-231.
13. Jiménez-Gallegos, R.; Galicia-Luna, L. A.; Elizalde-Solis, O. J. Chem. Eng. Data 2006, 51 (5), 1624-1628.
14. Ramjugernath, D.; Valtz, A.; Richon, D.; Williams-Wynn, M. D.; Coquelet, C. J. Chem. Eng. Data 2015, unpublished.
15. Ramjugemath, D.; Valtz, A.; Richon, D.; Williams-Wynn, M. D.; Coquelet, C. J. Chem. Eng. Data 2015, not published.
16. Williams-Wynn, M. D.; Naidoo, P.; Ramjugemath, D. J. Chem. Thermodyn. 2015, unpublished.
17. Williams-Wynn, M. D.; Naidoo, P.; Ramjugemath, D. Fluid Phase Equilib. 2015, unpublished.
18. Fredenslund, A.; Jones, R. L.; Prausnitz, J. M. AIChE J. 1975, 21 (6), 1086-1099.
19. Holderbaum, T.; Gmehling, J. Fluid Phase Equilib. 1991, 70, 251.
20. Lin, S.-T.; Sandler, S. I. Ind. Eng. Chem. Res. 2002, 41 (5), 899-913.
21. Hsieh, C.-M.; Sandler, S. I.; Lin, S.-T. Fluid Phase Equilibr. 2010, 297 (1), 90-97.
22. Saikawa, K.; Kijima, J.; Uematsu, M.; Watanabe, K. J. Chem. Eng. Data 1979, 24 (3), 165-167.
23. Kim, K. Y. Calorimetric studies on argon and hexafluoroethane and a generalized correlation of maxima in isobaric heat capacity. Ph.D. Dissertation, University of Michigan, Ann Arbour, MI, 1974.
24. Lide, D. R. CRC Handbook of Chemistry and Physics 2004-2005: A Ready-Reference Book of Chemical and Physical Data. CRC Press LLC: 2004.
25. O'Brien, R. N.; Quon, D. J. Chem. Eng. Data 1968, 13 (4), 517-517.
26. Garcia, I.; Cobos, J. C.; Gonzalez, J. A.; Casanova, C.; Cocero, M. J. J. Chem. Eng. Data 1988, 33 (4), 423.
27. Blanco, A.; Gayol, A.; Gómez-Díaz, D.; Navaza, J. M. J. Phys. Chem. Liq. 2013, 51 (3), 404-413.
28. Garcia, M.; Rey, C.; Villar, V. P.; Rodriguez, J. R. J. Chem. Eng. Data 1986, 31 (4), 481-483.
29. Ortega, J.; Gonzalez, E.; Matos, J. S.; Legido, J. L. J. Chem. Thermodyn. 1992, 24 (1), 15-22.
30. Wu, J.; Asfour, A.-F. A. Fluid Phase Equilib. 1994, 102 (2), 305-315.
31. González, B.; Dominguez, A.; Tojo, J. J. Chem. Thermodyn. 2003, 35 (6), 939-953.
32. Vrbka, P.; Dohnal, V.; Arlt, W. J. Chem. Eng. Data 2004, 49 (4), 867 -871.
33. Narasigadu, C.; Naidoo, P.; Coquelet, C.; Richon, D.; Ramjugernath, D. Fluid Phase Equilib. 2013, 338, 188-196.
34. Nandi, P.; Moodley, S.; Ramjugernath, D. Fluid Phase Equilib. 2013, 344, 84-91.
35. Taylor, B. N.; Kuyatt, C. E. NIST Technical Note 1994, 1297.
36. Taylor, B. N.; Mohr, P. J.; Douma, M. The NIST Reference on constants, units, and uncertainty. 2007.
37. Peng, D. Y.; Robinson, D. B. Ind. Eng. Chem. Fundam. 1976, 15, 59 -64.
38. Mathias, P. M.; Copeman, T. W. Fluid Phase Equilib. 1983, 13, 91-108.
39. Wong, D. S. H.; Sandler, S. I. AIChE J. 1992, 38, 671-680.
40. Renon, H.; Prausnitz, J. M. AIChE J. 1968, 14, 135-144.
41. Abrams, D. S.; Prausnitz, J. M. AIChE J. 1975, 21 (1), 116-128.
42. Wilson, G. M. J. Am. Chem. Soc. 1964, 86 (2), 127-130.
43. Aspen Technology. Aspen Plus V8.4 2012.
44. Ungerer, P.; Tavitian, B.; Boutin, A. Applications of molecular simulation in the oil and gas industry- Monte Carlo methods. 2005.
45. El Ahmar, E.; Valtz, A.; Naidoo, P.; Coquelet, C.; Ramjugernath, D. J. Chem. Eng. Data 2011, 56 (5), 1918-1924.
46. Heidemann, R. A.; Khalil, A. M. AIChE J. 1980, 26 (5), 769-779.
47. Stockfleth, R.; Dohrn, R. Fluid Phase Equilib. 1998, 45, 43-52.
48. Boukais-Belaribi, G.; Belaribi, B. F.; Ait-Kaci, A.; Jose, J. Fluid Phase Equilib. 2000, 167 (1), 83-97.
49. Dejoz, A.; González-Alfaro, V.; Miguel, P. J.; Vázquez, M. I. J. Chem. Eng. Data 1996, 41 (1), 93-96.
50. Gracia, M.; Sánchez, F.; Pérez, P.; Valero, J.; Losa, C. G. J. Chem. Thermodyn. 1992, 24 (8), 843-849.
51. Plesnar, Z.; Fu, Y.-H.; Sandler, S. I.; Orbey, H. J. Chem. Eng. Data 1996, 41 (4), 799-801.
52. Young, S. J. Chem. Soc. 1900, 77, 1145.
53. Young, S. Sci. Proc. R. Dublin Soc. 1910, 12, 374-443.
54. Young, S. Proc. Roy. Irish Acad. B 1928, 38, 65-92.
55. Hou, Y. C.; Martin, J. J. AIChE J. 1959, 5 (1), 125-129.
56. Rasskazov, D. S.; Petrov, E. K.; Spiridonov, G. A.; Ushmajkin, E. R. Teplofiz. Svoistva Veshchestv Mater. 1975, 8, 4-16.
57. Hori, K.; Okazaki, S.; Uematsu, M.; Watanabe, K. In An Experimental Study of Thermodynamic Properties of Trifluoromethane, 8th Symp. Thermophys. Prop., Gaithersburg, Sengers, J. V., Ed. ASME: Gaithersburg, 1982; pp 370-376.
58. Kijima, J.; Saikawa, K.; Watanabe, K.; Oguchi, K.; Tanishita, I. In Experimental study of thermodynamic properties of hexafluoroethane (R116), Proc. Symp. Thermophys. Prop., 7th, New York, Cezairliyan, A., Ed. ASME: New York, 1977; p 480.
59. Kao, C.-P. C.; Miller, R. N. J. Chem. Eng. Data 2000, 45 (2), 295-297.
60. Valtz, A.; Coquelet, C.; Richon, D. Fluid Phase Equilib. 2007, 258 (2), 179-185.
61. Madani, H.; Valtz, A.; Coquelet, C.; Meniai, A. H.; Richon, D. Fluid Phase Equilib. 2008, 268, 68-73.
62. Rainwater, J. C. Fluid Phase Equilib. 2001, 183-184, 41-51.
63. van Konynenburg, P. H.; Scott, R. L. Philos. Trans. R. Soc. 1980, 298, 495-540.

APPENDIX F

Isothermal vapour-liquid equilibrium data for the binary systems of CHF_3 with (n-nonane, n-decane, or n-undecane) and (C_2F_6 + n-decane)

Mark D. Williams-Wynn [a], Paramespri Naidoo [a] and Deresh Ramjugernath [a,*]

[a] Thermodynamics Research Unit, School of Engineering, University of KwaZulu-Natal, Howard College Campus, Durban, South Africa

ARTICLE INFO

Keywords:
static-analytic,
variable-volume,
trifluoromethane,
hexafluoroethane,
n-alkanes

ABSTRACT

The isothermal vapour-liquid and vapour-liquid-liquid equilibria of four binary refrigerant + n-alkane systems were measured using a static-analytic apparatus at near ambient temperatures. The R-23 + n-nonane and R-23 + n-decane systems were measured at temperatures of between (272.9 and 313.2) K, while the R-23 + n-undecane and R-116 + n-decane systems were measured at temperatures of between (293.1 and 313.3) K. For the R-23 + n-alkane systems, bubble pressures at temperatures of between (293.0 and 313.2) K at several compositions, measured with a variable-volume static-synthetic apparatus, were used to validate the data from the static-analytic apparatus.

The experimental phase equilibrium data was modelled with the PR EOS and the MC alpha function. The WS mixing rule, incorporating either the NRTL activity coefficient model or the UNIQUAC activity coefficient model, was used to apply the PR MC EOS to the mixture data. The temperature independent forms of the thermodynamic model were found to provide a more accurate representation of the experimental data than the corresponding temperature dependent forms. A single mixture critical point was determined using the indirect extended scaling laws of Ungerer et al. The calculation procedure of Heidemann and Khalil was used to estimate segments of the critical locus curves for the binary systems. The van Konynenburg and Scott classification of each of the systems were defined, based upon the characteristics of the critical locus curves, within the temperature ranges that were studied.

1. Introduction

The advantages behind the use of supercritical fluids in industrial applications have been fairly well documented over the last number of decades, with numerous reviews and monographs having been published [1-4]. There has been a steady increase in the types of industrial applications of supercritical fluids over the last number of years. Applications have branched out from the use of supercritical fluids solely as solvents for extraction purposes to other applications, such as solvents for reactions and for particle and polymer production, among others [5].

Carbon dioxide is generally recognised as the most suitable fluid for use as a supercritical solvent [1, 6]. In some applications, however, it is desirable to use a solvent with polar characteristics, especially when polar solutes are being used. In these cases, when it is desired to use a non-polar solvent, such as carbon dioxide, a co-solvent can be added to increase the polarity of the solvent [7, 8]. This co-solvent addition technique has the disadvantage of adding complexities to the downstream solvent-solute separation. It would therefore be useful to discover a polar solvent which would negate the need for the addition of co-solvents to effect a separation, while at the same time allowing the use of operating conditions similar to those required when using carbon dioxide as the solvent.

In the characterisation of the performance of a supercritical solvent, the most common technique is to investigate the phase equilibrium conditions of a small number of solutes that approximate the desired separation, yet do not require the measurement of an extensive set of binary systems [9-13]. n-Decane has been used as a 'base-normal-alkane' by several authors such as Huie et al. [14], Nagarajan et al. [15], Chou et al. [16] and Sánchez-Garcia et al. [12]. This 'base-normal-alkane' can be used for two purposes. It can be used as a benchmark for a single solvent, against which the solubilities of the other solutes are compared, but can also be used as a reference solute, against which the performance of different solvents can be compared.

The characterisation of the performance of a supercritical solvent with a smaller set of solutes can be undertaken by using a variety of phase equilibrium measurements. These range from solubility measurements to more complex vapour-liquid equilibrium (VLE) measurements. The advantage in the use of VLE measurements is the possibility for the correlation of the experimental data with thermodynamic models, and thereafter, the use of these models to calculate the phase behaviour of the system at any process conditions within the range of the experimental data.

As a continuation of the study to benchmark the performance of the two refrigerants, trifluoromethane (R-23, fluoroform) and hexafluoroethane (R-116, perfluoroethane), as supercritical solvents, VLE data for four binary refrigerant + n-alkane systems were measured. The VLE data of the R-23 + n-nonane system were measured at temperatures, T = (272.9 to 313.2) K, those of the R-23 + n-decane system at T = (272.9 to 313.3) K, those of the R-23 + n-undecane system at T = (293.1 to 313.3) K and those of the R-116 + n-decane system at T = (293.1 to 313.2) K.

2. Experimental

2.1. Materials and Chemicals

The n-nonane (C_9H_{20}, CAS Number 111-84-2) and n-undecane (C11H24, CAS Number 1120-21-4) that were used in this study were purchased from Merck Schuchardt OHG. The n-decane ($C_{10}H_{22}$, CAS Number 124-18-5) was purchased from Sigma-Aldrich Co. LLC. The trifluoromethane (CHF_3, CAS Number 75-46-7) and the hexafluoroethane (C_2F_6, CAS Number 76-16-4) were both obtained from A-Gas (South Africa) (Pty) Ltd. A gas chromatograph was operated with helium (Baseline 5.0), purchased from Afrox South Africa, as the carri-

Table 1.
Details of the chemicals used in this study: suppliers, stated purities, GC area fractions and critical properties, T_c and P_c.

	Supplier	Stated Purity	GC Area	T_c / K	P_c / MPa
Trifluoro-methane, CHF_3	A-Gas (South Africa)	> 0.999 [d]	0.9996	299.07 [c]	4.836 [c]
Hexafluoro-ethane, C_2F_6	A-Gas (South Africa)	> 0.999 [d]	0.9999	293.03 [b]	3.013 [a]
n-Nonane, C_9H_{20}	Merck Schu-chardt	> 0.990 [e]	0.9984	594.9 [c]	2.288 [c]
n-Decane, $C_{10}H_{22}$	Sigma-Aldrich	> 0.990 [e]	0.9964	617.65 [c]	2.104 [c]
n-Undecane, $C_{11}H_{24}$	Merck Schu-chardt	> 0.990 [e]	0.9973	638.85 [c]	1.955 [c]

[a] [17]
[b] [18]
[c] [19]
[d] volumetric basis
[e] mass basis

Table 2.
Experimentally measured densities, ρ, of n-nonane, n-decane and n-undecane at temperatures, T = (293.15 and 299.62) K, compared to data obtained from literature.

T / K	ρ (lit.) / [kg/m^3]	ρ (exp.) [l] / [kg/m^3]	ρ (lit.) / [kg/m^3]	ρ (exp.) [l] / [kg/m^3]	ρ (lit.) / [kg/m^3]	ρ (exp.) [l] / [kg/m^3]
	n-nonane		n-decane		n-undecane	
293.15	717.8 [a] 717.85 [b] 717.68 [c]	717.883	729.9 [g] 729.7 [h] 729.99 [i]	729.762	740.02 [c] 740.1 [h] 740.59 [k]	739.96
294.15	-	716.601		728.496		
295.15	-	715.824		727.738		737.96
296.15	-	715.045		726.983		
297.15	-	714.268		726.227		736.48
298.15	713.569 [d] 713.85 [e] 714.0 [f]	713.689	726.2 [g] 726.0 [h] 726.3 [b] 725.76 [j]	725.467	736.3 [c] 736.4 [h] 736.90 [k]	735.73
299.62	-	-		724.355		
299.75						734.56

[a] [20]
[b] [22]
[c] [25]
[d] [26]
[e] [23]
[f] [27]
[g] [29]
[h] [24]
[i] [28]
[j] [30]
[k] [21]
[l] combined uncertainties, $u(T) = 0.01$ K, $u(R^I) = 3\times10^{-4}$

Table 3.
Measured refractive indices (R^I) of n-nonane, n-decane and n-undecane at temperatures, T = (293.15 and 298.15) K, compared to data obtained from literature.

T / K	R^I (lit.)	R^I (exp.) [i]	R^I (lit.)	R^I (exp.) [i]	R^I (lit.)	R^I (exp.) [i]
	n-nonane		n-decane		n-undecane	
293.15		1.40595		1.41196	1.4173 [e]	1.41726
298.15	1.40336 [a] 1.4037 [b] 1.4034 [c] 1.4042 [d]	1.40329	1.40937 [a] 1.4113 [b] 1.4101 [c] 1.4098 [d]	1.40964	1.41473 [f] 1.41507 [g]	1.41502

[a] [34]
[b] [37]
[c] [32]
[d] [31]
[e] [35]
[f] [33]
[g] [36]
[i] $u(T) = 0.01$ K, $u(R^I) = 1\times10$-4

er gas.

To verify the stated purities of all of the pure components, their compositions were analysed with a gas chromatograph (GC). The GC peak area fraction for each component was used as a measure of the purity of that component. The suppliers of each component, the stated purities, the GC peak area fractions, and the pure component critical properties from literature [17-19], are reported in Table 1.

In addition to the GC analysis, the densities and refractive indices of the n-alkanes were also measured for the purposes of verifying the purity of the liquids. The densities of the n-alkanes were measured with an Anton Paar DMA 5000 density meter at temperatures of between (293.15 and 299.62) K. The estimated uncertainties of the DMA 5000 were 0.005 kg·m^{-3} and 0.05 K for density and temperature respectively. The measured densities of n-nonane, n-decane and n-undecane are reported in Table 2, and compared to measured densities obtained from literature sources [20-30].

The refractive indices of the n-alkanes were measured with an Atago RX7000 refractometer with uncertainties of 1×10^{-4} and 0.01 K for the refractive index and the temperature respectively. The measured refractive indices at temperatures of 293.15 and 298.15 K are reported in Table 3. To verify the purities of the components, these refractive indices were compared to data obtained from literature [31-37] which are also reported in Table 3.

2.2. Experimental Apparatus.

Two high-pressure phase equilibrium apparatuses were used to measure the vapour-liquid equilibrium (VLE) and vapour-liquid-liquid equilibrium (VLLE) of the four binary systems. These two apparatuses were, a static-analytic apparatus, developed by Narasigadu et al. [38], capable of measuring phase equilibrium data at temperatures of between 253 and 473 K and at pressures of up to 17 MPa; and a variable-volume, static-synthetic apparatus, developed by Ngema et al. [39], and modified for bubble point measurements by Williams-Wynn et al. [40]. This variable-volume cell is capable of measuring bubble point pressures of known loading compositions at temperatures of between 253 and 473 K and at pressures of up to 10 MPa.

2.3. Calibrations.

The pressure transducers and temperature probes were all calibrated against standards certified by WIKA Instruments. Four Pt100 temperature probes purchased from WIKA Instruments; two for each apparatus; were calibrated against a CTH 6500 temperature standard probe at temperatures of between (268.15 and 323.15) K. The standard probe was certified to have a maximum temperature uncertainty of 0.02 K.

The (0 to 25) MPa P-10 pressure transducer from the static-analytic apparatus and the (0 to 12) MPa P-10 pressure transducer from the variable-volume apparatus were both purchased from WIKA Instruments. These pressure transducers were calibrated against a (0 to 25) MPa CPT 6000 standard pressure transmitter with an uncertainty of less than 6.2 kPa for the full range. The standard deviations for calibrations between (0 and 10) MPa for the two transducers were 0.5 kPa and 1.5 kPa for the (0 to 25) MPa and (0 to 12) MPa respectively. The internal barometer of a Mensor CPC 3000 Pneumatic High-Speed Pressure Controller (uncertainty of 0.01 kPa or 0.02 % of the full range) was used to measure the atmospheric pressure for the static-analytic apparatus. For the variable-volume apparatus, the internal barometer of a Mensor CPC 8000 Automated High Pressure Calibrator (uncertainty of 0.005 kPa or

0.01% of the full range) was used to measure the atmospheric pressure.

The calibration curve for the thermal conductivity detector (TCD) of the GC was obtained by comparing measured peak response areas to the known number of moles injected through the GC. For each component, several accurately known volumes were injected into the GC, with each volume being repeated at least five times. The number of moles of each injection was determined using either the ideal gas equation for gas volumes, or the liquid molar density in the case of the liquid n-alkanes. For the gases, a 500 µl gas-tight SGE syringe was used (accuracy of 1 % of volume) and for the liquids, a 1.0 µl SGE liquid syringe was used (accuracy of 2 % of volume). The calibration uncertainties for the number of moles of R-23 and R-116 from the GC were 1.68×10^{-7} moles and 2.1×10^{-8} moles respectively. For the n-alkanes, the calibration uncertainties were 3.21×10^{-7} moles, 2.0×10^{-8} moles and 1.5×10^{-8} moles for the n-nonane, n-decane and n-undecane respectively.

2.4. Experimental Procedure.

Degassing of the liquids was performed in situ within the static-analytic equilibrium cell. Once the liquid had been introduced into the cell, a vacuum pump was used to pull a vacuum (capability of reducing pressure down to 0.2 kPa abs. with an empty cell) for approximately 10 minutes. The vacuum created within the cell caused the n-alkanes to boil whilst at room temperature. Once degassing of the liquid was complete, the cell was cooled and the refrigerant was added to the cell as a liquid.

The refrigerants were added to the cell at temperatures sufficiently low for the refrigerants to be liquids, for the purpose of creating a pressure gradient between the gas cylinder and the cell, and thus increasing the speed at which the loading could be performed. Once the refrigerant had been loaded into the cell, it was heated to the temperature at which the measurements would be made, and the contents of the cell were degassed. Due to the large relative volatility of the two components within the cell, degassing of the refrigerant could also be performed in situ, simply by venting a portion of the vapour phase and thereafter allowing this to be re-generated from the liquid phase. This degassing procedure could be repeated a number of times until negligible amounts of the volatile impurities were present within the cell. The presence of impurities could be verified by GC analysis, as well as by comparing the equilibrium pressure before and after a purge.

With the variable-volume static-synthetic cell, the liquid was degassed prior to being added to the cell, while no degassing of the refrigerant was performed. Every care was taken during the loading of the cell to prevent the ingression of impurities. These included pulling a vacuum in the cell overnight and purging of the cell and the loading lines with the refrigerant prior to loading of the components. The ingression of any air into the system during loading would have resulted erroneous experimental data due to elevated bubble point pressures.

Detailed descriptions of the experimental procedures for undertaking measurements of similar systems with the static-analytic apparatus and the variable volume static-synthetic apparatus have been described previously [40, 41].

2.5. Data Treatment.

The combined expanded uncertainties in the reported pressures, temperatures and compositions were estimated according to the guidelines issued by the National Institute of Standards and Technology (NIST) [42, 43]. To calculate the combined expanded uncertainties, the estimated uncertainties were multiplied by a coverage factor of k equal to 2.

Many gas-liquid high pressure VLE systems have been adequately described with a cubic equation of state and a simple mixing rule [40, 44, 45]. These simple thermodynamic models are, however, unable to accurately predict liquid-liquid immiscibility, and therefore performed poorly with systems containing either trifluoromethane or hexafluoroethane with n-alkanes consisting of 7 or more carbon atoms [46]. Several authors have used a more complex model to describe systems involving n-nonane, n-decane and n-undecane with carbon dioxide [47, 48] and systems involving n-alkanes with hexafluoroethane [49, 50]. This model consisted of the Peng-Robinson equation of state (PR EOS) [51] with the Mathias-Copeman (MC) alpha function [52] along with the Wong-Sandler (WS) mixing rule [53] and the Non-Random Two-Liquid (NRTL) activity coefficient model [54]. This PR-MC + WS/NRTL model was utilised in this study.

The replacement of the NRTL activity coefficient model within the WS mixing rule with the Universal Quasi-Chemical (UNIQUAC) activity coefficient model [55] was also investigated. The MC alpha function parameters for the pure components are regressed from vapour pressure data. The remaining three parameters; one parameter from the WS mixing rule and two from the activity coefficient model; could be regressed as temperature independent parameters for each isotherm individually, or as temperature dependent parameters for all of the data from the system concurrently.

The regression of the experimental data was performed using the regression tool in Aspen Plus V8.4. A Deming algorithm [56] was used to minimise a modified Barker's objective function for the regression of the data. Using these methods, the deviations between experimental and calculated values for pressure and vapour phase composition were minimised.

The average relative deviation (ARD) and the absolute average relative deviation (AARD) for both the pressure and vapour phase compositions were used to evaluate the fit of the thermodynamic models to the experimental data. The ARDs can be calculated using Equation 1, and the AARDs can be calculated using Equation 2.

$$ARD(\theta) = \frac{100}{N_p}\sum_{1}^{N_p}\frac{\theta_{exp} - \theta_{calc}}{\theta_{exp}} \qquad \text{Eqn. 1}$$

$$AARD(\theta) = \frac{100}{N_p}\sum_{1}^{N_p}\frac{\left|\theta_{exp} - \theta_{calc}\right|}{\theta_{exp}} \qquad \text{Eqn. 2}$$

θ refers to the data point, with the subscripts '*exp*' and '*calc*' denoting the experimental data and the calculated data respectively. N_p denotes the number of data points in the regressed data set.

Vapour-liquid equilibrium data from near critical conditions is also useful for extrapolation to the mixture critical loci. Two methods were used to estimate the critical loci of the systems. The method of Ungerer et al. [57], as used by El Ahmar et al. [58] was applied only to isotherms containing vapour-liquid mixture critical loci. This method used extended scaling laws to extrapolate from the subcritical co-existence points to the mixture critical point for a specific isotherm.

The second method for the estimation of the mixture critical loci was that of Heidemann and Khalil [59], in the form discussed by Stockfleth and Dohrn [60]. The Heidemann and Khalil method estimates the

Table 4.
The Mathias-Copeman alpha function parameters (κ_i) for the pure components investigated in this study, in the temperature range (T) of the literature data to which the parameters were regressed.

	T / K	κ_1	κ_2	κ_3
Trifluoromethane	252.93 – 299.07 [b]	0.776	0 [a]	0 [a]
Hexafluoroethane	273.10 – 292.90 [c]	0.777	0 [a]	0 [a]
n-Nonane	273.15 – 353.13 [d]	1.001	-0.009	0.299
n-Decane	273.15 – 333.15 [e]	1.107	-0.330	0.843
n-Undecane	298.09 – 333.11 [f]	0.412	3.965	-7.000

[a] Set to zero for this study.
[b] [40].
[c] [46].
[d] Regressed to literature data [20, 61-66].
[e] Regressed to literature data [28, 64, 67-73].
[f] Regressed to literature data [61, 69, 74-79].

critical locus curves from a thermodynamic model fitted to the experimental data. For a more accurate critical locus curve, the thermodynamic model must describe the experimental data as accurately as possible. The calculation procedures for the two critical loci estimation methods were described in further detail by Williams-Wynn et al. [40].

3. Results and discussion

The vapour pressures of n-nonane for the regression of the MC alpha function parameters were obtained from the work of Young [61], Schaefer et al. [62], Wolff et al. [63], Carruth and Kobayashi [64], Kolasinska et al. [65], Paul et al. [20] and Ahmad et al. [66]. For n-decane, data was obtained from Woringer [67], Reamer and Sage [68], Wadsö [69], Carruth and Kobayashi [64], Brunner [70], Allemand and co-workers [71], Chirico et al. [72], Belaribi et al. [73] and Dejoz and co-workers [28].

The vapour pressures for n-undecane were obtained from the works of Krafft [74], Young [61], Kohlraush and Koppl [75], Letsinger and Traynham [76], Tilicheev et al. [77], Wadsö [69], Marsh and co-workers [78] and Schmelzer et al. [79]. The single MC alpha function parameters for R-23 reported by Williams-Wynn et al. [40] and those for R-116 reported by Williams-Wynn and co-workers [46] were used in this study. The regressed MC alpha function parameters for the n-alkanes are reported in Table 4, alongside the parameters for R-23 and R-116.

The *P-x-x-y* phase equilibrium data for the R-23 (1) + n-nonane (2), R-23 (1) + n-decane (2) and R-23 (1) + n-undecane (2) systems are tabulated in Tables 5, 6 and 7 respectively. For the R-116 (1) + n-decane (2) system, the *P-x-x-y* phase equilibrium data are presented in Table 8. The combined expanded uncertainties for the temperatures, pressures and compositions are included in Tables 5 to 8 alongside of the corresponding data. The bubble pressure measurements for the systems containing R-23 + (n-nonane, n-decane or n-undecane) were performed to verify the VLE data from the static-analytic apparatus. This data, measured for each of the three systems, are presented in Tables 9, 10 and 11. The combined expanded uncertainties of the data are included alongside the bubble pressure data in these tables.

The two thermodynamic models were correlated to the experimental *P-x-x-y* and *P-x-y* data for all four systems. Both temperature dependent and temperature independent parameters were fitted to the data for each model. The parameters for R-23 with n-nonane, n-decane or n-decane are presented in Tables 12 to 14 respectively. The parameters for R-116 + n-decane are presented in Table 15. The statistical information for each of the regressions is also included in Tables 12 through 15. The pressure deviations between the experimental and the modelled data with the temperature dependent parameters were substantially larger than the corresponding deviations with the temperature independent parameters.

Table 5.
Experimental P-x_1^{I}-x_1^{II}-y_1- data with combined expanded uncertainties (U) for the binary system of R-23 (1) + n-nonane (2) at temperatures, T = (272.9 to 313.2) K. The combined expanded uncertainties were calculated with a coverage factor of k = 2.

T / K	U (T) / K	P /MPa	U(P) /MPa	x_1^{I}	$U(x_1^{I})$	x_1^{II}	$U(x_1^{II})$	y_1	$U(y_1)$
272.91	0.07	1.050	0.009	0.076	0.004			0.9959	0.0006
272.94	0.09	1.310	0.004	0.113	0.003			0.9984	0.0010
272.91	0.07	1.540	0.006	0.135	0.003			0.9969	0.0009
272.90	0.07	1.809	0.004	0.165	0.004			0.9992	0.0006
272.92	0.09	1.989	0.010	0.186	0.005			0.9993	0.0001
272.93	0.09	2.235	0.004	0.218	0.005			0.9990	0.0004
272.90	0.08	2.477	0.005	0.248	0.006	0.9803	0.0012	0.9985	0.0006
272.91	0.07	2.526	0.008	0.9942	0.0003			0.9999	0.0001
272.91	0.07	2.527	0.005	0.9944	0.0003			0.9998	0.0001
282.98	0.07	1.117	0.004	0.077	0.004			0.9897	0.0004
282.99	0.07	1.663	0.005	0.128	0.004			0.9968	0.0010
282.99	0.07	1.967	0.005	0.156	0.005			0.9980	0.0005
282.97	0.07	2.355	0.008	0.195	0.005			0.9981	0.0005
282.97	0.07	2.716	0.008	0.231	0.005			0.9967	0.0013
282.96	0.07	3.069	0.007	0.270	0.006			0.9993	0.0002
282.98	0.07	3.188	0.006	0.283	0.006	0.9725	0.0013	0.9978	0.0007
283.00	0.08	3.241	0.004	0.9932	0.0005			0.9997	0.0002
283.00	0.07	3.270	0.005	0.9964	0.0006			0.9995	0.0001
293.06	0.07	1.189	0.005	0.078	0.003			0.9939	0.0010
293.07	0.07	1.778	0.006	0.125	0.004			0.9975	0.0010
293.06	0.07	2.114	0.007	0.150	0.004			0.9979	0.0002
293.06	0.07	2.517	0.006	0.182	0.004			0.9979	0.0003
293.05	0.07	2.929	0.007	0.217	0.005			0.9985	0.0008
293.04	0.07	3.351	0.008	0.258	0.006			0.9984	0.0019
293.05	0.07	3.674	0.008	0.285	0.007			0.9993	0.0005
293.05	0.07	4.015	0.011	0.321	0.007			0.9988	0.0008
293.07	0.07	4.031	0.007	0.318	0.007	0.9802	0.0016	0.9990	0.0005
293.08	0.07	4.092	0.004	0.9892	0.0011			0.9994	0.0001
303.13	0.07	1.257	0.005	0.074	0.003			0.9942	0.0005
303.15	0.07	1.884	0.007	0.118	0.004			0.9972	0.0012
303.14	0.07	2.245	0.009	0.145	0.004			0.9979	0.0009
303.14	0.07	2.674	0.008	0.176	0.005			0.9977	0.0006
303.13	0.07	3.125	0.010	0.209	0.006			0.9984	0.0006
303.11	0.07	3.603	0.010	0.243	0.006			0.9980	0.0008
303.13	0.07	3.989	0.005	0.272	0.007			0.9988	0.0004
303.14	0.07	4.557	0.009	0.316	0.007			0.9976	0.0009
303.14	0.07	4.938	0.009	0.344	0.008			0.9987	0.0004
303.14	0.07	5.059	0.006	0.352	0.007	0.9877	0.0008	0.9979	0.0007
303.17	0.07	5.097	0.009	0.9909	0.0003			0.9947	0.0002
313.23	0.07	1.029	0.004	0.050	0.003			0.9957	0.0005
313.23	0.07	2.146	0.004	0.121	0.004			0.9946	0.0008
313.23	0.07	2.815	0.009	0.168	0.004			0.9963	0.0010
313.21	0.07	3.305	0.011	0.202	0.005			0.9982	0.0011
313.20	0.08	3.831	0.011	0.238	0.006			0.9973	0.0006
313.22	0.07	4.232	0.008	0.262	0.006			0.9973	0.0007
313.24	0.07	4.821	0.005	0.303	0.007			0.9978	0.0005
313.24	0.07	5.410	0.009	0.340	0.007			0.9976	0.0004
313.24	0.08	6.000	0.005	0.366	0.007			0.9954	0.0002
313.23	0.07	6.247	0.007	0.373	0.007			0.9918	0.0003
313.24	0.07	6.297	0.006	0.370	0.007			0.9901	0.0004

P-x-y plots were produced for each of the four systems (Figures 1 through 4). These P-x-y plots include the experimental data from the static-analytic apparatus and the variable-volume apparatus, as well as the VLE curves calculated from the thermodynamic models. The points along these curves were calculated using the thermodynamic models with temperature independent parameters. This was due to the substantially better fit that was achieved when temperature dependency was not accounted for in the thermodynamic models.

Only one isotherm from the R-23 + n-nonane system contained vapour-liquid coexistence points near to the critical point, and the method of Ungerer et al. could therefore only be applied to this isotherm. This critical locus was included on Figure 1. The critical locus curve

Table 6.
Experimental P-x_1^{I}-x_1^{II}-y_1 data with combined expanded uncertainties (U) for the binary system of R-23 (1) + n-decane (2) at temperatures, T = (272.9 to 313.3) K. The combined expanded uncertainties were calculated with a coverage factor of k = 2.

T / K	U (T) / K	P /MPa	U(P) /MPa	x_1^{I}	U(x_1^{I})	x_1^{II}	U(x_1^{II})	y_1	U(y_1)
272.90	0.07	0.928	0.005	0.032	0.001			0.9947	0.0020
272.90	0.07	1.194	0.004	0.043	0.001			0.9920	0.0017
272.90	0.07	1.595	0.004	0.062	0.003			0.9905	0.0029
272.89	0.07	2.028	0.006	0.083	0.003			0.9922	0.0024
272.90	0.07	2.218	0.007	0.094	0.003			0.9910	0.0012
272.89	0.07	2.251	0.004	0.096	0.003			0.9910	0.0029
272.90	0.08	2.485	0.004	0.108	0.004	0.9533	0.0026	0.9970	0.0013
272.89	0.08	2.504	0.004	0.9710	0.0010			0.9962	0.0013
272.89	0.08	2.513	0.004	0.9837	0.0018			0.9980	0.0009
272.89	0.08	2.517	0.004	0.9867	0.0008			0.9995	0.0001
293.08	0.08	0.845	0.004	0.023	0.001			0.9923	0.0025
293.09	0.08	1.366	0.006	0.040	0.002			0.9913	0.0021
293.09	0.08	1.909	0.004	0.058	0.002			0.9905	0.0025
293.09	0.08	2.572	0.007	0.084	0.003			0.9929	0.0013
293.07	0.07	2.948	0.008	0.098	0.003			0.9944	0.0012
293.07	0.07	3.518	0.005	0.122	0.004			0.9936	0.0030
293.08	0.08	4.015	0.009	0.140	0.005			0.9994	0.0003
293.09	0.08	4.088	0.005	0.144	0.004	0.9652	0.0019	0.9962	0.0009
293.08	0.07	4.092	0.004	0.9892	0.0011			0.9994	0.0005
293.07	0.07	4.106	0.004	0.9775	0.0013			0.9990	0.0002
293.06	0.07	4.115	0.004	0.9840	0.0011			0.9987	0.0005
303.15	0.08	0.906	0.004	0.023	0.001			0.9900	0.0015
303.14	0.08	1.327	0.004	0.035	0.001			0.9940	0.0006
303.15	0.08	1.779	0.006	0.049	0.001			0.9943	0.0008
303.14	0.08	2.582	0.005	0.076	0.002			0.9954	0.0010
303.14	0.08	3.138	0.007	0.095	0.003			0.9978	0.0002
303.14	0.08	3.730	0.007	0.116	0.004			0.9954	0.0016
303.14	0.08	4.983	0.004	0.158	0.004			0.9900	0.0016
303.14	0.08	5.178	0.004	0.162	0.005			0.9868	0.0021
303.15	0.07	5.212	0.007	0.163	0.004			0.9816	0.0008
313.26	0.08	0.965	0.004	0.023	0.001			0.9882	0.0012
313.26	0.08	1.795	0.004	0.045	0.002			0.9910	0.0016
313.27	0.08	2.529	0.006	0.066	0.003			0.9930	0.0014
313.26	0.08	3.310	0.009	0.091	0.003			0.9963	0.0020
313.27	0.08	4.118	0.006	0.115	0.004			0.9953	0.0009
313.26	0.10	4.843	0.010	0.139	0.004			0.9918	0.0010
313.27	0.09	5.477	0.007	0.158	0.004			0.9921	0.0018
313.27	0.09	6.208	0.010	0.174	0.004			0.9926	0.0018
313.25	0.08	6.335	0.007	0.178	0.004			0.9846	0.0035
313.29	0.08	6.595	0.004	0.180	0.005			0.9751	0.0032

estimation procedure of Heidemann and Khalil was used to produce curves for all four systems at refrigerant compositions of between 0.9 and 1.0. Several points for each critical locus curve are reported in Table 16, and the curves were included on Figures 1 to 4. Outside of the composition range for which the mixture critical loci were estimated, the critical temperatures were significantly higher than the measurement ranges. The likelihood of significant errors being introduced into the critical loci due to poor description of the systems by extrapolation of the models to these temperatures was large and therefore avoided.

On Figure 1, the critical locus that was extrapolated from the experimental data agreed with the critical locus curve that was calculated using the thermodynamic model. The inability of the temperature dependent thermodynamic model to precisely correlate the pressures of the system did not appear to adversely affect the critical locus curve. The effect of the poor pressure prediction could, however, have been masked by the steepness of the slope relating the critical pressure to the critical temperature, .

Table 7.
Experimental P-x_1^{I}-x_1^{II}-y_1 data with combined expanded uncertainties (U) for the binary system of R-23 (1) + n-undecane (2) at temperatures, T = (293.1 to 313.3) K. The combined expanded uncertainties were calculated with a coverage factor of k = 2.

T / K	U (T)/ K	P / MPa	U(P) / MPa	x_1^{I}	U (x_1^{I})	x_1^{II}	U (x_1^{II})	y_1	U(y_1)
293.07	0.07	0.945	0.004	0.027	0.002			0.9965	0.0014
293.06	0.07	1.308	0.004	0.039	0.001			0.9959	0.0018
293.06	0.07	1.796	0.007	0.056	0.002			0.9965	0.0012
293.07	0.07	2.332	0.006	0.075	0.002			0.9967	0.0010
293.07	0.07	2.889	0.006	0.096	0.003			0.9952	0.0006
293.07	0.07	3.418	0.007	0.115	0.003			0.9949	0.0011
293.06	0.08	3.763	0.010	0.127	0.003			0.9970	0.0008
293.07	0.07	4.128	0.006	0.140	0.004	0.984	0.001	0.9969	0.0008
293.07	0.07	4.136	0.004	0.986	0.001			0.9993	0.0003
293.07	0.07	4.165	0.004	0.993	0.001			0.9998	0.0002
303.16	0.08	1.063	0.004	0.029	0.001			0.9965	0.0013
303.16	0.08	1.491	0.006	0.042	0.002			0.9980	0.0010
303.16	0.08	2.096	0.007	0.061	0.002			0.9988	0.0005
303.16	0.08	3.486	0.005	0.107	0.003			0.9978	0.0014
303.16	0.08	4.118	0.007	0.128	0.004			0.9965	0.0019
303.15	0.08	4.693	0.009	0.144	0.004			0.9980	0.0007
303.17	0.07	4.904	0.007	0.149	0.004			0.9951	0.0008
303.15	0.08	5.173	0.006	0.154	0.005			0.9986	0.0002
303.17	0.08	5.215	0.004	0.155	0.004			0.9933	0.0008
303.16	0.08	5.252	0.004	0.156	0.004			0.9924	0.0020
313.26	0.09	0.886	0.004	0.021	0.001			0.9964	0.0015
313.26	0.09	1.552	0.005	0.040	0.001			0.9962	0.0013
313.25	0.09	2.271	0.004	0.061	0.002			0.9968	0.0013
313.25	0.10	3.057	0.005	0.084	0.003			0.9960	0.0012
313.25	0.10	3.855	0.007	0.108	0.003			0.9943	0.0010
313.26	0.09	4.540	0.007	0.130	0.003			0.9941	0.0006
313.27	0.08	5.191	0.007	0.146	0.004			0.9943	0.0018
313.26	0.09	5.424	0.006	0.152	0.004			0.9971	0.0009
313.26	0.08	5.876	0.010	0.162	0.005			0.9917	0.0017
313.27	0.08	6.301	0.008	0.168	0.005			0.9920	0.0006
313.26	0.09	6.458	0.005	0.171	0.004			0.9900	0.0013

Table 8.
Experimental P-x_1^{I}-x_1^{II}-y_1 data with combined expanded uncertainties (U) for the binary system of R-116 (1) + n-decane (2) at temperatures, T = (293.1 to 313.2) K. The combined expanded uncertainties were calculated with a coverage factor of k = 2.

T / K	U (T) / K	P / MPa	U(P) / MPa	x_1^{I}	U (x_1^{I})	x_1^{II}	U (x_1^{II})	y_1	U(y_1)
293.13	0.04	0.979	0.006	0.038	0.001			0.993	0.004
293.13	0.04	1.267	0.006	0.049	0.002			0.994	0.004
293.14	0.04	1.584	0.008	0.062	0.002			0.992	0.005
293.14	0.04	1.925	0.004	0.075	0.003			0.994	0.001
293.13	0.04	2.365	0.005	0.098	0.004			0.991	0.002
293.13	0.04	2.692	0.004	0.109	0.003			0.990	0.004
293.13	0.04	2.959	0.005	0.115	0.004			0.989	0.005
293.13	0.04	2.983	0.004	0.116	0.003	0.983	0.003	0.989	0.003
293.14	0.06	3.367	0.005	0.117	0.004	0.982	0.002		
303.15	0.04	0.896	0.004	0.032	0.002			0.9940	0.0005
303.14	0.04	1.271	0.007	0.049	0.007			0.9959	0.0043
303.14	0.04	1.428	0.004	0.052	0.002			0.9957	0.0005
303.14	0.04	1.988	0.007	0.072	0.003			0.9935	0.0010
303.14	0.04	2.356	0.009	0.087	0.004			0.9934	0.0013
303.14	0.04	2.767	0.006	0.101	0.004			0.9943	0.0013
303.14	0.04	3.201	0.007	0.111	0.003			0.9944	0.0009
303.15	0.04	3.628	0.007	0.123	0.004			0.9957	0.0010
303.15	0.04	4.412	0.005	0.130	0.004			0.9890	0.0008
313.17	0.04	0.993	0.004	0.035	0.010			0.9958	0.0007
313.17	0.04	1.456	0.007	0.053	0.005			0.9950	0.0007
313.17	0.05	2.133	0.012	0.079	0.009			0.9971	0.0012
313.17	0.05	2.653	0.005	0.096	0.006			0.9946	0.0010
313.17	0.05	3.089	0.005	0.109	0.005			0.9954	0.0010
313.17	0.04	3.540	0.010	0.125	0.005			0.9944	0.0005
313.17	0.04	4.164	0.006	0.141	0.004			0.9927	0.0006
313.16	0.04	4.596	0.005	0.146	0.004			0.9927	0.0011
313.17	0.04	5.441	0.004	0.152	0.005			0.9875	0.0008

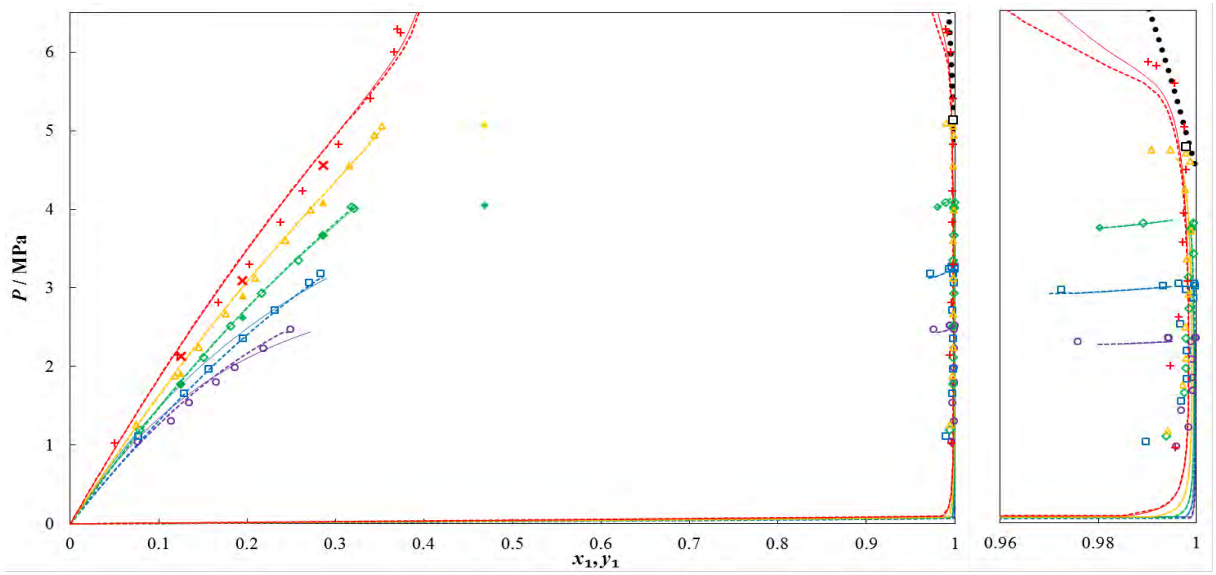

Fig. 1. P-x_1^I-x_1^{II}-y_1 data for the binary system of trifluoromethane (1) + n-nonane (2). Data was measured using a static-analytic apparatus at the temperatures, T = ○, 272.9 K; □, 283.0 K; ◇, 293.1 K; △, 303.1 K; +, 313.2 K. Data measured using a variable-volume apparatus at temperatures, T = ◆, 293.0 K; ▲, 303.1 K; X, 313.2 K. Solid lines, PR MC + WS/NRTL model; dashed line, PR MC + WS/UNIQUAC model; □, mixture critical point (Ungerer et al. method); ••••, mixture critical locus curve (Heidemann and Khalil method).

.

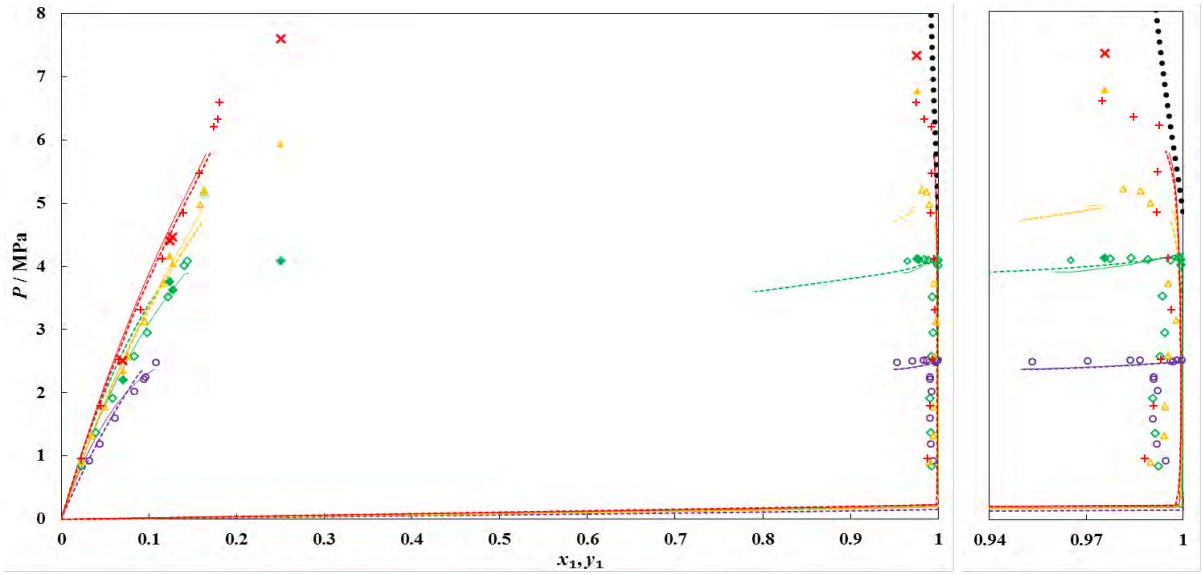

Fig. 2. P-x_1^I-x_1^{II}-y_1 data for the binary system of trifluoromethane (1) + n-decane (2). Data was measured using a static-analytic apparatus at temperatures, T = ○, 272.9 K; ◇, 293.1 K; △, 303.1 K; +, 313.3 K. Data measured using a variable-volume apparatus at temperatures of T = ◆, 293.0 K; ▲, 303.1 K; X, 313.2 K. Solid lines, PR MC + WS/NRTL model; dashed line, PR MC + WS/UNIQUAC model; ••••, mixture critical locus curve (Heidemann and Khalil method).

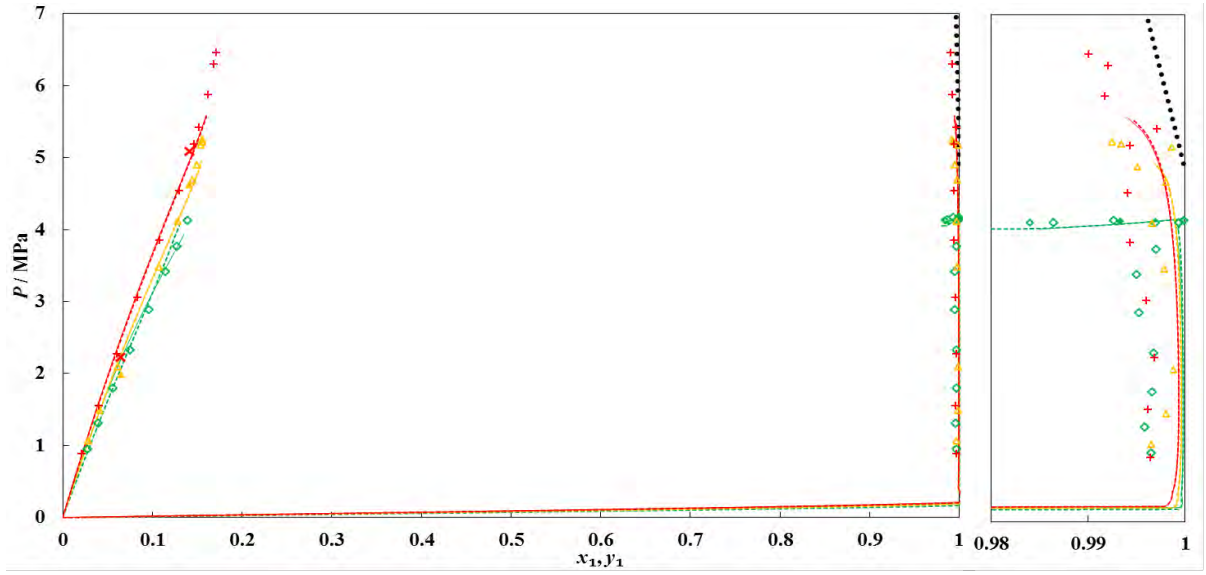

Fig. 3. P-x_1^{II}-x_1^{II}-y_1 data for the binary system of trifluoromethane (1) + n-undecane (2). Data was measured using a static-analytic apparatus at temperatures of T = ◇, 293.1 K; △, 303.2 K; +, 313.3 K. Data was also measured using a variable-volume apparatus at temperatures of T = ◆, 293.0 K; ▲, 303.1 K; X, 313.2 K. Solid lines, PR MC + WS/NRTL model; dashed line, PR MC + WS/UNIQUAC model; ••••, mixture critical locus curve (Heidemann and Khalil method).

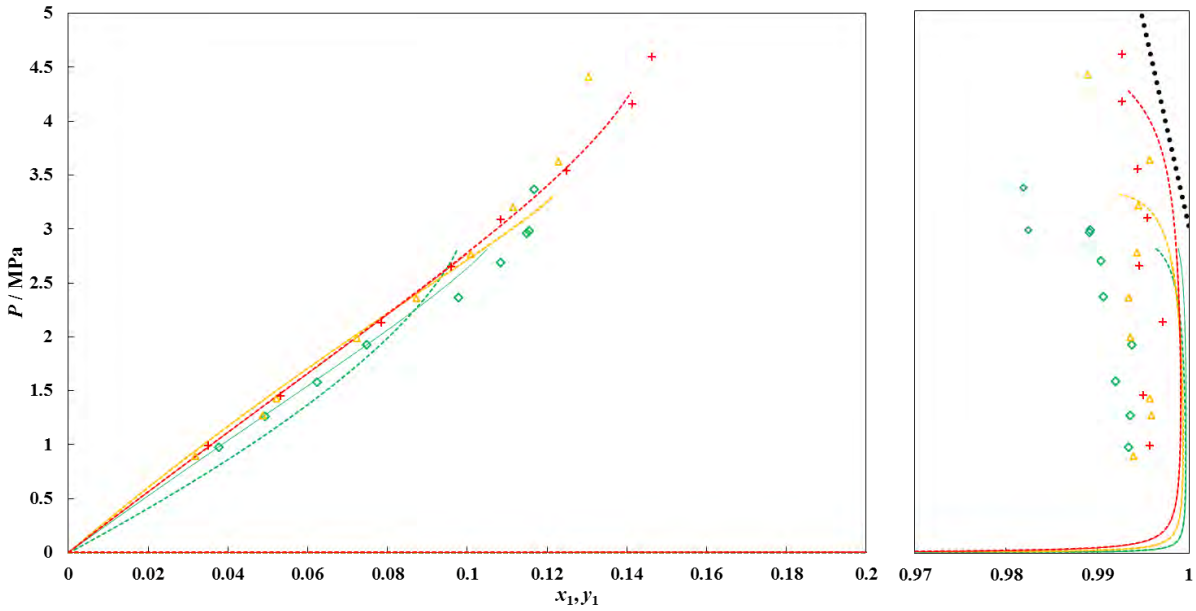

Fig. 4. P-x_1^{I}-x_1^{II}-y_1 data for the binary system of hexafluoroethane (1) + n-decane (2). Data was measured using the static-analytic apparatus at temperatures of T = ◇, 293.1 K; △, 303.1 K; +, 313.2 K. Solid lines, PR MC + WS/NRTL model; dashed line, PR MC + WS/UNIQUAC model; ••••, mixture critical locus curve (Heidemann and Khalil method).

Table 9.
Experimental bubble point P-x_1 data with combined expanded uncertainties (U) for the binary system of trifluoromethane (1) and n-nonane (2) at temperatures, T = (293.1 to 313.2) K. The combined expanded uncertainties were calculated with k = 2.

T / K	U(T) / K	P / MPa	U(P) / MPa	x_1	U(x_1)
293.16	0.03	1.778	0.005	0.125	0.003
293.14	0.03	2.623	0.006	0.195	0.001
293.14	0.03	3.667	0.010	0.286	0.001
293.13	0.03	4.049	0.007	0.469	0.001
303.18	0.03	1.908	0.006	0.125	0.003
303.16	0.03	2.899	0.008	0.195	0.001
303.16	0.04	4.092	0.007	0.286	0.001
303.15	0.03	5.088	0.007	0.469	0.001
313.21	0.04	2.130	0.005	0.125	0.003
313.20	0.03	3.097	0.007	0.195	0.001
313.19	0.03	4.560	0.014	0.286	0.001

Table 10.
Experimental bubble point P-x_1 data with combined expanded uncertainties (U) for the binary system of trifluoromethane (1) and n-decane (2) at temperatures, T = (293.0 to 313.3) K. The combined expanded uncertainties were calculated with a coverage factor of k = 2 .

T / K	U(T) / K	P / MPa	U(P) / MPa	x_1	U(x_1)
293.15	0.03	2.203	0.007	0.070	0.003
293.05	0.03	3.758	0.011	0.124	0.002
293.16	0.03	3.632	0.008	0.127	0.011
293.03	0.04	4.086	0.008	0.250 [a]	0.001
293.03	0.03	4.124	0.004	0.976	0.002
303.06	0.03	2.350	0.006	0.070	0.003
303.05	0.03	4.168	0.007	0.124	0.002
303.18	0.03	4.047	0.005	0.127	0.011
303.09	0.03	5.943	0.010	0.250 [a]	0.001
303.03	0.03	6.776	0.007	0.976	0.002
313.26	0.03	2.509	0.010	0.070	0.003
313.06	0.03	4.407	0.012	0.124	0.002
313.21	0.03	4.464	0.007	0.127	0.011
313.05	0.06	7.602	0.009	0.250	0.001
313.05	0.03	7.339	0.005	0.976	0.002

[a] VLLE region

Table 11.
Experimental bubble point P-x_1 data with combined expanded uncertainties (U) for the binary system of trifluoromethane (1) and n-undecane (2) at temperatures, T = (293.0 to 313.1) K. A coverage factor of k = 2 was used in the calculation of the combined expanded uncertainties .

T / K	U(T) / K	P / MPa	U(P) / MPa	x_1	U(x_1)
293.08	0.03	1.873	0.010	0.065	0.004
293.07	0.03	4.118	0.005	0.141	0.002
293.05	0.03	4.131	0.009	0.862 [a]	0.001
293.07	0.03	4.154	0.004	0.993	0.002
303.09	0.04	1.990	0.011	0.065	0.004
303.09	0.03	4.626	0.008	0.141	0.002
313.05	0.04	2.228	0.009	0.065	0.004
313.05	0.03	5.089	0.009	0.141	0.002

[a] VLLE region

The poor fit of the temperature dependent models to the experimental data is likely due to the different trends of the parameters above and below the critical temperature of the refrigerant. These trends are shown in Figures 5 to 8. The temperature dependent models are not capable of providing sufficient flexibility for the parameters above and below the critical points, and therefore the model correlation is compromised. A possible solution to this problem would be to separate the data into two subsets, one set containing data from below the critical temperature of the lighter component, and the other set containing data from above it.

There was little difference between the two thermodynamic models when comparing the degree to which they fitted the experimental data. For the R-23 and n-nonane system, the UNIQUAC containing model appeared to provide a slightly better description of the phase equilibrium. This was especially noticeable when observing the MRDs and AARDs of the temperature dependent regressions. With R-23 + n-decane, on the other hand, the NRTL containing model provided better correlation of the data. Convergence difficulties were encountered for the higher temperatures. This was especially so at higher pressures where liquid-liquid equilibrium occurred. Both of the models predicted a three phase region at 303.1 K, but this was not observed experimentally.

An observation from the R-23 + n-undecane system (Figure 3) is the ability of both models to predict the occurrence of VLLE at temperatures below the R-23 critical point, but not for the temperatures above it. For this system, there was no clear difference between the performances

of the two models. There was poor convergence to the phase equilibrium conditions of the system at higher temperatures and pressures. With R-116 and n-decane system, the calculations using the UNIQUAC containing model continued to converge at substantially higher pressures, and therefore gave a better description of the system at higher temperatures. At the lowest temperature (293.0 K), however, the deviations between the experimental and calculated pressures were substantially larger when using the UNIQUAC model than with the NRTL model.

All three of the systems that contained R-23 exhibited the 'bird's beak phenomenon', described by Rainwater [80]. The thermodynamic models were able to describe this behaviour with a fair degree of accuracy. The models were, however, not particularly accurate in describing the upper critical end points (UCEP) for the systems. At the UCEPs, the VLLE curve ends as it intersects the critical curve extending from the pure component critical point of the more volatile component. The poor prediction of the UCEPs is related to the erroneous prediction of a three-phase solution by the thermodynamic models, at temperatures at which only two phases were found experimentally.

The R-116 + n-decane system exhibited VLLE at temperatures near to the critical temperature of R-116. This phenomenon was more difficult to observe in this system than in the systems involving R-23, due to the low solubilities of n-decane in the R-116 rich phases. The R-116 rich phases contained similar, small concentrations of n-decane. The thermodynamic models did not accurately predict the UCEP for this system. An interesting observation was made with the 293.0 K isotherm. VLLE was observed to occur at this temperature; with one n-

Table 12.

The temperature dependent and temperature independent model parameters (k_{12} and τ_{ij} or Δu_{ij}) and regression statistics for the binary system of trifluoromethane (1) + n-nonane (2). The temperature dependent parameters were regressed at temperatures, T = (272.9 to 313.2) K. The average relative deviations (ARD) and the absolute average relative deviations (AARD) in the pressure and vapour mole fraction are included for each of the regressions .

T / K	k_{12}	τ_{12} / K [a] || $\Delta u\text{-}_{12}$ [b] / J·mol^{-1}	τ_{21} / K [a] || Δu_{21} [b] / J·mol^{-1}	*ARD* [c]		*AARD* [d]	
				P	y	P	y
PRMC + WS/NRTL							
272.9	0.591	1699.8	427.5	-2.77	-0.19	3.82	0.29
283.0	0.581	1656.2	371.8	-0.69	-0.16	2.70	0.19
293.1	0.600	1699.3	287.2	-0.20	-0.10	0.72	0.15
303.1	0.654	886.8	177.5	-0.38	-0.07	1.47	0.11
313.2	0.659	809.6	175.4	-0.34	-0.05	4.51	0.16
(272.9 – 313.2)	0.670	647.0	281.1	-2.73	-0.06	6.06	0.18
PRMC + WS/UNIQUAC							
272.9	0.666	-283.2	-3637.3	-0.70	-0.15	3.28	0.27
283.0	0.637	-580.9	-3182.0	1.21	-0.12	1.23	0.12
293.1	0.657	-386.8	-3287.2	-0.18	-0.10	0.81	0.15
303.1	0.654	-287.9	-3369.2	-0.36	-0.07	1.51	0.11
313.2	0.648	-140.0	-3594.5	-0.13	-0.02	4.90	0.17
(272.9 – 313.2)	0.660	4.5	-3865.2	-0.54	0.01	3.95	0.23

[a] τ_{12}, τ_{21} for the NRTL activity coefficient model
[b] Δu_{12}, Δu_{21} for the UNIQUAC activity coefficient model

[c] absolute average deviation, $$ARD(\theta) = \frac{100}{N_p}\sum_{1}^{N_p}\frac{\theta_{exp} - \theta_{calc}}{\theta_{exp}}$$

[d] absolute average relative deviation, $$AARD(\bar{\theta}) = \frac{100}{N_p}\sum_{1}^{N_p}\frac{|\bar{\theta}_{exp} - \bar{\theta}_{calc}|}{\bar{\theta}_{exp}}$$

Table 13.

The temperature dependent and temperature independent model parameters (k_{12} and τ_{ij} or Δu_{ij}) and regression statistics for the binary system of trifluoromethane (1) + n-decane (2). The temperature dependent parameters were regressed at temperatures, T = (272.9 to 313.2) K. The average relative deviations (ARD) and the absolute average relative deviations (AARD) in the pressure and vapour mole fraction are included for each of the regressions .

T / K	k_{12}	τ_{12} / K [a] || $\Delta u\text{-}_{12}$ [b] / J·mol^{-1}	τ_{21} / K [a] || Δu_{21} [b] / J·mol^{-1}	*ARD*		*AARD*	
				P	y	P	y
PRMC + WS/NRTL							
272.9	0.573	1882.9	737.5	-0.64	-0.55	5.72	0.55
293.1	0.587	1944.6	657.4	-0.30	-0.40	3.15	0.41
303.1	0.612	520.9	838.2	-0.68	0.26	1.60	1.38
313.3	0.664	538.4	572.1	-2.11	-0.44	3.76	0.45
(272.9 – 313.3)	0.608	520.2	626.9	-2.29	0.69	6.75	1.65
PRMC + WS/UNIQUAC							
272.9	0.650	-59.4	-5343.3	0.74	-0.55	3.18	0.55
293.1	0.668	94.7	-5417.1	-6.68	-0.37	7.46	0.38
303.1	0.605	360.2	-5938.4	0.60	-0.60	1.96	0.60
313.3	0.659	501.7	-6096.0	0.23	-0.15	3.31	0.66
(272.9 – 313.3)	0.615	-688.5	-4192.3	10.43	0.98	20.25	1.85

[a] τ_{12}, τ_{21} for the NRTL activity coefficient model
[b] Δu_{12}, Δu_{21} for the UNIQUAC activity coefficient model

Table 14.

The temperature dependent and temperature independent model parameters (k_{12} and τ_{ij} or Δu_{ij}) and regression statistics for the binary system of trifluoromethane (1) + n-undecane (2). The temperature dependent parameters were regressed at temperatures, T = (293.1 to 313.3) K. The average relative deviations (ARD) and the absolute average relative deviations (AARD) in the pressure and vapour mole fraction are included for each of the regressions.

T / K	k_{12}	τ_{12} / K [a] || $\Delta u\text{-}_{12}$ [b]	τ_{21} / K [a] || Δu_{21} [b]	*ARD*		*AARD*	
				P	y	P	y
PRMC + WS/NRTL							
293.1	0.674	1651.9	613.7	-2.61	-0.27	3.66	0.29
303.2	0.689	931.6	500.0	2.20	-0.13	2.61	0.19
313.3	0.669	789.1	519.3	1.06	0.04	2.74	0.50
(293.1 – 313.3)	0.706	620.3	595.8	-7.14	0.10	8.68	0.52
PRMC + WS/UNIQUAC							
293.1	0.707	-165.6	-5260.7	0.30	-0.27	2.08	0.27
303.2	0.691	202.3	-5761.4	3.36	-0.12	3.82	0.18
313.3	0.674	315.8	-5991.3	1.82	-0.04	2.77	0.46
(293.1 – 313.3)	0.690	-231.0	-5044.8	1.88	1.00	8.39	1.42

[a] τ_{12}, τ_{21} for the NRTL activity coefficient model
[b] Δu_{12}, Δu_{21} for the UNIQUAC activity coefficient model

Table 15.

The temperature dependent and temperature independent model parameters (k_{12} and τ_{ij} or Δu_{ij}) and regression statistics for the binary system of hexafluoroethane (1) + n-decane (2). The temperature dependent parameters were regressed at temperatures, T = (293.1 to 313.2) K. The average relative deviations (ARD) and the absolute average relative deviations (AARD) in the pressure and vapour mole fraction are included for each of the regressions .

T / K	k_{12}	τ_{12} / K [a] || Δu_{12} [b] / J·mol^{-1}	τ_{21} / K [a] || Δu_{21} [b] / J·mol^{-1}	*ARD*		*AARD*	
				P	y	P	y
PRMC + WS/NRTL							
293.1	0.527	662.5	420.2	-1.41	-0.76	3.65	0.78
303.1	0.446	482.9	501.0	0.56	-0.31	6.35	0.33
313.2	0.556	534.4	389.8	0.30	0.07	1.57	0.46
(293.1 – 313.2)	0.559	332.8	536.2	-1.80	-0.25	6.99	0.76
PRMC + WS/UNIQUAC							
293.1	0.340	-3780.4	-407.0	-0.16	-0.69	11.15	0.69
303.1	0.453	856.4	-3565.3	0.57	-0.31	6.32	0.34
313.2	0.563	718.3	-3103.8	0.23	0.06	1.74	0.46
(293.1 – 313.2)	0.564	948.4	-3545.7	1.26	-0.26	7.29	0.78

[a] τ_{12}, τ_{21} for the NRTL activity coefficient model
[b] Δu_{12}, Δu_{21} for the UNIQUAC activity coefficient model

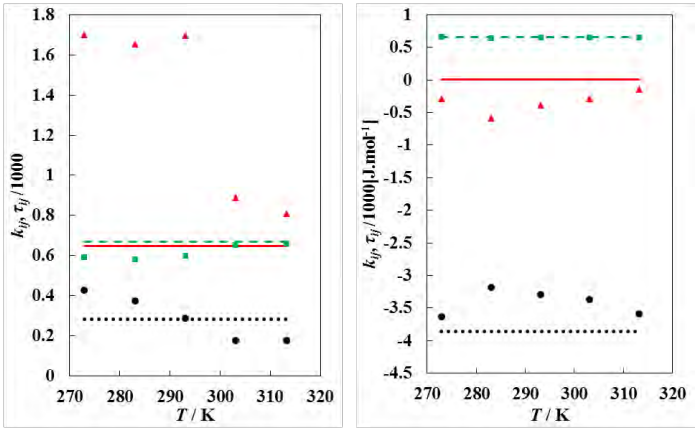

Fig. 5. The thermodynamic model parameters for the system of R-23 (1) + n-nonane (2). Symbols represent parameters regressed independently for each isotherm, while lines represent parameters regressed for all isotherms simultaneously. *Left*: (NRTL) ■/- - -, k_{12}; ●/·····, τ_{12}; ▲/——, τ_{21}. *Right*: (UNIQUAC) ■/- - -, k_{12}; ●/·····, Δu_{12}; ▲/——, Δu_{21}.

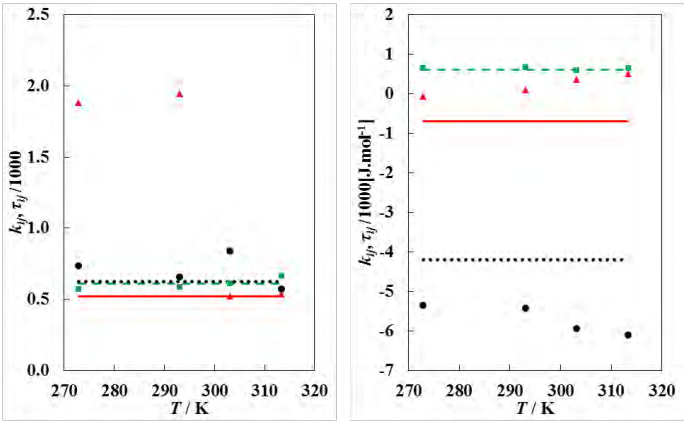

Fig. 6. The thermodynamic model parameters for the system of R-23 (1) + n-decane (2). Symbols represent parameters regressed independently for each isotherm, while lines represent parameters regressed for all isotherms simultaneously. *Left*: (NRTL) ■/- - -, k_{12}; ●/·····, τ_{12}; ▲/——, τ_{21}. *Right*: (UNIQUAC) ■/- - -, k_{12}; ●/·····, Δu_{12}; ▲/——, Δu_{21}.

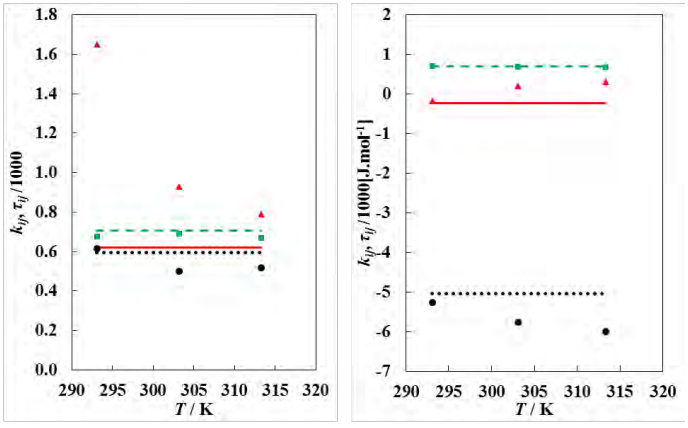

Fig. 7. The thermodynamic model parameters for the system of R-23 (1) + n-undecane (2). Symbols represent parameters regressed independently for each isotherm, while lines represent parameters regressed for all isotherms simultaneously. *Left*: (NRTL) ■/- - -, k_{12}; ●/·····, τ_{12}; ▲/——, τ_{21}. *Right*: (UNIQUAC) ■/- - -, k_{12}; ●/·····, Δu_{12}; ▲/——, Δu_{21}.

decane rich phase and two R-116 rich phases (vapour and liquid). Upon increasing the system pressure, by the addition of R-116, the two R-116 rich phases became homogeneous, but had a phase composition that was of greater similarity to the composition of the previous R-116 rich liquid phase than to that of the previous R-116 rich vapour phase. This

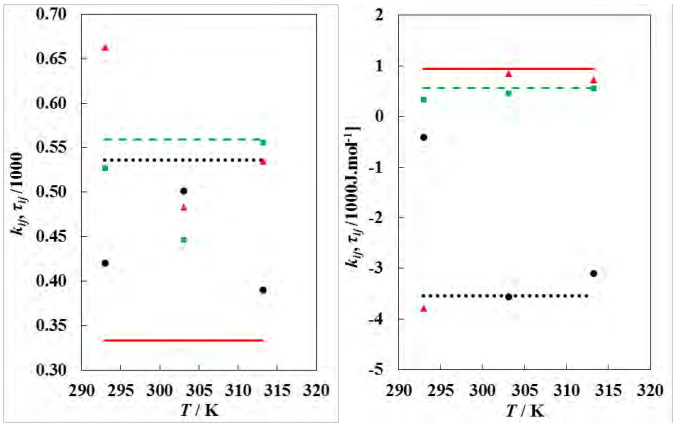

Fig. 8. The thermodynamic model parameters for the system of R-116 (1) + n-decane (2). Symbols represent parameters regressed independently for each isotherm, while lines represent parameters regressed for all isotherms simultaneously. *Left*: (NRTL) ■/- - -, k_{12}; ●/·····, τ_{12}; ▲/——, τ_{21}. *Right*: (UNIQUAC) ■/- - -, k_{12}; ●/·····, Δu_{12}; ▲/——, Δu_{21}.

Table 16.
Critical locus curves (T_c, P_c, $x_{c,i}$) estimated from the thermodynamic models by the method of Heidemann and Khalil [59], and extrapolated mixture critical locus by the method of Ungerer et al. [57] .

Critical Locus Curves					
T_c / K	P_c / MPa	$x_{c,1}$	T_c / K	P_c / MPa	$x_{c,1}$
R-23 (1) + n-nonane (2)			*R-23 (1) + n-decane (2)*		
318.2	7.07	0.99	306.2	8.84	0.99
351.6	12.66	0.96	343.5	27.00	0.96
376.5	18.53	0.93	350.1	53.10	0.93
399.8	25.5	0.90			
R-23 (1) + n-undecane (2)			*R-116 (1) + n-decane (2)*		
309.36	10.56	0.99	328.36	6.79	0.99
340.62	30.60	0.96	339.64	30.43	0.96

Extrapolated Critical Point (*R-23 (1) + n-nonane (2)*)		
T_c / K	P_c / MPa	$x_{c,1}$
303.1	5.14	0.998

phenomenon was repeated a number of times, as it was suspected to be an erroneous point, but found to occur with every measurement. A possible explanation for this phenomenon could be the occurrence of the UCEP at this temperature.

The experimental data that was available implied that all three of the systems containing R-23 were type IV systems of the van Konynenburg and Scott classification scheme [81]. This type of system contains three critical lines; a gas-liquid critical line from C_1 to the UCEP, a liquid-liquid critical line from the UCEP to a critical point at infinite pressure (Cm), and a third critical line (liquid-liquid and gas-liquid) from the lower critical end point (LCEP) to C_2. C_1 and C_2 are the pure component critical points for the lighter and heavier component respectively. The classifications of these systems as type IV were based upon there being a gas-liquid critical line between C_1 and the UCEP, and a liquid-liquid critical line above this towards a possible C_m point. At the temperatures that were investigated, it was not possible to investigate the occurrence of a LCEP. The R-116 + n-decane system was also estimated to be a type IV system, as it exhibited similar characteristics to the systems containing R-23. However, the strange phenomenon that occurred at 293.0 K is not explained by this classification, unless this point was in fact the UCEP.

When comparing the dew curves predicted by the models to the experimental vapour phase data in the expanded views, the discrepancies appear to increase with increased n-alkane chain length. With the R-23 + n-nonane system, the difference between the experimental and

calculated vapour phase values was less than the experimental uncertainty, whereas with the R-23 + n-undecane system, this was no longer the case. This could possibly be due to the increased liquid viscosities with increased chain length. These increase viscosities could have resulted in residual amounts of the n-alkanes remaining in the capillary and contaminating the vapour phase samples. In stating this, however, the capillary was purged between 30 and 50 times before sampling the vapour phase, and thereafter, repeatability of at least 5 consecutive samples was mandatory for these measurements. It is therefore unlikely that additional residual amounts of the heavier component could have been entrained in the sample, especially with the elevated temperatures at which the ROLSI™ was maintained during measurements (453.15 K).

4. Conclusions

The VLE and VLLE for four gas-liquid systems, R-23 + n-nonane, R-23 + n-decane, R-23 + n-undecane and R-116 + n-decane were measured, at temperatures of between (272.9 and 313.3) K, with a static-analytic apparatus. Bubble pressure data was measured for the systems containing R-23, at temperatures of between (293.1 and 313.3) K, with a variable-volume static-synthetic apparatus. The experimental data was correlated with two thermodynamic models. These models consisted of the PR EOS with the MC alpha function and the WS mixing rule, with either the NRTL or the UNIQUAC activity coefficient models. The temperature independent forms of these models were found to fit the experimental data better, due to differences in the trends of the parameters above and below the critical temperature of the more volatile component. Neither of the thermodynamic models were able to accurately describe the occurrence of the UCEP, although the 'bird's beak phenomenon' was described fairly well.

The critical locus extrapolation technique of Ungerer et al. was used to extrapolate a single critical locus for the R-23 + n-nonane system. The Heidemann and Khalil calculation procedure was used for all four systems, to estimate the critical locus curves based upon the thermodynamic models that were fitted to the experimental data. All four of the systems were characterised as type IV systems in the van Konynenburg and Scott classification, although LCEPs were not observed for any of the systems in the range of conditions that were studied.

Acknowledgements

This work is based upon research supported by the South African Research Chairs Initiative of the Department of Science and Technology and the National Research Foundation.

References

[1] McHugh, M.A.; Krukonis, V.J., Supercritical Fluid Extraction Principles and Practice, Butterworths: Stoneham, MA, 1986.

[2] Hauthal, W.H. Advances with supercritical fluids [review]. Chemosphere 2001, 43 (1), 123-135.

[3] Knox, D.E. Solubilities in Supercritical Fluids. Pure Appl. Chem. 2005, 77 (3), 513-530.

[4] Knez, Ž.; Markočič, E.; Leitgeb, M.; Primožič, M.; Knez Hrnčič, M.; Škerget, M. Industrial applications of supercritical fluids: A review. Energy 2014, 77, 235-243.

[5] Teja, A.S.; Eckert, C.A. Commentary on supercritical fluids: Research and applications. Ind. Eng. Chem. Res. 2000, 39 (12), 4442-4444.

[6] Sheng, Y.J.; Chen, P.C.; Chen, Y.P.; Wong, D.S.H. Calculations of solubilities of aromatic compounds in supercritical carbon dioxide. Ind. Eng. Chem. Res. 1992, 31 (3), 967-973.

[7] Kurnik, R.T.; Reid, R.C. Solubility of solid mixtures in supercritical fluids. Fluid Phase Equilib. 1982, 8 (1), 93-105.

[8] Dobbs, J.M.; Wong, J.M.; Johnston, K.P. Nonpolar co-solvents for solubility enhancement in supercritical fluid carbon dioxide. J. Chem. Eng. Data 1986, 31 (3), 303-308.

[9] de Leeuw, V.V.; de Loos, T.W.; Kooijman, H.A.; de Swaan Arons, J. The experimental determination and modelling of VLE for binary subsystems of the quaterhary system N2 + CH4 + C4H10 + C14H30 UP to 1000 bar and 440 K. Fluid Phase Equilib. 1992, 73 (3), 285-321.

[10] Peters, C.J.; de Roo, J.L.; de Swaan Arons, J. Measurements and calculations of phase equilibria in binary mixtures of propane + tetratriacontane. Fluid Phase Equilib. 1992, 72, 251-266.

[11] Peters, C.J.; de Roo, J.L.; de Swaan Arons, J. Phase equilibria in binary mixtures of propane and hexacontane. Fluid Phase Equilib. 1993, 85, 301-312.

[12] Sánchez-García, C.; Vázquez-Hernández, K.E.; Galicia-Luna, L.A.; Elizalde-Solis, O. Vapor-liquid equilibrium measurements for the ternary systems of CO 2 + n-hexane + n-decane and CO2 + n-octane + n-decane. Ind. Eng. Chem. Res. 2011, 50 (21), 12254-12258.

[13] Mendo-Sánchez, R.P.; Sánchez-García, C.; Galicia-Luna, L.A.; Elizalde-Solis, O. Vapor-liquid equilibrium for the ternary carbon dioxide+ethanol+n-hexane and quaternary carbon dioxide+ethanol+n-hexane+thiophene systems. Fluid Phase Equilib. 2012, 315, 40-45.

[14] Huie, N.C.; Luks, K.D.; Kohn, J.P. Phase-equilibria behavior of systems carbon dioxide-n-eicosane and carbon dioxide-n-decane-n-eicosane. J. Chem. Eng. Data 1973, 18 (3), 311-313.

[15] Nagarajan, N.; Gasem, K.A.M.; Robinson, R.L. Equilibrium phase compositions, phase densities, and interfacial tensions for carbon dioxide + hydrocarbon systems. 6. Carbon dioxide + n-butane + n-decane. J. Chem. Eng. Data 1990, 35 (3), 228-231.

[16] Chou, G.F.; Forbert, R.R.; Prausnitz, J.M. High-pressure vapor-liquid equilibria for CO2/n-decane, CO2/tetralin, and CO2/n-decane/tetralin at 71.1 and 104.4°C. J. Chem. Eng. Data 1990, 35 (1), 26-29.

[17] Kim, K.Y., 1974. Calorimetric studies on argon and hexafluoroethane and a generalized correlation of maxima in isobaric heat capacity, Thesis, University of Michigan, Ann Arbour, MI

[18] Saikawa, K.; Kijima, J.; Uematsu, M.; Watanabe, K. Determination of the critical temperature and density of hexafluoroethane. J. Chem. Eng. Data 1979, 24 (3), 165-167.

[19] Lide, D.R., CRC Handbook of Chemistry and Physics 2004-2005: A Ready-Reference Book of Chemical and Physical Data, CRC Press LLC, 2004.

[20] Paul, H.-I.; Krug, J.; Knapp, H. Measurements of VLE, hE and vE for binary mixtures of n-alkanes with n-alkylbenzenes. Thermochimica Acta 1986, 108, 9-27.

[21] Garcia, M.; Rey, C.; Villar, V.P.; Rodriguez, J.R. Excess volumes of (n-octane + n-undecane) between 288.15 and 308.15 K. J. Chem. Eng. Data 1986, 31 (4), 481-483.

[22] Garcia, M.; Rey, C.; Villar, V.P.; Rodriguez, J.R. Excess volumes of (n-nonane + n-undecane) between 288.15 and 308.15 K. J. Chem. Eng. Data 1988, 33 (1), 46-48.

[23] Ortega, J. Excess enthalpies of (a methyl alkanoate + n-nonane or n -undecane) at the temperature 298.15 K. J. Chem. Thermodyn. 1991, 23 (11), 1057-1061.

[24] Wu, J.; Asfour, A.-F.A. Densities and excess molar volumes of eight n-alkane binary systems at 293.15 and 298.15 K. Fluid Phase Equilib. 1994, 102 (2), 305-315.

[25] Aucejo, A.; Burguet, M.C.; Munoz, R.; Marques, J.L. Densities, Viscosities, and Refractive Indices of Some n-Alkane Binary Liquid Systems at 298.15 K. J. Chem. Eng. Data 1995, 40 (1), 141-147.

[26] Postigo, M.A.; Garcia, P.H.; Ortega, J.; Tardajos, G. Excess Molar Volumes of Binary Mixtures Containing a Methyl Ester (Ethanoate to Tetradecanoate) with Odd n-Alkanes at 298.15 K. J. Chem. Eng. Data 1995, 40 (1), 283-289.

[27] Aminabhavi, T.M.; Patil, V.B.; Aralaguppi, M.I.; Phayde, H.T.S. Density, Viscosity, and Refractive Index of the Binary Mixtures of Cyclohexane with Hexane, Heptane, Octane, Nonane, and Decane at (298.15, 303.15, and 308.15) K. J. Chem. Eng. Data 1996, 41

(3), 521-525.
[28] Dejoz, A.; González-Alfaro, V.; Miguel, P.J.; Vázquez, M.I. Isobaric Vapor−Liquid Equilibria for Binary Systems Composed of Octane, Decane, and Dodecane at 20 kPa. J. Chem. Eng. Data 1996, 41 (1), 93-96.
[29] González, B.; Dominguez, A.; Tojo, J. Viscosities, densities and speeds of sound of the binary systems: 2-propanol with octane, or decane, or dodecane at T=(293.15, 298.15, and 303.15) K. J. Chem. Thermodyn. 2003, 35 (6), 939-953.
[30] Domańska, U.; Kozłowska, M.K.; Rogalski, M. Solubilities, Partition Coefficients, Density, and Surface Tension for Imidazoles + Octan-1-ol or + Water or + n-Decane†. J. Chem. Eng. Data 2002, 47 (3), 456-466.
[31] Yanes, C.; Maestre, A.; Perez-Tejeda, P.; Calvente, J.J. Excess molar volumes and refractive indices of cis-9-octadecenoic acid + n -alkanes or alkan-1-ols at 298.15 K. J. Chem. Eng. Data 1993, 38 (4), 512-515.
[32] Aminabhavi, T.M.; Bindu, G. Densities, Viscosities, Refractive Indices, and Speeds of Sound of the Binary Mixtures of Bis(2-methoxyethyl) Ether with Nonane,Decane, Dodecane, Tetradecane, and Hexadecane at 298.15, 308.15, and 318.15 K. J. Chem. Eng. Data 1994, 39 (3), 529-534.
[33] Thermodynamic Research Center, TRC Thermodynamic Tables, Thermodynamic Research Center, A.M.U., Editor 1994: College Station, Texas.
[34] Touriño, A.; Gayol, A.; Hervello, M.; Moreno, V.; Iglesias, M. Changes of refractive indices of the ternary mixtures chlorobenzene + n-hexane + (n-nonane or n-decane) at 298.15 K. Phys. Chem. Liq. 2004, 42 (1), 63-74.
[35] Yao, M., Removal of Volatile Organic Compounds from Indoor Air Using Regenerative Activated Carbon Fiber Cloth, Michigan Technological University, 2008.
[36] Gayol, A.; Touriño, A.; Iglesias, M. Temperature dependence of the derived properties of mixtures containing chlorobenzene and aliphatic linear alkanes (C6–C12). Phys. Chem. Liq. 2010, 48 (5), 661-681.
[37] Baragi, J.G.; Maganur, S.; Malode, V.; Baragi, S.J. Excess molar volumes and refractive indices of binary liquid mixtures of acetyl acetone with n-Nonane, n-Decane and n-Dodecane at (298.15, 303.15, and 308.15) K. J. Molecular Liq. 2013, 178, 175-177.
[38] Narasigadu, C.; Naidoo, P.; Coquelet, C.; Richon, D.; Ramjugernath, D. A novel static analytical apparatus for phase equilibrium measurements. Fluid Phase Equilib. 2013, 338, 188-196.
[39] Ngema, P.T.; Nelson, W.M.; Naidoo, P.; Ramjugemath, D.; Richon, D. Isothermal method for hydrate studies using a transparent variable volume cell. Rev. Sci. Instrum. 2014, 85, 045123.
[40] Williams-Wynn, M.D.; Naidoo, P.; Ramjugemath, D. 1. Isothermal vapour-liquid equilibrium data for the binary systems of (CO2 + n-hexane) and (CHF3 + n-hexane). J. Chem. Thermodyn. 2015, unpublished.
[41] Nandi, P.; Moodley, S.; Ramjugernath, D. Isothermal vapor–liquid equilibrium of R170 + perfluorooctane at 308–338 K: Measurement, equation of state modelling, and molecular simulation. Fluid Phase Equilib. 2013, 344, 84-91.
[42] Taylor, B.N.; Kuyatt, C.E. Guidelines for Evaluating and Expressing the Uncertainty of NIST Measurement Results. NIST Technical Note 1994, 1297.
[43] Taylor, B.N.; Mohr, P.J.; Douma, M., The NIST Reference on constants, units, and uncertainty, 2007.
[44] Wagner, Z.; Wichterle, I. High-pressure vapour-liquid equilibrium in systems containing carbon dioxide, 1-hexene, and n-hexane. Fluid Phase Equilib. 1987, 33 (1-2), 109-123.
[45] Iwai, Y.; Hosotani, N.; Morotomi, T.; Koga, Y.; Arai, Y. High-Pressure Vapor-Liquid Equilibria for Carbon Dioxide + Linalool. J. Chem. Eng. Data 1994, 39 (4), 900-902.
[46] Williams-Wynn, M.D.; Naidoo, P.; Ramjugemath, D. 2. Isothermal vapour-liquid equilibrium data for the binary systems of (CHF3 + n -heptane) and (CF6 + n-heptane). Fluid Phase Equilib. 2015, unpublished.
[47] Jiménez-Gallegos, R.; Galicia-Luna, L.A.; Elizalde-Solis, O. Experimental vapor-liquid equilibria for the carbon dioxide + octane and carbon dioxide + decane systems. J. Chem. Eng. Data 2006, 51 (5), 1624-1628.
[48] Camacho-Camacho, L.E.; Galicia-Luna, L.A.; Elizalde-Solis, O.; Martínez-Ramírez, Z. New isothermal vapor–liquid equilibria for the CO2+n-nonane, and CO2+n-undecane systems. Fluid Phase Equilib. 2007, 259 (1), 45-50.
[49] Ramjugernath, D.; Valtz, A.; Coquelet, C.; Richon, D. Isothermal Vapor−Liquid Equilibrium Data for the Hexafluoroethane (R116) + Propane System at Temperatures from (263 to 323) K. J. Chem. Eng. Data 2009, 54 (4), 1292-1296.
[50] Ramjugernath, D.; Valtz, A.; Richon, D.; Williams-Wynn, M.D.; Coquelet, C. Isothermal Vapour-Liquid Equilibrium Data for the Hexafluoroethane (R116) + n-Butane System at Temperatures from (273 to 323) K. J. Chem. Eng. Data 2015, unpublished.
[51] Peng, D.Y.; Robinson, D.B. A New Two-Constant Equation of State. Ind. Eng. Chem. Fundam. 1976, 15, 59-64.
[52] Mathias, P.M.; Copeman, T.W. Extension of the Peng-Robinson Equation of State to Complex Mixtures: Evaluation of the Various Forms of the Local Composition Concept. Fluid Phase Equilib. 1983, 13, 91-108.
[53] Wong, D.S.H.; Sandler, S.I. Theoretically Correct Mixing Rule for Cubic Equations of State. AIChE J. 1992, 38, 671-680.
[54] Renon, H.; Prausnitz, J.M. Local Compositions in Thermodynamic Excess Functions for Liquid Mixtures. AIChE J. 1968, 14, 135-144.
[55] Abrams, D.S.; Prausnitz, J.M. Statistical thermodynamics of liquid mixtures: A new expression for the excess Gibbs energy of partly or completely miscible systems. AIChE J. 1975, 21 (1), 116-128.
[56] Deming, W.E., Statistical Adjustment of Data, Dover Books: Mineola, NY, 1964.
[57] Ungerer, P.; Tavitian, B.; Boutin, A., Applications of molecular simulation in the oil and gas industry- Monte Carlo methods, 2005.
[58] El Ahmar, E.; Valtz, A.; Naidoo, P.; Coquelet, C.; Ramjugernath, D. Isothermal Vapor−Liquid Equilibrium Data for the Perfluorobutane (R610) + Ethane System at Temperatures from (263 to 353) K. J. Chem. Eng. Data 2011, 56 (5), 1918-1924.
[59] Heidemann, R.A.; Khalil, A.M. The calculation of critical points. AIChE J. 1980, 26 (5), 769-779.
[60] Stockfleth, R.; Dohrn, R. An algorithm for calculating critical points in multicomponents mixtures. Fluid Phase Equilib. 1998, 45, 43-52.
[61] Young, S. On the Boiling Points of the Normal Paraffins at Different Pressures. Proc. Roy. Irish Acad. B 1928, 38, 65-92.
[62] Schaefer, K.; Rall, W.; Wirth-Lindemann, F.C. Thermodynamic experiments on the systems acetone + n-heptane and acetone + n-nonane. Z. Phys. Chem. (Munich) 1958, 14, 197-207.
[63] Wolff, H.; Höpfner, A.; Höpfner, H.M. Die Assoziation von Methyl-, Äthyl- und n-Propylamin in gesättigten aliphatischen Kohlenwasserstoffen (nach Dampfdruckmessungen). Ber. Bunsenges. Phys. Chem. 1964, 68 (4), 410-417.
[64] Carruth, G.F.; Kobayashi, R. Vapor pressure of normal paraffins ethane through n-decane from their triple points to about 10 mm mercury. J. Chem. Eng. Data 1973, 18 (2), 115-126.
[65] Kolasinska, G.; Goral, M.; Giza, J. Vapor-Liquid Equilibrium and Excess Gibbs Free Energy in Binary Systems of Acetone with Aliphatic and Aromatic Hydrocarbons. Z. Phys. Chem. (Leipzig) 1982, 263, 151.
[66] Ahmad, S.; Giesen, R.; Lucas, K. Vapor−Liquid Equilibrium Studies for Systems Containing n-Butylisocyanate at Temperatures between 323.15 K and 371.15 K. J. Chem. Eng. Data 2004, 49 (4), 826-831.
[67] Woringer, B. Vapor Pressures of a Series of Benzene Derivatives. Z. Phys. Chem., Stoechiom. Verwandschaftsl. 1900, 34, 257.
[68] Reamer, H.H.; Sage, B.H. Phase Equilibria in Hydrocarbon Systems. Volumetric and Phase Behavior of the n-Decane-CO2 System. J. Chem. Eng. Data 1963, 8 (4), 508-513.
[69] Wadsö, I. A Heat of Vaporisation Calorimeter for Work at 25C and for Small Amounts of Substances. Acta Chemica Scandinavica 1966, 20, 536-543.

[70] Brunner, E. Solubility of hydrogen in 10 organic solvents at 298.15, 323.15, and 373.15 K. J. Chem. Eng. Data 1985, 30 (3), 269-273.
[71] Allemand, N.; Jose, J.; Merlin, J.C. Mesure des pressions de vapeur d'hydrocarbures C10 A C18n-alcanes etn-alkylbenzenes dans le domaine 3-1000 pascal. Thermochimica Acta 1986, 105, 79-90.
[72] Chirico, R.D.; Nguyen, A.; Steele, W.V.; Strube, M.M.; Tsonopoulos, C. The vapor pressure of n-alkanes revisited. New high-precision vapor pressure data on n-decane, n-eicosane, and n-octacosane. J. Chem. Eng. Data 1989, 34 (2), 149-156.
[73] Belaribi, B.F.; Ait-Kaci, A.; Jose, J., Liquid vapor equilibrium. Decane-1-hexyne system, in Int. DATA Ser., Sel. Data Mixtures, Ser. A1991. p. 74-76.
[74] Krafft, F. Ueber neunzehn höhere Normalparaffine Cn H2n + 2 und ein einfaches Volumgesetz für den tropfbar flüssigen Zustand. I. Ber. Dtsch. Chem. Ges. 1882, 15 (2), 1687-1711.
[75] Kohlraush, K.W.F.; Koppl, F. Z. Phys. Chem. Abt. B 1934, 26, 209.
[76] Letsinger, R.L.; Traynham, J.G. The Reaction of Allylsodium with 2-Bromoöctane1. J. Am. Chem. Soc. 1948, 70 (10), 3342-3344.
[77] Tilicheev, M.D.; Peshkov, V.P.; Yuganova, S.A. Cryoscopic Constants and Transition Temperatures of Normal Alkanes. Zh. Obshch. Khim. 1951, 21 (1229-1237).
[78] Marsh, K.N.; Ott, J.B.; Richards, A.E. Excess enthalpies, excess volumes, and excess Gibbs free energies for (n-hexane + n-undecane) at 298.15 and 308.15 K. J. Chem. Thermodyn. 1980, 12 (9), 897-902.
[79] Schmelzer, J.; Lieberwirth, I.; Krug, M.; Pfestorf, R. Vapour-liquid equilibria and heats of mixing in alkane-alcohol(1) systems. I. Vapour-liquid equilibria in 1-alcohol-undecane systems. Fluid Phase Equilib. 1983, 11 (2), 187–200.
[80] Rainwater, J.C. An asymptotic expression for the critical-region "bird's beak" isotherm and adjacent isotherms on the vapor-liquid phase diagram of a simple binary mixture. Fluid Phase Equilib. 2001, 183-184, 41-51.
[81] van Konynenburg, P.H.; Scott, R.L. Critical Lines and Phase Equilibria in Binary Van Der Waals Mixtures. Philos. Trans. R. Soc. 1980, 298, 495-540.

APPENDIX G

Isothermal vapour-liquid equilibrium data for binary systems of (CHF_3 or C_2F_6) with (1-hexene or 3-methylpentane)

Mark D. Williams-Wynn [a], Paramespri Naidoo [a] and Deresh Ramjugernath [a,*]

[a] Thermodynamics Research Unit, School of Engineering, University of KwaZulu-Natal, Howard College Campus, Durban, South Africa

ARTICLE INFO

Keywords:
VLE,
Phase equilibria,
trifluoromethane,
hexafluoroethane,
1-hexene,
3-methylpentane

ABSTRACT

The isothermal vapour-liquid equilibria of R-23 + 1-hexene, R-23 + 3-methylpentane, R-116 + 1-hexene and R-116 + 3-methylpentane were measured at temperatures of between (293.1 and 313.3) K with a static-analytic apparatus. Vapour-liquid-liquid equilibria was exhibited by the R-116 + 1-hexene system. The equilibrium data was modelled with the PR EOS, modified with the MC alpha function, and the WS mixing rule with either the NRTL or the UNIQUAC activity coefficient model. Both the temperature dependent and the temperature independent forms of the models were regressed to the experimental data. The method of Ungerer et al. was used to extrapolate the subcritical co-existence data to the mixture critical loci, while the method of Heidemann and Khalil was used to estimate the critical locus curves for the systems. Each of the four systems were also categorised according to the classification system of van Konynenburg and Scott. .

1. Introduction

As a continuation of the investigation into alternative supercritical (SC) solvents, the phase equilibrium data for the systems of trifluoromethane (R-23) + 1-hexene, R-23 + 3-methylpentane, hexafluoroethane (R-116) + 1-hexene and R-116 + 3-methylpentane were measured [1-4]. At present, the almost sole supercritical solvent that is used in processes involving supercritical fluids is carbon dioxide (CO_2) [5]. When polar solutes are involved, a co-solvent, such as ethanol, must be added to the CO2 to increase the solubilities [6, 7]. It was therefore proposed that alternative solvents be investigated, for which the addition of co-solvents would not be required.

The work that has been previously reported from this study investigated the performance of the SC solvents with n-alkanes alone [1-4]. The performance of the alternative solvents has not as yet been investigated with hydrocarbons containing other functional groups, such as alkenes and branched alkanes. The phase behaviour of R-23 and R-116 with either 1-hexene or 3-methylpentane were therefore investigated at temperatures of between (293.1 and 313.3) K in a static-analytic microcell apparatus.

2. Experimental

2.1. Materials and Chemicals

The 1-hexene (C_6H_{12}, CAS Number 592-41-6) that was used in this study was obtained from Merck Schuchard OHG. Fluka analytical grade 3-methylpentane (C_6H_{14}, CAS Number 96-14-0) was purchased from Sigma-Aldrich. Trifluoromethane (CHF3, CAS Number 75-46-7) and hexafluoroethane (C2F6, CAS Number 76-16-4) were obtained from A-Gas (South Africa) (Pty) Ltd. Helium (Baseline 5.0), from Afrox South Africa was used as the carrier gas in a gas chromatograph (GC) for composition analysis. The suppliers, the purities and the critical temperature and pressure [8-10] of the four components used in the binary VLE measurements are tabulated in Table 1. The purities of the pure components were confirmed by GC analysis. The peak area percentages from the GC analysis are also reported in Table 1.

Densities and refractive indices of the two hydrocarbons, 1-hexene and 3-methylpentane, were measured to complete the pure component characterisation. An Anton-Paar DMA 5000 density meter was used to measure the densities at temperatures of between T = (293.15 to 301.35) K. The measured densities were compared against density data that has been reported in literature [11-18]. The standard combined uncertainties in the density measurements were given by Anton-Paar as 0.005 $kg{\cdot}m^{-3}$ and 0.05 K for density and temperature respectively. Table 2 provides the measured density values alongside data that has been reported previously in literature. There was a favourable comparison of the data.

The refractive indices of the 1-hexene and 3-methylpentane were measured at T = 293.15 K and T = 298.15 K with an Atago RX7000 refractometer. The standard combined uncertainties of this refractometer were specified to be 1×10^{-4} and 0.01 K for refractive index and temperature respectively. The refractive indices were compared against data that was obtained from literature [14, 15, 17-21]. Both the experimental data and the previously reported data are tabulated in Table 3. The experimentally measured refractive indices were very similar to those obtained from literature.

2.2. Experimental Apparatus.

The static-analytic apparatus developed by Narasigadu et al. [22], and used in this study, was capable of measuring phase equilibrium data at temperatures of between (253 and 473) K and at pressures of up to 17 MPa. A more detailed description of the experimental apparatus was given by Williams-Wynn et al. [1].

2.3. Calibrations.

Standards, certified by WIKA Instruments, were used to calibrate the equipment for temperature measurements (WIKA CTH 6500 temperature standard probe) and pressure measurements (CPT 6000 pressure standard transducer). Two Pt100 temperature probes were calibrated at temperatures of between (268.15 and 323.15) K for measurement of the equilibrium temperatures. The temperature standard probe that was used for the calibrations was certified to have a maximum temperature uncertainty of 0.02 K. A (0 to 25) MPa P-10 pressure transducer, for measuring the equilibrium pressure, was calibrated at pressures of between (0 and 10) MPa, with an uncertainty of 0.5 kPa. The standard

Table 1.
Details of the chemicals used in this study: suppliers, stated purities, GC area fractions and critical properties, T_c and P_c.

	Supplier	Stated Purity	GC Area	T_c / K	P_c / MPa
Trifluoromethane, CHF_3	A-Gas (South Africa)	> 0.999 [d]	0.9996	299.07 [c]	4.836 [c]
Hexafluoroethane, C_2F_6	A-Gas (South Africa)	> 0.999 [d]	0.9999	293.03 [b]	3.013 [a]
1-Hexene, C_6H_{12}	Merck Schuchardt	> 0.990 [e]	0.9992	504.5 [c]	3.126 [c]
3-Methylpentane, C_6H_{14}	Fluka Analytic	> 0.990 [e]	0.9980	504.1 [c]	3.206 [c]

[a] [8]
[b] [9]
[c] [10]
[d] volumetric basis
[e] mass basis

Table 2.
Experimentally measured densities, ρ, of 1-hexene and 3-methylpentane at temperatures of between T = (293.15 and 301.35) K, compared to data obtained from literature .

T / K	ρ (lit.) / [kg/m^3]	ρ (exp.) [l] / [kg/m^3]	ρ (lit.) / [kg/m^3]	ρ (exp.) [l] / [kg/m^3]
	1-hexene		*3-methylpentane*	
293.15	673.28 [a]	673.227	664.2 [e]	664.225
295.15		670.871		662.39
297.15		668.986		660.589
	668.46 [b]		659.72 [f]	
298.15	668.05 [c]	668.033	659.67 [g]	659.736
	668.28 [d]		659.68 [h]	
298.60				659.308
301.35		664.998		

[a] [11]
[b] [12]
[c] [13]
[d] [14]
[e] [15]
[f] [16]
[g] [17]
[h] [18]
[l] $u(T)$ = 0.05 K, $u(\rho)$ = 0.04 kg·m^{-3}

Table 3.
Measured refractive indices (R^l) of 1-hexene and 3-methylpentane at temperatures of T = (293.15 and 298.15) K, compared to data reported in literature at the same temperature .

T / K	R^l (*lit.*)	R^l (*exp.*) [i]	R^l (*lit.*)	R^l (*exp.*) [i]
	1-hexene		*3-methylpentane*	
293.15	1.38790 [a]	1.38796	1.3768 [e]	1.37654
	1.38788 [b]			
298.15	1.38539 [c]	1.38510	1.3742 [f]	1.37387
	1.38235 [d]		1.37386 [b]	
			1.3739 [g]	

[a] [14]
[b] [19]
[c] [20]
[d] [21]
[e] [15]
[f] [17]
[g] [18]
[i] $u(T)$ = 0.01 K, $u(R^l)$ = 1×10^{-4}

pressure transmitter used for the calibrations had an uncertainty of less than 6.2 kPa over the full range. The atmospheric pressure was obtained from the internal barometer of a Mensor CPC 3000 Pneumatic High-Speed Pressure Controller (uncertainty of 0.01 kPa).

For the analysis of composition of the phases present within the cell, the thermal conductivity detector (TCD) of a GC was used. The calibration of the TCD was performed by correlating the response to known numbers of moles of a given component injected into the GC. The injection of different known amounts allowed a calibration curve to be produced. For gases, several known volumes of the gas were injected using a 500 µl gas-tight SGE syringe with an accuracy of 1 % of the volume. The number of moles that was injected was determined by using the ideal gas equation. The liquids were injected with a 1.0 µl SGE liquid syringe, which had an uncertainty of 2 % of the volume. The number of moles comprising each injection was calculated using the molar density of the liquids. All of the injected volumes were repeated a minimum of five times to ensure the repeatability of the calibrations. The calibration uncertainties for trifluoromethane and hexafluoroethane were 2.6×10^{-7} moles and 6.0×10^{-8} moles respectively. For 1-hexene and 3-methylpentane, the uncertainties were 2.6×10^{-8} moles and 5.8×10^{-8} moles respectively .

2.4. Experimental Procedure.

The experimental method for high pressure VLE measurements with the static-analytic apparatus were presented previously by Williams -Wynn et al. [1, 2]. Degassing of the components was performed in situ in the equilibrium cell. For further information on the degassing procedure, the reader is referred to the previous papers.

2.5. Data Treatment.

The uncertainties in the experimental data were treated according to the guidelines which were issued by the National Institute of Standards and Technology (NIST) [23, 24]. A coverage factor, k, equal to 2 was used for the calculation of the combined expanded uncertainties.

The Peng-Robinson Equation of State (PR EOS) [25] modified with the Mathias-Copeman (MC) alpha function [26] was used to model the systems. The Wong-Sandler (WS) mixing rule [27] with either the Non-Random Two-Liquid (NRTL) activity coefficient model [28] or the Universal Quasi-Chemical (UNIQUAC) activity coefficient model [29] were incorporated into the model. Regression of both temperature dependent and temperature independent parameters were undertaken using the regression toolkit of Aspen Plus V8. The regression was performed by minimising a modified Barker's objective function (comprising vapour composition residuals and pressure residuals), with a Deming-type algorithm [30].

The ability of the model to adequately describe the systems was evaluated using the average relative deviation (ARD) and the absolute average relative deviation (AARD) of the pressure and the vapour phase compositions. Equations 1 and 2 describe the calculation of these two terms.

$$ARD(\theta) = \frac{100}{N_p}\sum_{1}^{N_p}\frac{\theta_{exp} - \theta_{calc}}{\theta_{exp}} \qquad \text{Eqn. 1}$$

$$AARD(\theta) = \frac{100}{N_p}\sum_{1}^{N_p}\frac{\left|\theta_{exp} - \theta_{calc}\right|}{\theta_{exp}} \qquad \text{Eqn. 2}$$

In Equations 1 and 2, θ refers to the individual data points that were measured, with the subscripts '*exp*' and '*calc*' denoting the experimental and calculated data points respectively. N_p denotes the size of the measured data set

The extended scaling law method of Ungerer et al. [31], as described by El Ahmar et al. [32], and the calculation procedure of Heidemann and Khalil [33], as described by Stockfleth and Dohrn [34], were

used to estimate the mixture critical loci. The method of Ungerer et al. relies on the availability of sub-critical co-existence points, which are extrapolated to the critical point. The method of Heidemann and Khlail, on the other hand, relies on thermodynamic models which have been fitted to experimental data. For further discussion of these methods, the reader is referred to the work of Williams-Wynn et al. [1].

Table 4.
The Mathias-Copeman alpha function parameters (κ_i) for the pure components investigated in this study, in the temperature range (T) of the literature data to which the parameters were regressed.

	T / K	κ_1	κ_2	κ_3
trifluoromethane [b]	252.93 – 299.07	0.776	0 [a]	0 [a]
hexafluoroethane [c]	273.10 – 292.90	0.777	0 [a]	0 [a]
1-hexene [d]	283.15 – 323.15	0.823	-0.291	0.778
3-methylpentane [e]	283.10 – 333.15	0.772	-0.076	0.378

[a] Set to zero for this study.
[b] [1].
[c] [2].
[d] Regressed from literature data [21, 35-42]
[e] Regressed from literature data [16, 43-47]

Table 5.
Experimental P-x_1-y_1 data with combined expanded uncertainties (U) for the binary system of R-23 (1) + 1-hexene (2) at temperatures of T = (293.06 to 313.27) K. The combined expanded uncertainties were calculated using a coverage factor of k = 2.

T / K	U(T) / K	P / MPa	U(P) / MPa	x_1	U(x_1)	y_1	U(y_1)
293.08	0.08	0.927	0.005	0.042	0.002	0.932	0.003
293.08	0.07	1.431	0.004	0.073	0.003	0.955	0.001
293.08	0.08	2.019	0.005	0.123	0.004	0.964	0.003
293.08	0.07	2.511	0.007	0.184	0.004	0.966	0.002
293.08	0.08	2.958	0.005	0.280	0.005	0.968	0.002
293.07	0.08	3.082	0.005	0.325	0.005	0.968	0.002
293.06	0.07	3.258	0.004	0.423	0.005	0.970	0.001
293.08	0.07	3.381	0.004	0.549	0.006	0.971	0.001
293.08	0.08	3.491	0.004	0.674	0.005	0.972	0.001
293.07	0.07	3.588	0.004	0.756	0.004	0.974	0.001
293.06	0.07	3.707	0.004	0.822	0.004	0.978	0.002
293.07	0.07	3.954	0.004	0.931	0.002	0.984	0.001
293.08	0.07	4.080	0.004	0.968	0.001	0.994	0.001
303.17	0.08	0.875	0.005	0.033	0.001	0.901	0.002
303.18	0.08	1.352	0.004	0.058	0.002	0.934	0.003
303.18	0.08	1.980	0.006	0.098	0.003	0.948	0.003
303.17	0.08	3.138	0.006	0.215	0.004	0.958	0.002
303.17	0.08	3.624	0.006	0.315	0.005	0.958	0.001
303.16	0.08	3.933	0.008	0.431	0.005	0.957	0.001
303.17	0.08	4.032	0.006	0.483	0.006	0.956	0.002
303.17	0.08	4.195	0.004	0.624	0.005	0.958	0.002
303.16	0.08	4.335	0.004	0.716	0.005	0.959	0.002
303.16	0.08	4.492	0.004	0.795	0.004	0.959	0.002
303.17	0.08	4.708	0.004	0.875	0.004	0.964	0.001
303.18	0.08	4.941	0.004	0.936	0.002	0.978	0.002
313.24	0.10	0.973	0.004	0.033	0.002	0.853	0.003
313.24	0.10	1.436	0.004	0.054	0.002	0.888	0.004
313.27	0.08	2.313	0.006	0.103	0.002	0.931	0.003
313.27	0.08	3.112	0.006	0.162	0.003	0.939	0.002
313.27	0.08	3.710	0.006	0.228	0.004	0.942	0.002
313.27	0.08	4.224	0.004	0.308	0.005	0.941	0.002
313.27	0.08	4.622	0.009	0.418	0.005	0.940	0.002
313.26	0.08	4.887	0.004	0.529	0.005	0.935	0.002
313.23	0.09	5.115	0.004	0.662	0.005	0.931	0.002
313.24	0.09	5.254	0.005	0.730	0.005	0.930	0.002
313.24	0.09	5.434	0.005	0.809	0.004	0.927	0.002
313.24	0.09	5.514	0.004	0.844	0.003	0.924	0.003

3. Results and discussion

The MC alpha function parameters for the PR MC model were fitted to the vapour pressures of 1-hexene which were reported in several literature sources [21, 35-42]. For 3-methylpentane, the MC parameters for the PR MC model were also fitted to vapour pressure data obtained from literature [16, 43-47]. The MC alpha parameters that were reported by Williams-Wynn et al. [1, 2], for R-23 and R-116, were used in this study. A one parameter model was used for both R-23 and R-116, as some of the VLE data was measured above the refrigerant critical temperatures, where the second and third terms become trivial. The MC alpha function parameters that were used in this study are reported in Table 4.

The measured isothermal P-x-y and P-x-x-y data for the four systems that were investigated in this study are presented in Table 5 through 8. The estimated expanded combined uncertainties in temperature, pressure and composition are presented alongside the data. The parameters for the PR MC + WS/NRTL and the PR MC + WS/UNIQUAC thermodynamic models were obtained by fitting the models to the experimental data. The model parameters for each of the systems are tabulated in Tables 9 to 12. Both temperature dependent and tem-

Table 6.
Experimental P-x_1-y_1 data with combined expanded uncertainties (U) for the binary system of R-23 (1) + 3-methylpentane (2) at temperatures of T = (293.06 to 313.27) K. A coverage factor of k = 2 was used for the calculation of the combined expanded uncertainties.

T / K	U(T) / K	P / MPa	U(P) / MPa	x_1	U(x_1)	y_1	U(y_1)
293.07	0.07	0.987	0.005	0.034	0.002	0.903	0.003
293.07	0.07	1.552	0.004	0.063	0.004	0.947	0.003
293.09	0.07	1.658	0.004	0.068	0.002	0.952	0.003
293.06	0.07	2.080	0.004	0.099	0.003	0.951	0.004
293.06	0.07	2.639	0.005	0.147	0.003	0.966	0.002
293.06	0.07	3.143	0.004	0.225	0.004	0.969	0.001
293.09	0.07	3.470	0.005	0.416	0.005	0.970	0.001
293.06	0.07	3.514	0.004	0.470	0.005	0.965	0.001
293.08	0.07	3.547	0.004	0.618	0.006	0.971	0.001
293.08	0.07	3.682	0.004	0.795	0.004	0.974	0.001
293.08	0.07	3.775	0.004	0.868	0.004	0.977	0.003
293.07	0.07	3.854	0.004	0.900	0.003	0.980	0.001
293.07	0.07	3.994	0.004	0.948	0.001	0.982	0.002
293.08	0.07	4.105	0.004	0.979	0.001	0.994	0.001
303.17	0.08	0.784	0.005	0.027	0.001	0.904	0.002
303.17	0.08	1.611	0.004	0.056	0.002	0.936	0.002
303.16	0.08	3.082	0.006	0.147	0.003	0.956	0.002
303.16	0.08	3.750	0.005	0.241	0.006	0.956	0.002
303.16	0.08	4.039	0.004	0.320	0.005	0.955	0.003
303.17	0.08	4.241	0.006	0.488	0.006	0.956	0.002
303.17	0.08	4.258	0.005	0.511	0.006	0.954	0.002
303.16	0.08	4.392	0.004	0.687	0.005	0.956	0.001
303.16	0.08	4.514	0.004	0.783	0.004	0.954	0.001
303.17	0.08	4.695	0.004	0.872	0.003	0.956	0.001
303.17	0.08	4.733	0.004	0.879	0.003	0.959	0.002
303.17	0.08	4.894	0.004	0.933	0.002	0.975	0.002
313.26	0.10	0.761	0.005	0.020	0.001	0.861	0.003
313.25	0.10	1.485	0.004	0.045	0.002	0.915	0.003
313.25	0.10	2.304	0.008	0.079	0.002	0.934	0.002
313.25	0.10	3.050	0.009	0.122	0.003	0.943	0.002
313.24	0.10	4.064	0.007	0.209	0.004	0.944	0.002
313.24	0.10	4.638	0.005	0.305	0.005	0.939	0.002
313.25	0.10	4.963	0.008	0.430	0.006	0.936	0.002
313.26	0.10	5.134	0.005	0.556	0.006	0.932	0.002
313.25	0.10	5.377	0.006	0.757	0.004	0.924	0.002
313.26	0.10	5.499	0.006	0.818	0.004	0.921	0.002
313.27	0.09	5.561	0.004	0.868	0.003	0.921	0.002
313.26	0.09	5.611	0.009	0.882	0.003	0.882	0.003

Table 7.
Experimental P-x_1^{I}-x_1^{II}-y_1 data with combined expanded uncertainties (U) for the binary system of R-116 (1) + 1-hexene (2) at temperatures of T = (293.09 to 313.15) K. The combined expanded uncertainties were calculated with a coverage factor of k = 2.

T / K	U(T) / K	P / MPa	U(P)/ MPa	x_1^{I}	U (x_1^{I})	x_1^{II}	U (x_1^{II})	y_1	U(y_1)
293.09	0.05	0.867	0.006	0.056	0.004			0.973	0.001
293.10	0.06	1.190	0.004	0.083	0.003			0.973	0.003
293.10	0.06	1.493	0.005	0.110	0.004			0.981	0.001
293.11	0.07	1.832	0.005	0.147	0.004			0.980	0.002
293.10	0.06	2.114	0.007	0.196	0.006			0.974	0.002
293.10	0.06	2.338	0.006	0.253	0.006			0.976	0.001
293.10	0.06	2.479	0.006	0.320	0.007			0.979	0.002
293.12	0.05	2.506	0.004	0.341	0.007	0.793	0.005	0.978	0.001
293.10	0.06	2.549	0.004	0.863	0.005			0.981	0.002
293.10	0.05	2.624	0.004	0.912	0.003			0.982	0.002
293.11	0.06	2.715	0.004	0.944	0.003			0.986	0.006
293.10	0.05	2.815	0.004	0.961	0.002			0.982	0.002
303.13	0.05	0.965	0.004	0.054	0.003			0.960	0.002
303.14	0.04	1.312	0.005	0.080	0.003			0.969	0.001
303.12	0.04	1.692	0.006	0.114	0.004			0.969	0.002
303.13	0.04	2.094	0.007	0.158	0.005			0.975	0.004
303.14	0.04	2.440	0.006	0.208	0.005			0.975	0.004
303.14	0.04	2.792	0.008	0.287	0.006			0.969	0.003
303.14	0.04	2.980	0.006	0.382	0.007			0.969	0.002
303.13	0.05	3.023	0.004	0.423	0.007	0.749	0.005	0.969	0.001
303.13	0.04	3.075	0.004	0.840	0.005			0.969	0.003
303.13	0.04	3.181	0.004	0.900	0.003			0.969	0.002
303.13	0.05	3.229	0.004	0.916	0.003			0.975	0.001
303.12	0.04	3.509	0.007	0.968	0.002			0.980	0.002
313.15	0.06	0.853	0.004	0.042	0.003			0.933	0.003
313.14	0.07	1.349	0.005	0.074	0.002			0.957	0.002
313.14	0.07	1.885	0.007	0.116	0.004			0.964	0.001
313.14	0.07	2.355	0.006	0.161	0.004			0.966	0.001
313.11	0.06	2.949	0.004	0.244	0.006			0.959	0.002
313.11	0.07	3.399	0.005	0.356	0.007			0.953	0.002
313.13	0.04	3.574	0.004	0.506	0.007			0.950	0.002
313.13	0.05	3.590	0.004	0.606	0.007			0.952	0.002
313.15	0.07	3.591	0.004	0.602	0.007			0.954	0.003
313.15	0.07	3.624	0.005	0.799	0.005			0.951	0.003
313.15	0.07	3.688	0.010	0.862	0.004			0.954	0.003
313.14	0.06	3.718	0.004	0.882	0.005			0.969	0.002
313.14	0.06	3.749	0.005	0.921	0.003			0.978	0.001

Table 8.
Experimental P-x_1-y_1 data with combined expanded uncertainties (U) for the binary system of R-116 (1) + 3-methylpentane (2) at temperatures of T = (293.09 to 313.12) K. A coverage factor of k = 2 was used to estimate the combined expanded uncertainties .

T / K	U(T) / K	P / MPa	U(P) / MPa	x_1	U(x_1)	y_1	U(y_1)
293.09	0.06	0.895	0.004	0.061	0.004	0.951	0.003
293.09	0.07	1.159	0.004	0.085	0.004	0.977	0.002
293.09	0.07	1.483	0.004	0.120	0.004	0.978	0.003
293.09	0.06	1.780	0.005	0.171	0.004	0.983	0.001
293.09	0.07	2.093	0.006	0.254	0.006	0.983	0.001
293.09	0.06	2.298	0.006	0.348	0.007	0.982	0.001
293.10	0.05	2.410	0.004	0.533	0.008	0.975	0.003
293.10	0.06	2.430	0.004	0.645	0.007	0.978	0.002
293.09	0.06	2.505	0.004	0.853	0.005	0.980	0.001
293.09	0.05	2.569	0.004	0.886	0.004	0.983	0.003
293.10	0.06	2.677	0.004	0.935	0.003	0.986	0.001
293.10	0.06	2.786	0.004	0.961	0.002	0.984	0.001
293.11	0.06	2.851	0.005	0.971	0.002	0.987	0.001
303.09	0.05	0.973	0.004	0.063	0.003	0.960	0.002
303.10	0.05	1.350	0.004	0.100	0.004	0.971	0.001
303.10	0.04	1.752	0.006	0.146	0.004	0.974	0.002
303.09	0.05	2.176	0.007	0.212	0.005	0.976	0.002
303.08	0.04	2.565	0.007	0.308	0.007	0.975	0.002
303.08	0.04	2.762	0.007	0.398	0.007	0.970	0.002
303.08	0.04	2.850	0.006	0.482	0.008	0.971	0.001
303.09	0.04	2.919	0.004	0.630	0.007	0.973	0.001
303.11	0.04	3.005	0.004	0.823	0.005	0.970	0.002
303.11	0.05	3.088	0.004	0.879	0.004	0.974	0.001
303.10	0.05	3.210	0.004	0.919	0.004	0.983	0.001
303.11	0.05	3.547	0.005	0.974	0.001	0.992	0.001
313.11	0.07	0.975	0.004	0.061	0.003	0.947	0.003
313.11	0.06	1.412	0.006	0.094	0.003	0.971	0.001
313.12	0.06	1.949	0.004	0.149	0.004	0.966	0.001
313.12	0.07	2.403	0.005	0.208	0.005	0.967	0.001
313.12	0.07	2.817	0.005	0.281	0.006	0.967	0.001
313.12	0.07	3.152	0.008	0.379	0.007	0.964	0.002
313.11	0.07	3.315	0.006	0.466	0.007	0.960	0.002
313.10	0.07	3.437	0.004	0.616	0.007	0.959	0.003
313.10	0.06	3.495	0.004	0.708	0.006	0.954	0.003
313.12	0.06	3.650	0.004	0.862	0.004	0.949	0.003
313.12	0.06	3.787	0.006	0.901	0.003	0.949	0.002

perature independent parameters, for the thermodynamic models, were fitted to the data. The estimated mixture critical locus curves, calculated by the method of Heidemann and Khalil, and the extrapolated mixture critical loci, extrapolated by the method of Ungerer et al., are presented in Table 13.

The experimental data for each of the four binary systems are plotted alongside the modelled data on Figures 1 to 4. The critical loci and the critical locus curves are also included on Figures 1 to 4. Each of the four P-x-y- plots included an expanded view of the region between compositions of 0.9 and 1.0 for component 1. This enabled the data in these regions to be discernible for the different isotherms. The temperature dependent and the temperature independent thermodynamic model parameters for each of the binary systems were compared in Figures 5 to 8.

For the R-23 + 1-hexene binary system (Table 5, Figure 1), both of the thermodynamic models appeared to over-predict the bubble pressures, particularly away from the dilute regions. Additionally, the description of the vapour phase compositions was fairly poor, with a deviation of between 0.03 and 0.04 between the experimental and the modelled vapour-phase compositions. There was little difference between the descriptions of the phase behaviour by the two models, as is observable from the statistical analysis of the regression in Table 9. The NRTL model appeared to provide a better description of the pressure, whereas the UNIQUAC model provided a marginally better description of the vapour phase composition. These may, however, have been artefacts of the regression Both of the thermodynamic models were able to describe the 'bird's-beak' behaviour of the system around the critical point of the R-23, despite not describing the nearby vapour phase behaviour very well.

The PR MC + WS/UNIQUAC model provided a substantially better description of the experimental data for the R-23 + 3-methylpentane system than the PR MC + WS/NRTL model (Table 6,

Figure 2). In particular, at R-23 compositions of between 0.15 and 0.75, the NRTL model over-predicted the bubble pressures of the system. The UNIQUAC model, in contrast provides a good description of the bubble pressures. For this system, the deviations between the vapour phase compositions predicted by both of the thermodynamic models and those measured experimentally are once again between 0.03 and 0.04. The poor description of the vapour phase is highlighted by the size of the MRDs and the AARDs of the fitted models in Table 10.

The R-116 + 1-hexene system (Table 7, Figure 3) exhibited VLLE behaviour for the lower two of the isotherms that were measured (293.1 and 303.1) K. Both of the thermodynamic models were able to accu-

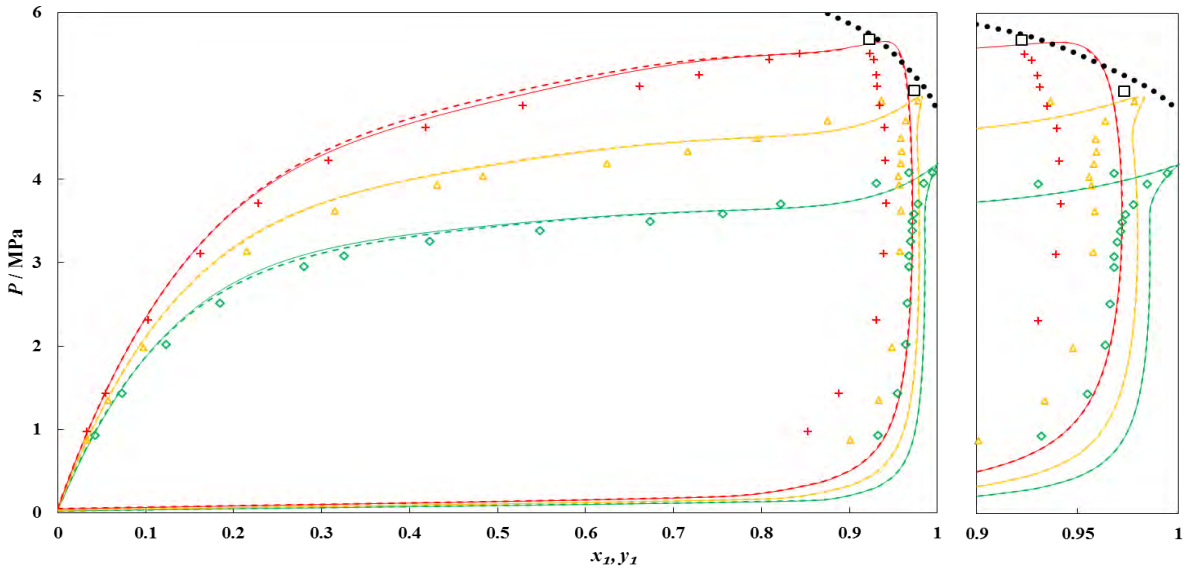

Fig. 1. P-x_1-y_1 data for the binary system of trifluoromethane (1) + 1-hexene (2). Data measured at temperatures of T = ◇, 293.1 K; △, 303.1 K; +, 313.3 K. Solid lines, PR MC + WS/NRTL model; dashed lines, PR MC + WS/UNIQUAC model; □, mixture critical point (Ungerer et al. method); ••••, mixture critical locus curve (Heidemann and Khalil method).

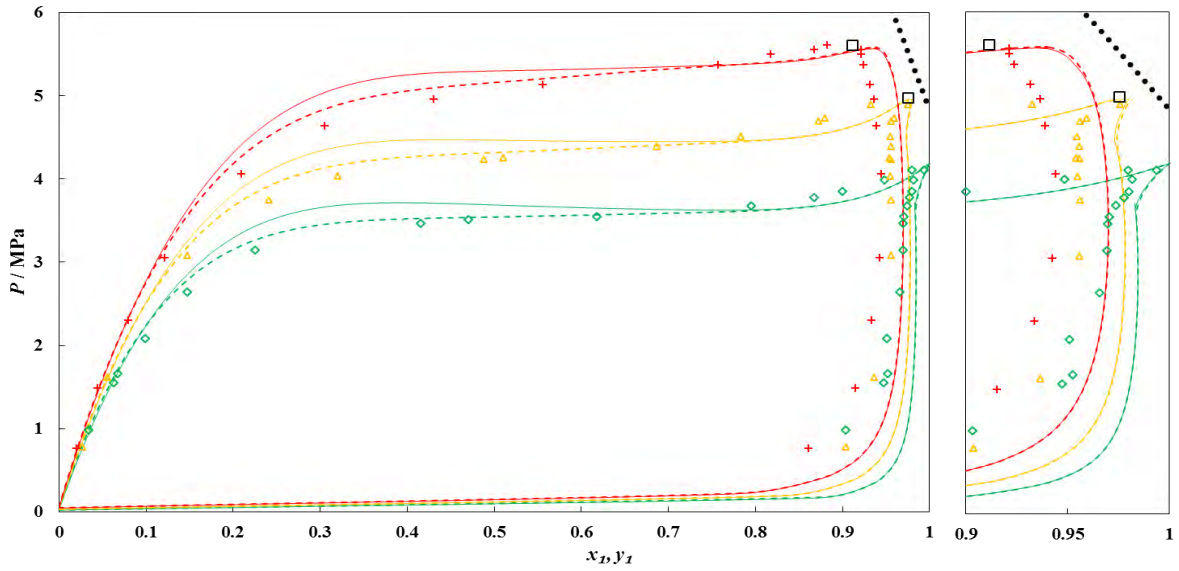

Fig. 2. P-x_1-y_1 data for the binary system of trifluoromethane (1) + 3-methylpentane (2). Data measured at temperatures of T = ◇, 293.1 K; △, 303.2 K; +, 313.3 K. Solid lines, PR MC + WS/NRTL model; dashed lines, PR MC + WS/UNIQUAC model; □, mixture critical point (Ungerer et al. method); ••••, mixture critical locus curve (Heidemann and Khalil method)

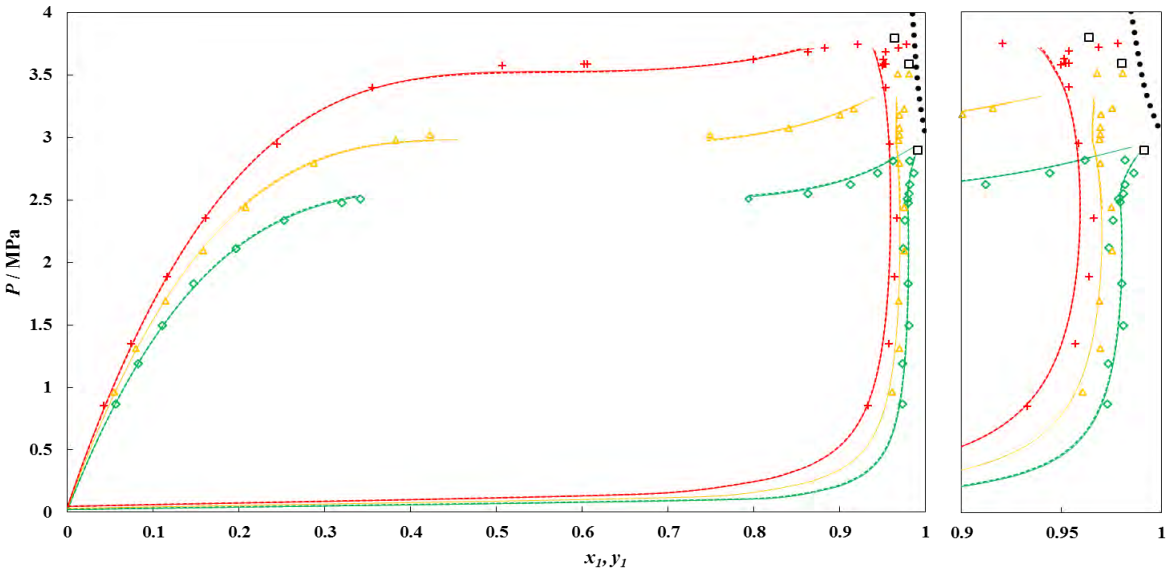

Fig. 3. P-x_1^{I}-x_1^{II}-y_1 data for the binary system of hexafluoroethane (1) + 1-hexene (2). Data measured at temperatures of T = ◇, 293.1 K; △, 303.1 K; +, 313.1 K. Solid lines, PR MC + WS/NRTL model; dashed lines, PR MC + WS/UNIQUAC model; □, mixture critical point (Ungerer et al. method); ••••, mixture critical locus curve (Heidemann and Khalil method)

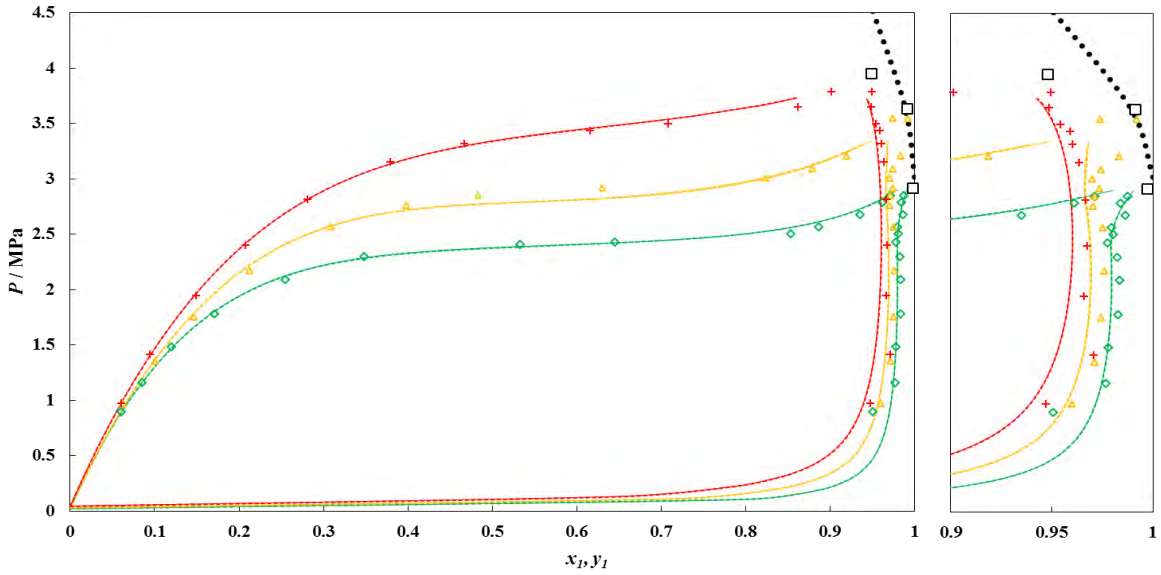

Fig. 4. P-x_1-y_1 data for the binary system of hexafluoroethane (1) + 3-methylpentane (2). Data was measured at temperatures of T = ◇, 293.1 K; △, 303.1 K; +, 313.1 K. Solid lines, PR MC + WS/NRTL model; dashed lines, PR MC + WS/UNIQUAC model; □, mixture critical point (Ungerer et al. method); ••••, mixture critical locus curve (Heidemann and Khalil method) .

rately predict the LLE for the systems, as well as predicting the occurrence of the upper end to the three-phase region at between (303.1 and 313.2) K. The model provided an excellent description of both the bubble and dew point curves. In addition, the occurrence of the 'bird's-beak' phenomenon [48] at 293.1 K was also described by the model. There was, however, a partial failure of the model to accurately describe the behaviour of the system in the dilute 1-hexene region at the higher temperatures. Observing the MRDs and AARDs for the regression of the models to this system (Table 11) gives an additional confirmation of the good description of the experimental data with the model.

Lastly, the R-116 + 3-methylpentane system (Table 8, Figure 4) was also well described by both of the thermodynamic models, with little to distinguish between their performances. Once again, the model was not capable of accurately modelling the 'bird's-beak' behaviour of the system at the two higher isotherms, but gave a reasonable description of it at 293.1 K. An observation of the statistical data for the regressions of the two models (Table 12) shows the high similarity between the performances of the two models. This system did not exhibit any LLE at the temperatures that were investigated. It is, however, possible that all of the measurements were conducted above the temperatures at which LLE occurs in this system.

The critical loci, extrapolated by the method of Ungerer et al., were fairly similar to the critical locus curves produced using the method of Heidemann et al. Difficulties arose with the Ungerer et al. extrapolations at conditions at which the 'bird's-beak' phenomenon occurred. The sudden inflection in the slope of the dew point curve, caused by this phenomenon, translated into a drastic reduction in the amount of data that provided meaningful extrapolation results. The critical points estimated using the method of Ungerer and co-workers, for isotherms where 'bird's-beak' behaviour occurred, were therefore extrapolated from only two or three co-existence points. In contrast, the critical locus

Table 9.

The temperature dependent and temperature independent model parameters (k_{12} and τ_{ij} or Δu_{ij}) and regression statistics for the binary system of trifluoromethane (1) + 1-hexene (2). The temperature dependent parameters were regressed at temperatures, T = (293.1 to 313.3) K. The average relative deviations (ARD) and the absolute average relative deviations (AARD) in the pressure, P, and vapour mole fraction, y, are included for each of the regressions.

T / K	k_{12}	τ_{12} / K [a] || Δu_{12} [b] / J·mol^{-1}	τ_{21} / K [a] || Δu_{21} [b] / J·mol^{-1}	ARD [c]		AARD [d]	
				P	y	P	y
PRMC + WS/NRTL							
293.1	0.514	398.9	454.3	-1.12	-1.73	2.53	1.77
303.2	0.512	429.6	453.9	-0.05	-1.53	2.40	3.70
313.3	0.498	446.2	470.6	0.90	-1.81	1.81	5.25
(293.1 to 313.3)	0.558	310.3	495.9	0.48	-0.45	3.18	4.47
PRMC + WS/UNIQUAC							
293.1	0.514	-143.7	4294.5	-0.78	-1.73	2.18	1.77
303.2	0.514	-114.5	4347.2	-0.16	-1.47	2.38	3.75
313.3	0.496	-67.1	4451.4	0.42	-1.80	2.19	5.21
(293.1 to 313.3)	0.558	-391.3	4616.5	2.11	-1.72	4.29	3.86

[a] τ_{12}, τ_{21} for the NRTL activity coefficient model
[b] Δu_{12}, Δu_{21} for the UNIQUAC activity coefficient model

[c] average relative deviation, $$ARD(\theta) = \frac{100}{N_p}\sum_{1}^{N_p}\frac{\theta_{exp} - \theta_{calc}}{\theta_{exp}}$$

[d] absolute average relative deviation, $$AARD(\bar{\theta}) = \frac{100}{N_p}\sum_{1}^{N_p}\frac{|\bar{\theta}_{exp} - \bar{\theta}_{calc}|}{\bar{\theta}_{exp}}$$

Table 10.

The temperature dependent and temperature independent model parameters (k_{12} and τ_{ij} or Δu_{ij}) and regression statistics for the binary system of trifluoromethane (1) + 3-methylpentane (2). The temperature dependent parameters were regressed at temperatures, T = (293.1 to 313.3) K. The average relative deviations (ARD) and the absolute average relative deviations (AARD) in the pressure, P, and vapour mole fraction, y, are included for each of the regressions .

T / K	k_{12}	τ_{12} / K [a] || Δu_{12} [b] / J·mol^{-1}	τ_{21} / K [a] || Δu_{21} [b] / J·mol^{-1}	ARD		AARD	
				P	y	P	y
PRMC + WS/NRTL							
293.1	0.537	444.1	540.7	-0.25	-2.09	3.95	2.09
303.2	0.516	538.4	465.5	-1.53	-2.47	3.53	2.47
313.3	0.520	465.5	556.0	0.57	-1.36	4.47	4.97
(293.1 to 313.3)	0.555	469.0	512.6	2.42	1.63	4.34	6.45
PRMC + WS/UNIQUAC							
293.1	0.535	-160.1	4916.9	0.69	-2.14	2.58	2.14
303.2	0.518	32.3	4655.7	-0.80	-2.61	1.87	2.61
313.3	0.525	-202.5	5149.8	1.23	-2.22	3.27	5.32
(293.1 to 313.3)	0.558	-238.3	4993.2	-0.41	-2.77	3.38	3.09

[a] τ_{12}, τ_{21} for the NRTL activity coefficient model
[b] Δu_{12}, Δu_{21} for the UNIQUAC activity coefficient model

Table 11.

The temperature dependent and temperature independent model parameters (k_{12} and τ_{ij} or Δu_{ij}) and regression statistics for the binary system of hexafluoroethane (1) + 1-hexene (2). The temperature dependent parameters were regressed at temperatures, T = (293.1 to 313.1) K. The average relative deviations (ARD) and the absolute average relative deviations (AARD) in the pressure, P, and vapour mole fraction, y, are included for each of the regressions.

T / K	k_{12}	τ_{12} / K [a] || Δu_{12} [b] / J·mol^{-1}	τ_{21} / K [a] || Δu_{21} [b] / J·mol^{-1}	ARD		AARD	
				P	y	P	y
PRMC + WS/NRTL							
293.1	0.397	250.9	435.1	-0.50	-0.07	0.97	0.24
303.1	0.366	278.3	433.8	-0.13	0.39	0.81	0.39
313.1	0.420	75.1	582.9	0.91	0.72	1.17	0.72
(293.1 to 313.1)	0.391	242.1	444.2	-1.03	0.26	1.74	0.38
PRMC + WS/UNIQUAC							
293.1	0.407	-351.7	2208.7	-0.63	-0.07	1.03	0.24
303.1	0.368	-266.4	2158.4	0.21	0.38	1.11	0.38
313.1	0.369	-330.1	2209.0	0.99	0.67	1.33	0.67
(293.1 to 313.1)	0.400	-372.7	2237.9	-1.16	0.29	2.08	0.40

[a] τ_{12}, τ_{21} for the NRTL activity coefficient model
[b] Δu_{12}, Δu_{21} for the UNIQUAC activity coefficient model

Table 12.

The temperature dependent and temperature independent model parameters (k_{12} and τ_{ij} or Δu_{ij}) and regression statistics for the binary system of hexafluoroethane (1) + 3-methylpentane (2). The temperature dependent parameters were regressed at temperatures, T = (293.1 to 313.1) K. The average relative deviations (ARD) and the absolute average relative deviations (AARD) in the pressure, P, and vapour mole fraction, y, are included for each of the regressions .

T / K	k_{12}	τ_{12} / K [a] || Δu_{-12} [b] / J·mol^{-1}	τ_{21} / K [a] || Δu_{21} [b] / J·mol^{-1}	ARD		AARD	
				P	y	P	y
PRMC + WS/NRTL							
293.1	0.399	184.0	482.6	-0.42	-0.16	0.99	0.38
303.1	0.347	282.8	395.9	0.09	1.01	1.92	1.01
313.1	0.376	216.5	406.1	-0.23	0.77	0.70	0.77
(293.1 to 313.1)	0.356	258.6	415.3	0.51	0.45	2.68	0.62
PRMC + WS/UNIQUAC							
293.1	0.403	-632.7	2603.2	-0.44	-0.17	1.02	0.39
303.1	0.354	-363.8	2183.7	0.62	0.59	1.67	0.59
313.1	0.378	-532.0	2308.6	-0.24	0.75	0.69	0.75
(293.1 to 313.1)	0.380	-491.0	2333.2	-0.54	0.35	2.75	0.55

[a] τ_{12}, τ_{21} for the NRTL activity coefficient model
[b] Δu_{12}, Δu_{21} for the UNIQUAC activity coefficient model

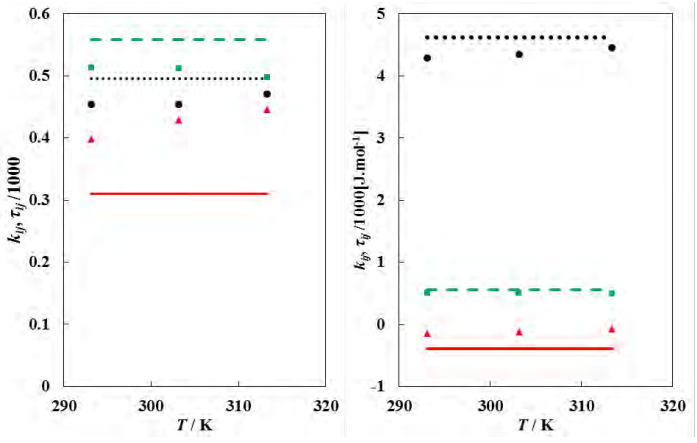

Fig. 5. The thermodynamic model parameters for the system of R-23 (1) + 1-hexene (2). Temperature independent parameters are represented by symbols, while the temperature dependent parameters are represented by lines. *Left*: (NRTL) ■/- - -, k_{12}; ●/·····, τ_{12}; ▲/——, τ_{21}. *Right*: (UNIQUAC) ■/- - -, k_{12}; ●/·····, Δu_{12}; ▲/——, Δu_{21}.

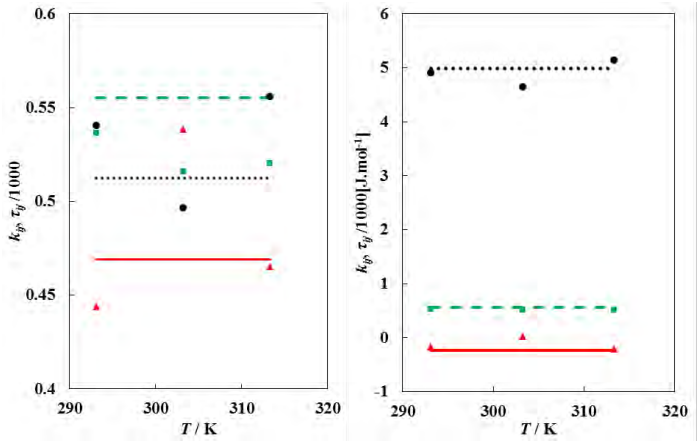

Fig. 6. The thermodynamic model parameters for the system of R-23 (1) + 3-methylpentane (2). Temperature independent parameters are represented by symbols, while the temperature dependent parameters are represented by lines. *Left*: (NRTL) ■/- - -, k_{12}; ●/·····, τ_{12}; ▲/——, τ_{21}. *Right*: (UNIQUAC) ■/- - -, k_{12}; ●/·····, Δu_{12}; ▲/——, Δu_{21}.

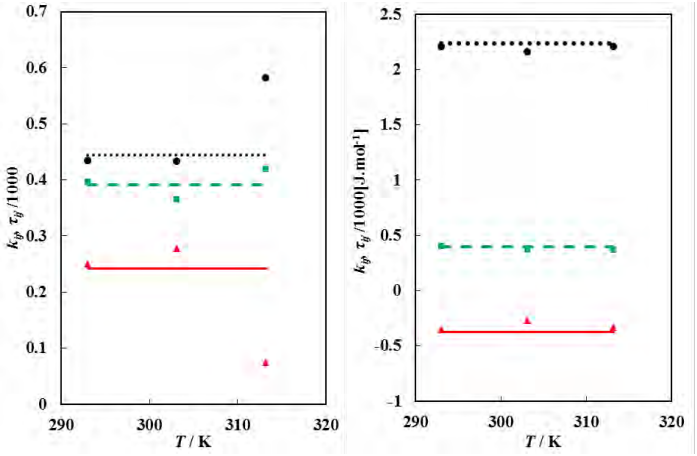

Fig. 7. The thermodynamic model parameters for the system of R-116 (1) + 1-hexene (2). Temperature independent parameters are represented by symbols, while the temperature dependent parameters are represented by lines. *Left*: (NRTL) ■/- - -, k_{12}; ●/·····, τ_{12}; ▲/——, τ_{21}. *Right*: (UNIQUAC) ■/- - -, k_{12}; ●/·····, Δu_{12}; ▲/——, Δu_{21}.

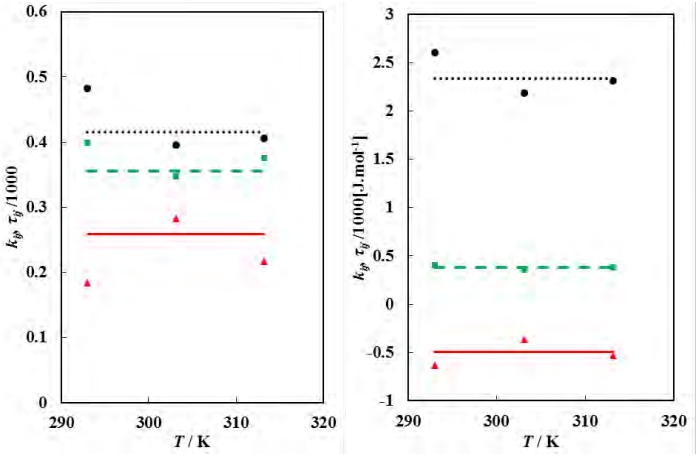

Fig. 8. The thermodynamic model parameters for the system of R-23 (1) + 3-methylpentane (2). Temperature independent parameters are represented by symbols, while the temperature dependent parameters are represented by lines. *Left*: (NRTL) ■/- - -, k_{12}; ●/·····, τ_{12}; ▲/——, τ_{21}. *Right*: (UNIQUAC) ■/- - -, k_{12}; ●/·····, Δu_{12}; ▲/——, Δu_{21}.

curves that were calculated by the method of Heidemann and Khalil were dependent on the temperature dependent thermodynamic models. When these models provided a poor description of the phase behaviour, this was translated into a poor description of the critical locus curve for the system. An example of this is the critical locus curve for R-23 + 3-methylpentane (Figure 2), in which there is a substantial difference between the extrapolated and calculated critical loci.

Table 13.

Critical locus curves (T_c, P_c, $x_{c,i}$) estimated from the thermodynamic models by the method of Heidemann and Khalil [33], and extrapolated mixture critical loci by the method of Ungerer et al. [31].

Critical Locus Curves (Heidemann & Khalil)					
T_c / K	P_c / MPa	$x_{c,1}$	T_c / K	P_c / MPa	$x_{c,1}$
R-23 (1) + 1-hexene (2)			*R-23 (1) + 3-methylpentane (2)*		
302.1	5.03	0.99	302.5	5.12	0.99
304.4	5.18	0.98	307.3	5.39	0.98
308.7	5.40	0.96	314.0	5.94	0.96
311.4	5.52	0.95	325.9	6.65	0.93
314.9	5.61	0.94	337.3	7.26	0.90
320.3	5.77	0.92	355.4	7.93	0.85
336.1	6.10	0.85			
350.5	6.20	0.80			
381.5	6.45	0.70			
R-116 (1) + 1-hexene (2)			*R-116 (1) + 3-methylpentane (2)*		
295.5	3.51	0.99	296.0	3.61	0.99
307.4	5.64	0.97	307.6	4.31	0.96
342.3	11.27	0.93	321.4	4.91	0.93
364.8	15.10	0.90	336.9	5.37	0.90
			361.7	6.10	0.85
			393.6	6.65	0.80
Critical Loci (Ungerer et al.)					
T_c / K	P_c / MPa	$x_{c,1}$	T_c / K	P_c / MPa	$x_{c,1}$
R-23 (1) + 1-hexene (2)			*R-23 (1) + 3-methylpentane (2)*		
303.2	5.07	0.973	303.2	4.98	0.975
313.3	5.68	0.922	313.3	5.61	0.911
R-116 (1) + 1-hexene (2)			*R-116 (1) + 3-methylpentane (2)*		
293.1	2.90	0.991	293.1	2.92	0.997
303.1	3.59	0.980	303.1	3.64	0.991
313.1	3.80	0.964	313.1	3.95	0.948

The temperature dependent and independent parameters of each of the systems investigated in this study were fairly similar, with no cases of extreme differences in the parameters. The measurements involving R-116 were all supercritical with respect to the R-116. There were therefore not expected to be any drastic changes in the parameters, as would have been expected were the data sets from both above and below the R-116 critical temperature. The critical temperature of R-23, in contrast (Tc = 299.07 K), lies between the 293.1 and 303.2 K isotherms. It was therefore expected that the parameters would display different trend above and below this critical point, as was experienced by Williams-Wynn et al. [1, 2]. However, with only three isotherms measured, it was not possible to discern whether the trend continued into these systems.

From the experimental data available for these four binary systems, it was not possible to conclusively define the systems according to the van Konynenburg and Scott classification scheme [49]. It is, however, a possibility that all four systems could be type II systems. Only the R-116 + 1-hexene system exhibited VLLE at the temperatures that were studied, with the upper limit to the three-phase region of this system occurring at a temperature above the critical temperature of R-116. This meant that this system was likely a being a type III system. Because no VLLE was observed, it was not possible to determine whether the other three systems would exhibit upper critical end points (UCEPs). Since these systems were, however, not 'simple' systems, it is assumed that they would most likely therefore be classified as type II systems, with one critical line from C_1 to C_2 (the pure component critical points), and another from the UCEP to a fictitious 'critical point at infinite pressure'.

4. Conclusions

The isothermal phase equilibrium data for binary systems of R-23 or R-116 with either 1-hexene or 3-methylpentane at temperatures of (293.1 to 313.3) K were measured with a static-analytic apparatus. Several VLLE data points were measured for the R-116 + 1-hexene system, but the remainder of the data consisted solely of *P-x-y* data. The PR MC + WS/NRTL and the PR MC + WS/UNIQUAC models were fitted to the experimental data, both dependent on and independent of temperature. The temperature independent models provided a better description of the phase behaviour than the temperature dependent models.

The models were found to describe the systems containing R-116 better than those containing R-23. The 'bird's-beak' phenomenon occurred with all four systems. The thermodynamic models were able to model this behaviour, although not with a great degree of accuracy. Both of the thermodynamic models were able to accurately describe the VLLE for the R-116 + 1-hexene system.

Mixture critical points were extrapolated from the subcritical coexistence points by the method of Ungerer et al., and were compared to the critical locus curves calculated by the method of Heidemann and Khalil. They were found to be fairly similar. With only three isotherms measured per system, it was difficult to define the systems according to the van Konynenburg and Scott classification. However, after some deduction, all of the systems investigated in this study were estimated to be type II systems.

Acknowledgements

This work is based upon research supported by the South African Research Chairs Initiative of the Department of Science and Technology and the National Research Foundation.

References

[1] M.D. Williams-Wynn, P. Naidoo, D. Ramjugemath, J. Chem. Thermodyn. unpublished (2015).

[2] M.D. Williams-Wynn, P. Naidoo, D. Ramjugemath, Fluid Phase Equilib. unpublished (2015).

[3] M.D. Williams-Wynn, P. Naidoo, D. Ramjugemath, J. Chem. Thermodyn. unpublished (2015).

[4] M.D. Williams-Wynn, P. Naidoo, D. Ramjugemath, Fluid Phase Equilib. unpublished (2015).

[5] Y.J. Sheng, P.C. Chen, Y.P. Chen, D.S.H. Wong, Ind. Eng. Chem. Res. 31 (3) (1992) 967-973.

[6] R.T. Kurnik, R.C. Reid, Fluid Phase Equilib. 8 (1) (1982) 93-105.

[7] J.M. Dobbs, J.M. Wong, K.P. Johnston, J. Chem. Eng. Data 31 (3) (1986) 303-308.

[8] K.Y. Kim, 1974. Calorimetric Studies on Argon and Hexafluoroethane and a Generalized Correlation of Maxima in Isobaric Heat Capacity, Thesis, University of Michigan, Ann Arbour, MI

[9] K. Saikawa, J. Kijima, M. Uematsu, K. Watanabe, J. Chem. Eng. Data 24 (3) (1979) 165-167.

[10] D.R. Lide, Crc Handbook of Chemistry and Physics 2004-2005: A Ready-Reference Book of Chemical and Physical Data, CRC Press Llc, 2004.

[11] R.K. Burkat, A.J. Richard, J. Chem. Thermodyn. 7 (3) (1975) 271-277.

[12] R. Bravo, M. Pintos, A. Amigo, J. Chem. Thermodyn. 23 (10) (1991) 905-910.

[13] E. Aicart, E. Junquera, T.M. Letcher, J. Chem. Eng. Data 40 (6) (1995) 1225-1227.

[14] A.J. Treszczanowicz, T.S. Pawłowski, T. Treszczanowicz, A.M. Szafrański, J. Chem. Eng. Data 55 (12) (2010) 5478-5482.

[15] R.L. Denyer, F.A. Fidler, R.A. Lowry, Ind. Eng. Chem. 41 (12) (1949) 2727-2737.

[16] C. Berro, F. Laichoubi, E. Rauzy, J. Chem. Thermodyn. 26 (8) (1994) 863–869.

[17] A. Aucejo, M. Cruz Burguet, R. Munoz, J.L. Marques, J. Chem. Eng. Data 40 (4) (1995) 871-874.

[18] J. Ortega, F.J. Toledo-Marante, J. Chem. Thermodyn. 34 (9) (2002) 1439-1459.

[19] J.A. Riddick, W.B. Bunger, T.K. Sakano, Organic Solvents: Physical Properties and Methods of Purification Techniques of Chemistry, 4th ed, Vol. 2, Wiley, New York, 1986.
[20] J. Tojo, C. Diaz, J. Chem. Eng. Data 40 (1) (1995) 96-98.
[21] A.F. Forziati, D.L. Camin, F.D. Rossini, J. Res. NBS 45 (5) (1950) 406-410.
[22] C. Narasigadu, P. Naidoo, C. Coquelet, D. Richon, D. Ramjugernath, Fluid Phase Equilib. 338 (2013) 188-196.
[23] B.N. Taylor, C.E. Kuyatt, NIST Technical Note 1297 (1994).
[24] B.N. Taylor, P.J. Mohr, M. Douma, The Nist Reference on Constants, Units, and Uncertainty, 2007.
[25] D.Y. Peng, D.B. Robinson, Ind. Eng. Chem. Fundam. 15 (1976) 59-64.
[26] P.M. Mathias, T.W. Copeman, Fluid Phase Equilib. 13 (1983) 91-108.
[27] D.S.H. Wong, S.I. Sandler, AIChE J. 38 (1992) 671-680.
[28] H. Renon, J.M. Prausnitz, AIChE J. 14 (1968) 135-144.
[29] D.S. Abrams, J.M. Prausnitz, AIChE J. 21 (1) (1975) 116-128.
[30] W.E. Deming, Statistical Adjustment of Data, Dover Books, Mineola, NY, 1964.
[31] P. Ungerer, B. Tavitian, A. Boutin, Applications of Molecular Simulation in the Oil and Gas Industry- Monte Carlo Methods, 2005.
[32] E. El Ahmar, A. Valtz, P. Naidoo, C. Coquelet, D. Ramjugernath, J. Chem. Eng. Data 56 (5) (2011) 1918-1924.
[33] R.A. Heidemann, A.M. Khalil, AIChE J. 26 (5) (1980) 769-779.
[34] R. Stockfleth, R. Dohrn, Fluid Phase Equilib. 45 (1998) 43-52.
[35] D.L. Camin, F.D. Rossini, J. Phys. Chem. 60 (10) (1956) 1446-1451.
[36] L. Negadi, A. Blondel, I. Mokbel, A. Ait-Kaci, J. Jose, Int. Data Ser., Sel. Data Mixtures Ser. A 21 (1993) 169-194.
[37] J.J. Segovia, M.C. Martín, C.R. Chamorro, M.A. Villamañán, J. Chem. Eng. Data 43 (6) (1998) 1021-1026.
[38] H. Segura, E. Lam, R. Reich, J. Wisniak, Phys. Chem. Liq. 39 (1) (2001) 43-54.
[39] C.R. Chamorro, J.J. Segovia, M.a.C. Martín, M.A. Villamañán, Fluid Phase Equilib. 193 (1-2) (2002) 289-301.
[40] E. Sapei, A. Zaytseva, P. Uusi-Kyyny, K.I. Keskinen, J. Aittamaa, J. Chem. Eng. Data 51 (6) (2006) 2203-2208.
[41] L. Negadi, A. Belabbaci, A. Ait Kaci, J. Jose, J. Chem. Eng. Data 52 (1) (2007) 47-55.
[42] B. Marrufo, A. Aucejo, M. Sanchotello, S. Loras, Fluid Phase Equilib. 279 (1) (2009) 11-16.
[43] C.B. Willingham, W.J. Taylor, J.M. Pignocco, F.D. Rossini, J. Res. Natl. Bur. Stand. (U. S.) 35 (1945) 219.
[44] E.W. Funk, F.-C. Chai, J.M. Prausnitz, J. Chem. Eng. Data 17 (1) (1972) 24-27.
[45] E.K. Liu, R.R. Davison, J. Chem. Eng. Data 26 (1) (1981) 85-88.
[46] R. Garriga, F. Sanchez, P. Perez, J. Valero, M. Gracia, Fluid Phase Equilib. 101 (1994) 227-236.
[47] P. Uusi-Kyyny, J.-P. Pokki, J. Aittamaa, S. Liukkonen, J. Chem. Eng. Data 46 (3) (2001) 754-758.
[48] J.C. Rainwater, Fluid Phase Equilib. 183-184 (2001) 41-51.
[49] P.H. van Konynenburg, R.L. Scott, Philos. Trans. R. Soc. 298 (1980) 495-540.

APPENDIX H

Isothermal vapour-liquid equilibrium data for binary systems of (CHF_3 or C_2F_6) with (methylcyclohexane or toluene)

Mark D. Williams-Wynn [a], Paramespri Naidoo [a] and Deresh Ramjugernath [a,*]

The isothermal vapour-liquid and vapour-liquid-liquid equilibria of four binary refrigerant-hydrocarbon systems were measured using a static-analytic apparatus at temperatures of between (293.0 and 313.2) K and at pressures of up to 6.1 MPa. The two refrigerants that were investigated were trifluoromethane and hexafluoroethane, and the hydrocarbons were methylcyclohexane and toluene. At the temperatures that were investigated, the R-23 + toluene system alone did not exhibit any liquid-liquid immiscibility. The "bird's-beak" phenomenon was observed for all of the systems. The experimental data were regressed with the PR MC EOS with the WS mixing rule. Either the NRTL or the UNIQUAC activity coefficient model was used within the WS mixing rule. The critical locus curves for the systems were calculated by the method of Heidemann and Khalil, and co-existence curves were extrapolated to the mixture critical points using the technique of Ungerer et al. The van Konynenburg and Scott classifications of the four binary systems were discussed.

Introduction

Carbon dioxide (CO_2) is presently by far the most commonly used supercritical (SC) solvent [1]. This is because it is non-flammable and non-toxic, and is therefore generally perceived to be a 'green' solvent. The major difficulty in the use of CO_2 as a SC solvent is its lack of polarity, which inhibits the extraction of any polar components with larger molecules. To overcome this, polar co-solvents, which improve the solubilities of these components in the solvent, are added to the solvent [2]. It is of interest to determine whether other gases exist which would provide better performance than CO_2, for the extraction of the more polar solutes, without the need for the addition of polar co-solvents. The requirements of these alternative gases would include the need to be non-flammable and non-toxic, as is the case for CO_2.

As a part of a study into SC solvents that could replace SC CO_2, the performance of two refrigerants, trifluoromethane (R-23) and hexafluoroethane (R-116) have been benchmarked with several different hydrocarbons, including n-alkanes [3-4] as well as an alkene and a branched alkane [5]. This current investigation expands the study to include the phase equilibria of R-23 or R-116 with either methylcyclohexane (MCH) or toluene. This study will therefore provide data for the refrigerants with an aromatic and a cycloalkane.

The phase equilibrium data for the four systems of R-23 + MCH, R-23 + toluene, R-116 + MCH and R-116 + toluene were measured using a static-analytic high-pressure vapour-liquid equilibrium (VLE) apparatus at temperatures of between (293.0 and 313.2) K.

Experimental

Materials and Chemicals. Both the methylcyclohexane (C_7H_{14}, CAS Number 108-87-2) and the toluene (C_7H_8, CAS Number 108-88-3) were purchased from Sigma-Aldrich Co. LLC. The trifluoromethane (CHF3, CAS Number 75-46-7) and hexafluoroethane (C_2F_6, CAS Number 76-16-4) were purchased from A-Gas (South Africa) (Pty) Ltd. Helium (Baseline 5.0, CAS Number 7440-59-7), purchased from Afrox South Africa, was used as the carrier gas for composition analysis using a gas chromatograph (GC). As well as composition analysis, the GC was also used to verify the purities of the four components, through the measurement of the individual peak area fractions. The suppliers, stated purities, GC peak area fractions as well as the critical temperatures and pressures are tabulated in Table 1.

Table 1.
The suppliers, stated purities, GC area fractions and critical properties (T_c, P_c) of the pure components used in these measurements.

	Supplier	Stated Purity	GC Area	T_c / K	P_c / MPa
Trifluoromethane, CHF_3	A-Gas (South Africa)	> 0.999 [d]	0.9996	299.07 [c]	4.836 [c]
Hexafluoroethane, C_2F_6	A-Gas (South Africa)	> 0.999 [d]	0.9999	293.03 [b]	3.013 [a]
Methylcyclohexane, C_7H_{14}	Sigma Aldrich	> 0.996 [e]	0.9989	572.2 [c]	3.471 [c]
Toluene, C_7H_8	Sigma Aldrich	> 0.995 [e]	0.9967	591.79 [c]	4.104 [c]

[a] Kim [43]
[b] Saikawa et al. [44]
[c] Lide [45]
[d] Volumetric basis
[e] mass basis

Table 2.
Experimentally measured (*exp.*) densities, ρ, of methylcyclohexane and toluene at temperatures of between T = (293.15 and 301.35) K, compared to data obtained from literature (*lit.*).

T / K	ρ (lit.) / [kg/m^3]	ρ (exp.) [h] / [kg/m^3]	ρ (lit.) / [kg/m^3]	ρ (exp.) [h] / [kg/m^3]
	methylcyclohexane		*toluene*	
293.15	769.39 [a]	768.849	866.98 [a]	866.510
			866.55 [b]	
295.15		767.186		864.691
296.69		765.899		
297.04		765.606		
297.15		765.512		862.861
298.15	764.83 [c]	764.667	861.87 [e]	861.941
	765.01 [d]		862.11 [f]	
	764.87 [e]		861.81 [g]	
298.69				861.451

[a] Richon et al. [7]
[b] Li et al. [6]
[c] Loras et al. [8]
[d] Carmona et al. [9]
[e] Martínez-Soria et al. [10]
[f] Domanska and Letcher [11]
[g] Sun et al. [12]
[h] $u(T)$ = 0.05 K, $u(\rho)$ = 0.04 kg·m^{-3}

The densities of the MCH and the toluene were measured using an Anton-Paar DMA 5000 density meter. The uncertainties from the

Table 3.
Experimentally measured (*exp.*) refractive indices (R^l) of methylcyclohexane and toluene at temperatures of T = (293.15 and 298.15) K, compared to data obtained from literature (*lit.*).

T / K	R^l (lit.)	R^l (exp.) [h]	R^l (lit.)	R^l (exp.) [h]
	methylcyclohexane		*toluene*	
293.15	1.4231 [a]	1.42314	1.49693 [b]	1.49658
	1.42312 [b]			
298.15	1.4194 [c]	1.42061	1.4940 [e]	1.49374
	1.4203 [d]		1.49410 [f]	
	1.4204 [e]		1.49417 [g]	

[a] Richon et al. [7]
[b] Riddick et al. [13]
[c] Loras et al. [8]
[d] Carmona et al. [9]
[e] Martínez-Soria et al. [10]
[f] Domanska et al. [11]
[g] Li et al. [6]
[h] $u(T)$ = 0.01 K, $u(R^l) = 1\times10^{-4}$

density meter, were 0.04 kg·m^{-3} and 0.05 K for density and temperature respectively. The measured densities were compared with data reported in literature [6-12]. The measured data and the literature data are reported in Table 2, and show a close agreement. The refractive indices of the MCH and the toluene were measured using an Atago RX7000 refractometer. The uncertainties for this unit, as reported by the manufacturers, were 1×10^{-4} and 0.01 K for refractive index and temperature respectively. The measured refractive indices were compared with data from literature [6-11, 13] in Table 3 and there was found to be a good agreement between the data sources.

Experimental Apparatus. The static-analytic high-pressure VLE apparatus that was developed by Narasigadu et al. [14] was used to perform these VLE measurements. This equipment was designed for the measurement of phase equilibria at temperatures of between (253 and 473) K and at pressures of up to 17 MPa. Williams-Wynn and co-workers 3 provided a detailed description of the apparatus.

Calibrations. The temperature probes, pressure transducer and the thermal conductivity detector (TCD) of the GC all required calibration. The Pt100 temperature probes, obtained from WIKA Instruments, were calibrated against a WIKA CTH 6500 temperature standard probe. This temperature standard probe had a maximum temperature uncertainty of 0.02 K. The maximum uncertainty in the calibration, at temperatures of between (268.15 and 323.15) K, was found to be 0.06 K.

A (0 to 25) MPa pressure transducer, also purchased from WIKA Instruments, was calibrated against a WIKA CPT 6000 pressure standard transducer. This standard pressure transducer had a maximum uncertainty of 6.2 kPa over its full span of (0 to 25) MPa. The calibration was performed at pressures of between (0 and 10) MPa, giving a standard deviation of 0.5 kPa. The internal barometer of a Mensor CPC 3000 Pneumatic High-Speed Pressure Controller, with an uncertainty of 0.01 kPa, was used to measure the atmospheric pressure.

The TCD of the GC was calibrated by relating the response of the TCD to the injection of known amounts of the chemicals through the GC. Several accurately known volumes of each component were injected into the GC with a syringe. This was repeated at least five times for each volume. The gases were injected with a 500 µl gas-tight SGE syringe and the liquids were injected with a 1.0 µl SGE liquid syringe. The uncertainties in the volumes injected were 1 and 2 % of the volume for the gases and liquids respectively. The number of moles of gas that was injected was calculated via the ideal gas equation, and the number of moles of liquid injected was calculated via the liquid densities. The uncertainties in the calibrations were 5.8×10^{-8} moles, 6.0×10^{-8} moles, 2.8×10^{-8} moles and 7.5×10^{-8} moles for trifluoromethane, hexafluoroethane, MCH and toluene respectively .

Experimental Procedure. The experimental procedure that was used to realise the data presented in this paper is similar to that which was presented by Nandi and co-workers [15]. In-situ degassing was performed despite the purities of the gases being very near to 1.0, as this removed any impurities that could have entered the cell during the loading procedure. An important change to the experimental procedure of Nandi and co-workers was the heating of the vaporisation chamber of the ROLSI™ to 453 K during sampling. This was to ensure that the MCH and toluene were vaporised before being transferred to the GC for analysis. The higher temperature was required because of the relatively lower volatilities of MCH and toluene.

Data Treatment. The guidelines for the estimation of uncertainties, published by the National Institute of Standards and Technology (NIST) [16-17], were used to estimate the uncertainties in the measured variables. The combined expanded uncertainties, calculated with a coverage factor of 2, were reported.

The Peng-Robinson equation of state (PR EOS) [18] with the Mathias -Copeman (MC) alpha function [19], coupled with the Wong-Sandler (WS) mixing rule [20], was used to model the system. The Gibbs' excess energy term within the mixing rule was described using either the Non-Random Two-Liquid (NRTL) [21] or the Universal Quasi-Chemical (UNIQUAC) activity coefficient model [22].

The regression tool-kit within Aspen Plus V8.0 was used to regress the model parameters to the experimental data. The regression was performed by minimising a modified Barker's objective function using a Deming-type algorithm. Both temperature-dependent and the temperature-independent parameters for the models were regressed, and their performances were compared.

The two statistical terms that were used to compare the performances of the different models were the average relative deviation (ARD) and the absolute average relative deviation (AARD). The equations used to determine these statistical terms are given by equations 1 and 2 .

$$ARD(\theta) = \frac{100}{N_p}\sum_{1}^{N_p}\frac{\theta_{exp} - \theta_{calc}}{\theta_{exp}} \quad (1)$$

$$AARD(\theta) = \frac{100}{N_p}\sum_{1}^{N_p}\frac{|\theta_{exp} - \theta_{calc}|}{\theta_{exp}} \quad (2)$$

where θ is the measured variable, the subscripts *exp* and *calc* represent the experimental and calculated data points respectively, and N_p is the number of data points in the set. .

Two methods were utilised for the estimation of the mixture critical points of the binary systems. The first method was the extended scaling law method of Ungerer et al. [23]. This method was applied to VLE data by El Ahmar et al. [24], and relies on the availability of sub-critical coexistence data, which is extrapolated to the critical point. The second critical point estimation technique was that of Heidemann and Khalil [25]. Stockfleth and Dohrn [26] provided an in-depth explanation of this technique, which requires a thermodynamic model, fitted to experimental phase equilibrium data, to enable the mixture critical locus curves to be constructed. Williams-Wynn and co-workers [3] have discussed both of these mixture critical point estimation techniques in greater detail .

Results and discussion

The parameters for the MC alpha function were fitted to vapour pressure data that was reported in literature for MCH [27-34] and for tolu-

Table 4.
The Mathias-Copeman alpha function parameters (κ_i) for the pure components investigated in this study in the temperature range, T, regressed from literature data.

	T / K	κ_1	κ_2	κ_3
trifluoromethane [b]	252.93 – 299.07	0.776	0 [a]	0 [a]
hexafluoroethane [c]	273.10 – 292.90	0.777	0 [a]	0 [a]
methylcyclohexane [d]	273.15 – 323.13	0.712	0.033	0.193
toluene [e]	283.10 – 333.15	0.744	0.063	0.122

[a] Set to zero for this study.
[b] Obtained from Williams-Wynn et al. [3].
[c] Obtained from Williams-Wynn et al. [4].
[d] Regressed to literature data [27-34]

ene [6, 27, 35-41]. The MC alpha parameters that were reported by Williams-Wynn et al. [3-4] for R-23 and R-116 were used in this study. A one parameter model was used for both R-23 and R-116, because of the measurement of some VLE data above the refrigerant critical temperatures. In these cases, the second and third terms of the model will become trivial. The MC alpha function parameters that were used in this study are reported in Table 4.

The measured phase equilibrium data for the four systems are reported in Tables 5 through 8. Alongside of the isothermal *P-x-x-y* data presented in these tables are the estimated combined expanded uncertainties for each measured variable (temperature, pressure and composition). The parameters for the PR MC + WS/NRTL and PR MC + WS/UNIQUAC thermodynamic models that were fitted to the experimental data are presented in Tables 9 to 12. Both the temperature dependent and the temperature independent parameters are reported. The statistical data for the regressions are included alongside the respective parameters. Table 13 contains several points along each of the four critical locus curves, which were calculated using the procedure of Heidemann and Khalil. Additionally, the mixture critical points for three of the systems, calculated by the procedure of Ungerer et al. are also included. No mixture critical points could be extrapolated for the R-116 + toluene system. This was due to only liquid-liquid critical points being present for this system. The method of Ungerer and co-workers fails for liquid-liquid critical points.

The experimental *P-x-x-y* data for the four systems are plotted alongside the curves produced by the thermodynamic models in Figures 1 to 4. These figures also include the calculated critical locus curves (by the method of Heidemann and Khalil) and the extrapolated mixture critical points (by the method of Ungerer et al.). For the investigation into the temperature dependency of the thermodynamic models, the temperature dependent and temperature independent parameters for each system are plotted on Figures 5 through 8.

The phase equilibria of the R-23 + MCH system (Tables 5 and 9, Figures 1 and 5) exhibited a large miscibility gap, including (vapour-liquid-liquid equilibrium) VLLE points at the lower two temperatures measured. At 313.2 K, only LLE was observed at the higher pressures, with no vapour phase being present. The pressure of the transition from VLLE to LLE was not measured in this study. The thermodynamic models provided a reasonable description of the system. The description of the bubble point curve by the models was fairly accurate, but the modelled vapour phase compositions were between 0.01 and 0.03 higher than the experimental values. Despite these deviations being further accentuated in the expanded view of the *P-x-x-y* plot, they were still greater than the expanded experimental uncertainties. The models provided good estimates of the VLLE which occurred at the lower temperatures, as well as being capable of predicting the occurrence of the "bird's-beak" phenomenon. There was little difference between the performances of the two models.

Table 5.
Experimental P-x_1^{I}-x_1^{II}-y_1 data with combined expanded uncertainties (U) for the binary system of R-23 (1) + methylcyclohexane (2) at temperatures of T = (293.03 to 313.23) K. Pressure, P, the 1st liquid phase composition, x_1^{I}, the 2nd liquid phase composition, x_1^{II}, and the vapour phase composition, y_1, along with their corresponding uncertainties are reported. The combined expanded uncertainties were calculated with a coverage factor of k = 2 .

T / K	U(T)/ K	P /MPa	U(P)/ MPa	x_1^{I}	U (x_1^{I})	x_1^{II}	U (x_1^{II})	y_1	U(y_1)
293.03	0.07	0.914	0.004	0.019	0.001			0.976	0.003
293.03	0.07	1.509	0.006	0.035	0.001			0.981	0.002
293.03	0.07	2.121	0.006	0.055	0.002			0.984	0.002
293.04	0.07	2.625	0.010	0.072	0.002			0.980	0.002
293.04	0.07	3.060	0.007	0.090	0.002			0.988	0.002
293.04	0.07	3.553	0.009	0.115	0.003			0.983	0.003
293.03	0.07	3.893	0.004	0.133	0.003	0.898	0.003	0.987	0.002
293.04	0.07	3.910	0.004	0.916	0.009			0.989	0.001
293.04	0.07	3.939	0.004	0.933	0.003			0.989	0.001
293.04	0.07	3.960	0.004	0.942	0.003			0.994	0.001
293.04	0.07	4.066	0.004	0.972	0.002			0.994	0.001
303.12	0.08	1.011	0.005	0.020	0.001			0.970	0.002
303.13	0.08	1.601	0.006	0.034	0.001			0.973	0.003
303.13	0.08	2.311	0.009	0.054	0.001			0.984	0.002
303.13	0.08	2.942	0.004	0.073	0.002			0.988	0.002
303.13	0.08	3.784	0.008	0.105	0.002			0.986	0.001
303.13	0.08	4.396	0.007	0.133	0.003			0.985	0.001
303.13	0.09	4.848	0.007	0.156	0.004	0.911	0.003	0.992	0.002
303.13	0.08	4.847	0.004	0.913	0.003			0.990	0.001
303.14	0.08	4.973	0.004	0.954	0.001			0.985	0.001
303.14	0.08	5.074	0.004	0.973	0.002			0.989	0.002
303.14	0.08	5.112	0.006	0.985	0.001			0.996	0.001
313.23	0.10	0.931	0.006	0.016	0.002			0.952	0.004
313.23	0.10	1.459	0.004	0.029	0.001			0.962	0.004
313.23	0.09	2.159	0.005	0.045	0.002			0.968	0.003
313.23	0.10	2.831	0.005	0.063	0.002			0.975	0.003
313.22	0.09	3.489	0.006	0.083	0.002			0.977	0.002
313.22	0.09	4.046	0.006	0.101	0.003			0.980	0.002
313.22	0.10	4.819	0.007	0.132	0.003			0.978	0.001
313.23	0.10	5.335	0.008	0.154	0.004			0.973	0.001
313.22	0.09	5.598	0.004	0.165	0.004			0.967	0.002
313.23	0.10	5.950	0.006	0.173	0.003			0.943	0.003
313.22	0.09	6.077	0.008	0.180	0.004			0.920	0.002

There was a substantial difference between the critical locus curve and the extrapolated mixture critical point for the R-23 + MCH system. This was likely due to the critical locus curve being dependent upon a thermodynamic model. Any discrepancies between the experimental data and the model was therefore projected onto the critical locus curve. Only a single mixture critical point could be extrapolated for this system, as the method of Ungerer and co-workers could only be applied to vapour-liquid critical points. Of the three isotherms that were measured for the system, only the 293.0 K isotherm contained vapour-liquid critical points. The other two isotherms exhibited liquid-liquid critical points.

The thermodynamic models provided reasonable descriptions of the three isotherms at which experimental data was measured for the R-23 + toluene system (Tables 6 and 10, Figures 2 and 6). The 293.1 K and 303.1 K bubble point curves were modelled fairly well, but the models did not provide a good description of the 313.2 K isotherm. For this system, there was once again little variance between the temperature-dependent and temperature-independent models. Both models over-

Table 6.
Experimental P-x_1-y_1 data with combined expanded uncertainties (U) for the binary system of R-23 (1) + toluene (2) at temperatures of T = (293.04 to 313.26) K. Pressure, P, the liquid phase composition, x_1, and the vapour phase composition, y_1, along with their corresponding uncertainties are reported. The combined expanded uncertainties were calculated with a coverage factor, k = 2 .

T/K	U(T) / K	P / MPa	U(P) /MPa	x_1	U(x_1)	y_1	U(y_1)
293.04	0.07	0.847	0.004	0.041	0.001	0.977	0.002
293.06	0.07	1.376	0.004	0.077	0.002	0.981	0.002
293.05	0.07	1.999	0.005	0.135	0.004	0.987	0.003
293.07	0.07	2.481	0.004	0.196	0.004	0.988	0.002
293.07	0.08	2.976	0.004	0.306	0.005	0.988	0.002
293.06	0.07	3.199	0.004	0.404	0.005	0.988	0.002
293.07	0.07	3.400	0.004	0.538	0.005	0.992	0.001
293.05	0.08	3.487	0.004	0.660	0.005	0.992	0.001
293.05	0.08	3.593	0.004	0.740	0.005	0.991	0.002
293.06	0.08	3.790	0.004	0.868	0.003	0.994	0.001
293.06	0.08	4.035	0.004	0.958	0.002	0.998	0.001
293.05	0.08	4.114	0.004	0.987	0.001	0.998	0.001
303.10	0.08	0.908	0.004	0.038	0.001	0.965	0.001
303.10	0.08	1.429	0.006	0.065	0.001	0.977	0.002
303.12	0.08	2.000	0.005	0.104	0.002	0.984	0.002
303.13	0.08	3.232	0.007	0.231	0.004	0.986	0.001
303.13	0.08	3.680	0.006	0.324	0.005	0.987	0.002
303.13	0.08	3.980	0.005	0.440	0.005	0.987	0.001
303.13	0.08	4.198	0.005	0.576	0.005	0.987	0.002
303.12	0.08	4.339	0.004	0.713	0.004	0.989	0.001
303.12	0.08	4.460	0.004	0.788	0.004	0.988	0.002
303.12	0.08	4.813	0.009	0.914	0.003	0.994	0.001
303.13	0.08	5.037	0.004	0.969	0.002	0.997	0.003
313.24	0.10	0.834	0.004	0.029	0.001	0.940	0.003
313.23	0.10	1.675	0.006	0.066	0.001	0.974	0.001
313.23	0.10	2.397	0.006	0.106	0.002	0.980	0.002
313.23	0.10	3.238	0.006	0.171	0.002	0.979	0.001
313.23	0.09	3.960	0.006	0.247	0.004	0.980	0.002
313.23	0.10	4.534	0.006	0.346	0.005	0.979	0.001
313.23	0.09	4.886	0.005	0.462	0.005	0.977	0.001
313.22	0.10	5.083	0.004	0.565	0.005	0.976	0.002
313.22	0.09	5.213	0.007	0.659	0.005	0.976	0.002
313.22	0.10	5.413	0.004	0.767	0.004	0.973	0.001
313.24	0.09	5.605	0.004	0.837	0.004	0.967	0.002
313.26	0.09	5.698	0.006	0.898	0.002	0.967	0.002

Table 7.
Experimental P-x_1^{I}-x_1^{II}-y_1- data with combined expanded uncertainties (U) for the binary system of R-116 (1) + methylcyclohexane (2) at temperatures of T = (293.10 to 313.15) K. Pressure, P, the 1st liquid phase composition, x_1^{I}, the 2nd liquid phase composition, x_1^{II}, and the vapour phase composition, y_1, along with their corresponding uncertainties are reported. The combined expanded uncertainties are calculated with the coverage factor, k = 2.

T / K	U(T) / K	P/ MPa	U(P)/ MPa	x_1^{I}	U (x_1^{I})	x_1^{II}	U (x_1^{II})	y_1	U(y_1)
293.11	0.11	0.941	0.004	0.030	0.003			0.974	0.002
293.10	0.10	1.240	0.004	0.038	0.003			0.982	0.002
293.10	0.09	1.517	0.006	0.046	0.002			0.980	0.001
293.10	0.09	1.871	0.008	0.061	0.004			0.985	0.002
293.10	0.09	2.164	0.007	0.074	0.003			0.984	0.002
293.12	0.11	2.464	0.004	0.088	0.003			0.983	0.002
293.11	0.10	2.737	0.004	0.103	0.004			0.987	0.003
293.11	0.09	2.778	0.005	0.102	0.003	0.925	0.003	0.992	0.002
293.11	0.09	2.830	0.004	0.941	0.003			0.995	0.001
293.10	0.07	2.928	0.006	0.982	0.001			0.994	0.001
293.11	0.08	3.010	0.007	0.994	0.001			0.998	0.001
303.11	0.06	0.912	0.005	0.028	0.001			0.942	0.003
303.11	0.06	1.129	0.004	0.037	0.002			0.971	0.002
303.11	0.06	1.342	0.004	0.041	0.002			0.978	0.003
303.11	0.06	1.667	0.005	0.052	0.002			0.975	0.002
303.10	0.06	1.990	0.005	0.065	0.003			0.981	0.003
303.11	0.06	2.337	0.007	0.075	0.003			0.978	0.002
303.12	0.06	2.651	0.006	0.086	0.003			0.978	0.001
303.12	0.07	2.966	0.004	0.100	0.004			0.982	0.002
303.12	0.06	3.212	0.006	0.107	0.004			0.983	0.003
303.12	0.06	3.384	0.004	0.118	0.004			0.977	0.002
303.12	0.06	3.451	0.004	0.121	0.004			0.971	0.003
303.12	0.07	3.486	0.009	0.123	0.003			0.960	0.003
313.14	0.07	0.962	0.004	0.029	0.002			0.971	0.001
313.14	0.07	1.264	0.004	0.038	0.002			0.975	0.001
313.15	0.07	1.516	0.005	0.045	0.002			0.976	0.002
313.14	0.07	1.994	0.005	0.064	0.002			0.978	0.003
313.13	0.06	2.416	0.007	0.078	0.003			0.982	0.003
313.14	0.07	2.807	0.005	0.093	0.003			0.973	0.006
313.13	0.06	3.057	0.004	0.102	0.003			0.979	0.002
313.14	0.06	3.361	0.006	0.112	0.003			0.976	0.003
313.13	0.05	3.656	0.006	0.124	0.004			0.976	0.002
313.13	0.06	3.819	0.006	0.128	0.004			0.976	0.002
313.12	0.06	3.972	0.005	0.131	0.005			0.977	0.002
313.12	0.07	4.220	0.005	0.134	0.004			0.966	0.002

Table 8.
Experimental P-x_1^{I}-x_1^{II}-y_1 data with combined expanded uncertainties (U) for the binary system of R-116 (1) + toluene (2) at temperatures of T = (293.10 to 313.12) K. Pressure, P, the 1st liquid phase composition, x_1^{I}, the 2nd liquid phase composition, x_1^{II}, and the vapour phase composition, y_1, along with their corresponding uncertainties are reported .

T / K	U (T)/ K	P/ MPa	U(P)/ MPa	x_1^{I}	U (x_1^{I})	x_1^{II}	U (x_1^{II})	y_1	U(y_1)
293.11	0.08	1.007	0.005	0.010	0.003			0.970	0.004
293.11	0.08	1.484	0.004	0.016	0.003			0.984	0.002
293.10	0.07	1.861	0.004	0.020	0.003			0.989	0.001
293.10	0.07	2.391	0.008	0.026	0.003			0.991	0.001
293.11	0.08	2.708	0.008	0.029	0.003			0.994	0.001
293.11	0.08	2.919	0.004	0.030	0.003	0.997	0.001	0.995	0.001
303.11	0.06	1.026	0.005	0.010	0.003			0.966	0.002
303.11	0.06	1.607	0.004	0.017	0.002			0.982	0.003
303.11	0.06	2.345	0.004	0.028	0.002			0.987	0.002
303.11	0.06	2.836	0.005	0.030	0.002			0.990	0.001
303.10	0.05	3.344	0.005	0.033	0.002			0.992	0.001
303.10	0.06	3.568	0.004	0.034	0.003			0.987	0.002
303.10	0.06	3.807	0.005	0.034	0.002			0.981	0.003
313.11	0.05	1.076	0.005	0.010	0.003			0.977	0.003
313.10	0.08	1.630	0.004	0.017	0.004			0.982	0.001
313.10	0.06	2.320	0.004	0.027	0.002			0.979	0.002
313.12	0.04	2.907	0.005	0.031	0.003			0.986	0.003
313.11	0.04	3.631	0.005	0.036	0.003			0.988	0.001
313.11	0.04	4.137	0.004	0.040	0.003			0.987	0.002
313.11	0.04	4.605	0.007	0.040	0.003			0.980	0.002

predicted the dew point compositions at all three temperatures. This over-prediction appeared to be worsened at higher temperatures and lower pressures. The models were capable of modelling the "bird's-beak" phenomenon occurring at lower temperatures.

From the critical locus curve that was calculated for this system, it appeared that the 313.2 K isotherm may also exhibit the "bird's-beak phenomenon". This was because the extrapolated mixture critical point at 313.2 K appeared to be incorrect when compared against the critical locus curve. Alternatively, the critical locus curve was incorrect due to the poor description of the vapour phase by the model at 313.2 K. The "bird's-beak" phenomenon was not observed experimentally, and therefore the second option would appear to be the more likely.

The two systems involving R-116 both exhibited very large miscibility gaps. This was possibly due to the molecules having unlike polarities. R-116 has a dipole moment of zero, while the non-symmetric MCH and toluene have small, non-zero, dipole moments, making them slightly polar.

The R-116 + MCH system (Tables 7 and 11, Figures 3 and 7) exhibited a vapour-liquid critical point, along with a three phase VLLE region at 293.1 K, and liquid-liquid critical points for the other two isotherms. The thermodynamic models provided fairly accurate descrip-

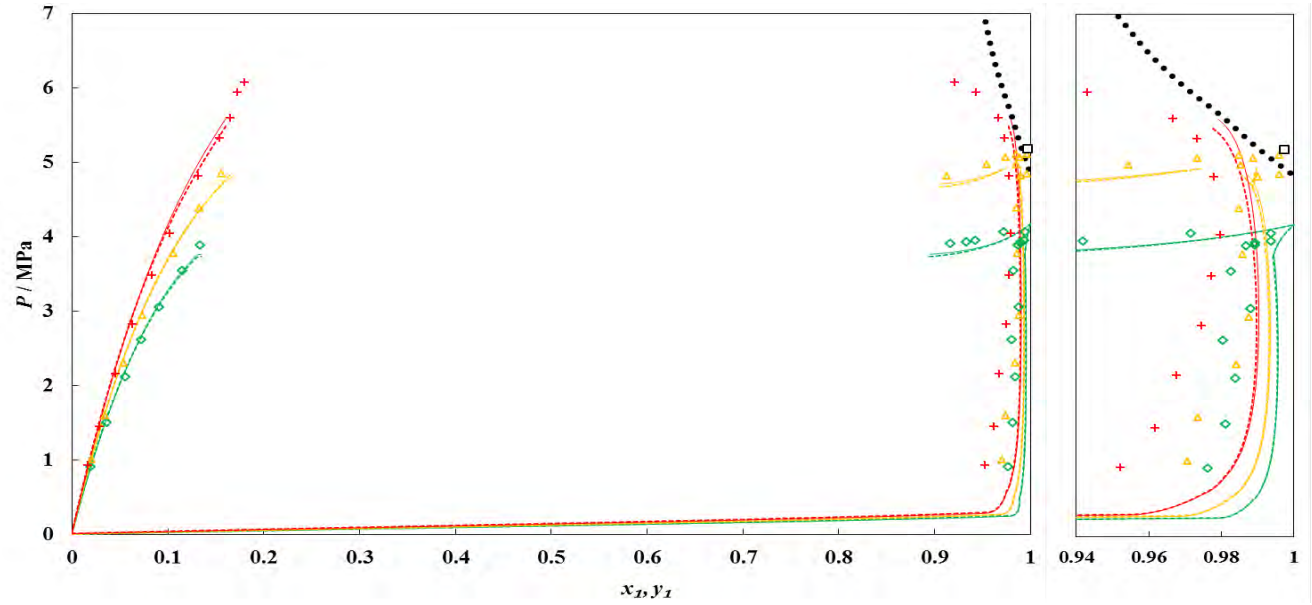

Figure 1. P-x_1^{I}-x_1^{II}-y_1 data for the binary system of trifluoromethane (1) + methylcyclohexane (2) at temperatures of ◇, 293.0 K; △, 303.1 K; +, 313.2 K. Solid lines: PR MC + WS/NRTL model; dashed lines: PR MC + WS/UNIQUAC model; □, mixture critical locus (Ungerer et al. method); ••••, mixture critical locus curve (Heidemann and Khalil method) .

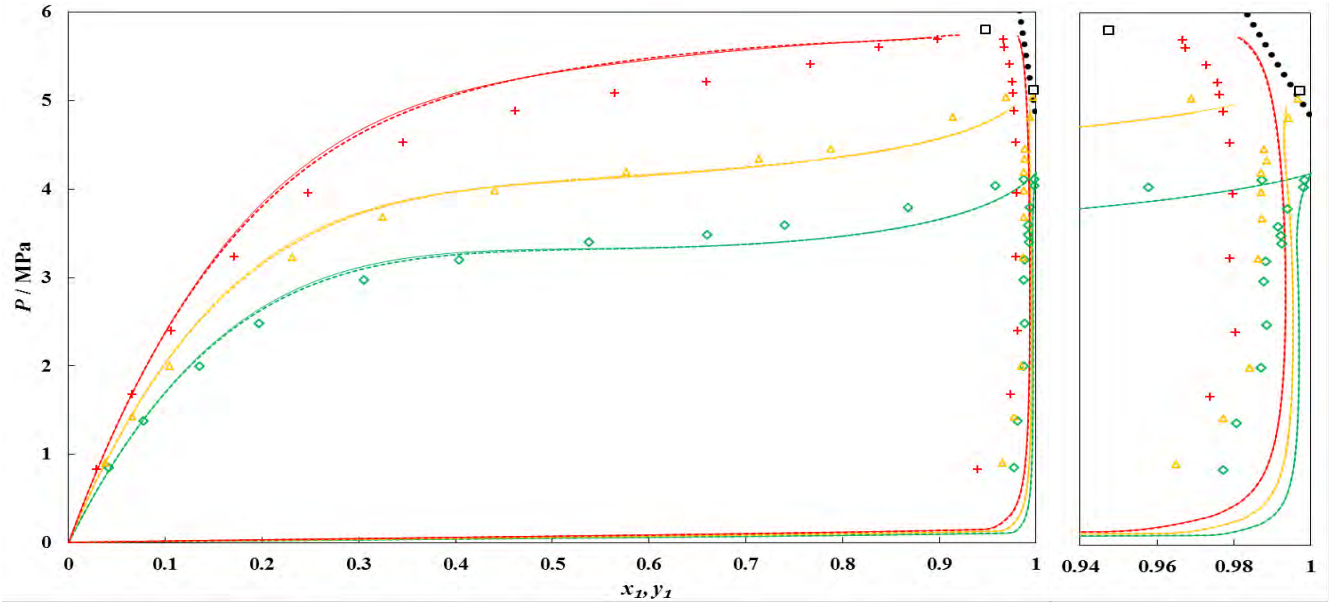

Figure 2. P-x_1-y_1 data for the binary system of trifluoromethane (1) + toluene (2) at temperatures of ◇, 293.1 K; △, 303.1 K; +, 313.2 K. Solid lines: PR MC + WS/NRTL model; dashed lines: PR MC + WS/UNIQUAC model; □, mixture critical loci (Ungerer et al. method); ••••, mixture critical locus curve (Heidemann and Khalil method) .

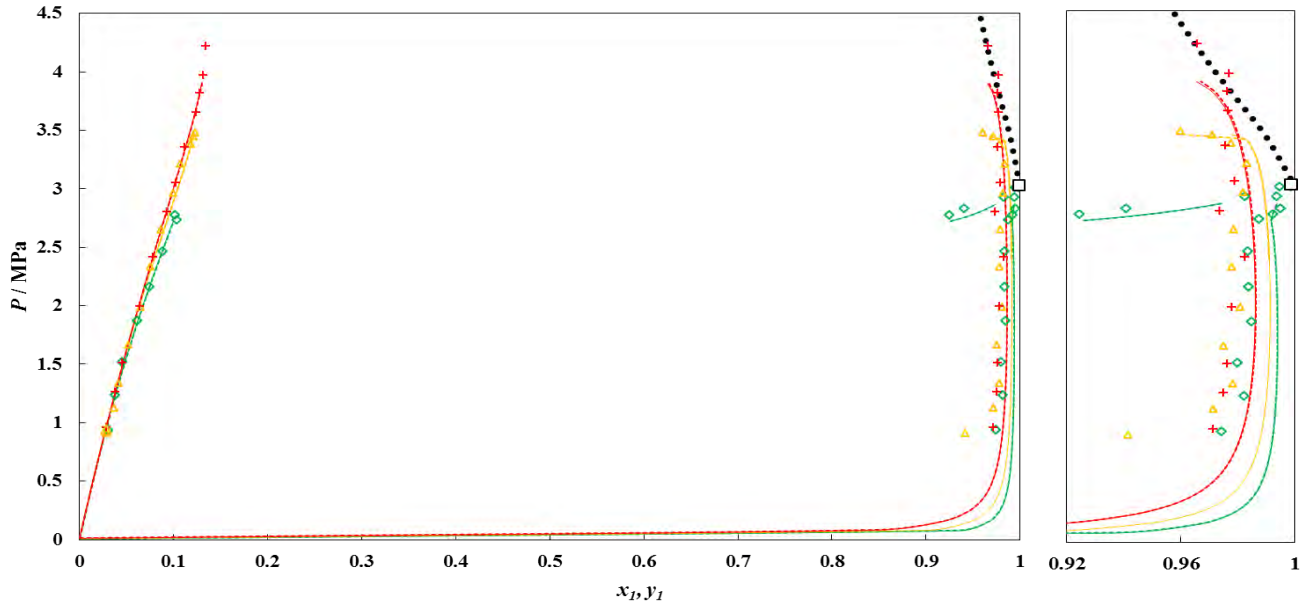

Figure 3. P-x_1^{I}-x_1^{II}-y_1 data for the binary system of hexafluoroethane (1) + methylcyclohexane (2) at temperatures of ◇, 293.1 K; △, 303.1 K; +, 313.1 K. Solid lines: PR MC + WS/NRTL model; dashed lines: PR MC + WS/UNIQUAC model; □, mixture critical locus (Ungerer et al. method); ••••, mixture critical locus curve (Heidemann and Khalil method) .

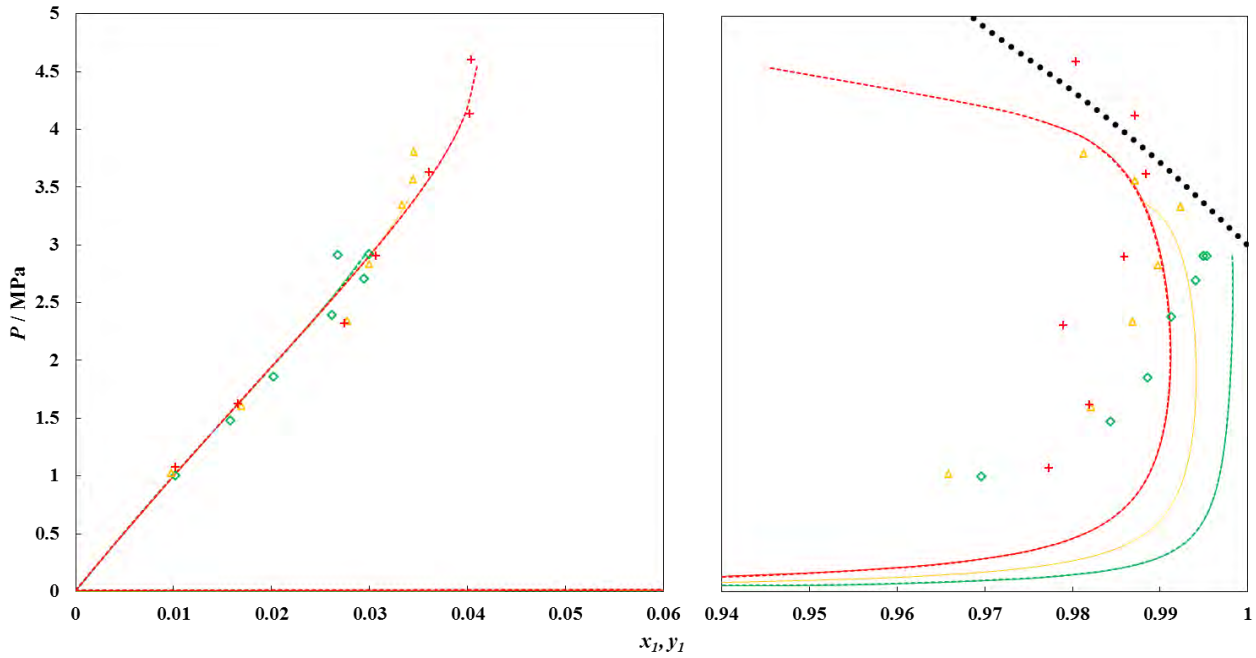

Figure 4. P-x_1^{I}-x_1^{II}-y_1 data for the binary system of hexafluoroethane (1) + methylcyclohexane (2) at temperatures of ◇, 293.1 K; △, 303.1 K; +, 313.1 K. Solid lines: PR MC + WS/NRTL model; dashed lines: PR MC + WS/UNIQUAC model; □, mixture critical locus (Ungerer et al. method); ••••, mixture critical locus curve (Heidemann and Khalil method) .

tions of the phase behaviour of this system. The description of the dew point curve was more accurate with this system than with the systems containing R-23. It was found that the temperature independent models were able to describe the system more accurately than the temperature dependent models. In particular, the temperature independent model was able to describe the VLLE and the "bird's-beak" phenomenon for the 293.1 K isotherm more accurately than the temperature-dependent model. The critical locus curve was calculated using the temperature dependent model by the method of Heidemann and Khalil. This critical locus curve agreed with the extrapolated mixture critical point.

Table 9.

The temperature dependent and temperature independent model parameters (k_{12} and τ_{ij} or Δu_{ij}) and regression statistics for the binary system of trifluoromethane (1) + methylcyclohexane (2). The temperature dependent parameters were regressed at temperatures, T = (293.0 to 313.2) K. The average relative deviations (ARD) and the absolute average relative deviations (AARD) in the pressure, P, and vapour mole fraction, y, are included for each of the regressions.

T / K	k_{12}	τ_{12} / K [a] || Δu_{12} [b] / J·mol^{-1}	τ_{21} / K [a] || Δu_{21} [b] / J·mol^{-1}	ARD [c]		AARD [d]	
				P	y	P	y
PR MC + WS/NRTL							
293.0	0.566	299.7	695.8	2.18	-0.94	2.58	0.94
303.1	0.568	288.2	703.1	1.47	0.09	2.90	1.24
313.2	0.557	313.9	692.0	-1.39	-0.98	2.40	3.58
(293.0 to 313.2)	0.562	313.4	689.1	0.50	-0.58	2.87	1.93
PR MC + WS/UNIQUAC							
293.0	0.549	-404.2	5507.9	2.43	-0.93	2.78	0.93
303.1	0.552	-464.0	5590.4	1.86	0.48	3.05	1.60
313.2	0.531	-464.5	5672.9	-0.90	-0.66	1.92	3.71
(293.0 to 313.2)	0.548	-408.6	5497.0	0.69	-0.61	2.97	1.89

[a] τ_{12}, τ_{21} for the NRTL activity coefficient model
[b] Δu_{12}, Δu_{21} for the UNIQUAC activity coefficient model

[c] absolute average deviation, $ARD(\theta) = \frac{100}{N_p}\sum_{1}^{N_p}\frac{\theta_{exp}-\theta_{calc}}{\theta_{exp}}$

[d] absolute average relative deviation, $AARD(\bar{\theta}) = \frac{100}{N_p}\sum_{1}^{N_p}\frac{|\bar{\theta}_{exp}-\bar{\theta}_{calc}|}{\bar{\theta}_{exp}}$

All three of the isotherms that were measured for the R-116 + toluene system (Tables 8 and 12, Figures 4 and 8) would likely have exhibited liquid-liquid critical points. The poor miscibility of the R-116 and toluene made measurement of the VLE fairly challenging in the static-analytic cell. A variable-volume cell with sampling capabilities for both the liquid and the vapour phases would have enabled the measurement of greater amounts of data for this system. The bubble point data of the three isotherms were very difficult to distinguish between, with the only tangible difference being the increased solubility of the R-116 in the toluene rich phase with increased temperature. The differences between the dew point curves of the three isotherms were larger than those of the bubble point curves. The models were not particularly capable of accurately modelling the phase behaviour of the system, with the performances of the temperature dependent models being worse than those of the temperature independent models. The poor modelling of the phase behaviour likely translated into a poor description of the critical locus curve. However, due to no isotherms exhibiting vapour-liquid critical

Table 10.

The temperature dependent and temperature independent model parameters (k_{12} and τ_{ij} or Δu_{ij}) and regression statistics for the binary system of trifluoromethane (1) + toluene (2). The temperature dependent parameters were regressed at temperatures, T = (293.0 to 313.2) K. The average relative deviations (ARD) and the absolute average relative deviations (AARD) in the pressure, P, and vapour mole fraction, y, are included for each of the regressions.

T / K	k_{12}	τ_{12} / K [a] || Δu_{12} [b] / J·mol^{-1}	τ_{21} / K [a] || Δu_{21} [b] / J·mol^{-1}	ARD		AARD	
				P	y	P	y
PR MC + WS/NRTL							
293.0	0.419	312.8	369.8	0.53	-0.94	3.88	0.94
303.1	0.441	319.6	383.5	0.24	-1.12	2.70	1.12
313.2	0.474	330.5	396.2	-2.55	-1.42	4.21	1.77
(293.1 to 313.2)	0.462	215.5	435.6	-2.18	-1.12	3.69	1.15
PR MC + WS/UNIQUAC							
293.0	0.420	-264.7	3452.8	1.49	-0.73	3.59	0.73
303.1	0.437	-452.3	3778.2	0.68	-1.00	2.65	1.01
313.2	0.471	-558.5	3918.1	-2.51	-1.40	3.93	1.77
(293.0 to 313.2)	0.460	-544.4	3856.9	-0.29	-0.96	2.59	1.24

[a] τ_{12}, τ_{21} for the NRTL activity coefficient model
[b] Δu_{12}, Δu_{21} for the UNIQUAC activity coefficient model

Table 11.

The temperature dependent and temperature independent model parameters (k_{12} and τ_{ij} or Δu_{ij}) and regression statistics for the binary system of hexafluoroethane (1) + methylcyclohexane (2). The temperature dependent parameters were regressed at temperatures, T = (293.1 to 313.1) K. The average relative deviations (ARD) and the absolute average relative deviations (AARD) in the pressure, P, and vapour mole fraction, y, are included for each of the regressions.

T / K	k_{12}	τ_{12} / K [a] || Δu_{12} [b] / J·mol^{-1}	τ_{21} / K [a] || Δu_{21} [b] / J·mol^{-1}	ARD		AARD	
				P	y	P	y
PR MC + WS/NRTL							
293.1	0.407	213.9	671.4	0.95	-0.54	2.19	0.61
303.1	0.423	212.9	636.5	0.67	-1.22	2.65	1.60
313.1	0.355	317.6	569.7	0.45	-0.29	1.10	0.82
(293.1 to 313.1)	0.411	202.4	656.1	0.30	-0.29	4.84	1.46
PR MC + WS/UNIQUAC							
293.1	0.405	-791.8	3227.8	0.92	-0.53	2.18	0.62
303.1	0.421	-795.5	3113.9	0.64	-1.22	2.70	1.59
313.1	0.362	-571.7	2776.9	0.37	-0.34	1.12	0.80
(293.1 to 313.1)	0.407	-791.5	3130.0	0.17	-0.50	6.12	1.23

[a] τ_{12}, τ_{21} for the NRTL activity coefficient model
[b] Δu_{12}, Δu_{21} for the UNIQUAC activity coefficient model

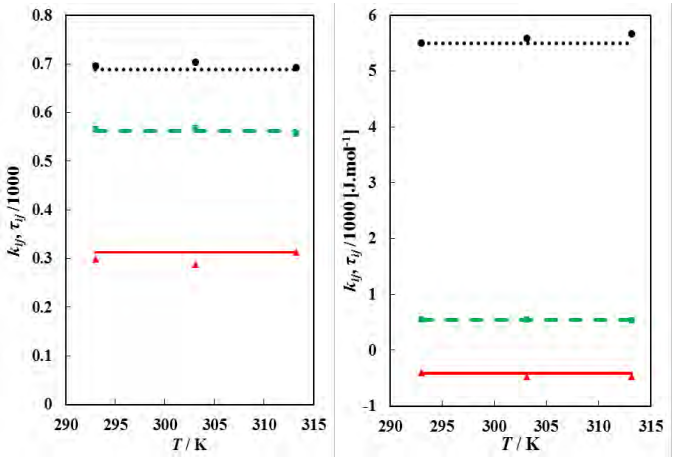

Figure 5. The thermodynamic model parameters for the system of R-23 (1) + methylcyclohexane (2) with the temperature independent parameters represented by symbols, and the temperature dependent parameters represented by lines Left: (PRMC + WS/NRTL model): ■ /- - -, k_{12}; ● /·····, τ_{12}; ▲ /——, τ_{21}. Right: (PRMC + WS/UNIQUAC model): ■ /- - -, k_{12}; ●/·····, Δu_{12}; ▲/——, Δu_{21}.

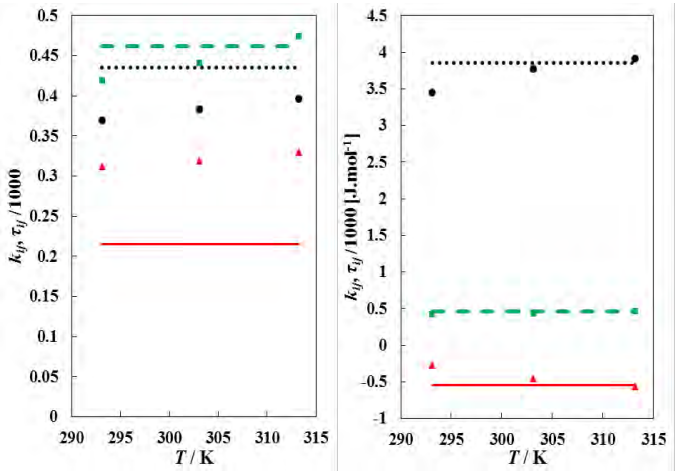

Figure 6. The thermodynamic model parameters for the system of R-23 (1) + toluene (2) with the temperature independent parameters represented by symbols, and the temperature dependent parameters represented by lines. Left: (PRMC + WS/NRTL model): ■ /- - -, k_{12}; ●/·····, τ_{12}; ▲ /——, τ_{21}. Right: (PRMC + WS/UNIQUAC model): ■ /- - -, k_{12}; ● /·····, Δu_{12}; ▲ /——, Δu_{21}.

Table 12.

The temperature dependent and temperature independent model parameters (k_{12} and τ_{ij} or Δu_{ij}) and regression statistics for the binary system of hexafluoroethane (1) + toluene (2). The temperature dependent parameters were regressed at temperatures, T = (293.1 to 313.1) K. The average relative deviations (ARD) and the absolute average relative deviations (AARD) in the pressure, P, and vapour mole fraction, y, are included for each of the regressions.

T / K	k_{12}	τ_{12} / K [a] || Δu-$_{12}$ [b] / J·mol^{-1}	τ_{21} / K [a] || Δu_{21} [b] / J·mol^{-1}	ARD		AARD	
				P	y	P	y
PR MC + WS/NRTL							
293.1	0.765	-108.9	1117.0	-2.44	-0.91	3.54	0.91
303.1	0.364	21.3	1135.9	-0.12	0.29	5.12	1.39
313.1	0.366	46.9	1094.8	0.30	-0.20	4.71	0.87
(293.1 to 313.1)	0.721	-20.5	1001.1	-3.62	-1.15	6.76	1.15
PR MC + WS/UNIQUAC							
293.1	0.750	-1452.8	4686.1	-2.48	-0.99	3.41	0.99
303.1	0.350	-1192.0	4695.0	0.56	-0.28	4.29	0.81
313.1	0.352	-1155.9	4564.0	0.23	-0.20	4.62	0.86
(293.1 to 313.1)	0.709	-1161.7	4080.8	-3.46	-1.13	8.23	1.13

[a] τ_{12}, τ_{21} for the NRTL activity coefficient model
[b] Δu_{12}, Δu_{21} for the UNIQUAC activity coefficient model

Table 13.

Critical locus curves, consisting of critical temperature, T_c, critical pressure, P_c, and the composition at these conditions, x_c, estimated from the thermodynamic models by the method of Heidemann and Khalil [25], and extrapolated mixture critical loci by the method of Ungerer et al. [23].

Critical Locus Curves (Heidemann & Khalil)					
T_c / K	P_c / MPa	$x_{c,1}$	T_c / K	P_c / MPa	$x_{c,1}$
R-23 (1) + methylcyclohexane (2)			*R-23 (1) + toluene (2)*		
301.7	5.21	0.99	305.5	5.52	0.99
306.8	5.64	0.98	312.8	6.24	0.98
316.3	6.02	0.97	322.4	6.99	0.97
330.8	6.48	0.96	336.7	7.81	0.96
348.0	7.06	0.95	365.9	9.52	0.94
371.2	8.14	0.93	401.2	11.34	0.92
382.0	10.05	0.90			
R-116 (1) + methylcyclohexane (2)			*R-116 (1) + toluene (2)*		
300.2	3.43	0.99	297.4	3.73	0.99
306.7	3.74	0.98	302.9	4.35	0.98
312.7	4.05	0.97	307.2	4.91	0.97
319.8	4.40	0.96	312.1	5.53	0.96
326.6	4.76	0.95	316.3	6.01	0.95
364.1	6.54	0.90	326.9	7.20	0.93
			351.2	9.19	0.90
			379.1	11.31	0.85
Critical Loci (Ungerer et al.)					
T_c / K	P_c / MPa	$x_{c,1}$	T_c / K	P_c / MPa	$x_{c,1}$
R-23 (1) + methylcyclohexane (2)			*R-23 (1) + toluene (2)*		
303.1	5.18	0.997	303.1	5.13	0.997
			313.2	5.81	0.948
R-116 (1) + methylcyclohexane (2)			*R-116 (1) + toluene (2)*		
293.1	3.03	0.998			

points being measured, it was impossible to verify the critical locus curve with critical loci extrapolated from the sub-critical co-existence data.

The plots of the temperature dependent and independent parameters for the thermodynamic models (Figures 5 to 8) reveal that the temperature dependency was, for the most part, sufficiently described using simple linear dependency of the models. In some cases, a substantial difference between the temperature dependent and temperature independent parameter sets occurred, but this may have been due to a number of factors surrounding the regression of the given parameter set, rather than due to the temperature dependency of the system. For the most part, the description of the phase behaviour was not substantially

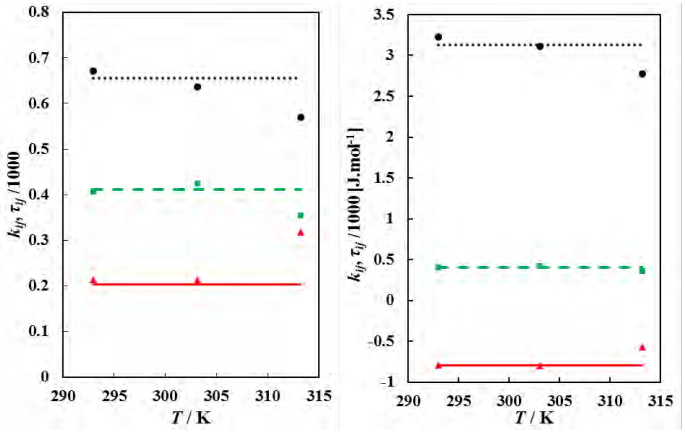

Figure 7. The thermodynamic model parameters for the system of R-116 (1) + methylcyclohexane (2) with the temperature independent parameters represented by symbols, and the temperature dependent parameters represented by lines. Left: (PRMC + WS/NRTL model): ■ /- - -, k_{12}; ● /·····, τ_{12}; ▲ /——, τ_{21}. Right: (PRMC + WS/UNIQUAC model): ■ /- - -, k_{12}; ●/·····, Δu_{12}; ▲/——, Δu_{21}.

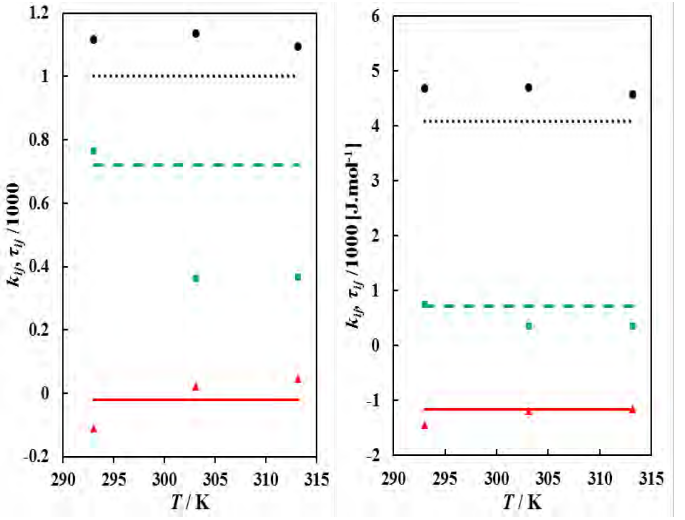

Figure 8. The thermodynamic model parameters for the system of R-116 (1) + toluene (2) with the temperature independent parameters represented by symbols, and the temperature dependent parameters represented by lines. Left: (PRMC + WS/NRTL model): ■ /- - -, k_{12}; ● /·····, τ_{12}; ▲ /——, τ_{21}. Right: (PRMC + WS/UNIQUAC model): ■ /- - -, k_{12}; ● /·····, Δu_{12}; ▲ /——, Δu_{21}.

different when using the temperature-dependent parameters as opposed to using the temperature-independent parameters. The temperature dependent parameters have a distinct advantage over the temperature-independent parameters, in that they can be applied to any temperature within the range of the experimental data to which they were regressed.

Since only three isotherms were measured per system, it was difficult to accurately characterise the systems according to the van Konynenburg and Scott [42] classification scheme. There were, however, a number of characteristics that could be used to shortlist the number of possible types that these systems could be classified by. All four systems exhibited liquid-liquid immiscibility, and therefore could not be classified as type I systems, which do not exhibit any immiscibilities. Additionally, the systems presented liquid-liquid critical loci at certain temperatures, and could therefore not be classified as type II systems. Thus, the systems were most likely either type III, type IV, or type V systems. Measurement of the systems at conditions near to the critical point of the heavier components would enable further classification of the systems from a *P-T* plot. This would make it possible to determine whether the critical locus curve emanating from the critical point of the heavier component traversed to the lower critical end point (LCEP) (for type IV or V systems) or to a critical point at infinite pressure (type III systems). To distinguish between type IV and type V systems would require a search for a low temperature upper critical solution temperature (UCST).

Conclusions

A static-analytic high-pressure phase equilibrium apparatus was used to measure VLE and VLLE for four binary refrigerant + hydrocarbon systems at temperatures of between (293.0 and 313.3) K. The four systems that were measured were R-23 + MCH, R-23 + toluene, R-116 + MCH and R-116 + toluene. Only the R-23 + toluene system did not exhibit liquid-liquid immiscibility at the temperatures that were studied. The "bird's-beak" phenomenon occurred near to the critical point for three of the systems, with only R-116 + toluene not displaying this behaviour.

The PR MC + WS/NRTL and the PR MC + WS/UNIQUAC thermodynamic models were fitted to the experimental data, and found to provide adequate descriptions of the phase behaviour. There was little difference between the two thermodynamic models, or between the temperature dependent and the temperature independent forms of the models. The performances of the models were poorest in their description of the vapour phase compositions. The critical locus curves were calculated from the temperature dependent models by the method of Heidemann and Khalil, and compared to the critical loci extrapolated from the experimental data by the method of Ungerer and co-workers. The agreement between the critical locus curves and the critical loci were closest at locations nearest to the critical point of component 1. The classification of the systems according to the van Konynenburg and Scott technique was discussed, and several of the classification types were shortlisted for these systems.

Acknowledgements

This work is based upon research supported by the South African Research Chairs Initiative of the Department of Science and Technology and the National Research Foundation. The authors would like to thank the NRF Focus Area Programme and the NRF Thuthuka Programme .

Literature Cited

1. Beckman, E. J. J. Supercritical Fluids 2004, 28 (2–3), 121-191.
2. Brunner, G. Fluid Phase Equilib. 1983, 10 (2-3), 289-298.
3. Williams-Wynn, M. D.; Naidoo, P.; Ramjugemath, D. J. Chem. Thermodyn. 2015, unpublished.
4. Williams-Wynn, M. D.; Naidoo, P.; Ramjugemath, D. Fluid Phase Equilib. 2015, unpublished.
5. Williams-Wynn, M. D.; Naidoo, P.; Ramjugemath, D. J. Chem. Eng. Data 2015, unpublished.
6. Li, I. P. C.; Wong, Y.-W.; Chang, S.-D.; Lu, B. C. Y. J. Chem. Eng. Data 1972, 17 (4), 492-498.
7. Richon, D.; Laugier, S.; Renon, H. J. Chem. Eng. Data 1991, 36 (1), 104-111.
8. Loras, S.; Montón, J. B.; España, F. J. Chem. Eng. Data 1997, 42 (5), 914-918.
9. Carmona, F. J.; González, J. A.; García de la Fuente, I.; Cobos, J. C. J. Chem. Eng. Data 1999, 44 (5), 892-895.
10. Martínez-Soria, V.; Peña, M. P.; Montón, J. B. J. Chem. Eng. Data 1999, 44 (1), 148-151.
11. Domanska, U.; Letcher, T. M. J. Chem. Thermodyn. 2000, 32 (12), 1635-1645.
12. Sun, Y.; Su, L.; Wang, H. J. Chem. Thermodyn. 2009, 41 (10), 1154 -1161.
13. Riddick, J. A.; Bunger, W. B.; Sakano, T. K. Organic Solvents: Physical Properties and Methods of Purification Techniques of

Chemistry. 4th ed.; Wiley: New York, 1986; Vol. 2.
14.Narasigadu, C.; Naidoo, P.; Coquelet, C.; Richon, D.; Ramjugernath, D. Fluid Phase Equilib. 2013, 338, 188-196.
15.Nandi, P.; Moodley, S.; Ramjugernath, D. Fluid Phase Equilib. 2013, 344, 84-91.
16.Taylor, B. N.; Kuyatt, C. E. NIST Technical Note 1994, 1297.
17.Taylor, B. N.; Mohr, P. J.; Douma, M. The NIST Reference on constants, units, and uncertainty. 2007.
18.Peng, D. Y.; Robinson, D. B. Ind. Eng. Chem. Fundam. 1976, 15, 59 -64.
19.Mathias, P. M.; Copeman, T. W. Fluid Phase Equilib. 1983, 13, 91-108.
20.Wong, D. S. H.; Sandler, S. I. AIChE J. 1992, 38, 671-680.
21.Renon, H.; Prausnitz, J. M. AIChE J. 1968, 14, 135-144.
22.Abrams, D. S.; Prausnitz, J. M. AIChE J. 1975, 21 (1), 116-128.
23.Ungerer, P.; Tavitian, B.; Boutin, A. Applications of molecular simulation in the oil and gas industry- Monte Carlo methods. 2005.
24.El Ahmar, E.; Valtz, A.; Naidoo, P.; Coquelet, C.; Ramjugernath, D. J. Chem. Eng. Data 2011, 56 (5), 1918-1924.
25.Heidemann, R. A.; Khalil, A. M. AIChE J. 1980, 26 (5), 769-779.
26.Stockfleth, R.; Dohrn, R. Fluid Phase Equilib. 1998, 45, 43-52.
27.Willingham, C. B.; Taylor, W. J.; Pignocco, J. M.; Rossini, F. D. J. Res. Natl. Bur. Stand. (U. S.) 1945, 35, 219.
28.Bonhorst, C. W.; Althouse, P. M.; Triebold, H. O. Ind. Eng. Chem. 1948, 40 (12), 2379-2384.
29.Nicolini, E.; Laffitte, P. C. R. Hebd. Séances Acad. Sci. 1949, 229, 757-759.
30.Heady, R. B.; Cahn, J. W. J. Chem. Phys. 1973, 58 (3), 896-910.
31.Castellari, C.; Francesconi, R.; Comelli, F. Can. J. Chem. Eng. 1988, 66 (1), 131-135.
32.Wu, H. S.; Pividal, K. A.; Sandler, S. I. J. Chem. Eng. Data 1991, 36 (4), 418-421.
33.Pividal, K. A.; Sterner, C.; Sandler, S. I.; Orbey, H. Fluid Phase Equilib. 1992, 72, 227-250.
34.Mokbel, I.; Rauzy, E.; Loiseleur, H.; Berro, C.; Jose, J. Fluid Phase Equilib. 1995, 108 (1-2), 103–120.
35.Kahlbaum, G. W. A. Ber. Dtsch. Chem. Ges. 1884, 17 (1), 1245-1262.
36.Kahlbaum, G. W. A. Z. Phys. Chem., Stoechiom. Verwandschaftsl. 1898, 26 (577-658).
37.Woringer, B. Z. Phys. Chem., Stoechiom. Verwandschaftsl. 1900, 34, 257.
38.Forziati, A. F.; Norris, W. R.; Rossini, F. D. J. Res. Natl. Bur. Stand. (U. S.) 1949, 43 (6), 555-564.
39.Besley, L. M. J. Chem. Thermodyn. 1974, 6 (6), 577–580.
40.Mokbel, I.; Rauzy, E.; Meille, J. P.; Jose, J. Fluid Phase Equilib. 1998, 147, 271-284.
41.Negadi, L.; Mokbel, I.; Negadi, A.; Kaci, A. A.; Jose, J.; Gmehling, J. J. Chem. Eng. Data 2009, 54 (7), 2045-2048.
42.van Konynenburg, P. H.; Scott, R. L. Philos. Trans. R. Soc. 1980, 298, 495-540.
43.Kim, K. Y. Calorimetric studies on argon and hexafluoroethane and a generalized correlation of maxima in isobaric heat capacity. Ph.D. Dissertation, University of Michigan, Ann Arbour, MI, 1974.
44.Saikawa, K.; Kijima, J.; Uematsu, M.; Watanabe, K. J. Chem. Eng. Data 1979, 24 (3), 165-167.
45.Lide, D. R. CRC Handbook of Chemistry and Physics 2004-2005: A Ready-Reference Book of Chemical and Physical Data. CRC Press LLC: 2004.